Synthesis and Evaluation of Novel Azaindolocarbazole Derivatives as Cancer Chemotherapeutics

Michael Cahill, B.Sc.

ucc

Coláiste na hOllscoile Corcaigh, Éire
University College Cork, Ireland

Thesis presented for the degree of Doctor of Philosophy
to National University of Ireland, Cork.

Department of Chemistry

Supervisor: Dr. Florence McCarthy

Head of Department: Prof. Michael Morris

March 2013

Table of Chapters

Acknowledgments

To try and convey my deepest gratitude to everybody who has given me such help and support over the past few years is a feat in itself, but I'll try my best. Firstly, I would like to sincerely thank Dr. Florence McCarthy for his encouragement and supervision throughout the duration of this project. It was a real honour and privilege for me to have been able to join such a dedicated research group.

There is an enormous wealth of technical expertise within UCC, and the assistance of so many different staff members has been vital towards the completion of this work. I would like to thank Dr. Dan McCarthy and Dr. Lorraine Bateman for NMR services, Dr. Ken Devine for topoisomerase I and II testing, Mick O'Shea for mass spectrometry services and Derry Kearney for glassblowing. I would also like to thank all of the other members of staff for their help, including Chrissie O'Flaherty, Noel Browne, Johnny Ryan, Terry Horgan, Pat O'Connell, Dr. Michael Cronin, Dr. Tom O'Mahony and Tina Kent.

To all the past and present members of the FMC research group, I would like to give my utmost thanks for their companionship and shared knowledge over the years, namely Larry, Charlotte, Fiona, Kieran, Hannah, Elaine and Niamh. To the new members Kevin and Quentin, I wish them all the best for the future. To Denis L., Donncha, Denis B., Harry, Colm and Tina, those who also had the misfortune of sharing a lab with me, thanks for the banter! I would also like to give my gratitude to the other organic postgrads and postdocs for their help and guidance – I'm leaving UCC with so many fond memories. The exploits of Synthos F.C. in particular will live long in the folklore of the department! Thanks to my good friends in both Cork and Ennis for all of the great shared experiences, it has certainly been emotional!

Most especially, I would like to thank my family for their constant love and support throughout this work, as it made every single day so much easier. Mum and Dad, I can't even begin to tell you how grateful I am for everything. Thank you so much.

Declaration

I hereby confirm that the body of work described within this thesis, for the degree of Doctor of Philosophy, is the result of my own research work, which was carried out under the supervision of Dr. Florence McCarthy, and has not been previously submitted for any other degree, either at University College Cork or elsewhere.

_____ Date: _____

For Mum and Dad

with all my love, as always

Abstract

This thesis details the design and implementation of novel chemical routes towards a series of highly propitious 7-azaindolyl derivatives of the indolocarbazole (ICZ) and bisindolylmaleimide (BIM) families, with subsequent evaluation for use as cancer chemotherapeutic agents.

A robust synthetic strategy was devised to allow the introduction of a 7-azaindolyl moiety into our molecular template. This approach allowed access to a range of β-keto ester and β-keto nitrile intermediates from simple starting materials such as succinonitrile and ethyl formate. Critical analysis identified F-ring modulation as a major theme towards the advancement of ICZ and BIM derivatives in drug therapy. Thus, the employment of cyclocondensation methodology furnished a number of novel aminopyrazole, isoxazolone, pyrazolone and pyrimidinone analogues, considerably widening the scope of the prevalent maleimide functionality.

Photochemical cyclisation provided for the first reported aza ICZ containing a six-membered F-ring, though similar application to other aza BIM derivatives had limited success. A second, more durable method towards achieving the aza ICZ core involved use of a Perkin-type condensation approach, with chemical elaboration of the headgroup instigated after rather than prior to aromatisation. The subsequent use of a modified Lossen rearrangement allowed access to further analogues containing a six-membered F-ring.

Extensive screening of the novel aza ICZ and BIM derivatives was carried out against the NCI-60 cancer cell array, with nine prospective candidates selected for further biological evaluation. From the resulting five-dose assays, a number of compounds were shown to inhibit cancer cell growth at concentrations of below 10 nM. Indeed, the most active aza ICZ tested is currently under assessment by the Biological Evaluation Committee of the NCI due to excellent antiproliferative activity demonstrated across the panel of cell lines, with a mean GI_{50} of 34 nM, a mean total growth inhibition (TGI) of 4.6 μM and a mean cytotoxicity (LC_{50}) of 63.1 μM.

Correlation to known topoisomerase I (topo I) inhibitors was revealed by COMPARE analysis, and the resulting topo I-mediated DNA cleavage assays showed inhibitory activity below 1 μM for several derivatives. On completion of this work, it is evident that there exists enormous potential within the aza ICZ family for the development of novel anticancer agents.

Abbreviations

AML	Acute myeloid leukemia
ATP	Adenosine triphosphate
aza ICZ	Azaindolocarbazole
bs	Broad singlet
bd	Broad doublet
BIM	Bisindolylmaleimide
Bn	Benzyl
Boc	*tert*-Butoxycarbonyl
CDI	1,1'-Carbonyldiimidazole
CDK	Cyclin-dependent kinase
$CDCl_3$	Deuterated chloroform
CHK1	Checkpoint kinase 1
CNS	Central nervous system
CPT	Camptothecin
d	Doublet
DCM	Dichloromethane
dd	Doublet of doublets
DDQ	2,3-Dichloro-5,6-dicyano-*p*-benzoquinone
DEPT	Distortionless enhancement of polarisation transfer
DMAP	*N*,*N*-Dimethylaminopyridine
DMF	*N*,*N*-Dimethylformamide
DMSO-d_6	Deuterated dimethyl sulfoxide
DNA	Deoxyribonucleic acid
DTP	Developmental Therapeutics Program
EGFR	Epidermal growth factor receptor
EtOH	Ethanol
g	Gram
FLT3	Fms-like tyrosine kinase

GI_{50}	50% Growth inhibition concentration
GSK-3	Glycogen synthase kinase-3
IC_{50}	50% Inhibition concentration
ICZ	Indolocarbazole
J	Coupling constant
JNK	c-Jun *N*-terminal kinase
HCl	Hydrochloric acid
HMBC	Heteronuclear multiple bond correlation
HRMS	High resolution mass spectrometry
HSQC	Heteronuclear single quantum correlation
Hz	Hertz
IR	Infrared
LC_{50}	50% Lethal concentration
LDA	Lithium diisopropylamide
LiHMDS	Lithium hexamethyldisilazane
lit.	Literature
m	Multiplet
MAPK	Mitogen-activated protein kinase
Me	Methyl
MeOH	Methanol
mg	milligram
MHz	Megahertz
mL	millilitre
MLK	Multiple lineage kinase
µM	micromolar
mmol	millimole
mol	mole
m.p.	melting point
nM	nanomolar

NMR	Nuclear magnetic resonance
NSCLC	Non-small cell lung cancer
PDB	Protein Data Bank
PDK1	Phosphoinositide-dependent kinase 1
PKA	cAMP-dependent protein kinase
PKC	Protein kinase C
p-TSA	*para*-Toluenesulfonic acid
q	Quartet
REB	Rebeccamycin
RET	Rearranged during transfection kinase
r.t.	Room temperature
s	Singlet
SAR	Structure activity relationship
SEM	2-(Trimethylsilyl)ethoxymethyl
STA	Staurosporine
t	Triplet
TBAF	Tetrabutylammonium fluoride
TBDMS	*tert*-Butyldimethylsilyl
TGI	Total growth inhibition
THF	Tetrahydrofuran
TLC	Thin-layer chromatography
TMS	Trimethylsilane
Topo I	Topoisomerase I
UV	Ultraviolet
VEGFR	Vascular endothelial growth factor receptor

Chapter 1

Biological Introduction

Contents

1.0 Biological Introduction

1.1 Cancer

One of the major causes of death in the world, cancer is estimated to be responsible for one out of every four deaths in the United States alone.[1] There is significant regional variability in the incident and mortality rates of different cancers, partly reflected by differences in lifestyle, prevalence and distribution of the major risk factors, detection practices and the availability and use of treatment services. For example, incident rates for breast cancer are highest in Western Europe but relatively low in sub-Saharan Africa and Asia, while half of the total number of cases and deaths worldwide due to liver cancer are estimated to occur in China.[2]

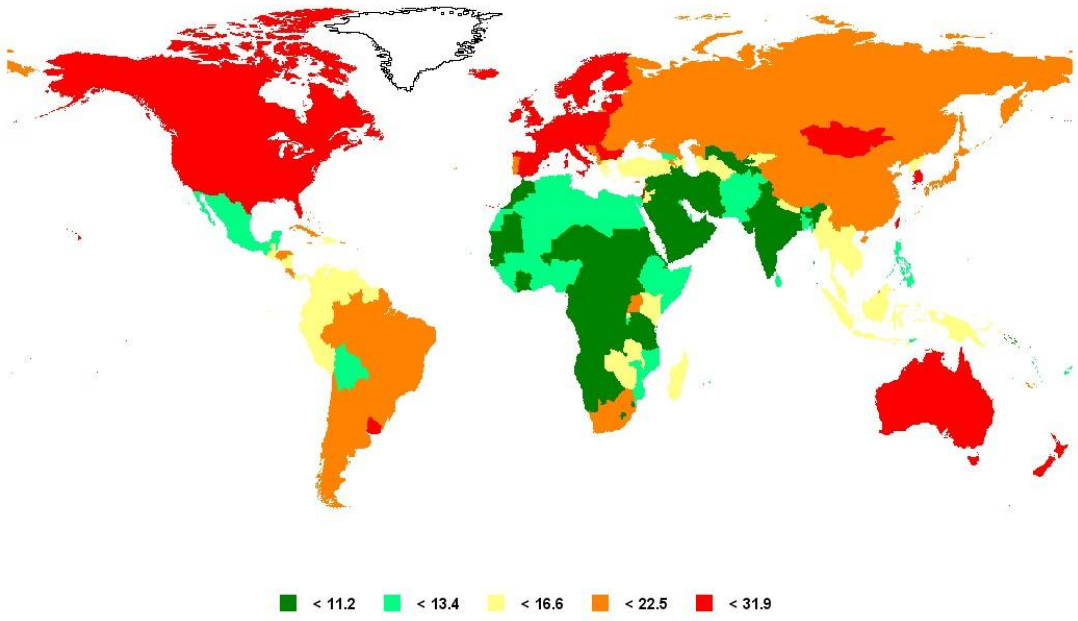

Fig. 1.1 *Estimated worldwide cumulative incidence (%) for all cancers, excluding non-melanoma skin cancer*[3]

In a European context, Ireland was ranked second behind Denmark in 2008 in terms of cancer incidence, but was much closer to the average with regard to cancer mortality rates across the countries surveyed (***Figure 1.2***).[4] Depending on the type of cancer, prognostic estimates can differ quite significantly in this country. For example, five year survival rates for testicular and prostate cancer have been determined to be 97% and 88% respectively, while cancers of

the pancreas, lung, brain and stomach have survival rates of below 25% over the same time period.[5]

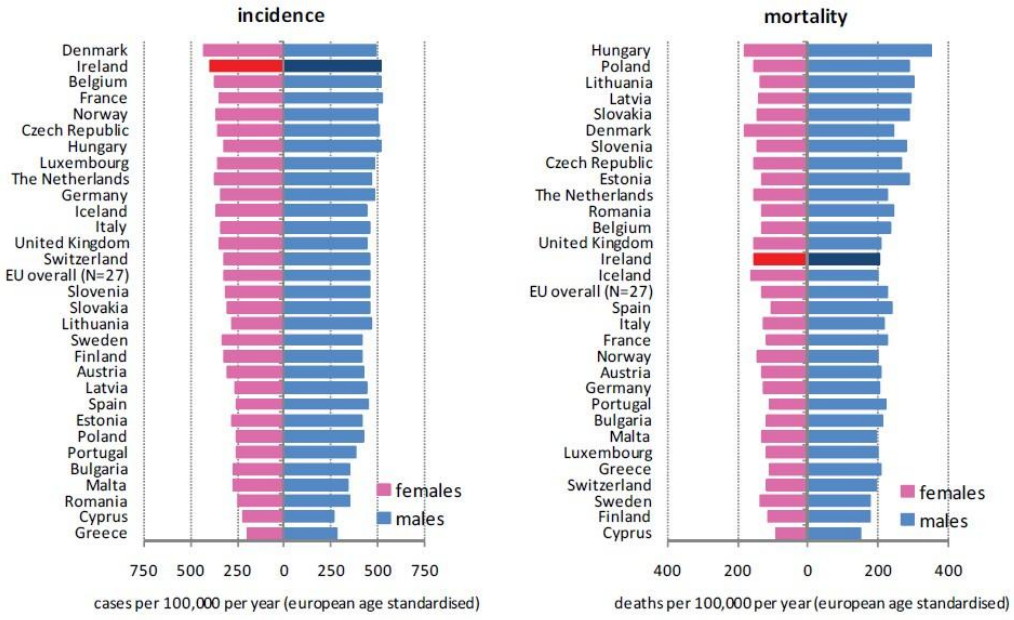

Fig. 1.2 *Estimated cancer incidence and mortality rates in Europe*[5]

Whilst commonly and most frequently referred to as an ailment in a singular sense, cancer is in fact a collection of different diseases that have a number of common features, with the most prominent being the uncontrolled growth and spread within the body of abnormal forms of the body's own cells. The actual term "cancer" refers to a malignant neoplasm, i.e. new growth. It can be quite difficult to classify and account for cancers as a particular group due to the fact that if a generalisation is made for this collection of diseases, there will always be an exception to disprove the rule. Despite this, it is possible to broadly define cancer as a set of diseases characterised by unregulated cell growth, leading to invasion of surrounding tissues and metastasis to other parts of the body.[6]

Though surgery is a primary method of treating cancer, it can only be effective if the cancer has not already undergone metastasis to other sites within the body. Other forms of treatment for cancer such as immunotherapy, chemotherapy and irradiation are thought to mediate their effects via induction of apoptosis in cancer cells.[7] In order to achieve the successful treatment of the vast majority of cancers, it has become apparent that only combinations of therapeutic

agents chosen for the highest possible individual activity against a specific type of cancer will effect a desirable outcome.[8] As a result, there is an even greater need for the development of novel drug templates with which to pursue targeted cancer therapies.

1.2 Indolocarbazole alkaloids

1.2.1 Discovery of staurosporine

The indolo[2,3-*a*]carbazole alkaloids, with a core pentacyclic structure **1**, represent a family of compounds upon which much research has been focused in recent years. Within the indolocarbazole class of compounds, four other isomeric ring systems are possible due to different orientations of the indolyl unit fused to one of the benzenoid rings of carbazole moiety. However, nearly all of the indolocarbazoles that have been isolated from nature contain an indolo[2,3-*a*]carbazole core, and as a whole, most scientific focus has been paid to this isomeric class.[9] While the first synthesis of an indolo[2,3-*a*]carbazole (ICZ) was reported by Tomlinson *et al*. in 1956, little attention was actually paid to this class of compounds until 1977, when the first isolation of an ICZ from nature was reported by Omura and co-workers.[10,11] Discovered in the course of screening extracts of the bacterium *Streptomyces staurosporeus*, this alkaloid was initially called AM-2282, but was subsequently renamed staurosporine (STA) **2**.

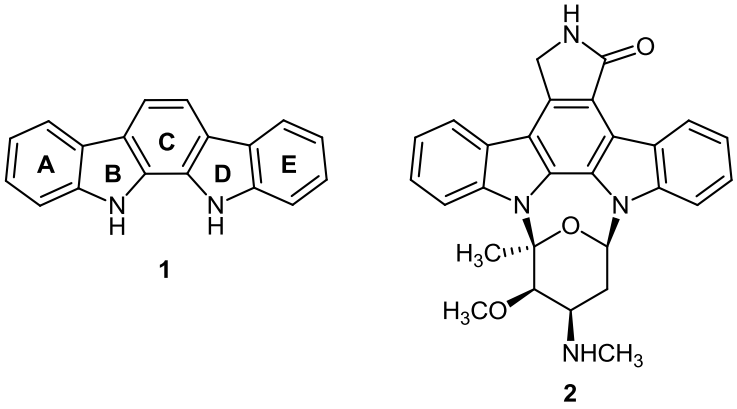

Fig. 1.3 *Indolo[2,3-a]carbazole **1** and STA **2** structures*

Early biological studies were to show that staurosporine **2** exhibited inhibitory activity toward fungi and also possessed strong hypotensive activity. The realisation of the potential of staurosporine **2** as a lead compound in anti-cancer treatment was to follow in 1986, when it was shown to be an extraordinarily potent inhibitor of protein kinase C (PKC) (IC_{50} = 2.7 nM) and was strongly cytotoxic towards cancer cells.[12] Unfortunately, STA **2** ultimately proved unsuitable to be brought forward as a pharmaceutical candidate due the wide variety of biological activities brandished by the compound, such as its ability to inhibit many more protein kinases in the low nanomolar range.[13]

1.2.2 Isolation of indolocarbazoles from natural sources

The isolation of further indolocarbazoles displaying intriguing biological profiles served to propagate the potential use of this class of compounds as anti-cancer agents. In 1985, rebeccamycin (REB) **3**, named after the daughter of the scientist who isolated the compound, was reported from cultures of the microorganism *Nocardia aerocolonigenes*.[14] Containing just one *N*-glycosidic bond instead of two as in the case of STA **2**, REB **3** was later shown to be active against leukemia and melanoma in mice, and to inhibit the growth of human lung adenocarcinoma cells, producing single-strand breaks in the DNA of these cells.[15]

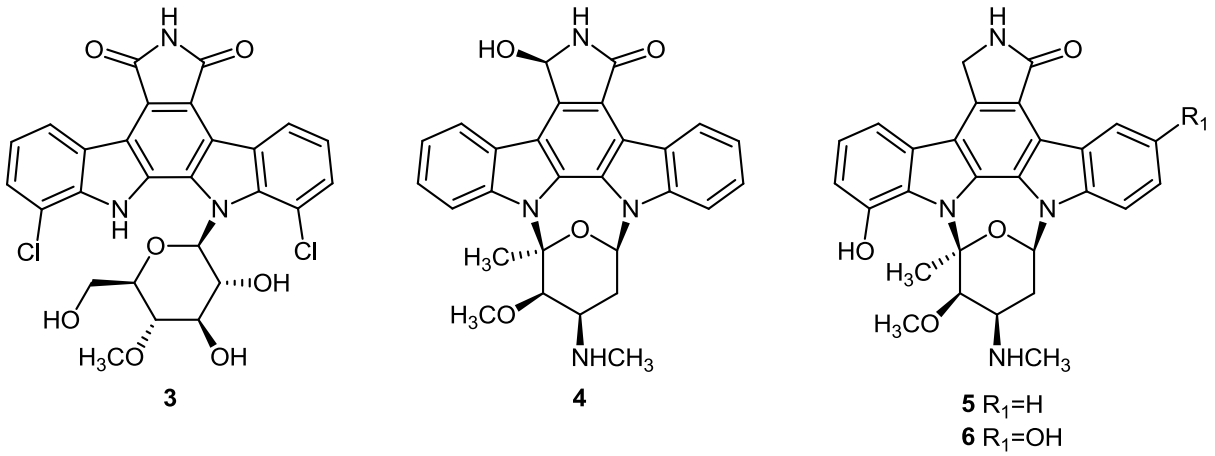

***Fig. 1.4** REB **3**, UCN-01 **4**, 11-hydroxy STA **5** and 3,11-dihydroxy STA **6** structures*

Isolated from *Streptomyces* sp. N-71, UCN-01 **4**, also known as 7-hydroxystaurosporine, was found to be a potent inhibitor of PKC and to exhibit significant *in vivo* antitumour activity.[16] Kinnel and Scheuer reported the isolation of 11-hydroxystaurosporine **5** and 3,11-

dihydroxystaurosporine **6** from the Pohnpei tunicate *Eudistoma* sp. in 1992, the first examples of naturally occurring indolocarbazoles from a marine organism. Both 11-hydroxy STA **5** and 3,11-dihydroxy STA **6** were shown to be active against cancer cell lines, with **5** proving to be a more potent PKC inhibitor than STA **2**.[17]

Many aglycone ICZ derivatives have also been identified from natural sources, such as arcyriaflavin A **7**, arcyriaflavin B **8** and arcyriaflavin C **9** which were reported to be contained in *Arcyria denudata* and *Arcyria nutans* slime moulds by Steglich *et al*.[18] Interestingly, in the same course of work, a series of bisindolylmaleimides, arcyriarubin A **10**, arcyriarubin B **11** and arcyriarubin C **12**, which are biosynthetically related to the ICZ class, were also isolated from the same moulds. Due to the close structural and biosynthetic relationship that is shared by both classes, bisindolylmaleimides are generally considered to be part of the broader ICZ family of compounds, despite their relative overall lack of planarity.[9] The aglycone of STA **2** itself, K252c **13**, was reported to be isolated from a different actinomycete strain, *Nocardiopsis* sp. K-290, by Nakanishi and co-workers in 1985.[19] However, since that time, both STA **2** and K252c **13** have been identified as coming from the same strains of microorganisms on a number of occasions, indicating that a complimentary biosynthetic pathway is involved.[20,21]

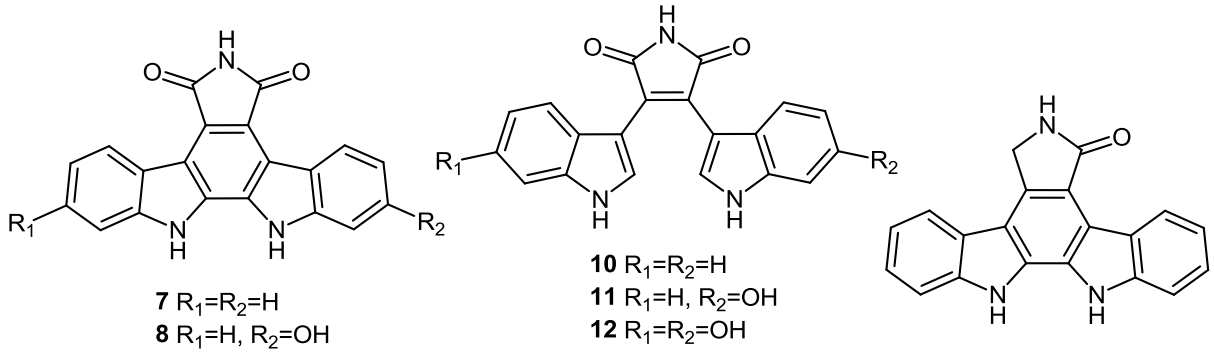

Fig. 1.5 *Arcyriaflavins A, B and C (**7**, **8**, **9**), arcyriarubins A, B and C (**10**, **11**, **12**) and K252c **13** structures*

Though not possessing a sugar moiety, as in the case of STA **2** and REB **3** for example, the arcyriaflavins and arcyriarubins were still shown to mediate significant biological activity. Arcyriaflavin A **7** displays micromolar and submicromolar inhibition against a number of

PKC isoforms and strongly inhibits the proliferation of non-small cell lung cancer A549 and murine leukemia P388 cell lines.[22] Arcyriarubin A **10**, while being the simplest bisindolylmaleimide structure, is a relatively effective nanomolar inhibitor of PKC (IC_{50} = 87 nM), along with the STA **2** aglycone, K252c **13** (IC_{50} = 110 nM).[19,23]

Ultimately, a wide variety of indolocarbazoles have been isolated from many different organisms over the past 35 years, including bacteria, fungi and marine invertebrates. Screening programmes to isolate further indolocarbazoles from natural sources have continued unabated, due to the potent antiproliferative activity and other biological responses mediated by numerous members within the compound class. Much focus has also been paid to the total syntheses of these natural products, as well as the development of synthetic ICZ analogues - a number of which are currently undergoing clinical trials.[24]

1.2.3 Biosynthesis of indolocarbazoles

With the isolation of indolocarbazoles from natural sources leading to the discovery of an extensive array of novel compounds with immense therapeutic potential, much work has also been carried out towards the elucidation of ICZ biosynthesis. From a biotechnology standpoint, the identification of genes involved in the biosynthesis of the naturally occurring members of this class, as well as the disclosure of their metabolic precursors and intermediates, has resulted in significant breakthroughs in the past 25 years.[9]

The biosyntheses of some of the more prominent members of the ICZ family have been widely studied, resulting in the identification of a number of similar key metabolic precursors (***Scheme 1.1***). The utilisation of isotope-labelled precursors in the fermentation of *Streptomyces staurosporeus*, the microorganism producer of STA **2**, and *Nocardia aerocolonigenes*, the producer of REB **3**, has led to the discovery that the core indolocarbazole structure is derived from two tryptophan **14** units.[25,26] Concomitantly, glucose **15** and methionine **16** were found to be the precursors responsible for the derivation of the sugar moiety in each case. However, it was not possible to determine the origin of the nitrogen of the lactam unit in STA **2** and maleimide unit in REB **3** in the course of these studies.

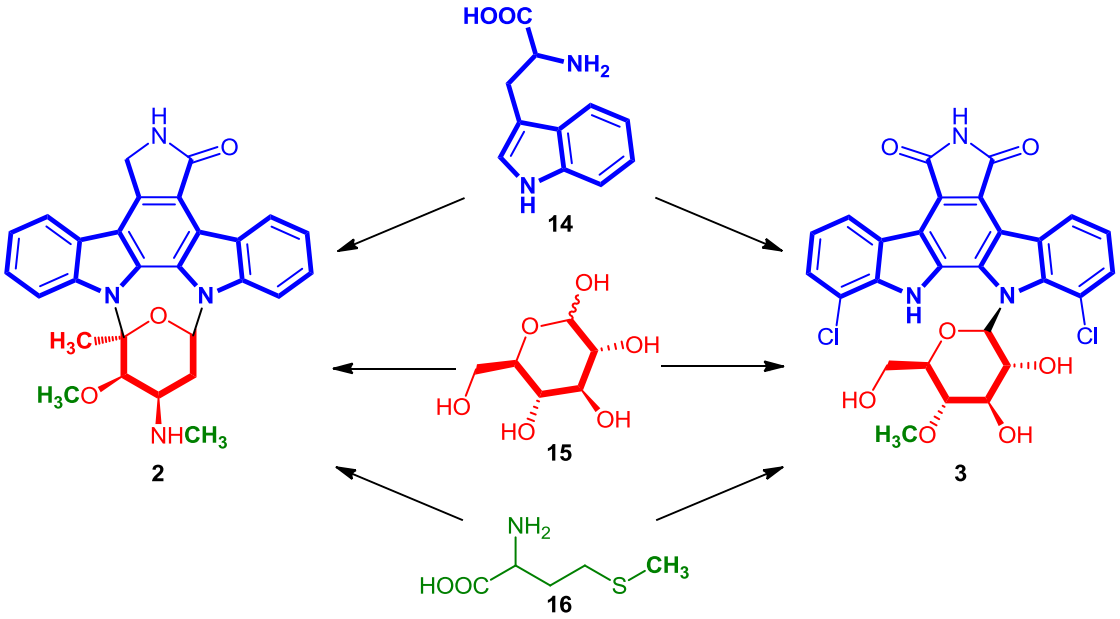

Scheme 1.1 *Metabolic precursors of STA* ***2*** *and REB* ***3***

By examining and testing the biosynthetic mechanics involved in ICZ production in the natural world, it has been possible to develop a number of new ICZ analogues via the use of altered precursors and also by varying the fermentation conditions of the microorganisms involved. For example, the use of potassium bromide in the fermentation of *Nocardia aerocolonigenes* lead to the production of 1,11-dibromorebeccamycin **17**, while the use of 7-azatryptophan in the cultivation of strain NPS012745 was shown to result in the production of 3-indolyl-4-(7-azaindolyl)pyrrole analogue **18.**[27,28]

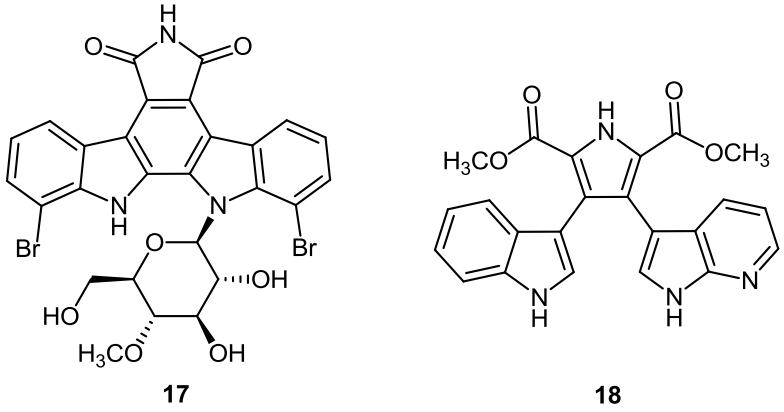

Fig. 1.6 *1,11-Dibromo REB* ***17*** *and 3-(indolyl)-4-(7-azaindolyl)pyrrole* ***18*** *structures*

1.3 Biological mechanisms of indolocarbazoles

A significant number of both synthetic and naturally occurring indolo[2,3-*a*]carbazoles have demonstrated excellent antitumour activity, and are thought to contribute their antiproliferative effects via protein kinase inhibition, as in the case of STA **2**, or by topoisomerase I inhibition, such as with derivatives of REB **3**.[29-31]

1.3.1 Protein kinases

Protein kinases represent one of the largest families of proteins in humans, and sequencing of the human genome has revealed there to be over 500 distinct kinases that can be grouped into about 20 known families on the basis of structural similarity.[32] Kinase enzymes catalyse the phosphorylation of amino acid residues, i.e. the transfer of the terminal phosphate residue of adenosine triphosphate (ATP) to the hydroxyl group of serine, threonine or tyrosine residues (***Scheme 1.2***).

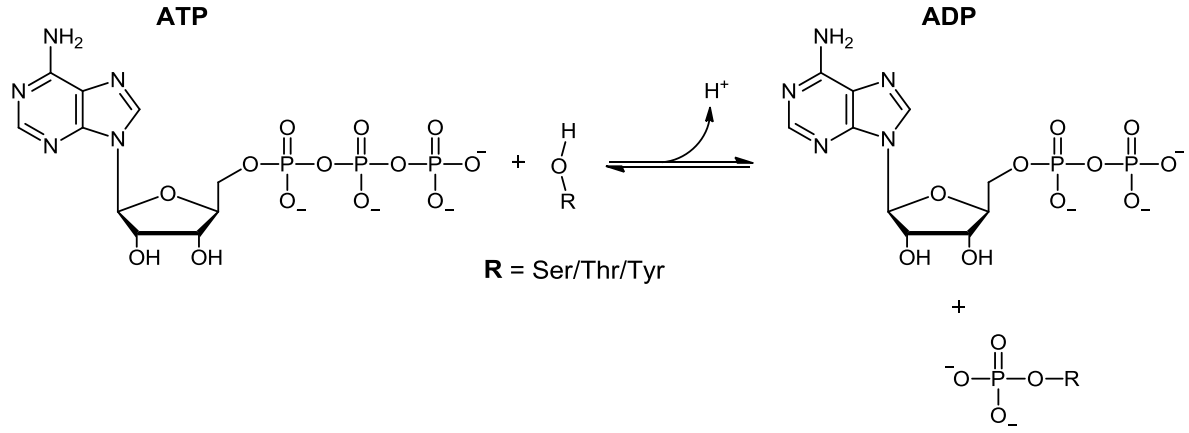

Scheme 1.2 *Phosphorylation of serine/threonine/tyrosine residues*

Research into protein kinases originated in 1955, when Fischer and Krebs perceived ATP-dependent enzymatic activity, leading to the discovery of the serine/threonine kinase phosphorylase b kinase.[33,34] Since then, kinase enzymes have played a central role in the elucidation of signal transduction pathways, and have been found to be involved in almost all critical cellular functions, such as growth, development and homeostasis.[35]

In 1991, Knighton and co-workers solved the first crystal structure of a protein kinase catalytic domain, cAMP-dependent protein kinase (PKA) co-crystallised with a bound, high-affinity inhibitor peptide, and since that time, about 1500 structures of around 200 unique kinases have been lodged on the Protein Data Bank (PDB).[36,37] The catalytic domain is relatively conserved in both sequence and structure across all members of the kinase family, with most small molecule kinase inhibitors binding to this site and competing with ATP.[38] This approach of ATP antagonism can be limited in terms of selectivity due to the similarity between the catalytic domains in different kinases.[39]

1.3.1.1 Structural features of kinase catalytic domain

The protein kinase catalytic domain consists of two major subdomains: a smaller N-terminal "lobe" and a larger C-terminal "lobe". The N-terminus comprises five β-strands with one critical α-helix (αC-helix), while the C-terminus is primarily α-helical (***Figure 1.7***).

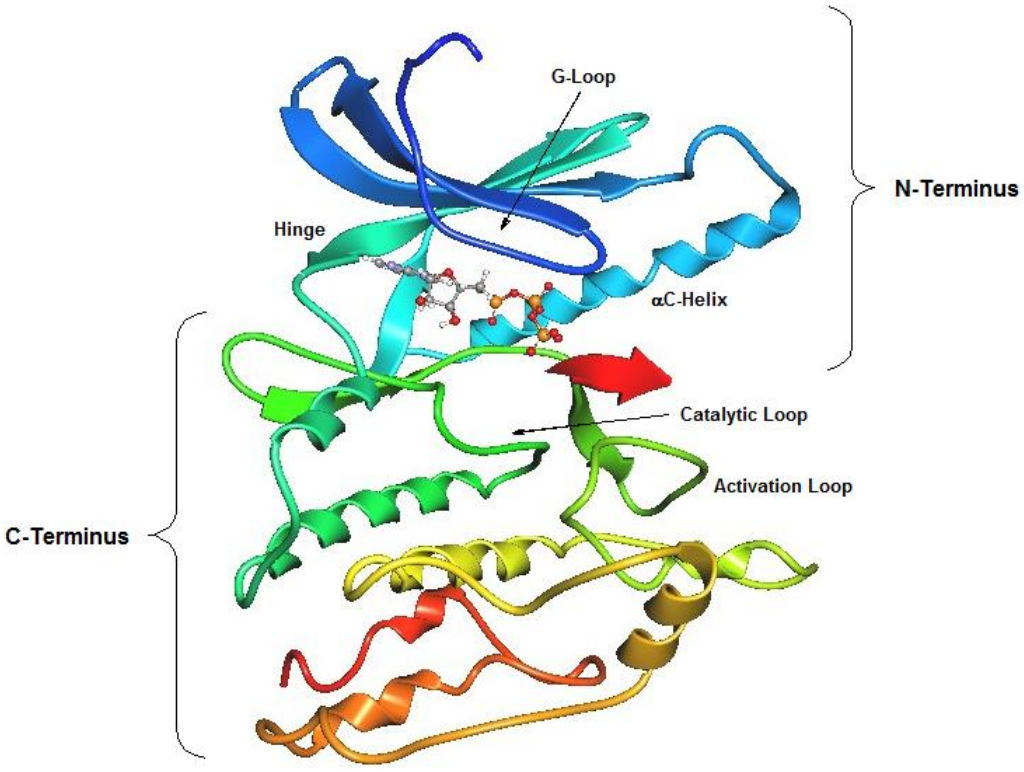

Fig. 1.7 *Phosphorylase kinase (PhK) complexed with ATP (PDB code 2PHK)*[40,41]

Connecting the two domains is a peptide strand, which forms the hinge region (***Figure 1.7***). The active site of the catalytic domain is then formed by the cleft situated between the two subdomains and the hinge region. This cleft has a front pocket containing the residues which are directly involved in catalysis or the binding of ATP, while towards the back of the cleft, a hydrophobic pocket supports regulatory functions.[42]

The adenine ring system of ATP binds to the amide backbone of the hinge region in the front pocket of the cleft of the domain (***Figure 1.8***). The orientation of the αC-helix within the N-terminus, in part, regulates enzymatic activation, i.e. in active state, it is oriented towards the active site. This αC-helix frequently interacts with the C-terminal activation loop to alter the alignment of key catalytic residues. The activation loop of the C-terminus contains a number of elements which are vital for effective enzyme function. For example, it contains a Mg^{2+} orienting loop which is critical for catalysis, mainly due to the fact that an aspartate residue binds directly to the magnesium ion cofactor (highlighted in green) orientating the γ-phosphate of ATP for transfer.

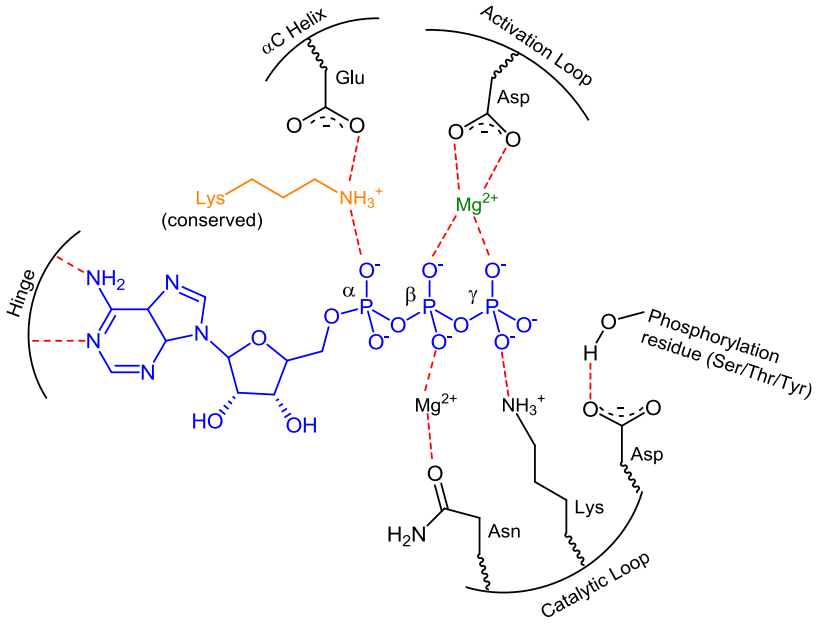

Fig. 1.8 *Molecular contacts between ATP and conserved active site residues and cofactors*

Phosphorylation sites essential to the regulation of catalytic activity are contained on the activation loop. A network of strong hydrogen bonds is created by the incorporation of a

phosphate group on an activation loop residue, thus facilitating the organisation of catalytic active site residues and the phosphorylation residue binding site. The conserved lysine residue (highlighted in orange) which helps to orient ATP for catalysis is not in a flexible loop, unlike many of the essential catalytic residues, and is held in a more rigid conformation. This conserved lysine residue, along with another "gatekeeper" residue, control access to the hydrophobic pocket that contains kinase regulatory elements. The gatekeeper residue can have either a large amino acid side chain (e.g. phenylalanine in CDK2) which blocks ligand access to the back pocket, or a small side chain (e.g. threonine in EGFR) which allows access.[42]

1.3.1.2 Deregulation of kinases and disease: attractive biological targets

In 1980, it was first reported that protein kinases played a crucial role in oncogenesis and the progression of tumours.[43] Since then, the development and advancement of such tools as genetic modulation, RNAi technology and bioinformatics, has implicated the deregulation of kinases in almost all human diseases, including diabetes, cardiovascular disease and neurological disease, as well as cancer.[44] As a result, the targeted inhibition of kinases has become an attractive therapeutic strategy in the treatment of relevant diseases. They are considered to be the second most important group of drug targets after G-protein coupled receptors.[45]

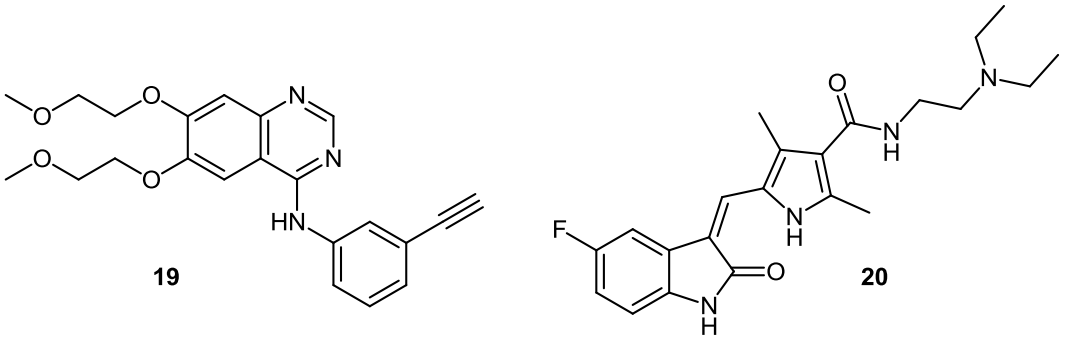

Fig. 1.9 *Structures of erlotinib **19** and sunitinib **20***

Currently, there are 14 kinase inhibitors approved by the FDA, including erlotinib **19**, which is marketed as a non-small cell lung cancer inhibitor, and sunitinib **20**, which is marketed for the treatment of renal cell carcinoma and imatinib-resistant gastrointestinal stromal tumour.[46,47] It has been estimated that the global market for kinase-directed therapies is estimated to be

US$35 billion in 2013.[39] A number of ICZ derivatives are currently undergoing clinical trials, including UCN-01 **4**, which is currently being examined for the treatment of cancer.[48]

1.3.1.3 Staurosporine: a non-selective kinase inhibitor

Ever since the disclosure of low nanomolar activity against PKC (IC_{50} = 2.7 nM), STA **2** has become a lead compound for the development of potential anticancer agents.[12] Due to the wide biological profile with which STA **2** operates, in particular its lack of specificity as a kinase inhibitor, progression of this natural product towards clinical trials was not possible. Although there was some initial debate due to aberrant kinetic data, STA **2** was found to effectuate kinase inhibition due to competition with respect to ATP.[13] This was later proven when crystal structures of the ICZ alkaloid in complex with the ATP-binding sites of cyclin-dependent kinase 2 (CDK2) and PKA were resolved.[49,50]

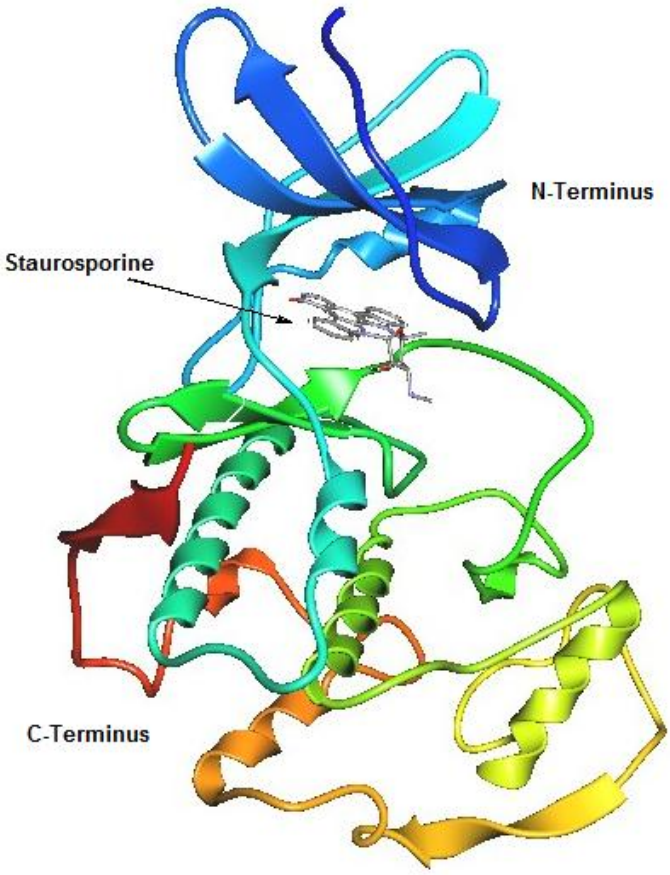

Fig. 1.10 *STA **2** in complex with CDK2 (PDB code 1AQ1)*[40,51]

To date, coordinate sets of roughly 40 kinase catalytic domains co-crystallised with STA **2** have been deposited with the PDB, for example in ***Figure 1.10***. These structures demonstrate the existence of an almost universal common binding mode of STA **2** to these ATP-binding sites. In a similar manner to the binding of the adenine ring to the hinge region of the kinase catalytic domain (***Figure 1.8***), the lactam moiety of STA **2** forms two conserved hydrogen bonds to two amino acid residues in order to anchor the inhibitor inside the ATP-binding site. Shown in ***Figure 1.11*** is STA **2** bound to the active site of phosphoinositide-dependent kinase 1 (PDK1), clearly illustrating the hydrogen bond formed between the NH of the lactam ring and the backbone carbonyl of Ser-160, and also the bond formed between the lactam carbonyl and the backbone NH of the Ala-162 residue of the hinge. Another hydrogen bond also exists between the methylamino group of the STA **2** carbohydrate moiety and a backbone carbonyl group of a glutamate residue, Glu-209, which also helps to anchor the ATP-competitive inhibitor to the active site.

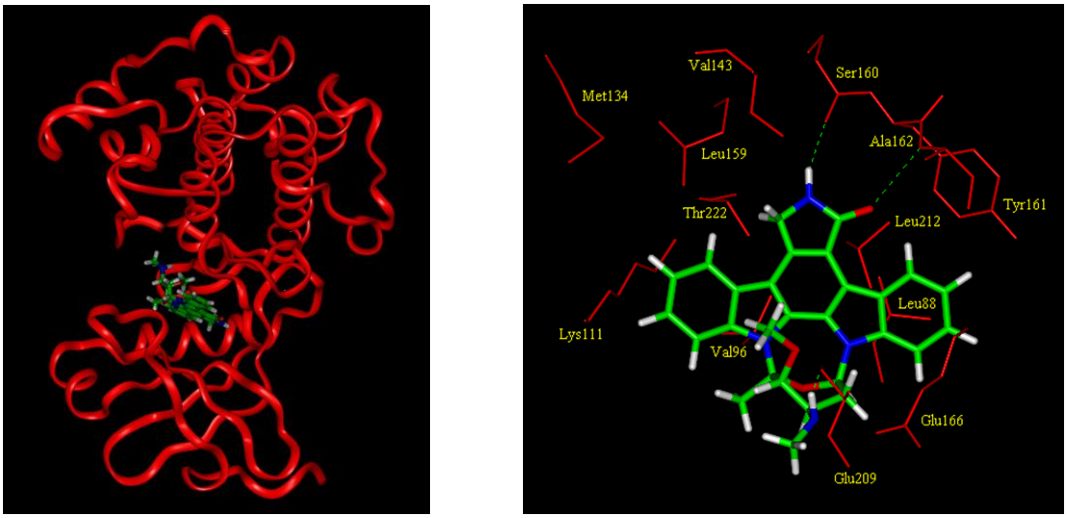

Fig. 1.11 *STA **2** in complex with PDK1 (PDB code 1OKYO)*[52,53]

While the relatively conserved nature of the kinase catalytic domain across the kinome can help to account for the lack of specificity of STA **2** and a number of other inhibitors across the kinome, there exists the potential to exploit subtle differences within the active site to generate a narrower selectivity profile for kinase inhibitors. For example, hydrophobic interactions are dominated by side-chain interactions which involve residues that are less conserved, such as the Leu-88, Leu-212 and Thr-222 residues of PDK1 (***Figure 1.11***). The residues involved in

these hydrophobic interactions are also subject to induced fit structural rearrangements on ligand binding. Overall, the exploitation of discreet differences in active site residues and conformations can help to confer or induce selectivity throughout the pan-kinase domain.[48]

1.3.1.4 ICZs as protein kinase inhibitors

Though the wide-ranging biological mode of action of STA **2** rendered it unsuitable as a clinical candidate, many other ICZ derivatives have since been investigated for their potential use as anticancer agents and in other diseases. UCN-01 **4** is currently undergoing clinical trials due to its highly potent antiproliferative activity, and as an inhibitor of PKC (IC_{50} = 10 nM) is comparable to STA **2** (IC_{50} = 2.7 nM).[54] UCN-01 **4** is also a strong inhibitor of CHK1 (K_i = 5.6 nM), PDK1 (IC_{50} = 5.0 nM), and other isoforms of PKC ($IC_{50} \leq 1$ µM), and is unique in being the only naturally occurring ICZ analogue being evaluated for clinical use at present.[53,55] Greater success has been seen with regard to synthetic ICZ derivatisation programmes, leading to the development of a number of highly promising chemotherapeutic candidates with the potential to widen the relatively narrow field of established kinase inhibitors on the market. To date, structural modifications to the STA **2** pharmacophore have included: (i) derivatisation of the lactam heterocycle, (ii) substitutions on aromatic rings **A** or **E** and (iii) structural variation of the sugar moiety (***Figure 1.12***).

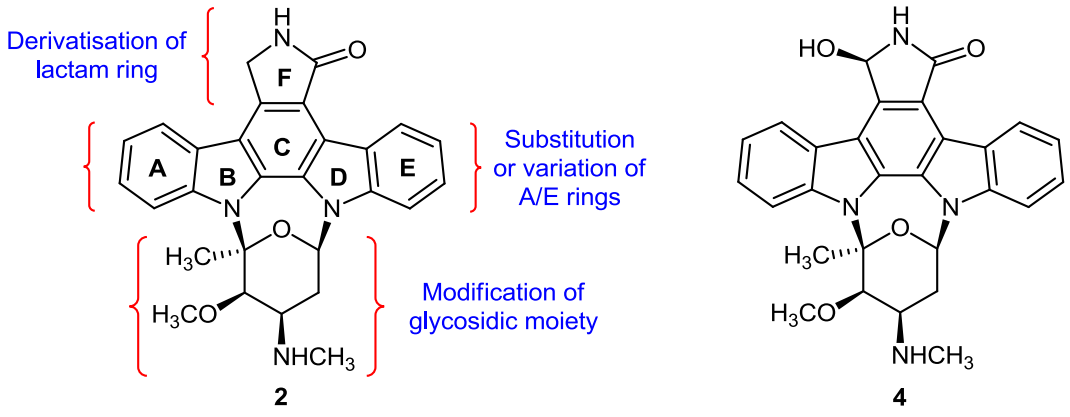

Fig. 1.12 *Derivatisation of STA **2** pharmacophore; structure of UCN-01 **4***

Replacement of the substituted pyranose sugar of STA **2** with a reduced furan ring, and the lactam group with a maleimide functionality furnished SB-218078 **21**, which proved to be a far more selective kinase inhibitor. SB-218078 **21** demonstrated a 15-fold selectivity for

CHK1 (IC_{50} = 15 nM) compared to CDK1 (IC_{50} = 250 nM), and a 65-fold selectivity against PKC (IC_{50} = 1000 nM).[56] This contrasts with STA **2**, which inhibits the same kinases in a narrow IC_{50} range of 2.7 to 8 nM. Similarly, CEP-1347 **22** retains the lactam moiety of STA **2**, but contains a substituted furan ring instead of the glycoside functionality and two ethylthiomethyl substituents on aromatic rings **A** and **E**. ICZ derivative **22** was shown to exhibit potent inhibitory activity against MLK kinases, which are key participants in the activation of the JNK signalling cascade.[57] The JNK signalling cascade has been of particular therapeutic interest in the treatment of the effects of Parkinson's disease, as it has been implicated in the governing of neuronal dysfunction and subsequent death. This approach towards treating the disease offers an attractive alternative to existing remedies, helping prevent disease progression by targeting the mechanisms involved in the pathogenesis of the ailment.[58]

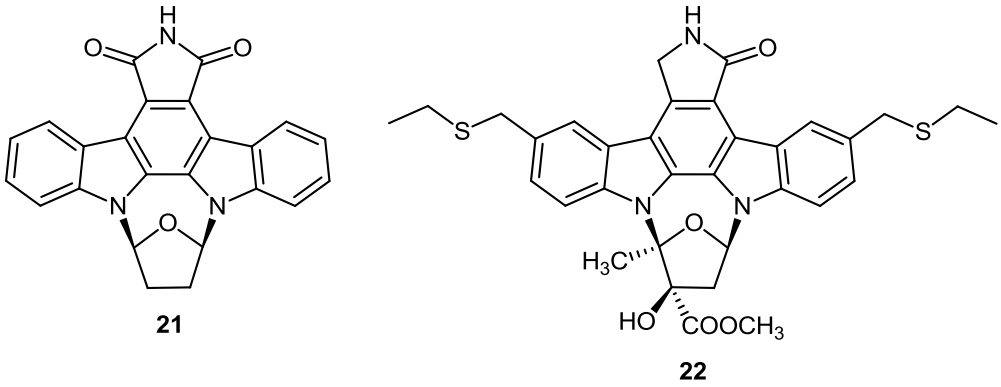

Fig. 1.13 *Structures of SB-218078* ***21*** *and CEP-1347* ***22***

Other highly promising pharmaceutical candidates arising from the derivatisation of the STA **2** pharmacophore include midostaurin **23**, a potent, non-specific inhibitor of a number of different kinases, including PKC, VEGFR2 and FLT3. Midostaurin **23** is currently under examination for treatment of acute myeloid leukemia (AML), as well as a number of different cancer types.[59] Suppression of tumour growth by ICZ **23** is thought to occur by inhibition of tumour angiogenesis, in addition to directly inhibiting cancer cell proliferation.[60] One of the main kinases targeted by **23**, FLT3, is a receptor tyrosine kinase which is activated by mutation in approximately a third of AML patients.

Lestaurtinib **24** has also entered trials for treatment of acute myeloid leukemia, as well as for treatment of myelofibrosis and prostate cancer.[61] While **24** has been shown to inhibit autophosphorylation and signalling of neurotrophin-specific Trk receptors, and to display potent antitumour activity, it has also been demonstrated to act on epidermal growth factor receptor, FLT3, RET and a number of other kinases.[62]

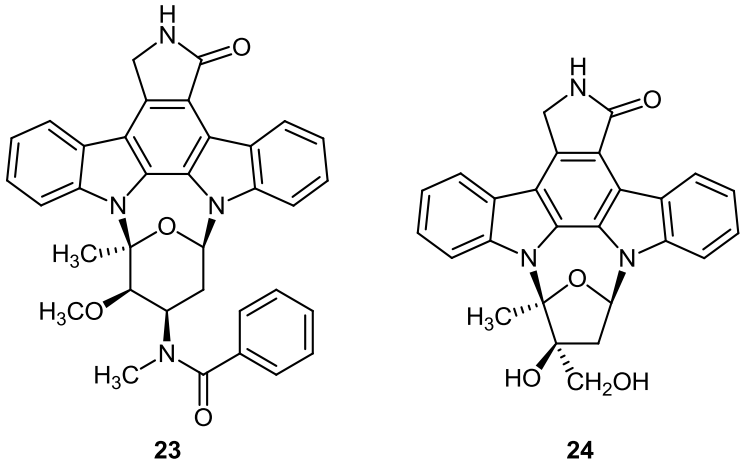

Fig. 1.14 *Midostaurin **23** and lestaurtinib **24** structures*

1.3.1.5 Bisindolylmaleimides: non-planar ICZ derivatives

Biosynthetically related and often used as synthetic precursors to ICZs, bisindolylmaleimides have proven to be worthy of much research focus in their own right, again due to the wide variety of biological activities modulated by this class, particularly as kinase inhibitors. Bisindolylmaleimide GF109203X **25** was originally proposed by Toullec *et al*. to be a selective inhibitor of PKC, though this was later discounted due to its inhibition of a number of other kinases.[63,64] It was also found to target a number of other unexpected proteins, such as P-glycoprotein and 5-hydroxytryptamine$_3$ (5-HT$_3$) receptor.[65,66]

Further elaboration of the bisindolylmaleimide template has since resulted in the development of ruboxistaurin **26**, a specific inhibitor of the PKC isoforms, PKCβ_1 (IC_{50} =4.7 nM) and PKCβ_2 (IC_{50} = 5.9 nM). This BIM derivative **26** displays a high degree of selectivity compared with other protein kinases and PKC isoforms, such as PKCα (IC_{50} = 360 nM), PKCγ (IC_{50} = 300 nM), PKCε (IC_{50} = 600 nM) and PDK1 (IC_{50} = 750 nM).[67,68] Due to the long-chain linker between the two indolic nitrogen atoms, macrocycle **26** has reduced

conformational freedom relative to other bisindolylmaleimides such as GF109203X **25**, but without the planarity of its ICZ analogues. At present used to treat diabetic peripheral retinopathy, ruboxistaurin **26** is the first chemotherapeutic agent used in the treatment of this serious complication of diabetes.[69]

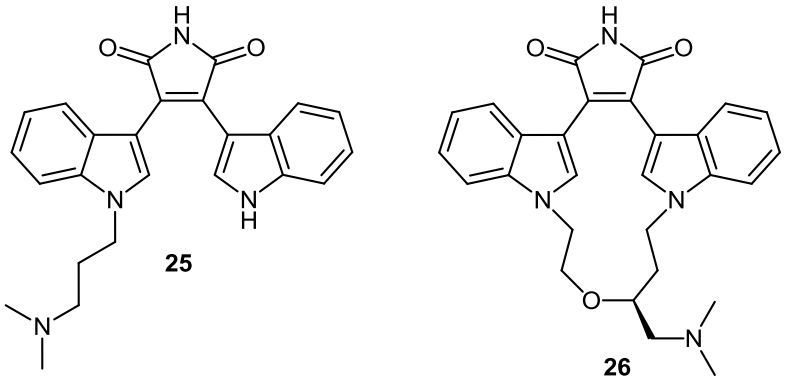

Fig. 1.15 *Structures of GF109203X* ***25*** *and ruboxistaurin* ***26***

Another modified bisindolylmaleimide, enzastaurin **27**, was found to be a highly potent inhibitor of PKCβ (IC_{50} = 6 nM) and the AKT/PI3 pathway, and is currently under clinical evaluation for such cancers as glioblastoma, non-small cell lung cancer and colorectal cancer. It displays significant selectivity over other isoforms of PKC, including PKCα (IC_{50} = 39 nM), PKCγ (IC_{50} = 83 nM) and PKCε (IC_{50} = 110 nM). With the activation of PKC, particularly PKCβ, implicated in tumour initiation and progression, orally administered BIM **27** induces apoptosis in a number of cancer cell lines and also inhibits VEGF-mediated angiogenesis.[70]

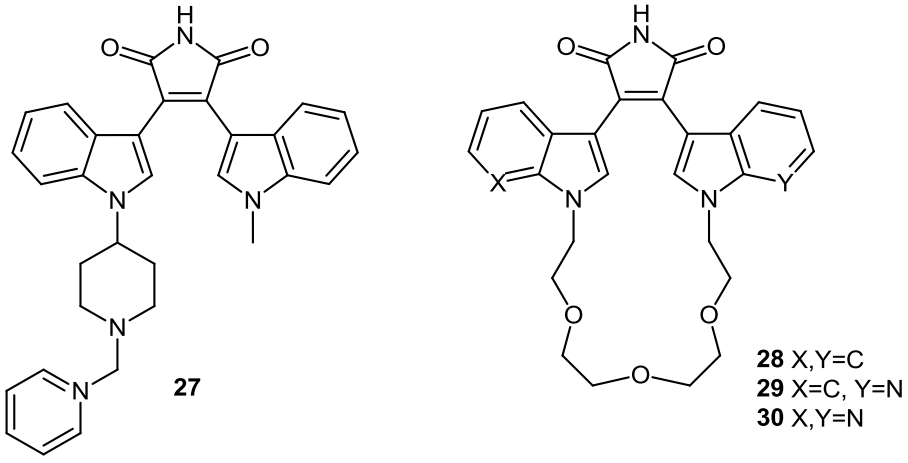

Fig. 1.16 *Structures of enzastaurin* ***27****, BIM* ***28****, and aza BIM derivatives* ***29*** *and* ***30***

The bioisosteric replacement of 7-azaindolyl subunits instead of either indolyl moiety in the BIM series has also been shown to mediate significant kinase inhibitory activity. In 2003, Kuo and co-workers reported the synthesis of a series of macrocyclic BIM derivatives, such as BIM **28** and azaindolylmaleimide analogues **29** and **30**, as potent inhibitors of glycogen synthase kinase-3 (GSK-3).[71] Inhibition of GSK-3 has previously been shown to attenuate apoptotic signals, leading to the potential use of inhibitors of this kinase in the treatment of Alzheimer's disease and other conditions.[72,73]

Kinase Assay	28	29	30
GSK-3β	0.022	0.017	0.034
CDK1	1.251	4.428	> 10
CDK2	0.922	2.439	> 10
VEGFR	1.450	3.560	> 10
PKCα	0.086	0.673	> 10
PKCβII	0.006	0.046	1.163
PKCθ	0.065	0.835	> 10
PKA	> 10	> 10	> 10

Table 1.1 *IC_{50} (μM) of kinase assays for BIM derivatives **28**, **29** and **30**[71]*

It was found that the kinase selectivity profiles of the macrocyclic BIM derivatives, illustrated in ***Table 1.1***, were dramatically altered by the incorporation of one and especially two 7-azaindolyl functionalities. Aza BIM analogue **30** displayed excellent ATP-competitive activity against the GSK-3β isoform (IC_{50} = 34 nM), while simultaneously showing very weak inhibition against almost every member of a panel of 50 kinases, such as PKCα, PKA and CDK1 (IC_{50} > 10 μM for all three). Conversely, BIM analogue **28**, while also observed to have excellent activity against GSK-3β, was shown to strongly inhibit a number of other kinases such as PKCα (IC_{50} = 86 nM), PKCβII (IC_{50} = 6 nM) and PKCθ (IC_{50} = 65 nM).

Molecular modelling studies suggested that concomitant to the conserved hydrogen-bonding between the backbone residues of GSK-3β and the maleimide ring of macrocycle **30**, a

significant hydrogen-bonding interaction also occurs between one of the azaindolic nitrogen atoms of **30** and a guanidine functionality of a side chain Arg-141 residue (***Figure 1.17***). It was posited that this particular hydrogen bond with Arg-141 is unique to GSK-3β, thus helping to explain the degree of selectivity observed for this series of 7-azaindolylmaleimides.[71]

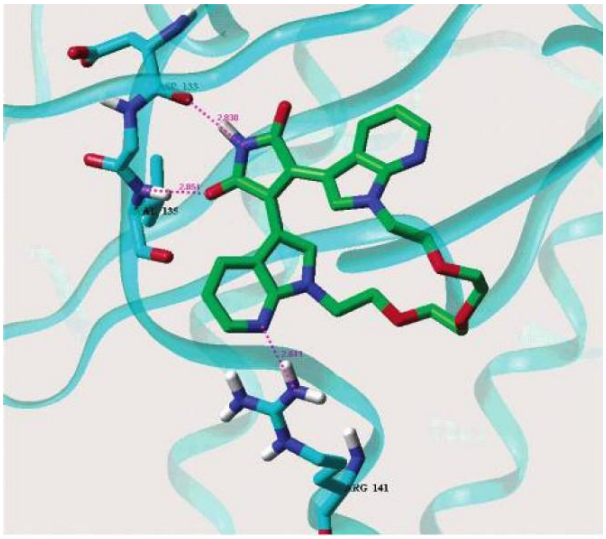

Fig. 1.17 *Binding mode of aza BIM analogue* ***30*** *in GSK-3β active site*[71]

1.3.1.6 Heteroaryl ICZ analogues as kinase inhibitors

Further diversification of the ICZ pharmacophore, with the appropriation of heteroaryl subunits, has served to potentiate kinase inhibitory activity in a number of reported instances.

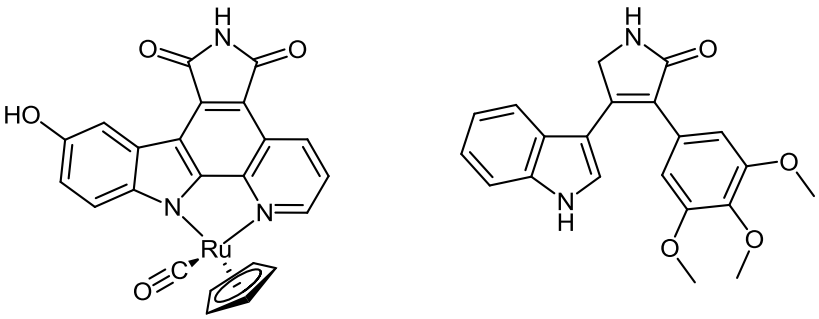

31 **32**

Fig. 1.18 *Structures of ruthenium complex* ***31*** *and VEGFR inhibitor* ***32***

In 2005, Meggers *et al*. described the synthesis of a series of ICZ derivatives (containing a pyridine ring in place of an indolyl unit) bound in a ruthenium complex.[74] These cyclometalated compounds were found to be highly efficacious inhibitors of the GSK-3α isoform of glycogen synthase kinase 3 (GSK-3), such as with complex **31** (IC_{50} = 0.3 nM), which is regarded as one of the most potent inhibitors of this kinase yet to be discovered.

In 2008, Peifer and co-workers described the synthesis of a series of BIM analogues containing a 3,4,5-trimethoxyphenyl moiety, such as derivative **32**, as potent inhibitors of vascular endothelial growth factor receptor (VEGFR).[75] The VEGFR family of kinases play pivotal roles in the mediation of the effects of hypoxia-induced VEGFs on angiogenesis such as in pancreatic, gastric and colorectal carcinomas.[76] Heteroaryl BIM/Combretastatin analogue **32** was found to be a potent inhibitor of the isoforms VEGFR-2 (IC_{50} = 31 nM) and VEGFR-3 (IC_{50} = 37 nM), while also blocking angiogenesis in an endothelial cell sprouting assay at a concentration of 1.3 μM using human lung-derived microvascular endothelial cells (HLMEC).[75]

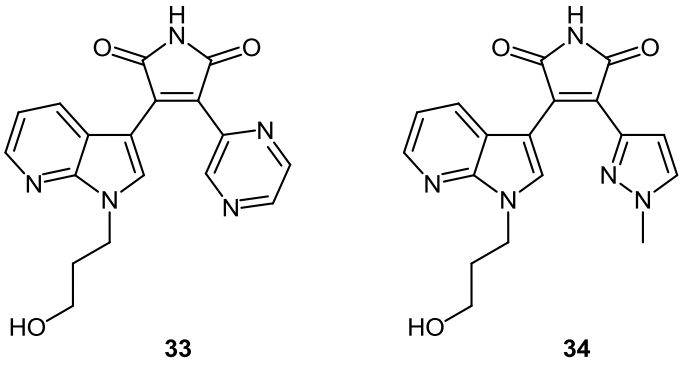

Fig. 1.19 *Structures of 3-(7-azaindolyl)-4-heteroaryl BIM derivatives **33** and **34***

Elaborating on previous work featuring macrocyclic BIM derivatives (Section *1.3.1.5*), Kuo *et al.* achieved similar GSK-3β inhibitory activity and selectivity with the development of a panel of 7-azaindolyl-heteroarylmaleimides. Dispensing with a long-chain linker, and utilising an entire series of heteroaryl units instead of one of the 7-azaindolyl moieties, a number of potent GSK-3β inhibitors were developed, including derivatives **33** (K_i = 25 nM) and **34** (K_i = 48 nM), both of which were shown to display good selectivity against a panel of 80 kinases.[77]

1.3.1.7 Kinase inhibitors containing a 7-azaindolyl nucleus

Despite constituting a key component of a number of potent kinase inhibitors described in the previous section, the 7-azaindolyl functionality has been found to occur in a very limited number of natural products.[78] In one such instance, structural elucidation of the variolins, a series of alkaloids isolated from the rare Antarctic sponge *Kirkpatricka varialosa*, revealed a common pyrido[3,2:4,5]pyrrolo[1,2-*c*]pyrimidine skeleton.[79] A member of the class, variolin B **35**, was found to be a potent inhibitor of the CDK and GSK-3 kinases, and to display cytotoxicity against a number of human cancer cell lines.[80]

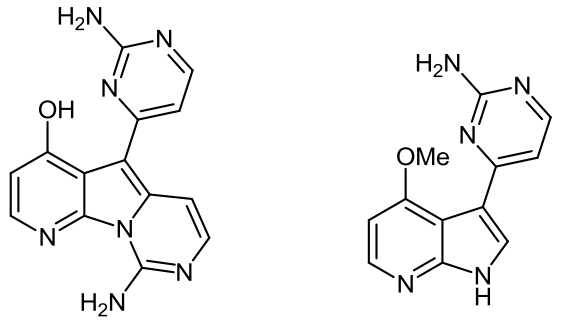

35 **36**

Fig. 1.20 *Structures of variolin B **35** and meriolin 3 **36***

Synthetic derivatisation of the variolin B **35** structure subsequently led to the development of the meriolin series of compounds, such as meriolin 3 **36**, with enhanced potency and selectivity towards the CDK kinases, along with increased antiproliferative and proapoptotic properties.[81] While displaying potent inhibition against CDKs such as CDK9 (IC_{50} = 6 nM), meriolin 3 **36** was found to be less efficacious against other kinases such as GSK-3 (IC_{50} = 230 nM) compared with variolin B **35** (IC_{50} = 70 nM).

1.3.2 Topoisomerase I

Topoisomerase I (topo I) is a ubiquitous enzyme found in all mammals and plays an essential role in many important cellular functions such as replication and transcription. In 1985, Sternglanz and co-workers detailed experimentally, using topo I gene mutants, how the enzyme was not a prerequisite for cell growth in yeast.[82] However, further genetic studies of topo I gene mutants showed that the enzyme was vital for the growth and development of the fruit fly, *Drosophila melanogaster*.[83] This led to the inference that topo I played an essential role in more complex eukaryotic cells. Morham *et al.* illustrated this by later demonstrating how the inactivation of the topo I gene caused the death of mice early in embryogenesis.[84]

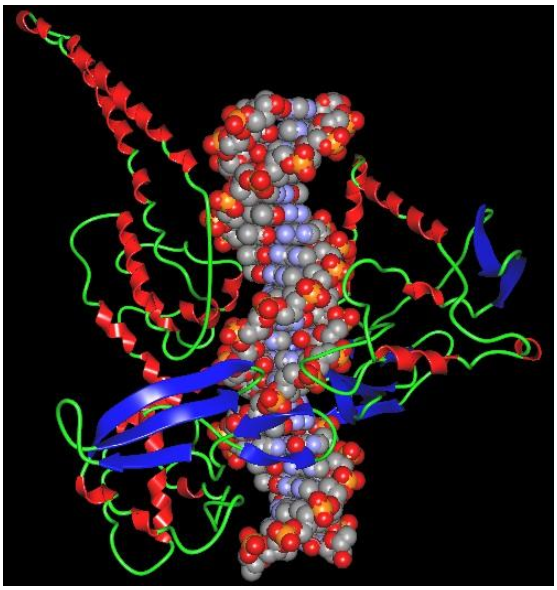

Fig. 1.21 *Topo I cleavage complex with human DNA (PDB code 1A36)*[40,85]

In the human genome, there are four genes which encode for topo I: the nuclear topo I and mitochondrial topo I genes, along with the topo IIIα and topo IIIβ genes. The cellular function of topo I is to produce a transient single strand break in DNA, thus relaxing the torsional strain built up from the unwinding process, and allowing the DNA to be effectively transcribed and replicated. The single strand break is then religated, resulting in the restoration of the DNA double strand. A cleavage complex is formed when topo I binds to and cuts the phosphate backbone of DNA, with the enzyme encircling the DNA tightly like a clamp (***Figure 1.21***).[86]

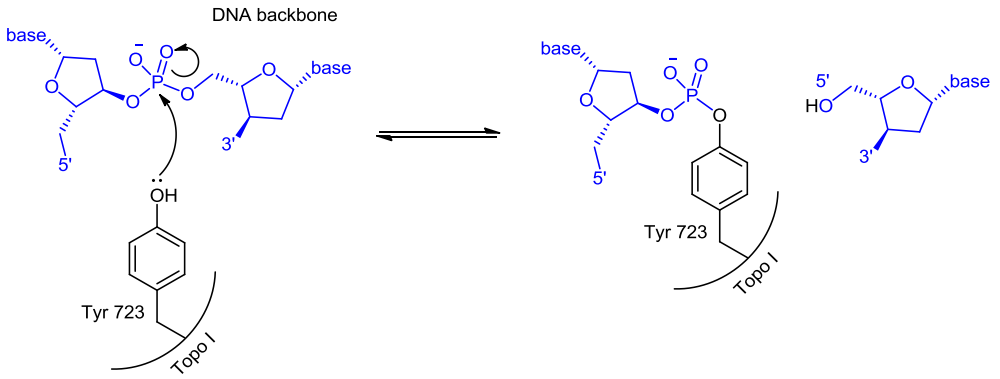

Scheme 1.3 *Nucleophilic attack from tyrosyl residue of topo I to DNA phosphodiester bond*

The mechanism by which topo I induces a single strand break in DNA, called the nicking step, results from the nucleophilic attack of the phenolic oxygen of an active site tyrosine residue (Tyr-723 in human topo I) on a DNA phosphodiester bond (***Scheme 1.3***). Topo I then forms a covalent linkage to the 3'-end of the broken DNA strand, while generating a 5'-hydroxyl group at the other end of the break.[87] Controlled rotation of the 5'-hydroxyl end of the broken strand around the intact DNA strand allows for the relaxation of the DNA (***Scheme 1.4***).

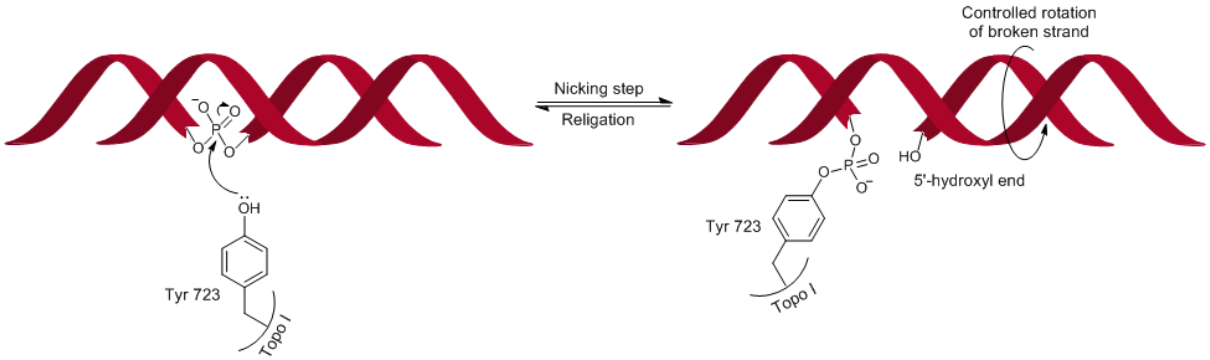

Scheme 1.4 *Single strand DNA break allows for controlled rotation of 5'-hydroxyl end*

1.3.2.1 Topo I as a chemotherapeutic target

There has been widespread research interest in the development of topo I-directed chemotherapeutic drugs over the past few decades, with levels of topo I catalytic activity shown to be significantly elevated in a number of different cancers, such as colon, prostate and ovarian carcinomas.[88,89] Wall *et al.* reported the isolation of a potent anticancer alkaloid,

camptothecin (CPT) **37**, from the Chinese tree *Camptotheca acuminata* in 1966, which was later found to inhibit topo I by interacting with the topo I-DNA cleavage complex.[90,91]

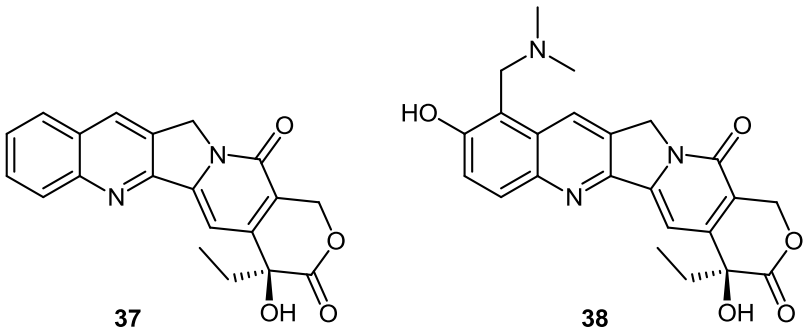

Fig. 1.22 *Structures of camptothecin **37** and topotecan **38***

Topo I is reported to be the sole cellular target of CPT **37**, and trapping the enzyme-DNA complex prevents religation of the broken strand of DNA. In acting as a topo I poison, CPT **37** converts topo I into a DNA-damaging agent, resulting in cellular cytotoxicity and apoptosis. Though trials of CPT **37** were discontinued due to its harmful side-effects, derivatives such as topotecan **38** have since been developed and brought into clinical use.[92]

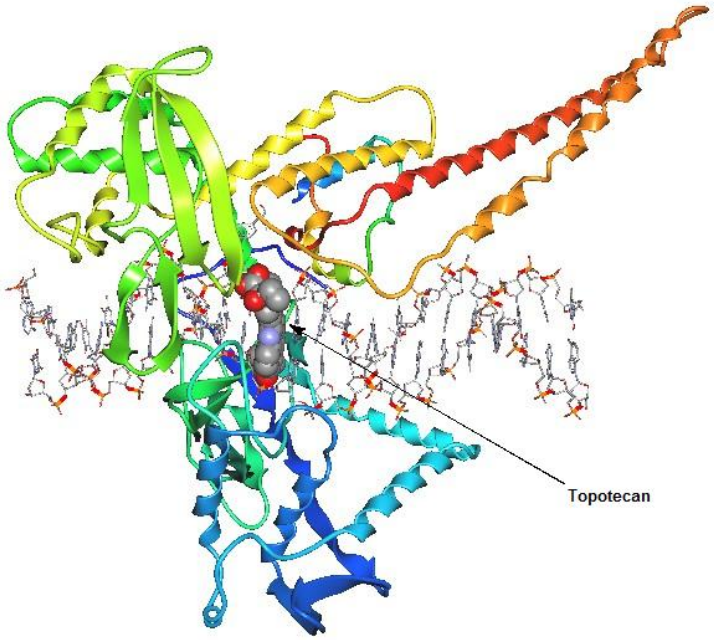

Fig. 1.23 *Intercalation of topotecan **38** into the topo I-DNA cleavage complex (PDB code 1K4T)*[40,93]

Topo I poisons, such as topotecan **38**, act as uncompetitive inhibitors by specifically binding to the enzyme-substrate complex. Topotecan **38** mimics a DNA base pair and binds at the site of DNA cleavage by intercalating between the upstream and downstream base pairs (***Figure 1.23***). The downstream DNA is displaced due to the intercalation, which prevents religation of the cleaved strand.[93] Topotecan hydrochloride is marketed under the registered trademark Hycamtin, and is commonly used to treat ovarian, cervical and non-small cell lung carcinomas amongst others, and was the first topoisomerase I inhibitor approved for oral use.[94]

1.3.2.2 ICZ Topo I Inhibitors

Though CPT **37** derivatives, such as topotecan **38**, have shown highly significant promise as anticancer agents, they still suffer drawbacks such as low tumour response rates and dose-limiting toxicity.[95] As a result of these problems, and due to the excellent potential shown by topo I poisons for the treatment of cancer, significant efforts have been made to identify non-CPT inhibitors of this enzyme. It is in this effort that ICZ derivatives have displayed a burgeoning proficiency.

After the isolation of rebeccamycin **3**, the exact mechanism of its potent antitumour action was initially unclear, but subsequent studies identified that REB **3** was able to induce *in vitro* DNA cleavage mediated by the topo I enzyme.[14] In the same assay, two other ICZ derivatives, KT6006 **39** and KT6528 **40**, exhibited even more potent activity.

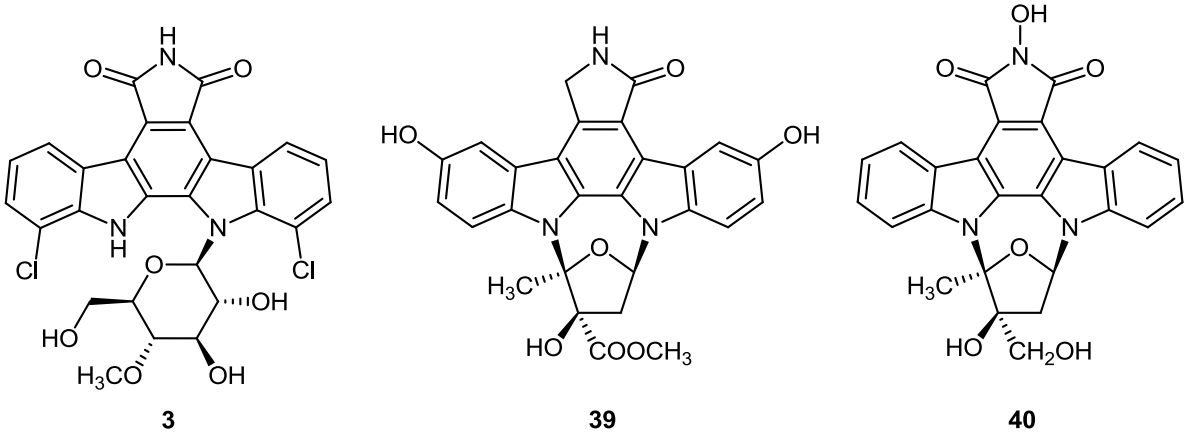

Fig. 1.24 *Structures of REB **3**, KT6006 **39** and KT6528 **40***

In a similar manner seen for topotecan **38**, KT6006 **39** and KT6528 **40** stabilised the topo I-DNA cleavage complex and prevented religation, and furthermore, in the absence of the topo I enzyme, KT6528 **40** behaved as a DNA intercalator.[96]

The aglycone indolocarbazole, BE-13793C **41**, was reported to be isolated from *Streptoverticillium mobaraense* BA13793 by Kojiri and co-workers in 1991.[97] While ICZ **41** was shown to be an effective inhibitor of topo I and to have remarkable activity in Ehrlich ascites carcinoma (EAC) cells, its low aqueous solubility prevented further biological evaluation.[98] The synthesis of a glycosidic analogue, ED-110 **42**, increased the water solubility of aglycone **41**, while retaining significant inhibition of topo I and highly potent antitumour activity, including against cell lines resistant to established chemotherapeutic agents, vincristine and doxorubicin.[98]

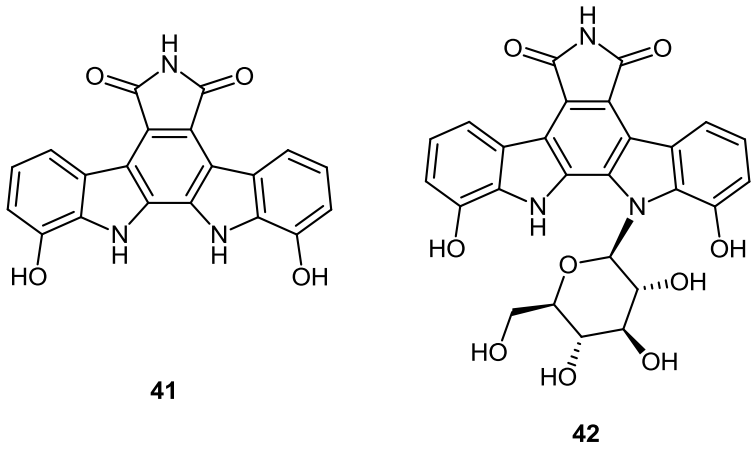

***Fig. 1.25** BE-13793C **41** and ED-110 **42** structures*

Further chemical elaboration from the aglycone core **41**, with the incorporation of a *N*-formylamino substituent, yielded NB-506 **43**, another ICZ displaying excellent anticancer potential.[99] NB-506 **43** inhibits the kinase activity and DNA-relaxing activity of topo I, as well as acting as a DNA-binding agent in its own right.[100] Despite entering clinical trials for the treatment of solid tumours in 1994, NB-506 **43** has since been discontinued from evaluation for use as a chemotherapeutic agent.[101]

Numerous derivatives of REB **3** and NB-506 **43** have been synthesised and evaluated, providing vital information for structure-activity relationship (SAR) studies. Using NB-506 **43**

as an example, the ICZ pharmacophore can be divided into three distinct regions on the basis of topo I inhibitory activity (***Figure 1.26***). The planar ICZ core (rings A – E) partially intercalates between two consecutive DNA base pairs, as seen also for topotecan **38**, while the glycosidic moiety was proposed to project into a groove of the DNA double helix. The substituent attached to the F-ring imide nitrogen then protrudes toward the opposite groove, where it interacts with residues of the catalytic domain of topo I.[102]

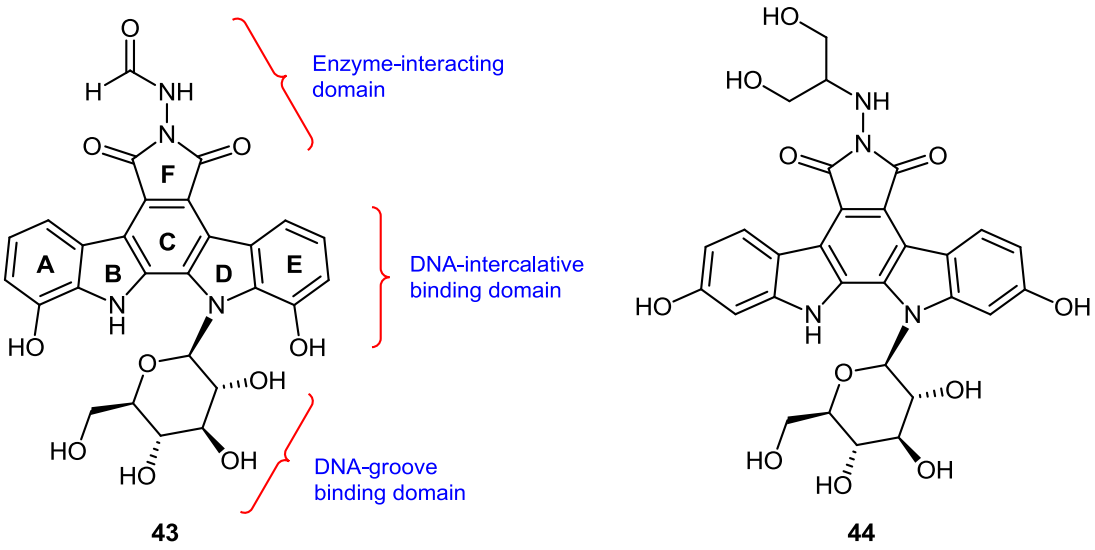

Fig. 1.26 *SAR of NB-506* ***43*** *and structure of edotecarin* ***44***

Progressive modification of the NB-506 **43** structural framework led Ohkubo *et al.* to what remains to date one of the most promising ICZ chemotherapeutic candidates, edotecarin **44**.[103] The formyl unit on the F-ring was replaced with a more polar 1,3-dihydroxypropane group, while the two hydroxyl substituents on the A- and E-rings were shifted from the C_1 and C_{11} positions to the C_2 and C_{10} positions. These discrete changes increased the overall aqueous solubility and plasma stability of the molecule, while retaining topo I activity and increasing cytotoxicity.[104] In fact, ICZ derivative **44** induces single-strand DNA cleavage more effectively and also gives rise to more stable topo I-DNA complexes than CPT **37** or NB-506 **43**. Edotecarin **44** is at present being trialled in the clinic for the treatment of amongst others, breast cancer, glioblastoma multiforme and gastric cancer.[105]

The crystal structure of the indolocarbazole SA315F **45** bound to the human topo I-DNA covalent complex was reported by Burgin *et al.* in 2005, highlighting a similar intercalative

binding mode to that seen for topotecan **38** and other topo I inhibitors.[106] The indole ring with the glycosidic substituent was shown to stack with bases on the intact strand side of the duplex DNA, with the other indole stacked with bases on the cleaved strand side. The maleimide ring of ICZ **45** is placed on the minor groove side of the intercalation binding pocket, with the glucose moiety positioned in the major groove of the ternary complex (***Figure 1.27***).

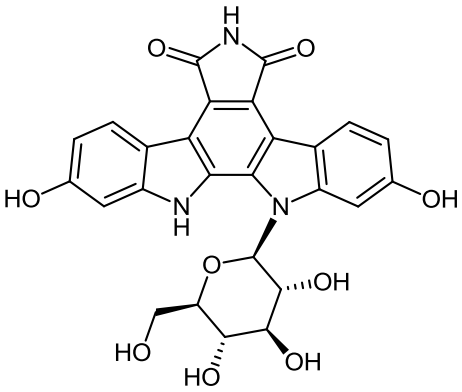

45

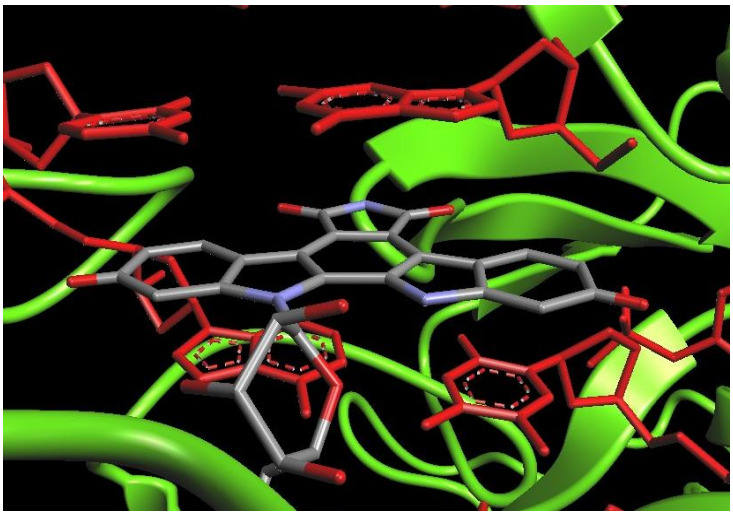

Fig. 1.27 *Structure of SA315F **45** and bound to topo I-DNA complex (PDB code 1SEU)*[40,106]

1.3.2.3 7-Azarebeccamycin derivatives: greater selectivity than parent ICZs

The incorporation of 7-azaindole subunits into the REB **3** pharmacophore has been shown to confer highly significant selectivity profiles towards tumour cell lines. Prudhomme *et al*. demonstrated that replacing indole units in REB **3** analogues with 7-azaindolyl bioisosteres, i.e. azaindolocarbazole derivatives **46** and **47**, conferred relatively significant differences to their cytotoxicity profiles in comparison with their parent ICZs.[107]

While both were found to exert considerable topo I inhibition, 7-aza ICZ derivative **47** was shown to be more potent than its isomeric analogue **46**. This was found to correlate with its higher DNA affinity and greater cytotoxicity against a series of tumour cell lines. The most intriguing aspect to the biological evaluation of 7-aza ICZ derivatives **46** and **47** was that they demonstrated a relatively high degree of selectivity for some tumour lines, resulting in markedly different cytotoxicity profiles to their parent ICZs. For example, derivative **46** displayed considerable selectivity for SK-N-MC neuroblastoma (IC_{50} = 59 nM) and NCI-H69

non-small cell lung cancer (IC_{50} = 10 nM) cell lines relative to IGROV1 ovarian cancer (IC_{50} = 68.8 µM) and HT29 colon carcinoma (IC_{50} = >100 µM) lines. This starkly contrasted with its parent ICZ, which was found to be highly cytotoxic across all cell lines tested.[107] Thus, in altering just one atom, it is possible to significantly modulate biological activity.

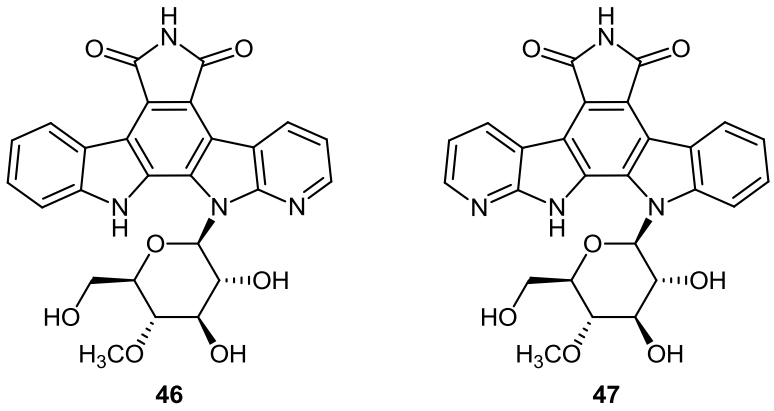

Fig. 1.28 *Structures of 7-aza REB* ***3*** *derivatives* ***46*** *and* ***47***

Prudhomme *et al.* further demonstrated that aza ICZ **48**, containing two 7-azaindolyl moieties, was more cytotoxic against a number of cancer cell lines, such as L1210 leukemia (IC_{50} = 0.067 µM) and HT29 non-small cell lung cancer (IC_{50} = 0.57 µM) lines, compared to REB **3** (IC_{50} = 0.14 and 0.3 µM respectively).[108] In comparison, *N*-methyl derivative **49** was found to be about ten times less potent against L1210 cells (IC_{50} = 0.58 µM) and inactive against HT29 cells (IC_{50} = 97 µM), indicating that a free imide nitrogen is highly important for activity.

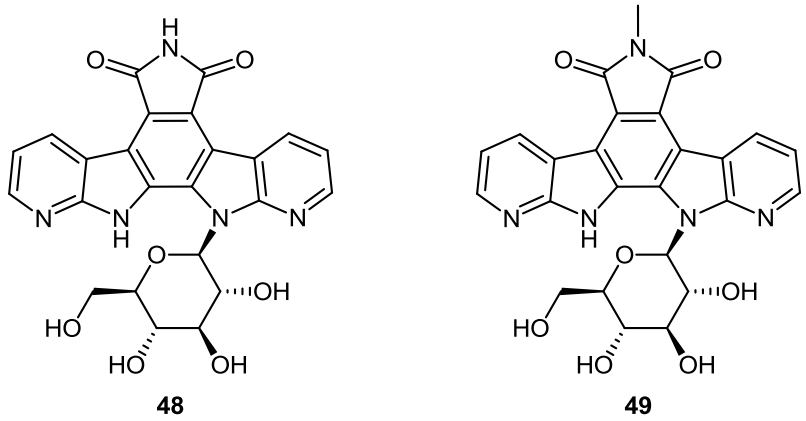

Fig. 1.29 *Structures of REB* ***3*** *analogues bearing two 7-azaindole moieties*

1.4 Conclusion

The ICZ alkaloids represent a privileged scaffold with which to explore the development of novel chemotherapeutic drugs due to the wide range of biological activities mediated by members of the class. Two main modes of action exist within the paradigm of ICZ derivatives as anticancer agents: inhibition of protein kinases and the topoisomerase I enzyme. For example, candidates such as lestaurtinib **24** and enzastaurin **27**, which are both currently undergoing clinical trials, have been shown to demonstrate excellent kinase activity (Sections *1.3.1.4* and *1.3.1.5*), while other derivatives such as edotecarin **42** act primarily as topoisomerase I inhibitors (Section *1.3.2.2*).[65,73,105]

Of the various synthetic derivatisations that have been described and documented, one of the most interesting developments has been seen with the bioisosteric assimilation of 7-azaindolyl subunits into the ICZ core. In these instances, the replacement of just one or two atoms has often resulted in the conferring of remarkable selectivity profiles relative to their parent ICZs (Sections *1.3.1.5* and *1.3.2.3*).[74,108]

1.5 References

1. Siegel, R.; Ward, E.; Brawley, O.; Ahmedin, J. *CA Cancer J. Clin.* **2011**, 61, 212-236
2. Jemal, A.; Bray, F.; Center, M.M.; Ferlay, J.; Ward, E.; Forman, D. *CA Cancer J. Clin.* **2011**, 61, 69-90
3. Ferlay, J.; Shin, H.R.; Bray, F.; Forman, D.; Mathers, C.; Parkin, D.M. *GLOBOCAN 2008 v2.0*, Cancer Incidence and Mortality Worldwide: IARC CancerBase No. 10 [Internet]. Lyon, France: International Agency for Research on Cancer; **2010**. Available from: http://globocan.iarc.fr, accessed on 12/2/2012
4. Rang, H.P.; Dale, M.M.; Ritter, J.M. *Pharmacology* **1999**, 4th Edition, Churchill Livingstone
5. Ferlay, J.; Parkin, D.; Stelianova-Foucher, E. *Eur. J. Cancer* **2010**, 46, 765-781
6. Cancer in Ireland *National Cancer Institute Ireland* **2011**, *Annual Statistical Report*
7. Fulda, S.; Debatin, K.-M. *Oncogene* **2006**, 25, 4798-4811
8. Kummar, S.; Chen, H.X.; Wright, J.; Holbeck, S.; Davis Millin, M.; Tomaszewski, J.; Zweibel, J.; Collins, J.; Doroshow, J.H. *Nat. Rev. Drug Discovery* **2010**, 9, 843-856
9. Sánchez, C.; Méndez, C.; Salas, J.A. *Nat. Prod. Rep.* **2006**, 23, 1007-1045
10. Brunton, R.J.; Drayson, F.K.; Plant, S.G.P.; Tomlinson, M.L. *J. Chem. Soc.* **1956**, 4783-4785
11. Omura, S.; Iwai, Y.; Hirano, A.; Nakagawa, A.; Awaya, J.; Tsuchiya, Y.; Takahashi, Y.; Masuma, R. *J. Antibiot.* **1977**, 30, 275-282
12. Tamaoki, T.; Nomoto, H.; Takahashi, I.; Kato, Y.; Morimoto, M.; Tomita, F. *Biochem. Biophys. Res. Commun.* **1986**, 135, 397-402
13. Omura, S.; Sasaki, Y.; Iwai, Y.; Takeshima, H. *J. Antibiot.* **1995**, 48, 535-548
14. Nettleton, D.E.; Doyle, T.W.; Krishnan, B.; Matsumoto, G.K.; Clardy, J. *Tet. Lett.* **1985**, 26, 4011-4014
15. Bush, J.A.; Long, B.H.; Catino, J.J.; Bradner, W.T.; Tomita, K. *J. Antibiot.* **1987**, 40, 668-678
16. Takahashi, I.; Kobayashi, E.; Asano, K.; Yoshida, M.; Nakano, H. *J. Antibiot.* **1987**, 40, 1782-1784
17. Kinnel, R.B.; Scheuer, P.J. *J. Org. Chem.* **1992**, 57, 6327-6329
18. Steglich, W.; Steffan, B.; Kopanski, L.; Eckhardt, G. *Angew. Chem. Int. Ed. Engl.* **1980**, 19, 459-460
19. Nakanishi, S.; Matsuda, Y.; Iwahashi, K.; Kase, H. *J. Antibiot.* **1986**, 39, 1066-1071
20. Takahashi, H.; Osada, H.; Uramoto, M.; Isono, K. *J. Antibiot.* **1990**, 43, 168-173
21. Osada, H.; Takahashi, H.; Tsunoda, K.; Kusakabe, H.; Isono, K. *J. Antibiot.* **1990**, 43, 163-167
22. Horton, P.A.; Longley, R.E.; McConnell, O.J.; Ballas, L.M. *Cell. Mol. Life Sci.* **1994**, 50, 843-845

23. McCombie, S.W.; Bishop, R.W.; Carr, D.; Dobek, E.; Kirkup, M.P.; Kirschmeier, P.; Lin, S.-I.; Petrin, J.; Rosinski, K.; Shankar, B.B.; Wilson, O. *Bioorg. Med. Chem. Lett.* **1993**, 3, 1537-1542
24. Butler, M.S. *Nat. Prod. Rep.* **2005**, 22, 162-195
25. Yang, S.W.; Lin, L.J.; Cordell, G.A.; Wang, P.; Corley, D.G. *J. Nat. Prod.* **1999**, 62, 1551-1553
26. Lam, K.S.; Forenza, S.; Doyle, T.W.; Pearce, C.J. *J. Ind. Microbiol.* **1990**, 6, 291-294
27. Lam, K.S.; Schroeder, D.R.; Veitch, J.M.; Matson, J.A.; Forenza, S. *J. Antibiot.* **1991**, 44, 934-939
28. Gullo, V.P.; McAlpine, J.; Lam, K.S.; Baker, D.; Petersen, F. *J. Ind. Microbiol. Biotechnol.* **2006**, 33, 523-531
29. Gray, N.; Détivaud, L.; Doerig, C.; Meijer, L. *Curr. Med. Chem.* **1999**, 6, 859-875
30. Prudhomme, M. *Curr. Med. Chem.* **2000**, 7, 1189-1212
31. Schupp, P.; Eder, C.; Proksch, P.; Wray, V.; Schneider, B.; Herderich, M., Paul, V. *J. Nat. Prod.* **1999**, 62, 959-962
32. Manning, G.; Whyte, D.B.; Martinez, R.; Hunter, T.; Sudarsanam, S. *Science* **2002**, 298, 1912-1934
33. Fischer, E.H.; Krebs, E.G. *J. Biol. Chem.* **1955**, 216, 121-132
34. Krebs, E.G.; Kent, A.B.; Fischer, E.H. *J. Biol. Chem.* **1958**, 231, 73-83
35. Liu, J.; Hu, Y.; Waller, D.L.; Wang, J.; Liu, Q. *Nat. Prod. Rep.* **2012**
36. Knighton, D.R.; Zheng, J.H.; Ten Eyck, L.F.; Ashford, V.A.; Xuong, N.H.; Taylor, S.S.; Sowadski, J.M. *Science* **1991**, 253, 407-414
37. Schwartz, P.A.; Murray, B.W. *Bioorg. Chem.* **2011**, 39, 192-210
38. McGregor, M.J. *J. Chem. Info. Model.* **2007**, 47, 2374-2382
39. Fischer, P.M. *Curr. Med. Chem.* **2004**, 11, 1563-1583
40. ArgusLab 4.0.1; Thompson, M.A. *Planaria Software LLC*, Seattle, WA, USA http://www.arguslab.com, accessed on 26/1/2012
41. Lowe, E.D.; Noble, M.E.M.; Skamnaki, V.T.; Oikonomakos, N.G.; Owen, D.J.; Johnson, L.N. *EMBO J.* **1997**, 16, 6646-6658
42. Kornev, A.P.; Taylor, S.S. *Biochim. Biophys. Acta* **2009**, 1804, 440-444
43. Sefton, B.M.; Hunter, T.; Beemon, K.; Eckhart, W. *Cell* **1980**, 20, 807-816
44. Liao, J.J.-L. *J. Med. Chem.* **2007**, 50, 409-424
45. Weinmann, H.; Metternich, R. *ChemBioChem* **2005**, 6, 455-459
46. Chandregowda, V; Venkateswara Rao, G.; Chandrasekara Reddy, G. *Org. Process Res. Dev.* **2007**, 11, 813-816
47. Goodman, V.L.; Rock, E.P.; Dagher, R.; Ramchandani, R.P.; Abraham, S.; Gobburu, J.V.S.; Booth, B.P.; Verbois, S.L.; Morse, D.E.; Liang, C.Y.; Chidambaram, N.; Jiang, J.X.; Tang, S.; Mahjoob, K.; Justice, R.; Pazdur, R. *Clin. Cancer Res.* **2007**, 13,1367-1373
48. Gani, O.; Engh, R. *Nat. Prod. Rep.* **2010**, 27, 489-498
49. Toledo, L.M.; Lydon, N.B. *Structure* **1997**, 5, 1551-1556
50. Prade, L.; Engh, R.A.; Girod, A.; Kinzel, V.; Huber, R.; Bossemeyer, D. *Structure* **1997**, 5, 1627-1637
51. Lawrie, A.M.; Noble, M.E.; Tunnah, P.; Brown, N.R.; Johnson, L.N.; Endicott, J.A. *Nat. Struct. Biol.* **1997**, 4, 796-801

52. *Cerius^2 Modeling Environment*, **2007**. San Diego: Molecular Simulations Inc., 2000
53. Komander, D.; Kular, G.S.; Bain, J.; Elliott, M.; Alessi, D.R.; Van Aalten, D.M. *Biochem. J.* **2003**, 375, 255-262
54. Jiang, X.; Zhao, B.; Britton, R.; Lim, L.Y.; Leong, D.; Sanghera, J.S.; Zhou, B.B.; Piers, E.; Andersen, R.J.; Roberge, M. *Mol. Cancer Ther.* **2004**, 3, 1221-1227
55. Zhao, B.; Bower, M.J.; McDevitt, P.J.; Zhao, H.; Davis, S.T.; Johanson, K.O.; Green, S.M.; Concha, N.O.; Zhou, B.B. *J. Biol. Chem.* **2002**, 277, 46609-46615
56. Jackson, J.R.; Gilmartin, A.; Imburgia, C.; Winkler, J.D.; Marshall, L.A.; Roshak, A. *Cancer Res.* **2000**, 60, 566-572
57. Mucke, H.A. *IDrugs* **2003**, 6, 377-383
58. Parkinson Study Group *Neurology* **2004**, 62, 330-332
59. Butler, M.S. *Nat. Prod. Rep.* **2005**, 22, 162-195
60. Stone, R.M.; Deangelo, D.J.; Klimek, V.; Galinsky, I.; Estey, E.; Nimer, S.D.; Grandin, W.; Lebwohl, D.; Wang, Y.; Cohen, P.; Fox, E.A.; Neuberg, D.; Clark, J.; Gilliland, D.G.; Griffin, J.D. *Blood* **2005**, 105, 54-60
61. Smith, B.D.; Levis, M.; Beran, M.; Giles, F.; Kantarjian, H.; Berg, K.; Murphy, K.M.; Dauses, T.; Allebach, J.; Small, D. *Blood* **2004**, 103, 3669-3676
62. Strock, C.J.; Park, J.I.; Rosen, D.M.; Dionne, C.; Ruggeri, B.; Jones-Bolin, S.; Denmeade, S.R.; Ball, D.W.; Nelkin, B.D. *Cancer Res.* **2003**, 63, 5559-5563
63. Toullec, D.; Pianetti, P.; Coste, H.; Bellevergue, P.; Grand-Perret, T.; Ajakane, M.; Baudet, V.; Boissin, P.; Boursier, E.; Loriolle, F.; Duhamel, L.; Charon, D.; Kirilovsky, J. *J. Biol. Chem.* **1991**, 266, 15771-15781
64. Davies, S.P.; Reddy, H.; Caivano, M.; Cohen, P. *Biochem. J.* **2000**, 351, 95-105
65. Conseil, G.; Perez-Victoria, J.M.; Jault, J.M.; Gamarro, F.; Goffeau, A.; Hofmann, J.; Di Petro, A. *Biochemistry* **2001**, 40, 2564-2571
66. Coultrap, S.J.; Sun, H.; Tenner Jr., T.E.; Machu, T.K. *J. Pharmacol. Exp. Ther.* **1999**, 290, 76-82
67. Jirousek, M.R.; Gillig, J.R.; Gonzalez, C.M.; Heath, W.F.; McDonald III, J.H.; Neel, D.A.; Rito, C.J.; Singh, U.; Stramm, L.E.; Melikian-Badalian, A.; Baevsky, M.; Ballas, L.M.; Hall, S.E.; Winneroski, L.L.; Faul, M.M. *J. Med. Chem.* **1996**, 39, 2664-2671
68. Komander, D.; Kular, G.S.; Schüttelkopf, A.W.; Deak, M.; Prakash, K.R.C.; Bain, J.; Elliott, M.; Garrido-Franco, M.; Kozikowski, A.P.; Alessi, D.R.; Van Aalten, D.M.F. *Structure* **2004**, 12, 215-226
69. Gálvez, M.I. *Curr. Phar. Biotechnol.* **2011**, 12, 386-391
70. Graff, J.R.; McNulty, A.M.; Ross Hanna, K.; Konicek, B.W.; Lynch, R.L.; Bailey, S.N.; Banks, C.; Capen, A.; Goode, R.; Lewis, J.E.; Sams, L.; Huss, K.L.; Campbell, R.M.; Iversen, P.W.; Lee Neubauer, B.; Brown, T.J.; Musib, L.; Geeganage, S.; Thornton, D. *Cancer Res.* **2005**, 65, 7462-7469
71. Kuo, G.-H.; Prouty, C.; DeAngelis, A.; Shen, L.; O'Neill, D.J.; Shah, C.; Connolly, P.J.; Murray, W.V.; Conway, B.R.; Cheung, P.; Westover, L.; Xu, J.Z.; Look, R.A.; Demarest, K.T.; Emanuel, S.; Middleton, S.A.; Jolliffe, L.; Beavers, M.P.; Chen, X. *J. Med. Chem.* **2003**, 46, 4021-4031
72. Cross, D.; Cubert, A.A.; Chalmers, K.A.; Facci, L.; Skaper, S.D.; Reith, A.D. *J. Neurochem.* **2001**, 77, 94-102

73. Castro, A.; Martinez, A. *Expert Opin. Ther. Pat.* **2000**, 10, 1519-1527
74. Bregman, H.; Williams, D.S.; Meggers, E. *Synthesis* **2005**, 9, 1521-1527
75. Peifer, C.; Selig, R.; Kinkel, K.; Ott, D.; Totzke, F.; Schächtele, C.; Heidenreich, R.; Röcken, M.; Schollmeyer, D.; Laufer, S. *J. Med. Chem.* **2008**, 51, 3814-3824
76. Kiselyov, A.; Balakin, K.V.; Tkachenko, S.E. *Expert Opin. Invest. Drugs* **2007**, 16, 83-107
77. O'Neill, D.J.; Shen, L.; Prouty, C.; Conway, B.R.; Westover, L.; Xu, J.Z.; Zhang, H.-C.; Maryanoff, B.E.; Murray, W.V.; Demarest, K.T.; Kuo, G.-H. *Bioorg. Med. Chem.* **2004**, 12, 3167-3185
78. Popowycz, F.; Routier, S.; Joseph, B.; Mérour, J.-Y. *Tetrahedron* **2007**, 63, 1031-1064
79. Perry, N. B.; Ettouati, L.; Litaudon, M.; Blunt, J. W.; Munro, M. H. G.; Parkin, S.; Hope, H. *Tetrahedron* **1994**, 50, 3987–3992
80. Simone, M.; Erba, E.; Damia, G.; Vikhanskaya, F.; Di Francesco, A.M.; Riccardi, R.; Bailly, C.; Cuevas, C.; Sousa-Faro, J.M.F.; D'Incalci, M. *Eur. J. Cancer* **2005**, 41, 2366-2377
81. Echalier, A.; Bettayeb, K.; Ferandin, Y.; Lozach, O.; Clément, M.; Valette, A.; Liger, F.; Marquet, B.; Morris, J.C.; Endicott, J.A.; Joseph, B.; Meijer, L. *J. Med. Chem.* **2008**, 51, 737-751
82. Thrash, C.; Bankier, A.T.; Barrell, B.G.; Sternglanz, R. *Proc. Natl. Acad. Sci. USA* **1985**, 82, 4374-4378
83. Lee, M.P.; Brown, S.D.; Chen, A.; Hsieh, T.-S. *Proc. Natl. Acad. Sci. USA* **1993**, 90, 6656-6660
84. Morham, S.G.; Kluckman, K.D.; Voulomanos, N.; Smithies, O. *Mol. Cell. Biol.* **1996**, 16, 6804-6809
85. Stewart, L.; Redinbo, M.R.; Qiu, X.; Hol, W.G.; Champoux, J.J. *Science* **1998**, 279, 1534-1541
86. Pommier, Y. *Nat. Rev. Cancer* **2006**, 6, 789-802
87. Tse-Dinh, Y.-C.; Kirkegaard, K.; Wang, J.C. *J. Biol. Chem.* **1980**, 255, 5560-5565
88. Van der Zee, A.G.J.; Hollema, H.; Jong, S.; Boonstra, H.; Gouw, A.; Willemse, P.H.B.; Zijlstra, J.G.; Varies, E.G.E. *Cancer Res.* **1991**, 51, 5915-5920
89. Husain, I.; Mohler, J.L.; Seigler, H.F.; Besterman, J.M. *Cancer Res.* **1994**, 54, 539-546
90. Wall, M.E.; Wani, M.C.; Cooke, C.E.; Palmer, K.H.; McPhail, A.T.; Slim, G.A. *J. Am. Chem. Soc.* **1966**, 88, 3888-3890
91. Hsiang, Y.H.; Hertzberg, R.; Hecht, S.; Liu, L.F. *J. Biol. Chem.* **1985**, 260, 14873-14878
92. Staker, B.L.; Feese, M.D.; Cushman, M.; Pommier, Y.; Zembower, D.; Stewart, L.; Burgin, A.B. *J. Med. Chem.* **2005**, 48, 2336-2345
93. Staker, B.L.; Hjerrild, K.; Feese, M.D.; Behnke, C.A.; Burgin Jr., A.B.; Stewart, L. *Biochemistry* **2002**, 99, 15387-15392
94. Pommier, Y. *Chem. Rev.* **2009**, 109, 2894-2902
95. Ulukan, H.; Swaan, P.W. *Drugs* **2002**, 62, 2039-2057
96. Yamashita, Y.; Fujii, N.; Murakata, C.; Ashizawa, T.; Okabe, M.; Nakano, H. *Biochemistry* **1992**, 31, 12069-12075

97. Kojiri, K.; Kondo, H.; Yoshinari, T.; Arakawa, H.; Nakajima, S.; Satoh, F.; Kawamura, K.; Okura, A.; Suda, H.; Okanishi, M. *J. Antibiot.* **1991**, 44, 723-728
98. Yoshinari, T.; Yamada, A.; Uemura, D.; Nomura, K.; Arakawa, H.; Kojiri, K.; Yoshida, E.; Suda, H.; Okura, A. *Cancer Res.* **1993**, 53, 490-494
99. Ohkubo, M.; Nishimura, T.; Jona, H.; Honma, T.; Ito, S.; Morishima, H. *Tetrahedron* **1997**, 53, 5937-5950
100. Yoshinari, T.; Matsumoto, M.; Arakawa, H.; Okada, H.; Noguchi, K.; Suda, H.; Okura, A.; Nishimura, S. *Cancer Res.* **1995**, 55, 1310-1315
101. Arakawa, H.; Iguchi. T.; Yoshinari, T.; Kojiri, K.; Suda, H.; Okura, A. *Cancer Res.* **1995**, 55, 1316-1320
102. Bailly, C.; Qu, X.; Chaires, J.B.; Colson, P.; Houssier, C.; Ohkubo, M.; Nishimura, S.; Yoshinari, T. *J. Med. Chem.* **1999**, 42, 2927-2935
103. Ohkubo, M.; Nishimura, T.; Kawamoto, H.; Nakano, M.; Honma, T.; Yoshinari, T.; Arakawa, H.; Suda, H.; Morishima, H.; Nishimura, S. *Bioorg. Med. Chem. Lett.* **2000**, 10, 419-422
104. Goossens, J.F.; Kluza, J.; Vezin, H.; Kouach, M.; Briand, G.; Baldeyrou, B.; Wattez, N.; Bailly, C. *Biochem. Pharmacol.* **2003**, 65, 25-34
105. Sheng, C.; Miao, Z.; Zhang, W. *Curr. Med. Chem.* **2011**, 18, 4389-4409
106. Staker, B.L.; Feese, M.D.; Cushman, M.; Pommier, Y.; Zembower, D.; Stewart, L.; Burgin, A.B. *J. Med. Chem.* **2005**, 48, 2336-2345
107. Marminon, C.; Pierré, A.; Pfeiffer, B.; Pérez, V.; Léonce, S.; Joubert, A.; Bailly, C.; Renard, P.; Hickman, J.; Prudhomme, M. *J. Med. Chem.* **2003**, 46, 609-622
108. Marminon, C.; Pierré, A.; Pfeiffer, B.; Pérez, V.; Léonce, S.; Renard, P.; Prudhomme, M. *Bioorg. Med. Chem.* **2003**, 11, 679-687

Chapter 2

Chemical Introduction

Contents

2.0 Chemical Introduction

2.1 Synthetic routes to indolo[2,3-*a*]carbazoles

The first natural product found to contain the indolocarbazole core, staurosporine **2**, was isolated from nature in 1977, with members of this structural class previously garnering little attention aside from purely synthetic interest.[1] Of the five different isomeric ring systems available to the ICZ family of compounds, it is the indolo[2,3-*a*]carbazole **1** class that has been the subject of the greatest research interest, as it is this structural framework that has been found to be the main constituent of many natural products with a diverse range of potent biological activities.

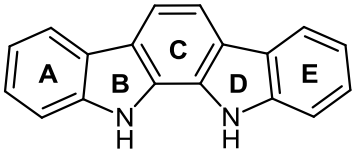

1

Fig. 2.1 *Indolo[2,3-a]carbazole structural core **1***

Numerous diverse routes have been reported in reference to the formation of ICZs since the first synthetic protocol towards these polycyclic ring systems was described in 1956.[2] For review purposes we have broadly classified an overview of the chemical techniques involved on the basis of the final step to yield the ICZ core, namely Fischer indole synthesis (Section ***2.1.1***), aromatisation of bisindole precursors (Section ***2.1.2***), nitrene insertion (Section ***2.1.3***) and palladium(0)-catalysed polyannulation (Section ***2.1.4***).

Initial synthetic efforts carried out in this field in the 1950's were relatively sparse and limited in scope, predominantly involving variations of the Fischer indolisation. Once the potent biological activities of a number of ICZ alkaloids were realised in the late 1970's and early 1980's, great emphasis was placed in the medicinal chemistry field on both the total syntheses of natural products from this series and on synthetic derivatisation programmes in order to develop new clinical candidates. Although perhaps by far the most heavily utilised means of access has involved the aromatisation of bisindolyl precursors, an ever expanding level of endeavour has meant that many other methodologies have been employed and developed.

2.1.1 Fischer indolisation towards ICZs

As part of a wider synthetic effort towards the development of carbazole chemistry, Tomlinson *et al.* reported the first formation of an indolo[2,3-*a*]carbazole (ICZ) ring system in 1956 as an *N*-methyl derivative **52** (***Scheme 2.1***).[2] This ICZ **52** was accessed through the condensation of 8-amino-1,2,3,4-tetrahydro-9-methyl-9*H*-carbazole **50** with 2-hydroxycyclohexanone **51**, followed by dehydrogenation. Unfortunately, attempts to utilise this method to form parent ICZ **1** met with little success.

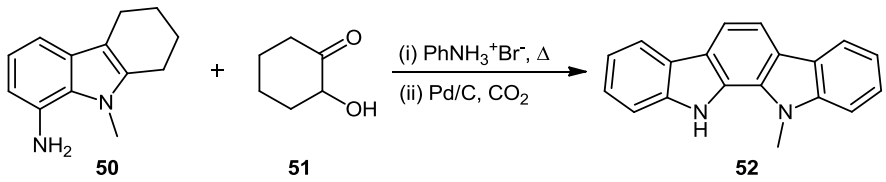

Scheme 2.1 *Synthesis of* N*-methyl ICZ derivative* ***52***

However, the successful synthesis of ICZ **1** was reported in 1958 by Willcox *et al.*, utilising the methodology of a Fischer indolisation of 2-hydroxycyclohexanone **51** with phenylhydrazine **53** (***Scheme 2.2***).[3]

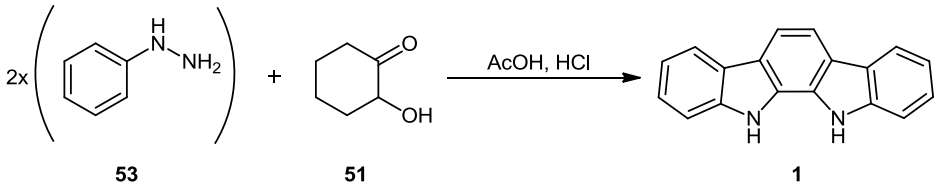

Scheme 2.2 *Synthesis of parent ICZ* ***1***

In recent years, Hu and Chen reported a series of ICZs from a neat one-pot reaction by means of Fischer indolisation, starting from substituted 2-aminocyclohexanone derivatives and a number of hydrazine hydrochlorides.[4] One such representative reaction (illustrated in ***Scheme 2.3***) involves the synthesis of ICZ **56** from 2-amino-4-phenylcyclohexanone hydrochloride **54** and (4-chlorophenyl)hydrazine hydrochloride **55** in a mixture of acetic acid and trifluoroacetic acid. The authors noted the simple efficiency and robust nature of the novel procedure, which is insensitive to air and moisture, with a panel of 16 ICZs being formed using this methodology.

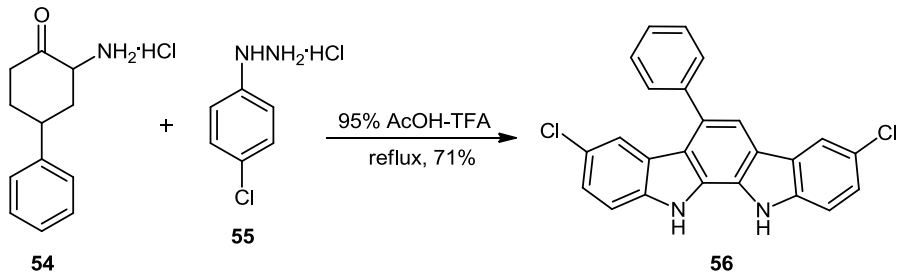

Scheme 2.3 *Accessing ICZs via one-pot Fischer indolisation*

2.1.2 Accessing ICZs: aromatisation of bisindolyl precursors

Perhaps due to ease of access and the provision of significant scope for elaboration, the primary means reported in the literature towards the formation of the pentacyclic ICZ core involves the cyclisation of bisindolyl precursors. Methods employed include the aromatisation of bisindolyl lactams (Section *2.1.2.1*) and bisindolylmaleimides (Section *2.1.2.2*), Diels-Alder and metathesis reactions of 2,2'-bisindoles (Section *2.1.2.3*), and the cyclisation of unsymmetrical 3,3'-bisindole derivatives (Section *2.1.2.4*).

2.1.2.1 Utilisation of bisindolyl lactam precursors

The first synthesis of the STA **2** aglycone K252c **13** was described by Winterfeldt and Sarstedt in 1983, three years before it was first reported to be isolated from a natural source.[5]

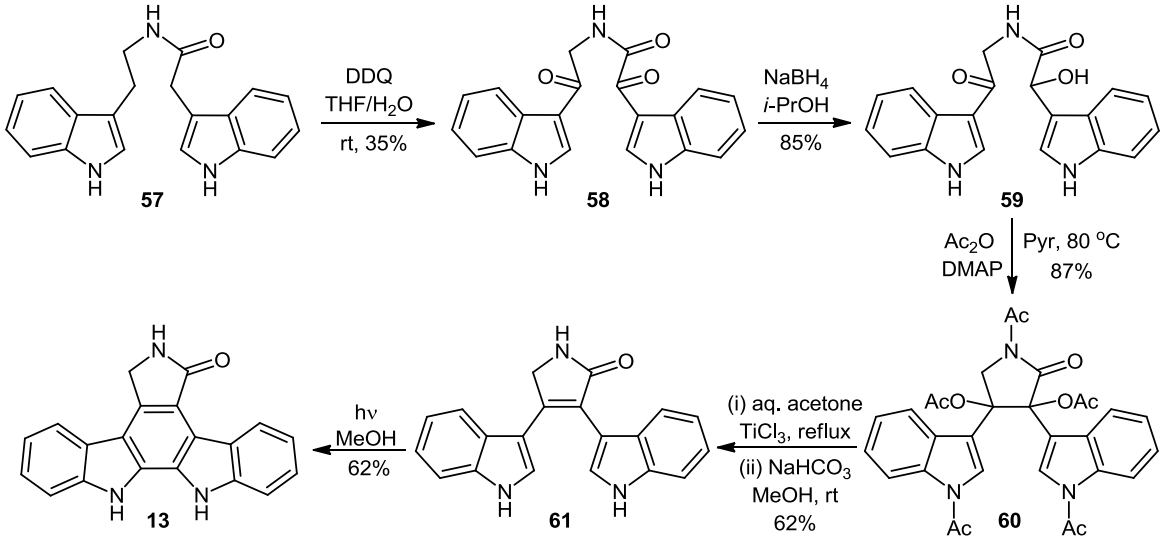

Scheme 2.4 *The first reported synthesis of K252c* ***13***

Oxidation of amide **57**, itself derived from tryptamine and indolyl-3-acetyl chloride, with DDQ in a mixture of THF and water provided diketone **58**, which was then selectively reduced to hydroxy ketone **59** using sodium borohydride (***Scheme 2.4***). Cyclisation of hydroxy ketone **59** towards acetylated derivative **60** was effectuated using acetic anhydride and a base catalyst, which was subsequently reduced and deacetylated using $TiCl_3$ in aqueous acetone followed by sodium bicarbonate in methanol respectively, yielding bisindolyl lactam **61**. The final oxidative ring closing step was accomplished by irradiation of lactam **61** in methanol, resulting in the formation of K252c **13**.

A novel synthesis of K252c was reported by Mahboobi *et al.* in 1999, where an intermolecular Michael addition of 1-(indol-3-yl)-2-nitroethene **62** to methyl 2-(indol-3-yl)acetate **63** initially yielded methyl 2,3-bis(indol-3-yl)-4-nitrobutanoate **64**.[6] Catalytic hydrogenation and cyclisation of nitrobutanoate **64** afforded lactam **65** in high yield of 87%, with subsequent oxidative cyclisation using DDQ and *p*-TSA then yielding K252c **13** (***Scheme 2.5***)

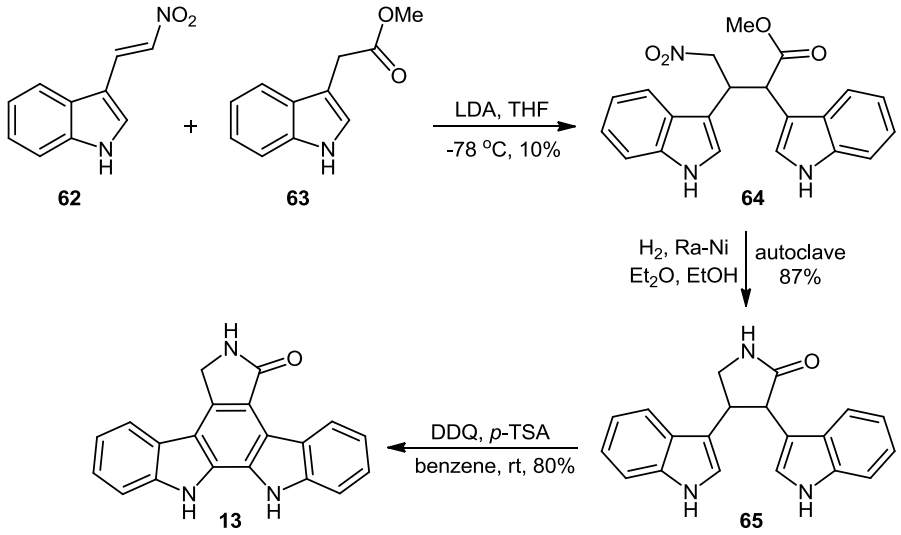

Scheme 2.5 *Synthesis of K252c **13** described by Mahboobi et al.*[6]

2.1.2.2 Cyclisation of bisindolylmaleimides

In 1980, Steglich *et al.* described the neat synthesis of a bisindolylmaleimide for the first time, derivative **68**, which would later lead to the development of relatively efficient synthetic routes towards ICZs.[7] The condensation of indolylmagnesium iodide **67** with *N*-methyl

dibromomaleimide **66** in benzene at room temperature with a catalytic amount of HMPA afforded BIM **68** in a good yield of 60% (***Scheme 2.6***).

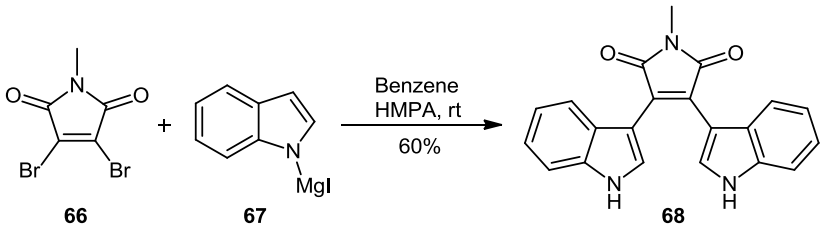

Scheme 2.6 *Synthesis of BIM* ***68***

Employing a variation of Steglich's approach, Weinreb and co-workers reported the synthesis of *N*-benzyl K252c **73** in 1984.[8] The initial formation of benzylated BIM **71** was achieved via the reaction of *N*-benzyl dibromomaleimide **70** with indolylmagnesium bromide **69**. Oxidative cyclisation of BIM **71** with *p*-TSA and DDQ afforded ICZ **72**, which was then reduced under Clemmensen conditions to give *N*-benzyl K252c **73** (***Scheme 2.7***).

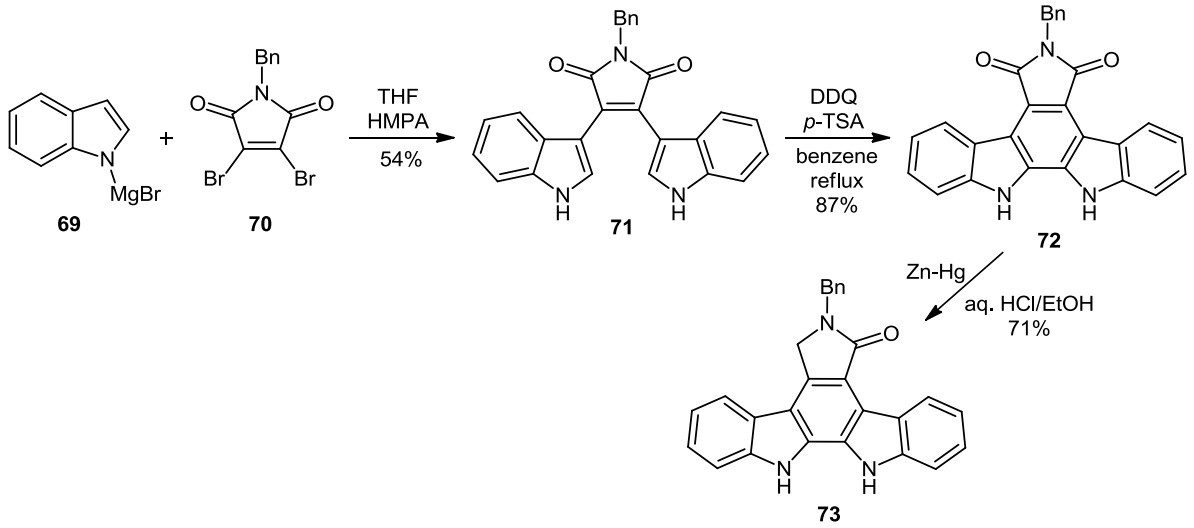

Scheme 2.7 *Synthesis of* N*-benzyl K252c* ***73***

In 1993, Hill and co-workers reported the synthesis of K252c **13** via two other naturally occurring ICZ derivatives, arcyriarubin A **10** and arcyriaflavin A **7** (***Scheme 2.8***).[9] Natural product **10** was afforded by reaction of dibromomaleimide **74** with indolylmagnesium bromide **69** in benzene. Oxidative cyclisation of bisindolylmaleimide **10** using palladium(II) acetate in acetic acid then formed the ICZ arcyriaflavin A **7**. The subsequent reduction of ICZ

7 using lithium aluminium hydride yielded hydroxy lactam **75**, with a hydrogenolysis in the presence of 10% Pd/C yielding K252c **13** in quite an efficient synthesis, with an overall yield of 14% from dibromomaleimide **74**.

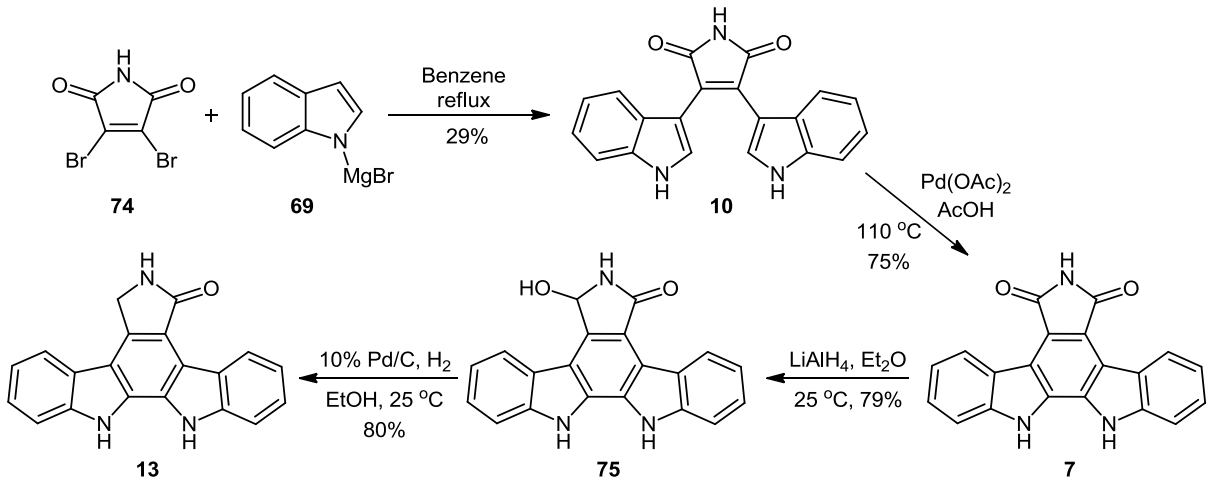

Scheme 2.8 *Synthesis of K252c* ***13*** *via arcyriarubin A* ***10*** *and arcyriaflavin A* ***7***

A higher yielding route to K252c **13** was described by Xie and Lown in 1994, incorporating the same benzylated BIM **71** as that first reported by Weinreb *et al*, though with a slightly modified coupling reaction (***Scheme 2.9***).[8,10]

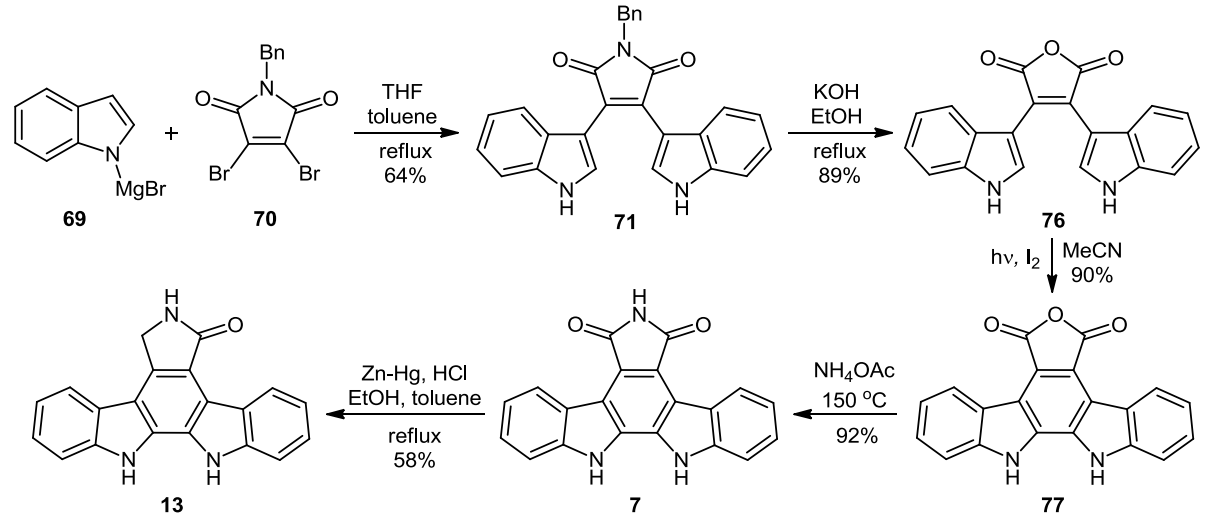

Scheme 2.9 *Synthesis of K252c* ***13*** *by Xie and Lown*[10]

N-Benzyl dibromomaleimide **70**, synthesised from dibromomaleimide **74** in 92% yield, was condensed with indolylmagnesium bromide **69** under reflux conditions to give BIM **71** (***Scheme 2.9***). Base-induced conversion to maleic anhydride **76** was followed by photocyclisation to yield ICZ **77**. Reaction of anhydride **77** with ammonium acetate then gave arcyriaflavin A **7**, with consequent reduction to K252c **13** accomplished with zinc amalgam, with an overall yield from dibromomaleimide **74** of 25%.

Ohkubo and co-workers disclosed the synthesis of a number of the arcyriaflavins in 1996, starting from dibromo-*N*-methylmaleimide **66** and 6-benzyloxyindole **78** (***Scheme 2.10***).[11]

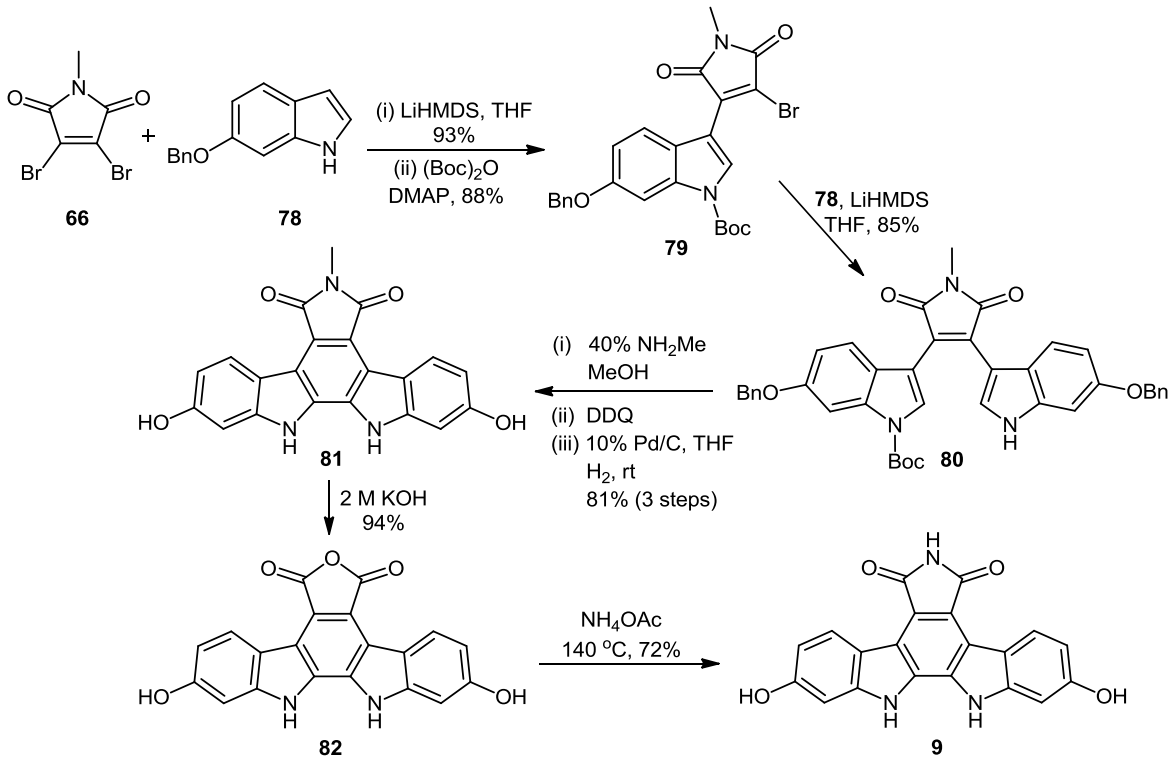

Scheme 2.10 *Route towards arcyriaflavin C* ***9***

Maleimide **66** and indole **78** were initially coupled using lithium hexamethyldisilazide as base, resulting in the formation of a monoindole derivative, with the subsequent Boc-protection of the indolic nitrogen giving **79** (***Scheme 2.10***). Further base-induced coupling of 6-benzyloxyindole **78** with intermediate **79** led to bisindolyl system **80**. Deprotection of the Boc group of bisindole **80** using methylamine, followed by oxidative cyclisation using DDQ and then subsequent debenzylation to give ICZ **81** was achieved in a high yield of 81% over three

steps. Maleic anhydride **82** was accessed by treatment of *N*-methyl maleimide **81** with a solution of aqueous potassium hydroxide, with consequent conversion to arcyriaflavin C **9** allowed using ammonium acetate. Ohkubo *et al.* were to later apply the same synthetic methodology to the synthesis of topo I inhibitors ED-110 **42** and NB-506 **43**.[12]

A novel route to arcyriarubin A **10** was reported by Faul *et al.* in 1998, where initially, following the reaction of indole **83** with oxalyl chloride, treatment of the glyoxyl chloride intermediate with sodium methoxide resulted in the formation of glyoxylate **84** (***Scheme 2.11***).[13] Arcyriarubin A **10** was then formed in a quantitative fashion by means of an intermolecular Perkin-type condensation of glyoxylate **84** with acetamide **85** in the presence of a 1 M solution of potassium *tert*-butoxide in THF. Despite requiring a step more than that described by Hill *et al.* (***Scheme 2.8***), the overall yield was significantly improved at 93%.

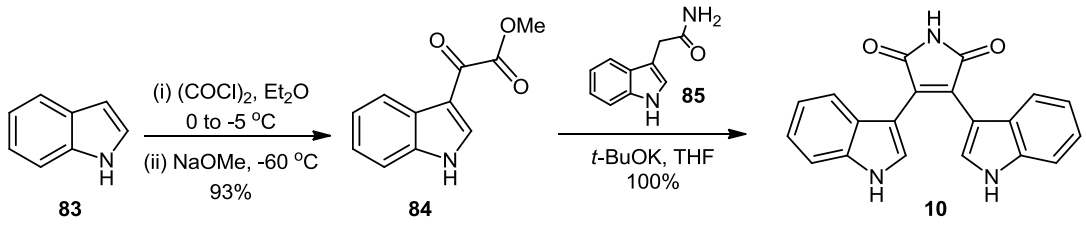

Scheme 2.11 *Synthesis of arcyriarubin A* ***10*** *reported by Faul et al.*[13]

Having established a new and efficient route towards BIMs such as arcyriarubin A **10**, Faul *et al.* subsequently applied their condensation method approach towards the total synthesis of rebeccamycin **3** and other ICZs.[14] Deprotonation of acetamide **86** with sodium hydride in acetonitrile, followed by treatment with α-1,2-anhydrosugar **87** resulted in the formation of *β*-*N*-glycoside **88**, which then underwent an intermolecular Perkin-type condensation (similar to that seen previously in ***Scheme 2.11***) with glyoxylate **89** to form the hydroxyimide **90** (***Scheme 2.12***). The ensuing i*n situ* treatment of reaction intermediate **90** with concentrated aqueous HCl under reflux conditions afforded bisindolylmaleimide **91**. Oxidative cyclisation of BIM **91** to form the ICZ core was then accomplished using palladium(II) triflate in DMF, with subsequent debenzylation of the glycosidic moiety by means of Pearlman's catalyst ultimately resulting in the formation of REB **3**.

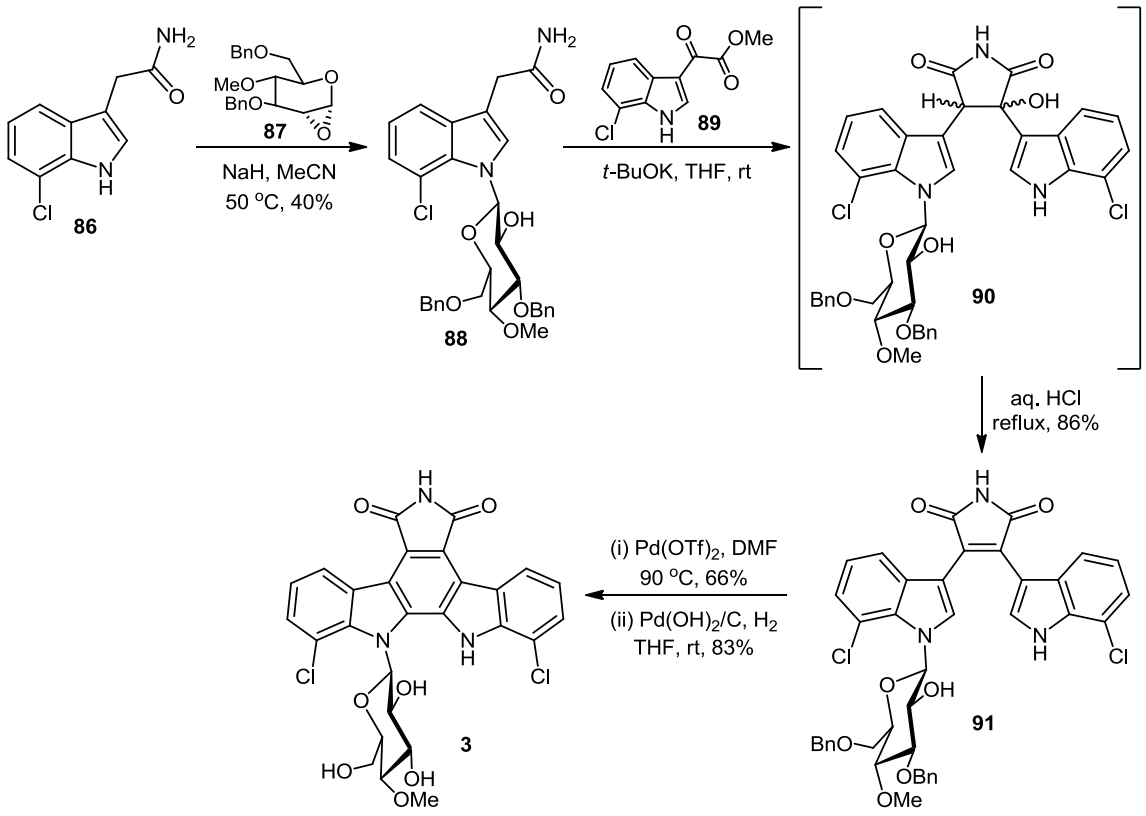

Scheme 2.12 *Total synthesis of rebeccamycin **3** by Faul et al.*[14]

2.1.2.3 Synthesis of ICZs via 2,2'-bisindole derivatives

Many routes to ICZs have been described using 2,2'-bisindole derivatives as precursors, with aromatisation to the pentacyclic core achieved by a variety of different methods. The synthesis of phenylarcyriaflavin A **96** was reported by Somei and Kodama in 1992, utilising the approach of a Diels-Alder cycloaddition.[15] Lithiation of 1-methoxyindole **92** was first of all carried out by treatment with *n*-butyl lithium, forming 2-lithio-1-methoxyindole, which then underwent oxidative coupling using anhydrous copper(II) sulfate and ultrasound stirring under an oxygen atmosphere to yield 2,2'-bis(1-methoxyindole) **93** in a yield of 54% (***Scheme 2.13***). Catalytic hydrogenation of the methoxy functionalities then gave 2,2'-bisindole **94**, which was subjected to Diels-Alder cycloaddition with *N*-phenylmaleimide **95** in the presence of catalytic 10% palladium on carbon in *o*-dichlorobenzene under reflux conditions to give phenylarcyriaflavin A **96** in 30% yield. Without the presence of 10% Pd/C, the yield of ICZ **96** was almost halved to 17%.

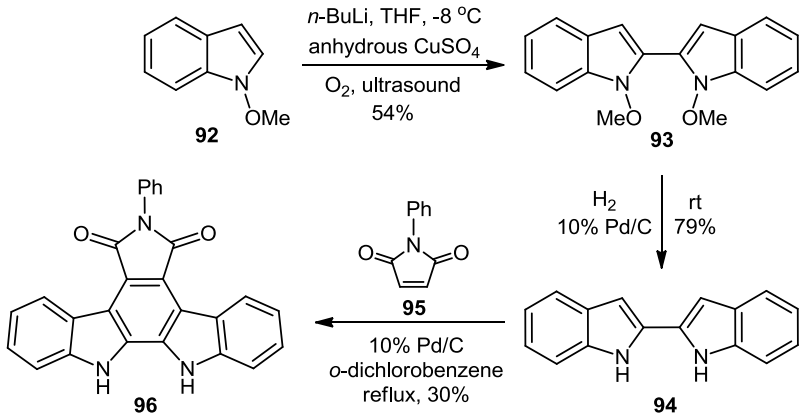

Scheme 2.13 *Synthesis of phenylarcyriaflavin A* ***96*** *via 2,2'-bisindole* ***93***

In 1995, Pindur and co-workers also reported the synthesis of an ICZ using a 2,2'-bisindole intermediate, 6-benzyl-12,13-dimethylarcyriaflavin A **102**, employing a different method to that used by Somei and Kodama.[14,16] Two units of *N*-methyl indole **97** were initially oxidatively coupled using copper(II) chloride, having previously been lithiated by means of *n*-butyl lithium, to afford 2,2'-bis(1-methylindole) **98** (***Scheme 2.14***).

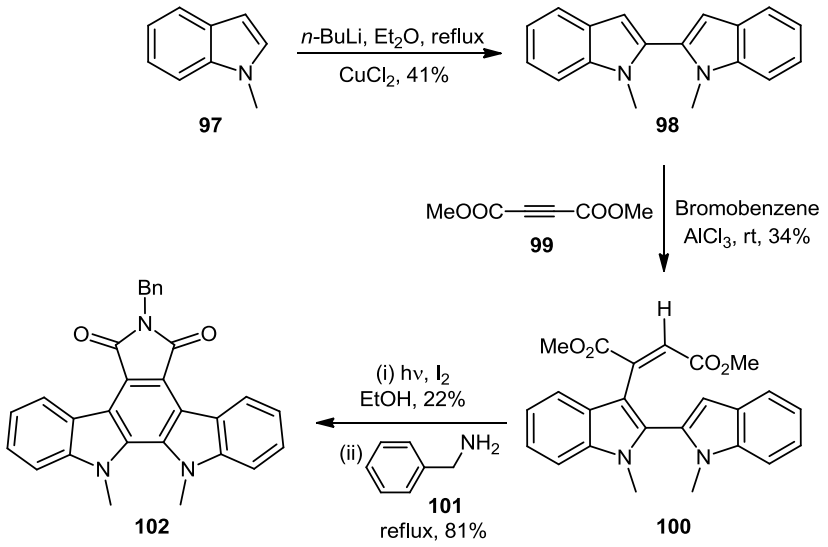

Scheme 2.14 *Synthesis of 6-benzyl-12,13-dimethylarcyriaflavin A* ***102***

2,2'-Bisindole **98** was then reacted with dimethyl acetylenedicarboxylate **99** in the presence of aluminium trichloride in bromobenzene, furnishing 2,2'-bisindol-3-yl dimethyl maleate **100**.

Following photochemical cyclisation of dimethyl maleate **100**, treatment with benzylamine **101** resulted in the formation of 6-benzyl-12,13-dimethylarcyriaflavin A **102** (***Scheme 2.14***).

Wood *et al.* described the synthesis of K252c **13** and a whole range of other ICZs in 1997 from the coupling 2,2'-bisindole **94** with different α-diazo-β-keto-γ-lactams.[17] A mixture of bisindole **94** and diazolactam **103** in degassed pinacolone was treated with rhodium(II) acetate in a sealed tube at 120 ^{o}C, resulting in the formation of K252c **13**, with the annulation posited to proceed via intermediates **104** and **105** (***Scheme 2.15***). The choice of degassed pinacolone, which is quite compatible with carbenoid chemistry, as solvent had a significant effect on the yield of ICZ aglycon **13**, as when the reaction had been carried out in benzene, a yield of only 3% was recorded.

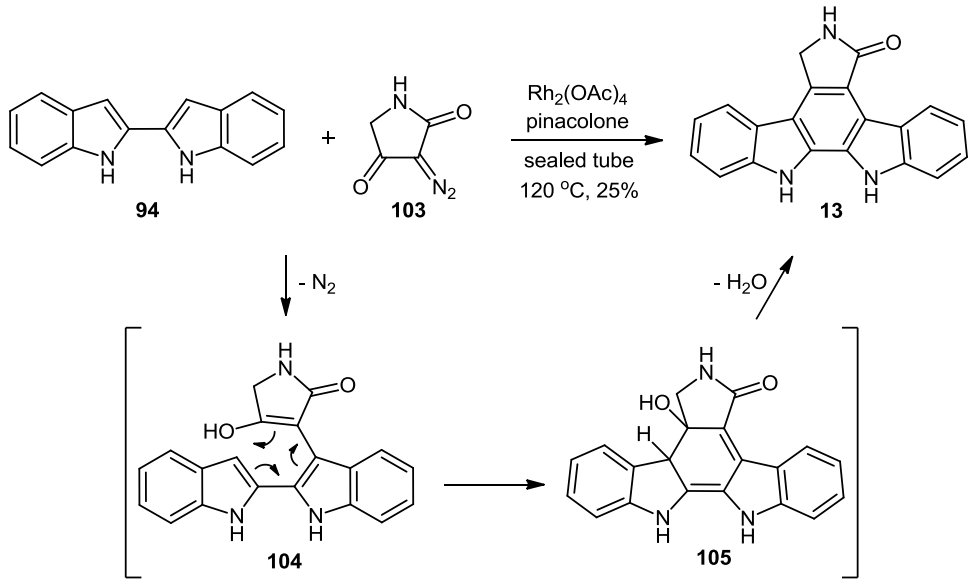

Scheme 2.15 *Synthesis of K252c* ***13*** *from 2,2'-bisindole* ***94***

In 2005, de Koning and co-workers described the novel use of a metathesis reaction to fashion an ICZ core **109** starting from precursor 2,2'-bisindole **94** (***Scheme 2.16***).[18] Standard Vilsmeier-Haack conditions on bisindole **94**, followed by Boc-protection led to dialdehyde **106**. Wittig olefination of dialdehyde **106** then lead to the required dialkene precursor **107** for the subsequent use of metathesis. Exposure of dialkene **107** to Grubbs' second generation catalyst **108** resulted in aromatisation to ICZ **109**.

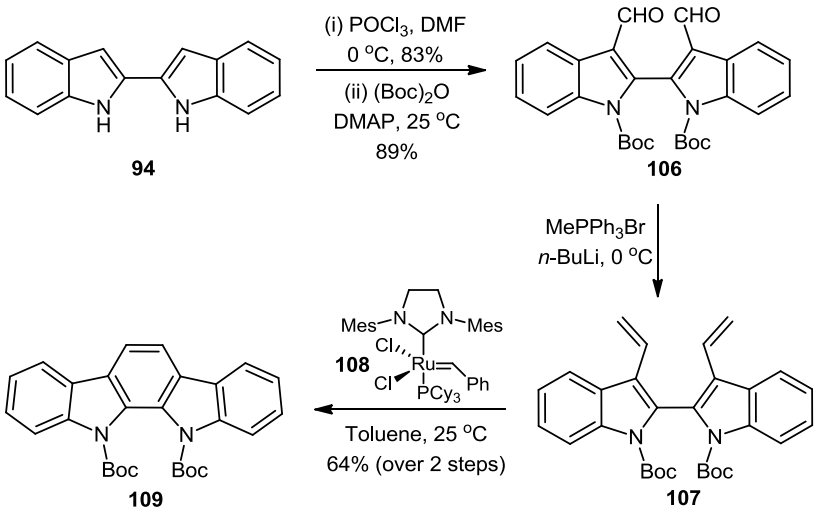

Scheme 2.16 *Formation of ICZ* ***109*** *via metathesis reaction*

Another novel route towards ICZ alkaloids featuring 2,2'-bisindole precursors was divulged when Snieckus and Cai reported the use of a Stille cross-coupling strategy in the synthesis of ICZ **115** (***Scheme 2.17***).[19] Initial attempts to fashion a 2,2'-bisindolyl bond between differentially *N*-protected 3-substituted indole coupling partners using Suzuki-Miyaura cross-coupling protocol had proven to be unsuccessful prior to the use of the corresponding Stille tactic.

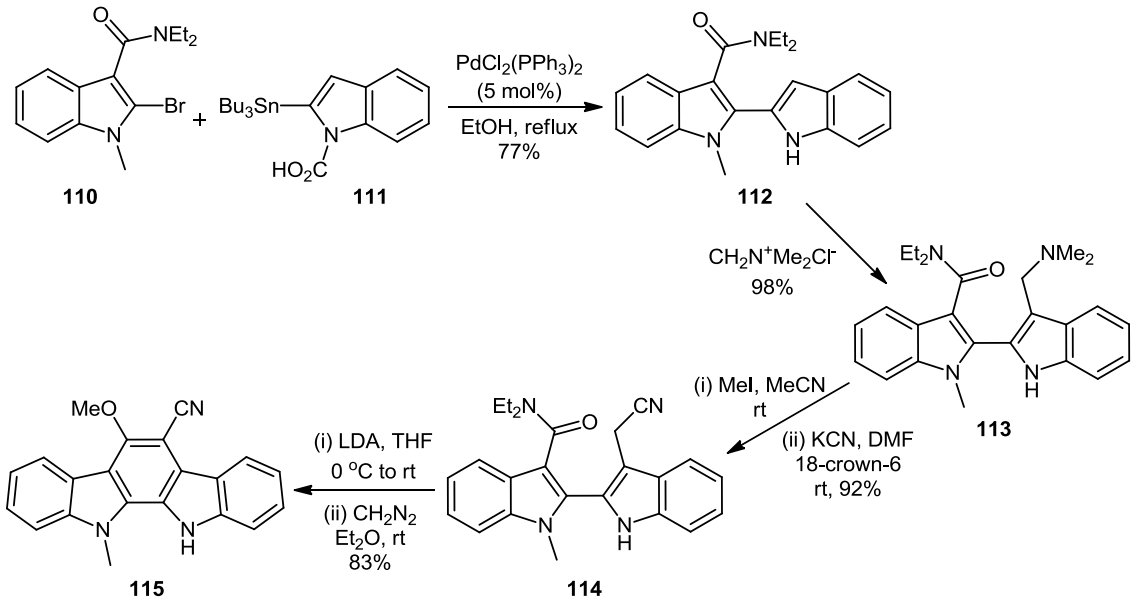

Scheme 2.17 *Route to ICZ* ***115*** *via metalation-cross coupling sequence*

The Stille coupling of 2-bromo indolo-3-carboxamide **110** with 2-stannylated *N*-carboxyindole **111** provided 2,2'-bisindole **112** in good yield, which upon treatment with Eschenmoser's salt afforded 2-substituted gramine **113**. The sequential reaction of bisindole **113** with methyl iodide and potassium cyanide/18-crown-6 resulted in the formation of acetonitrile **114**. Base-mediated cyclisation of intermediate **114**, followed by the immediate methylation of the relatively unstable phenol gave ICZ **115**.

2.1.2.4 Utilisation of 3,3'-bisindolyl precursors towards unsymmetrical ICZs

Orito *et al.* announced the availability of a new route towards the formation of unsymmetrical ICZs in 2007 when describing the synthesis of a series of *N*-protected ICZ aglycones.[20] Gramine methiodide **117** was initially coupled with 2-(1-benzyl-1*H*-indol-3-yl)acetonitrile **116** using *t*-BuLi to afford bisindole precursor **118** in excellent yield of 96% (***Scheme 2.18***).

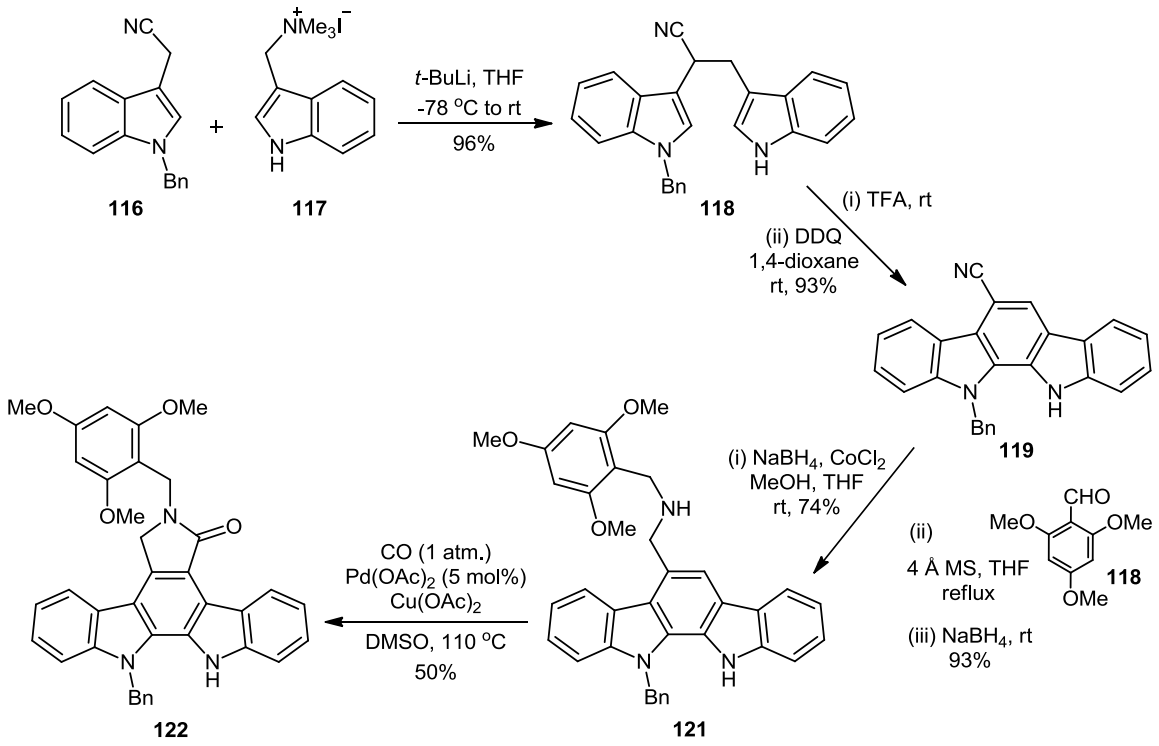

Scheme 2.18 *Route to N-benzylated ICZ* ***122***

Subsequent cyclisation of bisindole **118** by treatment with trifluoroacetic acid, followed by DDQ oxidation of the resulting cyclisation product gave ICZ **119**, again in a high yield of 93%. Reduction and condensation of ICZ **119** with 2,4,6-trimethoxybenzaldehyde **120**,

followed by a second reduction using sodium borohydride resulted in the formation of *N*-(2,4,6-trimethoxy)benzylamine **121**. Carbonylation of benzylamine **121** was then carried out using palladium(II) acetate and copper(II) acetate in DMSO under a carbon monoxide atmosphere to give lactam **122**. With each of the three nitrogen atoms of ICZ **122** bearing a different substituent, it has been postulated that this route could be prove useful in potential application to the synthesis of staurosporine **2** and related glycosidic ICZs.

2.1.3 Formation of ICZ core via nitrene insertion

The use of nitrene insertions to form the pentacyclic ICZ core has also been frequently documented in the literature. In one of the earliest examples, Raphael *et al.* described the synthesis of arcyriaflavin B **8** in 1983 by means of nitrene insertion following an initial Diels-Alder cycloaddition (***Scheme 2.19***).[21] 2-Nitrocinnamaldehyde **123** was initially condensed with a Wittig reagent obtained from 4-methoxy-2-nitrobenzylbromide **124** to give 1,4-diarylbutadiene **125**. The neat thermal cycloaddition of butadiene **125** with maleimide **126** was followed by oxidation with DDQ to give terphenyl imide **127**. A double nitrene insertion of imide **127** allowed for the formation of the ICZ core, with ether cleavage by heating in molten pyridine hydrochloride subsequently yielding arcyriaflavin B **8**.

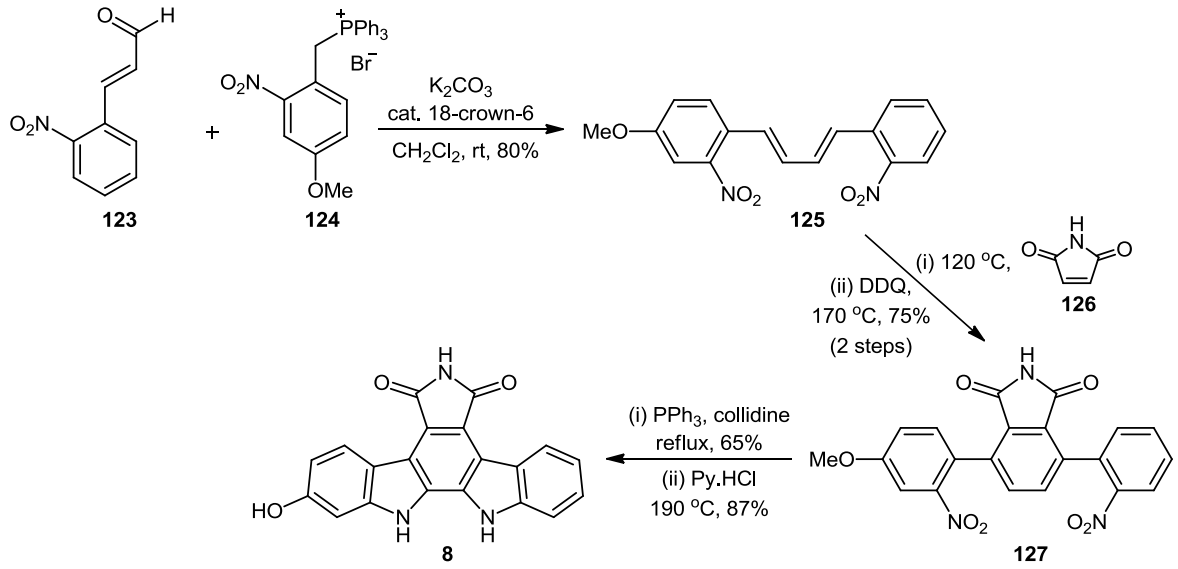

Scheme 2.19 *Route towards arcyriaflavin B **8** via Diels-Alder cycloaddition*

A new strategy towards ICZ ring systems was described in 2000, when Tomé and co-workers reported the synthesis of arcyriaflavin A **7** starting from commercially available 2-nitrobenzaldehyde **128**.[22] Ketone **130** was initially formed by the Wittig reaction of aldehyde **128** with corresponding keto-ylide **129**, which was then treated with TBDMS triflate in the presence of triethylamine to afford diene **131**. Diels-Alder cycloaddition of diene **131** with maleimide **126**, followed by silyl ether hydrolysis, gave solely *endo*-cycloadduct **132** in quantitative yield (***Scheme 2.20***).

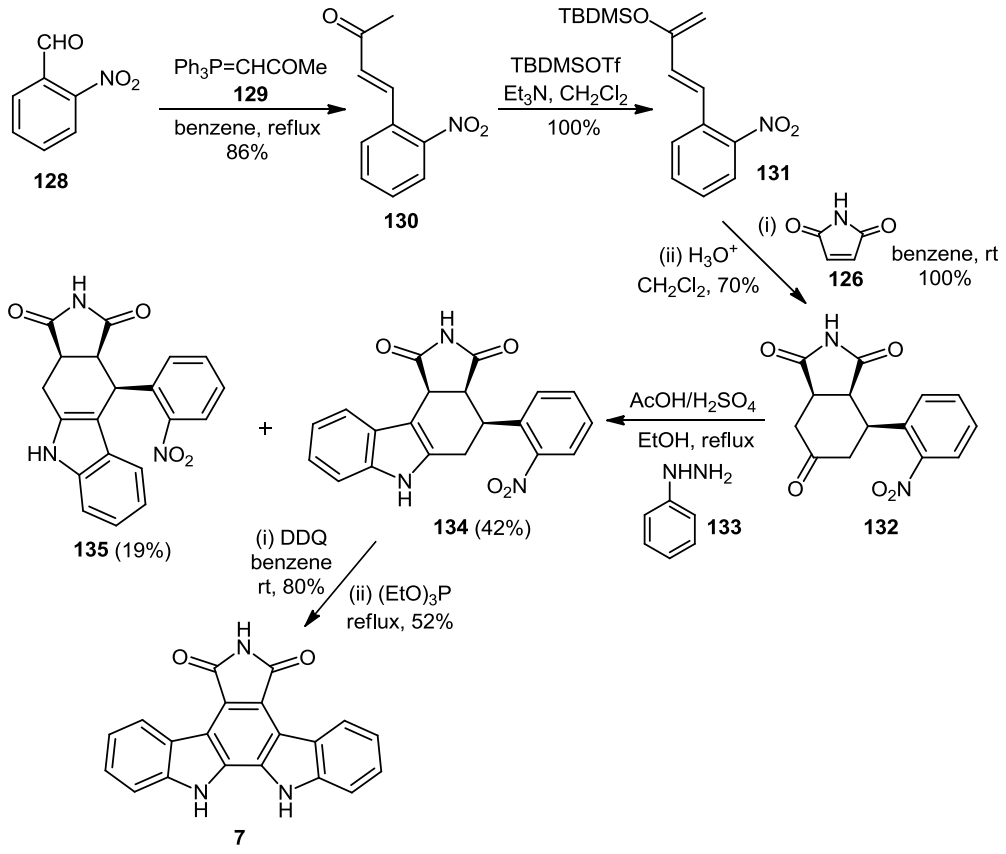

Scheme 2.20 *Synthesis of arcyriaflavin A* ***7*** *via Fischer indolisation*

Fischer indolisation of trione **132** with phenylhydrazine **133** subsequently yielded regioisomers **134** and **135** in a ratio of 2.2:1. After chromatographic separation of the regioisomers, aromatisation of major isomer **134** was effected using DDQ, with the final ring closure carried out via formal nitrene insertion using triethyl phosphite to give arcyriaflavin A **7** (***Scheme 2.20***).

2.1.4 Palladium(0)-catalysed polyannulation

In a relatively unique departure from the standard methodology of forming ICZs, a novel synthesis of *N*-benzyl arcyriaflavin A **72** featuring a palladium(0)-catalysed polyannulation was disclosed by Saulnier *et al.* in 1995.[23] Treatment of diacetylene **136** with trifluoroacetic anhydride resulted in the formation of the corresponding bistrifluoroacetanilide **137** in high yield of 96% (***Scheme 2.21***).

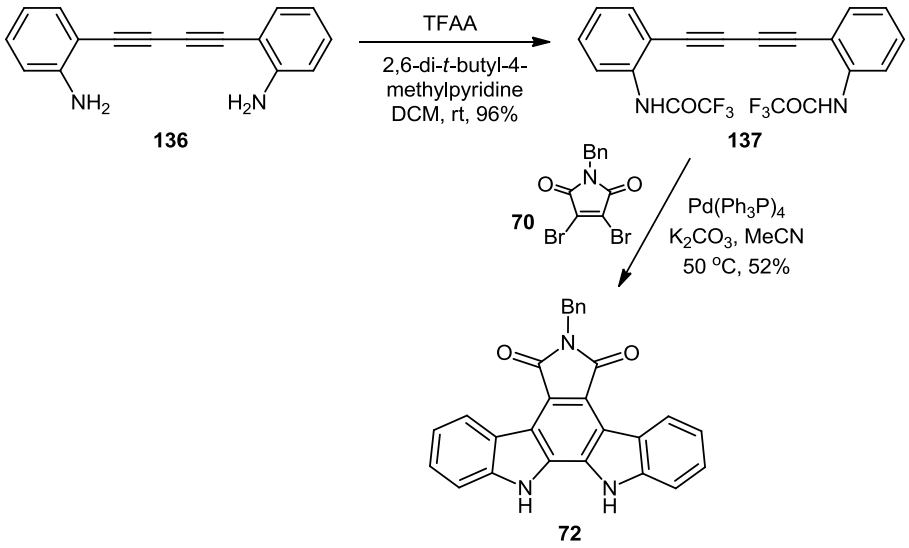

Scheme 2.21 *Synthesis of ICZ **72** via palladium(0)-catalysed polyannulation*

The reaction of the generated acetanilide **137** with *N*-benzyldibromomaleimide **70** and anhydrous potassium carbonate in the presence of tetrakis(triphenylphosphine)-palladium(0) in dry acetonitrile led to the formation of *N*-benzyl arcyriaflavin A **72**. In the synthesis of ICZ **72**, this highly interesting novel polyannulation reaction generates four bonds and three rings in a straightforward one-pot process.

2.2 Synthetic routes towards azaindolocarbazoles

The incorporation of azaindolyl moieties into the ICZ pharmacophore represents a relatively new development in medicinal chemistry, with the first reported synthesis of an azaindolocarbazole (aza ICZ) detailed in 2002.[24] As a result, there exists only a limited number of routes detailed in the literature towards these ICZ bioisosteres, meaning that further advancement of the synthetic accessibility of aza ICZs represents a privileged field to further explore the possibility of new chemotherapeutic agents.

2.2.1 First reported synthesis of aza ICZs

Routier *et al.* described the first synthesis of symmetrical and non-symmetrical azaindolocarbazole derivatives in 2002, invoking methodology that had its origins in Steglich's first approach towards the BIM template (Section *2.1.2.2*).[7,24] Initially, the reaction of 7-azaindole **139** with *N*-methyl dibromomaleimide **66**, using ethyl magnesium bromide in a mixture of toluene and DCM, resulted in the formation of C-3 alkylated derivative **140** (***Scheme 2.22***). Previous utilisation of LiHMDS instead of the Grignard reagent had culminated only in substitution on the indolic nitrogen of 7-azaindole **139**.

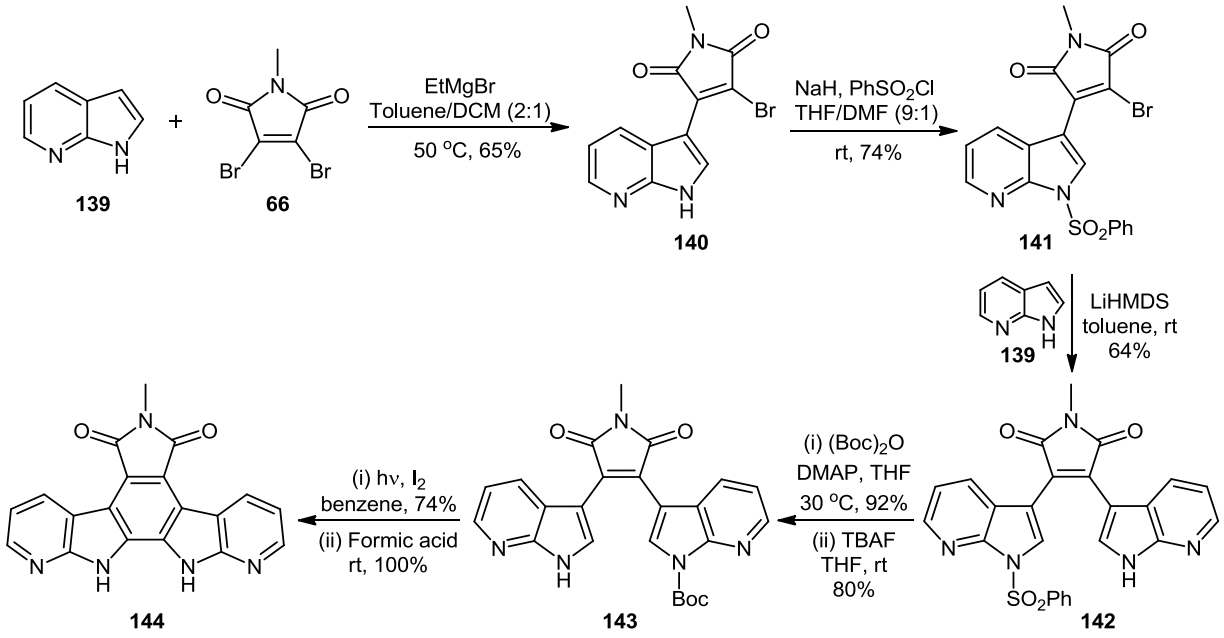

Scheme 2.22 *First described route to azaindolocarbazole* ***144***

Following *N*-phenylsulphonyl protection of 3-substituted azaindole **140**, reaction of intermediate **141** with the lithium salt of 7-azaindole **139** then generated bisazaindolylmaleimide **142** in moderate yield of 64%. Boc-protection of the free indolic nitrogen of BIM analogue **142**, followed by the selective cleavage of the phenylsulphonyl group, afforded another bisazaindolylmaleimide **143**. Oxidative photocyclisation of mono-Boc substituted **143** was carried out in the presence of molecular iodine, with a final deprotection step performed using formic acid then ultimately leading to aza arcyriaflavin A derivative **144**. The choice of protecting group for the photocyclisation step was seemingly crucial, with decomposition of starting materials observed when other substituents had been employed (***Scheme 2.22***).

A similar approach was exercised in the synthesis of unsymmetrical aza ICZ **147**, with the bioisosteric replacement of just one of the indole units of the ICZ pharmacophore with a 7-azaindolyl moiety (***Scheme 2.23***).[24] The lithio derivative of 7-azaindole **139** was coupled with 2-bromo-3-(*N*-Boc-indol-3-yl)-1-methylmaleimide **145** to form maleimide **146** in 67% yield. Photocyclisation of maleimide **146**, accompanied by Boc-deprotection using TBAF in THF under reflux conditions, effectuated the formation of monoaza arcyriaflavin A derivative **147**.

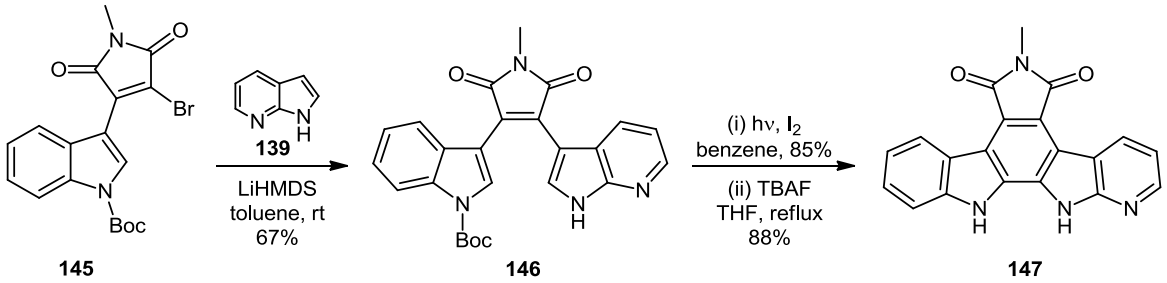

Scheme 2.23 *Synthesis of first unsymmetrical aza ICZ **147***

2.2.2 Synthesis of 7-azarebeccamycin analogues

In the wake of the work carried out by Routier *et al.*, Prudhomme and co-workers implemented further progression of the azaindolocarbazole core towards the development of a series of azarebeccamycin derivatives which were to display biological properties of considerable interest.[24,25] At first, beginning from previously synthesised precursors such as maleimide **146**, Prudhomme *et al*. focused on *N*-glycosylation (***Scheme 2.24***).

N-Glycosylation of maleimide precursor **146** was carried out by means of a Mitsunobu reaction using 2,3,4,6-tetra-*O*-acetyl-α-D-glucopyranose **148** in the presence of DEAD and triphenylphosphine, yielding β-*N*-glycoside **149** (***Scheme 2.24***). Subsequent Boc-deprotection to afford glycosidic BIM analogue **150** was only achieved using formic acid, as the attempted use of tetrabutylammonium fluoride resulted in concomitant deacetylation of the sugar functionality and the formation of a sparingly soluble compound unsuitable for further elaboration. Oxidative photocyclisation of BIM analogue **150** and sequential cleavage of the acetate moieties using aqueous ammonium hydroxide in methanol finally furnished azarebeccamycin analogue **151**.[25]

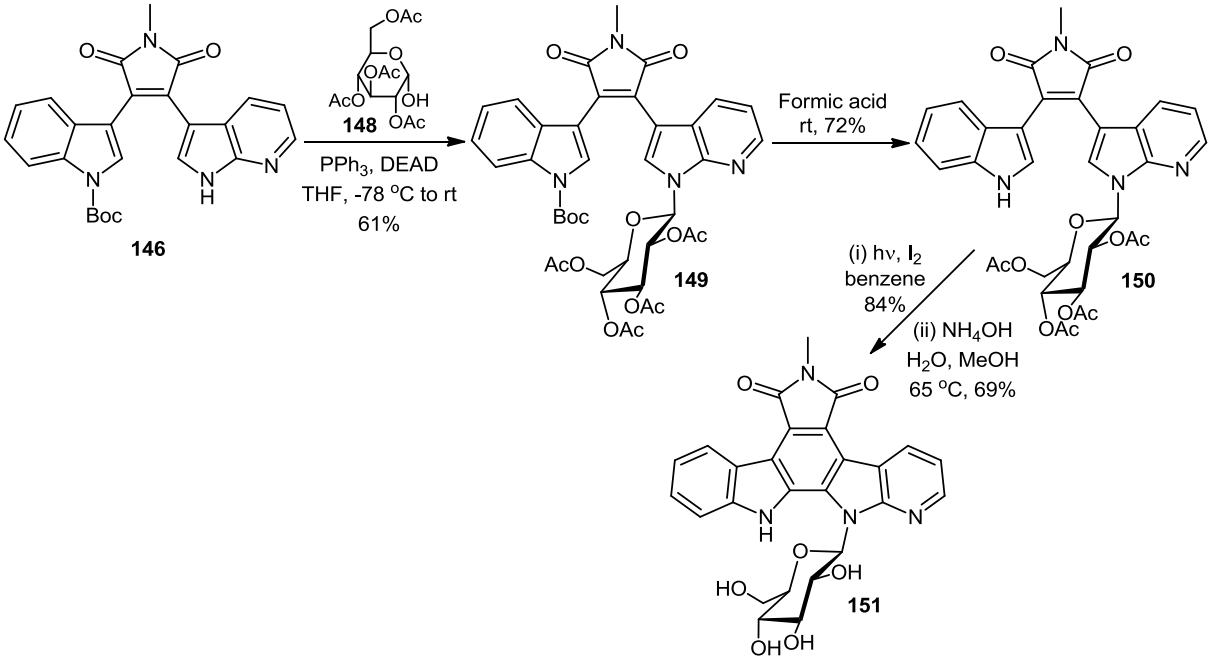

Scheme 2.24 *Route to azarebeccamycin derivative* ***151***

Substitution on the imide nitrogen of BIM analogue **150** was made possible via conversion to maleic anhydride intermediate **152** (***Scheme 2.25***). This was accomplished by the initial treatment of *N*-methyl maleimide **150** with aqueous sodium hydroxide in THF, followed by photochemical aromatisation to yield anhydride **152**. Reaction of anhydride **152** with a range of amines, in this case hydrazine hydrate, allowed for the formation of a series of *N*-substituted derivatives, such as *N*-amino maleimide **153**.[26]

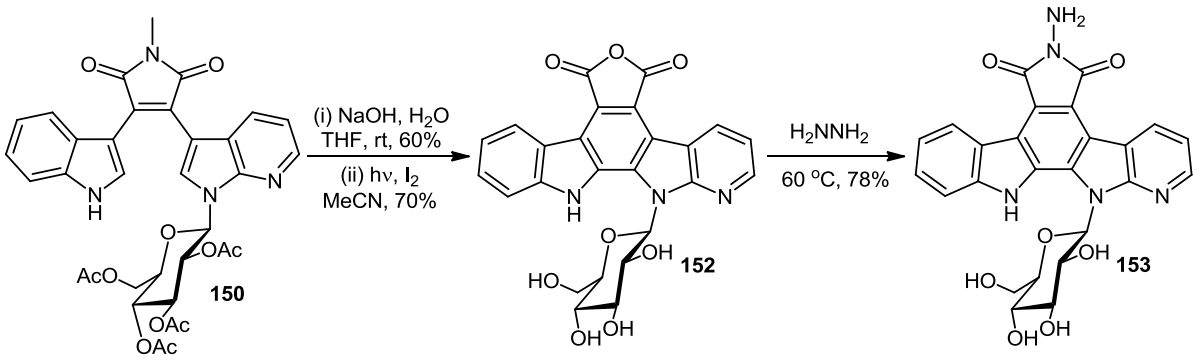

Scheme 2.25 *Formation of* N*-amino maleimide aza-ICZ* ***153***

In order to fashion azarebeccamycin analogues containing two 7-azaindolyl units, Prudhomme *et al.* synthesised a series of bisazaindolylmaleimide precursors, such as *N*-benzyloxymethyl derivative **154**, using similar methodology to that established previously by Routier *et al*.[24,27] Aromatisation of maleimide **154** under photochemical conditions lead to ICZ **155**, with deprotection then carried out in two steps to give 7-aza REB analogue **156** (***Scheme 2.26***).[27]

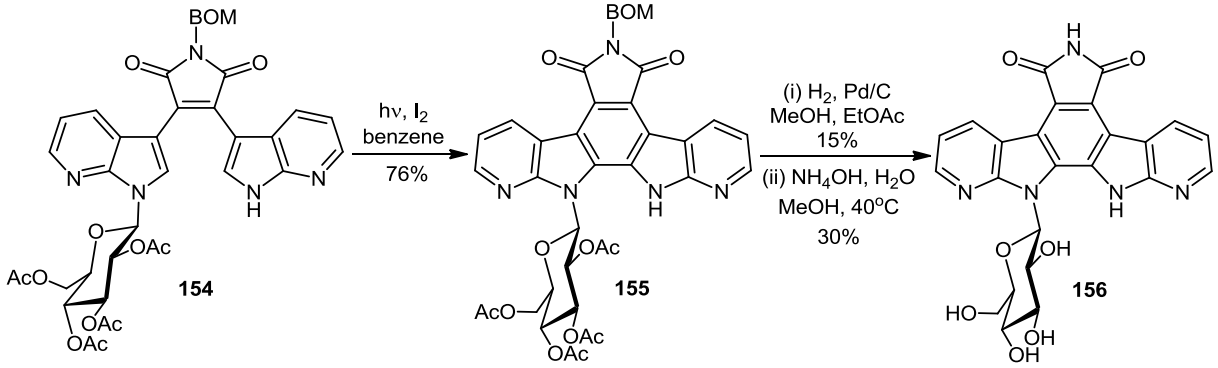

Scheme 2.26 *Synthesis of azarebeccamycin derivative* ***156*** *containing two azaindolyl units*

2.2.3 Routes to bridged 7-azarebeccamycin derivatives

Prudhomme and co-workers found that bridged azarebeccamycin derivatives were relatively accessible from aza ICZs such as aglycone **147**.[28] The initial glycosidic linkage was formed by means of the coupling of 1-chloro-2-*O*-tosyl-3,4,6-tri-*O*-benzyl-α-D-glucopyranose **157** with aza ICZ **147** in the presence of potassium hydroxide and the phase transfer catalyst tris(2-(2-methoxyethoxy)ethyl)amine (TDA-1) in acetonitrile (***Scheme 2.27***).

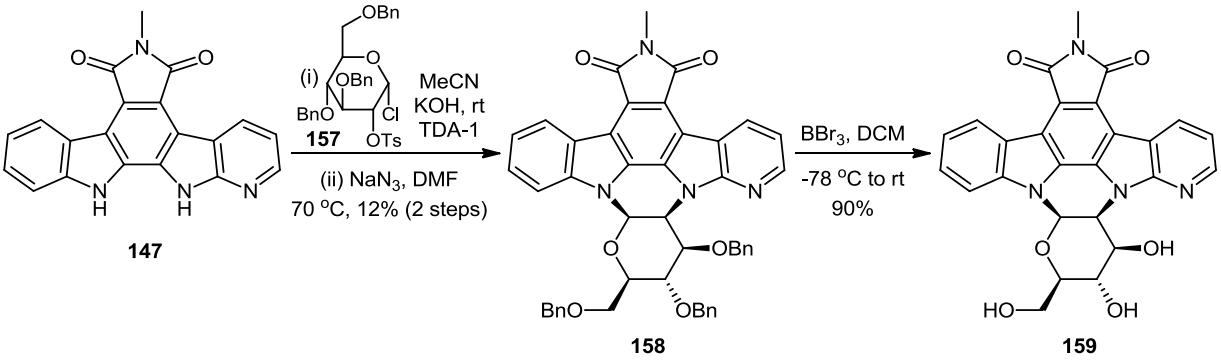

Scheme 2.27 *Synthesis of 7-aza REB analogue* ***159***

Formation of the second *N*-glycosyl bond, affording bridged derivative **158**, was achieved by subsequent treatment with sodium azide in DMF, though the yield was quite low at 12% over two steps. Debenzylation of the sugar group was carried out using boron tribromide in DCM, which gave bridged 7-aza REB analogue **159** in 90% yield (***Scheme 2.27***).

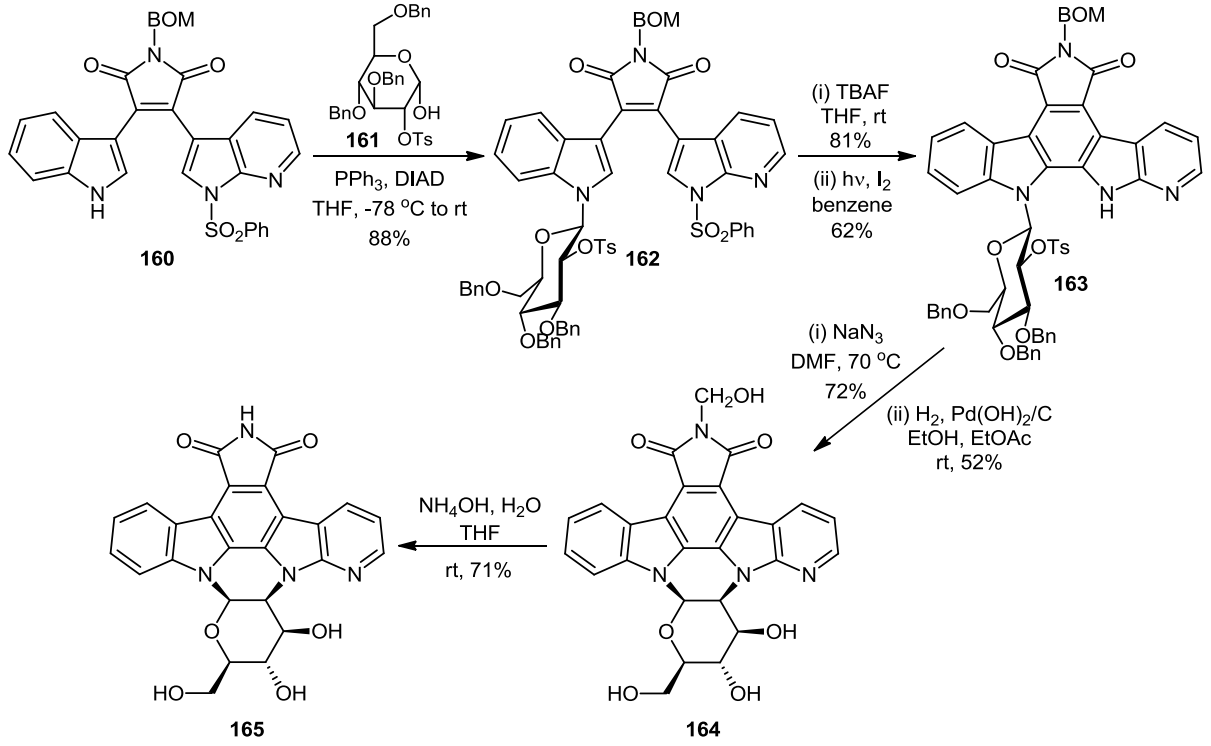

Scheme 2.28 *Route to bridged 7-aza REB analogue* ***165***

Using a similar but more efficient strategy, Prudhomme *et al.* later focused on forming the first *N*-glycosyl bond prior to the photochemical aromatisation of the aza ICZ (***Scheme***

2.28).[29] A Mitsunobu coupling of maleimide **160** and 1-hydroxy-2-*O*-tosyl-3,4,6-tri-*O*-benzyl-α-D-glucopyranose **161** led to the formation of *N*-glycoside **162** in high yield of 88%. Deprotection of the phenylsulphonyl group, followed by oxidative photocyclisation afforded aza ICZ **163**. Bridging of the sugar moiety to the second indolic nitrogen was then carried out by reaction of aza ICZ **163** with sodium azide, with debenzylation consequently occurring by treatment with Pearlman's catalyst, giving bridged glycoside **164**. Finally, aminolysis using aqueous ammonium hydroxide in methanol allowed the formation of bridged 7-aza REB analogue **165**.[29]

2.3.4 Synthesis of 5-azaindolocarbazoles

A synthetic route towards 5-azaindolocarbazoles was reported for the first time by Coudert *et al.* in 2008, whereby a series of 5-aza ICZ derivatives were fashioned using two key steps: a Stille reaction and photochemical cyclisation (***Scheme 2.29***).[30]

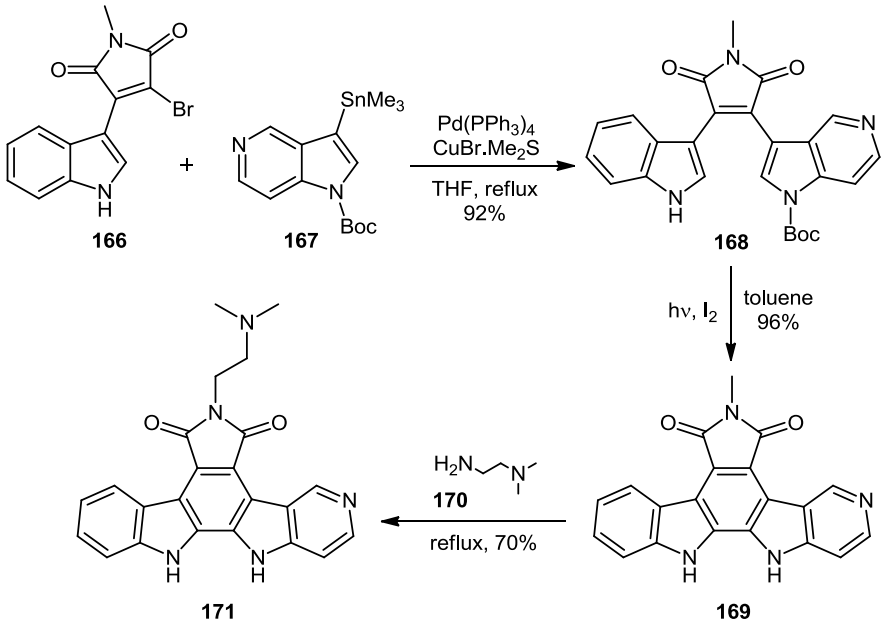

Scheme 2.29 *Synthesis of 5-aza ICZs **169** and **171***

Monobromoindolylmaleimide **166** was initially engaged in a Stille coupling reaction with 1-Boc-3-trimethylstannyl-5-azaindole **167** to yield the 5-aza BIM analogue **168** in high yield of 92%. Oxidative cyclisation of 5-aza BIM **168** in the presence of a tenfold excess of iodine led to the formation of 5-azaindolocarbazole **169**, with the cleavage of the Boc group occurring

during workup of the reaction. The treatment of 5-aza ICZ **169** with dimethylaminoethylamine **170** under reflux conditions subsequently furnished *N*-amino 5-aza ICZ **171** in 70% yield (***Scheme 2.29***).[30]

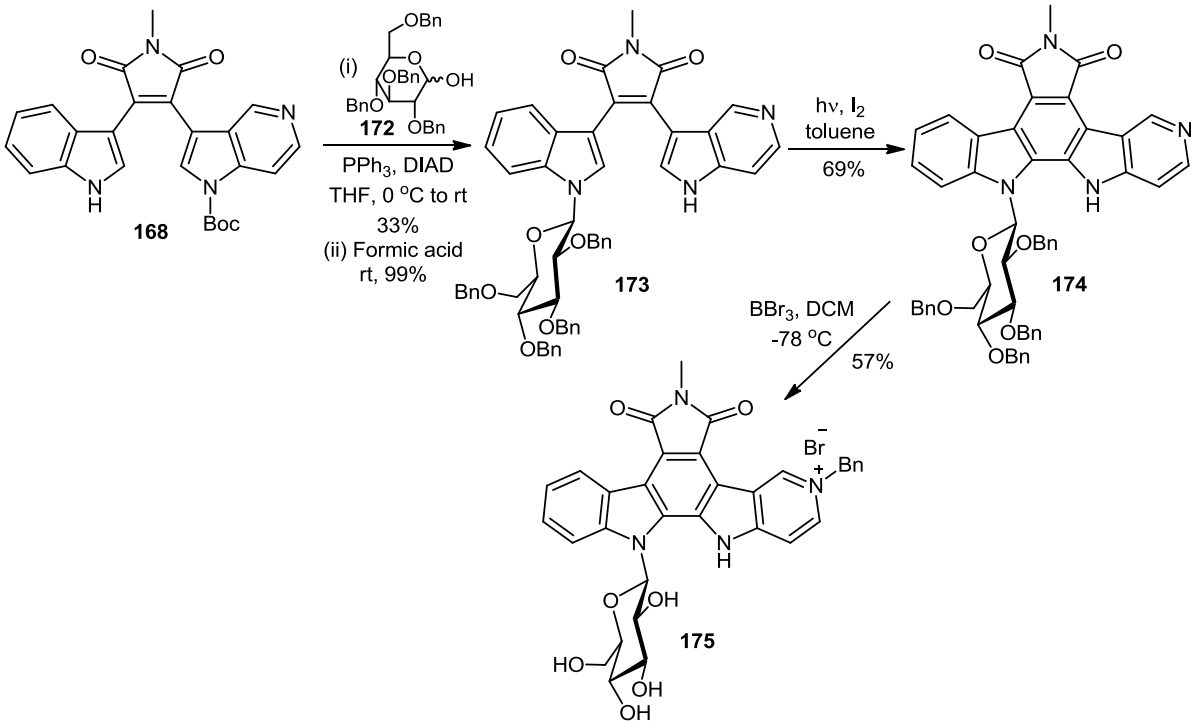

Scheme 2.30 *Route to glycosidic 5-aza ICZ **175***

The synthesis of glycosylated 5-aza ICZs was also examined, beginning with 5-aza BIM **168** (***Scheme 2.30***). Glycosidic 5-aza BIM **173** was prepared by the initial Mitsunobu reaction of 5-aza BIM **168** with tetrabenzyl-D-glucopyranose **172**, followed by deprotection of the Boc group using formic acid at room temperature. Following photochemical cyclisation to yield the pentacyclic 5-aza ICZ core, debenzylation of 5-aza ICZ **174** using boron tribromide resulted in the formation of derivative **175**, which bore an unexpected quaternary pyridine nitrogen atom.[30]

2.3 Targeted synthesis of bisindolylmaleimide analogues

While extremely useful as precursors in the synthesis of ICZs, bisindolylmaleimide derivatives have served as target compounds in their own right as a result of excellent biological activities exhibited by some members of the class. The development of a number of BIM analogues as clinical candidates has meant that the synthetic elaboration of this family of compounds continues to be of major interest to medicinal chemists.

2.3.1 Synthesis of macrocyclic BIM: ruboxistaurin 26

The synthesis of a series of macrocyclic BIM analogues was disclosed by Jirousek *et al*. in 1996, which would ultimately lead to the development of one member, ruboxistaurin **26**, for clinical use in the treatment of diabetic peripheral retinopathy, as a specific inhibitor of PKC isoforms PKCβ_1 and PKCβ_2.[31]

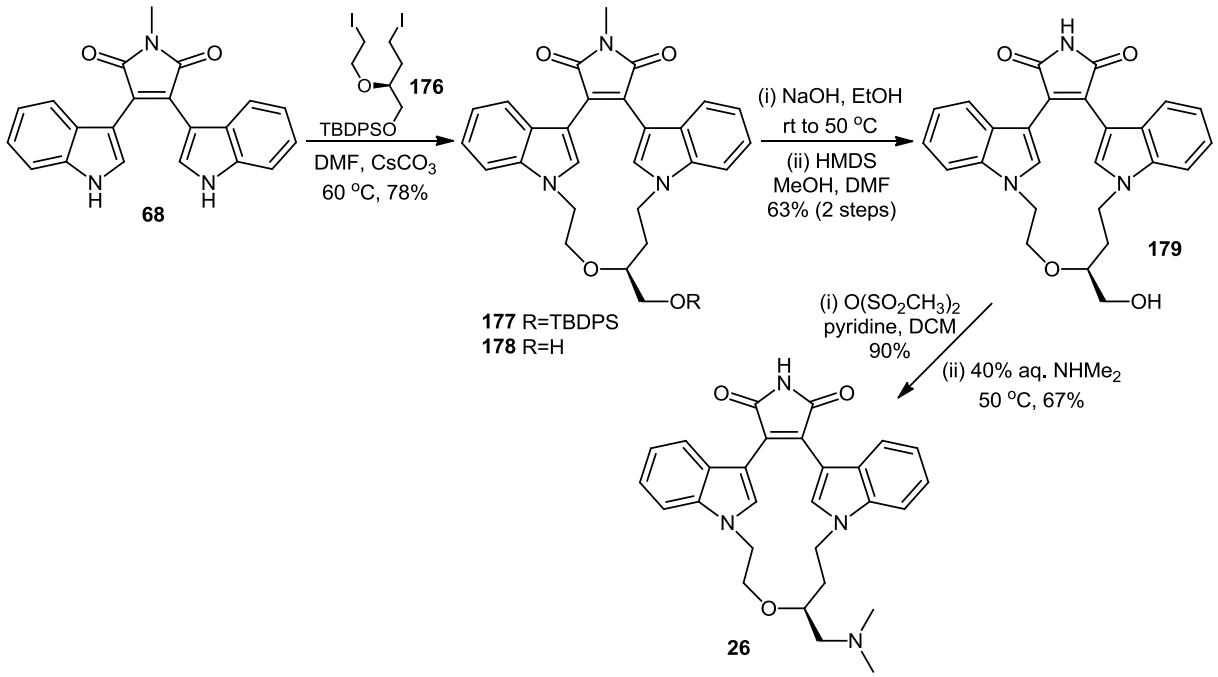

Scheme 2.31 *Route towards ruboxistaurin* ***26***

Reaction of *N*-methyl-2,3-bisindolylmaleimide **68** with bisiodide **176** gave a mixture of macrocyclic products comprising of silyl ether **177** and alcohol **178** with a combined yield of 78% (***Scheme 2.31***). Partial loss of the silyl protecting group during the reaction was deemed

inconsequential in terms of the overall synthesis as it was intended to be removed in the ensuing step. Base hydrolysis followed by an acidic work-up and subsequent treatment with 1,1,3,3-hexamethyldisilazane resulted in the formation of bisindolylmaleimide macrocycle **179**. Mesylation of the alcohol moiety of BIM **179** was carried out using methanesulfonic anhydride, affording a mesylate intermediate which then underwent displacement with dimethylamine to give ruboxistaurin **26**.[31]

2.3.2 Route towards N-*(azacycloalkyl) BIM: enzastaurin* 27

Further derivatisation of the BIM pharmacophore led to the discovery of another selective inhibitor of PKCβ, enzastaurin **27**, which is currently undergoing clinical trials as a chemotherapeutic agent.[32]

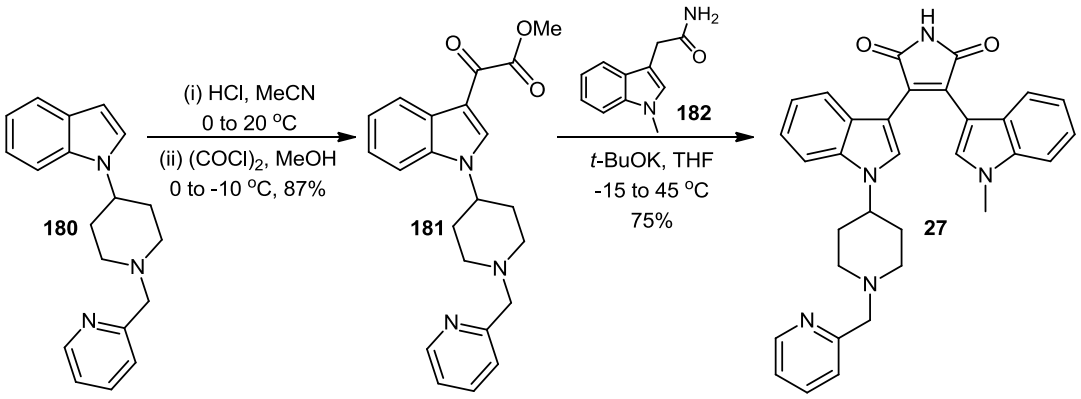

Scheme 2.32 *Synthesis of enzastaurin* ***27***

Faul and co-workers initially carried out the *in situ* treatment of the hydrochloride salt of *N*-(1-pyridin-2-yl methyl-piperidin-4-yl) indole **180** with oxalyl chloride and methanol to furnish glyoxylate **181** (***Scheme 2.32***). Utilising the same intermolecular Perkin-type condensation methodology previously developed within their group (Section *2.1.2.2*), glyoxylate **181** was reacted with acetamide **182** to form BIM derivative enzastaurin **27**.[13,32]

2.3.3 Accessing bisazaindolylmaleimide derivatives

In incorporating 7-azaindolyl functionalities into the BIM pharmacophore, Kuo *et al.* synthesised a series of macrocyclic bisazaindolylmaleimides, such as derivative **30**, from an *N*-methyl-2,3-dichloromaleimide unit **185** (***Scheme 2.33***).[33] Trimethylstannane **184** was

formed from treatment of iodide **183** with trimethyltin chloride and *n*-BuLi in THF at -78 °C. A palladium cross-coupling reaction of stannane **184** with maleimide **185** then gave deprotected bisazaindolylmaleimide **186** in 41% yield. Subsequent alkylation of BIM analogue **186** with bismesylate **187** afforded *N*-methyl macrocycle **188**, with further hydrolysis and aminolysis yielding macrocyclic bisazaindolylmaleimide **30**.[33]

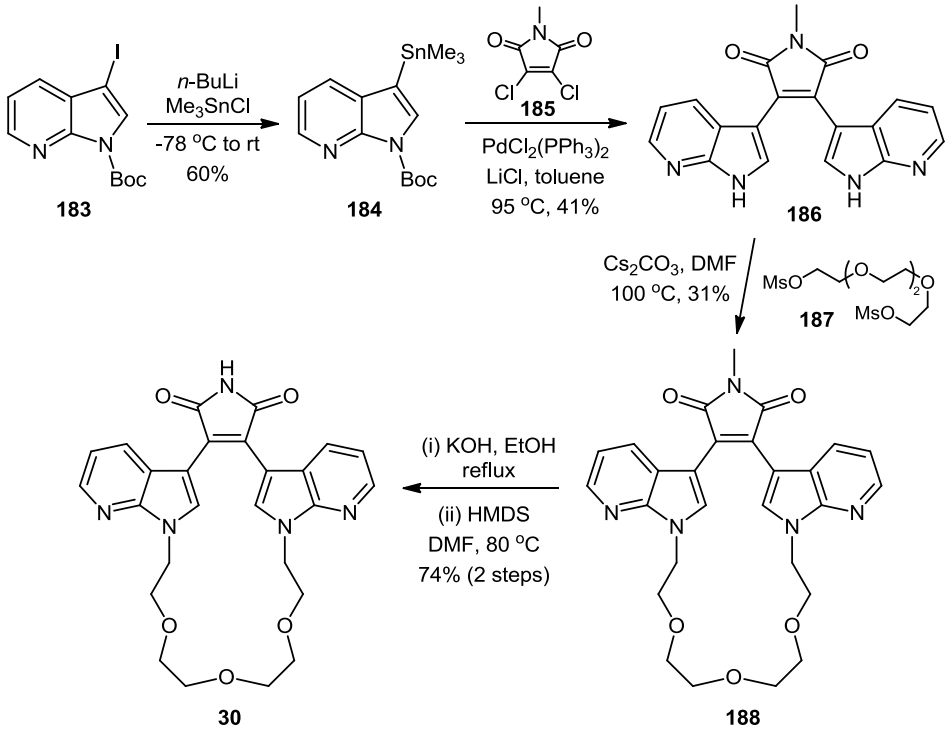

Scheme 2.33 *Synthesis of macrocyclic bisazaindolylmaleimide **30***

A route was also devised by Kuo and co-workers towards acyclic bisazaindolylmaleimides, beginning from 7-azaindole **139** (***Scheme 2.34***).[34] The Grignard of precursor **139** was initially formed using ethylmagnesium bromide, which upon treatment with methyl oxalyl chloride afforded methyl 7-azaindole-3-glyoxylate **189**. *N*-Alkylation of the indolic nitrogen of glyoxylate **189** with 3-(*tert*-butyldimethylsilyloxy)propyl bromide was then carried out in the presence of caesium carbonate in DMF, forming α-keto ester **190**. Utilisation of standard Perkin-type conditions allowed for maleimide formation, in which ester **190** was condensed with 2-(*N*-ethyl-7-azaindolyl)acetamide **191** using potassium *tert*-butoxide in THF at 0 °C. Application of concentrated aqueous HCl resulted in cleavage of the silyl protecting group, yielding acyclic bisazaindolylmaleimide **192**.[34]

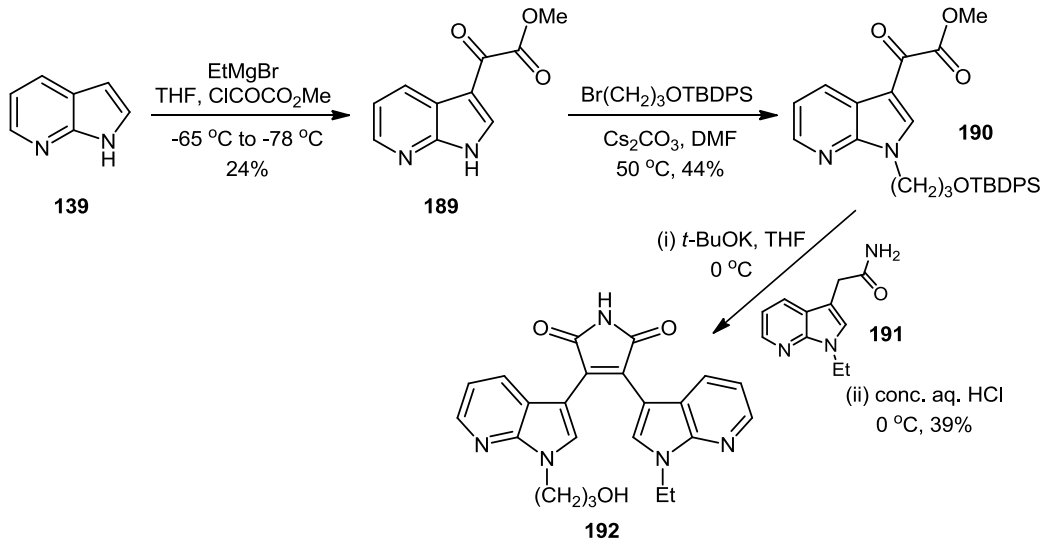

Scheme 2.34 *Route towards acyclic bisazaindolylmaleimide* ***192***

2.3.4 Synthesis of 4-azaindolyl-indolylmaleimides

In 2009, Hu and co-workers, in the search for novel GSK-3β inhibitors, reported the synthesis of a series of BIM analogues bearing a 4-azaindolyl moiety.[35] The reported compounds contained a maleimide ring substituted either at the azaindolic nitrogen (as seen for derivative **196**) or at the 3-position of the 4-azaindolyl unit (e.g. analogue **200**). Reaction of indolyl-3-maleimide intermediate **193** with 4-azaindole **194** in the presence of LDA in THF furnished protected BIM analogue **195** (***Scheme 2.35***). Respective treatment with TBAF and ammonium acetate then afforded desired 4-azaindolyl-indolylmaleimide **196**.

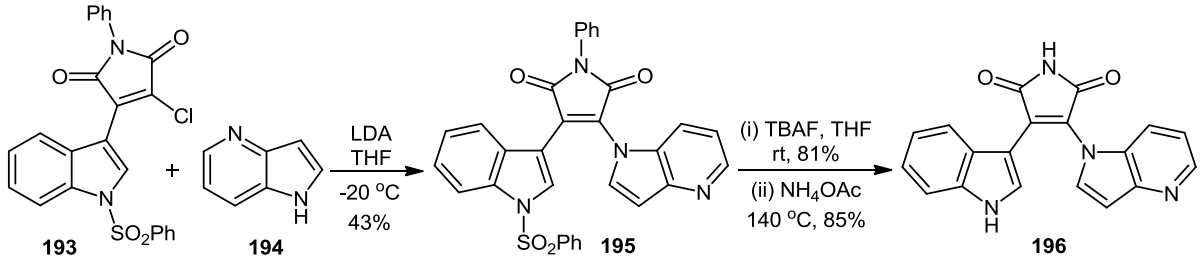

Scheme 2.35 *Synthesis of 4-azaindolyl-indolylmaleimide* ***196***

To achieve the formation of 4-aza BIM analogue **200**, *N*-methyl-4-azaindole **197** was initially reacted with aluminium trichloride and ethyl oxalyl monochloride, resulting in glyoxylate **198** (***Scheme 2.36***). Employing similar methodology to Faul and co-workers (Section *2.1.2.2*),

condensation of acetamide **199** with glyoxylate **198**, followed by removal of the silyl ether using TBAF, afforded the formation of 4-azaindolyl-indolylmaleimide **200** in a poor yield of 12%.[13,35]

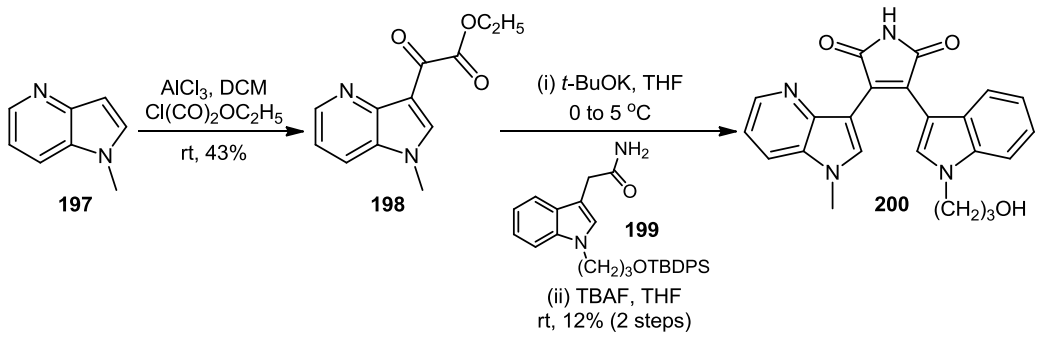

197 **198** **199** **200**

Scheme 2.36 *Intermolecular Perkin-type condensation towards 4-aza BIM analogue **200***

2.4 Routes towards heteroaryl ICZ analogues

Diversification of the ICZ pharmacophore has not just been limited to the bioisosteric replacement of indole units with azaindole moieties (Section **2.2**) or the development of bisindolylmaleimides as clinical candidates (Section **2.3**). Continued efforts to potentiate the biological effects of ICZ analogues has seen the incorporation of a wide range of aryl subunits in place of one of the indole functionalities, thus helping to broaden our knowledge of the associated structure-activity relationships.

2.4.1 Cyclometalation of ICZ analogues

The use of ICZ derivatives as organometallic enzyme inhibitors has been explored by Meggers *et al.* in the synthesis of a series of pyrido[2,3-*a*]pyrrolo[3,4-*c*]carbazole-5,7(6*H*)-diones as constituents of half-sandwich ruthenium complexes (e.g. complex **210**).[36] Reaction of 2-acetylpyridine **201** and 4-methoxyphenylhydrazine hydrochloride **202** lead to the formation of hydrazone **203**, which then underwent Fischer indolisation using trimethylsilyl polyphosphate as Lewis acid (***Scheme 2.37***). Demethylation in the presence of boron tribromide led to the formation of 5-hydroxypyridoindole **204**. Following TBDMS protection, lithiation and subsequent reaction with dibromomaleimide **206** afforded monobromo

intermediate **207**, which was then subjected to photochemical cyclisation to yield carbazole **208**. Cyclometalation of TBDMS-protected ligand **208** was achieved upon reaction with ruthenium precursor **209** in the presence of potassium carbonate. Finally, TBAF-induced silyl deprotection resulted in the formation of carbazole ruthenium complex **210**.[36]

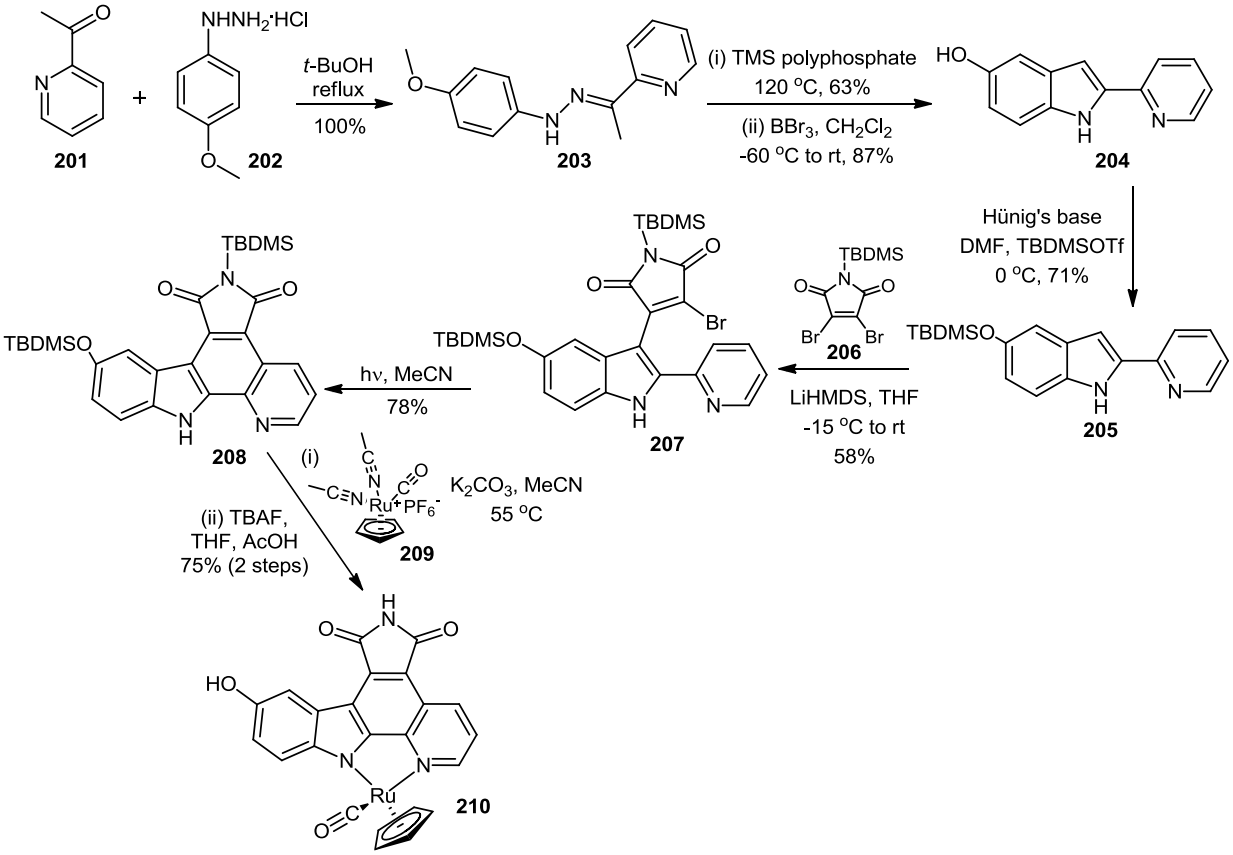

Scheme 2.37 *Synthesis of carbazole ruthenium complex* ***210***

2.4.2 Aza derivatives of isogranulatimide 211

The synthetic access to a series of analogues of the natural product isogranulatimide **211** bearing an azaindolyl moiety instead of an indolyl subunit was described by Prudhomme *et al.* in 2007.[37] One of the routes reported involved the treatment of 3-substituted azaindole **212** with imidazole magnesium bromide to yield diaryl maleimide adduct **213**, with concomitant loss of the carbamate protecting group (***Scheme 2.38***). Following another Boc-protection, owing to the insolubility of maleimide **213**, cyclisation under photochemical conditions led to products **214** and **215**, which were separated by chromatography. Further oxidation of both

derivatives using manganese dioxide, followed by Boc-deprotection using formic acid, afforded aza analogues **216** and **217** of isogranulatimide **211** respectively.[37]

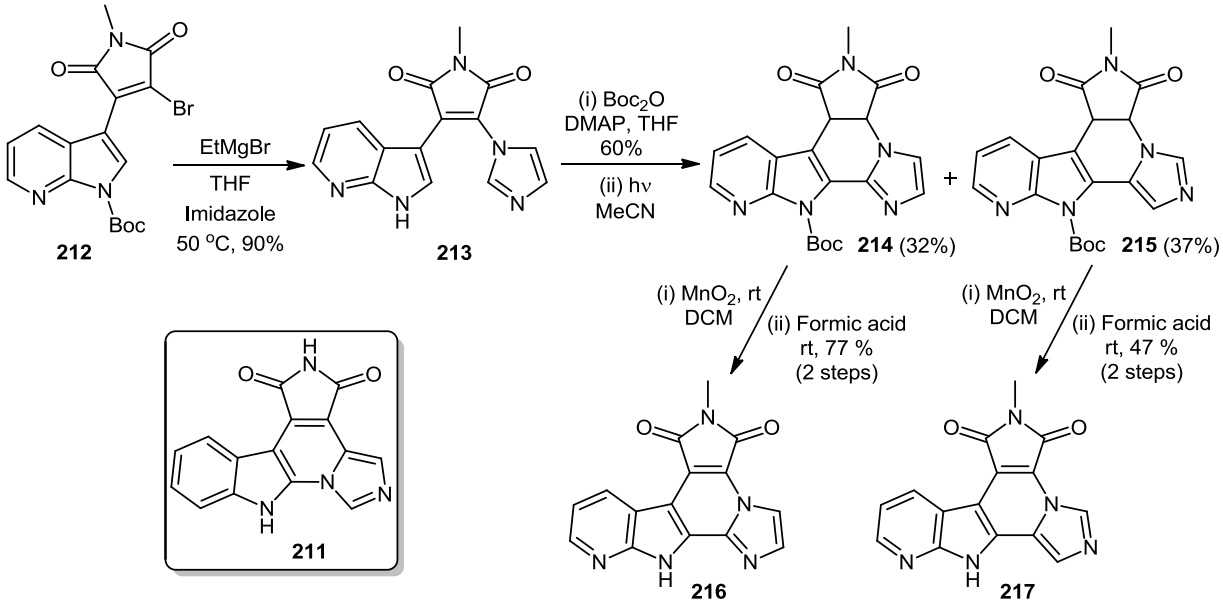

Scheme 2.38 *Accessing 7-azaindolyl derivatives* ***216*** *and* ***217*** *of isogranulatimide* ***211***

2.4.3 Synthesis of 3,4-diaryl-2H-pyrrole-2-ones

In a bid for the rational design and synthesis of novel vascular endothelial growth factor receptor (VEGFR) inhibitors, Peifer and co-workers reported a series of 3,4-diaryl-2*H*-pyrrole-2-ones in 2008, based on a previously synthesised lead compound.[38,39] For example, the fashioning of 3-(3,4,5-trimethoxyphenyl)-4-(indolyl)-2*H*-pyrrole-2-one **220** was described from precursor **218** in an adaptation of Faul's Perkin-type condensation methodology (***Scheme 2.39***).[13] The cyclisation of precursor **218** to yield pyrrolone **219** was carried out under thermodynamic Knoevenagel reaction conditions, with the 2-(trimethylsilyl)ethoxymethyl (SEM) protecting group on the indolic nitrogen deemed crucial towards formation of the desired product. It was discovered that as a consequence of having no protecting group in place, deprotonation of the indolic nitrogen led to anionic delocalisation, therefore resulting in deactivation of carbonyl activity necessary for the condensation to occur. The removal of the SEM protecting group to yield target compound **220** subsequently proved to be much more difficult than expected. For example, the application of commonly-used deprotecting agent TBAF resulted in the oxidation of the

pyrrolone ring to a pyrrole-2,5-dione group. Reaction of SEM-protected **219** with HCl in *tert*-butyl alcohol ultimately resulted in the formation of desired pyrrolone **220** (albeit in low yield of 10%), as well as hemiaminal **221**. Following separation and isolation, it was possible to convert byproduct **221** to target compound **220** by treatment with sodium methoxide in methanol (***Scheme 2.39***).[39]

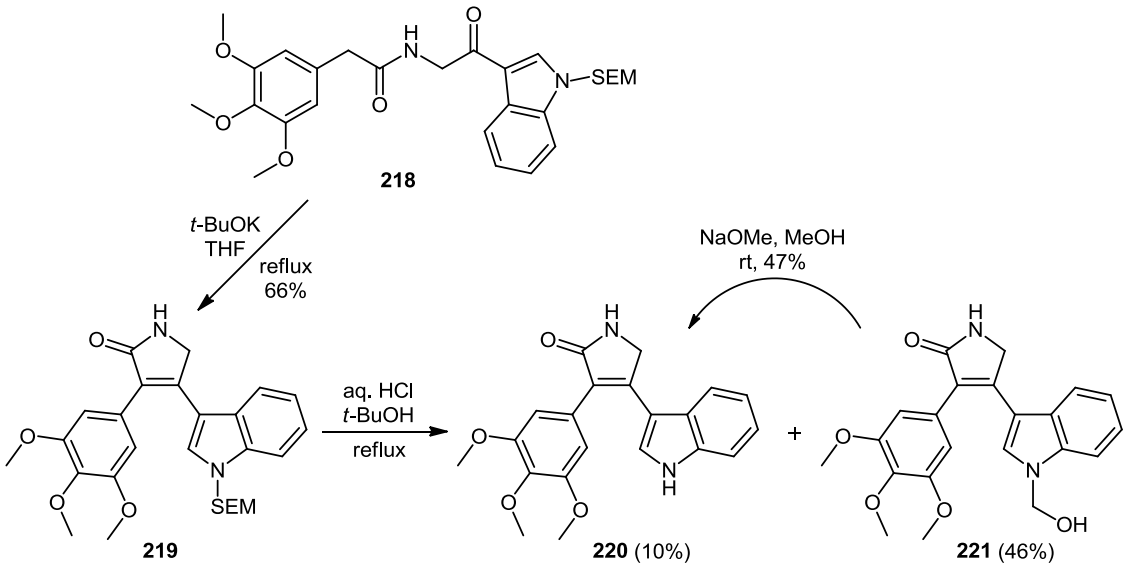

Scheme 2.39 *Synthesis of 3-(3,4,5-trimethoxyphenyl)-4-(indolyl)-2*H*-pyrrole-2-one* ***220***

2.4.5 Synthesis of 7-azaindolyl-heteroarylmaleimides

Expanding on the syntheses of acyclic and macrocyclic bisazindolylmaleimides (Section ***2.3.3***), Kuo *et al.* reported the development of a series of 7-azaindolyl heteroarylmaleimides, effecting the replacement of one of the 7-azaindolyl units with a diverse range of aryl cogeners.[40] One of the approaches described involved the initial oxidation and *N*-alkylation of 7-azaindole-3-acetonitrile **222** to afford acetamide **223** (***Scheme 2.40***). The reaction of acetamide **223** with diethyl oxalate in the presence of potassium *tert*-butoxide then gave 4-hydroxy maleimide **224**, which was then treated with oxalyl chloride to yield key intermediate **225**, from which a range of 7-azaindolyl-heteroarylmaleimide derivatives could be fashioned. For example, the Stille coupling of chloride **225** with 2-tributylstannylpyrazine **226** was effectuated in the presence of $Pd(P(t\text{-}Bu)_3)_2$. Removal of the silyl protecting group using

TBAF subsequently led to desired 3-(1-(3-hydroxypropyl)-7-azaindolyl)-4-pyrazin-2-yl-pyrrole-2,5-dione **227**.[40]

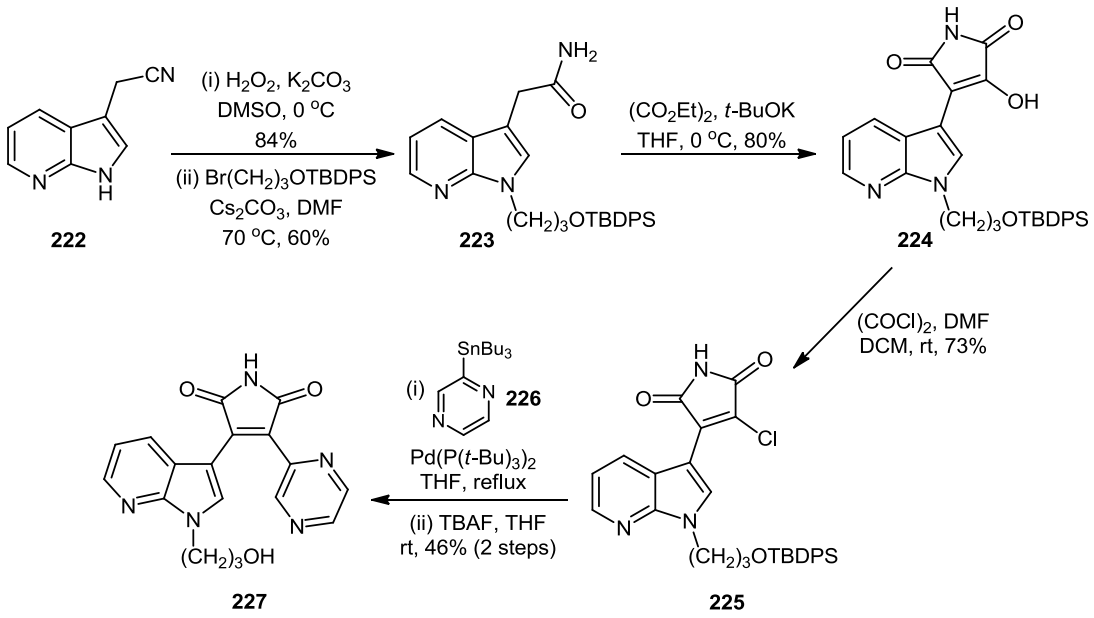

Scheme 2.40 *Route to 3-(7-azaindolyl)-4-pyrazin-2-yl-maleimide* ***227***

2.5 Conclusion

Much progress has been observed in the development of synthetic routes to indolo[2,3-*a*]carbazole derivatives over the past thirty years. Initial efforts were focused mainly on the use of Fischer indolisation methodology to achieve the pentacyclic ICZ core, however many limitations arise from this approach, such as regiochemical constraints or the sensitivity of reaction intermediates to acidic conditions employed. Burgeoning scientific interest in these alkaloids has meant that a number of novel conduits, such the palladium(0)-catalysed polyannulation method proffered by Saulnier and co-workers (Section ***2.1.4***), were uncovered and detailed in the literature. The most widely utilised techniques remain firmly rooted in the cyclisation of bisindolyl congeners towards the central benzenoid ring of the ICZ template, due to the fundamental accessibility of the precursors, and the well-established precedence of a variety of coupling modes extended by Steglich and Faul, amongst others (Section ***2.1.2***).

In contrast, the advancement of strategies towards bioisosteric azaindolocarbazole derivatives has been far more limited and underdeveloped. Of the relatively few approaches detailed, Prudhomme and Routier devised means of access to azaindolylmaleimide progenitors via an adaptation of Steglich's substitution procedure of indolyl subunits with halogenated maleimides, with subsequent aromatisation to aza-ICZ systems (Section **2.2**). Kuo and co-workers, with specific interest in bisazaindolylmaleimides, examined the usage of Stille coupling reactions and Perkin-type condensation techniques enroute to the progression of a series of novel BIM analogues (Section ***2.3.3***).

Given the highly appealing biological modes of action attributed to a number of aza ICZ derivatives, and the conferring of unique selectivity profiles relative to analogous ICZs (Sections *1.3.1.5* and *1.3.2.3*), the exploration of new synthetic routes to this chemical family is of paramount interest to the further enhancement of this area of medicinal chemistry.

2.6 References

1. Omura, S.; Iwai, Y.; Hirano, A.; Nakagawa, A.; Awaya, J.; Tsuchiya, Y.; Takahashi, Y.; Masuma, R. *J. Antibiot.* **1977**, 30, 275-282
2. Brunton, R. J.; Drayson, F. K.; Plant, S. G. P.; Tomlinson, M. L. *J. Chem. Soc*. **1956**, 4783-4785
3. Mann, F.G.; Willcox, T.J. *J. Chem. Soc.* **1958**, 1525-1529
4. Hu, Y.-Z.; Chen, Y.-Q. *Synlett* **2005**, 42-48
5. Sarstedt, B.; Winterfeldt, E. *Heterocycles* **1983**, 20, 469-476
6. Mahboobi, S.; Eibler, E.; Koller, M.; Kumar, K.C.S.; Popp, A. *J. Org. Chem.* **1999**, 64, 4697-4704
7. Steglich, W.; Steffan, B.; Kopanski, L.; Eckhardt, G. *Angew. Chem., Int. Ed. Engl.* **1980**, 19, 459-460
8. Weinreb, S.M.; Garigipati, R.S.; Gainor, J.A. *Heterocycles* **1984**, 21, 309-324
9. Harris, W.; Hill, C. H.; Keech, E.; Malsher, P. *Tetrahedron Lett*. **1993**, 34, 8361-8364
10. Xie, G.; Lown, J.W. *Tetrahedron Lett.* **1994**, 35, 5555-5558
11. Ohkubo, M.; Nishimura, T.; Jona, H.; Honma, T.; Morishima, H. *Tetrahedron* **1996**, 52, 8099-8112
12. Ohkubo, M.; Nishimura, T.; Jona, H.; Honma, T.; Ito, S.; Morishima, H. *Tetrahedron* **1997**, 53, 5937-5950
13. Faul, M.M.; Winneroski, L.L.; Krumrich, C.A. *J. Org. Chem.* **1998**, 63, 6053-6058
14. Faul, M.M.; Winneroski, L.L.; Krumrich, C.A. *J. Org. Chem.* **1999**, 64, 2465-2470
15. Somei, M.; Kodama, A. *Heterocycles* **1992**, 34, 1285-1288
16. Pindur, U.; Kim, Y.-S.; Schollmeyer, D. *J. Het. Chem.* **1995**, 32, 1335-1339
17. Wood, J.L.; Stoltz, B.M.; Dietrich, H.-J.; Pflum, D.A.; Petsch, D.T. *J. Am. Chem. Soc.* **1997**, 119, 9641-9651
18. Pelly, S.C.; Parkinson, C.J.; van Otterlo, W.A.L.; de Koning, C.B. *J. Org. Chem.* **2005**, 70, 10474-10481
19. Cai, X.; Snieckus, V. *Org. Lett.* **2004**, 6, 2293-2295
20. Wada, Y.; Nagasaki, H.; Tokuda, M.; Orito, K. *J. Org. Chem.* **2007**, 72, 2008-2014
21. Hughes, I.; Raphael, R.A. *Tetrahedron Lett.* **1983**, 24, 1441-1444
22. Adeva, M.; Buono, F.; Caballero, E.; Medarde, M.; Tomé, F. *Synlett* **2000**, 832-834
23. Saulnier, M.G.; Frennesson, D.B.; Deshpande, M.S.; Vyas, D.M. *Tetrahedron Lett.* **1995**, 36, 7841-7844
24. Routier, S.; Coudert, G.; Mérour, J.-Y.; Caignard, D.H. *Tetrahedron Lett.* **2002**, 43, 2561-2564
25. Marminon, C.; Pierré, A.; Pfeiffer, B.; Pérez, V.; Léonce, S.; Joubert, A.; Bailly, C.; Renard, P.; Hickman, J.; Prudhomme, M. *J. Med. Chem.* **2003**, 46, 609-622
26. Messaoudi, S.; Anizon, F.; Léonce, S.; Pierré, A.; Pfeiffer, B.; Prudhomme, M. *Eur. J. Med. Chem.* **2005**, 961-971

27. Marminon, C.; Pierré, A.; Pfeiffer, B.; Pérez, V.; Léonce, S.; Renard, P.; Prudhomme, M. *Bioorg. Med. Chem.* **2003**, 11, 679-687
28. Messaoudi, S.; Anizon, F.; Pfeiffer, B.; Golsteyn, R.; Prudhomme, M. *Tetrahedron Lett.* **2004**, 4643-4647
29. Messaoudi, S.; Anizon, F.; Pfeiffer, B.; Prudhomme, M. *Tetrahedron* **2005**, 61, 7304-7316
30. Lefoix, M.; Coudert, G.; Routier, S.; Pfeiffer, B.; Caignard, D.-H.; Hickman, J.; Pierré, A.; Golsteyn, R.M.; Léonce, S.; Bossard, C.; Mérour, J.-Y. *Bioorg. Med. Chem.* **2008**, 16, 5303-5321
31. Jirousek, M.R.; Gillig, J.R.; Gonzalez, C.M.; Heath, W.F.; McDonald III, J.H.; Neel, D.A.; Rito, C.J.; Singh, U.; Stramm, L.E.; Melikian-Badalian, A.; Baevsky, M.; Ballas, L.M.; Hall, S.E.; Winneroski, L.L.; Faul, M.M. *J. Med. Chem.* **1996**, 39, 2664-2671
32. Faul, M.M.; Grutsch, J.L.; Kobierski, M.E.; Kopach, M.E.; Krumrich, C.A.; Staszak, M.A.; Udodong, U.; Vicenzi, J.T.; Sullivan, K.A. *Tetrahedron* **2003**, 59, 7215-7229
33. Kuo, G.-H.; Prouty, C.; DeAngelis, A.; Shen, L.; O'Neill, D.J.; Shah, C.; Connolly, P.J.; Murray, W.V.; Conway, B.R.; Cheung, P.; Westover, L.; Xu, J.Z.; Look, R.A.; Demarest, K.T.; Emanuel, S.; Middleton, S.A.; Jolliffe, L.; Beavers, M.P.; Chen, X. *J. Med. Chem.* **2003**, 46, 4021-4031
34. Zhang, H.-C.; Ye, H.; Conway, B.R.; Derian, C.K.; Addo, M.F.; Kuo, G.-H.; Hecker, L.R.; Croll, D.R.; Li, J.; Westover, L.; Xu, J.Z.; Look, R.; Demarest, K.T.; Andrade-Gordon, P.; Damiano, B.P.; Maryanoff, B.E. *Bioorg. Med. Chem. Lett.* **2004**, 14, 3245-3250
35. Ye, Q.; Xu, G.; Lv, D.; Cheng, Z.; Li, J.; Hu, Y. *Bioorg. Med. Chem.* **2009**, 17, 4302-4312
36. Bregman, H.; Williams, D.S.; Meggers, E. *Synthesis* **2005**, 9, 1521-1527
37. Hugon, B.; Anizon, F.; Bailly, C.; Golsteyn, R.M.; Pierré, A.; Léonce, S.; Hickman, J.; Pfeiffer, B.; Prudhomme, M. *Bioorg. Med. Chem.* **2007**, 15, 5965-5980
38. Peifer, C.; Krasowski, A.; Haemmerle, N.; Kohlbacher, O.; Dannhardt, G.; Totzke, F.; Schächtele, C.; Laufer, S. *J. Med. Chem.* **2006**, 49, 7549-7553
39. Peifer, C.; Selig, R.; Kinkel, K.; Ott, D.; Totzke, F.; Schächtele, C.; Heidenreich, R.; Röcken, M.; Schollmeyer, D.; Laufer, S. *J. Med. Chem.* **2008**, 51, 3814-3824
40. O'Neill, D.J.; Shen, L.; Prouty, C.; Conway, B.R.; Westover, L.; Xu, J.Z.; Zhang, H.-C.; Maryanoff, B.E.; Murray, W.V.; Demarest, K.T.; Kuo, G.-H. *Bioorg. Med. Chem.* **2004**, 12, 3167-3185

Chapter 3

Aims and Objectives

3.0 Aims and Objectives

3.1 Overview of project

The isolation of staurosporine **2** in 1977 proved to be a significant milestone in the field of medicinal chemistry, with ensuing research yielding a number of indolocarbazole derivatives as clinical candidates for the treatment of cancer and other diseases.[1] In terms of synthetic elaboration, the incorporation of 7-azaindolyl subunits into the ICZ pharmacophore represents a highly appealing and incipient paradigm with which to pursue the development of novel chemotherapeutic agents. Contrary to the abundance of indolyl congeners, the 1*H*-pyrrolo[2,3-*b*]pyridine nucleus is considerably less abundant in natural products. One such compound, variolin B **35**, has been reported to display excellent antiproliferative properties in human tumour cell cultures, along with a synthetic analogue meriolin 3 **36** (Section *1.3.1.7*).[2,3]

3.2 Biological significance of 7-azaindole in ICZ template

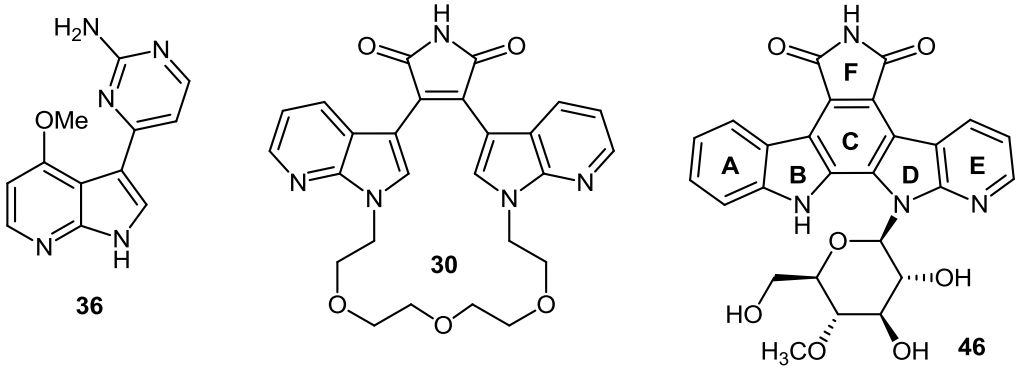

Figure 3.1 *Structures of meriolin 3* ***36****, bisazaindolylmaleimide* ***30*** *and aza REB derivative* ***46***

Appropriation of 7-azaindolyl subunits into the framework of ICZ derivatives has previously been shown to significantly alter the pharmacological properties of these compounds. In 2003, Kuo *et al.* discovered that the introduction of 7-azaindolyl functionalities into macrocyclic bisindolylmaleimide structures (such as **30**) conferred a dramatic increase in selectivity for glycogen synthase kinase-3 (GSK-3) due to additional discrete H-bonding (Section *1.3.1.5*).[4] Also in 2003, Prudhomme and co-workers reported greater cytotoxic selectivity of a series of

azarebeccamycin derivatives (e.g. aza ICZ **46**) for a number of cancer cell lines relative to their indolyl analogues (Section *1.3.2.3*).[5] Remarkably, given the scope for potential enhancement of biological profiles, there have been no aza analogues of STA **2** or UCN-01 **4** reported to date.

3.3 Development of synthetic targets

The incorporation of 7-azaindolyl subunits and novel F-ring constituents into the ICZ template forms the central tenet of our program of fragment-based drug discovery. Thus, the key aim in our synthetic strategy is to develop novel routes towards these alkaloid derivatives and to synthesise new analogues of biological significance.

Our initial focus assumes the chemical elaboration of bisindolylmaleimide scaffold **10**, a key bioactive precursor to the ICZ core, due to the prodigious chemotherapeutic potential exhibited by members of the class.[6] Previous endeavour within this area has primarily examined *N*-alkylation of the indolic nitrogens or heteroaryl derivatisation, shown in ***Figure 3.2***. For example, the use of benzofuranyl functionalities by Kozikowski *et al*. led to the synthesis of a series of BIM analogues, such as compound **228**, which display high selectivity for GSK-3β.[7]

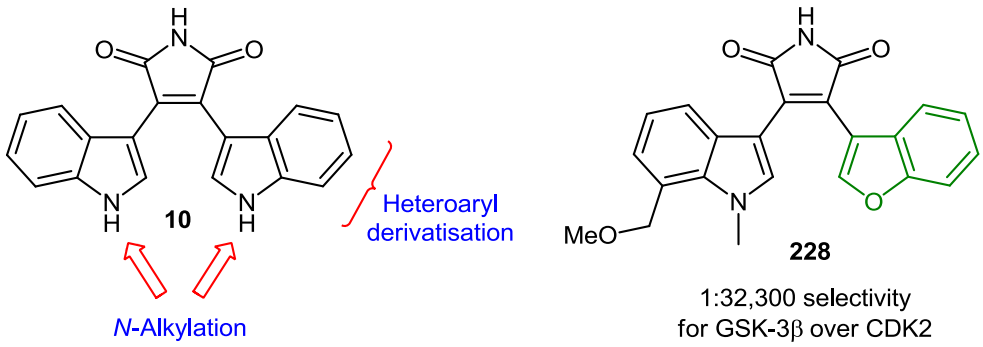

Fig. 3.2 *Structures of arcyriarubin A* ***10*** *and benzofuranyl analogue* ***228***

Expanding on the theme of heteroaryl derivatisation of BIM derivatives steered Peifer *et al*. to 3,4,5-trimethoxyphenyl analogues **32** and **230** from lead molecule **229**, a potent VEGFR inhibitor (***Figure 3.3***).[8] Modification of the maleimide moiety of **229** towards these isomeric

lactam derivatives produced strikingly different biological profiles. Though derivative **32** was found to potently inhibit VEGFR, its isomer **230** displayed significantly weaker activity, thus illustrating the importance of the orientation of the F-ring hydrogen bonding units within the active site.

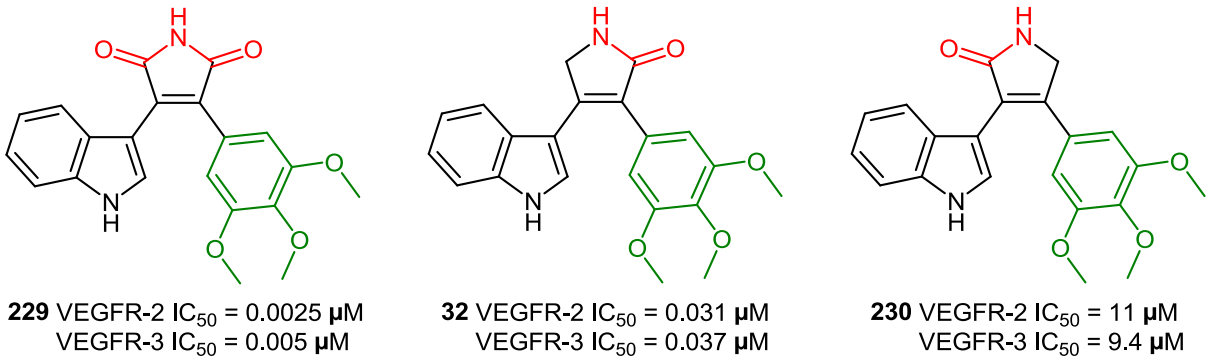

Fig. 3.3 *Structures of 3,4,5-trimethoxyphenyl BIM derivatives* ***229***, ***32*** *and* ***230***

Previous work within our research group has examined novel F-ring modification of the ICZ template towards 6-membered heterocyclic congeners such as bisindolylpyrimidinone **231**.[9] This attractive approach towards the development of new clinical candidates offers the possibility of enhancing existing physicochemical properties, such as the solubility and bioavailability of ICZs containing maleimide moieties. In extending this purpose towards the inclusion of 7-azaindolyl bioisosteres, as with general structure **232**, modulation of the ICZ F-ring can also be used as a vehicle by which to diversify H-bonding networks in ligand-target complexes.

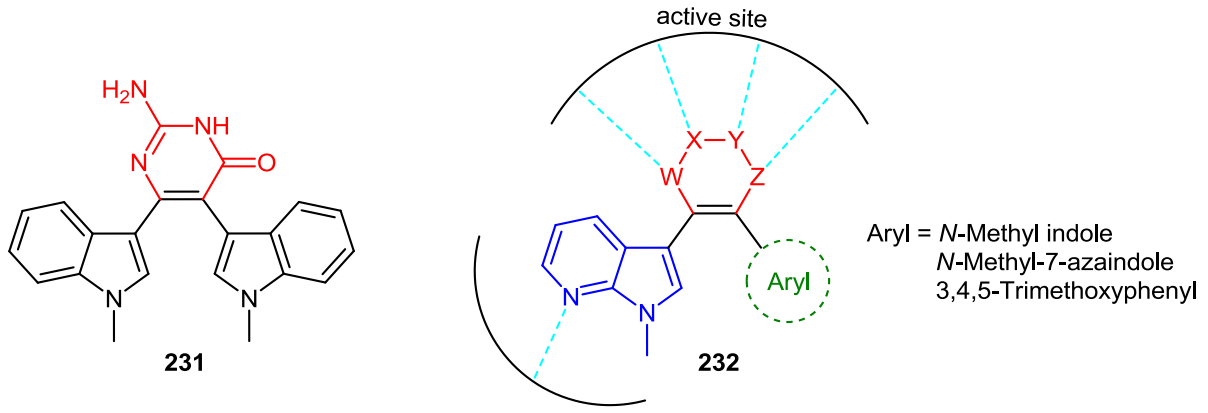

Fig. 3.4 *Structures of bisindolylpyrimidinone* ***231*** *and general azaindole scaffold* ***232***

3.4 Synthetic focus and application

The initial phase of diversity-oriented synthesis towards novel aza ICZ derivatives shall undertake to expand the VEGFR inhibitor template **32** towards novel isomeric congeners **233** and **234**, incorporating a 7-azaindolyl moiety and F-ring modulation. Concomitant to possessing the ability to mimic the conformation of the key lactam functionality, derivatisation of the aminopyrazole ring of **233** and **234** provides an excellent platform with which to probe active site interactions. Comparison of the biological profiles of both sets of isomers should afford an excellent basis for SAR study, given the different F-ring orientations within the binding pocket.

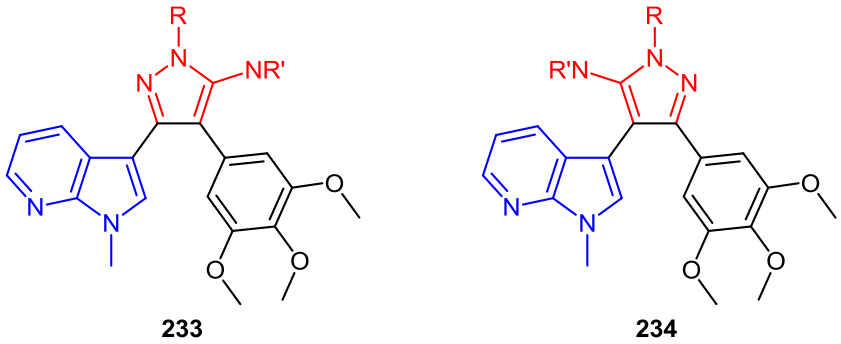

Fig. 3.5 *7-Azaindolyl analogues* ***233*** *and* ***234*** *of VEGFR inhibitors* ***32*** *and* ***229***

Further F-ring modification of the BIM pharmacophore should proffer a useful mechanism by which to further explore the essential protein-ligand interactions necessary for biological activity. We propose that accessing analogues such as aminopyrazole **235** and isoxazolone **236** shall result in a promising diversification of existing H-bonding networks within this structural class of compounds.

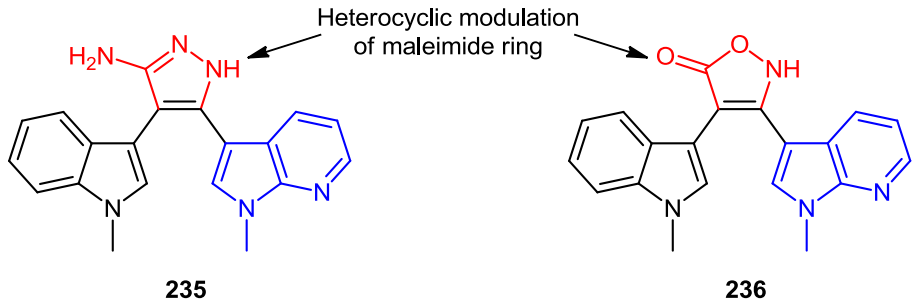

Figure 3.6 *Structures of aminopyrazole* ***235*** *and isoxazolone* ***236*** *BIM derivatives*

The ultimate goal of this work lies in the accomplishment of new routes towards novel azaindolocarbazoles of general structure **237**, as there is a significant paucity in the literature with regard to these alkaloids in comparison to ICZs.

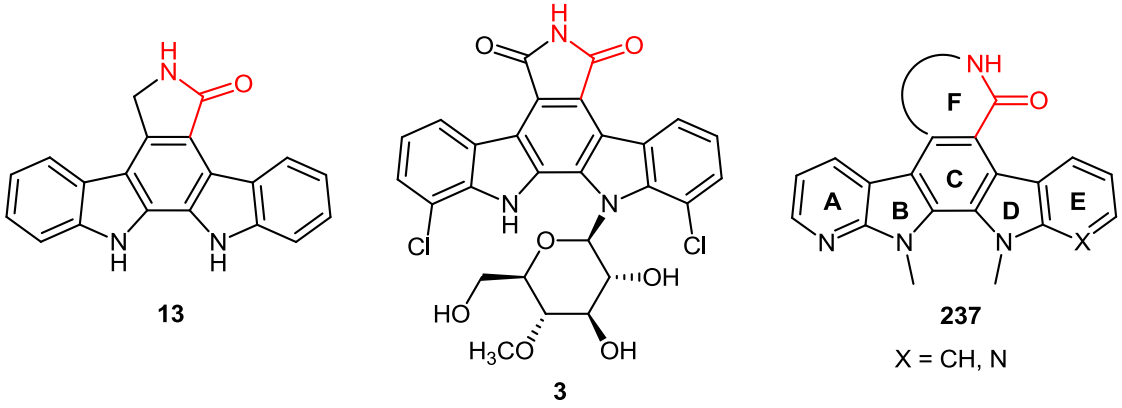

Fig. 3.7 *Structure of K252c* ***13****, REB* ***3*** *and general aza ICZ* ***237***

Little work has been carried out in this field with regard to alteration of the F-ring throughout the ICZ family, such as for K252c **13** and rebeccamycin **3**. It is envisaged that such modification of aza ICZ **237**, with the retention of an amide functionality, has the potential to confer more favourable pharmacological properties, such as increased bioavailability, greater stabilisation of the topo I-DNA complex and the exploitation of discrete differences in the kinase active site. Adaptation of the F-ring in order to encompass six-membered heterocycles, such as derivative **238**, represents a synthetic strategy carried out for the first time within this research group.[10,11] Given the rationale for use of 7-azaindolyl moieties in the ICZ template, the synthesis of aza analogues, such as **239**, is of primary interest in this body of work.

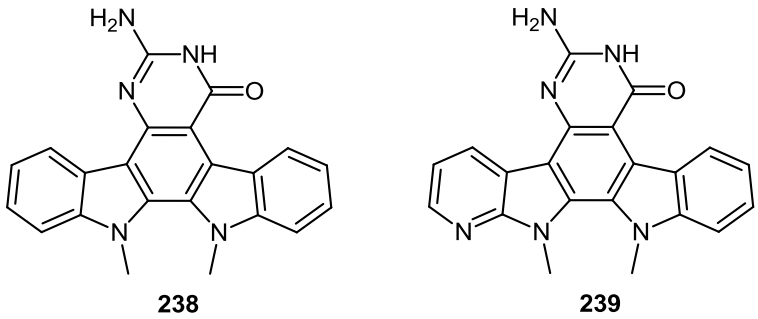

Fig. 3.8 *Structures of novel ICZs* ***238*** *and* ***239*** *containing 6-membered F-rings*

3.5 References

1. Gani, O.; Engh, R. *Nat. Prod. Rep.* **2010**, 27, 489-498
2. Perry, N.B; Ettouati, L.; Litaudon, M.; Blunt, J.W.; Munro, M.H.G.; Parkin, S.; Hope, H. *Tetrahedron* **1994**, 50, 3987-3992
3. Bettayeb, K.; Tirado, O.M.; Marionneau-Lambot, S.; Ferandin, Y.; Lozach, O.; Morris, J.C.; Mateo-Lozano, S.; Drueckes, P.; Schächtele, C.; Kubbutat, M.H.G.; Liger, F.; Marquet, B.; Joseph, B.; Echalier, A.; Endicott, J.A.; Notario, V.; Meijer, L. *Cancer Res.* **2007**, 67, 8325-8334
4. Kuo, G.-H.; Prouty, C.; DeAngelis, A.; Shen, L.; O'Neill, D.J.; Shah, C.; Connolly, P.J.; Murray, W.V.; Conway, B.R.; Cheung, P.; Westover, L.; Xu, J.Z.; Look, R.A.; Demarest, K.T.; Emanuel, S.; Middleton, S.A.; Jolliffe, L.; Beavers, M.P.; Chen, X. *J. Med. Chem.* **2003**, 46, 4021-4031
5. Marminon, C.; Pierré, A.; Pfeiffer, B.; Pérez, V; Léonce, S.; Joubert, A.; Bailly, C.; Renard, P.; Hickman, J.; Prudhomme, M. *J. Med. Chem.* **2003**, 46, 609-622
6. Sánchez, C.; Méndez, C.; Salas, J.A. *Nat. Prod. Rep.* **2006**, 23, 1007-1045
7. Gaisina, I.; Gallier, F.; Ougolkov, A.V.; Kim, K.H.; Kurome, T.; Guo, S.; Holzle, D.; Luchini, D.N.; Blond, S.Y.; Billadeau, D.D.; Kozikowski, A.P. *J. Med. Chem.* **2009**, 52, 1853-1863
8. Peifer, C.; Selig, R.; Kinkel, K.; Ott, D.; Totzke, F.; Schächtele, C.; Heidenreich, R.; Röcken, M.; Schollmeyer, D.; Laufer, S. *J. Med. Chem.* **2008**, 51, 3814-3824
9. Pierce, L.T.; Cahill, M.M.; McCarthy, F.O. *Tetrahedron* **2010**, 66, 9754-9761
10. Pierce, L.T. *PhD Thesis* **2011**
11. Pierce, L.T., Cahill, M.M.; Winfield, H.W.; McCarthy, F.O. *Eur. J. Med. Chem.* **2012**, 56, 292-300

Chapter 4

Chemical Results and Discussion

Contents

4.0 Chemical Results and Discussion

4.1 Initial strategy towards novel azaindolocarbazole derivatives

The inceptive aim of our project was to establish a route to novel BIM analogues containing a 7-azaindolyl moiety, such as **232** and **240**, replacing the maleimide ring with other heterocyclic congeners. Retrosynthetic analysis allowed the identification of key versatile intermediates β-keto ester **241** and β-keto nitrile **242**, from which it would be possible to access a range of BIM derivatives (***Scheme 4.1***). It was further theorised that intermediates **241** and **242** could be reached by the coupling of acyl chloride precursor **243** with either nitrile **244** or ester **245**.

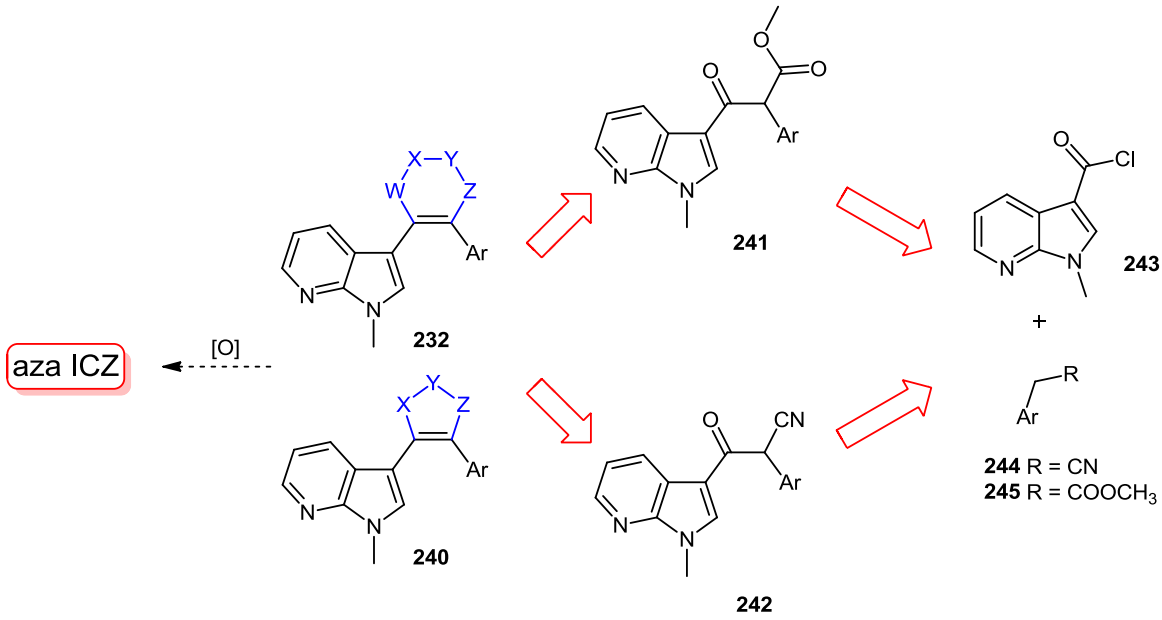

Scheme 4.1 *Retrosynthetic analysis to access aza BIM derivatives **232** and **240***

The basis of this formative strategy had its origins in work concomitantly carried out by Braňa *et al*. and our research group towards derivatives of the BIM template.[1-3] In 2006, Braňa and co-workers described the synthesis of β-keto ester **248**, which was initially obtained from the coupling of acyl chloride **246** and ester **247** in the presence of LDA (***Scheme 4.2***). A series of pyrazolones, such as derivative **249**, were fashioned from intermediate **248** following treatment with the appropriate hydrazine in the presence of camphoric acid.[1]

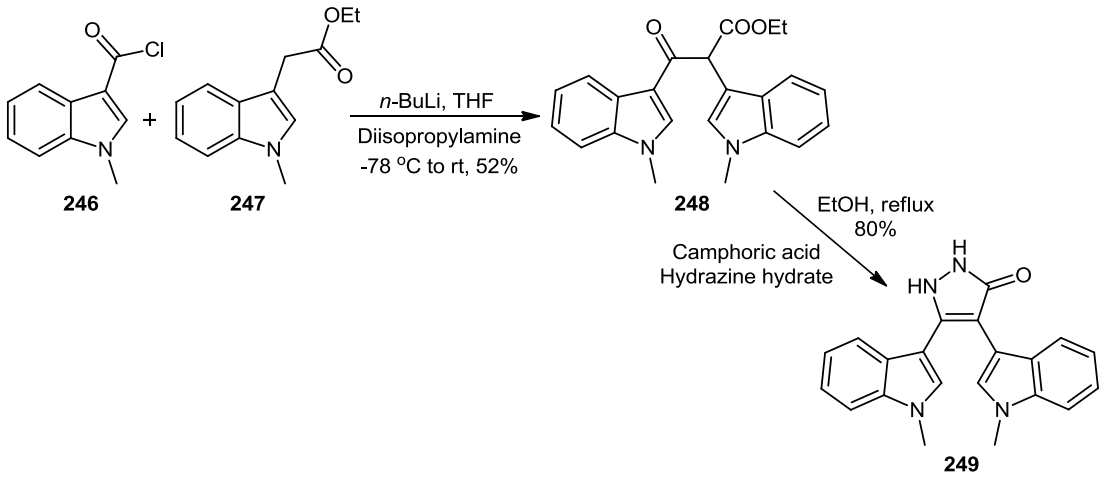

Scheme 4.2 *Route towards pyrazolone* ***249*** *described by Braňa et al.*[1]

Contemporary work within our research group, which was focused on the realisation of bisindolyl ICZ derivatives, utilised methyl ester **250** in place of ethyl ester **247** (***Scheme 4.3***).[2,3] Subsequent optimisation of reaction conditions led to the formation of β-keto ester **251** in a high yield of 80%. Illustrating the versatility of these key intermediates, cyclocondensation of oxopropanoate **251** with guanidine led to bisindolylpyrimidinone **231**, with subsequent photochemical cyclisation affording ICZ **238**.

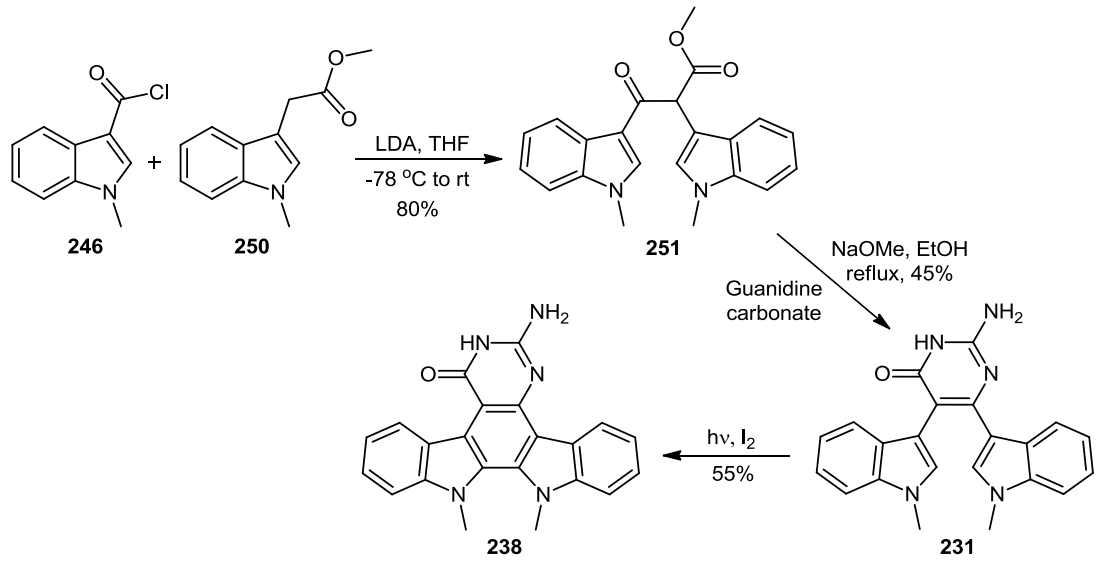

Scheme 4.3 *Synthesis of ICZ* ***238*** *via bisindolylpyrimidinone* ***231***[2,3]

In keeping with our goal of developing novel aza ICZ derivatives, we sought to develop innovative synthetic routes to better exploit the outstanding clinical potential proffered by members of this class of compounds. Initially, we focused on a strategic modification of the route used within our laboratory to access β-keto ester **251** (***Scheme 4.3***), whereby the inclusion of a 7-azaindolyl moiety would allow access to a range of intermediates such as **241** and **242**. Such an approach would differ from previously documented syntheses of aza ICZ derivatives, which have primarily employed methods such as Grignard or Stille coupling at the 3-position of 7-azaindolyl subunits (Sections **2.2**, ***2.3.3*** and ***2.3.4***).[4,5] A program of diversity oriented synthesis from these intermediates would extend our knowledge of the F-ring binding motifs associated with ICZ and BIM derivatives. The accessibility of novel heterocyclic congeners of the ICZ pharmacophore is key to the exploration of new H-bonding contacts within targeted enzymatic active sites.

4.2 Routes to azaindolyl precursors and key intermediates

While a number of azaindolyl subunits are freely available to purchase commercially, there are relatively high costs associated with these molecular building blocks compared to their indolyl analogues. Therefore, a cost-effective synthetic route to these precursors was necessary for the significant undertaking involved with this project.

4.2.1 Synthesis of 7-azaindolyl precursors

In order to achieve β-keto ester intermediate **241**, it was first of all necessary to obtain the precursor 7-azaindolyl-3-carboxylic acid **252** (***Scheme 4.4***).

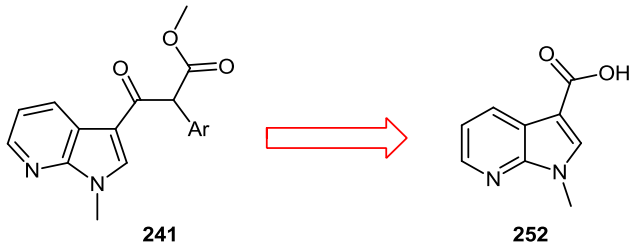

Scheme 4.4 *7-Azaindolyl precursor **252** of β-keto ester **241***

In 2003, enroute to the industrial scale synthesis of an antitussive drug, Allegretti *et al.* reported the fashioning of 7-azaindolyl-3-carboxylic acid **255** over five steps from the inexpensive starting materials of succinonitrile **253** and ethyl formate **254** (***Scheme 4.5***).[6] It was subsequently decided to adapt this route to the laboratory scale required for our needs.

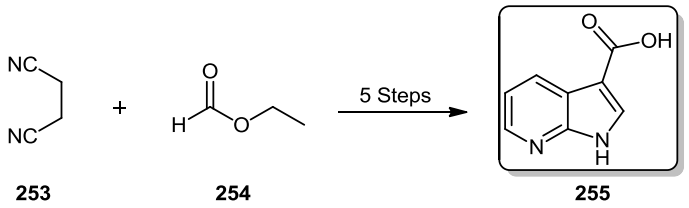

Scheme 4.5 *Route towards 7-azaindolyl-3-carboxylic acid **255** reported by Allegretti et al.*[6]

The first step in this synthesis was the condensation of succinonitrile **253** and ethyl formate **254** under a nitrogen atmosphere in the presence of sodium methoxide in toluene to yield the corresponding salt of 2-(hydroxymethylene)succinonitrile **256** (***Scheme 4.6***). The cream-coloured mixture was treated *in situ* with *t*-butyl amine and acetic acid and subsequently heated to reflux, resulting in the formation of enaminonitrile **257** as a brown solid in 81% yield. Base-catalysed intramolecular condensation of intermediate **257** was then carried out using potassium hydroxide in ethanol to give pyrrole **258** as a light brown crystalline material in a yield of 65%. Use of the *t*-butyl protecting group was noted to be unusual, as it is not normally utilised as protecting group for indolic or pyrrolic nitrogens.[6]

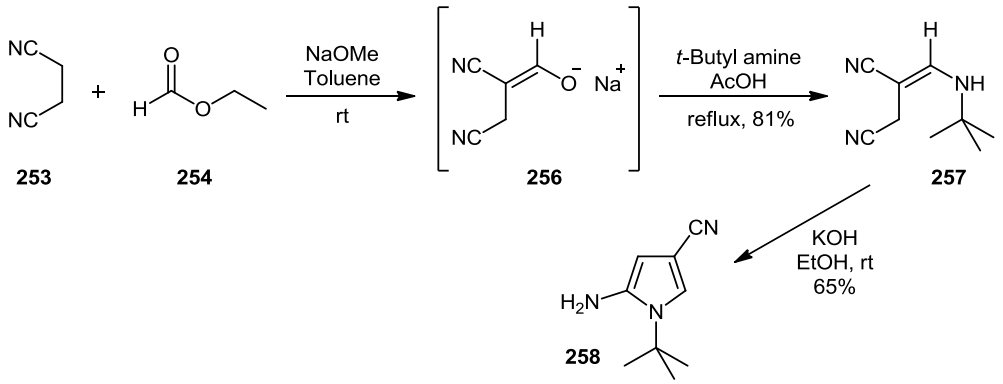

Scheme 4.6 *Synthesis of pyrrole **258** from succinonitrile **253** and ethyl formate **254***

Completion of the pyridine functionality of the 7-azaindolyl nucleus was afforded by the reaction of pyrrole **258** with 1,1,3,3-tetramethoxypropane in the presence of a catalytic

amount of *p*-toluenesulfonic acid, with the driving force for the completion of the reaction being the azeotropic removal of the methanol by-product (***Scheme 4.7***). Deprotection of azaindole **259** was achieved using three equivalents of the Lewis acid, aluminium trichloride, in chlorobenzene under reflux conditions, forming 3-cyano-7-azaindole **260** as an off-white solid in 81% yield. Previous use of benzyl protecting groups had been described by the authors to be fruitless when deprotection was required.[6]

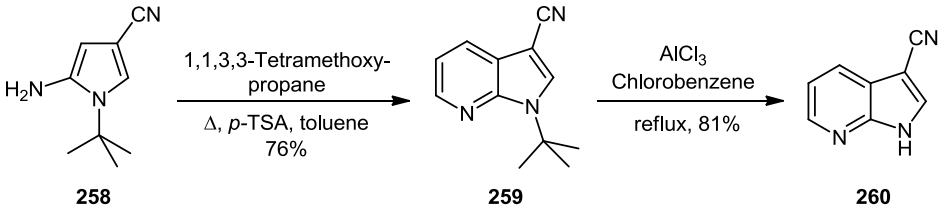

Scheme 4.7 *Synthesis of 3-cyano-7-azaindole* ***260***

The pyridine functionality of a 7-azaindolyl subunit gives rise to a characteristic set of signals in ^{1}H NMR spectra, corresponding to the three adjacent aromatic protons. The C-H_5 proton is almost always the most shielded of the three, and is observed by a doublet of doublets at 7.22 ppm in the case of azaindole **259** (***Figure 4.1***).

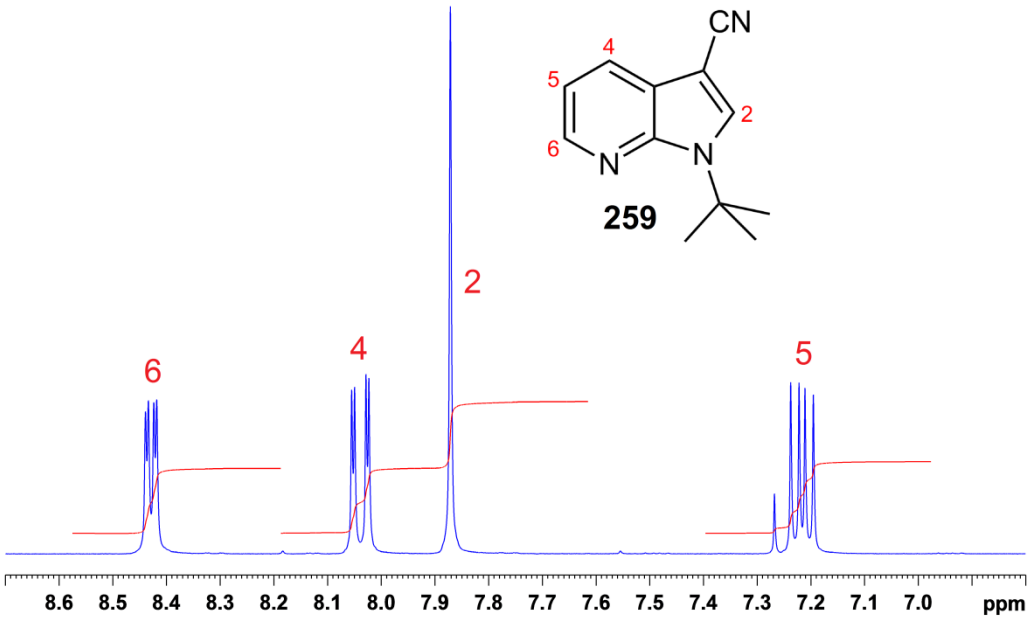

Fig. 4.1 *Aromatic region of ^{1}H NMR spectrum of azaindole* ***259*** *($CDCl_3$, 300 MHz)*

While the other two aromatic protons are also split into distinct doublets of doublets, they are easily distinguishable by their coupling constants, with that of the C-H_4 proton being almost twice that of the C-H_6 (8.0 and 4.7 Hz respectively in the case of azaindole **259**).

Depending on the reaction conditions, 3-cyano-7-azaindole **260** could either be hydrolysed to 7-azaindolyl-3-carboxylic acid **255** or converted to 7-azaindole **139**, another useful precursor (***Scheme 4.8***). Treatment of nitrile **260** with concentrated aqueous hydrochloric acid at a controlled temperature of 70 ^{o}C led to the formation of carboxylic acid **255** as a white solid in 91% yield. The use of harsher reaction conditions, i.e. heating to reflux for 48 hours, led to the formation of 7-azaindole **139** in 62% yield via intermediate decarboxylation of acid **255**.

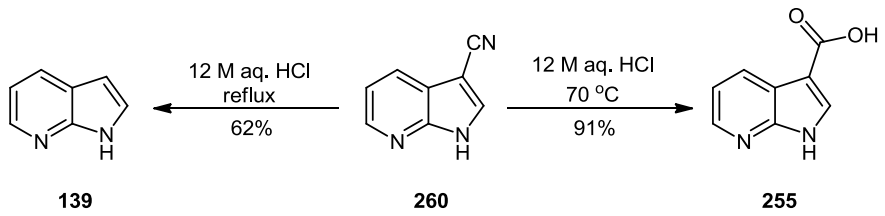

Scheme 4.8 *Synthesis of 7-azaindole **139** and 7-azaindolyl-3-carboxylic acid **255***

4.2.2 Initial routes towards β-keto ester intermediates

The use of 7-azaindolyl-3-carboxylic acid **255** as a precursor towards the formation of β-keto ester **263** was attempted via a number of base-mediated coupling methods with indolyl ester **250** (***Scheme 4.9***).

4.2.2.1 Attempted base-mediated condensation

Initially, esterification of commercially available indole-3-acetic acid **261** was achieved following treatment with dimethyl carbonate (serving as methylating agent) in the presence of potassium carbonate, affording *N*-methyl ester **250** as a golden oil in 84% yield (***Scheme 4.9***).[7] 7-Azaindolyl acyl chloride **262** was then generated in quantitative yield as a yellow solid following stirring of acid **255** in excess thionyl chloride with a few drops of DMF at room temperature. Employing the same base-mediated methodology described by Braňa *et al.* and previously utilised within our research group, the coupling of ester **250** with acyl chloride **262** to form β-keto ester **263** was attempted.[1-3] A solution of *N*-methyl ester **250** was added to

a vessel containing 2.2 equivalents of LDA in dry THF at -78 °C under a nitrogen atmosphere, with the resulting mixture maintained at this temperature for one hour. A suspension of acyl chloride **262** in THF was then added to the reaction vessel, containing the corresponding α-anion of ester **250**, in a dropwise manner.

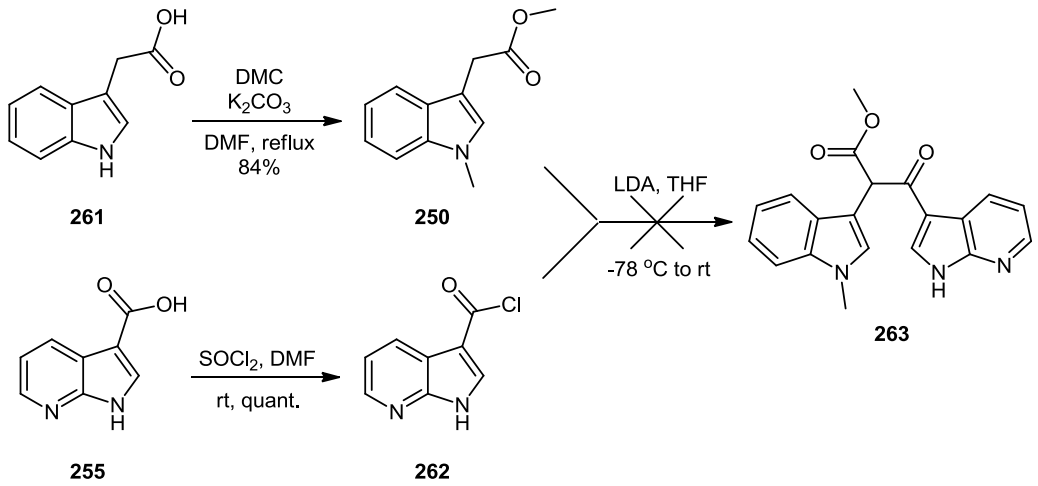

Scheme 4.9 *Attempted synthesis of β-keto ester* ***263***

Upon completion of the additions, the dark mixture was allowed to warm to room temperature over a period of 14 hours. Following workup, analysis of the crude product revealed that β-keto ester **263** had not formed, with starting material primarily identified. Systematic variation of the reaction conditions, such as using different equivalents of base and acyl chloride **262**, similarly did not result in the desired outcome.

4.2.2.2 Utilisation of N-protected acyl chloride

Having been unable to access β-keto ester **263**, the next attempted route involved the use of *N*-protected acyl chloride **266** towards the synthesis of β-keto ester **267** (***Scheme 4.10***). Methylation of 3-cyano-7-azaindole **260** using sodium hydride and iodomethane in DMF at 0 °C gave *N*-methyl-3-cyano-7-azaindole **264** in 68% yield, which was then hydrolysed to carboxylic acid **265** using concentrated aqueous HCl. Treatment of acid **265** with oxalyl chloride in DCM led to the formation of acyl chloride **266** as a white solid in quantitative yield. Using a similar procedure to that described in Section *4.2.2.1*, acyl chloride **266** was added to the anion of indolyl ester **250** at -78 °C under an inert atmosphere, with the resulting

mixture being allowed to warm to room temperature overnight. However, analysis of the crude product revealed that the desired β-keto ester **267** had not been formed.

In fact, limited formation of the self-condensation product **268** of ester **250** was detected by spectroscopic analysis of the crude mixture, illustrating the lack of reactivity of azaindolic electrophile **266**.

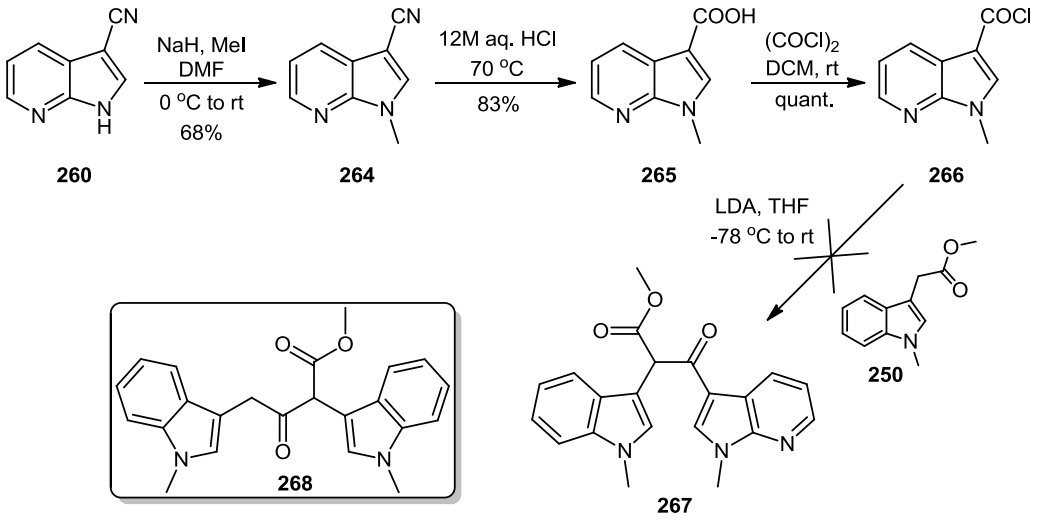

Scheme 4.10 *Attempted route towards β-keto ester* ***267***

4.2.2.3 Claisen condensation approach

An approach to β-keto ester **267** using Claisen condensation conditions was next to be implemented (***Scheme 4.11***).

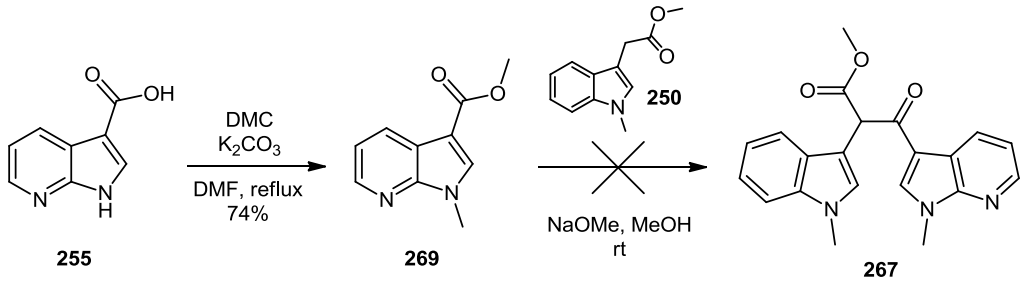

Scheme 4.11 *Attempted Claisen condensation approach towards β-keto ester* ***267***

Conversion of carboxylic acid **255** to *N*-methyl methyl ester **269** was achieved in 74% yield following treatment with dimethyl carbonate and potassium carbonate in DMF. Subsequent to

the deprotonation of ester **250** using sodium methoxide in methanol, a solution containing azaindolic ester **269** was slowly added, with the resulting reaction mixture then allowed to stir at room temperature for four hours. Once more however, the desired β-keto ester **267** was not formed, with only the presence of starting materials detected in analysis of the crude product mixture. Modification of the experimental conditions, such as varying the equivalents of starting materials and increasing the reaction temperature to reflux, again could not effect a desirable outcome.

*4.2.2.4 Activation of acid **265** using 1,1'-carbonyldiimidazole*

The use of a CDI-activated carboxylic acid instead of an acyl chloride was next to be examined in the coupling step towards β-keto ester **267** (***Scheme 4.12***). 1,1'-Carbonyldiimidazole (CDI) was added to a solution of acid **265** in DMF, with the resulting mixture heated to 50 ^{o}C for 1.5 hours before then being cooled to -10 ^{o}C. Indolyl ester **250** was subsequently added, followed by sodium hydride in a portionwise manner over a 20 minute period. The reaction mixture was then stirred at -10 ^{o}C for 30 minutes before being allowed to warm to room temperature over 3 hours. Upon workup, analysis of the crude product showed that the desired β-keto ester **267** had not formed and that once more, the self-condensation product **268** of ester **250** was present along with unreacted starting material.

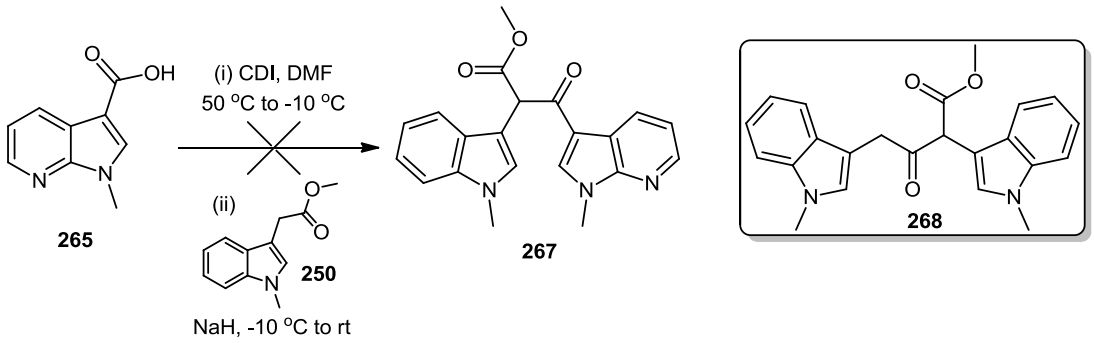

***Scheme 4.12** Activation of carboxylic acid **265** using CDI*

4.2.3 N-*Benzyl protecting group on 7-azaindolyl moiety*

It was clear that the problem with the coupling reactions lay with the 7-azaindolyl functionality, as the employment of analogous indolyl electrophiles had previously proven to be successful (Section **4.1**).[1-3] As evidence of the self-condensation of indolyl ester **250** demonstrated the suitable nucleophilicity of the anion, our focus turned towards the solubility of the 7-azaindolyl subunit. Thus, instead of a methyl protecting group, the use of an *N*-benzyl group was pursued as a means to bestow greater organic solubility (***Scheme 4.13***). Benzylation of 3-cyano-7-azaindole **260** was carried out using sodium hydride and benzyl bromide in DMF, forming the *N*-protected product **270** as an off-white solid in 72% yield. Hydrolysis of the nitrile functionality of azaindole **270** using concentrated aqueous HCl then afforded carboxylic acid **271** in high yield of 94%. Treatment of a suspension of acid **271** in DCM with 2.1 equivalents of oxalyl chloride at room temperature led to the formation of acyl chloride **272** as a white solid in quantitative yield. It was observed that the characteristic IR carbonyl stretch shifted from 1689 cm^{-1} in acid **271** to 1739 cm^{-1} in acyl chloride **272.**

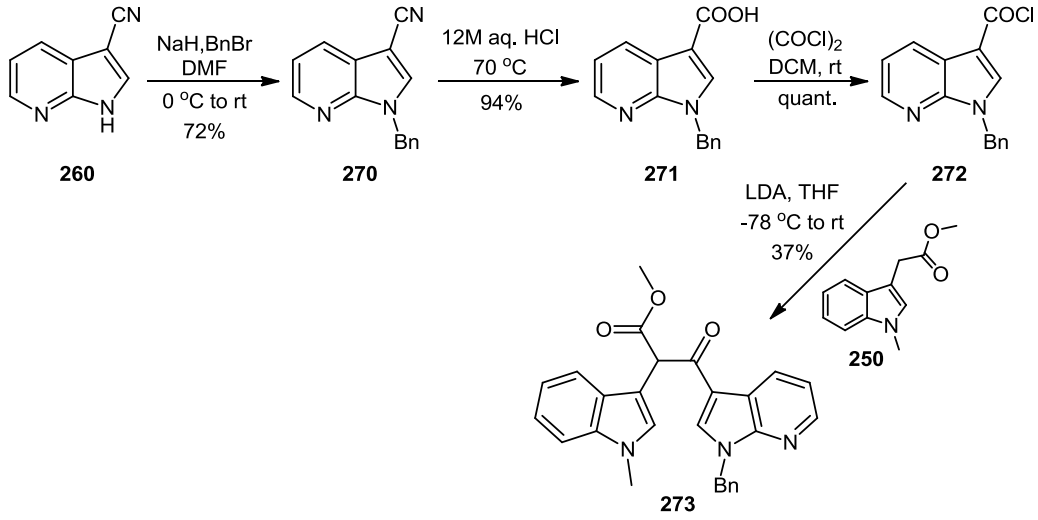

Scheme 4.13 *Route towards successful formation of β-keto ester **273***

Employing the methodology of Braňa *et al.*, a partial suspension of acyl chloride **272** in THF was added to the anion of ester **250** in THF at -78 °C under a nitrogen atmosphere, with the resulting mixture then allowed to warm to room temperature overnight.[1] Following workup, spectroscopic analysis of the crude residue revealed that the desired β-keto ester **273** had been

formed, with purification by flash column chromatography affording the pure product **273** as an orange/brown crystalline solid in 37% yield.

The two benzylic CH_2 protons of β-keto ester **273** are nonequivalent, leading to an AB system in the ^{1}H NMR spectrum (***Figure 4.2***). The two doublets arising from the geminal coupling (*J* = 15.0 and 15.1 Hz respectively) display a classic distortion of peak heights associated with AB systems, i.e. an increase in intensity of the inner peaks. This contrasts with the ^{1}H spectra of nitrile **270** and carboxylic acid **271**, in which the same protons, H_A and H_B, give rise to a singlet in each case. The lone Hα proton of ester **273** displays a chemical shift of 5.62 ppm, which is seen to be characteristic across similar β-keto esters. Interesting to note also is the effect of the β-keto ester functionality on the 7-azaindolyl aromatic protons in **273** relative to the carboxylic acid of precursor **271**. The C-$H_{2'}$ proton becomes more shielded, moving from a multiplet between 8.33-8.37 ppm to 7.88 ppm in ester **273**, while in contrast, C-$H_{4'}$ becomes more deshielded, shifting to 8.65 ppm. No significant change was observed for the C-$H_{5'}$ and C-$H_{6'}$ protons.

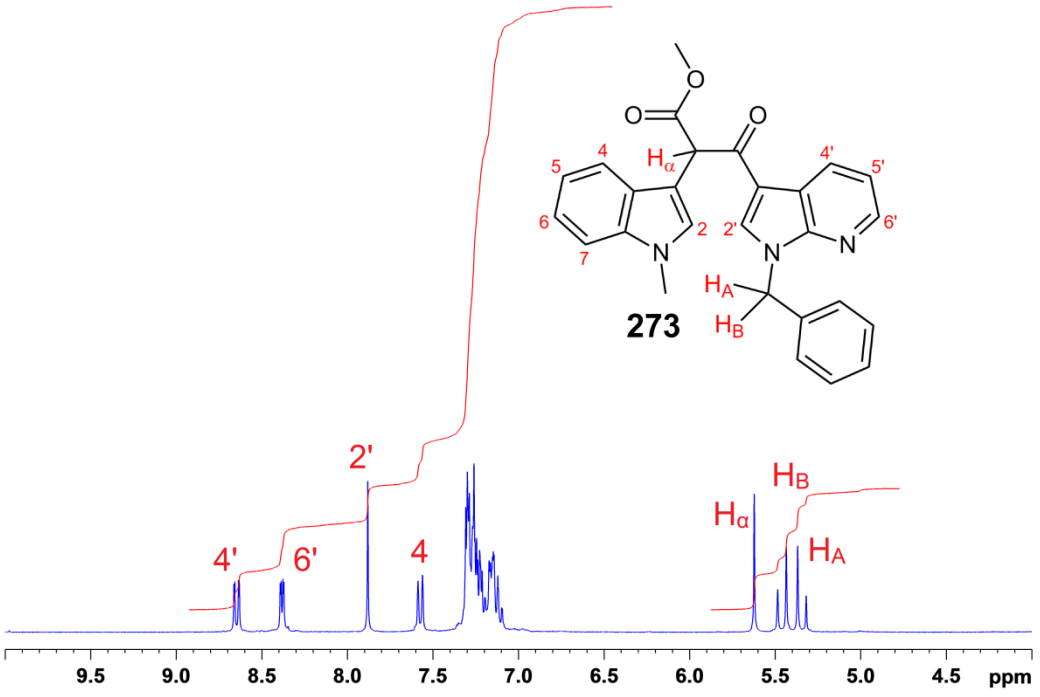

Fig. 4.2 *Expansion of aromatic region: ^{1}H NMR spectrum of β-keto ester **273** ($CDCl_3$, 300 MHz)*

4.2.4 Temperature studies with N-*methyl acyl chloride* 266

Given the successful formation of β-keto ester **273** (Section ***4.2.3***), it was concluded that the original problems encountered with the coupling step had resulted not from the lack of reactivity of the 7-azaindolyl subunit, but rather as a result of solubility. Calculation of the partition coefficient (ClogP) of acid chlorides used within the group indicated that *N*-methyl acyl chloride **266** was considerably more polar than the other acid chlorides utilised (***Figure 4.3***).

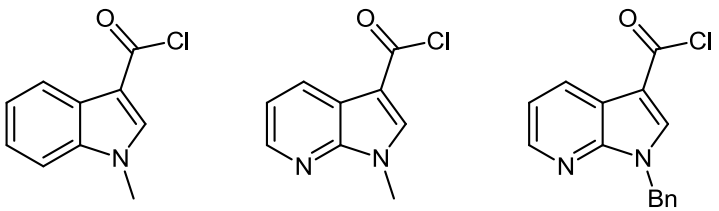

Fig. 4.3 *Structures and calculated partition coefficients of acyl chlorides* ***246****,* ***266*** *and* ***272***

While indolyl acyl chloride **246** had previously been employed within our laboratory in the proficient synthesis of analogous β-keto esters (Section **4.1**), utilisation of 7-azaindolyl acyl chloride **266** under similar conditions could not effectuate a successful outcome, despite numerous attempts. The introduction of a benzyl protecting group, seen for acyl chloride **272**, finally led to the successful attainment of a viable β-keto ester **273** containing a 7-azaindolyl moiety. Ultimately, after much examination of experimental parameters, it was found that increasing the reaction temperature immediately after the addition of acyl chloride **266** resulted in the successful formation of desired oxopropanoate **267** (***Scheme 4.14***).

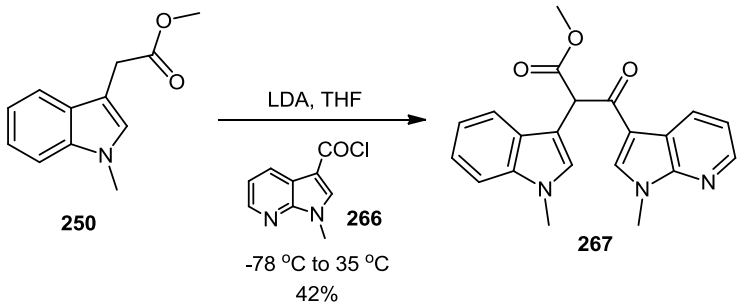

Scheme 4.14 *Synthesis of β-keto ester* ***267***

Subsequent optimisation afforded β-keto ester **267** in a yield of 42% as a yellow crystalline solid when the reaction vessel temperature was increased from -78 ^{o}C to 35 ^{o}C after the final addition of acyl chloride **266**. The development of this methodology was to prove vital in the synthesis of a number of other key aza ICZ precursors (Sections ***4.2.5***, ***4.2.6***, ***4.2.8*** and ***4.2.9***).

4.2.5 Synthesis of β-keto nitrile intermediate 276

Having successfully accessed β-keto esters **267** and **273** containing 7-azaindolyl functionalities, the attainment of other useful intermediates was examined. Accessing β-keto nitrile **276** represented one such judicious route (***Scheme 4.15***). Reaction of commercially available indole-3-acetonitrile **274** with sodium hydride and iodomethane in DMF at 0 ^{o}C led to the formation of *N*-methyl indole-3-acetonitrile **275** as an off-white solid in 84% yield. After stirring acetonitrile **275** in a solution of LDA in THF at -78 ^{o}C for 1 hour under a nitrogen atmosphere, a suspension of acyl chloride **266** in THF was added in a dropwise manner.

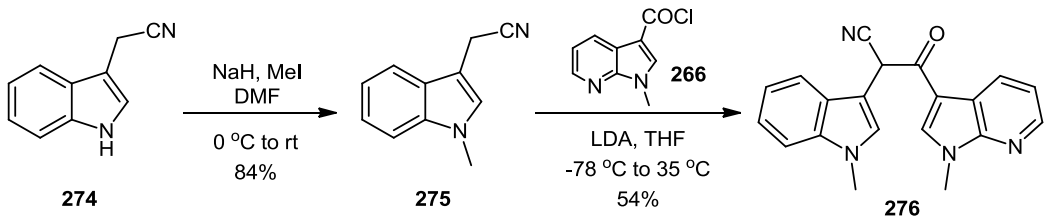

Scheme 4.15 *Route towards β-keto nitrile* ***276***

The temperature of the vessel was then raised to 35 ^{o}C upon completion of the addition, with the reaction subsequently allowed to stir at this temperature overnight. Following quenching of the reaction and workup, purification of the crude brown residue by flash column chromatography led to the isolation of oxopropanenitrile **276** as a reddish/brown solid in 54% yield.

4.2.6 Synthesis of bis-7-azaindolyl oxopropanoate 281

Bis-7-azaindolyl oxopropanoate **281** was the next target intermediate, beginning from 7-azaindole **139** (***Scheme 4.16***). Methylation of azaindole **139** was achieved under standard sodium hydride/methyl iodide conditions, affording *N*-protected 7-azaindole **277** as a green oil

in 94% yield. The dropwise addition of oxalyl choride to a solution of azaindole **277** in diethyl ether allowed for intermediary glyoxyl chloride formation, which was subsequently treated with potassium hydroxide in a mixture of water and acetone to give glyoxylate **278** as a white solid in 47% yield following acidic workup.

The Wolff-Kishner reduction of oxoacetic acid **278** towards acetic acid **279** was carried out in a one-pot procedure involving the heating of a mixture of acid **278**, hydrazine hydrate and sodium methoxide in ethylene glycol to 150 ^{o}C for 3 hours, allowing the solvent to concentrate down to roughly half the volume in that time. Acidic workup led to the precipitation of acetic acid **279** as a pure white solid in 84% yield, following copious water washes to remove all traces of remaining ethylene glycol.

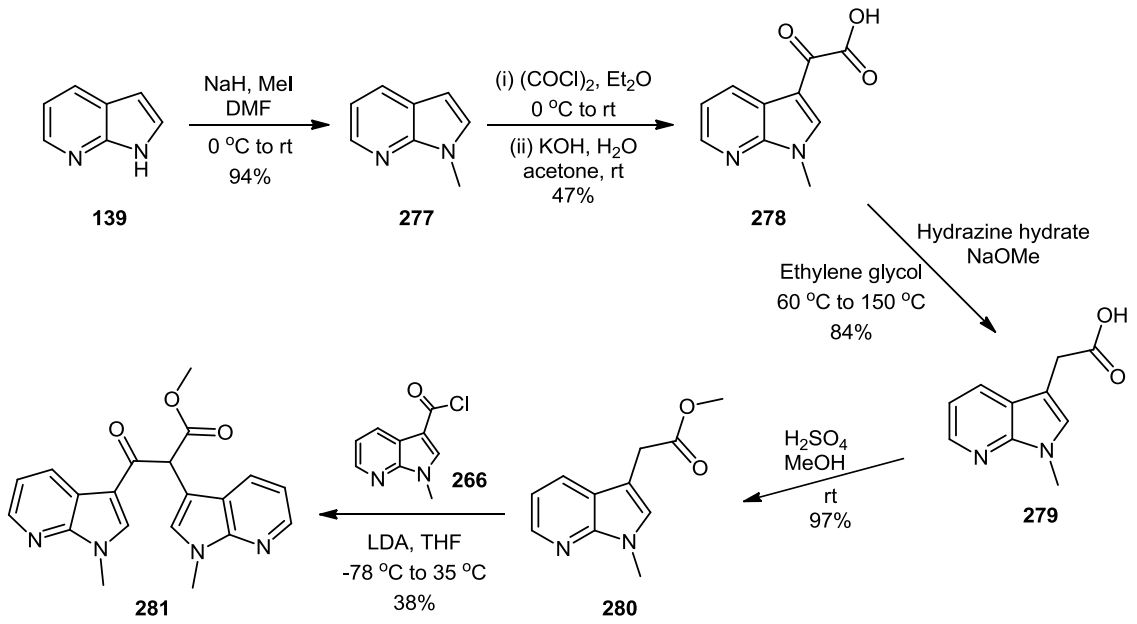

Scheme 4.16 *Route to bis-7-azaindolyl oxopropanoate **281***

The highly efficient conversion of acetic acid **279** to ester **280** was carried out by treatment of a solution of **279** in methanol with neat sulfuric acid, with the resulting mixture allowed to stir for 2 hours at room temperature. After the pH of the acidic solution was carefully adjusted to 9 using saturated aqueous sodium bicarbonate, extraction with ethyl acetate allowed for the isolation of ester **280** as a yellow oil in 97% yield. The LDA-mediated condensation of ester **280** with acyl chloride **266** subsequently resulted in the formation of bis-7-azaindolyl

oxopropanoate **281** as a golden crystalline solid in 38% yield (***Scheme 4.16***), with a characteristic signal corresponding to the C-Hα proton observed at 5.63 ppm in the ^{1}H NMR spectrum.

4.2.7 Route towards oxopropanenitrile 287

The next step in our synthetic strategy of fragment-based drug discovery was to incorporate a 3,4,5-trimethoxyphenyl functionality into our template for aza BIM derivatives. Bisindolylmaleimide analogues containing this aryl subunit had previously been shown by Peifer and co-workers to elicit potent VEGFR inhibitory activity.[8] To this end, it was initially necessary to fashion 7-azaindolyl-3-acetonitrile **283** to allow access to β-keto nitrile intermediate **287**. The Mannich reaction of diethylamine hydrochloride and formaldehyde with 7-azaindole **139** led to gramine **282** as an orange solid in excellent yield of 88% (***Scheme 4.17***). However, all subsequent endeavour to convert diethyl gramine **282** to acetonitrile **283** was met with failure. As well as attempting to protonate the gramine moiety of **282** under acidic conditions followed by nucleophilic attack of a cyanide anion, a strategy of alkylating the same functional group using dimethyl sulfate was also pursued, but to no avail.

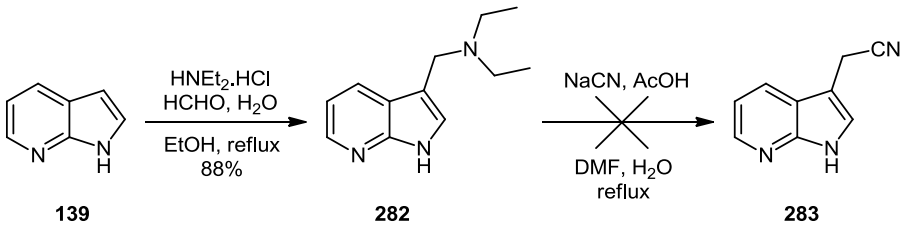

Scheme 4.17 *Attempted synthesis of 7-azaindolyl-3-acetonitrile* ***283***

This problem was later overcome when it was found that dimethyl gramine analogue **284**, also prepared in excellent yield from 7-azaindole **139**, could readily undergo cyanolysis to form nitrile **283** as a white crystalline material in 52% yield (***Scheme 4.18***). Given that the conversion to acetonitrile **283** proved unsuccessful under similar reaction conditions using diethyl gramine **282**, it suggests that perhaps difficulties arise with substitution of the cyanide anion on the corresponding quaternary salt of **282**. Further examination of this reaction could provide a topic for future work.

Reaction of acetonitrile **283** with sodium hydride and iodomethane resulted in *N*-methyl derivative **285**, albeit in relatively low yield of 46%. Formation of a dimethylated by-product, arising as a consequence of the highly acidic nature of the protons adjacent to the nitrile, accounted for the comparatively low yield of desired product **285**.

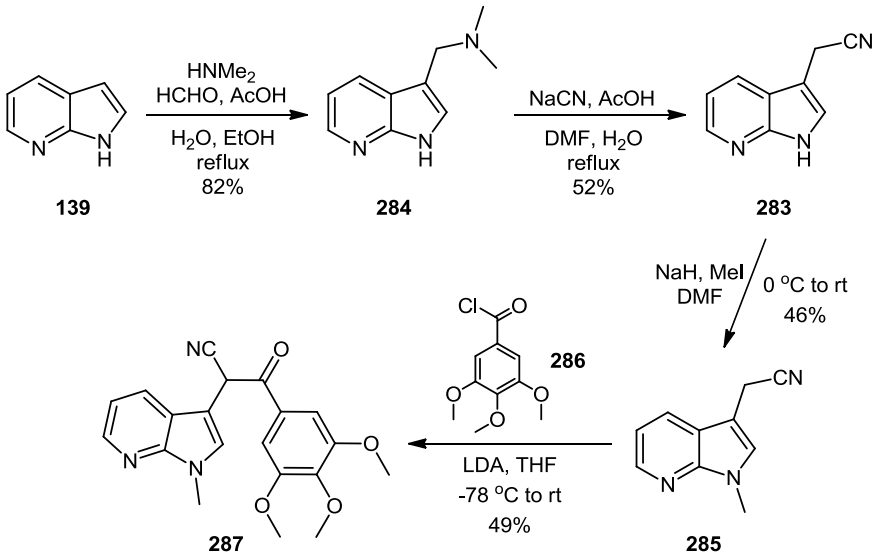

Scheme 4.18 *Route to β-keto nitrile* ***287***

The base-catalysed condensation of acetonitrile **285** with acyl chloride **286**, generated quantitatively from the reflux of 3,4,5-trimethoxybenzoic acid in chloroform and excess thionyl chloride, afforded β-keto nitrile **287** as a yellow solid in 49% yield. Due to negligible solubility issues with acyl chloride **286**, there was no need for immediate adjustment of temperature upon completion of additions.

4.2.8 Synthesis of oxopropanenitrile 289

Synthesis of the regioisomer of β-keto nitrile **287**, oxopropanenitrile **289**, proved to be relatively straightforward, given the previous establishment of methodology involving the use of acyl chloride **266** (Section ***4.2.4***). The anion of commercially available 3,4,5-trimethoxyphenyl acetonitrile **288** was initially generated at -78 °C using a solution of LDA in THF under a nitrogen atmosphere (***Scheme 4.19***).

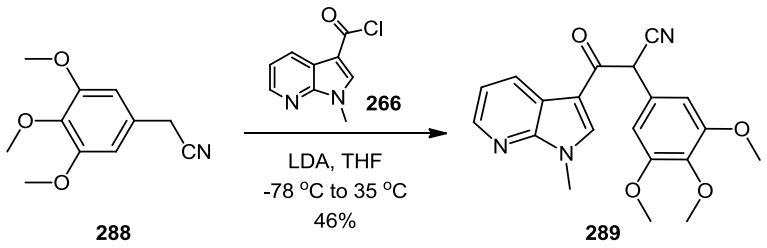

Scheme 4.19 *Synthesis of oxopropanenitrile* ***289***

A suspension of acyl chloride **266** in THF was then added to the mixture, at which point the reaction vessel was warmed to 35 °C and left to stir overnight. Following workup, the β-keto nitrile **289** product was isolated as a yellow solid in 46% yield by flash column chromatography, employing an ethyl acetate/hexane (70:30) eluent system.

4.2.9 Synthesis of oxopropanoate 292

Oxopropanoate **292** was synthesised in two steps from 3,4,5-trimethoxyphenyl acetic acid **290** via ester **291** (***Scheme 4.20***). Initial attempts to effect the esterification of acid **290** using oxalyl chloride with a drop of anhydrous DMF in THF followed by stirring in methanol, resulted in only a moderate yield of 28%.

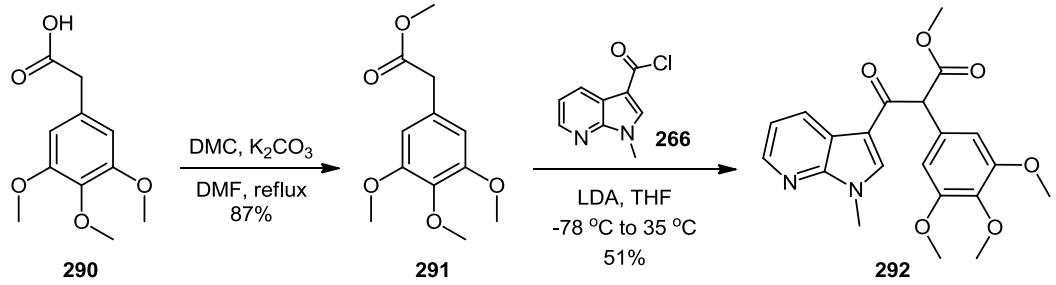

Scheme 4.20 *Route to β-keto ester* ***292***

However, treatment of acid **290** with potassium carbonate and dimethyl carbonate in DMF under reflux conditions for 16 hours resulted in a significant improvement in the yield of ester **291** to 87%, which was isolated as a colourless oil after column chromatography. Reaction of acyl chloride **266** with the anion of ester **291** under similar conditions to that seen previously (Section ***4.2.4***) led to the formation of oxopropanoate **292** in 51% yield as a pale yellow solid following chromatographic purification.

4.3 Cyclocondensation reactions: accessing aza BIM derivatives

With the successful establishment of a viable methodology to allow access to a series of oxopropanoate and oxopropanenitrile intermediates (Section **4.2**), it was now possible to proceed with the next stage of our synthetic strategy. To achieve our goal of developing novel aza BIM and aza ICZ derivatives of biological interest, we next examined the cyclocondensation of these intermediates, and their subsequent elaboration.

4.3.1 Synthesis and derivatisation of 5-aminopyrazole 293

Reaction of β-keto nitrile **287** (Section ***4.2.7***) with hydrazine hydrate in the presence of hydrochloric acid led to the formation of 3-(3,4,5-trimethoxyphenyl)-4-(1-methyl-1*H*-pyrrolo[2,3-*b*]pyridin-3-yl)-1*H*-pyrazol-5-amine **293**, a highly promising heterocyclic bioisostere of the potent VEGFR inhibitor **229** (***Scheme 4.21***).[9]

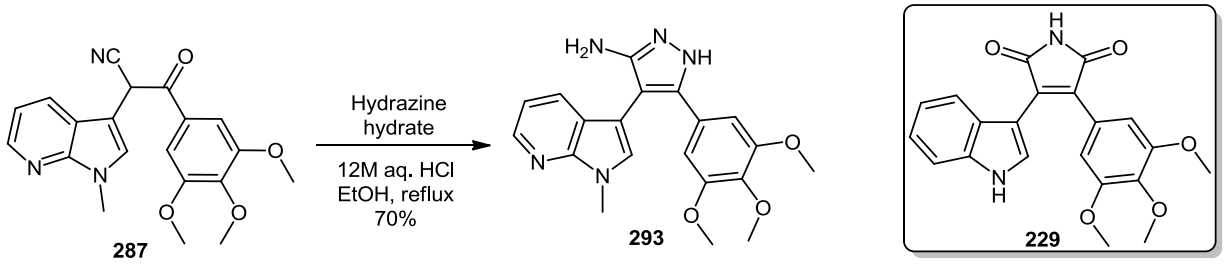

Scheme 4.21 *Synthesis of 5-aminopyrazole* ***293***

Monitoring of the reaction by TLC revealed that no starting material remained after 20 hours under reflux, with the pure product **293** subsequently isolated by column chromatography (10% methanol in ethyl acetate) as a light brown solid in 70% yield. The use of camphoric acid instead of hydrochloric acid as catalyst for the transformation, as detailed by Braňa *et al.* in the synthesis of an analogous series of pyrazolones (***Scheme 4.2***), resulted in a significant reduction in yield to 28% over a similar reaction time.

As well as acting as a useful congener to established kinase inhibitor **229**, aminopyrazole **293** offers an appealing template with which to pursue further synthetic diversification towards the potential enhancement of enzyme-inhibitor contacts.

Although structural confirmation of aminopyrazole **293** was provided for by ^{1}H NMR and mass spectrometry data, the apparent absence of four quaternary carbon signals in the 75 MHz ^{13}C NMR spectrum was problematic. A detailed comparison with the precursor, β-keto nitrile **287**, served to indicate that the missing signals belong to carbon atoms constituent of the aminopyrazole moiety, or those neighbouring the heterocyclic moiety.

Subsequent analysis of aminopyrazole **293** on a more powerful 125 MHz instrument led to the discovery of four additional peaks of broad and weak intensity at 95.2, 126.9, 141.8 and 152.3 ppm. To better understand the origin of these signals, a further series of ^{13}C NMR experiments were carried out, initially focused on alternating the probe temperature and pulse frequency. Following the incremental variation of both parameters, best resolution of the four peaks was obtained with a pulse time delay of 7 seconds and with the probe temperature set to 315 K (***Figure 4.3***).

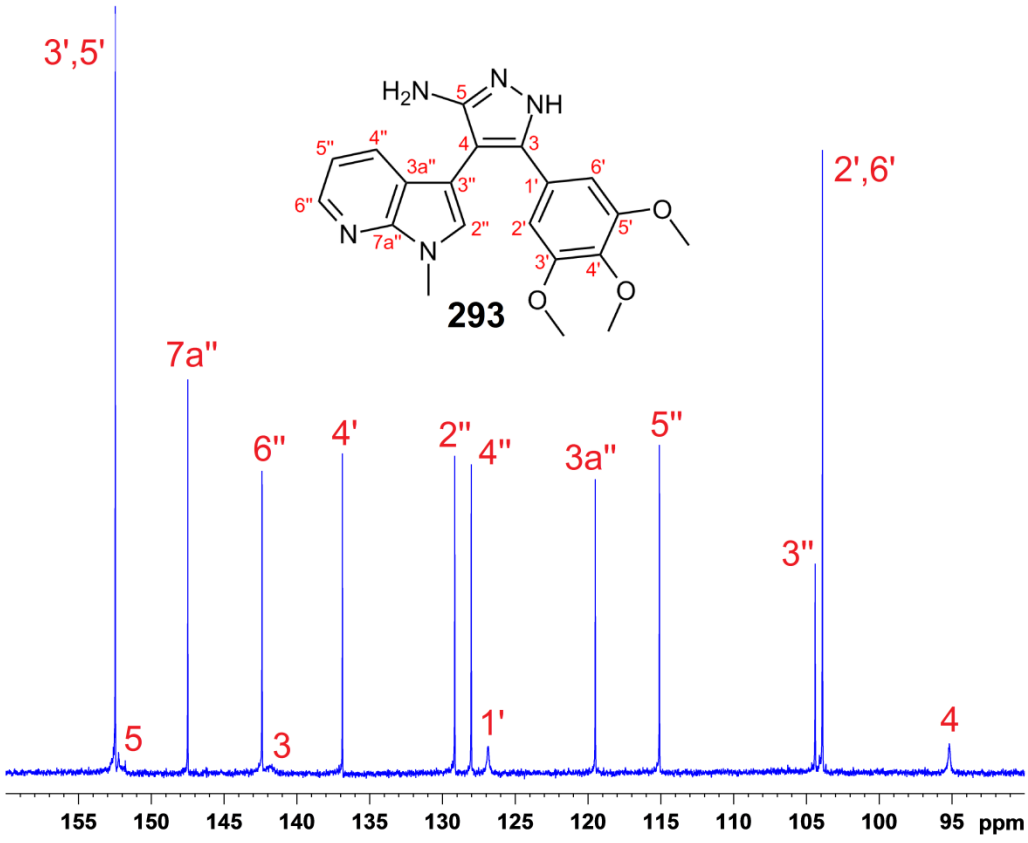

Fig. 4.3 *Expansion of ^{13}C NMR spectrum of aminopyrazole **293***
(DMSO-d$_6$, 150 MHz, 315 K, τ = 7 sec)

With the unambiguous assignment of all CH and CH_3 carbon nuclei within the molecule provided for by the application of DEPT and 2D HSQC experiments, establishment of all quaternary carbons was then necessary in apportioning the identity of the four suppressed ^{13}C peaks. Consequently, a 2D HMBC (heteronuclear multiple bond correlation) technique was employed, whereby correlation between protons and quaternary carbons is obtained via coupling over two or more bond lengths (***Figure 4.4***). For purposes of clarity, ^{13}C NMR signals on the y-axis are labelled: (i) green for CH aromatic peaks, (ii) orange for quaternary carbon peaks of normal intensity and (iii) red for broad quaternary carbon peaks.

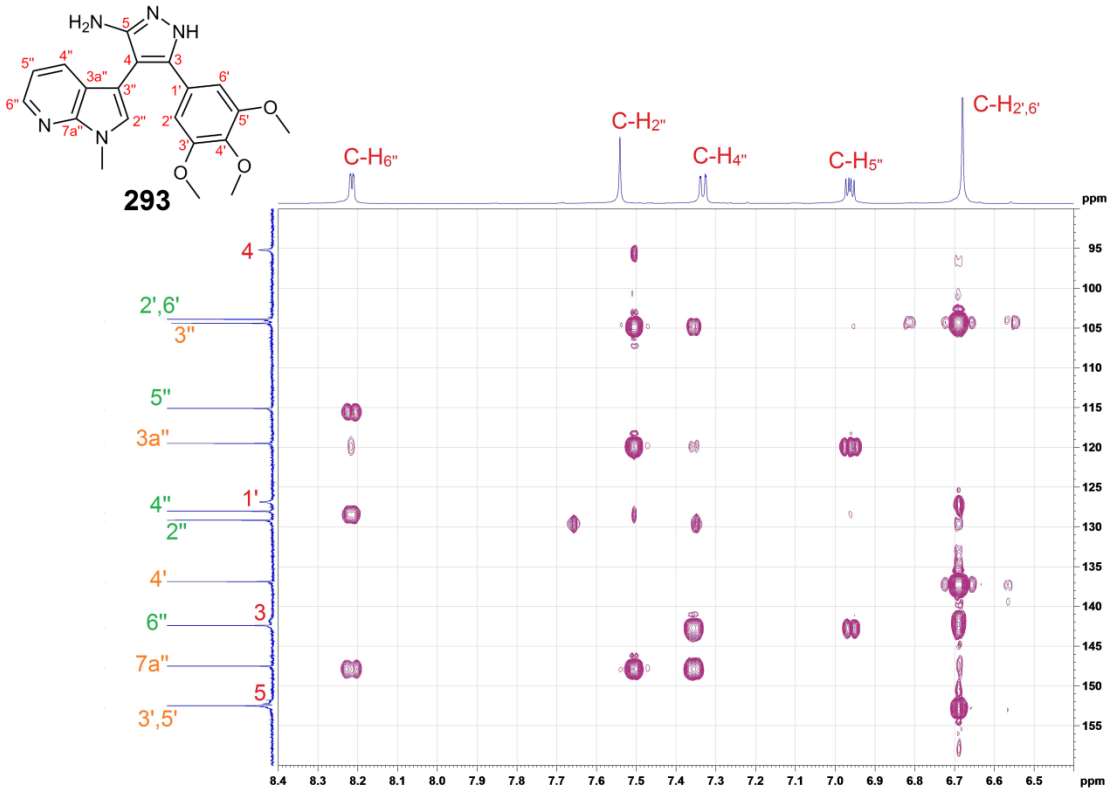

Fig. 4.4 *2D HMBC spectrum of aminopyrazole* ***293*** *(^{13}C NMR on y axis, ^{1}H NMR on x axis)*

Examining the quaternary signals (orange annotation) of normal intensity first, C(3'') of aminopyrazole **293** shows distinct correlation to the C-$H_{2''}$ proton, and less so to C-$H_{4''}$, which is a further bond length away. The bridgehead carbon C(3a'') at 119.5 ppm is seen to couple to C-$H_{2''}$ and C-$H_{5''}$ over three bond lengths, though correlation to the more proximal C-$H_{4''}$ is somewhat suppressed. The opposing bridgehead carbon C(7a'') clearly correlates to the C-$H_{2''}$, C-$H_{4''}$ and C-$H_{6''}$ protons, all of which are three bonds distant. The equivalent quaternary

carbons of the trimethoxyphenyl moiety, C(3') and C(5'), give rise to a single signal at 152.5 ppm, with coupling seen to the corresponding equivalent protons of the ring, C-$H_{2'}$ and C-$H_{6'}$. Stronger correlation is shown to occur between the same two protons and the carbon at the *para*-position, C(4'), despite the further bond length.

Eliminating the assigned quaternary carbons, it is possible to designate the four weak peaks (red annotation) in the ^{13}C NMR spectrum as C(1'), C(3), C(4) and C(5), all of which lie in or adjacent to the aminopyrazole ring. Of these signals, two are more readily identifiable, with C(4) correlating to C-$H_{2''}$ and C(1') coupling to the C-$H_{2'}$ and C-$H_{6'}$ protons. The remaining two quaternary signals are weaker again and definitive correlation is difficult to prove, complicating the spectroscopic analysis. However, it is possible to surmise that C(5) is the more deshielded of the two nuclei, as it is bonded to two heteroatoms as opposed to just one.

From the series of ^{13}C NMR experiments conducted, it was found that the C(4) and C(1') signals could be resolved by increasing the temperature of the probe. However, it was not possible to distinguish the even less pronounced C(3) and C(5) peaks until the delay time was also raised to 7 seconds, inferring a long spin-lattice relaxation of the ^{13}C nuclei involved. It is an intrinsic property of carbon nuclei in any molecule to have either a short or long relaxation time, with quaternary carbons in fixed structures typically showing longer relaxation times, often longer than that provided for under standard conditions.[10]

Broadening of the four quaternary carbon signals could possibly arise due to annular tautomerism of the aminopyrazole moiety of **293**, with interchange of the NH ring proton. Previous studies have noted a similar broadening of signals in the spectra of other aminopyrazoles.[11,12] For example, in a study examining the structure and tautomerism of a series of monoaryl-substituted aminopyrazoles in both solid state and in solution, Puello and co-workers observed broad ^{13}C NMR peaks corresponding to a coalescence of quaternary carbon signals from either tautomer.[11]

*4.3.1.1 Bicyclic derivatives of 5-aminopyrazole **293***

In the initial stage of this derivatisation study, it was possible to effect the formation of bicyclic systems **295** and **297** via reaction of 5-aminopyrazole **293** with respective bidentate electrophiles (***Scheme 4.22***). Treatment of a solution of **293** in DCM with two drops of triethylamine followed by *N*-chlorocarbonyl isocyanate **294** led to triazinedione **295** as a white precipitate in 56% yield, following quenching of the reaction by the addition of water. Confirmation of the formation of the barbiturate moiety was given by the appearance of a broad 2H singlet at 11.66 ppm in the ^{1}H NMR spectrum of product **295**, corresponding to the two free NH protons.

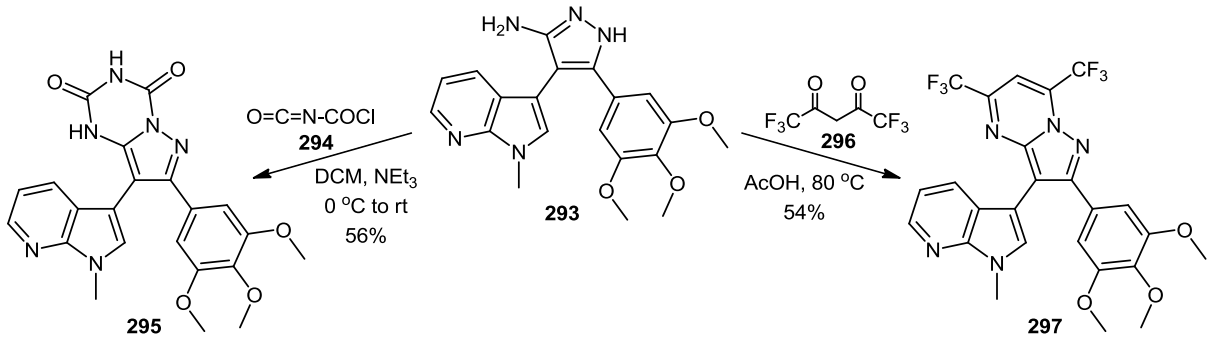

Scheme 4.22** Routes to bicyclic analogues **295** and **297

Treatment of aminopyrazole **293** with a 20-fold molar excess of hexafluoroacetylacetone **296** in acetic acid at 80 ^{o}C over 20 hours led to the formation of pyrazolo[1,5-*a*]pyrimidine **295** as a orange solid in 54% yield.

Interestingly, the coupling of fluorine to carbon is observed in the ^{13}C NMR spectrum of pyrimidine **297** in the form of four quartets (***Figure 4.5***). Large coupling constants ($J_{F\text{-}C}$ = 275.4 and 275.2 Hz respectively) were identified for the overlapping quartets of C_{α} and C_{β} as a consequence of substitution with three fluorine atoms. The effect is also noticeable over a distance of two bonds from the site of fluorine substitution, namely for the quaternary carbons C_5 and C_7. However, the magnitude of coupling is significantly diminished with increased remoteness from the fluorine atoms at $J_{F\text{-}C}$ = 37.8 and 34.7 Hz respectively. No coupling was observed beyond two bond lengths.

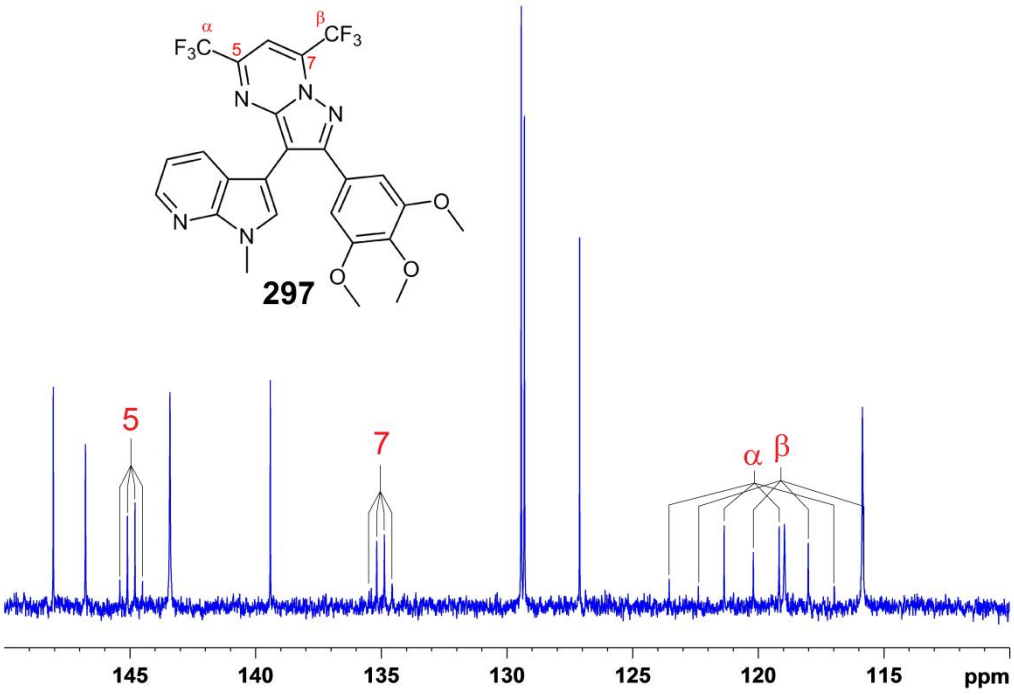

Fig. 4.5 *Expansion of ^{13}C NMR spectrum of pyrimidine* ***297*** *($CDCl_3$, 125 MHz)*

4.3.1.2 Reaction of 5-aminopyrazole ***293*** *with monodentate electrophiles*

Continuing with a synthetic derivatisation theme, the monosubstitution of 5-aminopyrazole **293** with a number of electrophiles was next to be investigated.

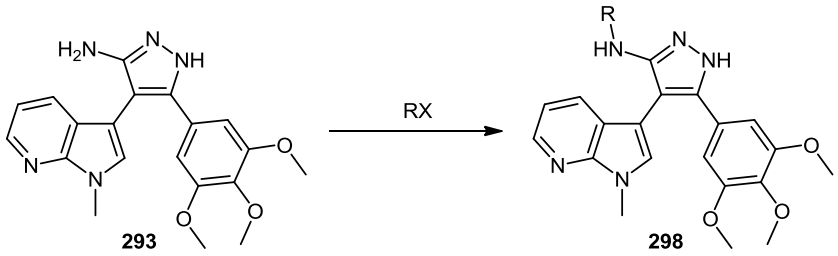

Scheme 4.23 *Monosubstitution of 5-aminopyrazole* ***293***

Consequent to the formation of bicyclic systems **295** and **297** (Section *4.3.1.1*), it was expected that the reaction of **293** with a given set of monodentate electrophiles would result in substitution on the exocyclic amine (***Scheme 4.23***).

The expected substitution on the exocyclic nitrogen of 5-aminopyrazole **293** was found to occur upon reaction with trifluoroacetic anhydride **299** in acetonitrile, resulting in the

formation of acetylated product **300** as a pale yellow solid in 41% yield (***Scheme 4.24***). Structural confirmation of the product **300** was afforded by the appearance of two broad singlets at 11.23 and 13.52 ppm in the ^{1}H NMR spectrum, corresponding to the acetamide NH and pyrazolic NH respectively.

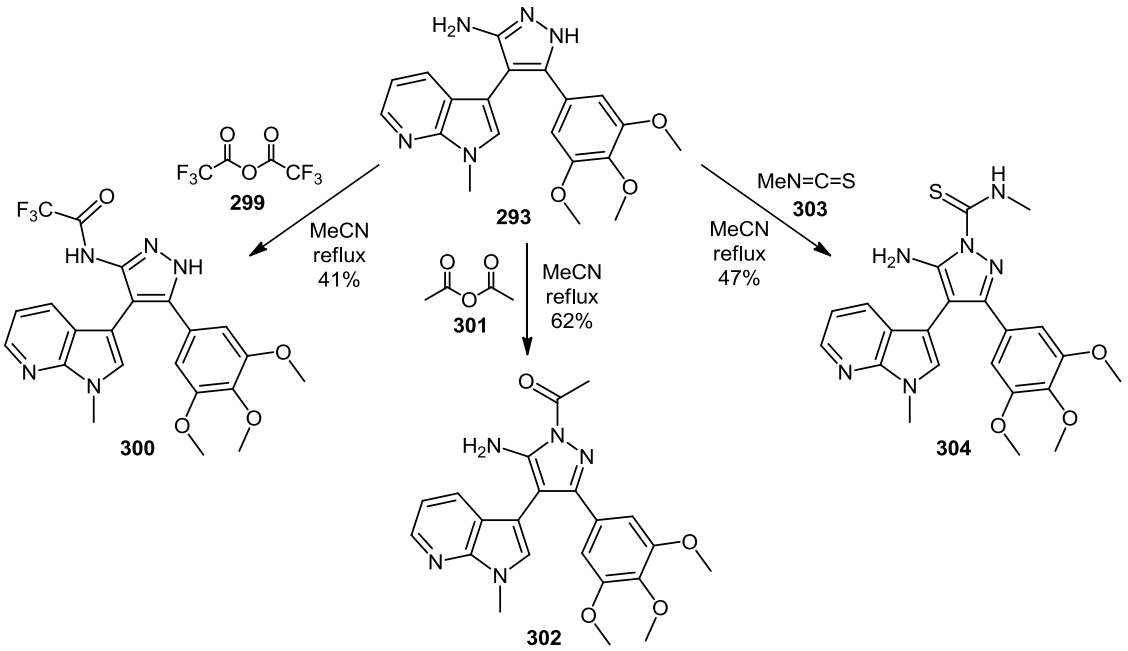

Scheme 4.24 *Synthesis of monosubstituted aminopyrazole derivatives **300**, **302** and **304***

It was therefore an unexpected result, when the treatment of aminopyrazole **293** with acetic anhydride **301** in acetonitrile at reflux temperature for 24 hours led to the formation of *N*-acetyl **302**, with the site of substitution lying at position 1 of the ring. Purification of the crude reaction residue by column chromatography (40% hexane in ethyl acetate) led to the isolation of acetylated derivative **302** as a pale yellow crystalline solid in good yield of 62%. The identification of a broad 2H singlet at 5.60 ppm in the ^{1}H NMR spectrum, corresponding to the free exocyclic amine, served to ascertain the correct structure of the product.

Reaction of aminopyrazole **293** with methyl isothiocyanate **303** led to the formation of carbothioamide **304** as a white solid in 47% yield, with substitution of the aminopyrazole again occurring on the nitrogen at position 1 of the pyrazole, in a similar fashion to acetylated analogue **302** (***Scheme 4.24***).

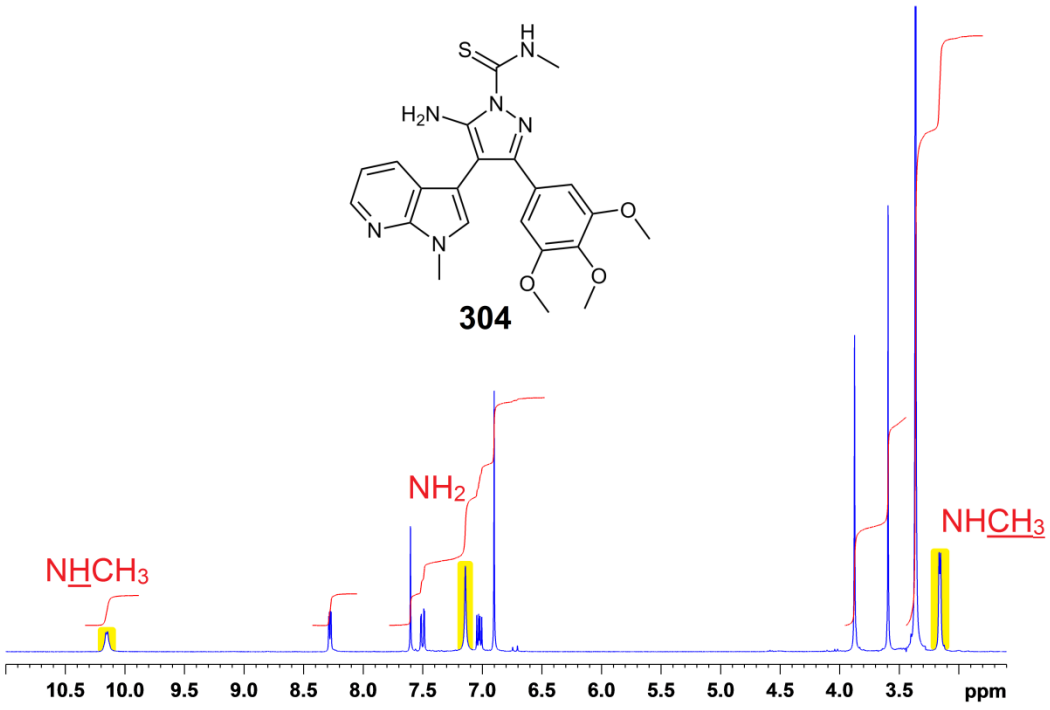

Fig. 4.6 *^{1}H NMR spectrum of carbothioamide **304** (DMSO-d_6, 300 MHz)*

The mode of substitution of carbothioamide **304** is illustrated by analysis of the ^{1}H NMR spectrum (***Figure 4.6***), with a broad 2H singlet at 7.14 ppm arising due to the free amino functionality of the aminopyrazole. Two characteristic signals are observed due to the presence of the thioamide substituent, with a broad 3H doublet at 3.16 ppm corresponding to the methyl group and a broad 1H doublet at 10.15 ppm as a result of the thioamide NH.

Comparison of the ^{13}C NMR spectra of monosubstituted aminopyrazoles **300**, **302** and **304** with that of their precursor **293** serves to illustrate an interesting trend. As in the case of parent aminopyrazole **293** (Section ***4.3.1***), a number of the quaternary carbon signals of trifluoroacetamide **300** appear as broad peaks, while all of the quaternary carbon signals in the ^{13}C NMR spectra of acetylated aminopyrazole **302** and carbothioamide **304** are of similar, normal intensity. This can perhaps be explained by the fact that by substituting at the N(1) position of the aminopyrazole, as in the case of derivatives **302** and **304**, there is no possibility of annular tautomerism, with the electronic configuration of the ring effectively "locked" in position. However, with trifluoroacetamide **300**, interchange of the NH ring proton is still

possible, therefore potentially resulting in the peak broadening of neighbouring quaternary carbons in the ^{13}C spectrum.

Precedence for the difference in regioselectivity observed for the substitution of aminopyrazole **293** exists within the literature. It has been noted that the structural nature of the end product depends on the type of reagent and reaction conditions used.[13]

While using different electrophiles and reaction parameters, Nie and co-workers described the substitution of various 5-aminopyrazoles of general structure **305** with ethoxycarbonyl isothiocyanate **306**, with the regioselectivity of the reaction dependant on both the conditions employed and the nature of the ring substituent at the C(4) position (***Scheme 4.25***).[14]

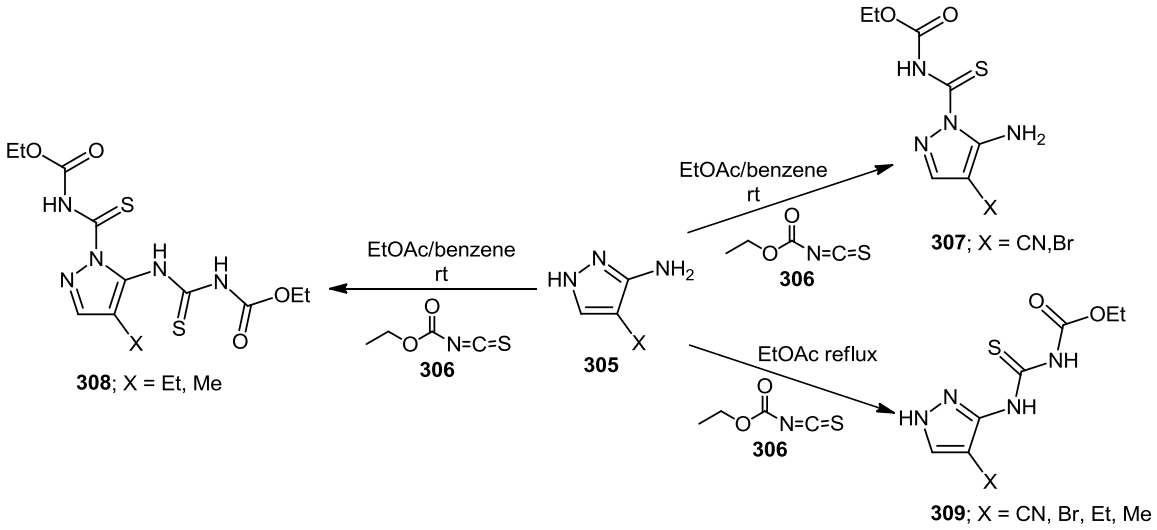

Scheme 4.25 *Reaction of aminopyrazole **305** with ethoxycarbonyl isothiocyanate **306**[14]*

When the reaction was carried out in mixture of ethyl acetate and benzene at room temperature, with an electron-withdrawing group such as CN or Br at the C(4) position of **305**, electrophilic substitution occurred solely at the N(1) position of the ring (general structure **307**). However, with an electron-donating group at the C(4) position, disubstitution occurred under the same reaction conditions (general structure **308**). Nie *et al*. later found that when the reaction was carried out in ethyl acetate at reflux temperature, substitution occurred solely on the exocyclic amine (general structure **309**), regardless of the nature of the ring substituent.[14] This suggests that while reaction at the N(1) position may be the more kinetically-favoured

process, substitution on the amino functionality is more thermodynamically-favoured due to the thermal stability of the resulting products.

Elnagdi *et al.* noted that heating a mixture of aminopyrazole **310** in neat acetic anhydride **301** to reflux led to the formation of acetamide **311** in 90% yield, with substitution on the exocyclic amine (***Scheme 4.26***).[15] Similar to that seen with Nie and co-workers (***Scheme 4.25***), the formation of acetamide **311** appears to arise as a result of being the more thermodynamically-favoured product, mirroring the situation with the formation of trifluroacetamide **300** (***Scheme 4.24***). To add to the complexity, this contradicts the substitution pattern we observed under modified conditions, hence the need for future investigation.

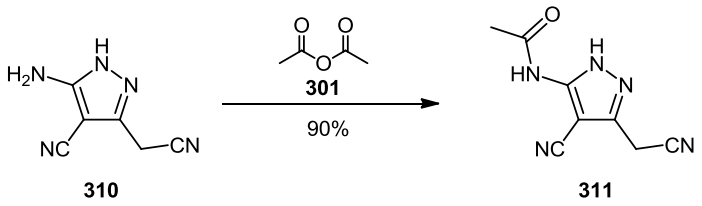

Scheme 4.26 *Synthesis of acetamide* ***311*** *from aminopyrazole* ***310***[15]

4.3.2 Synthesis and derivatisation of 5-aminopyrazole 312

In terms of biological mode of action, the spatial positioning of molecular functionalities can prove critical towards the exploitation of unique features in enzymatic binding pockets. Peifer and co-workers described how the regioisomer **230** of VEGFR inhibitor **32** was found to be completely inactive against the same kinase, simply with a different orientation of the lactam moiety (***Figure 4.7***).[8]

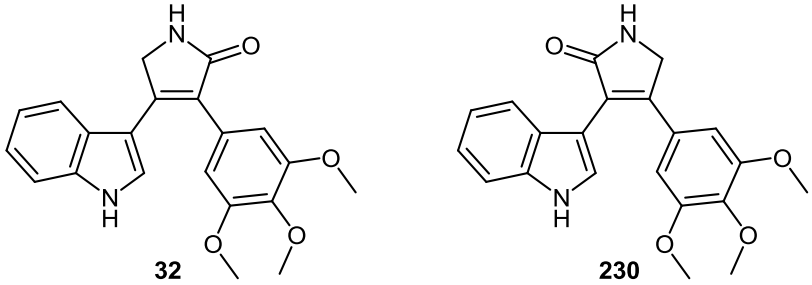

Fig. 4.7 *VEGFR inhibitor template described by Peifer et al.*[8]

Expanding our endeavour in the study of 5-aminopyrazoles (Section ***4.3.1***), our next aim was to fashion a series of regioisomers of our previous molecular template, realising the opportunity for the exploration of novel target-ligand binding motifs and SAR study. To this end, the synthesis and derivatisation of 3-(1-methyl-1*H*-pyrrolo[2,3-*b*]pyridin-3-yl)-4-(3,4,5-trimethoxyphenyl)-1*H*-pyrazol-5-amine **312** was undertaken, beginning from the previously formed oxopropanenitrile precursor **289** (Section ***4.2.8***).

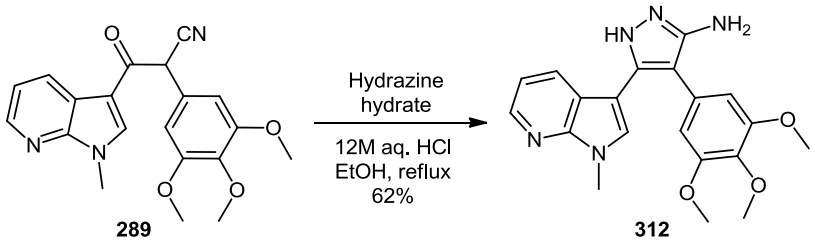

Scheme 4.27 *Synthesis of 5-aminopyrazole* ***312***

Reaction of β-ketonitrile **289** with hydrazine hydrate, with hydrochloric acid acting as catalyst, in absolute ethanol at reflux temperature led to the formation of aminopyrazole **312** as a brown solid in 62% yield (***Scheme 4.27***).

Understandably, the ^{1}H NMR spectrum of aminopyrazole **312** revealed a striking similarity in comparison to regioisomer **293** (***Figure 4.8***). The only major difference between the two spectra involves the signals arising from the C-H_2 and C-H_4 protons, which coalesce to form a broad singlet at 7.55 ppm in the case of aminopyrazole **312**, whereas they resolve into separate, distinct peaks in the case of aminopyrazole **293**.

In the ^{13}C NMR spectrum of aminopyrazole **312**, four quaternary carbons appear as broad, weak signals at 105.3, 107.0, 125.4, and 151.8 ppm, indicating the potential effect of annular tautomerism, with the possibility of interchange of the NH ring proton leading to a suppression of the observed peaks. This corresponds to the spectroscopic analysis carried out for its regiosomer, aminopyrazole **293**, which also contained four weak quaternary carbon signals.

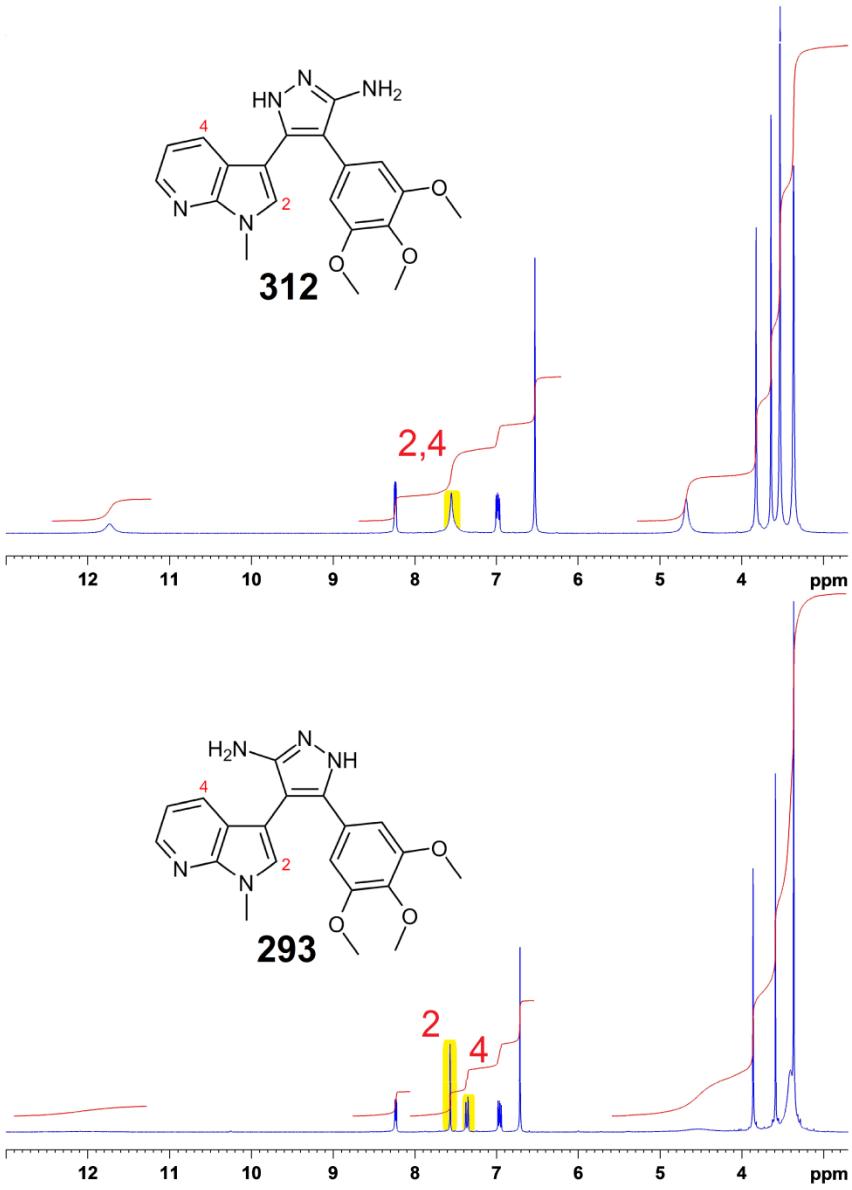

Fig. 4.8 *Comparison of* ^{1}H *NMR spectra of* ***293*** *and* ***312*** *(DMSO-*d_6*, 300 MHz)*

In analytical terms, the main feature to distinguish between the two regioisomers is by their melting point ranges, between which there is considerable difference. The melting point range of aminopyrazole **312** (135-137 ^{o}C) was found to be far lower than that of aminopyrazole **293** (266-267 ^{o}C). The relatively large disparity between the melting points of the regioisomers could perhaps be due to additional intramolecular hydrogen bonding in **312** due to the positioning of the amino moiety. This leads to the suggestion that aminopyrazole **312** should have better physicochemical characteristics than its regioisomer **293**.

*4.3.2.1 Bicyclic derivatives of 5-aminopyrazole **312***

As in the case of analogue **293**, derivatisation of aminopyrazole **312** can be effected in a straightforward manner as a result of its nucleophilic nature. Treatment of a cooled solution of aminopyrazole **312** and a few drops of triethylamine in DCM with *N*-chlorocarbonyl isocyanate **294** led to the formation of triazinedione **313** as a white solid in 45% yield (***Scheme 4.28***). Structural confirmation of the barbiturate moiety of triazinedione **313** is afforded by the two broad singlets arising from the NH protons at 11.59 and 11.74 ppm in the ^{1}H NMR spectrum.

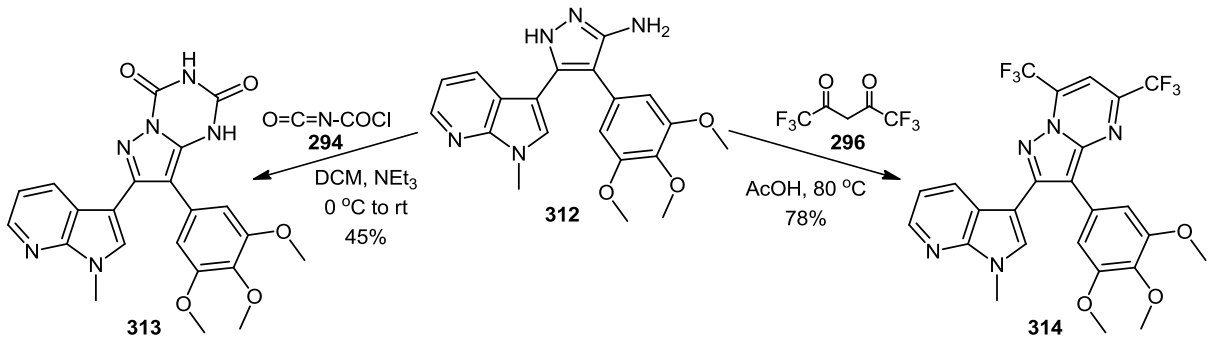

Scheme 4.28** Synthesis of bicyclic derivatives **313** and **314** of aminopyrazole **312

Condensation of aminopyrazole **312** with hexafluoroacetylacetone **296** in an acidic medium gave highly-conjugated pyrazolo[1,5-*a*]pyrimidine **314** as an orange/red solid in high yield of 78%, following purification by flash column chromatography (40% ethyl acetate in hexane).

*4.3.2.2 Reaction of 5-aminopyrazole **312** with monodentate electrophiles*

It was interesting to note that aminopyrazole **312** exhibited similar regioselectivity towards monodentate electrophiles as with its analogue **293**, despite the rearrangement of the 7-azaindolyl and 3,4,5-trimethoxyphenyl rings at the C(3) and C(4) ring positions. Though the overall presence of these two large aryl units may have some influence on the substitution pattern observed, their position on the aminopyrazole ring cannot be said to directly affect regioselectivity.

Reaction of aminopyrazole **312** with trifluoroacetic anhydride **299** afforded trifluoroacetamide **315** as an off-white solid in 68% yield (***Scheme 4.29***). The presence of two broad singlets at

11.37 and 13.30 ppm in the ^{1}H NMR spectrum confirm that substitution occurred on the exocyclic amino functionality rather than N(1) nitrogen. As observed for each of the other fluorinated aminopyrazole derivatives, fluorine-carbon coupling is evident in the ^{13}C NMR spectrum of **315**. Once more, a large coupling constant was recorded for the quartet arising from the trifluoromethyl carbon (J = 288.0 Hz), with the magnitude dropping significantly over a distance of two bond lengths to the carbonyl carbon (J = 36.2 Hz).

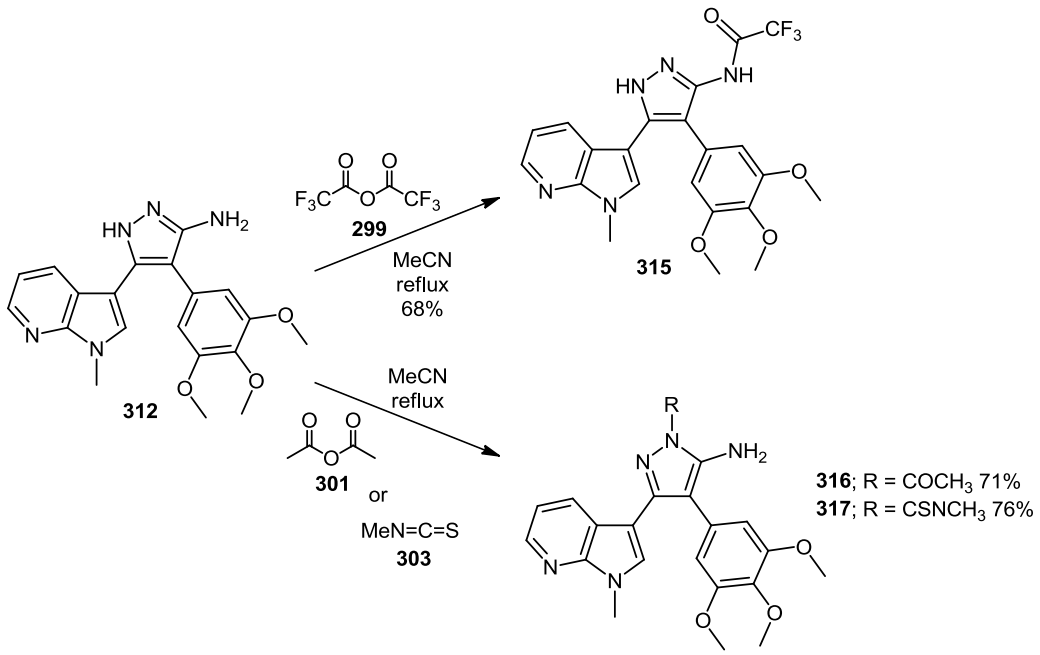

Scheme 4.29 *Monosubstitution of aminopyrazole* ***312*** *towards derivatives* ***315***, ***316*** *and* ***317***

Acetylated derivative **316** was synthesised as a greyish solid in a good yield of 71% following treatment of aminopyrazole **312** with acetic anhydride **301** in acetonitrile at reflux. The site of substitution was confirmed to be the N(1) position of the pyrazole due to the presence of a 2H broad singlet at 5.56 ppm in the ^{1}H NMR spectrum, corresponding to the exocyclic amino functionality.

Reaction of aminopyrazole **312** with methyl isothiocyanate **303** led to the formation of carbothioamide **317** as a white solid in 76% yield. Spectroscopic analysis again provided structural confirmation of substitution at the N(1) pyrazolic position.

The effect of the substituent on the N(1) position of carbothioamide **317** and acetylated aminopyrazole **316** is similar to that seen for their corresponding regioisomers (Section *4.3.1.2*), with the relative intensities of all quaternary carbon signals in the respective ^{13}C NMR spectra all being broadly similar. However, in the ^{13}C NMR spectrum of trifluoroacetamide **315**, with no substitution on the N(1) position of the aminopyrazole, a number of the quaternary carbons give rise to broad, weak peaks.

The monosubstitution yields of parent compound **312** were found to be considerably higher than those of its analogue **293**, despite similar reaction times being employed – perhaps indicative of a more nucleophilic aminopyrazole moiety.

4.3.3 Synthesis and derivatisation of 5-aminopyrazole 318

The next step in our synthetic strategy was to synthesise and derivatise aminopyrazole **318** from oxopropanenitrile **276** (***Scheme 4.30***). It was posited that aminopyrazole **318** could proffer an interesting novel bioisostere to acyriarubin A **10**.

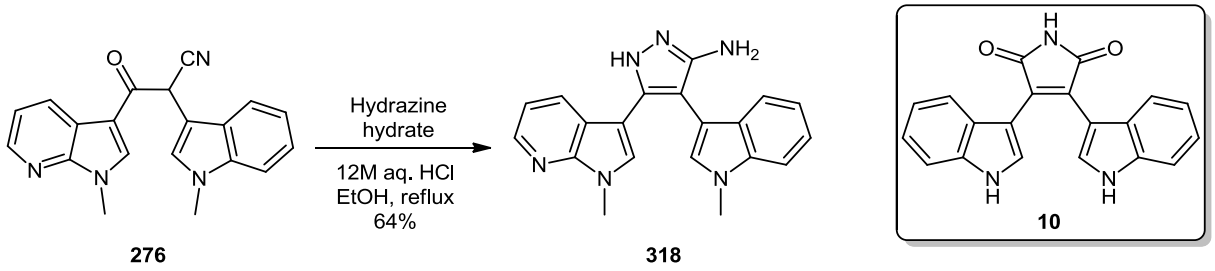

Scheme 4.30 *Synthesis of aminopyrazole* ***318*** *from oxopropanenitrile* ***276***

A similar synthetic methodology was employed to that previously used for the fashioning analogous aminopyrazoles **293** and **312** (Sections ***4.3.1*** and ***4.3.2***). Treatment of β-keto nitrile **276** (Section ***4.2.5***) with five equivalents of hydrazine hydrate in the presence of hydrochloric acid under reflux conditions led to the formation of 3-(1-methyl-1*H*-pyrrolo[2,3-*b*]pyridin-3-yl)-4-(1-methyl-1*H*-indol-3-yl)-1*H*-pyrazol-5-amine **318** as a light brown crystalline material in 64% yield after purification via flash column chromatography (10% methanol in ethyl acetate). The use of acetic acid has also been described in the literature as catalyst for the successful synthesis of aminopyrazole heterocycles from β-keto nitrile intermediates.[16]

However, when employed as acid catalyst for the synthesis of **318** under similar reaction conditions, a lower yield of 48% was obtained.

*4.3.3.1 Bicyclic derivatives of 5-aminopyrazole **318***

Extending the derivatisation methodology previously employed for 3-(3,4,5-trimethoxyphenyl)-4-(1-methyl-1*H*-pyrrolo[2,3-*b*]pyridin-3-yl)-1*H*-pyrazol-5-amine **293** (Section ***4.3.1***) and 3-(1-methyl-1*H*-pyrrolo[2,3-*b*]pyridin-3-yl)-4-(3,4,5-trimethoxyphenyl)-1*H*-pyrazol-5-amine **312** (Section ***4.3.2***) towards the BIM analogue aminopyrazole **318** proved to be relatively straightforward.

Following dissolution in dry DCM containing four drops of triethylamine, treatment of aminopyrazole **318** with *N*-chlorocarbonyl isocyanate **294** led to the formation of triazinedione **319** as a grey solid in 66% yield following aqueous workup (***Scheme 4.31***). The highly deshielded NH protons of the barbiturate moiety of bicyclic derivative **319** were observed at 11.55 and 11.68 ppm in the ^{1}H NMR spectrum.

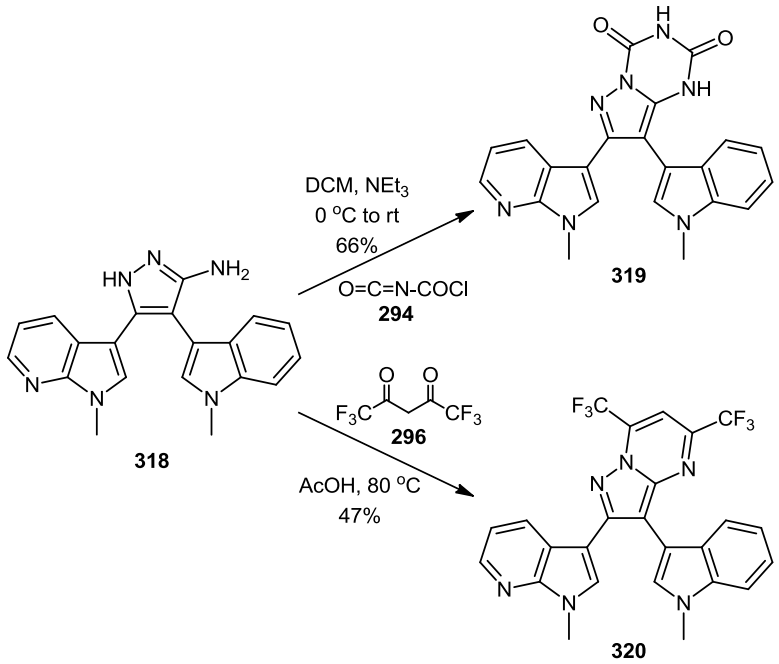

Scheme 4.31** Synthesis of bicyclic derivatives **319** and **320** from aminopyrazole **318

Formation of bis(trifluoromethyl)pyrimidine **320** was achieved following the heating of a mixture of aminopyrazole **318** in acetic acid and a 20-fold molar excess of

hexafluoroacetylacetone **296** to 80 ^{o}C for 20 hours. Column chromatography (40% ethyl acetate in hexane) provided the pure bicyclic product **320** as a bright red solid in 47% yield. As in the case of analogous bicyclic pyrimidine derivatives **297** and **312**, fluorine-carbon coupling is evident in the ^{13}C NMR spectrum of **320**. Two large quartets ($J_{F\text{-}C}$ = 275.2 and 275.7 Hz respectively) arise due to the two trifluoromethyl carbon nuclei, with fluorine-carbon coupling over a distance of three bond lengths to the adjacent quaternary carbons resulting in two smaller quartets ($J_{F\text{-}C}$ = 38.1 and 37.4 Hz respectively).

*4.3.3.2 Reaction of 5-aminopyrazole **318** with monodentate electrophiles*

No discernible difference in regioselectivity was observed for the reaction of aminopyrazole **318** with a series of monodentate electrophiles than that seen previously for aminopyrazoles **293** (Section *4.3.1.2*) and **312** (Section *4.3.2.2*).

Following application of trifluoroacetic anhydride **299** to solution of aminopyrazole **318** in acetonitrile, followed by heating to reflux for 20 hours, trifluoroacetamide **321** was isolated as a white solid in 35% yield from the resulting crude brown residue by flash column chromatography (30% hexane in ethyl acetate) (***Scheme 4.32***).

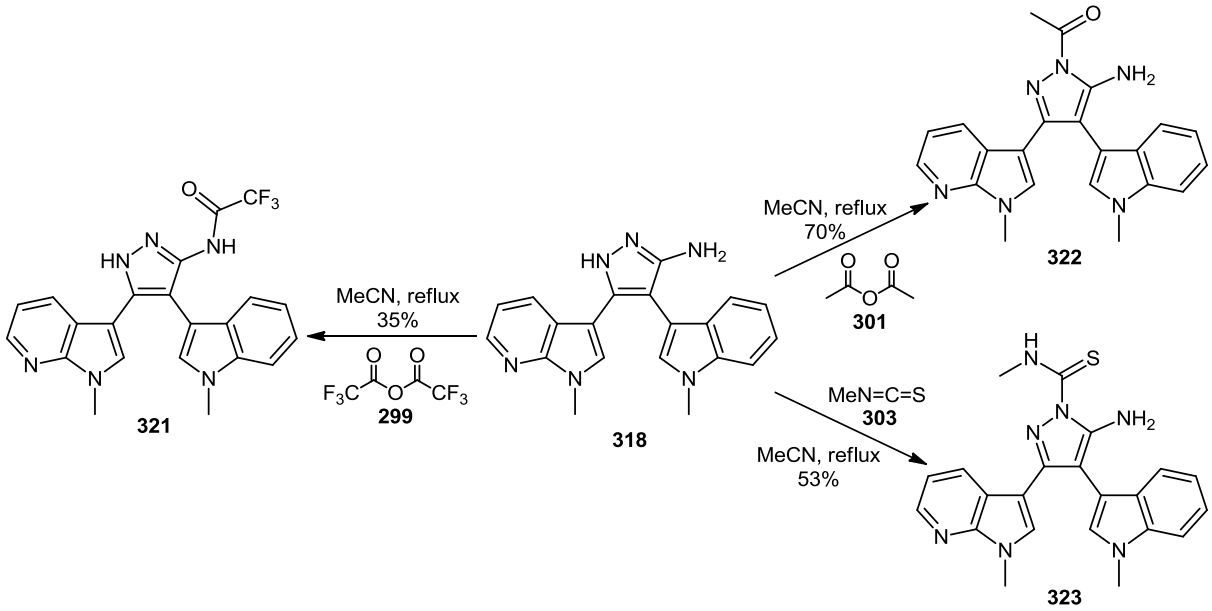

Scheme 4.32 *Synthesis of mono-substituted aminopyrazole derivatives **321**, **322** and **323***

Treatment of aminopyrazole **318** with 1.2 equivalents of acetic anhydride **301** in acetonitrile under reflux conditions led to the formation of acetylated derivative **322** as a white crystalline solid in good yield of 70%. Substitution at the N(1) position of the aminopyrazole ring was confirmed by the appearance of a broad singlet at 5.44 ppm in the ^{1}H NMR spectrum of **322** integrating for two protons, corresponding to the NH_2 exocyclic amino moiety.

In a similar manner, treatment of a solution of aminopyrazole **318** in acetonitrile with methyl isothiocyanate **303** also resulted in substitution at the N(1) pyrazolic position. Carbothioamide **323** was isolated as a white solid in 53% yield following purification by column chromatography, employing a 50:50 mixture of ethyl acetate and hexane as eluent. Once again, key to the discernment of the site of substitution was the appearance of a broad 2H singlet at 6.34 ppm in the ^{1}H NMR spectrum due to the NH_2 amino functionality, as well as the lack of any broad 1H singlet which could correspond to a highly deshielded NH ring proton.

Having successfully completed the synthesis of three series of derivatised aminopyrazoles (Sections ***4.3.1***, ***4.3.2*** and ***4.3.3***), it was evident that the pattern of regioselectivity with regard to reaction of the parent aminopyrazoles with monodentate electrophiles was not dependent on the nature of the aryl substituents. In the case of reaction with methyl isothiocyanate and acetic anhydride, substitution occurred at the N(1) position of the aminopyrazole ring in each case, i.e. the kinetic product of the reaction was more favourable than the thermodynamic product.

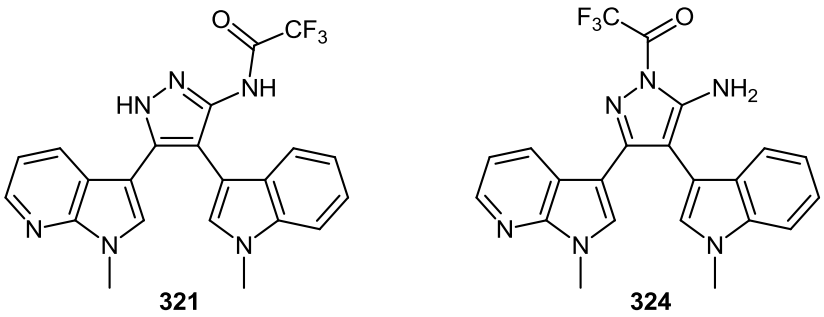

Fig. 4.9 *Structures of trifluoroacetamide **321** and hypothetical trifluoroacetylated aminopyrazole **324***

However, when treated under similar conditions with trifluoroacetic anhydride, the most reactive of the three monodentate electrophiles used, substitution occurred on the exocyclic amine of the aminopyrazole (such as with derivative **321**), i.e. the thermodynamic product was the more favourable of the two. In this scenario, it is possible that the kinetic product of the reaction (e.g. hypothetical compound **324**) was more unstable than the analogous carbothioamide and acetyl derivatives, due to the greater electron-withdrawing ability of the trifluoroacetyl moiety. Hence, substitution on the amino group may resulted in the more stable and favoured product **321**.

4.3.4 5-Membered heterocycles from oxopropanoate intermediates

The use of oxopropanoate intermediates in the formation of novel 5-membered heterocyclic BIM bioisosteres was also examined as part of this overall project. In a manner analogous to that previously employed by Braňa and co-workers in the synthesis of bisindolylpyrazolones (***Scheme 4.2***), β-keto ester **267** (Section ***4.2.4***) was treated with hydrazine hydrate in the presence of camphoric acid (***Scheme 4.33***).[1] However, it was not possible to isolate the desired pyrazolone **325** owing to a multitude of side-products formed, despite a number of attempts at purification by column chromatography. Spectroscopic analysis indicated that only a small proportion of the expected product **325** was formed, even after repeated attempts.

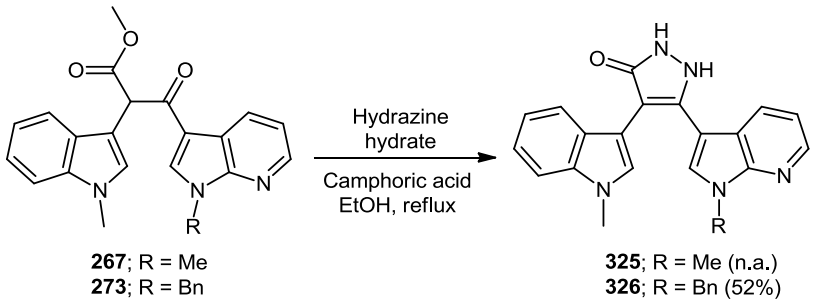

Scheme 4.33 *Synthesis of pyrazolone **325** and **326** from oxopropanoates **267** and **273***

In contrast, reaction of *N*-benzyl β-keto ester **273** with hydrazine hydrate under similar conditions resulted in the formation of an appreciable quantity of the expected pyrazolone product **326**. However, purification was not a straightforward task, as it was necessary to employ a number of different chromatographic eluent systems before it was possible to isolate the pure product **326** as a brown solid in 52% yield (2% methanol in DCM).

Despite the problematic reaction of β-keto ester **267** with hydrazine hydrate, it was found to readily undergo cyclocondensation to form isoxazolone **327** following treatment with five equivalents of hydroxylammonium chloride in methanol under reflux conditions (***Scheme 4.34***). Isoxazolone **327** was isolated in 64% yield as a light brown solid following flash column chromatography (5% methanol in ethyl acetate). Subsequent alkylation to *N*-methyl derivative **328** was achieved under standard conditions using sodium hydride and methyl iodide in DMF, with the product formed as an off-white solid in 88% yield.

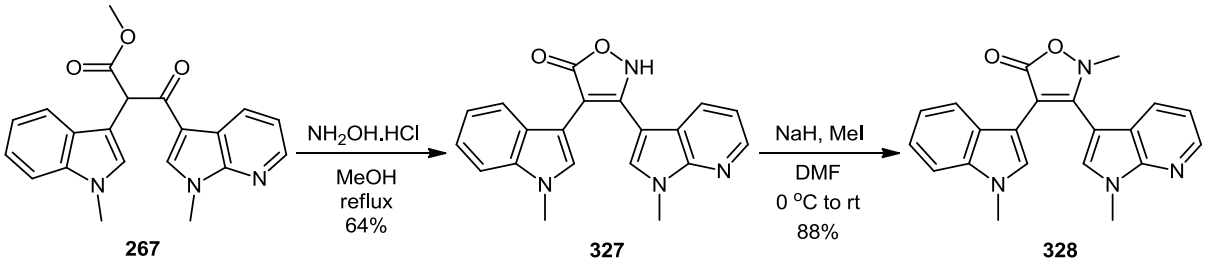

Scheme 4.34 *Synthesis of isoxazolone **327** and conversion to* N*-methyl derivative **328***

4.4 Accessing of 6-membered heterocyclic BIM derivatives

The synthesis of 6-membered heterocyclic derivatives of the BIM pharmacophore has previously been explored within our research group by Pierce and McCarthy (***Scheme 4.35***).[2,3]

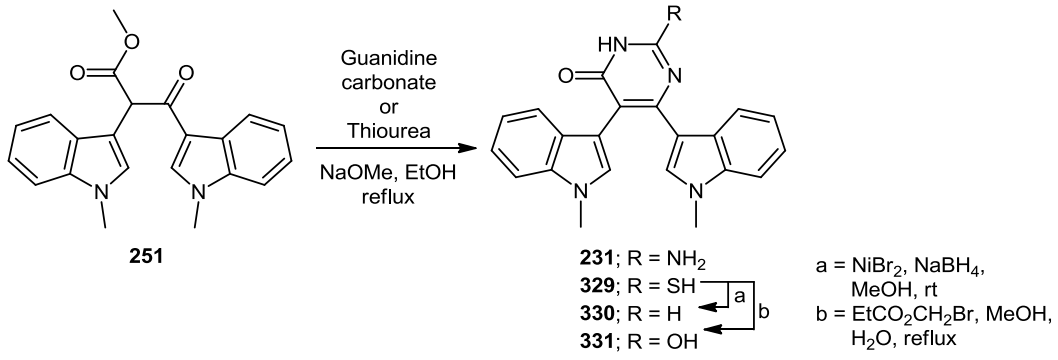

Scheme 4.35 *Synthesis of 6-membered pyrimidinone BIM derivatives **231**, **329**, **330** and **331***

Utilising nucleophiles such as guanidine and thiourea, base-mediated cyclocondensation of bisindolyl β-keto ester **251** led to the fashioning of 2-aminopyrimidin-4-one **231** and thiouracil

329 respectively. Further elaboration of thiouracil **329** afforded desulfurised pyrimidinone analogue **330** and uracil **331**.

It was discovered that the successful synthesis of 6-membered BIM analogues from β-keto ester **251**, such as pyrimidinone **231** and thiouracil **329**, was highly dependent on the reactive nature of the nucleophile. For example, reaction of ester **251** with urea failed to directly produce uracil **331**, which instead had to be accessed via thiouracil **329**. Similarly, the use of other nucleophiles such as *O*-methyl isourea and *N,N'*-dimethyl thiourea failed to produce the desired 6-membered products, with only starting material identified. As a result of the reagent-dependant nature of these cyclocondensation reactions involving precursor **251**, the development of a library of 6-membered BIM derivatives was pursued by secondary modification of pyrimidinone **231** and thiouracil **329**.[2,3]

4.4.1 Routes towards monoaza 6-membered BIM derivatives

Consequent to the previous synthetic effort towards bisindolyl derivatives such as pyrimidinone **231** (***Scheme 4.35***), accessing analogous systems containing 7-azaindolyl subunits represented a highly desirable endeavour in our program of fragment-based drug discovery, given the significant alteration of pharmacological properties that has occurred upon their inclusion in similar chemotherapeutic candidates (Sections *1.3.1.5* and *1.3.2.3*).

Initially, the reaction of β-keto ester **267** (Section ***4.2.4***) with guanidine under basic conditions was examined (***Scheme 4.36***).

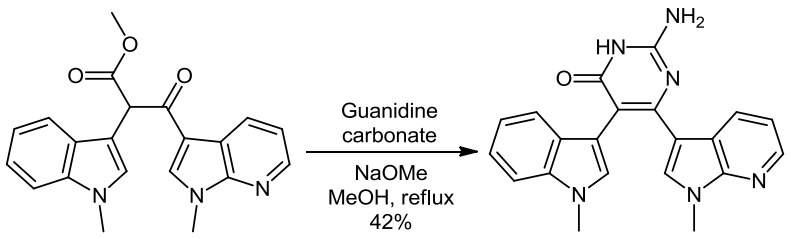

267 **332**

Scheme 4.36 *Synthesis of pyrimidinone **332** from β-keto ester **267***

Following the liberation of guanidine from the corresponding carbonate salt by treatment with sodium methoxide, ester **267** underwent cyclocondensation to form pyrimidinone **332**. The

crude product was isolated as a dark green precipitate following an acidic workup, with subsequent purification by column chromatography (10% methanol in ethyl acetate) furnishing the desired product **332** as a light brown solid in 42% yield.

Employing similar conditions to that used for the synthesis of pyrimidinone **332** (***Scheme 4.36***), the reaction of thiourea with β-keto ester **267** was next to be explored (***Scheme 4.37***). Once again, a crude precipitate was obtained following an acidic workup. While it was indicated by mass spectrometry that a very limited amount of desired thiouracil product **333** had been formed, it was not possible to isolate a pure sample, with numerous other products in evidence by TLC and ^{1}H NMR analysis. Varying the reaction conditions employed, significant effort was expended in an attempt to both increase the yield of desired thiouracil **333** and also to limit side-product formation, to no avail.

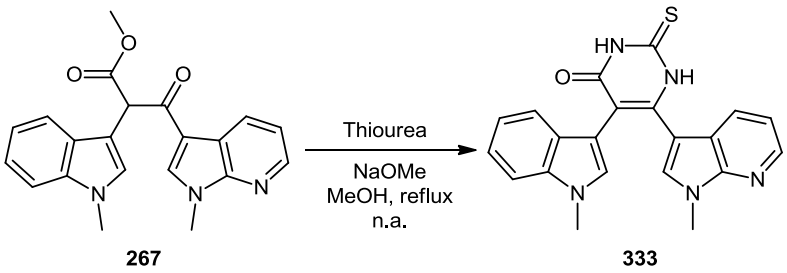

Scheme 4.37 *Synthesis of thiouracil **333** from β-keto ester **267***

The formation of uracil **334** from the reaction of β-keto ester **267** with urea in the presence of excess sodium methoxide was also attempted (***Scheme 4.38***). However, even with a prolonged reaction time of 96 hours, none of desired product **334** was afforded and only starting material was detected. This confirmed work by Pierce regarding the lack of nucleophilicity of urea and similar reagents necessary for effective heterocyclic formation from β-keto ester precursors.[2]

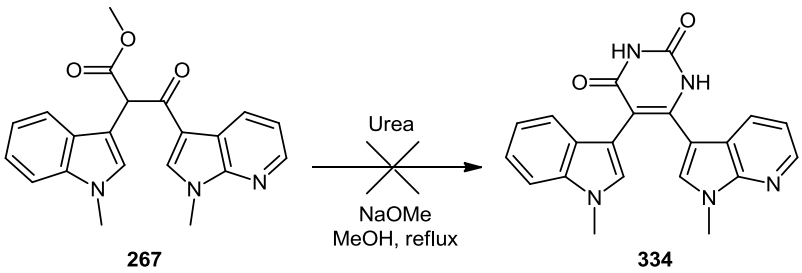

Scheme 4.38 *Attempted synthesis of uracil **334** from β-keto ester **267***

The use of β-keto ester **273**, with an *N*-benzyl protecting group on the azaindolic moiety (Section ***4.2.3***), towards the synthesis of similar monoaza 6-membered BIM derivatives was also explored (***Scheme 4.39***). However, attempts to access pyrimidinone **335** and thiouracil **336** via reaction of precursor **273** with guanidine and thiourea respectively proved unsuccessful. Degradation of the starting material was detected in each case, with no evidence of desired products **335** and **336** having formed.

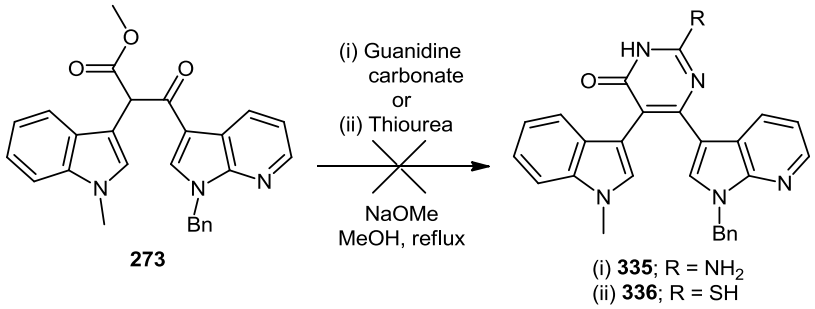

Scheme 4.39 *Attempted synthesis of pyrimidinone **335** and thiouracil **336***

Therefore, replacing the *N*-methyl protecting group of ester **267** with a benzyl functionality in analogous intermediate **273** meant that it was not possible to effectuate cyclocondensation towards 6-membered heterocyclic bioisosteres of the BIM series. Further investigation is required in order to determine the impact of such functionalities on this particular reaction.

4.4.2 Attempted syntheses of further 6-membered BIM derivatives

Having previously experienced variable success in the synthesis of 6-membered heterocyclic BIM derivatives using precursors containing both indolyl and 7-azaindolyl substituents (Section ***4.4.1***), the use of other oxopropanoate intermediates was examined.

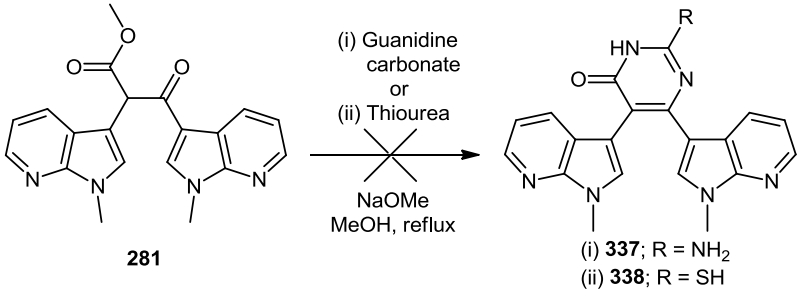

Scheme 4.40 *Attempted synthesis of pyrimidinone **337** and thiouracil **338***

However, it was found that the respective base-mediated reactions of bis-7-azaindolyl β-keto ester **281** (Section ***4.2.6***) with guanidine and thiourea only resulted in the recovery of starting material, without formation of desired products **337** and **338** (***Scheme 4.40***).

The unreliable nature of the cyclocondensation methodology towards these BIM analogues was further highlighted by the attempted syntheses of pyrimidinone **339** and thiouracil **340** (***Scheme 4.41***), from the 3,4,5-trimethoxyphenyl substituent-bearing oxopropanoate **292** (Section ***4.2.9***). As in the case of bis-7-azaindolyl β-keto ester **281** (***Scheme 4.40***), desired products **339** and **340** were not formed, with degradation of starting material in each case.

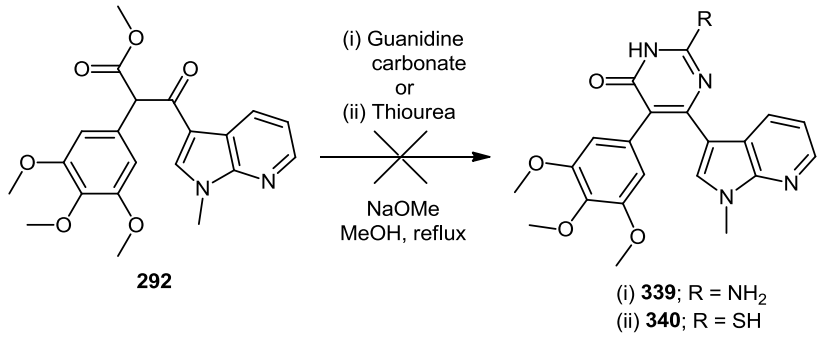

Scheme 4.41 *Attempted synthesis of pyrimidinone **339** and thiouracil **340***

As previously alluded to at the start of this section (Section **4.4**), Pierce had noted that the reactivity of the nucleophile utilised was of paramount importance in the successful synthesis of analogous 6-membered BIM derivatives from bisindolyl β-keto ester **251** (***Scheme 4.35***).[2] Given the application of a similar methodology towards the formation of 6-membered aza BIM derivatives (Sections ***4.4.1*** and ***4.4.2***), it can be concluded that the success of this type of cyclocondensation reaction is also highly dependent on the nature of substituents of the oxopropanoate precursor. For instance, it was found that where two 7-azaindolyl substituents (***Scheme 4.40***) or a 3,4,5-trimethoxyphenyl and 7-azaindolyl substituent (***Scheme 4.41***) were employed in reaction with guanidine or thiourea, the corresponding pyrimidinone and thiouracil derivatives were not afforded. However, it was possible to fashion pyrimidinone **232** from oxopropanoate **267**, giving rise to optimism towards future elaboration of this synthetic route in the development of novel aza BIM and aza ICZ derivatives.

4.5 Synthetic routes towards novel azaindolocarbazoles

Given the wealth of literature that exists in relation to the synthesis of ICZs, it is somewhat surprising that comparatively little focus has been paid towards azaindolocarbazoles, especially given how the replacement of one or more benzenoid rings with a pyridine moiety has been shown to confer unique biological selectivity in a number of cases (Section *1.3.2.3*).[17,18]

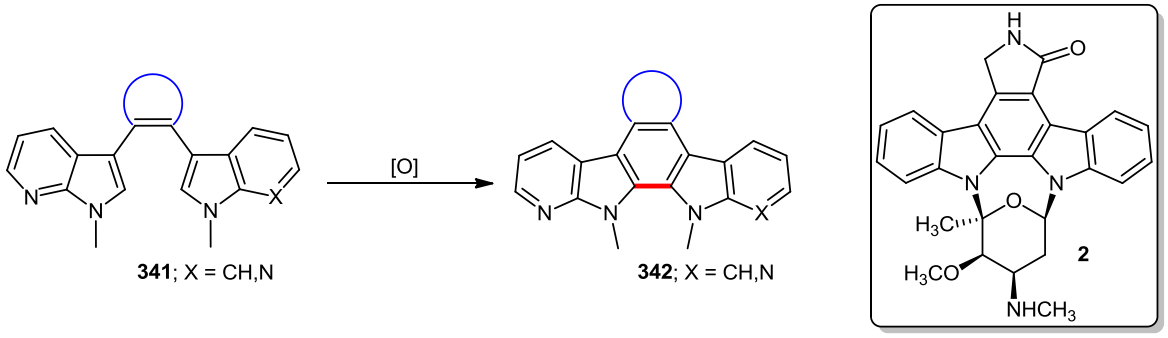

Scheme 4.42 *Aromatisation of aza BIM analogues of general structure* ***341*** *to aza ICZ* ***342***

Having previously accessed a wide number of aza BIM derivatives (Sections **4.3** and **4.4**), our ultimate aim was to examine the formation of the central C-C bond towards novel aza ICZs of general structure **342** with both 5- and 6-membered heterocyclic headgroups, thus continuing the medicinal chemistry effort in the development of chemotherapeutic agents based on the lead compound in the class, staurosporine **2** (***Scheme 4.42***). It has been well documented within the literature that ICZs often display more potent biological activity than their bisindolyl precursors.[19] For example, Sanchez-Martinez *et al*. detailed how a series of indolo[2,3-*a*]pyrrolo[3,4-*c*]carbazoles consistently showed greater inhibition towards CDK2 and CDK4 compared with their corresponding BIMs.[20]

4.5.1 Accessing aza ICZs via 6-membered aza BIM derivatives

The initial intention of our efforts in the synthesis of novel aza ICZs involved the aromatisation of 6-membered heterocyclic bioisosteres of the BIM pharmacophore by photocyclisation or other means (***Scheme 4.43***). However, as previously detailed (Section **4.4**), cyclocondensation methodology towards aza BIM derivatives of general structure **343**

proved to be unreliable, with pyrimidinone **332** the only compound successfully synthesised and isolated in this class of compounds.

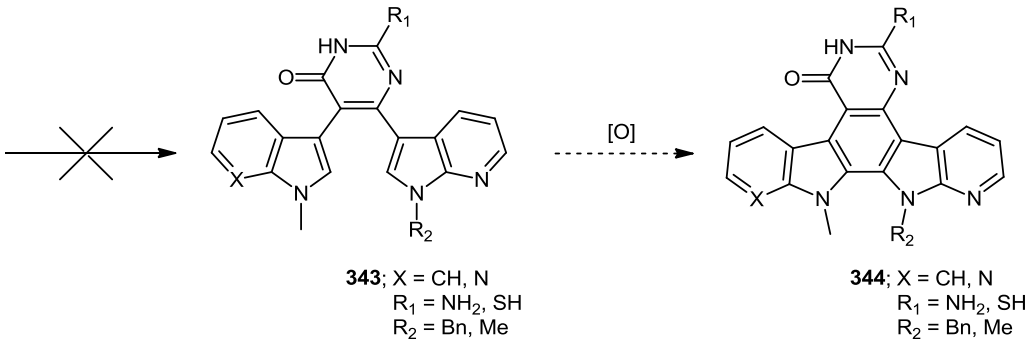

Scheme 4.43 *Envisaged route to aza ICZs with 6-membered F-rings*

Aromatisation of pyrimidinone **332** was completed by photochemical means with U.V. light and a catalytic amount of molecular iodine, thus forming the first aza ICZ with a 6-membered F-ring, derivative **239** (***Scheme 4.44***).

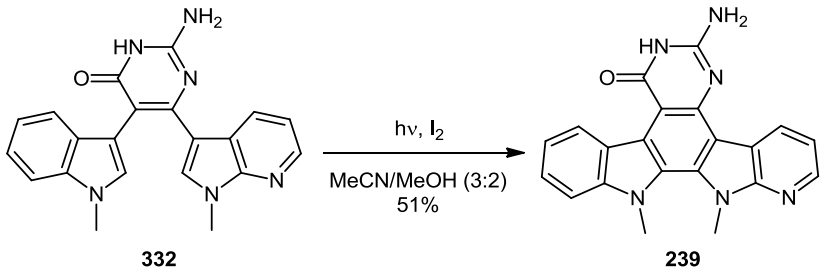

Scheme 4.44 *Synthesis of aza ICZ **239** from pyrimidinone **332***

Application of UV light to the stirred reaction mixture was achieved using a medium pressure mercury lamp. Optimisation of reaction conditions found that the highest yield of product was obtained by employing a solvent system of acetonitrile/methanol (3:2), with a high dilution factor of 0.08 g per 200 mL. The highly-conjugated aza ICZ product **239** was subsequently purified by flash column chromatography (1% methanol in ethyl acetate) as an off-white solid in a yield of 51%.

The increase in conjugation upon aromatisation of pyrimidinone **332** to aza ICZ **239** is accompanied by a significant deshielding effect on the ^{1}H NMR spectrum of **239**. As can be seen by direct comparison in ***Table 4.1***, all of the aromatic protons of aza ICZ **239** are more

deshielded than in precursor **332**. The effect is most pronounced on the C-H_4 and C-$H_{4'}$ protons of pyrimidinone **332**, which are shifted from a doublet at 7.48 ppm to 9.72 ppm and a doublet of doublets at 8.64 ppm to 9.27 ppm respectively, upon aromatisation to aza ICZ **239**. Formation of the central C-C bond of the azaindolocarbazole structure is also confirmed by the disappearance of the C-H_2 and C-$H_{2'}$ proton signals in the spectrum of **239**.

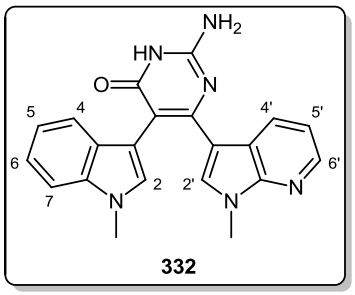

332

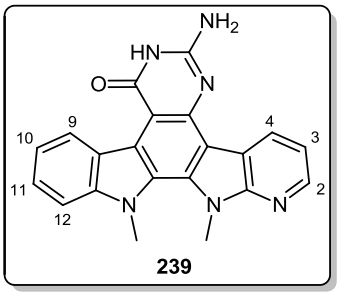

239

332	C-H_4	C-$H_{4'}$	C-H_5	C-$H_{5'}$	C-H_6	C-$H_{6'}$	C-H_7
	7.48 (1H, d)	8.64 (1H, dd)	6.85-6.89 (2H, m)	7.02-7.15 (3H, m)	7.02-7.15 (3H, m)	8.24 (1H, dd)	7.02-7.15 (3H, m)
239	C-H_9	C-H_4	C-H_{10}	C-H_3	C-H_{11}	C-H_2	C-H_{12}
	9.72 (1H, d)	9.27 (1H, dd)	7.23 (1H, t)	7.38 (1H, q)	7.50 (1H, t)	8.54 (1H, dd)	7.67 (1H, d)

Table 4.1 *Comparison of aromatic ^{1}H NMR chemical shifts (ppm) between pyrimidinone **33** and aza ICZ **239** (DMSO-d_6, 300 MHz)*

4.5.2 Attempted aromatisation of 5-membered aza BIM derivatives

Having successfully effectuated the aromatisation of 6-membered aza BIM derivative **332** towards aza ICZ **239** (Section ***4.5.1***), the synthesis of other novel aza ICZs from previously formed 5-membered aza BIM derivatives (Sections ***4.3.3*** and ***4.3.4***) was then examined. With aminopyrazole **318** proving more soluble than pyrimidinone **332**, acetonitrile was the sole solvent initially employed in the attempted photocyclisation towards aza ICZ **345** (***Scheme 4.45***). However, following application of UV light and the presence of a catalytic amount of

iodine, anticipated product **345** was not formed after 16 hours. The same solvent system (acetonitrile/methanol, 3:2) to that previously used in the synthesis of aza ICZ **239** (Section ***4.5.1***) was then used under similar photochemical conditions, but once more the desired aza ICZ **345** was not afforded, even when the reaction time was extended to 36 hours.

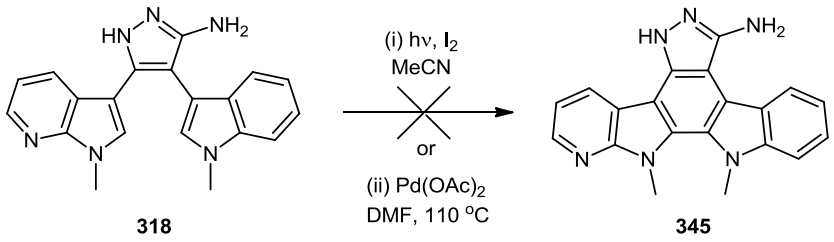

Scheme 4.45 *Attempted synthesis of aza ICZ **345** from aminopyrazole **318***

Another method to effect the central C-C bond formation towards aza ICZ **345** was then attempted by means of Pd(II)-mediated oxidation (***Scheme 4.45***). Palladium(II) acetate, a well-known mediator of this type of reaction, was added to a stirred solution of aminopyrazole **318** in anhydrous DMF, which was then heated to 110 ^{o}C for 20 hours. However, this alternative strategy once again failed to yield aza ICZ **345**, with only starting material recovered from the reaction.

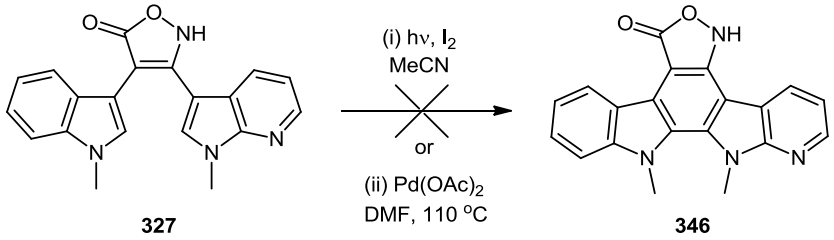

Scheme 4.46 *Attempted synthesis of aza ICZ **346** from isoxazolone **327***

Both photochemical cyclisation and Pd(II)-mediated oxidation methodology was also used in the attempted synthesis of aza ICZ **346** from isoxazolone **327** (***Scheme 4.46***). In the same manner as previously seen with aminopyrazole **318** (***Scheme 4.45***), the application of either chemical route once again failed to form desired aza ICZ **346**, with only the presence of starting material detected in either case. This is not unexpected due to limited literature precedent in the case where both indolic nitrogens are alkylated, and as such, perhaps removal of the methyl groups is key to a more successful outcome.

4.5.3 Further routes to aza ICZ precursors: accessing azaindolylmaleimides

Examining our effort towards the formation of novel aza ICZs, it was clear that accessibility was hindered in two key areas: (i) the cyclocondensation methodology used to synthesise these BIM derivatives proved too unreliable to allow for the establishment of a library of such compounds (Section **4.4**), and (ii) the nature of the precursor's headgroup/indolic substituent is essential for the formation of the central C-C bond, with heterocycles such as aminopyrazoles and isoxazolones proving ineffective in this regard (Section ***4.5.2***). As a result, a more robust synthetic strategy was required.

It has previously been shown by both Prudhomme and Routier (and indeed in the general ICZ class) that aromatisation towards aza ICZs can be carried out using precursors containing a dione moiety, such as azaindolylmaleimide or azaindolylmaleic anhydrides.[21,22] It was therefore posited that a series of aza ICZs of general structure **348** could be accessed from dione precursors **347**, with subsequent F-ring modification allowing for the synthesis of a range of both 5- and 6-membered aza ICZs (***Scheme 4.47***).

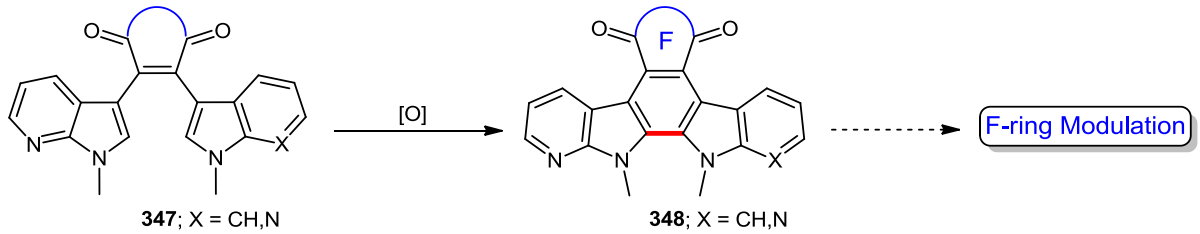

Scheme 4.47 *Aromatisation of dione precursor **347** to aza ICZ **348** with subsequent F-ring modification*

To date, the primary synthetic means utilised in this field of chemistry towards the formation of monoazaindolylmaleimide or bisazaindolylmaleimide precursors of aza ICZs has involved the coupling of 7-azaindoles with dibromomaleimide subunits, which can often lead to problems with regiospecificity (Section **2.2**). As a result, we sought to examine a novel mode of accession towards aza ICZ precursors such as **347**.

4.5.3.1 Synthesis of monoazaindolyl maleimide precursors

The Perkin-type condensation of indolyl-3-acetic acids with indolyl-3-glyoxyl chlorides in the presence of base, such as triethylamine, has previously been documented in the attainment of bisindolylmaleic anhydrides, such as by Gribble *et al*. in the synthesis of ICZs such as **353** (***Scheme 4.48***).[23] Anhydride **351** is converted to maleimide **352** using hexamethyldisilazane, which then undergoes Pd(II)-mediated oxidative cyclisation towards ICZ **353**, with the final transformation carried out in poor yield of 8% while requiring five equivalents of $Pd(CF_3CO_2)_2$ catalyst. This again shows the apparent influence of indolic alkyl substituents on this transformation, and their role in hindering aromatisation.

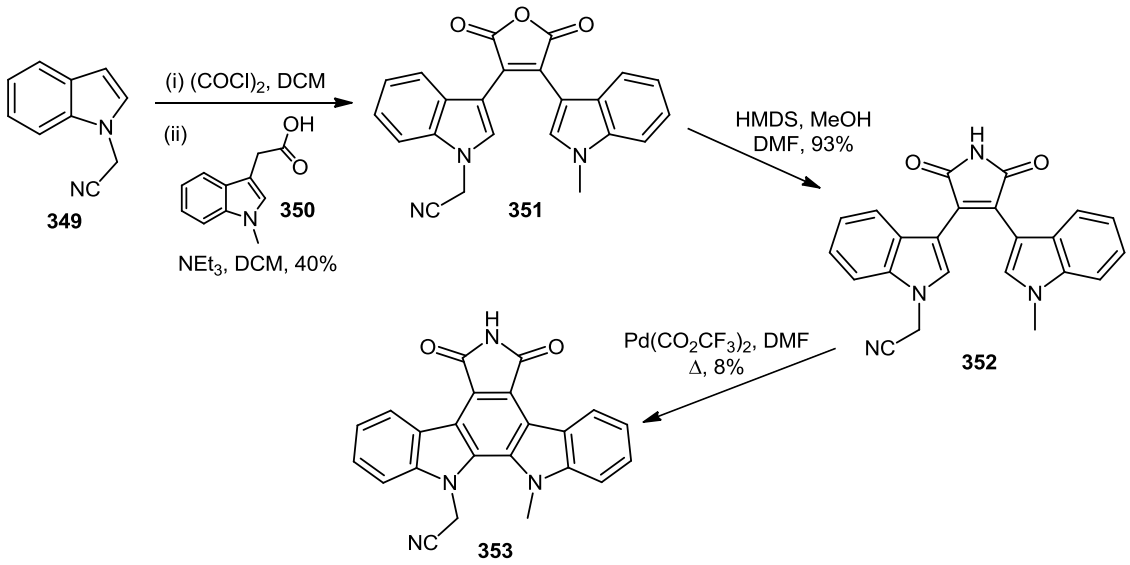

Scheme 4.48 *Route to ICZ **353** via maleic anhydride **351** and maleimide **352***[23]

The application of this Perkin-type condensation methodology towards the synthesis of novel maleic anhydride **355** proved to be a relatively straightforward accomplishment (***Scheme 4.49***). Initially, *N*-methyl indole-3-acetic acid **350** was formed by treatment of indole-3-acetic acid **261** with sodium hydride and methyl iodide in THF, with acid **350** formed as a light brown solid in 84% yield. Separately, a stirred solution of *N*-methyl-7-azaindole **277** in diethyl ether at 0 ^{o}C was treated with oxalyl chloride. After stirring at room temperature over 3 hours, glyoxyl chloride **354** was isolated as an off-white solid in quantitative yield following solvent evaporation under reduced pressure.

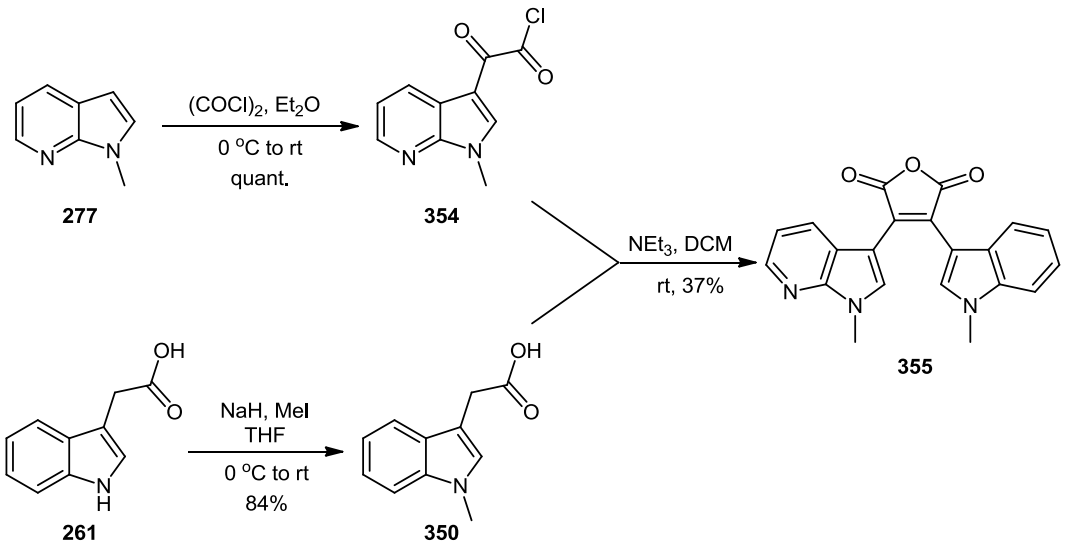

Scheme 4.49 *Synthesis of maleic anhydride* ***355*** *via Perkin-type condensation*

Glyoxyl chloride **354** was then added to a stirred solution containing *N*-methyl indole-3-acetic acid **350** and triethylamine in DCM, with the resulting reaction mixture being allowed to stir for 14 hours at room temperature. Isolation of maleic anhydride **355** as a bright red solid in 37% yield from the crude reaction residue was achieved by flash column chromatography (30% ethyl acetate in hexane) (***Scheme 4.49***).

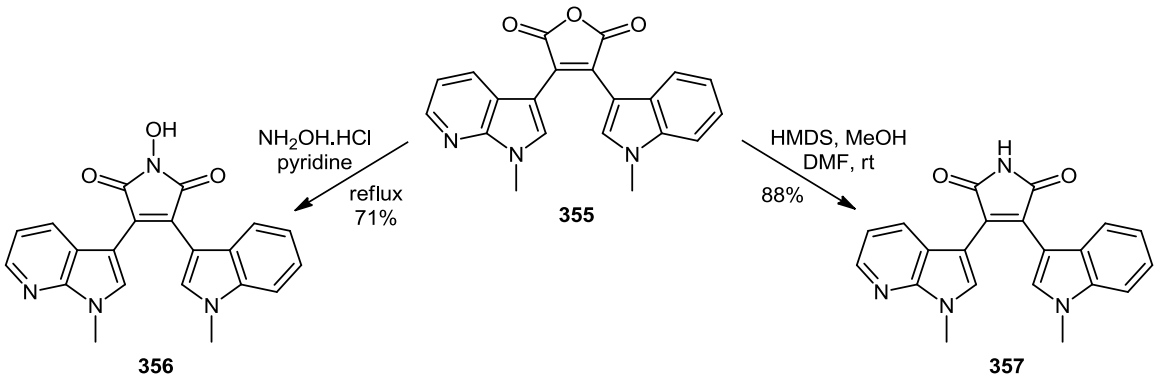

Scheme 4.50 *Synthesis of* N*-hydroxy maleimide* ***356*** *and maleimide* ***357***

Treatment of a solution of maleic anhydride **355** in dry pyridine with hydroxylammonium chloride under reflux conditions led to the formation of *N*-hydroxyl maleimide **356** as a red solid in 71% yield, following purification by column chromatography (hexane/ethyl acetate, 50:50) (***Scheme 4.50***). Conversion of maleic anhydride **355** to maleimide **357** occurred in

excellent yield of 88%. A solution of anhydride **355** in DMF was treated with 10 equivalents of hexamethyldisilazane, followed by 5 equivalents of methanol, with the resulting reaction mixture then being allowed to stir at room temperature for 24 hours. Following purification by column chromatography (hexane/ethyl acetate, 50:50), the highly-conjugated product, maleimide **357**, was isolated as a brilliant red solid.

4.5.3.2 Synthesis of bis(7-azaindol-3-yl)maleimide precursors

The synthesis of bis(7-azaindol-3-yl)maleic anhydride **358** was attempted using a similar methodology to that used in the synthesis of maleic anhydride **355** (***Scheme 4.49***). Glyoxyl chloride **354** was added to a stirred solution of acetic acid **279** (Section ***4.2.6***) and triethylamine in DCM, with the resulting mixture then allowed to stir for 14 hours at room temperature (***Scheme 4.51***). However, anhydride **358** was not formed, with only starting material recovered from the crude reaction residue. Likewise, heating the reaction mixture did not result in desired product formation. This indicated the relatively unreactive nature of *N*-methyl 7-azaindolyl-3-acetic acid **279** in comparison with its indolyl analogue **350**.

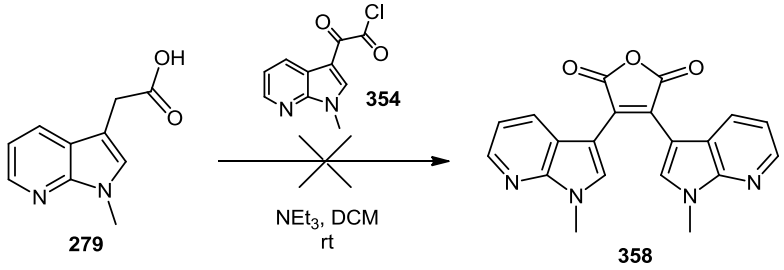

Scheme 4.51 *Attempted synthesis of maleic anhydride **358***

A different variation of the Perkin-type reaction towards anhydride **358** was then employed (***Scheme 4.52***). A solution of glyoxylate **278** (Section ***4.2.6***) in ethanol was treated with one equivalent of potassium hydroxide, with the resulting mixture stirred at room temperature for 4 hours. Following evaporation of the solvent and desiccation overnight at 50 ^{o}C, potassium salt **359** was isolated as a white solid in quantitative yield. A mixture of acetic acid **279** and potassium salt **359** in acetic anhydride was then heated to 130 ^{o}C for 4 hours. Pure maleic anhydride **358** was isolated by column chromatography (40% hexane in ethyl acetate) as a dark red solid in 45% yield.

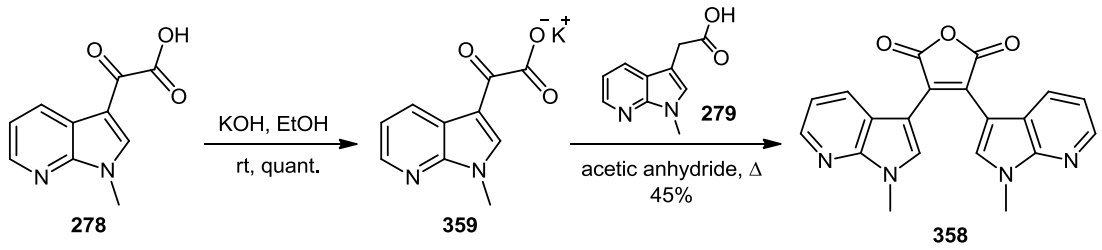

Scheme 4.52 *Route to anhydride* ***358*** *from glyoxylate* ***278***

Due to the symmetry of anhydride **358**, only half the number of signals arises in both the ^{1}H and ^{13}C NMR spectra of the compound. For example, in the ^{1}H NMR spectrum (***Figure 4.10***), both methyl groups give rise to one singlet at 3.90 ppm.

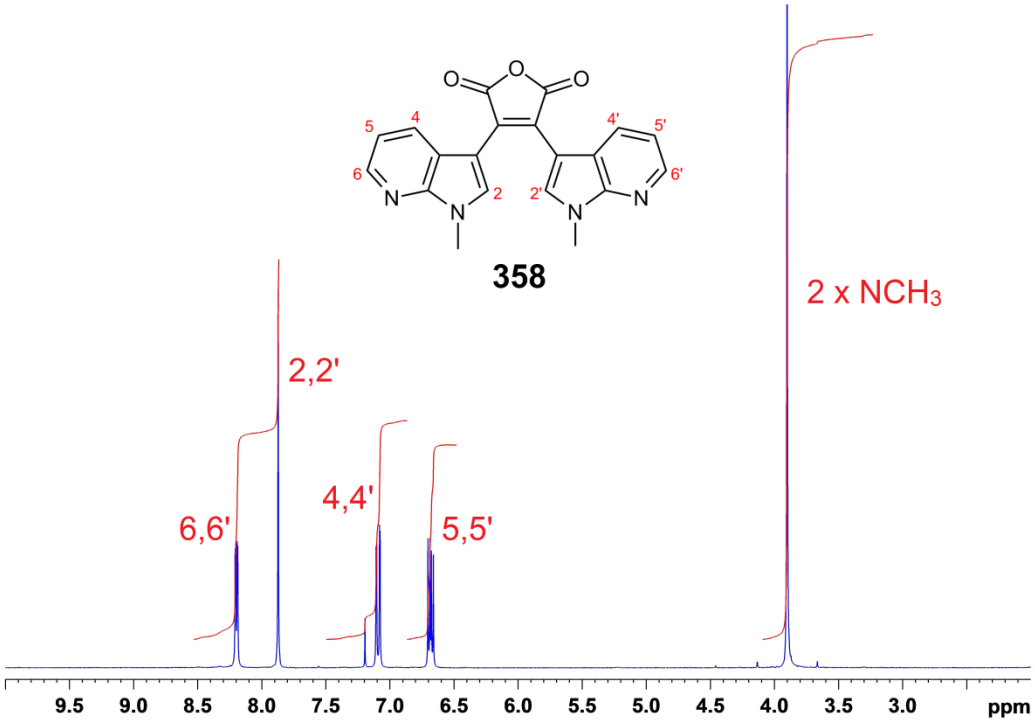

Fig. 4.10 *^{1}H NMR spectrum of maleic anhydride* ***358*** *($CDCl_3$, 300 MHz)*

The C-H_5 and C-$H_{5'}$ protons display a single quartet at 6.68 ppm, while the C-H_4 and C-$H_{4'}$ protons give rise to a doublet of doublets at 7.09 ppm. One singlet at 7.87 ppm is seen for the C-H_2 and C-$H_{2'}$ protons, leaving a doublet of doublets for the C-H_6 and C-$H_{6'}$ protons at 8.20 ppm (***Figure 4.10***).

Similar to its 3-(indol-3-yl)-4-(7-azaindol-3-yl) analogue **355** (Section *4.5.1.1*), anhydride **358** was readily converted to its *N*-hydroxy counterpart **360** by treatment with hydroxylammonium chloride in dry pyridine at reflux (***Scheme 4.53***). Following purification by column chromatography (30% hexane in ethyl acetate), *N*-hydroxy maleimide **360** was isolated as a red solid in 59% yield.

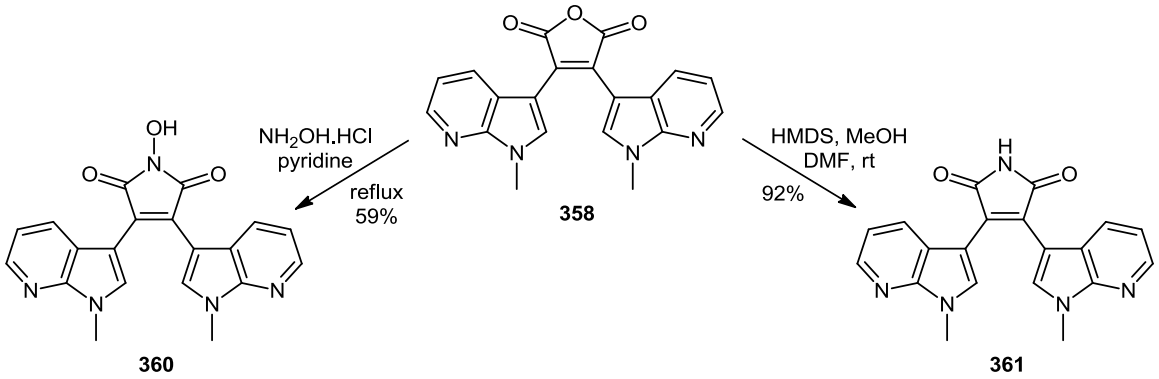

Scheme 4.53 *Synthesis of* N-*hydroxy maleimide* ***360*** *and maleimide* ***361***

Conversion of maleic anhydride **358** to maleimide **361** was achieved in excellent yield of 92%, following treatment of a solution of anhydride **358** in DMF at room temperature with hexamethyldisilazane, followed by methanol. Purification by column chromatography (20% hexane in ethyl acetate) afforded the highly-conjugated product as an orange-red solid.

4.5.4 Aromatisation studies towards monoaza ICZs and F-ring modulation

Initial attempts to effectuate the aromatisation of maleic anhydride **355** and *N*-hydroxy maleimide **356** (Section *4.5.3.1*) towards the respective aza ICZs **362** and **363** proved problematic (***Scheme 4.54***). Only the presence of starting material was detected in either case when both UV light and palladium(II) trifluoroactetate were engaged to mediate the cyclisation.

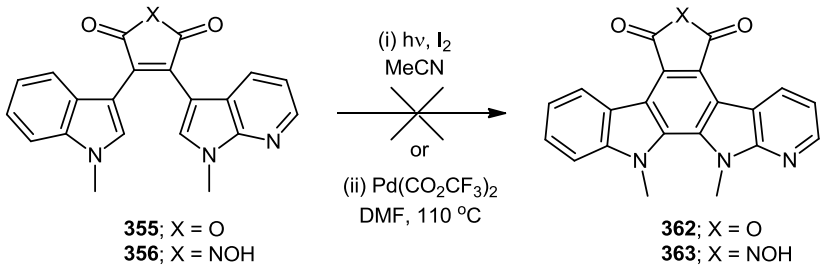

Scheme 4.54 *Attempted aromatisation of maleic anhydride **355** and N-hydroxymaleimide **356***

However, in the ensuing application of photochemical conditions to a solution of maleimide **357** and a catalytic amount of iodine in acetonitrile, it was found that formation of aza ICZ **364** occurred readily (***Scheme 4.55***). Optimisation of reaction conditions later allowed for the isolation of fully-aromatised product **364** in 81% yield.

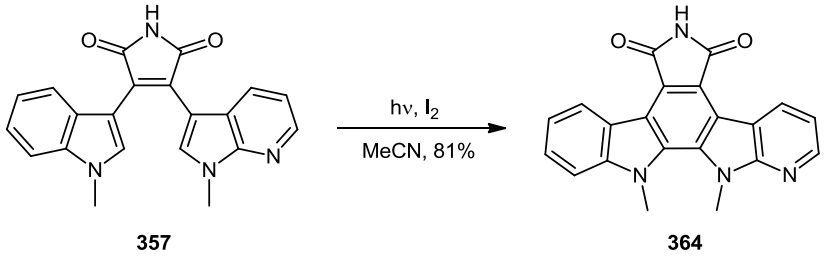

Scheme 4.55 *Cyclisation of maleimide **357** towards aza ICZ **364***

Prior to the elucidation of optimum reaction conditions, purification of aza ICZ **364** had proven extremely arduous, due to the co-elution of one or more side products under column chromatography, coupled with the sparing solubility of the compounds involved. Elimination of side product formation was subsequently achieved by increasing the dilution factor of the reaction mixture from 100 mg/150 mL of maleimide **357** in acetonitrile to 100 mg/300 mL. Addition of a saturated solution of aqueous sodium thiosulfate during workup resulted in the

precipitation of a brilliant yellow solid from the biphasic mixture. Following filtration, copious water washes and thorough desiccation, analysis of the solid revealed that aza ICZ **364** had been formed in high purity (***Figure 4.11***).

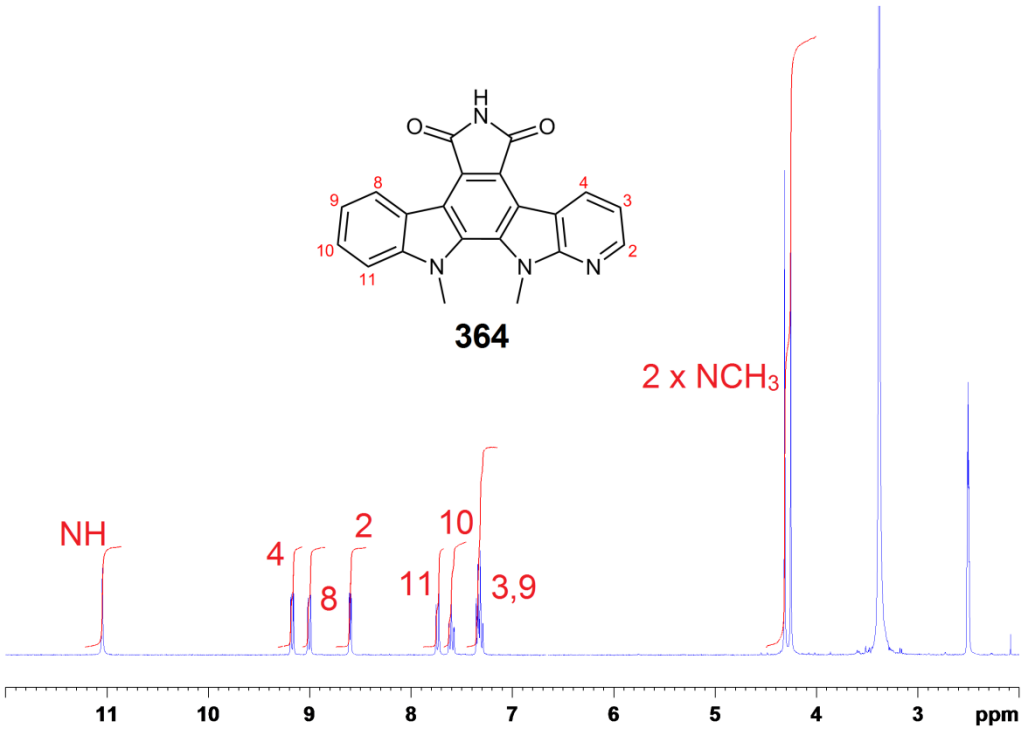

Fig. 4.11 *^{1}H NMR spectrum of aza ICZ **364** (DMSO-d$_6$, 300 MHz)*

Upon complete characterisation of aza ICZ **364**, it was possible to gain greater insight into the previous side product formation. As well as the expected molecular ion peak at 355 m/z appearing in mass spectra of the impure **364**, a peak also arose at 357 m/z, potentially corresponding to the starting material, maleimide **357**. However, from TLC analysis it was clear that no more starting material remained, which was further confirmed by NMR spectrometry. Although unable to isolate and definitively assign the side products formed within the reaction, a number of distinguishable peaks could be identified in the ^{1}H NMR spectrum (***Figure 4.12***).

Of the identifiable peaks within the spectrum, those which are worthy of immediate attention include the multiplet at 5.63 ppm and the two doublets at 6.62 and 6.64 ppm (J = 5.1 Hz for

both). That which initially appears to be a doublet at 2.73 ppm can actually be assigned as a pair of singlets at 2.72 and 2.74 ppm.

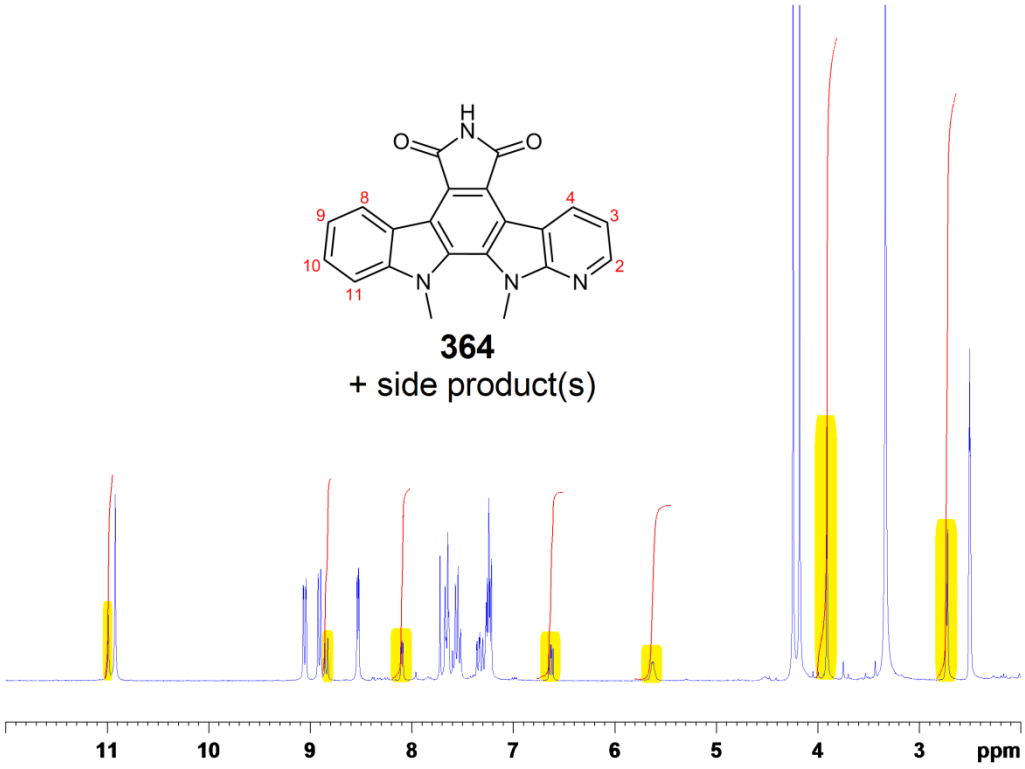

Fig. 4.12 *^{1}H NMR spectrum of aza ICZ **364** with distinguishable signals of side product(s) highlighted in yellow (DMSO-d_6, 300 MHz)*

Examining the aromatisation of maleimide **357**, it is likely that the reaction proceeds through dihydro intermediate **365** before conversion to the final product, aza ICZ **364** (***Scheme 4.56***). However, it is unlikely that reaction intermediate **365** is the side product contained in the impure sample of **364**, as there ought to be two distinct singlets in close proximity occurring near 4 ppm due to the two sets of methyl protons. Instead there is one singlet at 3.91 ppm, which integrates for the combined singlets at 2.72 and 2.74 ppm, leading to the conclusion that the protons for one of the methyl groups have become significantly more shielded.

It is possible that the shielding effect experienced by one of the methyl groups occurs due to a loss of conjugation, brought about by a [1,5] sigmatropic shift of dihydro intermediate **365** to give *cis* **366** and *trans* **367** side products. Coupling between the *cis* and *trans* protons in either

of the two proposed side products **366** and **367** can then account for the multiplet 5.63 ppm and the two doublets at 6.62 and 6.64 ppm.

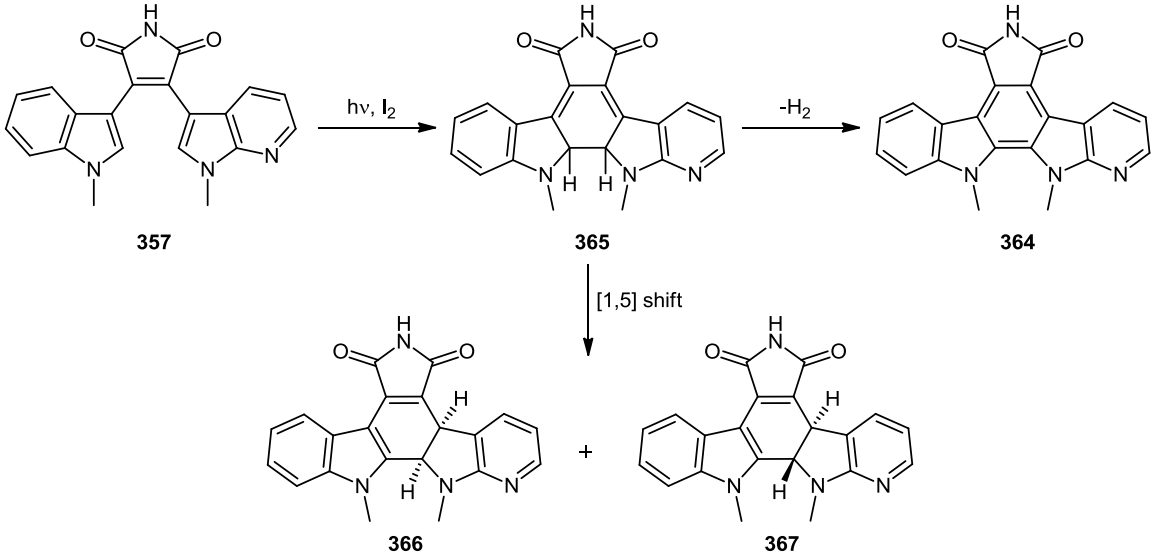

Scheme 4.56 *Formation of possible side products* ***366*** *and* ***367*** *of aza ICZ* ***364***

With insufficient dilution of the reaction mixture, precipitation of intermediary products such as **365** can occur, thus introducing the possibility of a [1,5] sigmatropic shift towards sideproducts **366** and **367**. A doubling of the dilution factor ensured that no precipitation of reaction intermediates occurred under exposure to UV light, therefore allowing for the formation of aza ICZ **364** in high yield of 81%.

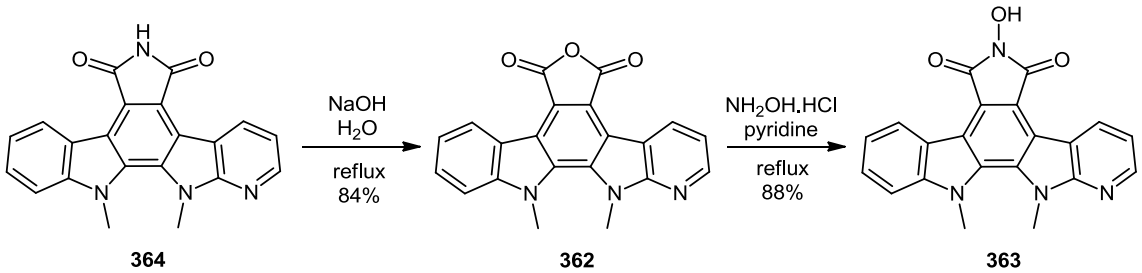

Scheme 4.57 *Formation of* N*-hydroxymaleimide* ***363*** *from maleimide* ***364*** *via maleic anhydride* ***362***

The base-catalysed conversion of aza ICZ maleimide **364** to maleic anhydride **362** was carried out under reflux in a 2 M solution of aqueous sodium hydroxide for 14 hours (***Scheme 4.57***).

Once cooled to room temperature, dropwise treatment of the reaction mixture with an aqueous 2 M HCl solution lead to the precipitation of anhydride **362** as a yellow solid in 84% yield, which was subsequently used without further purification. A considerable shift of the carbonyl stretch was noted in the IR spectrum of anhydride **362** (1747 cm^{-1}) compared to maleimide precursor **364** (1719 cm^{-1}).

The synthesis of hydroxymaleimide **363** was afforded by the application of hydroxylammonium chloride to a mixture of anhydride **362** in pyridine under reflux conditions for 12 hours (***Scheme 4.57***). Recrystallisation from absolute ethanol gave hydroxymaleimide **363** as a yellow solid in 88% yield.

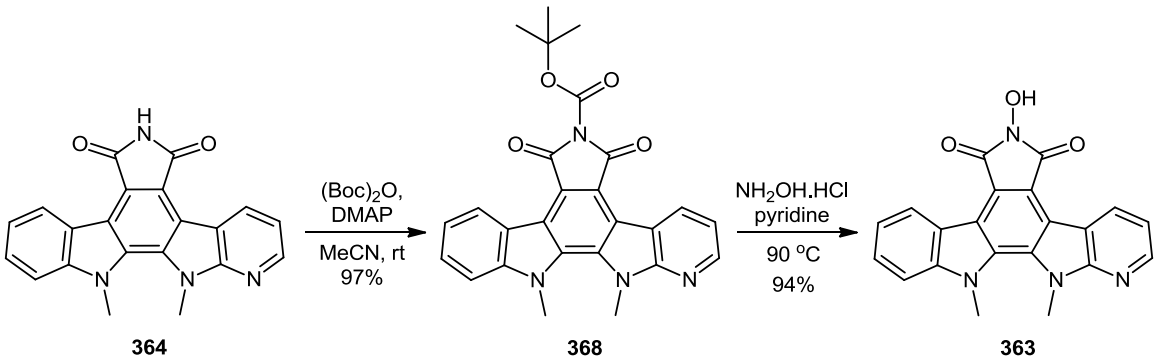

Scheme 4.58 *Alternative synthesis of* N-*hydroxymaleimide* ***363*** *via Boc-protected maleimide* ***368***

A more facile route towards hydroxymaleimide **363** was successfully undertaken via Boc-protected maleimide **368** (***Scheme 4.58***). A suspension of maleimide **364** in acetonitrile was treated with 2.2 equivalents of di-*tert*-butyl-dicarbonate (Boc anhydride) and then 0.1 equivalents of DMAP. After stirring at room temperature for 1 hour, removal of solvent under reduced pressure, followed by recrystallisation from ethanol, afforded Boc-protected maleimide **368** in excellent yield of 97%. In a similar manner to that previously seen (***Scheme 4.57***), formation of hydroxymaleimide **363** was achieved in 94% yield by heating a mixture of **368** and five equivalents of hydroxylammonium chloride in pyridine to 90 ^{o}C for 14 hours.

Seeking to expand the theme of F-ring modulation towards the synthesis of 6-membered heterocycles, a modified Lossen rearrangement involving the tosyl derivative of hydroxymaleimide **363** and hydrazine was examined (***Scheme 4.59***). Initially, tosyl chloride

was added to a solution of aza ICZ **363** and DMAP in pyridine and DMSO, with the resulting mixture allowed to stir for 4 hours at room temperature. The tosyl derivative of **363**, used without further purification, then underwent a modified Lossen rearrangement following reaction with hydrazine hydrate under reflux in ethanol. As a result, a mixture of regioisomers **369** and **370** was obtained, which proved inseparable by flash column chromatography. Employing preparative HPLC, the distance between the peaks of the two regioisomers was small and it was not possible to achieve sufficient purification of either regioisomer.

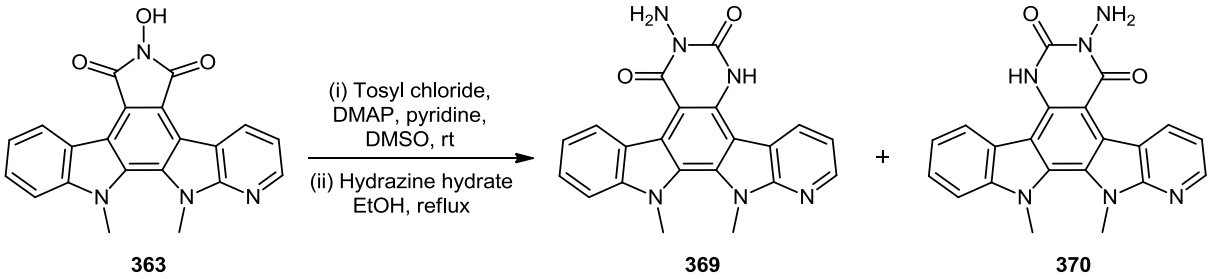

363 **369** **370**

Scheme 4.59 *Synthesis of aza ICZs* ***369*** *and* ***370*** *with 6-membered F-rings*

4.5.5 Aromatisation towards bisaza ICZ 373 *and F-ring modulation*

Employment of a similar synthetic methodology towards the development of bisaza ICZs to that applied in the monoaza series (Section ***4.5.4***) proved highly successful (***Scheme 4.60***).

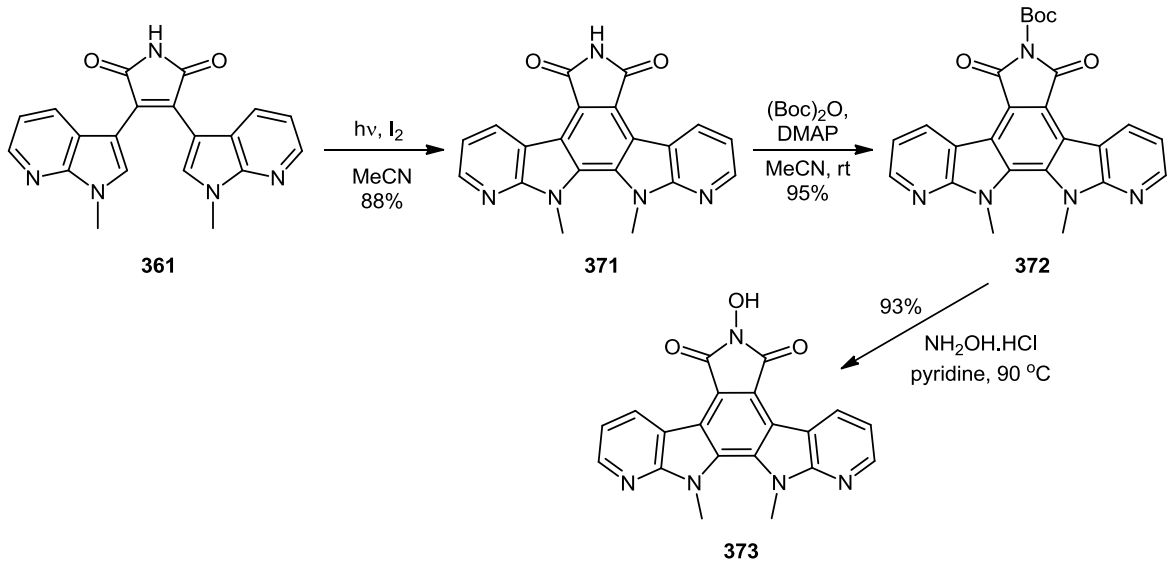

361 **371** **372** **373**

Scheme 4.60 *Synthesis of* N*-hydroxymaleimide aza ICZ* ***373*** *from maleimide* ***361***

Aromatisation of maleimide **361** to bisaza ICZ **371** was achieved in 88% yield (***Scheme 4.60***), greater than that obtained for its monoaza analogue **364** (***Scheme 4.55***). Following protection of maleimide **371** to Boc-derivative **372** in excellent yield of 95%, transformation to hydroxymaleimide **373** was achieved by reaction with hydroxylammonium chloride in pyridine, forming the desired product as a bright yellow solid in 93% yield.

Due to the symmetrical nature of hydroxymaleimide **373**, it was possible to effectuate the synthesis of aza ICZ **374** without the occurrence of regioisomers (***Scheme 4.61***). Following tosylation of **373** by treatment with tosyl chloride in the presence of DMAP and pyridine, reaction with hydrazine hydrate afforded aza ICZ **374**, containing a 6-membered F-ring, by means of a modified Lossen rearrangement. Purification by flash column chromatography (DCM/MeOH, 95:5) afforded aza ICZ **374** as an off-white solid in 44% yield.

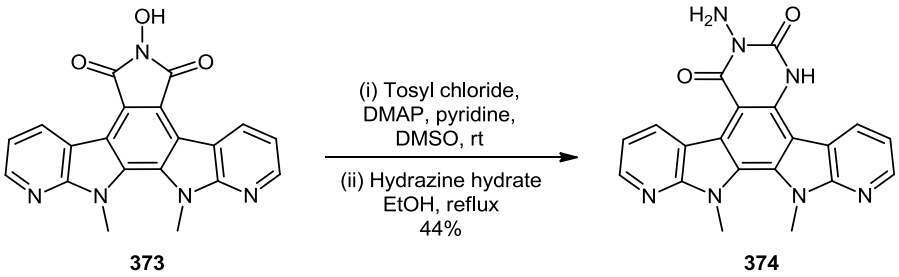

373 **374**

Scheme 4.61 Synthesis of aza ICZ **374** with 6-membered F-ring

4.6 Conclusion

The indolocarbazoles and their derivatives, such as the bisindolylmaleimides, offer enormous scope for the development of novel anticancer agents due to the profound nature in which they interact on a cellular level. Many synthetic routes towards the ICZs and the BIMs have been documented, predominantly since the 1980's. However, the azaindolocarbazole members of the ICZ family have been far less frequently researched - surprisingly so, given the excellent biological selectivity profiles that have been described for a number of derivatives. Hence, the aim of this project was to devise and implement novel synthetic routes towards aza ICZ and aza BIM derivatives, and to examine the paradigm of F-ring modulation as a means of potentiating anticancer activity.

Retrosynthetic analysis identified a series of oxopropanoate and oxopropanenitrile derivatives as key intermediates towards the development of aza BIM, and ultimately aza ICZ, targets of clinical interest. To this end, initial difficulties were encountered in the synthesis of oxopropanoate **267**, with only starting material or the self-condensation product **268** of ester **250** recovered from the reaction. However, following thorough examination of the experimental parameters, it was found that increasing the reaction temperature to 35 ^{o}C upon final addition of acyl chloride **266** allowed for the successful formation of desired product **267**. Further application of this methodology allowed for the synthesis of a range of analogous oxopropanoate and oxopropanenitrile intermediates.

Condensation of oxopropanenitrile intermediates **276**, **287** and **289** with hydrazine resulted in the formation of a series of 5-aminopyrazoles. These heterocyclic targets were to show excellent promise both as novel bioisosteres of the BIM core and also for their versatility in subsequent derivatisation studies, thus propagating the theme of F-ring modulation. Reaction of 5-aminopyrazoles **293**, **312** and **318** with bidentate electrophiles such as *N*-chlorocarbonyl isocyanate or hexafluoroacetylacetone afforded novel bicyclic triazinedione and pyrimidine systems respectively, while reaction with monodentate electrophiles led to a series of derivatives which were substituted either on the exocyclic amine or one of the ring nitrogens.[24]

The synthesis of 6-membered BIM analogues from oxopropanoates **267**, **273**, **281** and **292** was found to be significantly more challenging, with pyrimidinone **332** the only derivative to be successfully synthesised and purified. It is thought that the nature of the cyclocondensation reaction is dependent on the reactivity of nucleophiles such as guanidine and thiouracil, and also on the substituents of the oxopropanate electrophiles.

Aromatisation of pyrimidinone **332** under photochemical conditions led to the successful synthesis of the first aza ICZ **239** with a 6-membered F-ring to be described in the literature.[25] Subsequent attempts to effectuate similar cyclisations of aminopyrazole **318** and isoxazolone **327** did not achieve the desired result, perhaps due to the nature of the 5-membered F-rings or the alkyl substituents on the indolic nitrogens. Consequently, it was posited that greater success would be met in derivatisation of the F-ring after aromatisation had occurred. Maleimides **357** and **361** were found to readily undergo aromatisation towards derivatives **364** and **371**, and from these novel aza ICZs, it was possible to achieve desired F-ring modulation towards such highly promising candidates as hydroxymaleimides **363** and **373**, as well as aza ICZ **374** containing a 6-membered F-ring.

4.7 References

1. Braňa, M.F.; Gradillas, A.; Ovalles, A.G.; López, B.; Acero, N.; Llinares, F.; Muñoz Mingarro, D. *Bioorg. Med. Chem.* **2006**, 14, 9-16
2. Pierce, L.T. *PhD Thesis* **2011**
3. Pierce, L.T.; Cahill, M.M.; McCarthy, F.O. *Tetrahedron* **2010**, 66, 9754-9761
4. Popowycz, F.; Routier, S.; Joseph, B.; Mérour, J.-Y. *Tetrahedron* **2007**, 63, 1031-1064
5. O'Neill, D.J.; Shen, L.; Prouty, C.; Conway, B.R.; Westover, L.; Xu, J.Z.; Zhang, H.-C.; Maryanoff, B.E.; Murray, W.V.; Demarest, K.T.; Kuo, G.-H. *Bioorg. Med. Chem.* **2004**, 12, 3167-3185
6. Allegretti, M; Anacardio, R.; Candida Cesta, M.; Curti, R.; Mantovanini, M.; Nano, G.; Topai, A.; Zampella, G. *Org. Process Res. Dev.* **2003**, 7, 209-213
7. Jiang, X.; Tiwari, A.; Thompson, M.; Chen, Z.; Cleary, T.P.; Lee, T.B.K. *Org. Process Res. Dev.* **2001**, 5, 604-608
8. Peifer, C.; Selig, R.; Kinkel, K.; Ott, D.; Totzke, F.; Schächtele, C.; Heidenreich, R.; Röcken, M.; Schollmeyer, D.; Laufer, S. *J. Med. Chem.* **2008**, 51, 3814-3824
9. Peifer, C.; Krasowski, A.; Hämmerle, N.; Kohlbacher, O.; Dannhardt, G.; Totzke, F.; Schächtele, C.; Laufer, S. *J. Med. Chem.* **2006**, 49, 7549-7553
10. Friebolin, H. *Basic One- and Two-Dimensional NMR Spectroscopy* **2011**, 5th Edition, Wiley-VCH
11. Puello, J.Q.; Obando, B.I.; Foces-Foces, C.; Infantes, L.; Claramunt, R.M.; Jiménez, J.A.; Elguero, J. *Tetrahedron* **1997**, 53, 10783-10802
12. Michon, V.; Hervé du Penhoat, C.; Tombret, F.; Gillardin, J.M.; Lepage, F.; Berthon, L. *Eur. J. Med. Chem.* **2005**, 30, 147-155
13. Anwar, H.F.; Elnagdi, M.H. *ARKIVOC* **2009**, (*i*), 198-250
14. Nie, Z.; Perretta, C.; Erickson, P.; Margosiak, S.; Almassy, R.; Lu, J.; Averill, A.; Yagger, K.M.; Chu, S. *Bioorg. Med. Chem. Lett.* **2007**, 17, 4191-4195
15. Elkholy, A.; Al-Qalaf, F.; Elnagdi, M.H. *ARKIVOC* **2008**, (*xiv*), 124-131
16. Saito, T.; Obitsu, T.; Kondo, T.; Matsui, T.; Nagao, Y.; Kusumi, K.; Matsumura, N.; Ueno, S.; Kishi, A.; Katsumata, S.; Kagamiishi, Y.; Nakai, H.; Toda, M. *Bioorg. Med. Chem.* **2011**, 19, 5432-5445
17. Marminon, C.; Pierré, A.; Pfeiffer, B.; Pérez, V.; Léonce, S.; Joubert, A.; Bailly, C.; Renard, P.; Hickman, J.; Prudhomme, M. *J. Med. Chem.* **2003**, 46, 609-622
18. Marminon, C.; Pierré, A.; Pfeiffer, B.; Pérez, V.; Léonce, S.; Renard, P.; Prudhomme, M. *Bioorg. Med. Chem.* **2003**, 11, 679-687
19. Sánchez, C.; Méndez, C.; Salas, J.A. *Nat. Prod. Rep.* **2006**, 23, 1007-1045
20. Sanchez-Martinez, C.; Shih, C.; Zhu, G.; Li, T.; Brooks, H.B.; Patel, B.K.R.; Schultz, R.M.; DeHahn, T.B.; Spencer, C.D.; Watkins, S.A.; Ogg, C.A.; Considine, E.; Dempsey, J.A.; Zhang, F. *Bioorg. Med. Chem. Lett.* **2003**, 3841-3846
21. Routier, S.; Coudert, G.; Mérour, J.-Y.; Caignard, D.H. *Tetrahedron Lett.* **2002**, 43, 2561-2564
22. Marminon, C.; Pierré, A.; Pfeiffer, B.; Pérez, V.; Léonce, S.; Joubert, A.; Bailly, C.; Renard, P.; Hickman, J.; Prudhomme, M. *J. Med. Chem.* **2003**, 46, 609-622

23. Roy, S.; Eastman, A.; Gribble, G. *Tetrahedron* **2006**, 62, 7838-7845
24. Pierce, L.T.; Cahill, M.M.; McCarthy, F.O. *Tetrahedron* **2011**, 67, 4601-4611
25. Pierce, L.T.; Cahill, M.M.; Winfield, H.W.; McCarthy, F.O. *Eur. J. Med. Chem.* **2012**, 56, 292-300

Chapter 5

Biological Results and Discussion

Contents

5.0 Biological Results and Discussion

The aim of this project was to synthesise and evaluate novel azaindolocarbazole (aza ICZ) derivatives, a highly promising and underexploited class of compounds in the field of anticancer chemotherapy. Having generated a chemical library containing over 50 novel compounds, the biological profiling of potential candidates was imperative in order to exploit molecular targets associated with anticancer mechanisms. Considering the diverse chemical nature of the indolocarbazole family and associated derivatives, it is unsurprising that a vast array of biological modes of action have been associated with different members within the class. For example, concomitant to its potent antitumour activity (Section *1.3.2.2*), rebeccamycin **3** has also been shown to exert antibacterial activity.[1] Antifungal activity has been demonstrated by a number of staurosporine **2** analogues, such as RK-286C **375**, which is also a protein kinase C (PKC) inhibitor.[2] The antiviral properties of a number of members of the class have also been noted within the literature, such as in the case of the bisindole pyrrole, lycogarubin C **376**, which was shown in 1994 by Asakawa and co-workers to have moderate activity against the HSV-1 virus.[3]

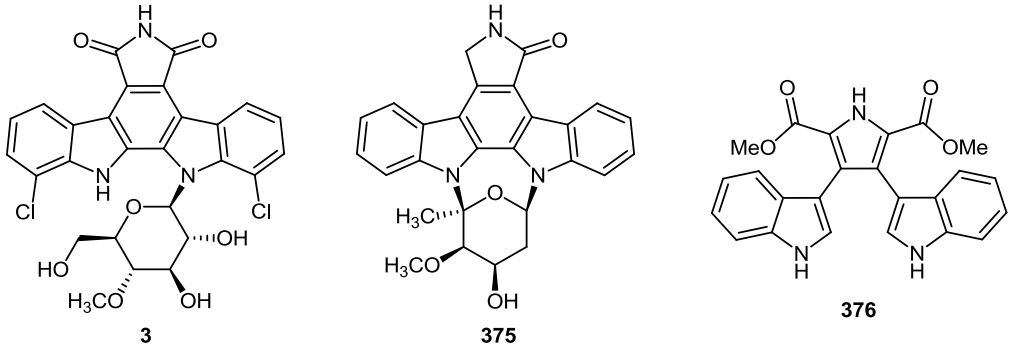

Fig. 5.1 *Structures of REB **3**, RK-286C **375** and lycogarubin C **376***

The anticancer action of ICZs, however, has been the most widely investigated and reported bioactive mechanism associated with this class of compounds.[4-7] Potent cytotoxic and antitumour properties have been documented for numerous ICZ and BIM derivatives, primarily occurring via inhibition of eukaryotic DNA topoisomerase I (topo I) or by protein kinase inhibition (Section **1.3**).[8] Given the vast importance of cancer research in modern society (Section **1.1**), it is upon this area that we will focus the evaluation of our panel of

novel aza ICZ derivatives. Aiming to realise and exploit suitable biological targets associated with such *in vivo* activity, initial testing involved screening against the NCI 60 cell panel, along with DNA topological assays.

5.1 NCI-60 cell screen

Potential candidates from our library of novel aza ICZ and aza BIM derivatives were initially tested against the US National Cancer Institute 60 human tumour cell line panel (NCI-60). Developed in the late 1980's as an *in vitro* drug-discovery tool, it was intended that the NCI-60 panel be used to identify compounds with growth-inhibitory or toxic effects on particular types of tumour.[9] However, it quickly became clear that much additional biological information could be provided by this screening model. The formation of distinctive patterns corresponding to differential sensitivities of the cell lines to particular compounds was found to occur, which could then be correlated to similar mechanisms of cell growth inhibition. As a result of these observations, Paull and co-workers were able to develop the COMPARE algorithm, which can be used to help predict the biological mechanisms by which potential chemotherapeutic candidates exert their activity.[10]

Within the NCI-60 panel, the cell lines employed represent leukemia and melanoma, as well as cancers of the lung, colon, brain, ovary, breast, prostate and kidney. Compounds submitted to this screening process are initially tested at a single dose (10 μM) against the 60 cell line panel. Subsequent to this initial testing, compounds which satisfy threshold inhibition criteria in a minimum number of cell lines are progressed to a full five-dose assay.

In the five-dose assay, the percentage growth is calculated at each of the five drug concentration levels using a series of absorbance measurements (time zero (Tz), control growth (C), and test growth in the presence of the drug at the five different levels (Ti)). The response parameters GI_{50} (concentration required for 50% inhibition of growth) and LC_{50} (concentration required for 50% cell death) are extracted from concentration-response curves by linear interpolation, while TGI (total growth inhibition) is read as the x-axis intercept from the five different drug concentrations.[11]

5.2 NCI-60 single-dose screen results

The *in vitro* activity of each selected compound against the NCI-60 cell panel was displayed in the form of an overall mean graph (Appendix *i* to *xxix*), comprising a series of horizontal bar graphs representing units of nominal growth percent, deviating from the mean growth inhibition for the 60 cell line array, i.e. centre line or '0' (a representative example is seen in ***Figure 5.2***).

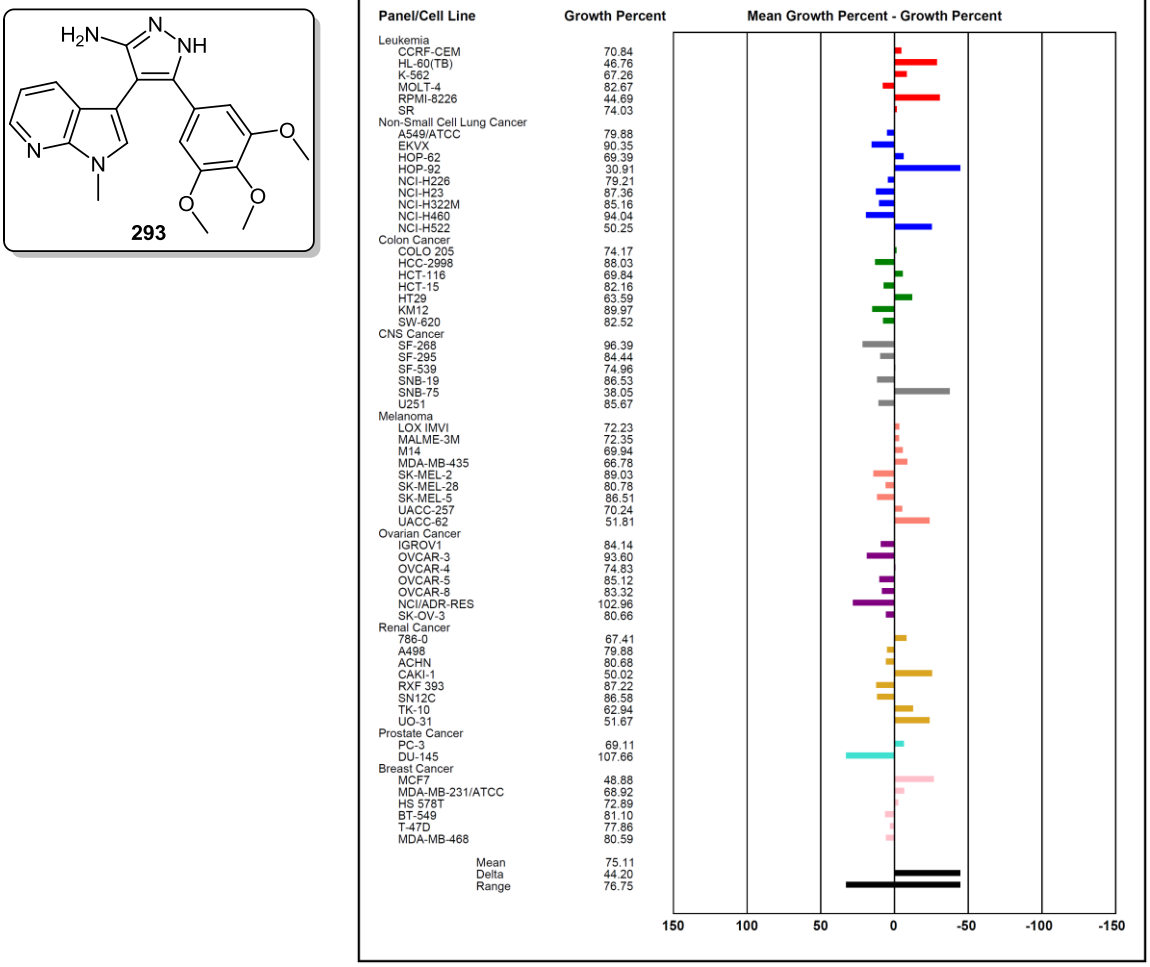

Fig. 5.2 *Structure of aminopyrazole* ***293*** *and corresponding single-dose NCI-60 cell array*

For each case against the overall mean growth of a compound, graphs which extend to the right (-) denote a relative cytotoxic or positive growth inhibitory effect on individual cell lines, while those which extend to the left (+) of centre line indicate a relative chemoprotective or

non-cytotoxic effect (***Figure 5.2***). From an early stage in the DTP program, it was recognised that identifiable trends across the NCI-60 cell array are characteristic of molecular mechanisms of action.

5.2.1 Aza BIM derivatives containing a 3,4,5-trimethoxyphenyl moiety

Single-dose mean graphs for parent aminopyrazoles **293** and **312**, along with derivatives **295**, **297**, **302**, **304**, **313**, **314**, **316** and **317** can be found in Appendices *i* to *x*.

With a mean growth of 75%, aminopyrazole **293** did not satisfy the threshold inhibition criteria in order to proceed to the five-dose assay (***Table 5.1***). However, appreciable selectivity was shown towards HL-60(TB) and RMPI-8226 leukemia, SNB-75 CNS cancer and in particular HOP-92 non-small cell lung cancer lines. Although extension of the aminopyrazole moiety towards bicyclic systems **295** and **297** resulted in an increase in the mean growth percentage in both cases, greater selectivity was achieved towards the HOP-92 cell line. This was particularly evident for pyrimidine **297** (Appendix *iii*), which completely arrests growth in this tumour cell line and even exhibits a degree of cytotoxicity after 48 hours incubation.

The selectivity exhibited towards the HOP-92 line by aminopyrazole **293** and derivatives **295** and **297** indicate the bioactive potential of this compound class, within which it is possible that interactions with various isoforms of PKC could have a role. COMPARE analysis has previously indicated that the HOP-92 line is one of the most responsive out of the NCI-60 panel towards PKC modulators.[12] Enzastaurin **27**, which is a BIM analogue and a selective inhibitor of PKCβ, has shown strong antiproliferative activity in the low micromolar range against the HOP-92 cell line, amongst others within the panel.[13] Hence, given the specificity exhibited by aminopyrazole **293** and its bicyclic derivatives towards HOP-92 cells, further biological evaluation could involve assays against the various isoforms of the PKC enzyme.

While the introduction of an acetyl functionality (derivative **302**) resulted in a significant loss of activity across the 60 cell line panel (Appendix *iv*), carbothioamide **304** displayed a lower mean growth (66.5%, Appendix *v*) to that of parent aminopyrazole **293**. Retaining remarkably similar activity against RMPI-8226 and SNB-75 cell lines to that of its precursor **293**,

thioamide substitution in **304** gave increased selectivity towards a number of other lines, notably in two renal carcinomas (CAKI-1 and UO-31).

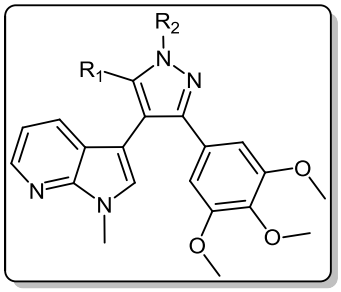

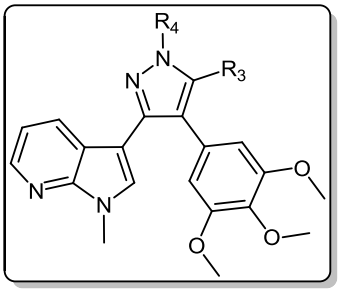

No.	Substituents		NSC No.	Mean (%)	Five Dose	Selected Cells (% Growth)				Regioisomer Correlation (COMPARE)
	R_1	R_2				HOP-92	SNB-75	CAKI-1	UO-31	
293	NH_2	H	754616	75.1	x	30.9	38.1	50.0	51.7	0.791
295	-NHCONHCO-		754617	104.3	x	53.5	99.7	118.4	94.8	0.366
297	$-NC(CF_3)CHC(CF_3)-$		754618	94.0	x	-3.1	67.2	-	73.7	0.632
302	NH_2	$COCH_3$	763899	104.2	x	86.4	101.9	81.0	92.8	0.475
304	NH_2	$CSNHCH_3$	763898	66.5	x	-	39.7	18.2	25.3	0.805
	R_3	R_4								
312	NH_2	H	763892	79.8	x	47.9	34.4	48.9	49.6	0.791
313	-NHCONHCO-		763893	101.5	x	87.7	67.2	89.8	94.2	0.366
314	$-NC(CF_3)CHC(CF_3)-$		763894	95.4	x	-	73.2	82.3	71.2	0.632
316	NH_2	$COCH_3$	763896	76.6	x	-	8.5	39.7	33.1	0.475
317	NH_2	$CSNHCH_3$	763895	78.6	x	-	26.5	34.1	35.9	0.805

***Table 5.1** Aminopyrazoles **293** and **312** and respective derivatives*

Examination of the single-dose data for aminopyrazole **312** and its derivatives serves to illustrate an interesting pattern of tumour chemoselectivity amongst these two isomeric classes. Parent aminopyrazole **312** (Appendix *vi*) and carbothioamide **317** (Appendix *x*) display similar growth inhibition against a number of cell lines including SNB-75, CAKI-1, UO-31 and UACC-62 (melanoma) lines, closely resembling the profiles obtained for their

isomers **293** and **304**. Accordance of the regioisomers is borne out by the high correlations obtained using COMPARE analysis, with 0.791 for aminopyrazoles **293** and **312**, and 0.805 for carbothioamides **304** and **317**, where 1 is an identical result (***Table 5.1***).

In stark contrast to its relatively inactive isomer **302**, acetylated aminopyrazole **316** (Appendix *ix*) exhibited significant growth inhibition against CAKI-1, UO-31 and especially SNB-75 cell lines, with correlation between the two regioisomers relatively modest at 0.475. Bicyclic derivatives **313** and **314** (Appendices *vii* and *viii*) displayed unremarkable growth inhibition across the NCI-60 cell panel. Unfortunately, pyrimidine **314** was not evaluated against the HOP-92 cell line, the line against which the isomeric pyrimidine system **297** had previously displayed excellent selective inhibition. Moderate correlation of 0.632 between the two pyrimidine systems across remaining lines within the NCI-60 panel indicate that the antiproliferative activity of derivative **314** against HOP-92 cells would be worthy of future assessment.

Upon overall appraisal of both sets of regioisomers, close agreement in the single-dose data for a number of compounds from either class, especially parent aminopyrazoles **293** and **312**, carbothioamides **304** and **317** and acetylated aminopyrazole **316**, denotes the possibility of a common biological mode of action. On the other hand, the lack of activity observed for derivative **302** in comparison with its isomer **316**, along with the poor correlation between triazinedione systems **295** and **313**, suggests that there is room for more extensive SAR study.

5.2.2 Derivatives of 5-aminopyrazole 318

Single-dose mean graphs for aminopyrazole **318** and derivatives **319**, **320**, **322** and **323** can be found in Appendices *xi* to *xv*.

While possible to distinguish a pattern of tumour chemoselectivity across a number of derivatives containing a 3,4,5-trimethoxyphenyl moiety (Sections ***5.2.1***), it was more difficult to do so across the NCI-60 profiles of aminopyrazole **318** and its derivatives, suggesting different biological targets (and hence molecular mechanisms of action) across the class. Thus, it appears that modulation of the F-ring leads to unique bioactivity profiles, a significant discovery in the BIM/ICZ field of research. Parent compound **318** (Appendix *xi*) displays

selective activity against a number of leukemia cell lines, especially the SR line, while being relatively nonactive across almost all melanoma, ovarian and prostate cell lines. Mean growth across the six leukemia lines was found to be 65.1%, while the least activity was seen for melanoma, with a mean growth of 95.4% across nine cell lines (***Table 5.2***).

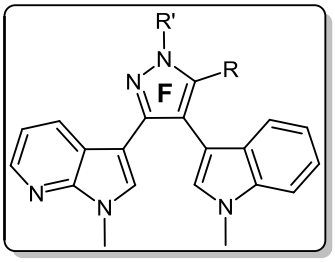

No.	Substituents		NSC No.	Mean (%)	Five Dose	Selected Cells (% Growth)			
	R	R'				SR	SNB-75	M14	MDA-MB-435
318	NH_2	H	754612	82.0	X	18.4	54.7	119.6	84.6
319	-NHCONHCO-		754613	94.6	X	61.4	73.4	117.4	104.9
320	$-NC(CF_3)CHC(CF_3)-$		754614	76.9	X	86.3	9.1	12.8	85.5
322	NH_2	$COCH_3$	762132	77.0	X	28.2	54.0	73.2	33.2
323	NH_2	$CSNHCH_3$	754615	73.8	X	46.2	53.3	27.5	25.6

Table 5.2 *Aminopyrazole* ***318*** *and derivatives* ***319***, ***320***, ***322*** *and* ***323***

Similar to its precursor **318**, triazinedione **319** is most active against SR leukemia and MCF7 cell lines, despite having the highest mean growth in this compound series (Appendix *xii*). In contrast, bicyclic congener, pyrimidine **320**, displays insignificant growth inhibition against any of the leukemia cell lines (Appendix *xiii*). However, excellent activity is shown for a number of other lines, especially SNB-75 CNS cancer cells (***Table 5.2***). Acetylated derivative **322** shows greatest growth inhibition against the SR leukemia cell line (Appendix *xiv*), mirroring the parent aminopyrazole **318**.

The trend in selectivity towards melanoma cell lines in this series makes for interesting comparative analysis, with parent aminopyrazole **318** initially displaying little activity in this regard. The introduction of a bicyclic system in the case of triazinedione **319** resulted in no improvement, however trifluoromethyl-substituted pyrimidine **320** induces significant growth

inhibition against M14 cells. Monosubstitution of the aminopyrazole in the case of acetylated derivative **322** gives good selectivity for the MDA-MB-435 line, and in the case of carbothioamide **323** the M14 and MDA-MB-435 lines. It is therefore seen that substitution on the F-ring induces different antiproliferative mechanisms in the cells tested, with the nature of the substituent leading to different selectivity profiles in the NCI-60 cell array. Worthy of further investigation, future work on this series could aim to look at increasing the potency of the aminopyrazole derivatives in order to better exploit the appealing bioactive characteristics observed.

5.2.3 Various aza BIM derivatives

Single-dose mean graphs for various aza BIM derivatives **326**, **327**, **328**, **332**, **356**, **357** and **361** can be found in Appendices *xvi* to *xxii*.

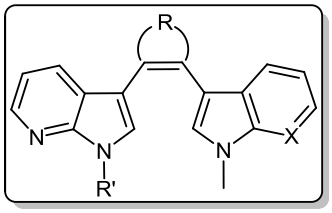

No.	Substituents		X	NSC No.	Mean (%)	Five Dose	Selected Cells (% Growth)					
	R	R'					SR	SF-295	SNB-75	MDA-MB-435	SK-MEL-2	A498
326	-NHNHCO-	Bn	CH	762134	95.3	x	91.3	94.2	49.5	104.8	-	118.1
327	-NHOCO-	Me	CH	762131	60.9	✓	9.3	51.6	49.2	2.6	36.0	79.4
328	-N(CH_3)OCO-	Me	CH	762133	92.5	x	83.5	92.2	73.3	100.7	87.0	105.9
332	-NC(NH_2)NHCO-	Me	CH	754611	97.6	x	90.4	98.2	87.6	98.8	105.1	85.7
356	-CON(OH)CO-	Me	CH	762130	97.8	x	53.1	93.1	79.8	104.9	109.8	113.1
357	-CONHCO-	Me	CH	762129	28.8	✓	12.1	9.5	10.4	12.9	-13.8	-19.9
361	-CONHCO-	Me	N	763897	56.1	✓	9.0	-14.1	-12.1	67.1	94.5	-15.7

Table 5.3 *Aza BIM derivatives* ***326***, ***327***, ***328***, ***332***, ***356***, ***357*** *and* ***361***

Due to the relative structural disparity between the various aza BIM derivatives featured in ***Table 5.3***, little correlation in activity is seen across the NCI-60 panel. Pyrazolone **326** displays insignificant inhibition against the majority of cell lines, with a mean growth of 95.3% (Appendix *xvi*). The only exception was in the case of SNB-75 CNS cancer, which was the only cell line to have less than 50% growth after 48 hours incubation.

Isoxazolone **327**, with a mean growth of 60.9%, passed the threshold inhibition criteria in order to proceed to five-dose testing (Appendix *xvii*). Good selectivity is seen for a number of cell lines, with growth almost completely arrested in the case of M14 melanoma cells, and excellent activity also seen against SR leukemia, NCI-H522 lung cancer and HT29 colon cancer lines. The introduction of a methyl protecting group on the isoxazolone moiety for derivative **328** resulted in an almost complete loss of growth inhibitory activity (Appendix *xviii*). However, some selectivity is retained for UO-31 renal, MCF7 and MDA-MB-468 breast cancer cells, against which parent isoxazolone **327** is also active. With a mean growth of 97.6%, six-membered pyrimidinone BIM derivative **332** was shown to have very little bioactivity across the NCI-60 panel, concomitant with relatively little selectivity evident for any particular cell lines (Appendix *xix*). The bisindolyl analogue of pyrimidinone **332**, previously synthesised within our research group, had also exhibited little antiproliferative activity, with a mean growth of 101.9%.[14]

Both monoaza maleimide **357** (Appendix *xxi*) and bisaza maleimide **361** (Appendix *xxii*) were brought forward for five-dose testing, given the promising nature of the single-dose data for both compounds. Although monoaza maleimide **357** had a lower mean growth of 28.8% compared with bisaza analogue **361** (56.1%), greater selectivity was seen for bisaza **361**, which displays a degree of cytotoxicity against SF-295 and SNB-75 CNS cancer, and A498 renal cancer lines. Monoaza maleimide **357** also displays cytotoxic effects against a number of lines within the panel, including SF-539 CNS, SK-MEL-2 melanoma and A498 renal cells. The greater degree of selectivity seen for bisaza maleimide **361** mirrors work carried out by Kuo and co-workers (Section *1.3.1.5*), who noted that a series of bisaza BIM derivatives were more selective inhibitors of glycogen synthase kinase-3 (GSK-3) than their monoaza analogues.[15] However, this is not a direct correlation, as Kuo *et al*. utilised a kinase inhibition assay, whereas this data arises from cellular growth inhibition assays.

The role of the maleimide moiety in the bioactivity of **357** and **361** was highlighted in the single-dose data obtained for hydroxymaleimide **356** (Appendix *xx*). The introduction of an *N*-hydroxy functionality to the maleimide ring for **356** resulted in a loss of activity across the NCI-60 array (mean growth 97.8%), with the only appreciable growth inhibition retained for the SR leukemia cell line (***Table 5.3***).

5.2.4 Azaindolocarbazoles

Single-dose mean graphs for aza ICZs **239**, **364**, **363**, **368**, **371**, **372** and **373** can be found in Appendices *xxiii* to *xxix*.

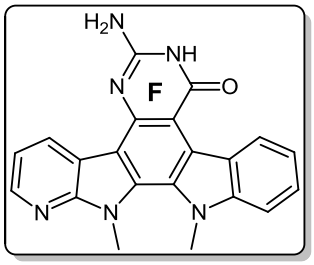

No.	NSC No.	Mean (%)	Five Dose	Selected Cells (% Growth)			
				NCI-H522	UO-31	MCF7	T-47D
239	762128	79.5	x	35.1	39.4	45.7	48.7

Table 5.4 *Six-membered aza ICZ* ***239***

Pyrimidinone **239** was the first aza ICZ with a six-membered F-ring to be tested against the NCI-60 cell screen (Appendix *xxiii*). Although formation of the central carbazole ring resulted in greater bioactivity in comparison with its unaromatised analogue **332**, aza ICZ did not meet the criteria for further analysis within the DTP program. Selectivity was observed against a number of cell lines, including NCI-H522 lung, UO-31 renal and MCF7 and T-47D breast carcinomas (***Table 5.4***). Using COMPARE analysis, it was shown that poor correlation of 0.441 exists between aza ICZ **239** and its ICZ analogue **231**, previously synthesised within this research group, and the introduction of an aza moiety resulted in a decrease in overall activity.[14] Hence, the discrete change of a single atom results in a different biological profile, as was described previously by Prudhomme *et al.* with other aza ICZ derivatives (Section *1.3.2.3*).[16]

In contrast, all of the aza ICZs containing a 5-membered F-ring to be tested against the NCI-60 panel were found to be sufficiently active in order to proceed to the five-dose screen (***Table 5.5***). Given the conserved structural nature of aza ICZs **364**, **363**, **368**, **371**, **372** and **373**, it is unsurprising that similar trends of bioactivity are observed across the series. For example, the SR leukemia cell line is consistently targeted by each compound to varying degrees. In the cases of maleimide **364**, hydroxymaleimide **363** and Boc-protected maleimides **368** and **372**, growth of SR leukemia cells is almost completely arrested, while in the case of maleimide **371** and hydroxymaleimide **373**, significant cytotoxicity was observed.

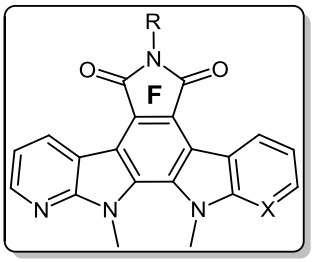

No.	Substituent R	X	NSC No.	Mean (%)	Five Dose	Selected Cells (% Growth)						
						MOLT-4	SR	SF-295	SNB-75	MCF7	T-47D	MDA-MB-468
364	H	CH	762125	63.1	✓	61.5	10.2	69.5	61.2	15.9	34.9	20.5
363	OH	CH	762126	37.7	✓	-8.6	3.3	18.2	-6.4	3.3	-7.7	41.5
368	Boc	CH	762127	50.7	✓	61.0	5.9	52.3	28.9	4.4	-0.6	5.5
371	H	N	763889	55.9	✓	-7.6	-30.2	6.5	16.1	20.3	61.8	24.3
372	Boc	N	763890	61.2	✓	-5.8	1.8	16.8	85.3	24.7	57.1	31.4
373	OH	N	763891	20.0	✓	-33.0	-25.1	-17.8	10.3	5.4	25.3	-14.9

Table 5.5 *Aza ICZs **364**, **363**, **368**, **371**, **372** and **373** containing 5-membered F-rings*

Bisaza maleimide **371** and bisaza hydroxymaleimide **373** were found to be more potent than their monoaza analogues **364** and **363**, in contrast with the single-dose data obtained for unaromatised monoaza and bisaza maleimides **357** and **361** (Section ***5.2.3***). Hydroxymaleimide **373** was the most bioactive compound in the series against the NCI-60 cell array, with the induction of cytotoxic effects against eight different cell lines after 48

hours of incubation, particularly in the case of MOLT-4 and SR leukemia and 786-0 renal cancer lines (Appendix *xxix*).

5.2.5 Conclusion

Of the twenty nine compounds submitted to the DTP for screening to date, nine were deemed to be sufficiently cytotoxic or have suitably interesting selectivity profiles to progress to five-dose testing. Much useful information was obtained from the single-dose testing, with a number of promising leads for future work. A number of aza BIM derivatives containing a 3,4,5-trimethoxyphenyl subunit displayed good selectivity towards the HOP-92 line (Section ***5.2.1***), which would make it worthwhile to further investigate the biological pathways responsible for apoptosis in these cells, in particular PKC interaction. It was also clear that F-ring modulation could profoundly impact on the anticancer activity of aza BIM derivatives (Section ***5.2.2***). For example, substitution of aminopyrazole **318** with either mono- or bidentate ligands resulted in different antiproliferative profiles and the conferring of good selectivity for a number of cancer cell lines, such as melanoma M14 or MDA-MB-435 lines.

The changing of even one atom significantly impacted on the single-dose data obtained for different candidates. For example, a second 7-azaindolyl subunit instead of an indolyl moiety in maleimide **361** lead to greater selectivity for a number of cell lines, though with a higher overall mean growth than its monoaza analogue **357**. Further exploitation of this paradigm could be of major benefit in future SAR studies. Interestingly, there is a complete drop off in activity between maleimide **357** to hydroxymaleimide **356**, whereas significant antiproliferation is evident for both corresponding monoaza ICZ derivatives **364** and **363**. Hence, it can be surmised that the maleimide functionality is of considerably greater importance towards antiproliferative activity in the unaromatised analogues compared to their corresponding planar aza ICZs.

Although not as detailed as results obtained from the five-dose assay, the single-dose NCI-60 screen allows for a higher throughput of compounds and is a valuable tool in the identification of potential leads for future chemotherapeutic candidates, and also for elucidating putative biological mechanisms of action.

5.3 NCI-60 five-dose screen results

Compounds which were successfully brought forward for five-dose testing were tested against the NCI-60 cell panel at five different concentrations ranging from 100 µM to 10 nM. As a result of the data obtained, dose-response curves were generated for cell growth inhibition as a function of inhibitor concentration for each cell line. The three characteristic *in vitro* parameters, GI_{50}, TGI and LC_{50}, were calculated for each cell line in response to the presence of the different drug candidates.

5.3.1 Five-dose data for isoxazolone 327

Having shown sufficient promise in initial screening, isoxazolone **327** was subsequently tested at five different concentrations against the NCI-60 cell array. Inhibition across the panel was observed to occur in a dose-dependent manner (***Figure 5.3***), with GI_{50} values predominantly in the low micromolar range (Appendices *xxx* and *xxxi*).

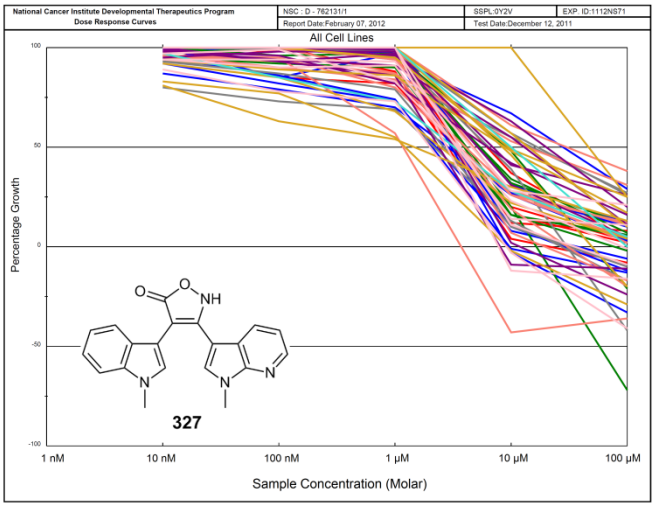

Fig. 5.3 *Dose-response curves for isoxazolone* ***327***

It was of significant interest to note that the MDA-MB-435 melanoma line, which had the lowest percentage growth after 48 hours in the single-dose screen, also had the lowest GI_{50} and TGI values (1.18 µM and 3.75 µM respectively) in response to isoxazolone **327** in the five-dose testing, illustrating a consistency in results. The lethal concentration required for the death of 50% of cell population (LC_{50}) was >100 µM in almost all cases across the panel. The

only appreciable cytotoxicity was found for the COLO 205 colon carcinoma line, with an LC_{50} value of 58 µM (***Figure 5.4***).

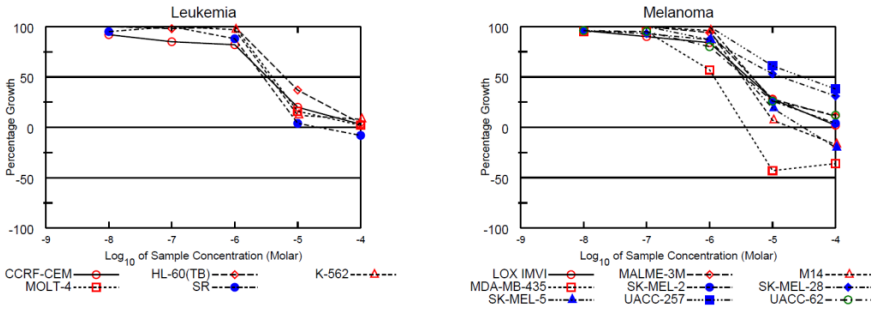

Fig. 5.4 *Dose response curves of isoxazolone* ***327*** *against colon cancer and melanoma cells*

The antiproliferative activity recorded against the MDA-MB-435 line suggests the potential role of isoxazolone **327** as a mitogen-activated protein kinase (MAPK) inhibitor. In 2000, Roberts *et al.* described how p38 MAP kinase plays a role in the adhesive properties of human tumour cells, specifically MDA-MB-435 cells.[17] Concomitantly, Laufer *et al.* demonstrated in 2008 that a series of diaryl-substituted isoxazolones functioned as potent inhibitors of the p38 MAP kinase enzyme.[18] Hence, in order to investigate MAPK inhibition as a potential biological mechanism for **327**, future investigation using the relevant enzyme assays is imperative.

5.3.2 Five-dose data for maleimides 357 *and* 361

With the second-lowest mean growth in the single-dose screen, monoazaindolyl maleimide **357** was a clear candidate for further biological examination. Pronounced cytotoxic effects are observed across many cell lines at higher concentrations, however there is a discernible drop-off in activity between the 10 µM and 100 nM levels (Appendices *xxxii* and *xxxiii*).

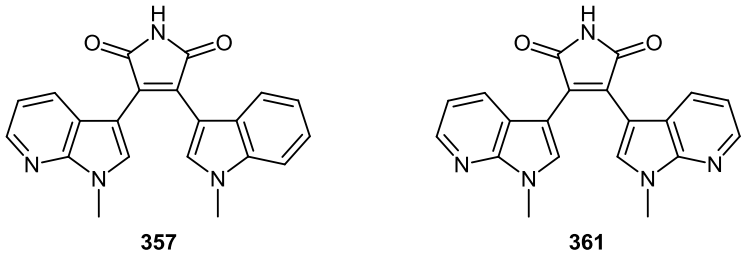

357 **361**

Fig. 5.5 *Structures of monoaza maleimide* ***357*** *and bisaza maleimide* ***361***

As seen for isoxazolone **327** (Section ***5.3.1***), correlation between the two screens is quite noticeable in the case of maleimide **357**. The A498 renal cancer cell line was observed to have the lowest TGI value (2.3 µM) out of the NCI-60 cell panel (***Figure 5.6***), thus complimenting the single-dose data for **357**, in which the lowest growth percent (-19.9%) was also seen for the same line.

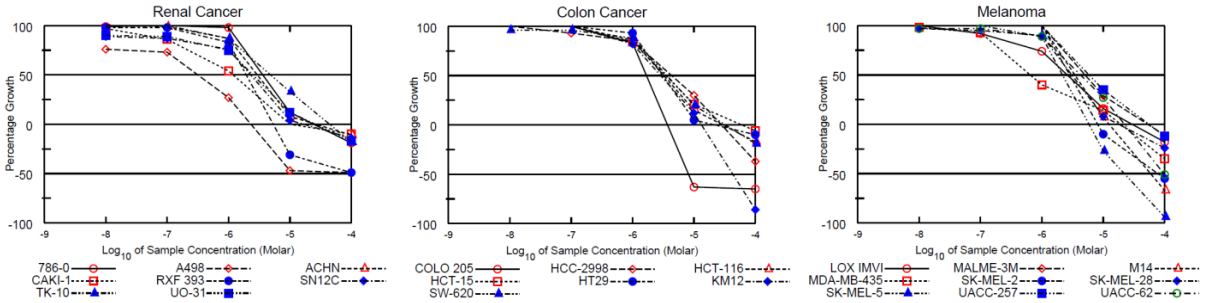

Fig. 5.6 *Dose-response curves for **357** against melanoma, renal and colon cancer cells*

Maleimide **357** is also seen to have cytotoxic effects across several cell lines, including COLO 205 (LC_{50} = 8.1 µM) and KM12 (LC_{50} = 43.2 µM) colon, SF-539 (LC_{50} = 42.4 µM) CNS, M14 (LC_{50} = 58.8 µM) and SK-MEL-5 (LC_{50} = 21.8 µM) melanoma lines. An interesting parallel between isoxazolone **327** and maleimide **357** is revealed by the fact that the most pronounced cytotoxicity is observed against the COLO 205 cell line in both cases.

Maleimide **361** displays a broadly similar dose-response curve to that of its monoaza analogue **357** (Appendices *xxxiv* and *xxxv*). However, at lower concentrations, admirable selectivity is seen for A498 renal cancer cells in the NCI-60 array, with a submicromolar dosage (0.9 µM) of malemide **361** required to totally arrest growth, and a GI_{50} of 157 nM (***Figure 5.7***).

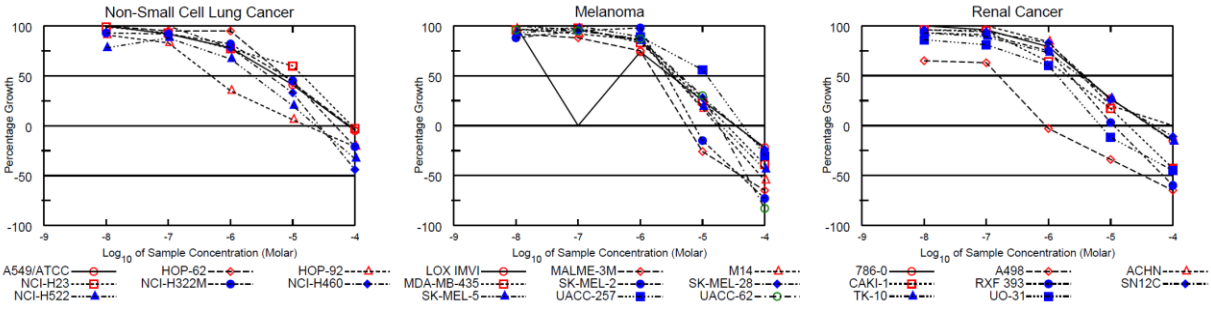

Fig. 5.7 *Dose-response curves for bisazaindolyl maleimide **361***

Bisaza maleimide **361** also displays considerable cytotoxicity against A498 cells with an LC_{50} of 33.2 µM. Significantly, analogous BIM enzastaurin **27**, which is most active against K562 and MOLT-4 leukemia, HOP-92 lung and PC-3 prostate cancer cells, does not exert any antiproliferative activity on the A498 line.[13]

As seen previously with isoxazolone **327** and monoaza maleimide **357**, bisaza maleimide **361** mediates anticancer activity primarily in a dose-dependent manner. Low TGI values are observed across a range of different cell lines, including MALME-3M (5.5 µM) and SK-MEL-2 (7.4 µM) melanoma, SK-OV-3 (7.6 µM) ovarian, UO-31 (6.8 µM) renal and HOP-92 (17.0 µM) cancer cell lines.

5.3.3 Five-dose data for monoaza ICZs

The dose-response curves for the aza ICZs with five-membered F-rings were found to be more atypical than those seen for isoxazolone **327** (Section ***5.3.1***) and maleimides **357** and **361** (Section ***5.3.2***). For example, greater antiproliferative activity is seen across almost all cell lines at a concentration of 10 µM than at 100 µM for monoaza ICZ **364** (Appendices *xxxvi* and *xxxvii*, ***Figure 5.9***). This may in part be due to the relatively insoluble nature of the compound, with reduced efficacy at higher concentration perhaps due to aggregation of the precipitated maleimide **364**.

Excellent activity at nanomolar concentrations is seen for **364** against a number of cell lines, highlighting its considerable potency. For example, low nanomolar activity is seen against SR leukemia cells (GI_{50} = <10 nM), and also against NCI-H460 lung (GI_{50} = 22.6 nM), MCF7 (GI_{50} = 31.0 nM) and MDA-MB-468 breast (GI_{50} = 27.4 nM) cancer cells (***Figure 5.8***).

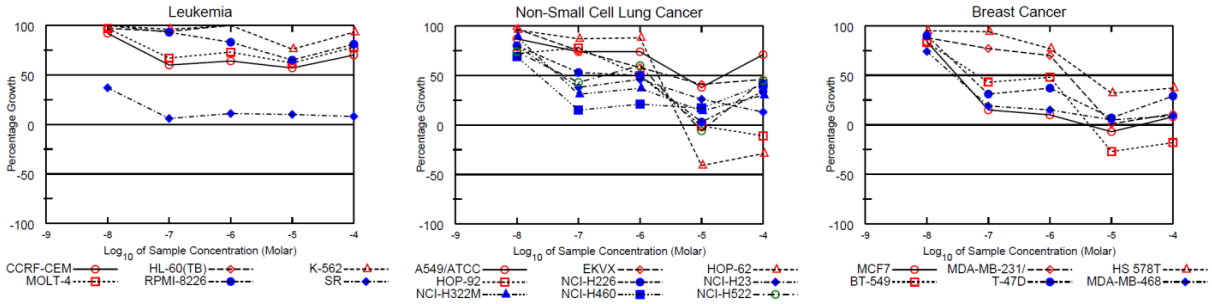

Fig. 5.8 *Dose-response curve for aza ICZ* ***364***

Though antiproliferative activity is quite potent even at lower concentrations for a number of cells, little cytotoxicity was seen for monoaza ICZ **364** across the panel. COMPARE analysis indicated a correlation of 0.679 with the mycotoxin, 5-methoxy sterigmatocystin (NSC S178249), which has previously been shown to have potent antitumour properties.[19]

Introduction of a Boc protecting group on the maleimide moiety of monoaza ICZ **368** resulted in a large increase in the solubility of the compound (for instance, dissolution occurs much more readily in DMSO at higher concentrations). This is seen to translate into a more typical dose-response curve across the NCI-60 cell array (***Figure 5.9***), with higher concentrations generally corresponding to greater antiproliferative activity for **368**.

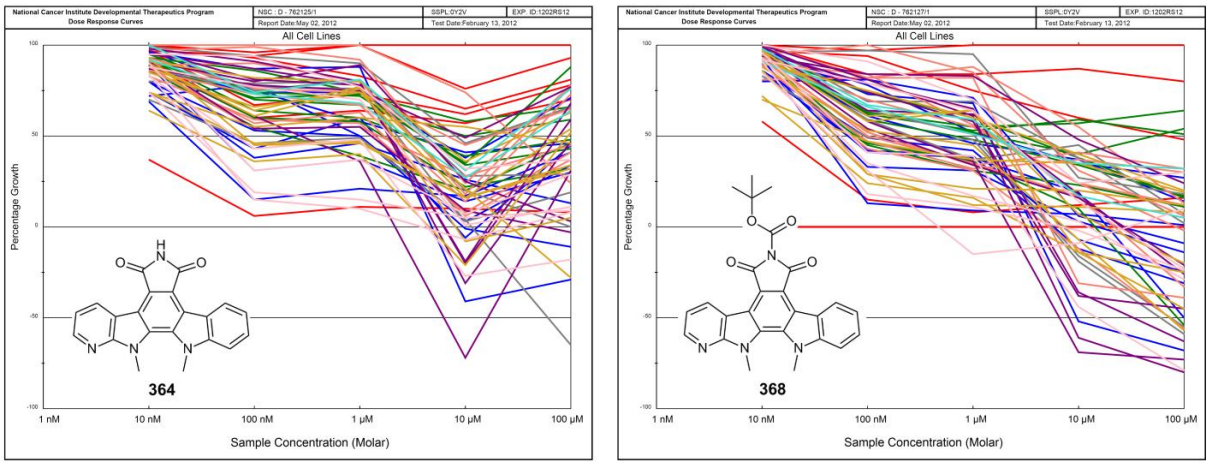

Fig. 5.9 *Dose-response curves for maleimide **364** and Boc-protected maleimide **368***

As was the case for maleimide **364**, greatest activity for **368** is seen against SR leukemia cells (GI_{50} = 15.4 nM), along with inhibition of several other lines in the nanomolar range, such as NCI-H460 lung (GI_{50} = 34.3 nM), ACHN (GI_{50} = 42.7 nM) and UO-31 (GI_{50} = 29.0 nM) renal, and MCF7 breast (GI_{50} = 36.2 nM) cancer cells (Appendices *xl* and *xli*, ***Figure 5.10***).

Boc-protected aza ICZ **370** exhibits cytotoxicity against several cell lines, such as HOP-62 lung (LC_{50} = 9.6 µM), OVCAR-3 (LC_{50} = 8.2 µM) and OVCAR-4 ovarian (LC_{50} = 6.7 µM), and BT-549 breast (LC_{50} = 14.6 µM) cancer cells. This contrasts starkly with maleimide **364**, which only shows discernible evidence of a cytotoxic effect against one cell line from the NCI-60 array, SNB-75 (LC_{50} = 61.2 µM). It is possible that the Boc functionality renders **368** into a pro-drug for maleimide **364**, resulting in greater solubility of the molecule and

increasing the ease with which it crosses the cell membrane. It is also possible that the Boc group could potentiate interactions with cellular targets. Using COMPARE, strong correlation of 0.811 is seen between Boc-protected maleimide **368** and maleimide **364**, with moderate correlations also seen between **368** and a phenanthridine derivative (0.614, NSC S125552) and camptothecin (0.538, NSC S651012), a known topo I inhibitor (Section *1.3.2.1*).

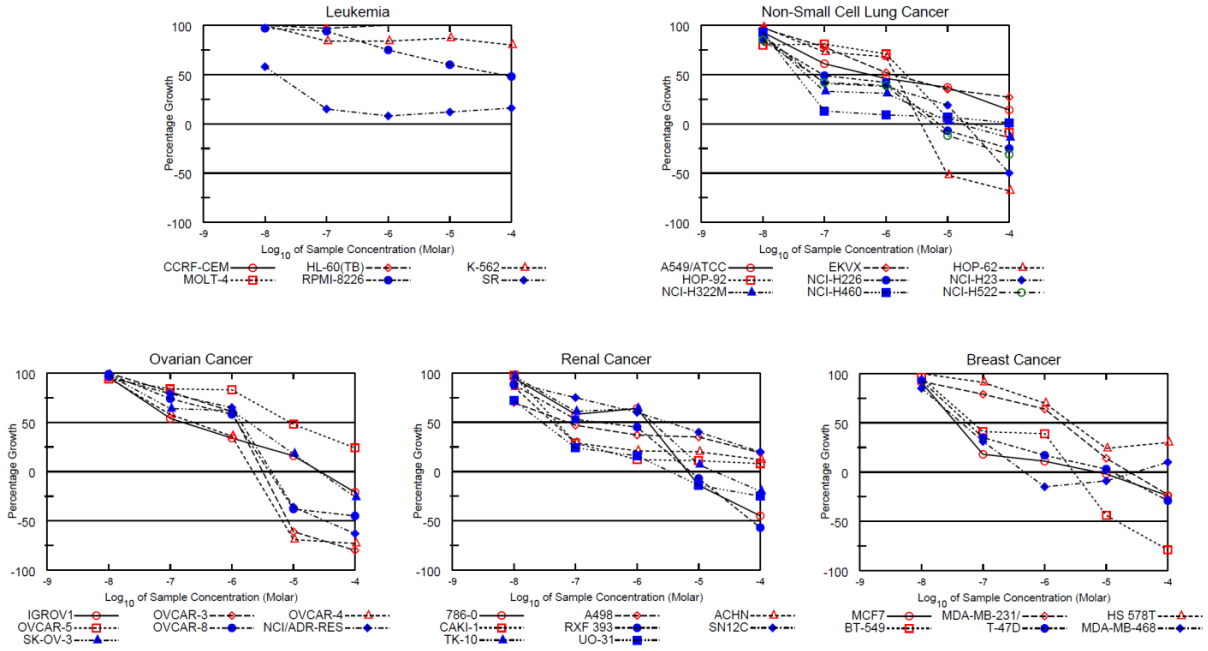

Fig. 5.10 *Dose-response curves for **368** against leukemia, lung, ovarian, renal and breast cancer cells*

Upon conversion of **368** to hydroxymaleimide **363**, most cytotoxicity is lost (Appendices *xxxviii* and *xxxix*). However, greatest antiproliferative activity is once more seen against SR leukemia cells (GI_{50} = 35.3 nM), suggesting a common target (***Figure 5.11***).

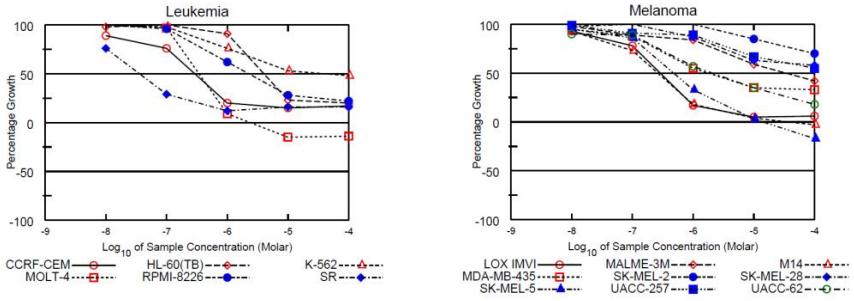

Fig. 5.11 *Dose-response curve for aza ICZ **363***

Useful bioactivity is also seen for **363** against a number of melanoma cell lines, such as M14 (GI_{50} = 259 nM) and SK-MEL-5 (GI_{50} = 470 nM) (***Figure 5.11***).

Further investigation using the COMPARE algorithm demonstrates a very high correlation between hydroxymaleimide **363** and a series of derivatives of camptothecin **37**, such as anticancer agent topotecan **38** (***Table 5.6***).

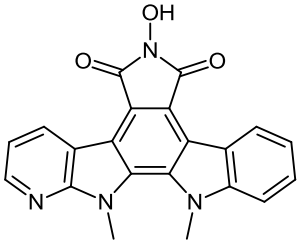

363

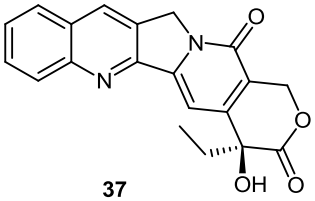

37

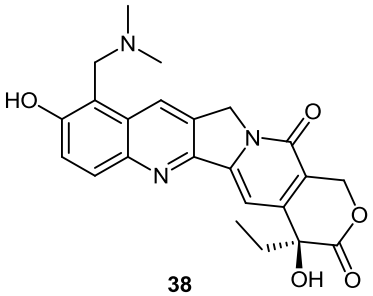

38

Correlation	Compound	NSC Number
0.848	Camptothecin prodrug	S374028
0.836	Camptothecin conjugate (+ etoposide)	S683556
0.825	Deoxycamptothecin	S105132
0.819	Camptothecin lysinate	S610457
0.811	Topotecan **38**	S609699

Table 5.6 *Correlation of aza ICZ **363** with derivatives of camptothecin **37** using COMPARE*

The strong correlation seen between aza ICZ **363** and the derivatives of camptothecin **37** indicate the existence of a similar biological mode of action. As camptothecin **37** and its derivatives are renowned as topo I inhibitors, it suggests that aza ICZ **363** could interact with the same enzyme or perhaps with DNA itself.

5.3.4 Five-dose data for bisaza ICZs

Having examined the chemotherapeutic potential of a series of monoazaindolyl ICZs (Section ***5.3.3***), attention was subsequently focused on derivatives containing two 7-azaindolyl moieties. Maleimide **371** was found to have a similarly unusual dose-response profile (Appendices *xlii* and *xliii*) to that of its monoaza analogue **364**, containing a general trend of increased bioactivity with decreasing concentration from 100 µM to 100 nM. Once more, poor solubility of maleimide **371** is thought to be a factor in this phenomenon.

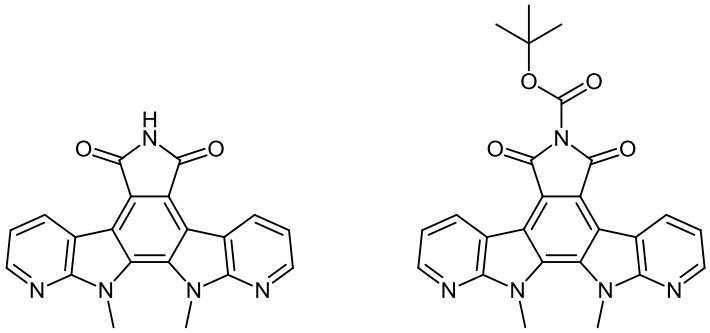

Fig. 5.12 *Structures of aza ICZs **371** and **372***

It was found that the addition of the second azaindolyl subunit in **371** did not significantly enhance antiproliferative activity against the NCI-60 array relative to monoaza ICZ **364**. Once more, however, excellent growth inhibition is seen against SR leukemia cells (GI_{50} = <10 nM), which have been consistently targeted by any aza ICZs tested that contain a five-membered F-ring (***Figure 5.13***).

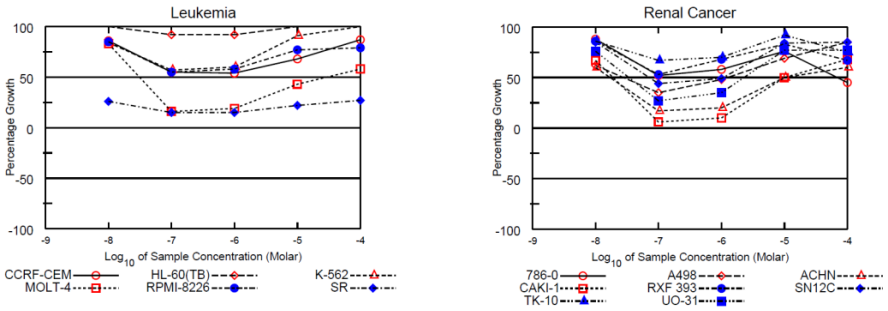

Fig. 5.13 *Dose-response curves of maleimide **371** against leukemia and renal cancer cells*

Due to the nature of the dose-response curves for bisaza ICZ **371**, it was not possible to calculate GI_{50} values for a number of cell lines, and reassessment against the panel is currently ongoing in order to ascertain more accurate information.

Protection of the maleimide moiety in **372** with a Boc group resulted in increased antiproliferative activity against a number of cell lines relative to its precursor **371**, again raising the possibility of **372** functioning as a prodrug (Appendices *xliv* and *xlv*). Unlike with its monoaza analogue **368**, however, a significant increase in cytotoxicity against a number of cell lines is not observed.

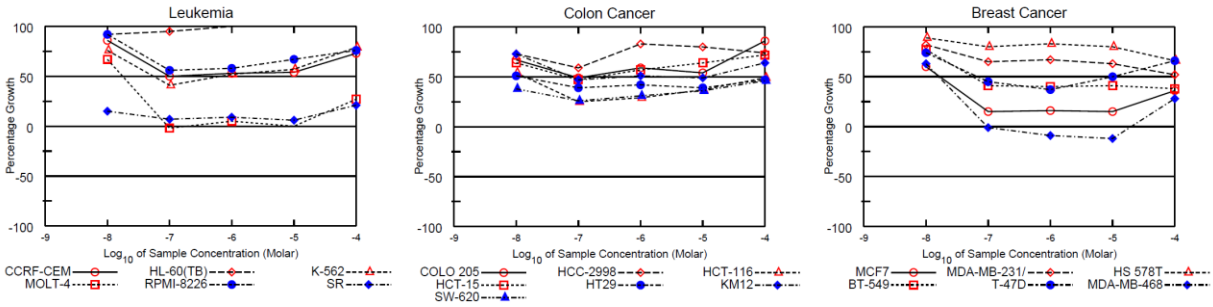

Fig. 5.14 *Dose-response curves for **372** against leukemia, colon and breast cancer cells*

As in the case of maleimide **371**, the nature of the dose-response curves recorded for Boc-protected **372** meant that GI_{50} values for a number of cell lines were unable to be calculated. However, amongst the figures that proved possible to obtain, considerable cytostatic effects are evident across a number of different cancer types, with only low nanomolar concentrations of **372** required to inhibit 50% of growth in many instances (***Figure 5.14***). As seen previously, a GI_{50} value of less than 10 nM is seen for the SR leukemia cell line, along with a number of other lines such as SW-620 colon, SF-295 CNS, ACHN and CAKI-1 renal cancers.

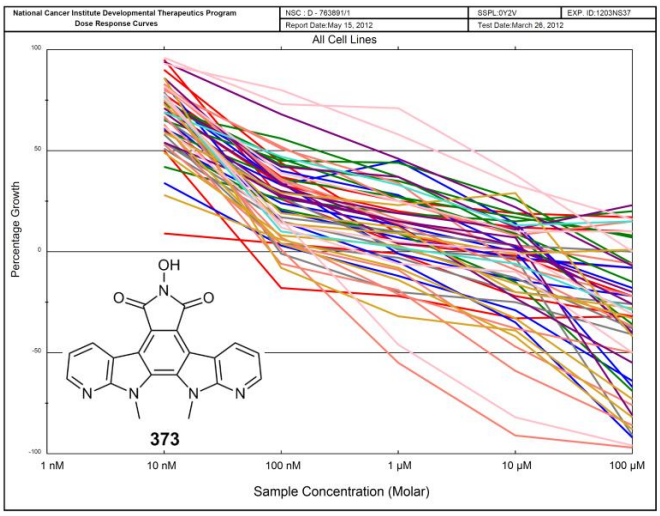

Fig. 5.15 *Dose-response curves for bisaza ICZ* ***373***

Upon conversion of Boc-protected maleimide **372** to hydroxymaleimide **373**, restoration of more typical dose-response curves were recorded, albeit with a large increase in cytotoxicity across most cell lines tested (***Figure 5.15***). Low nanomolar GI_{50} values of less than 10 nM were obtained for **373** against similar cell lines to those targeted by its precursor **372**, such as SR leukemia, SW-620 colon, ACHN and CAKI-1 renal cancer cells (***Figure 5.16***).

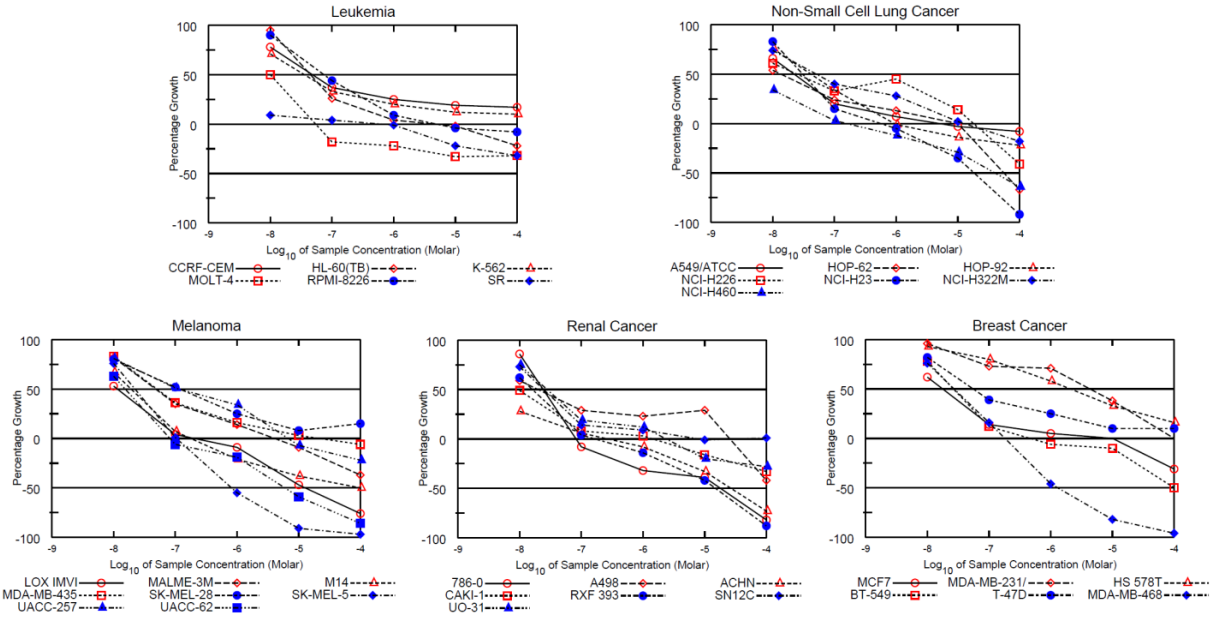

Fig. 5.16 *Dose-response curves for* ***373*** *against leukemia, lung, melanoma, renal and breast cancer cells*

There were also nanomolar TGI figures obtained for hydroxymaleimide **373** against a number of cancer lines, including MOLT-4 leukemia (54.0 nM), SF-539 CNS (97.8 nM) and UACC-62 melanoma (81.5 nM) cells. Unlike either of its bisazaindolyl analogues **371** and **372**, aza ICZ **373** displays cytotoxic effects across many cancer cells, such as MDA-MB-468 breast (LC_{50} = 1.3 μM), SK-MEL-5 (LC_{50} = 0.8 μM) and UACC-62 melanoma (LC_{50} = 5.9 μM) lines (Appendices *xlvi* and *xlvii*).

Utilisation of the COMPARE algorithm to help determine a putative biological mode of action for hydroxymaleimide **373** proved relatively successful, with strong correlation again seen for topotecan **38**. As was the case with its monoaza analogue **363**, strong correlation between hydroxymaleimide **373** and topotecan **38** was observed based on GI_{50} values (0.755). However, unlike with monoaza ICZ **363**, this correlation between bisaza ICZ **373** and topotecan **38** was upheld on comparison of TGI (0.611) and LC_{50} (0.745) values. In fact, **375** was found to have an identical potency to toptecan **38** in terms of mean cytotoxicity (LC_{50} = 63 μM), further corroborating evidence of a common biological mechanism. Strong correlation, based on LC_{50} values, was also noted between bisaza ICZ **373** and the clinical standard anticancer agent cisplatin (0.757).

Examination of the five-dose data for aza ICZs **363** and **373** illustrates that the hydroxymaleimide moiety is necessary for strong correlation to the bioactivity of topotecan **38**. Though both compounds exhibit excellent growth inhibition across many cell lines in the NCI-60 array, inclusion of the second azaindolyl functionality in **373** results in a large increase in cytotoxicity against a number of different cancer types, a fact which could prove very useful in future SAR work.

The use of topotecan **38** and other topo I inhibitors (particularly camptothecin **37** derivatives) has been of immense importance in the field of cancer chemotherapeutics over the last twenty years.[20] Due to an ever growing understanding of the role of topoisomerase I in the proliferation of different cancer types, new targets are constantly being uncovered. This year for example, using the Cancer Cell Line Encyclopaedia (CCLE), Barretina *et al.* predicted that expression of the SLFN11 gene was linked to sensitivity to topo I inhibitors.[21] Examining over 4,000 primary tumour samples spanning 39 lineages, it was found that Ewing's sarcomas

exhibited the highest SLFN11 expression, suggesting that topo I inhibitors could potentially offer an effective treatment option for this cancer type (***Figure 5.17***).

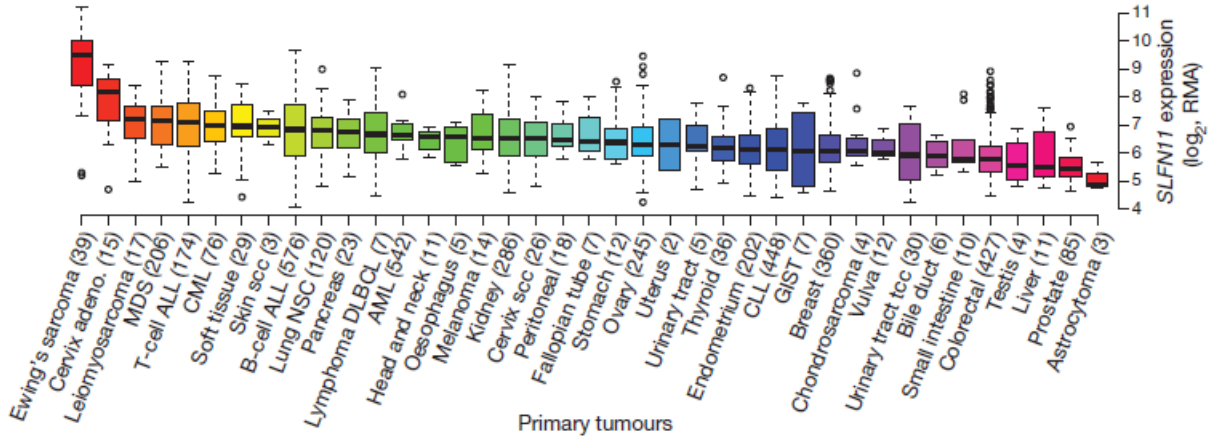

Figure 5.17 *Expression of SLFN11 in 4,103 primary tumour samples*[21]

Looking for markers which were predictive of response to several conventional chemotherapeutic agents, SLFN11 expression had emerged as the top correlate of sensitivity towards topotecan **38** and irinotecan **377**, another camptothecin **37** derivative. These latest findings confirm the preliminary results of a number of clinical trials currently underway to examine the use of topotecan **38** and irinotecan **377** in combinatorial regimens towards the treatment of Ewing's sarcoma.[22]

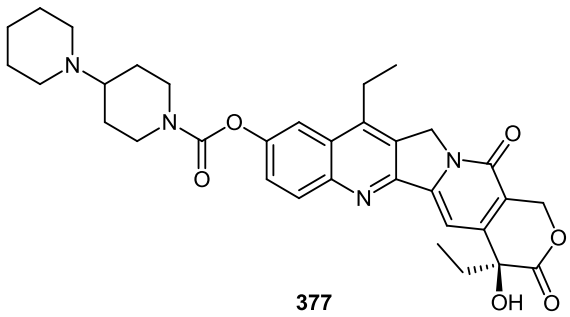

377

Figure 5.18 *Structure of irinotecan **377***

5.3.5 Conclusion

A vast amount of valuable information was obtained from the results of the five-dose assays on nine aza BIM and aza ICZ derivatives, which has lead to a number of potential leads for further biological evaluation. It was found that isoxazolone **323** exhibited good activity against the MDA-MB-435 cell line, suggesting a potential role as a MAPK inhibitor (Section ***5.3.1***). Although maleimides **357** and **361** show good selectivity for a number of cancer cell lines within the NCI-60 array, there is a drop off in activity at lower concentrations (Section ***5.3.2***). However, this issue with potency could be addressed in future SAR studies.

In contrast to maleimides **357** and **361**, most of the monoaza and bisaza ICZs exhibit excellent activity against a number of cell lines at lower concentrations (Sections ***5.3.3*** and ***5.3.4***). In particular, many of the candidates within this series show good selectivity for the SR leukemia cell line, warranting a need for further examination to establish the associated molecular targets. As evidenced by COMPARE analysis, there is a strong correlation between the biological profiles of hydroxymaleimides **363** and **373** and that of the known topoisomerase I inhibitor, topotecan **38**. Hence, the next mode of investigation in the elucidation of the biological targets associated with these aza ICZs assumes the form of a series of topological assays.

5.4 Topoisomerase I-mediated DNA cleavage assay

Results from the NCI-60 five dose screen had previously indicated a strong correlation between the bioactivities of several candidates from our aza ICZ panel and those of known topo I inhibitors, such as topotecan **38** (Sections ***5.3.3*** and ***5.3.4***). Initiating a series of DNA topological assays, selected derivatives were screened for their ability to inhibit topo I-mediated DNA cleavage. Each aza ICZ was examined at a number of different concentrations, with the experimental protocol adapted from Marminon *et al*. (Section ***7.2.1***).[16] By measuring the intensity of the nicked DNA in the lanes of each gel, it was possible to quantify the activity of each drug relative to the standard topo I inhibitor camptothecin **37**.

5.4.1 Monoaza ICZ assays

In the first assay, maleimide **364** showed excellent activity against topo I, comparing very favourably against camptothecin **37** (***Figure 5.19***).

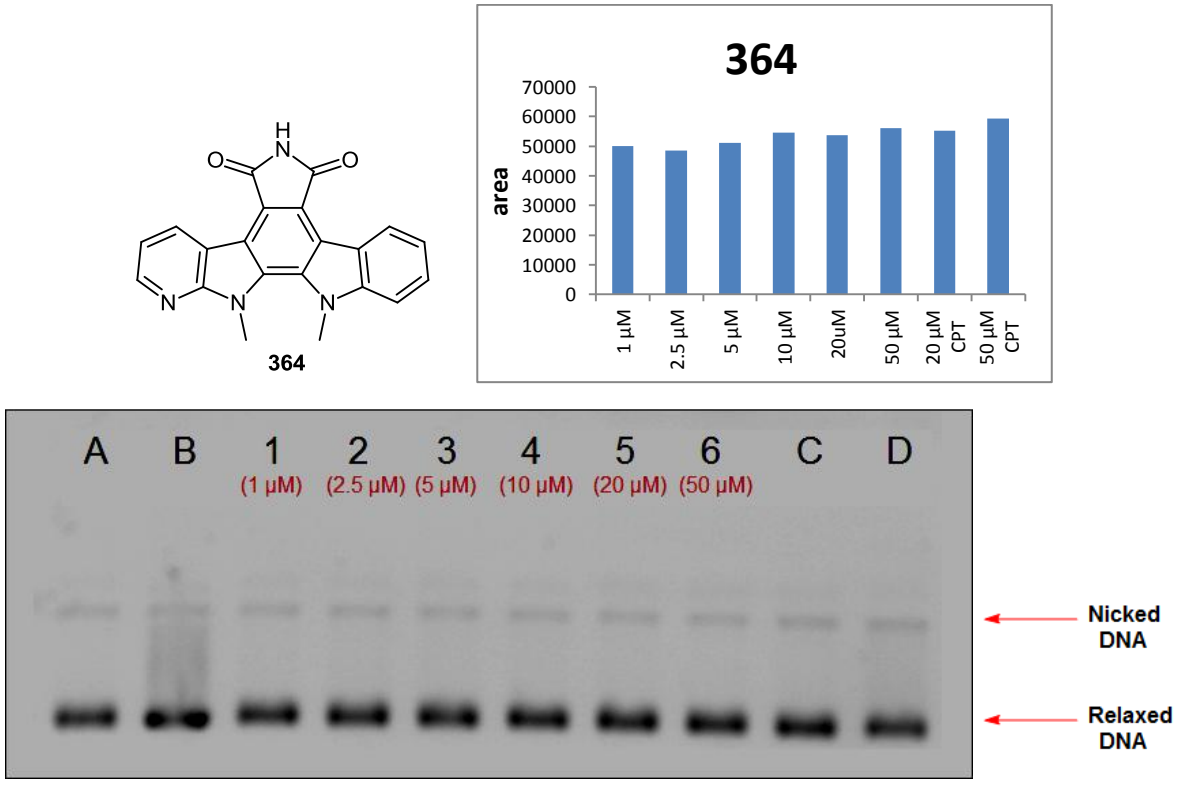

Fig. 5.19 *Topo I assay for maleimide **364** at different concentrations, with a graph of relative intensities of inhibition compared to CPT controls; **A** = positive control (DNA + topo I + water); **B** = negative control (DNA); **C** = camptothecin (20 µM); **D** = camptothecin (50 µM).*

The topo I inhibition displayed by maleimide **364** was found to be relatively consistent regardless of dosage, with only a small decrease in observed activity corresponding to a lowering of the drug concentration (***Figure 5.19***). The inhibitory activity of maleimide **364** was found to be almost identical to that shown by camptothecin **37**, albeit slightly lower. The pattern of topo I inhibition mirrors the unusually flat dose-response curve obtained for **364** in the NCI-60 five dose screen (Section ***5.3.3***), and is perhaps a function of the relatively insoluble nature of the compound.

The introduction of a Boc protecting group in aza ICZ **368** results in more typical concentration-dependent activity against topo I (***Figure 5.20***). However, despite the overall increase in solubility, Boc-protected **368** displays less inhibition than parent maleimide **364**.

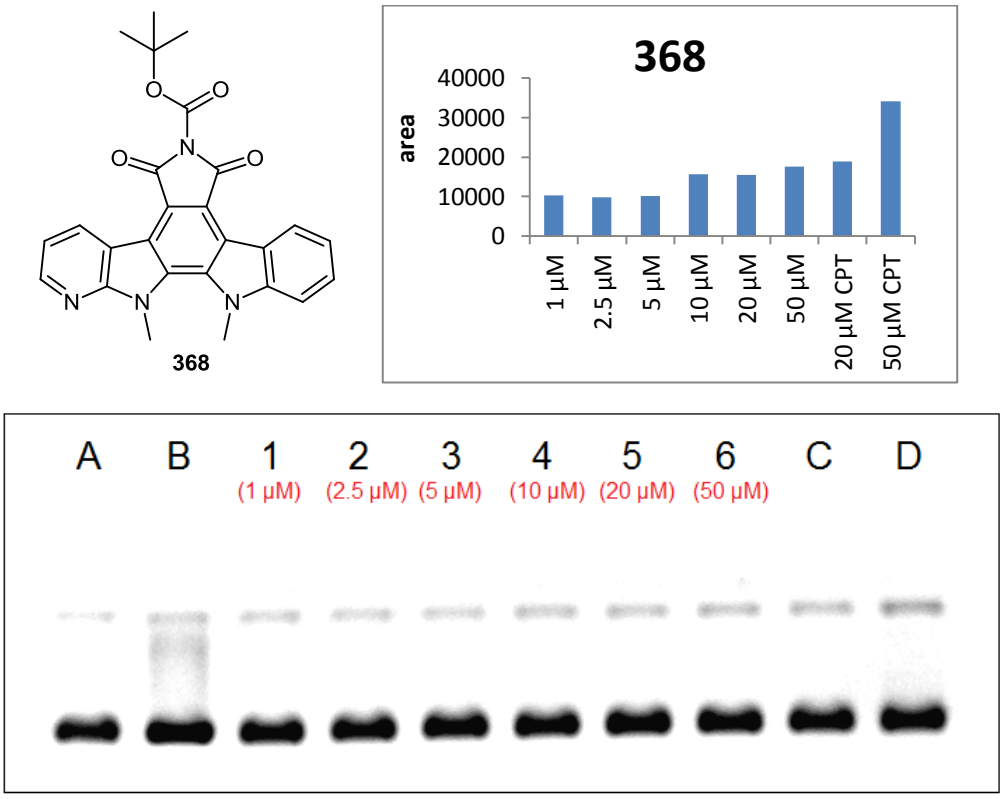

Fig. 5.20 *Topo I assay for Boc-protected maleimide **368** at different concentrations;* ***A*** *= positive control (DNA + topo I + water);* ***B*** *= negative control (DNA only);* ***C*** *= camptothecin (20 µM);* ***D*** *= camptothecin (50 µM).*

The third derivative in the monoaza ICZ series, hydroxymaleimide **363**, showed less topo I activity than maleimide **364**, Boc-protected maleimide **368** or the camptothecin controls

(***Figure 5.21***). This was an unexpected result, as a high correlation had previously been recorded between the bioactivity of hydroxymaleimide **363** in the NCI-60 five dose screen and those of a series of camptothecin derivatives (Section ***5.3.3***). Given the measured intensities of nicked DNA across the different concentrations, it can be seen that topo I inhibition by aza ICZ **363** in this assay is independent of dose.

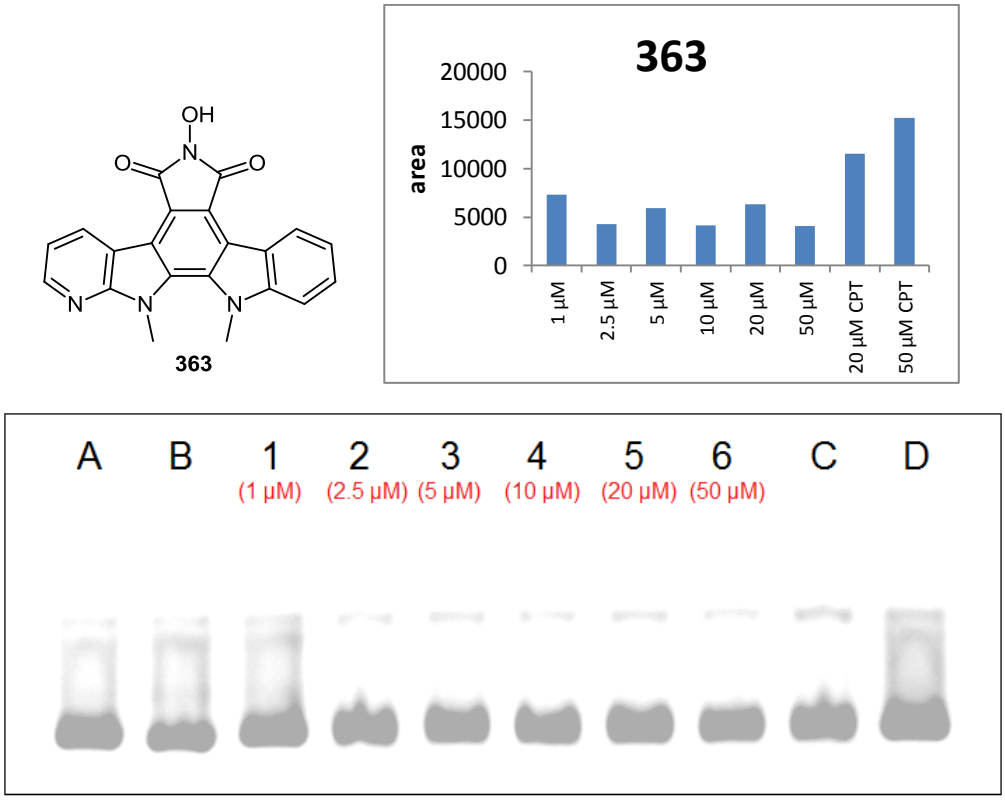

Fig. 5.21 *Topo I assay for hydroxymaleimide **363** at different concentrations;*
A *= positive control (DNA + topo I + water);* ***B*** *= negative control (DNA only);*
C *= camptothecin (20 µM);* ***D*** *= camptothecin (50 µM).*

The disparity between the NCI-60 data and the cleavage assay for hydroxymaleimide **363** is perhaps indicative of a different inhibitory mechanism than that of the topo I "poisoning" effectuated by derivatives of camptothecin **37**. It is possible that aza ICZ **363** instead acts as a topo I "suppressor", whereby the drug directly inhibits the enzyme without stabilising the intermediary topo I-DNA covalent complex. Inhibition of topo I in this manner prevents any binding of the enzyme to the cleavage site, thus halting all subsequent steps in the catalytic cycle, such as religation of the broken DNA strands.[23] As such, the interaction of

hydroxymaleimide **363** with topo I in this manner would not be illuminated in a cleavage assay, and could explain the low level of observed activity.

5.4.2 Bisaza ICZ assays

Maleimide **371**, containing two azaindolyl moieties, retains an almost uniform level of inhibition across the range from 50 µM down to 1 µM, illustrating activity which is relatively independent of concentration at the dosages tested in this assay (***Figure 5.22***).

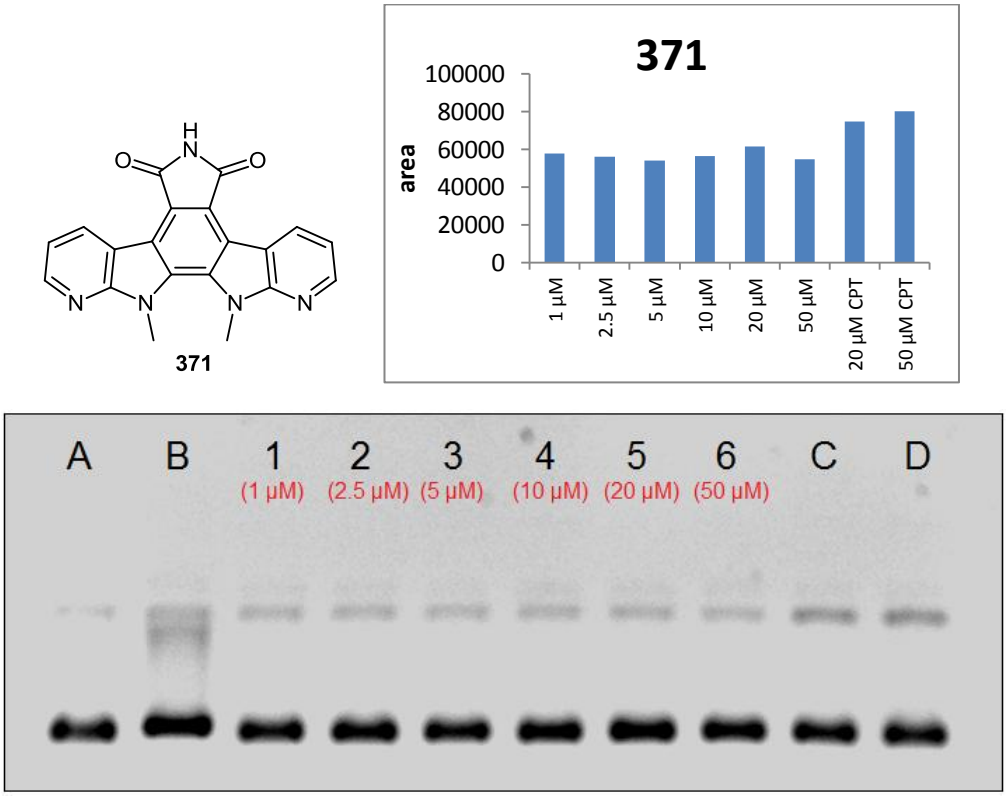

Fig. 5.22 *Topo I assay for maleimide **371** at different concentrations; **A** = positive control (DNA + topo I + water); **B** = negative control (DNA only); **C** = camptothecin (20 µM); **D** = camptothecin (50 µM).*

Much like the results of the cellular testing on the NCI-60 panel (Section ***5.3.4***), the incorporation of a second 7-azaindolyl subunit into the aza ICZ pharmacophore did not improve the efficacy of maleimide **371** compared with its monoaza analogue **364**. Lower levels of inhibition were also observed for **371** compared to the camptothecin controls.

However, introduction of a Boc protecting group in aza ICZ **372** (lending a structural similarity to the topo I inhibitor NB-506 **43**) resulted in a significant increase in the level of interaction with the topo I-DNA covalent complex, as evidenced in ***Figure 5.23***. Although the dose-response curve is not as typical as that recorded for monoaza analogue **368** (Section ***5.4.1***), there is a clear drop off in activity at concentrations of 1 µM and 2.5 µM for aza ICZ **372**, a property not readily seen for the other aza ICZ derivatives tested. Unlike with parent maleimide **371**, the inclusion of a second 7-azaindolyl functionality for Boc-protected derivative **372** resulted in an increase in topo I inhibition relative to its monoaza analogue **368**, again consistent with data obtained from the NCI-60 five-dose screen (Section ***5.3.4***).

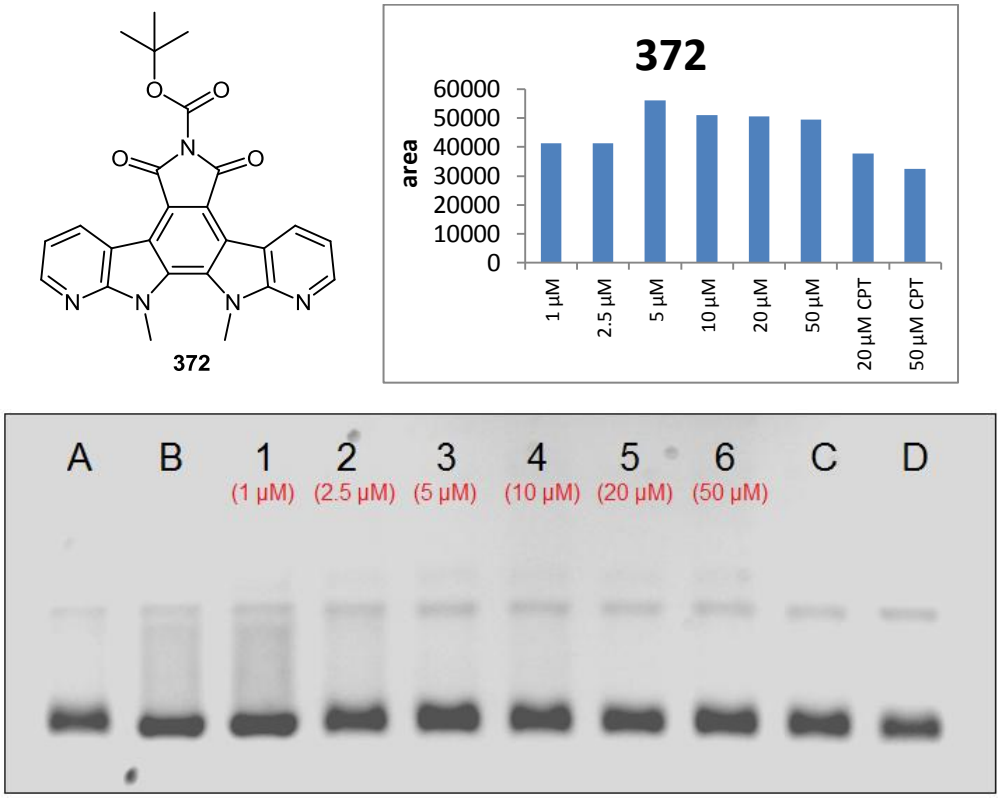

Fig. 5.23 *Topo I assay for Boc-protected maleimide **372** at different concentrations;* ***A*** *= positive control (DNA + topo I + water);* ***B*** *= negative control (DNA only);* ***C*** *= camptothecin (20 µM);* ***D*** *= camptothecin (50 µM).*

Hydroxymaleimide **373** was the most promising candidate to emerge from the NCI-60 five-dose screen, with excellent antiproliferative activity recorded across a range of different cancer cell lines, with a strong correlation to the bioactivity of topotecan **38** indicated by COMPARE analysis (Section ***5.3.4***). It was therefore of little surprise that hydroxymaleimide

373 displayed outstanding inhibitory activity in the topo I-mediated DNA cleavage assay (***Figure 5.24***). As in the case of Boc-protected maleimide **372**, it would appear that a second 7-azaindolyl subunit does much to increase the efficacy of aza ICZ **373** relative to its monoaza analogue **363**.

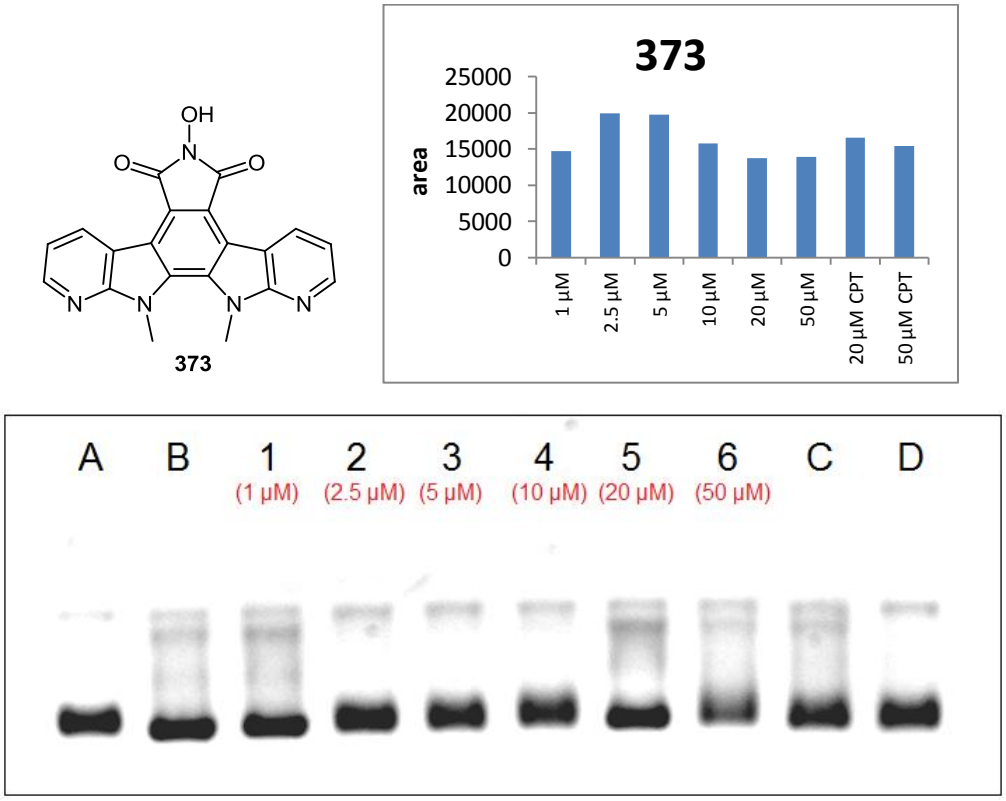

Fig. 5.24 *Topo I assay for hydroxymaleimide **373** at different concentrations;*
***A** = positive control (DNA + topo I + water); **B** = negative control (DNA only);*
***C** = camptothecin (20 µM); **D** = camptothecin (50 µM).*

5.4.3 Conclusion

The results of the assays indicate that significant interaction occurs between the tested aza ICZ candidates and the topo I-DNA covalent complex, a mode of action which could perhaps be at least partially responsible for the antiproliferative activities recorded in the NCI-60 screen. However, although hydroxymaleimide **373** was the most potent compound tested in the five dose screen, it did not display the greatest inhibition of topo I in the cleavage assay, indicating that perhaps there are other cellular targets or mechanisms involved. For example, it is possible that hydroxymaleimide **373** also acts as a topo I suppressor as well as a topo I poison.

Apart from Boc-protected maleimides **368** and **372**, unusual dose-response profiles were observed for the other aza ICZs tested, with activity seemingly independent of the dosage range. In order to ascertain a lower limit of topo I inhibition for these derivatives, it is necessary that further assays be carried out at concentrations below the previous lowest dosage of 1 μM.

5.5 Topoisomerase II decatenation assay

Furthering the examination of our library of novel aza BIM and aza ICZ derivatives against DNA topological assays, selected candidates were screened for their ability to inhibit topoisomerase II-mediated circular kinetoplast DNA (kDNA) decatenation. The standard topoisomerase II inhibitor, ellipticine **378**, was used as a reference compound in this study.

Topoisomerase II (topo II), which belongs to the same enzymatic family as topo I (Section ***1.3.2***), helps to modulate DNA processes via transient double-strand breaks in the DNA helix.[24] Topo II is involved in many vital cellular processes, such as replication, transcription, recombination and segregation, as well as cell proliferation.[25] With higher expression of topo II in proliferating cells than inactive cells, this enzyme is a useful target for the induction of cytotoxic effects in many cancer types. A number of anticancer agents, such as etoposide and doxorubicin, target topo II and trap the enzyme in a covalently-bound complex with DNA, thus interfering with its catalytic activity and leading to DNA damage and cell death.[26]

5.5.1 Topo II inhibition results

The candidates selected for topo II testing are listed in **Table 5.7** and **Table 5.8**. It was found that aza BIM derivatives **293**, **295**, **297**, **300** and **304**, all of which contain a 3,4,5-trimethoxyphenyl moiety, exhibited no inhibitory activity against topo II. Partial inhibition was seen at 100 µM for barbiturate **319** and pyrazolopyrimidine **320**.

Structure	Compound	Activity
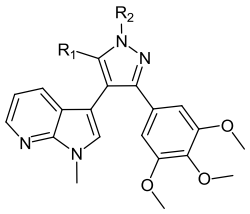	**293**; R_1=NH_2, R_2=H	-
	295; -NHCONHCO-	-
	297; -NC(CF_3)CHC(CF_3)-	-
	300; R_1=$COCF_3$, R_2=H	-
	304; R_1=H, R_2=$CSNHCH_3$	-

Table 5.7 *Topo II decatenation assay: (+*) partial inhibition at 100 µM; (+†) partial inhibition at 100 µM, inactive at 1 and 10 µM*

Structure	Compound	Activity
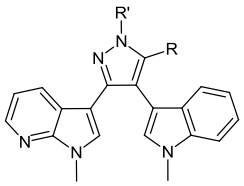	**319**; -NHCONHCO-	+*
	320; -NC(CF_3)CHC(CF_3)-	+*
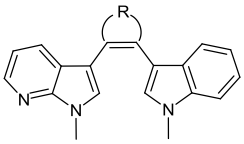	**327**; -NHOCO	+[†]
	328; -N(CH_3)OCO-	-
	332; NC(NH_2)NHCO-	-

Table 5.8 *Topo II decatenation assay: (+*) partial inhibition at 100 µM; (+[†]) partial inhibition at 100 µM, inactive at 1 and 10 µM*

Isoxazolone **327** is seen to partially inhibit topo II at a concentration of 100 µM, although at lower concentrations, however, of 10 µM and 1 µM, the level of inhibition drops off (**Table 5.8**). It was found that alkylation of isoxazolone **327** to methylated derivative **328** resulted in a loss of enzymatic inhibitory activity, mirroring the single-dose data from the NCI-60 cell array, where a loss of antiproliferative activity was recorded from **327** to **328** (Section ***5.2.3***). Pyrimidinone **332**, which was one of the least active compounds in the single-dose NCI-60 screen, was similarly found to exhibit no inhibition towards topo II.

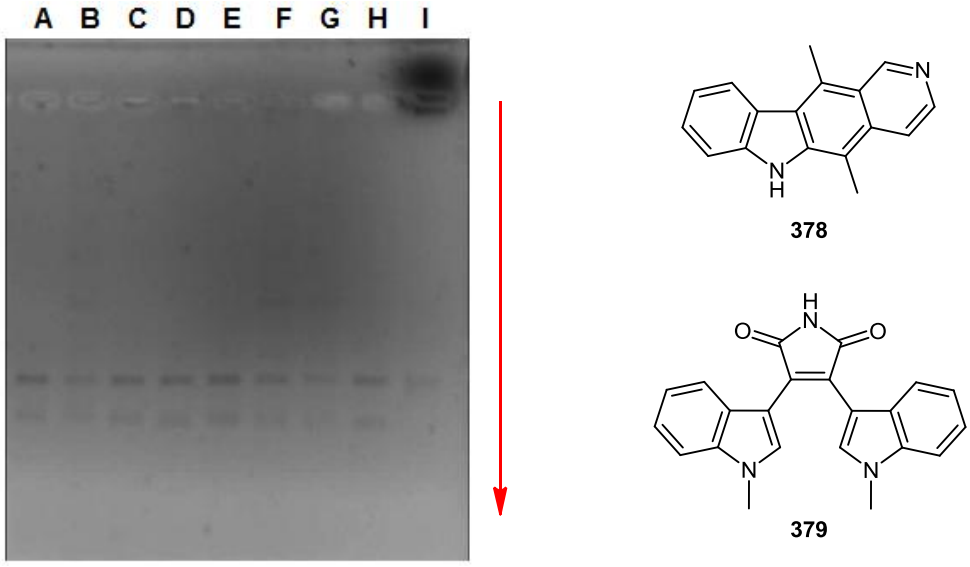

Fig. 5.25 *Representative topo II decatenation assay of screening panel and structures of ellipticine **378** and maleimide **379**; **H** = positive control (cDNA + ATP + topo II); **I** = negative control (cDNA + ATP + topo II + 100 µM ellipticine **378**)*

Lane No.	A	B	C	D	E	F	G
Compound No.	381	327	327	327	328	319	320
Concentration	100 µM	100 µM	10 µM	1 µM	100 µM	100 µM	100 µM
Topo II Inhibition	-	+*	-	-	-	+*	+*

Table 5.9 *Results of representative topo II decatenation assay; inhibitory activity: (+*) = partial inhibition; (-) = not active against topo II*

5.5.2 Conclusion

In the first phase of testing, partial inhibitory activity against topo II was seen for a number of candidates within the class of aza BIM derivatives. The lack of complete inhibition can perhaps be attributed to insufficient molecular planarity, which is required for efficient DNA intercalation, and is a key feature of many topo II inhibitors, such as ellipticine **378**. Further assays are planned towards the inclusion of previously synthesised aza ICZ derivatives, within

which it is anticipated that greater bioactivity will be observed, owing to their more rigid structural nature.

This key SAR feature can be further illustrated by the fact that none of the compounds containing an unrestricted 3,4,5-trimethoxyphenyl moiety exhibited any activity towards topo II. In comparison, it is likely that DNA intercalation is more easily achieved in the case of bicyclic systems **319** and **320** which contain greater conformational planarity, thus contributing to the partial topo II inhibition.

5.6 References

1. Bush, J.A.; Long, B.H.; Catino, J.J.; Bradner, W.T.; Tomita, K. *J. Antibiot.* **1987**, 40, 668-678
2. Koshino, H.; Osada, H.; Amano, S.; Onose, R.; Isono, K. *J. Antibiot.* **1992**, 45, 1428-1432
3. Hashimoto, T.; Yasuda, A.; Akazawa, K.; Takaoka, S.; Tori, M.; Asakawa, Y. *Tetrahedron Lett.* **1994**, 35, 2559-2560
4. Prudhomme, M. *Eur. J. Med. Chem.* **2003**, 38, 123-140
5. Knolker, H.J.; Reddy, K.R. *Chem. Rev.* **2002**, 102, 4303-4427
6. Long, B.H.; Rose, W.C.; Vyas, D.M.; Matson, J.A.; Forenza, S. *Curr. Med. Chem.: Anti-Cancer Agents* **2002**, 2, 255-266
7. Akinaga, S.; Sugiyama, K.; Akiyama, T. *Anti-Cancer Drug Design* **2000**, 15, 43-52
8. Sánchez, C.; Méndez, C.; Salas, J.A. *Nat. Prod. Rep.* **2006**, 23, 1007-1045
9. Shoemaker, R.H. *Nat. Rev. Cancer* **2006**, 6, 813-823
10. Paull, K.; Shoemaker, R.H.; Hodes, L.; Monks, A.; Scudiero, D.A.; Rubinstein, L.; Plowman, J.; Boyd, M.R. *J. Natl. Cancer. Inst.* **1989**, 81, 1088-1092
11. Alley, M.C.; Scudiero, D.A.; Monks, P.A.; Hursey, M.L.; Czerwinski, M.J.; Fine, D.L.; Abbott, B.J.; Mayo, J.G.; Shoemaker, R.H.; Boyd, M.R. *Cancer Res.* **1988**, 48, 589-601
12. Choi, S.H.; Hyman, T.; Blumberg, P.M. *Cancer Res.* **2006**, 66, 7261-7269
13. Graff, J.R.; McNulty, A.M.; Ross Hanna, K.; Konicek, B.W.; Lynch, R.L.; Bailey, S.N.; Banks, C.; Capen, A.; Goode, R.; Lewis, J.E.; Sams, L.; Huss, K.L.; Campbell, R.M.; Iversen, P.W.; Lee Neubauer, B.; Brown, T.J.; Musib, L.; Geeganage, S.; Thornton, D. *Cancer Res.* **2005**, 65, 7462-7469
14. Pierce, L.T.; Cahill, M.M.; Winfield, H.W.; McCarthy, F.O. *Eur. J. Med. Chem.* **2012**, 56, 292-300
15. Kuo, G.-H.; Prouty, C.; DeAngelis, A.; Shen, L.; O'Neill, D.J.; Shah, C.; Connolly, P.J.; Murray, W.V.; Conway, B.R.; Cheung, P.; Westover, L.; Xu, J.Z.;

Look, R.A.; Demarest, K.T.; Emanuel, S.; Middleton, S.A.; Jolliffe, L.; Beavers, M.P.; Chen, X. *J. Med. Chem.* **2003**, 46, 4021-4031

16. Marminon, C.; Pierré, A.; Pfeiffer, B.; Pérez, V.; Léonce, S.; Joubert, A.; Bailly, C.; Renard, P.; Hickman, J.; Prudhomme, M. *J. Med. Chem.* **2003**, 46, 609-622
17. Paine, E.; Palmantier, R.; Akiyama, S.K.; Olden, K.; Roberts, J.D. *J Biol. Chem.* **2000**, 275, 11284-11290
18. Laufer, S.A.; Mergutti, S. *J. Med. Chem.* **2008**, 51, 2580-2584
19. Essery, J.H.; O'Herron, F.A.; McGregor, D.N.; Bradner, W.T. *J. Med. Chem.* **1976**, 19, 1339-1342
20. Pommier, Y. *Chem. Rev.* **2009**, 109, 2894-2902
21. Barretina, J.; Caponigro, G.; Stransky, N.; Venkatesan, K.; Margolin, A.A.; Morrissey, M.P.; Sellers, W.R.; Schlegel, R.; Garraway, L.A. *et al. Nature* **2012**, 483, 603-607
22. Wagner, L.M. *Pediatr. Blood Cancer* **2007**, 48, 132-139
23. Bailly, C. *Curr. Med. Chem.* **2000**, 7, 39-58
24. Burden, B.A.; Osheroff, N. *Biochim. Biophys. Acta* **1998**, 1400, 139-154
25. Nitiss, J.L. *Nat. Rev. Cancer* **2009**, 9, 338-350
26. Baldwin, E.L.; Osheroff, N. *Curr. Med. Chem.: Anti-Cancer Agents* **2005**, 5, 363-372

Chapter 6

Current Perspectives

6.0 Current Perspectives

6.1 Overview

The definitive achievement of synthetic endeavour within this project involved successfully completing a panel of forty-one novel derivatives of the aza BIM **380** and aza ICZ **381** templates. Considerable success was met in propagating the previously underexploited theme of F-ring modulation, leading to the development of key heterocyclic analogues, containing isoxazolone, aminopyrazole or pyrimidinone headgroups, for instance.

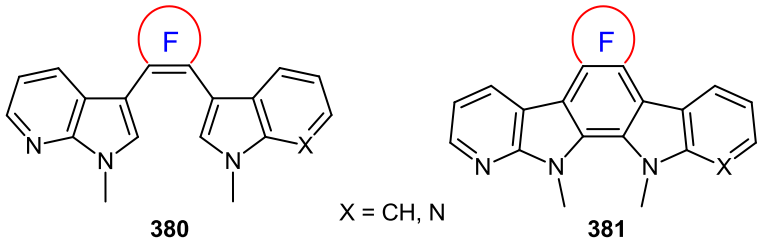

Fig. 6.1 *Key aza BIM* ***380*** *and aza ICZ* ***381***

Previous work in this field has focused on the coupling of azaindolyl moieties to dibromomaleimide subunits, a path which limits the scope of heteroaryl derivatisation within the resulting aza BIMs and aza ICZs. To this end, a series of β-keto ester and β-keto nitrile intermediates, initially identified via retrosynthetic analysis, were fashioned in order to advance our goal of diversity-oriented synthesis. The cyclocondensation of these intermediates with various nucleophiles such as hydrazine or guanidine, followed by several different modes of derivatisation, resulted in the formation of novel analogues of the BIM pharmacophore, later to prove of considerable biological interest.

Aromatisation studies involving these aza BIM derivatives later resulted in the photochemically-induced synthesis of the first reported aza ICZ with a six-membered F-ring. Limitations to this approach informed the design and progression of a second route, whereby the aza ICZ template, and subsequent F-ring modulation, was accomplished from maleimide precursors following Perkin-type methodology. Two novel routes ultimately leading towards aza ICZs were therefore developed in this project.

Preliminary biological evaluation of candidates from the panel of aza BIM and aza ICZ derivatives was achieved in the form of the NCI-60 cell screen and a series of DNA topological assays. The identification of several lead compounds, along with the disclosure of excellent selectivity in the bioactive profiles of numerous derivatives, confirmed the pursuance of F-ring elaboration as a viable paradigm to the medicinal chemist.

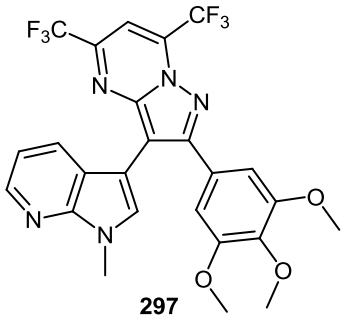

297

Mean growth = 94.0%
NSC lung cancer selectivity
(HOP-92: -3.1%)

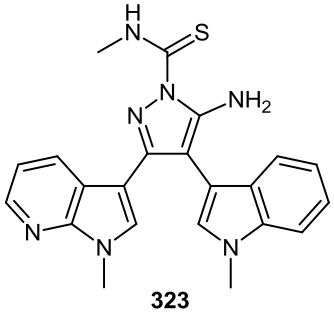

323

Mean growth = 73.8%
Melanoma potency
(M14 growth: 27.5%;
MDA-MB-435: 25.6%)

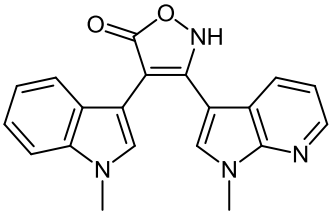

327

Mean growth = 60.9%
Melanoma, leukemia potency
(SR growth: 9.3%;
MDA-MB-435: 2.6%)

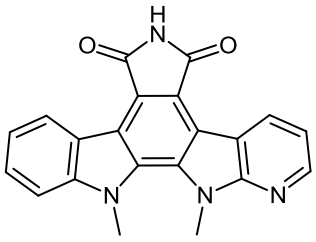

364

Topo I inhibitor (1 µM)
Mean GI_{50} = 1.44 µM

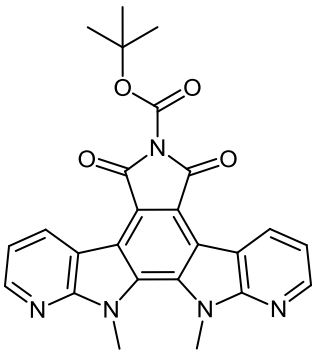

372

Topo I inhibitor (1 µM)
Mean GI_{50} = 0.22 µM

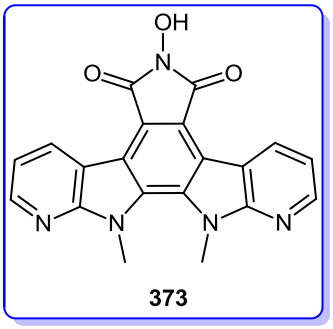

373

Topo I inhibitor (1 µM)
Mean GI_{50} = 0.03 µM

Fig. 6.2 *Novel aza BIM and aza ICZ derivatives with anticancer activity*

The selectivity profiles revealed by a number of candidates in the NCI-60 single dose screen illustrated the potential that exists for unique molecular targets within this class of compounds. For example, pyrimidine **297** was shown to be highly selective for the HOP-92 lung cancer cell line, with carbothioamide **323** targeting melanoma cell lines and isoxazolone displaying excellent activity against melanoma and leukemia cell lines (***Figure 6.2***).

Of the twenty-nine compounds submitted to the NCI-60 cell screen, nine were selected for further screening, representing an excellent return. Utilisation of the COMPARE algorithm revealed a correlation between the five dose data for a number of derivatives within the panel and a series of camptothecin analogues, highlighting the possibility of topo I inhibition as a putative mechanism of action. This was borne out in topo I-mediated DNA cleavage assays, with aza ICZs such as maleimide **364**, Boc-protected maleimide **372** and hydroxymaleimide **373** showing low micromolar inhibitory activity. The most bioactive compound from the five dose screen, hydroxymaleimide **373**, is currently being assessed by the Biological Evaluation Committee in the NCI, and is under consideration for further testing.

6.2 Future Work

The incorporation of a 3,4,5-trimethoxyphenyl functionality into the aza BIM template **382** was seen to confer admirable selectivity towards a number of cancer cell lines within the NCI-60 cell array (Section ***5.2.1***). Identification of targets associated with these cell lines, followed by molecular modelling of ligand-enzyme interactions, shall allow further functionalisation of the aminopyrazole pharmacophore towards the achievement of potential clinical candidates.

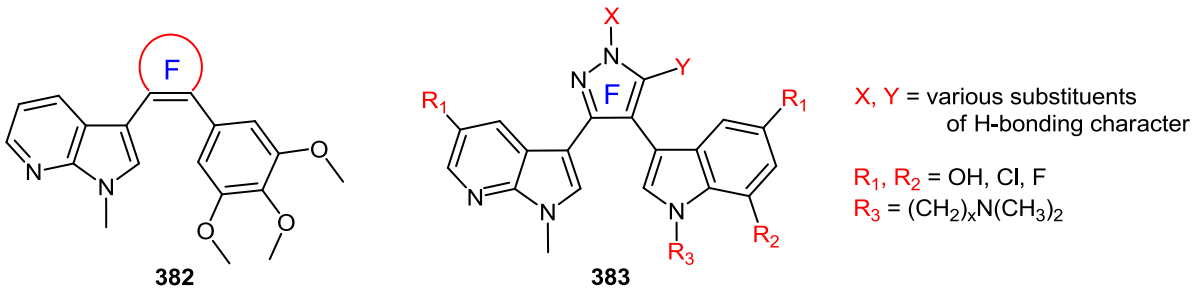

Fig. 6.3 *General structures of aza BIM derivatives*

As previously discussed, unique and specific bioactive profiles were obtained for more conventional aza BIM derivatives of general structure **383** (Sections ***5.2.2***, ***5.3.3*** and **6.1**). Second-generation endeavour towards increasing both selectivity and potency will involve substitution on the azaindolic rings using hydroxyl or halogen functionalities, removal of alkyl protecting groups or replacement with solubilising chains, and also further F-ring modulation.

It is proposed that isoxazolone **327** may be a potent inhibitor of mitogen-activated protein (MAP) kinase, given its activity against the MDA-MB-435 cell line and also that previous biological evaluation of compounds containing an isoxazolone heterocycle have been shown to exhibit good inhibition against p38 MAP kinase. Kinase and tubulin inhibition assays would form the next steps of biological evaluation for derivatives of **327**.

The most bioactive compounds within the library of aza BIM and aza ICZ derivatives proved to be the fully aromatised aza ICZs with 5-membered F-rings (Section ***5.3.4***), such as maleimide **364**, with excellent activity seen for this compound class down to a low nanomolar concentration against a number of cell lines. Given the antiproliferative nature of these aza ICZs, it will be important to carry out flow cytometry studies in order to ascertain the point in the cell cycle at which growth is arrested. From this, it will be possible to probe potential interactions with, for instance, checkpoint kinases, thus advancing further towards a complete understanding of the associated biological mode of action.

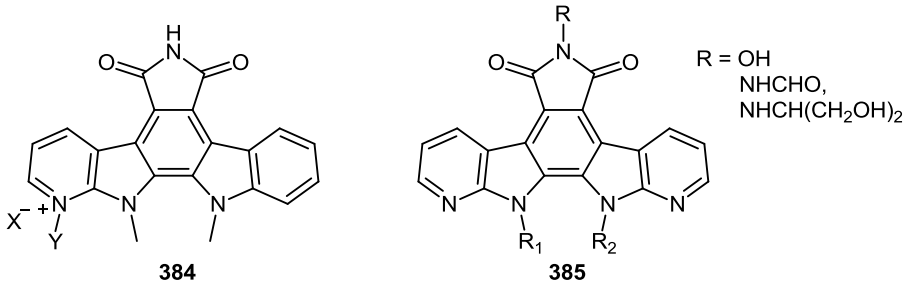

Fig. 6.4 *Structures of proposed aza ICZs* ***384*** *and* ***385***

Solubility can be regarded as a significant issue towards the future development of aza ICZs as clinical candidates, as evidenced by the dose-response curves in the 5-dose assays. The introduction of a lipophilic Boc group on the maleimide ring did help in this regard, and further resolution of this problem could possibly be accomplished by the formation of

quaternary salts at the azaindolic nitrogen atoms (**384**), for example by reaction with alkyl halides or inorganic complexes containing ruthenium or platinum. The introduction of more water soluble moieties, such as *N*-formyl or 2-aminopropane-1,3-diol groups (**385**), by substitution on the nitrogen atom of the maleimide ring could also help improve solubility, as in the well-known ICZs, NB-506 **43** and edotecarin **44** (Section *1.3.2.2*).

Given the excellent antiproliferative and topo I activity of hydroxymaleimide **373**, it should function as a lead compound for future work. It is envisaged that further SAR study would examine the use of various hydroxyl or halogen atom substituents on the peripheral benzenoid rings or long-chain amines on the indolic nitrogens (R_1 and R_2 of **385**). The synthesis of analogues containing 4-, 5- or 6-azaindolyl moieties also represents a worthy paradigm with which to investigate and pursue the development of novel anticancer chemotherapeutic agents.

Much effort remains to be expended towards F-ring modulation in the field of ICZ chemistry, as the enormous potential remains for the exploitation of discrete differences in the active sites of protein kinases. For example, the synthesis of derivatives containing sulfomaleic anhydride **387** or isothiazolone dioxide **389** headgroups could allow for the expansion of the hydrogen bonding networks in the ligand-enzyme complex.

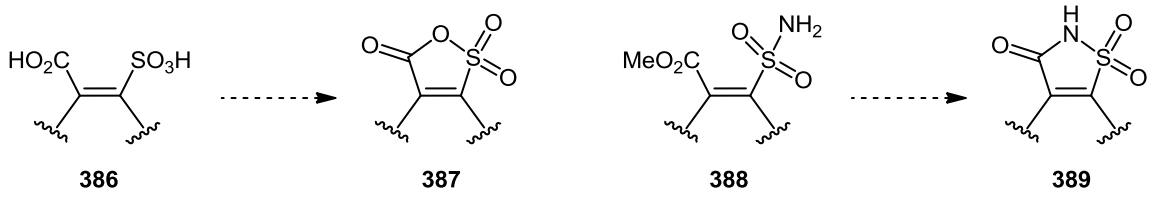

Fig. 6.5 *Proposed syntheses of sulfomaleic anhydride **387** and isothiazolone **389***

Overall, this project has examined many different aspects of the aza ICZ pharmacophore towards their use against cancer. Given the scarcity of literature precedent towards these derivatives within the wide spectrum of the broader ICZ family, it is envisaged that this work will help to inform and encourage future work within this field. As evidenced by extensive NCI-60 and topo I inhibitory data obtained, enormous potential exists within aza ICZs to develop viable candidates for use in the clinic. On a personal level, I have gained invaluable insight into the multifaceted discipline of medicinal chemistry, and a huge respect for both its scope and the possibilities that exist there within.

Chapter 7

Experimental

Contents

7.0 Experimental

7.1 General procedures

Solvents were distilled prior to use as follows: dichloromethane was distilled from phosphorous pentoxide; ethyl acetate was distilled from potassium carbonate; ethanol and methanol were distilled from magnesium in the presence of iodine and stored over 3 Å molecular sieves; toluene was distilled from sodium and benzophenone and stored over 4 Å molecular sieves; hexane was distilled prior to use; tetrahydrofuran was freshly distilled from sodium and benzophenone. Diethyl ether was obtained pure from Riedel-de Haën. HPLC grade acetonitrile was obtained from Fluka. Molecular sieves were dried by heating to >100 ^{o}C at 0.2 mbar overnight or at 140 ^{o}C for 24 hours. Organic phases were dried using anhydrous magnesium sulfate. All commercial reagents were used without further purification unless otherwise stated.

Melting points were measured in a uni-melt Thomas Hoover capillary melting point apparatus and are uncorrected. Thin layer chromatography was carried out on precoated silica gel plates (Merck 60 PF254), and visualisation was achieved by UV light detection (254 or 366 nm) or vanillin staining. Wet flash column chromatography was performed using Kieselgel silica gel 60, 0.040 – 0.063 mm (Merck).

Infrared spectra were recorded as a thin film on sodium chloride plates for liquids or a potassium bromide (KBr) disc for solids on a Perkin Elmer Spectrum 100 FT-IR spectrometer. Low resolution mass spectra were recorded on a Waters Quattro Micro triple quadrupole spectrometer (QAA102) in electrospray ionisation (ESI) mode using 50% acetonitrile – water containing 0.1% formic acid as eluent. High resolution mass spectra (HRMS) were recorded on a Waters LCT Premier Time of Flight spectrometer in electrospray ionisation (ESI) mode using 50% acetonitrile – water containing 0.1% formic acid as eluent. Samples (max. 1 mg) were dissolved in acetonitrile, methanol or a 1:1 acetonitrile/methanol mixture.

^{1}H (300 MHz) and ^{13}C (75 MHz) NMR spectra were recorded on a Bruker Avance 300 NMR spectrometer. ^{1}H (400 MHz) NMR spectra were recorded on a Bruker Avance 400 NMR spectrometer. ^{13}C (125 MHz) NMR spectra were recorded on a Bruker Avance 500 NMR

spectrometer. ^{1}H (600 MHz) and ^{13}C (150 MHz) NMR spectra were recorded on a Bruker Avance III 600 MHz NMR spectrometer equipped with a dual CH cryoprobe. Spectra were recorded at room temperature (~20 ^{o}C) unless otherwise stated, in deuterated chloroform ($CDCl_3$) with tetramethylsilane (TMS) as an internal standard, deuterated dimethylsulfoxide (DMSO-d_6), or deuterated methanol (CD_3OD). Chemical shifts (δ_H and δ_C) are expressed in parts per million (ppm) relative to the reference peak. Coupling constants (J) are expressed in Hertz (Hz). Splitting patterns in ^{1}H NMR spectra are designated as s (singlet), bs (broad singlet), d (doublet), bd (broad doublet), t (triplet), q (quartet), dd (doublet of doublets) and m (multiplet). ^{13}C NMR spectra were assigned (CH, CH_2, CH_3) with the aid of DEPT (Distortionless Enhancement by Polarisation Transfer) experiments.

7.2 Chemical data

7.2.1 Route towards 7-azaindolyl precursors

2-(*tert*-Butylaminomethylene)succinonitrile (257)[1]

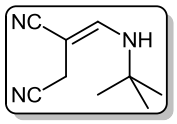

While stirring under a nitrogen atmosphere, sodium metal (4.720 g, 205 mmol) was carefully added in a portionwise manner to methanol (100 mL), which was cooled to 0 ^{o}C in an ice bath. Once complete, the excess solvent was evaporated under reduced pressure, leaving sodium methoxide as a white solid (11.023 g, 204 mmol). Also under a nitrogen atmosphere, anhydrous toluene (100 mL) was added to the sodium methoxide, with the resulting suspension cooled to 5 ^{o}C. To this stirred suspension, a solution of ethyl formate **254** (18.3 mL, 227 mmol) and succinonitrile **253** (15.026 g, 188 mmol) in anhydrous toluene (100 mL) was added dropwise over a 20 minute period. Once the addition was complete, the mixture was allowed to stir at room temperature for 2.5 hours. To the reaction mixture was then added *tert*-butylamine (20.2 mL, 192 mmol), followed by acetic acid (13.2 mL, 231 mmol), and the resulting mixture heated to reflux for 2.5 hours. Once cooled to room temperature, brine (50 mL) was added, and the two phases were separated. The aqueous layer was extracted with toluene (2 x 20 mL), before the combined organic extracts were washed with water (2 x 50 mL), dried over magnesium sulfate and evaporated under reduced pressure. The brown residue was desiccated overnight at 50 ^{o}C to yield **257** as a brown solid (24.875 g, 81 %) in a mixture of E and Z isomers (1:6): m.p. 114-117 ^{o}C (lit.[1] 118-119 ^{o}C); ν_{max}/cm^{-1} (KBr) 3319, 2977, 2191, 1638, 1227; δ_H (300 MHz, $CDCl_3$) 1.30 [9H, s, C(C$\underline{H}_3$)$_3$], 3.16 [2H, s, C$\underline{H}_2$CN], 5.21 [1H, bd, *J* 14.2, NH], 6.91 [1H, d, *J* 14.2, C=C$\underline{H}$ (E isomer)], 7.01 [1H, d, *J* 14.5, C=C$\underline{H}$ (*Z* isomer)]; δ_C (75 MHz, $CDCl_3$) 15.5 (CH_2, $\underline{C}H_2$CN), 30.1 (3CH_3, C($\underline{C}H_3$)$_3$), 53.4 (C, $\underline{C}$(CH$_3$)$_3$), 65.0 (C, $\underline{C}$=CHNH), 116.3 (C, CN), 122.1 (C, CN), 146.8 (CH, C=$\underline{C}$HNH); m/z (ES+) 164.1 [M+H]$^+$ (100%).

5-Amino-1-(*tert*-butyl)-1*H*-pyrrole-3-carbonitrile (258)[1]

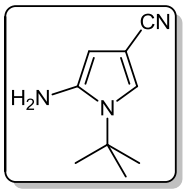

Potassium hydroxide (17.862 g, 271 mmol) was dissolved in absolute ethanol (150 mL) at 50 ^{o}C, with the resulting solution then cooled to room temperature. To the latter, a solution of 2-(*tert*-butylaminomethylene)succinonitrile **257** (24.004 g, 147 mmol) in absolute ethanol (40 mL) was added while stirring. The resulting mixture was stirred for 4 hours at room temperature before being concentrated under reduced pressure until a solid started to precipitate out. Water (120 mL) was then added and the mixture was stirred for 1 hour. The precipitate was filtered, washed with water and desiccated overnight to yield **258** as a brown solid (15.571 g, 65 %): m.p. 111-112 ^{o}C (lit.[1] 112-113 ^{o}C); ν_{max}/cm^{-1} (KBr) 3396, 3335, 2972, 2212, 1633, 1526, 1213; δ_H (300 MHz, DMSO-d_6) 1.53 [9H, s, C(C$\underline{H}_3$)$_3$], 4.46 [2H, bs, NH_2], 5.55 [1H, d, *J* 2.2, C-H_4], 7.15 [1H, d, *J* 2.3, C-H_2]; δ_C (75 MHz, DMSO-d_6) 29.1 ($3CH_3$, C($\underline{C}H_3$)$_3$), 56.5 (C, $\underline{C}$(CH$_3$)$_3$), 87.0 (C, aromatic C), 95.4 (CH, aromatic CH), 118.0 (C, CN), 121.0 (CH, aromatic CH), 139.6 (C, aromatic C); m/z (ES+) 164.1 $[M+H]^+$ (100%).

1-(*tert*-Butyl)-1*H*-pyrrolo[2,3-*b*]pyridine-3-carbonitrile (259)[1]

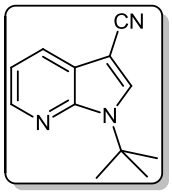

To a solution of 5-amino-1-(*tert*-butyl)-1*H*-pyrrole-3-carbonitrile **258** (15.008 g, 92.4 mmol) in toluene (150 mL) was added 1,1,3,3-tetramethoxypropane (16.9 mL, 102.6 mmol) and then *p*-toluenesulfonic acid monohydrate (1.863 g, 9.8 mmol). The reaction mixture was then slowly heated to reflux, utilising distillation apparatus to perform the azeotropic removal of methanol, a by-product of the reaction. After 1 hour, the reaction mixture was cooled to room temperature and the solvent evaporated under reduced pressure. Diethyl ether (100 mL) was added to residue, which was then heated to reflux for 20 minutes. Once cooled to room temperature, the latter mixture was filtered off, with the residue being washed with diethyl ether (20 mL). The combined organic layers were evaporated under reduced pressure, with the residue then being subjected to flash column chromatography (hexane/ethyl acetate, 70:30) to yield the pure product **259** as an orange crystalline solid (14.047 g, 76%): m.p. 90-

91 °C (lit.[1] 91-92 °C); ν_{max}/cm^{-1} (KBr) 2972, 2215, 1602, 1522, 1210; δ_H (300 MHz, $CDCl_3$) 1.83 [9H, s, C(C<u>H</u>$_3$)$_3$], 7.22 [1H, dd, *J* 8.0, 4.7, C-H$_5$], 7.87 [1H, s, C-H$_2$], 8.04 [1H, dd, *J* 8.0, 1.7, C-H$_4$], 8.43 [1H, dd, *J* 4.7, 1.6, C-H$_6$]; δ_C (75 MHz, $CDCl_3$) 29.1 (3CH$_3$, C(<u>C</u>H$_3$)$_3$), 58.5 (C, <u>C</u>(CH$_3$)$_3$), 83.1 (C, aromatic C), 115.6 (C, CN), 117.6 (CH, aromatic CH), 121.4 (C, aromatic C), 127.9 (CH, aromatic CH), 133.1 (CH, aromatic CH), 144.1 (CH, aromatic CH), 147.1 (C, aromatic C); m/z (ES+) 200.2 $[M+H]^+$ (100%).

1*H*-Pyrrolo[2,3-*b*]pyridine-3-carbonitrile (260)[1]

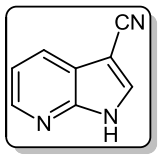

Under a nitrogen atmosphere at room temperature, 1-(*tert*-butyl)-1*H*-pyrrolo[2,3-*b*]pyridine-3-carbonitrile **259** (13.501 g, 67.8 mmol) was added portionwise to a stirred suspension of $AlCl_3$ (28.026 g, 210.2 mmol) in chlorobenzene (120 mL) over 30 minutes. Once the additions were complete, the reaction mixture was heated to reflux for 8 hours. Once cooled to room temperature, precooled 2 M aqueous HCl (150 mL) was carefully added to the reaction mixture, which was then allowed to stir for 2 hours. Celite (10 g) was then added to the mixture, which was subsequently filtered. The phases were separated and the organic layer was washed with 2 M aqueous HCl (3 x 25 mL), following which the combined aqueous extracts were washed with a further portion of chlorobenzene (25 mL). The pH of the strongly acidic aqueous layer was adjusted to 2.5 using 50 wt.% aqueous NaOH. The precipitate formed was filtered, washed with water and desiccated at 50 °C to give **260** as an off-white solid (7.840 g, 81%): m.p. 254-256 °C (lit.[1] 259-260 °C); ν_{max}/cm^{-1} (KBr) 3021, 2837, 2220, 1583, 1418, 1287; δ_H (300 MHz, DMSO-d_6) 7.29 [1H, dd, *J* 7.9, 4.7, C-H$_5$], 8.12 [1H, dd, *J* 8.0, 1.5, C-H$_4$], 8.41 [1H, dd, *J* 4.7, 1.4, C-H$_6$], 8.44 [1H, s, C-H$_2$], 12.84 [1H, bs, NH]; δ_C (75 MHz, DMSO-d_6) 83.2 (C, aromatic C), 115.6 (C, CN), 117.9 (CH, aromatic CH), 118.9 (C, aromatic C), 127.3 (CH, aromatic CH), 135.5 (CH, aromatic CH), 145.0 (CH, aromatic CH), 147.4 (C, aromatic C); m/z (ES+) 144.1 $[M+H]^+$ (100%).

1*H*-Pyrrolo[2,3-*b*]pyridine-3-carboxylic acid (255)[1]

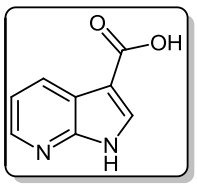

1*H*-Pyrrolo[2,3-*b*]pyridine-3-carbonitrile **260** (3.506 g, 24.5 mmol) was suspended in 12 M aqueous HCl (50 mL), and the resulting mixture was heated to 70 °C for 20 hours. Water (30 mL) and charcoal (0.4 g) were then added, and the mixture was stirred for 1 hour at 70 °C. Celite (0.4 g) was then added and the mixture was stirred for a further hour at 70 °C. The warm solution was then filtered, before being cooled to room temperature. The pH of the strongly acidic solution was adjusted to 2.5 using 50 wt.% aqueous NaOH, at which point a white precipitate formed. The suspension was then stirred for 2 hours at room temperature, before the precipitate was filtered off and washed with water, then desiccated overnight at 50 °C to yield carboxylic acid **255** as a white solid (3.616 g, 91%): m.p. 244-246 °C (lit.[1] 245-246°C); ν_{max}/cm^{-1} (KBr) 3416, 3145, 2545, 1679, 1531, 1320, 1186; δ_H (300 MHz, DMSO-d_6) 7.22 [1H, dd, *J* 7.8, 4.8, C-H$_5$], 8.14 [1H, s, C-H$_2$], 8.30-8.34 [2H, m, C-H$_{4,6}$], 12.46 [1H, bs, COOH]; δ_C (75 MHz, DMSO-d_6) 106.3 (C, aromatic C), 117.4 (CH, aromatic CH), 118.3 (C, aromatic C), 128.8 (CH, aromatic CH), 132.6 (CH, aromatic CH), 143.7 (CH, aromatic CH), 148.6 (C, aromatic C), 165.4 (C, C=O); m/z (ES+) 163.1 $[M+H]^+$ (100%).

1*H*-Pyrrolo[2,3-*b*]pyridine (139)[1]

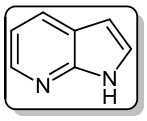

A mixture of 1*H*-pyrrolo[2,3-*b*]pyridine-3-carbonitrile **260** (3.450 g, 24.1 mmol) and 12 M aqueous HCl (40 mL) were heated to reflux for 24 hours. The reaction mixture was cooled to 70 °C and additional 12 M aqueous HCl (40 mL) was added. The mixture was then once again heated to reflux for 24 hours. Once the mixture was cooled to room temperature, water was added (50 mL) and was adjusted to pH 2.5 using 50 wt.% aqueous NaOH. Charcoal (0.4 g) and celite (0.4 g) were added to the mixture, which was then stirred for 1 hour at room temperature and subsequently filtered. The filtrate was adjusted to pH 12 using 50 wt.% aqueous NaOH, after which it was extracted with DCM (4 x 20 mL). The combined organic extracts were dried over magnesium sulfate and evaporated to yield **139** as a white solid (1.776 g, 62%): m.p. 106-108 °C (lit.[1] 105-106 °C); ν_{max}/cm^{-1} (KBr) 3067, 1600, 1584, 1422, 1279, 1107; δ_H (300 MHz, $CDCl_3$) 6.51 [1H, d, *J* 3.5,

C-H_3], 7.09 [1H, dd, *J* 7.9, 4.8, C-H_5], 7.40 [1H, d, *J* 3.5, C-H_2], 7.97 [1H, dd, *J* 7.9, 1.6, C-H_4], 8.35 [1H, dd, *J*, 4.8, 1.5, C-H_6], 11.89 [1H, bs, NH]; δ_C (75 MHz, $CDCl_3$) 100.5 (CH, aromatic CH), 115.7 (CH, aromatic CH), 120.6 (C, aromatic C), 125.4 (CH, aromatic CH), 129.1 (CH, aromatic CH), 142.2 (CH, aromatic CH), 148.9 (C, aromatic C); m/z (ES+) 119.1 $[M+H]^+$ (100%).

Methyl 1-methyl-1*H*-pyrrolo[2,3-*b*]pyridine-3-carboxylate (269)

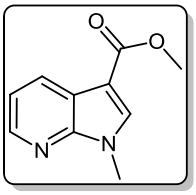

To a solution of 1*H*-pyrrolo[2,3-*b*]pyridine-3-carboxylic acid **255** (1.500 g, 9.3 mmol) in DMF (40 mL) was added dimethyl carbonate (5.8 mL, 68.9 mmol) and potassium carbonate (2.065 g, 14.9 mmol). The resulting mixture was heated to reflux for 14 hours. Once cooled to room temperature, water (50 mL) and ethyl acetate (50 mL) were added to the reaction mixture. The two phases were separated and the aqueous phase was further extracted with ethyl acetate (50 mL). The combined organic extracts were then washed with water (4 x 50 mL) and brine (50 mL), before being dried over magnesium sulfate and evaporated under reduced pressure. The crude residue was subjected to flash column chromatography to yield the product **269** as a white solid (1.307 g, 74%): m.p. 116-118 ^oC; ν_{max}/cm^{-1} (KBr) 3123, 3012, 1712, 1599, 1359, 1266; δ_H (300 MHz, $CDCl_3$) 3.91 [3H, s, OCH_3], 3.93 [3H, s, NCH_3], 7.22 [1H, dd, *J* 7.8, 4.9, C-H_5], 7.91 [1H, s, C-H_2], 8.39 [1H, dd, *J* 4.9, 1.6, C-H_6], 8.41 [1H, dd, *J* 7.8, 1.6, C-H_4]; δ_C (75 MHz, $CDCl_3$) 31.8 (CH_3, NCH_3), 51.1 (CH_3, OCH_3), 105.5 (C, aromatic C), 117.9 (CH, aromatic CH), 119.0 (C, aromatic C), 129.9 (CH, aromatic CH), 135.0 (CH, aromatic CH), 144.0 (CH, aromatic CH), 148.0 (C, aromatic C), 164.9 (C, C=O); m/z (ES+) 191.3 $[M+H]^+$ (100%); HRMS (ES+): Exact mass calculated for $C_{10}H_{11}N_2O_2$ 191.0821. Found 191.0812.

1-Methyl-1*H*-pyrrolo[2,3-*b*]pyridine-3-carbonitrile (264)

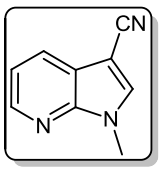

1*H*-Pyrrolo[2,3-*b*]pyridine-3-carbonitrile **260** (17.343 g, 121 mmol) was dissolved in DMF (150 mL), and the resulting solution was cooled to 0 ^{o}C in an ice bath. Sodium hydride (55 wt.% oil dispersion, 7.390 g, 169 mmol) was then added portionwise over 10 minutes, ensuring that the reaction did not become too vigorous. Once the addition was complete, the reaction mixture was stirred at 0 ^{o}C for a further 30 minutes. At this point, a solution of iodomethane (10.5 mL, 169 mmol) in DMF (40 mL) was added in a dropwise manner. Upon completion, the reaction mixture was allowed to warm to room temperature and was stirred for 3 hours. Water (50 mL) was then carefully added to quench the reaction. The reaction mixture was extracted with ethyl acetate (3 x 100 mL), and the combined organic extracts were then washed with water (5 x 100 mL) and brine (100 mL), dried over magnesium sulfate and evaporated under reduced pressure to yield the crude product as a reddish solid. This was then purified by flash column chromatography (hexane/ethyl acetate, 50:50) to yield the pure product **264** as an off-white solid (12.741 g, 68%): m.p. 102-104 ^{o}C; ν_{max}/cm^{-1} (KBr) 3117, 3053, 2221, 1602, 1574, 1533, 1450, 1412, 1304, 1122; δ_H (300 MHz, $CDCl_3$) 3.96 [3H, s, N-CH_3], 7.26 [1H, dd, *J* 7.9, 4.7, C-H_5], 7.75 [1H, s, C-H_2], 8.07 [1H, dd, *J* 7.9, 1.5, C-H_4], 8.46 [1H, dd, *J* 4.7, 1.5, C-H_6]; δ_C (75 MHz, $CDCl_3$) 32.0 (CH_3, NCH_3), 84.2 (C, aromatic C), 115.1 (C, CN), 118.1 (CH, aromatic CH), 120.0 (C, aromatic C), 128.2 (CH, aromatic CH), 135.9 (CH, aromatic CH), 145.3 (CH, aromatic CH), 146.8 (C, aromatic C); m/z (ES+) 158.2 $[M+H]^+$ (100%); HRMS (ES+): Exact mass calculated for $C_9H_8N_3$ 158.0718. Found 158.0711.

1-Methyl-1*H*-pyrrolo[2,3-*b*]pyridine-3-carboxylic acid (265)[2]

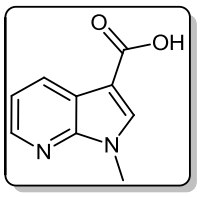

1-Methyl-1*H*-pyrrolo[2,3-*b*]pyridine-3-carbonitrile **264** (12.624 g, 80 mmol), was suspended in 12 M aqueous HCl (100 mL), and the suspension was heated to 70 ^{o}C to give a dark red homogenous solution, which was stirred at this temperature for 20 hours. At this point, the reaction mixture was diluted with water (100 mL) and charcoal (0.8 g) was added. The mixture was stirred at 70 ^{o}C for 30 minutes, before celite (0.8 g) was added, with the reaction

mixture then being stirred for a further 30 minutes. The warm solution was filtered and the filtrate was then allowed to cool to room temperature. The strongly acidic solution was carefully adjusted to pH 2.5 using 50 wt.% aqueous NaOH, at which point a white precipitate was formed. This suspension was stirred at room temperature for 2 hours before the precipitate was filtered off, washed with water and desiccated at 50 ^{o}C overnight to yield the pure product **265** as a white solid (11.628 g, 83%): m.p. 253-255 ^{o}C (lit.[2] 249-251 ^{o}C); ν_{max}/cm^{-1} (KBr) 3488, 3109, 2922, 2498, 1674, 1599, 1538, 1466, 1268, 1135; δ_H (300 MHz, DMSO-d_6) 3.87 [3H, s, N-CH_3], 7.26 [1H, dd, *J* 7.9, 4.7, C-H_5], 8.24 [1H, s, C-H_2], 8.32 [1H, dd, *J* 7.9, 1.6, C-H_4], 8.35 [1H, dd, *J* 4.7, 1.6, C-H_6], 12.25 [1H, bs, COOH]; δ_C (75 MHz, DMSO-d_6) 31.3 (CH_3, NCH_3), 104.9 (C, aromatic C), 117.6 (CH, aromatic CH), 118.6 (C, aromatic C), 129.0 (CH, aromatic CH), 136.2 (CH, aromatic CH), 143.5 (CH, aromatic CH), 147.6 (C, aromatic C), 165.1 (C, C=O); m/z (ES+) 176.1 $[M+H]^+$ (100%).

7.2.2 Synthesis of key intermediates

7.2.2.1 Routes towards oxopropanoates

Methyl 2-(1-methyl-1H-indol-3-yl)acetate (250)[3]

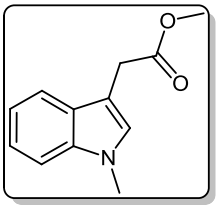

To a solution of indole-3-acetic acid **261** (6.000 g, 34.2 mmol) in DMF (50 mL) was added potassium carbonate (6.002 g, 43.4 mmol) and dimethyl carbonate (8.6 mL, 102.1 mmol). The resulting mixture was heated to reflux for 16 hrs. The reaction mixture was cooled to room temperature, then water (80 mL) and ethyl acetate (60 mL) were added. Following separation of the two layers, the aqueous layer was extracted with ethyl acetate (2 x 40 mL). The combined organic extracts were then washed with water (4 x 50 mL), followed by brine (50 mL) and then dried over magnesium sulfate. The solvent was evaporated under reduced pressure to yield the crude product as a dark red oil. This was then subjected to flash column chromatography (hexane/ethyl acetate, 75:25), isolating **250** as a golden oil which was used without further purification (5.866 g, 84%): ν_{max}/cm^{-1} (NaCl) 2951, 1736, 1617, 1475, 1332, 1163; δ_H (300 MHz, $CDCl_3$) 3.66 [3H, s, OCH_3], 3.67 [3H, s, NCH_3], 3.74 [2H, s,

$C\underline{H_2}COOCH_3$], 6.97 [1H, s, C-H_2], 7.11 [1H, t, *J* 7.8, C-H_5], 7.21 [1H, t, *J* 7.9, C-H_6], 7.25 [1H, d, *J* 7.9, C-H_7], 7.58 [1H, d, *J* 8.0, C-H_4]; δ_C (75 MHz, $CDCl_3$) 31.1 (CH_2, $\underline{C}H_2COOCH_3$), 32.7 (CH_3, NCH_3), 52.0 (CH_3, OCH_3), 106.8 (C, aromatic C), 109.4 (CH, aromatic CH), 119.0 (CH, aromatic CH), 119.3 (CH, aromatic CH), 121.8 (CH, aromatic CH), 127.7 (C, aromatic C), 127.8 (CH, aromatic CH), 137.0 (C, aromatic C) 172.7 (C, C=O); m/z (ES+) 204.4 $[M+H]^+$ (100%).

1-Methyl-1*H*-pyrrolo[2,3-*b*]pyridine-3-carbonyl chloride (266)

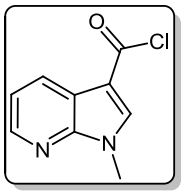

1-Methyl-1*H*-pyrrolo[2,3-*b*]pyridine-3-carboxylic acid **265** (4.301 g, 24.4 mmol) was ground into a fine powder, then suspended in DCM (80 mL) under an inert atmosphere. While cooling in an ice bath, oxalyl chloride (4.5 mL, 51.2 mmol) was added in a dropwise fashion. Once the addition was complete, the reaction mixture was stirred for 16 hours at room temperature. The solvent and excess oxalyl chloride was removed under reduced pressure, to yield acyl chloride **266** in quantitative yield as a white solid, which was subsequently used without further purification: ν_{max}/cm^{-1} (KBr) 2916, 2553, 1695, 1641, 1551, 1273, 1124.

Methyl 2-(1-methyl-1*H*-indol-3-yl)-3-(1-methyl-1*H*-pyrrolo[2,3-*b*]pyridin-3-yl)-3-oxopropanoate (267)

<u>Method A:</u>

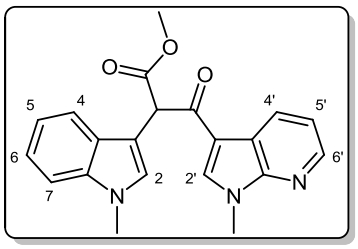

A solution of LDA (1.8 M, 33.3 mL, 59.9 mmol) in THF (30 mL) was cooled to -78 ^oC under a nitrogen atmosphere. A second solution of methyl 2-(1-methyl-1*H*-indol-3-yl)acetate **250** (4.512 g, 22.2 mmol) in THF (10 mL) was then added in a dropwise manner, with the resulting mixture being stirred for 1 hour at -78 ^oC. A suspension of 1-methyl-1*H*-pyrrolo[2,3-*b*]pyridine-3-carbonyl chloride **266** (4.735 g, 24.3 mmol) in THF (40 mL) was slowly added

to the reaction mixture over a 20 minute period. Once the addition was complete, the reaction mixture was warmed to 35 ^{o}C and left to stir for 12 hours. The solvent was removed under reduced pressure and the residue was dissolved in ethyl acetate (80 mL) and washed successively with a saturated aqueous sodium bicarbonate solution (50 mL), water (50 mL) and then brine (50 mL), before being dried over magnesium sulfate. Removal of the organic solvent under reduced pressure yielded the crude product as a brown solid, which was then subjected to column chromatography (hexane/ethyl acetate, 50:50) to yield **267** as a yellow crystalline solid (3.360 g, 42%): m.p. 101-103 ^{o}C; ν_{max}/cm^{-1} (KBr) 2951, 1737, 1651, 1533, 1449, 1375; δ_H (300 MHz, $CDCl_3$) 3.77 [3H, s, OCH_3], 3.77 [3H, s, NCH_3], 3.87 [3H, s, NCH_3], 5.69 [1H, s, CH_α], 7.13 [1H, dd, *J* 7.9, 4.7, C-$H_{5'}$], 7.14-7.32 [4H, m, C-$H_{2,5,6,7}$], 7.67 [1H, d, *J* 7.7, C-H_4], 7.92 [1H, s, C-$H_{2'}$], 8.38 [1H, dd, *J* 4.7, 1.6, C-$H_{6'}$], 8.65 [1H, dd, *J* 7.9, 1.6, C-$H_{4'}$]; δ_C (75 MHz, $CDCl_3$) 32.0 (CH_3, NCH_3), 32.9 (CH_3, NCH_3), 52.7 (CH_3, OCH_3), 53.0 (CH, $\underline{C}HCOOCH_3$), 107.1 (C, aromatic C), 109.6 (CH, aromatic CH), 113.4 (C, aromatic C), 118.3 (CH, aromatic CH), 118.8 (CH, aromatic CH), 119.3 (C, aromatic C), 119.7 (CH, aromatic CH), 121.9 (CH, aromatic CH), 127.1 (C, aromatic C), 128.9 (CH, aromatic CH), 131.2 (CH, aromatic CH), 135.7 (CH, aromatic CH), 136.7 (C, aromatic C), 144.8 (CH, aromatic CH), 148.3 (C, aromatic C), 170.0 (C, C=O), 188.1 (C, C=O); m/z (ES+) 362.2 $[M+H]^+$ (100%); HRMS (ES+): Exact mass calculated for $C_{21}H_{20}N_3O_3$ 362.1505. Found 362.1509.

Method B:

To a solution of LDA (1.8 M, 6.1 mL, 3.39 mmol) in THF (15 mL) under a nitrogen atmosphere at -78 ^{o}C was added, in a dropwise manner, a solution of methyl 2-(1-methyl-1*H*-indol-3-yl)acetate **250** (1.005 g, 4.9 mmol) in THF (5 mL). Following stirring at -78 ^{o}C for 1 hour, a suspension of 1-methyl-1*H*-pyrrolo[2,3-*b*]pyridine-3-carbonyl chloride **266** (1.054 g, 5.4 mmol) in THF (10 mL) was added over a period of 20 minutes. Once the addition was complete, the reaction mixture was allowed to warm to room temperature under stirring over 14 hours. The solvent was evaporated under reduced pressure and the residue was dissolved in ethyl acetate (40 mL), before being washed with saturated aqueous sodium bicarbonate solution (30 mL), water (30 mL) and brine (30 mL), before being dried over magnesium sulfate. The solvent was removed under reduced pressure, and the crude residue was

subsequently subjected to flash column chromatography (hexane/ethyl acetate, 50:50). However, the desired product was not formed, with only the self-condensation product **268** of ester **250** identified: δ_H (300 MHz, $CDCl_3$) 3.68 [2H, s, C<u>H</u>$_2$COCH], 3.68 [3H, s, OCH_3], 3.73 [3H, s, NCH_3], 3.90 [3H, s, NCH_3], 5.16 [1H, s, CH_α], 6.82 [1H, d, *J* 11.7, C-H_5], 6.98-7.31 [7H, m, C-$H_{2,2',5',6,6',7,7'}$], 7.34 [1H, d, *J* 8.2, C-H_4], 7.41 [1H, d, *J* 7.9, C-$H_{4'}$]; m/z (ES+) 375.1 $[M+H]^+$ (100%).

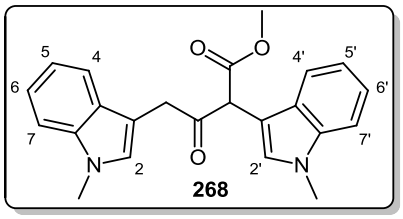

1-Benzyl-1*H*-pyrrolo[2,3-*b*]pyridine-3-carbonitrile (270)

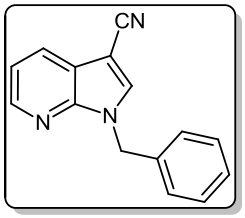

A stirred solution of 1*H*-pyrrolo[2,3-*b*]pyridine-3-carbonitrile **260** (1.010 g, 7.1 mmol) in anhydrous DMF (10 mL) was cooled to 0 ^oC. Sodium hydride (60 wt.% oil dispersion, 0.426 g, 10.7 mmol) was carefully added to the mixture in a portionwise manner, which was then left to stir for 30 minutes at 0 ^oC. Benzyl bromide (1.0 mL, 8.5 mmol) was subsequently added dropwise to the reaction mixture, which was then allowed to warm to room temperature and stirred for 3 hours. Water (20 mL) was carefully added to quench the reaction, and the resulting mixture was extracted with ethyl acetate (3 x 20 mL). The combined organic extracts were washed with water (4 x 50 mL) and brine (50 mL), then dried over magnesium sulfate. The solvent was removed under reduced pressure and the crude residue was subjected to flash column chromatography (hexane/ethyl acetate, 80:20) to yield **270** as an off-white solid (1.188 g, 72%): m.p. 94-95 ^oC; ν_{max}/cm^{-1} (KBr) 3106, 2215, 1573, 1528, 1424, 1306, 1177; δ_H (300 MHz, $CDCl_3$) 5.52 [2H, s, C<u>H</u>$_2$Bn], 7.25-7.39 [6H, m, C-$H_{5,2'-6'}$], 7.68 [1H, s, C-H_2], 8.08 [1H, dd, *J* 7.9, 1.5, C-H_4], 8.48 [1H, dd, *J* 4.7, 1.5, C-H_6]; δ_C (75 MHz, $CDCl_3$) 48.7 (CH_2, <u>C</u>H_2Bn), 85.0 (C, aromatic C), 115.0 (C, CN), 118.4 (CH, aromatic CH), 120.0 (C, aromatic C), 127.9 (2CH, 2 x aromatic CH), 128.3 (CH, aromatic CH), 128.5 (CH, aromatic CH), 129.1 (2CH, 2 x aromatic CH), 134.8 (CH, aromatic CH), 135.7 (C, aromatic C), 145.5 (CH, aromatic CH), 146.7 (C, aromatic C); m/z (ES+) 234.4 $[M+H]^+$ (100%). HRMS (ES+): Exact mass calculated for $C_{15}H_{12}N_3$ 234.1031. Found 234.1020.

1-Benzyl-1*H*-pyrrolo[2,3-*b*]pyridine-3-carboxylic acid (271)

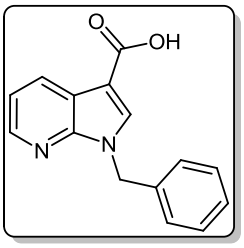

1-Benzyl-1*H*-pyrrolo[2,3-*b*]pyridine-3-carbonitrile **270** (1.005 g, 4.3 mmol) was suspended in 12 M aqueous HCl (30 mL), with the resulting mixture then being heated to 70 ^{o}C for 28 hours. Water (15 mL) and charcoal (0.1 g) were then added, and the reaction mixture was allowed to stir for 1 hour at 70 ^{o}C. Celite (0.1 g) was added to the mixture, which was allowed to stir for a further hour at 70 ^{o}C. The warm solution was then filtered, and allowed to cool to room temperature. Through the cautious addition of 50 wt.% aqueous NaOH, the strongly acidic solution was adjusted to pH 2.5, at which point a white precipitate formed. The mixture was allowed to stir for 2 hours at room temperature before the precipitate was filtered off, washed with copious water, then desiccated overnight at 50 ^{o}C to yield the pure product **271** as a white solid (0.984 g, 94%): m.p. 188-190 ^{o}C; ν_{max}/cm^{-1} (KBr) 2921, 2573, 1689, 1534, 1432, 1261; δ_H (300 MHz, DMSO-d_6) 5.55 [2H, s, CH_2], 7.28 [1H, dd, *J* 7.9, 4.7, C-H_5], 7.31-7.33 [5H, m, C-$H_{2'-6'}$], 8.33-8.37 [3H, m, C-$H_{2,4,6}$], 12.29 [1H, bs, COOH]; δ_C (75 MHz, DMSO-d_6) 66.3 (CH_2, $\underline{C}H_2$Bn), 105.7 (C, aromatic C), 117.9 (CH, aromatic CH), 118.7 (C, aromatic C), 127.5 (2CH, 2 x aromatic CH), 127.6 (CH, aromatic CH), 128.6 (2CH, 2 x aromatic CH), 129.2 (CH, aromatic CH), 135.2 (CH, aromatic CH), 137.5 (C, aromatic C), 143.7 (CH, aromatic CH), 147.3 (C, aromatic C), 165.1 (C, C=O); m/z (ES+) 253.3 $[M+H]^+$ (100%). HRMS (ES+): Exact mass calculated for $C_{15}H_{13}N_2O_2$ 253.0977. Found 253.0977.

1-Benzyl-1*H*-pyrrolo[2,3-*b*]pyridine-3-carbonyl chloride (272)

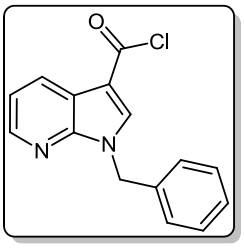

1-Benzyl-1*H*-pyrrolo[2,3-*b*]pyridine-3-carboxylic acid **271** (0.902 g, 3.6 mmol) was ground into a fine powder, then suspended in DCM (25 mL) under an inert atmosphere. While cooling in an ice bath, oxalyl chloride (0.64 mL, 7.5 mmol) was added in a dropwise fashion. Once complete, the reaction mixture was stirred for 12 hours at room temperature. The solvent and excess oxalyl chloride was removed under reduced pressure,

to yield acyl chloride **272** in quantitative yield as a white solid, which was subsequently used without further purification: ν_{max}/cm^{-1} (KBr) 3090, 3033, 2531, 1739, 1636, 1525, 1393, 1171.

Methyl 3-(1-benzyl-1*H*-pyrrolo[2,3-*b*]pyridin-3-yl)-2-(1-methyl-1*H*-indol-3-yl)-3-oxopropanoate (273)

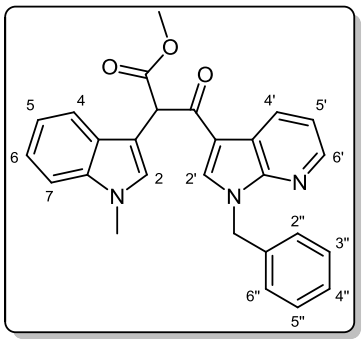

A solution of LDA (1.8 M, 3.24 mL, 5.8 mmol) in THF (10 mL) was cooled to -78 ^{o}C under a nitrogen atmosphere. A second solution of methyl 2-(1-methyl-1H-indol-3-yl)acetate **250** (0.535 g, 2.6 mmol) in THF (3 mL) was then added in a dropwise manner, with the reaction mixture being stirred for 1 hour at -78 ^{o}C. A suspension of acyl chloride **272** (0.862 g, 3.2 mmol) in THF (5 mL) was then added to the reaction mixture in a dropwise manner over a 15 minute period, which was subsequently allowed to slowly warm to room temperature and left to stir for 14 hours. The solvent was removed under reduced pressure, with the resulting reddish brown residue being dissolved in ethyl acetate (40 mL), then washed with a saturated aqueous sodium bicarbonate solution (30 mL), water (30 mL) and brine (30 mL), before being dried over magnesium sulfate. The solvent was removed under reduced pressure and the crude residue was subjected to flash column chromatography (hexane/ethyl acetate, 65:35) to yield the pure product **273** as a light orange/brown crystalline solid (0.424 g, 37%): m.p. 89-91 ^{o}C; ν_{max}/cm^{-1} (KBr) 2949, 1748, 1652, 1527, 1425, 1393, 1187; δ_H (300 MHz, $CDCl_3$) 3.71 [3H, s, NCH_3], 3.73 [3H, s, OCH_3], 5.34 [1H, d, H_A of AB, *J* 15.0, C$\underline{H}_2$Ph], 5.46 [1H, d, H_B of AB, *J* 15.1, C$\underline{H}_2$Ph], 5.62 [1H, s, C-H_α], 7.09-7.31 [10H, m, C-$H_{2,5,6,7,5',2''-6''}$], 7.57 [1H, d, *J* 8.0, C-H_4], 7.88 [1H, s, C-$H_{2'}$], 8.38 [1H, dd, *J* 4.7, 1.6, C-$H_{6'}$], 8.65 [1H, dd, *J* 7.9, 1.6, C-$H_{4'}$]; δ_C (75 MHz, $CDCl_3$) 32.9 (CH_3, NCH_3), 48.4 (CH_2, $\underline{C}H_2$Ph), 52.7 (CH_3, OCH_3), 53.0 (CH, $\underline{C}$HCOOCH_3), 107.0 (C, aromatic C), 109.6 (CH, aromatic CH), 113.8 (C, aromatic C), 118.3 (CH, aromatic CH), 119.0 (CH, aromatic CH), 119.3 (C, aromatic C), 119.7 (CH, aromatic CH), 121.9 (CH, aromatic CH), 127.0 (C, aromatic C), 127.9 (2CH, 2 x aromatic CH), 128.2 (CH, aromatic CH), 128.9 (CH, aromatic CH), 129.0 (2CH, 2 x aromatic CH), 131.2 (CH, aromatic CH),

134.6 (CH, aromatic CH), 135.9 (C, aromatic C), 136.7 (C, aromatic C), 144.9 (CH, aromatic CH), 148.1 (C, aromatic C), 170.0 (C, C=O), 188.3 (C, C=O); m/z (ES+) 438.1 $[M+H]^+$ (100%); HRMS (ES+): Exact mass calculated for $C_{27}H_{24}N_3O_3$ 438.1802. Found 438.1818.

1-Methyl-1*H*-pyrrolo[2,3-*b*]pyridine (277)[4]

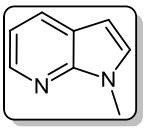

A solution of 7-azaindole **139** (4.002 g, 33.9 mmol) in DMF (60 mL) was cooled to 0 ^oC in an ice bath. Sodium hydride (60 wt.% oil dispersion, 2.033 g, 50.8 mmol) was then added in a portionwise manner. The resultant mixture was then allowed to stir at 0^oC for 30 minutes. A solution of methyl iodide (2.53 mL, 40.6 mmol) in DMF (20 mL) was then added in a dropwise manner, after which the reaction mixture was allowed to warm to room temperature and stirred for 3 hours. Water (80 mL) was carefully added to quench the reaction. The aqueous layer was extracted with ethyl acetate (3 x 60 mL), and then the combined organic extracts were washed with water (4 x 100 mL) and brine (100 mL), before being dried over magnesium sulfate and evaporated under reduced pressure to yield the crude product as a brown oil. The crude product was subjected to flash column chromatography (hexane/ethyl acetate, 75:25) to yield *N*-methyl product **277** as a green oil which was used without further purification (4.229 g, 94%): ν_{max}/cm^{-1} (NaCl) 3053, 2941, 1595, 1570, 1516, 1439, 1409, 1297; δ_H (300 MHz, $CDCl_3$) 3.88 [3H, s, NCH_3], 6.44 [1H, d, *J* 3.5, C-H_3], 7.04 [1H, dd, *J* 7.8, 4.7, C-H_5], 7.15 [1H, d, *J* 3.5, C-H_2], 7.90 [1H, dd, *J* 7.8, 1.5, C-H_4], 8.33 [1H, dd, *J* 4.7, 1.4, C-H_6]; δ_C (75 MHz, $CDCl_3$) 31.3 (CH_3, NCH_3), 99.3 (C, aromatic CH), 115.5 (C, aromatic CH), 120.7 (C, aromatic C), 128.9 (C, aromatic CH), 129.1 (C, aromatic CH), 142.6 (C, aromatic CH), 147.6 (C, aromatic C); m/z (ES+) 133.3 $[M+H]^+$ (100%).

2-(1-Methyl-1*H*-pyrrolo[2,3-*b*]pyridin-3-yl)-2-oxoacetic acid (278)

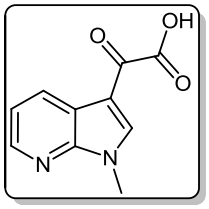

A solution of 1-methyl-1*H*-pyrrolo[2,3-*b*]pyridine **277** (4.002 g, 30.3 mmol) in diethyl ether (60 mL) was cooled to 0 ^{o}C using an ice bath. Oxalyl chloride (3.07 mL, 36.3 mmol) was then added in a dropwise manner over a period of 20 minutes. Once the addition was complete, the resulting mixture was allowed to slowly warm to room temperature over 3 hours. The solvent and excess oxalyl chloride was then removed by evaporation under reduced pressure. The solid residue was then suspended in acetone (80 mL), with the resulting mixture then being treated with a solution of potassium hydroxide (6.813 g, 121.4 mmol) in water (80 mL) before being left to stir at room temperature for 14 hours. The ensuing deep brown solution was acidified to pH 2 using 2M aqueous HCl, with the subsequent precipitate being filtered, washed with water and to dried to give oxoacetic acid **278** as a white solid (2.891 g, 47%): m.p. 266-267 ^{o}C; ν_{max}/cm^{-1} (KBr) 3130, 2408, 1709, 1654, 1591, 1522, 1365, 1277; δ_H (300 MHz, DMSO-d_6) 3.93 [3H, s, NCH_3], 7.37 [1H, dd, *J* 7.8, 4.8, C-H_5], 8.44 [1H, dd, *J* 4.7, 1.4, C-H_6], 8.49 [1H, dd, *J* 7.8, 1.4, C-H_4], 8.69 [1H, s, C-H_2], 13.92 [1H, bs, COOH]; δ_C (75 MHz, DMSO-d_6) 31.7 (CH_3, NCH_3), 109.7 (C, aromatic C), 118.3 (C, aromatic C), 119.1 (CH, aromatic CH), 129.7 (CH, aromatic CH), 141.4 (CH, aromatic CH), 144.7 (CH, aromatic CH), 148.1 (C, aromatic C), 164.6 (C, C=O), 180.3 (C, C=O); m/z (ES+) 205.2 $[M+H]^+$ (100%); HRMS (ES+): Exact mass calculated for $C_{10}H_9N_2O_3$ 205.0613. Found 205.0604.

2-(1-Methyl-1*H*-pyrrolo[2,3-*b*]pyridin-3-yl)acetic acid (279)

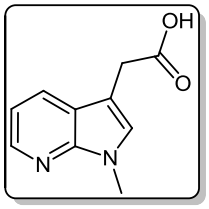

A solution of 2-(1-methyl-1*H*-pyrrolo[2,3-*b*]pyridin-3-yl)-2-oxoacetic acid **278** (1.763 g, 8.6 mmol) in ethylene glycol (20 mL) was treated with hydrazine hydrate (2.71 mL, 43.2 mmol), and the resulting mixture was heated to 60 ^{o}C. Sodium methoxide (4.989 g, 92.4 mmol) was then added in a portionwise manner, following which the reaction mixture was slowly heated to 150 ^{o}C. The mixture was stirred at 150 ^{o}C for 3 hours, allowing the solvent to concentrate to roughly half the original volume, before being cooled to room temperature and

then carefully diluted with water (100 mL). Using an ice bath, the resulting solution was cooled to 0 ^{o}C and then acidified to pH 2 using 12 M aqueous hydrochloric acid. The precipitate formed was filtered, washed with water and dried to yield pure acetic acid **279** as a white solid (1.382 g, 84%): m.p. 235-236 ^{o}C; ν_{max}/cm^{-1} (KBr) 2933, 2475, 1704, 1585, 1542, 1359, 1294; δ_H (300 MHz, DMSO-d_6) 3.61 [2H, s, C$\underline{H}_2$COOH], 3.72 [3H, s, NCH$_3$], 7.01 [1H, dd, *J* 7.8, 4.7, C-H$_5$], 7.34 [1H, s, C-H$_2$], 7.87 [1H, dd, *J* 7.8, 1.6, C-H$_4$], 8.19 [1H, dd, *J* 4.7, 1.5, C-H$_6$], 12.23 [1H, bs, COOH]; δ_C (75 MHz, DMSO-d_6) 30.5 (CH$_3$, NCH$_3$), 30.7 (CH$_2$, $\underline{C}$H$_2$COOH), 105.8 (C, aromatic C), 114.9 (CH, aromatic CH), 119.7 (C, aromatic C), 127.2 (CH, aromatic CH), 128.3 (CH, aromatic CH), 142.3 (CH, aromatic CH), 147.3 (C, aromatic C), 172.8 (C, C=O); m/z (ES+) 191.2 [M+H]$^+$ (100%); HRMS (ES+): Exact mass calculated for $C_{10}H_{11}N_2O_2$ 191.0821. Found 191.0814.

Methyl 2-(1-methyl-1*H*-pyrrolo[2,3-*b*]pyridin-3-yl)acetate (280)

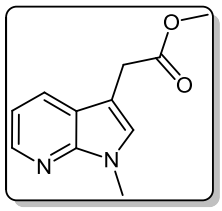

2-(1-Methyl-1*H*-pyrrolo[2,3-*b*]pyridin-3-yl)acetic acid **279** (0.701 g, 3.7 mmol) was dissolved in methanol (25 mL), and the resulting solution was carefully treated with neat sulphuric acid (1 mL). This mixture was then stirred at room temperature for 2 hours. Saturated aqueous sodium bicarbonate solution was added to the reaction mixture in a portionwise manner until pH 9 was reached. The resulting alkaline solution was extracted with ethyl acetate (3 x 15 mL), and the combined organic extracts were washed with water (20 mL) and brine (20 mL), before being dried over magnesium sulfate. The solvent was removed under reduced pressure to yield the ester product **280** as a yellow oil which was used without further purification (0.734 g, 97%): ν_{max}/cm^{-1} (NaCl) 2951, 1736, 1617, 1475, 1332, 1163; δ_H (300 MHz, CDCl$_3$) 3.68 [3H, s, NCH$_3$], 3.72 [2H, s, C$\underline{H}_2$COOCH$_3$], 3.82 [3H, s, OCH$_3$], 7.03 [1H, dd, *J* 7.9, 4.7, C-H$_5$], 7.12 [1H, s, C-H$_2$], 7.88 [1H, dd, *J* 7.9, 1.5, C-H$_4$], 8.33 [1H, dd, *J* 4.7, 1.4, C-H$_6$]; δ_C (75 MHz, CDCl$_3$) 30.0 (CH$_3$, NCH$_3$), 30.1 (CH$_2$, $\underline{C}$H$_2$COOCH$_3$), 52.0 (CH$_3$, OCH$_3$), 105.3 (C, aromatic C), 115.3 (CH, aromatic CH), 120.0 (C, aromatic C), 127.2 (CH, aromatic CH), 127.7 (CH, aromatic CH), 143.0 (CH, aromatic CH), 147.8 (C, aromatic C),

172.1 (C, C=O); m/z (ES+) 205.2 $[M+H]^+$ (20%), 100.1 (100%); HRMS (ES+): Exact mass calculated for $C_{11}H_{13}N_2O_2$ 205.0977. Found 205.0967.

Methyl 2,3-bis(1-methyl-1*H*-pyrrolo[2,3-*b*]pyridin-3-yl)-3-oxopropanoate (281)

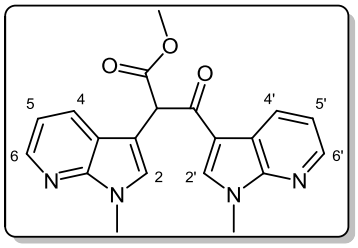

A solution of LDA (1.8 M, 1.54 mL, 2.8 mmol) in THF (20 mL) was cooled to -78 ^oC under a nitrogen atmosphere. A second solution of methyl 2-(1-methyl-1*H*-pyrrolo[2,3-*b*]pyridin-3-yl)acetate **280** (0.257 g, 1.3 mmol) in THF (5 mL) was then added in a dropwise manner, with the resulting mixture being stirred for 1 hour at -78 ^oC. A suspension of 1-methyl-1*H*-pyrrolo[2,3-*b*]pyridine-3-carbonyl chloride **266** (0.294 g, 1.5 mmol) in THF (10 mL) was added in a dropwise manner to the reaction mixture over a 15 minute period. Once the addition was complete, the mixture was warmed to 35 ^oC and left to stir under a nitrogen atmosphere for 14 hours. The solvent was then evaporated under reduced pressure, and the crude residue dissolved in ethyl acetate (40 mL). The organic phase was extracted with saturated aqueous sodium bicarbonate solution (30 mL), water (30 mL) and brine (30 mL), before being dried over magnesium sulfate. The solvent was removed under reduced pressure and the crude product was purified by flash column chromatography (hexane/ethyl acetate, 20:80) to yield **281** as a golden crystalline solid (0.178 g, 38%): m.p. 94-95 ^oC; ν_{max}/cm^{-1} (KBr) 2950, 1747, 1651, 1598, 1533, 1448, 1302; δ_H (300 MHz, $CDCl_3$) 3.78 [3H, s, NCH_3], 3.88 [3H, s, NCH_3], 3.91 [3H, s, OCH_3], 5.63 [1H, s, C-H_α], 7.09 [1H, dd, *J* 7.9, 4.7, C-$H_{5'}$], 7.25 [1H, dd, *J* 7.9, 4.7, C-H_5], 7.43 [1H, s, C-H_2], 7.95 [1H, s, C-$H_{2'}$], 8.02 [1H, dd, *J* 7.9, 1.5, C-H_4], 8.34 [1H, dd, *J* 4.7, 1.5, C-H_6], 8.40 [1H, dd, *J* 4.8, 1.6, C-$H_{6'}$], 8.65 [1H, dd, *J* 7.9, 1.6, C-$H_{4'}$]; δ_C (75 MHz, $CDCl_3$) 31.4 (CH_3, NCH_3), 32.1 (CH_3, NCH_3), 52.9 (CH_3, OCH_3), 53.4 (CH, $\underline{C}HCOOCH_3$), 105.7 (C, aromatic C), 113.3 (C, aromatic C), 115.8 (CH, aromatic CH), 118.9 (CH, aromatic CH), 119.2 (C, aromatic C), 119.5 (C, aromatic C), 127.5 (CH, aromatic CH), 128.8 (CH, aromatic CH), 131.2 (CH, aromatic CH), 135.7 (CH, aromatic CH), 143.3 (CH, aromatic CH), 144.9 (CH, aromatic CH), 147.7 (C, aromatic C), 148.3 (C,

aromatic C), 169.7 (C, C=O), 187.5 (C, C=O); m/z (ES+) 363.1 $[M+H]^+$ (100%); HRMS (ES+): Exact mass calculated for $C_{20}H_{19}N_4O_3$ 363.1457. Found 363.1453.

Methyl 2-(3,4,5-trimethoxyphenyl)acetate (291)[5]

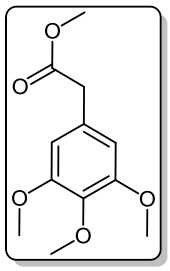

A solution of 3,4,5-trimethoxyphenyl acetic acid **290** (1.503 g, 6.6 mmol) in DMF (30 mL) was treated with potassium carbonate (1.100 g, 8.0 mmol) and dimethyl carbonate (1.1 mL, 13.3 mmol). The resulting mixture was heated to reflux for 16 hours before being cooled to room temperature. Water (50 mL) was added to the reaction mixture, which was then extracted with ethyl acetate (3 x 30 mL). The combined organic extracts were washed with water (4 x 50 mL) and brine (50 mL), before being dried over magnesium sulfate. The solvent was removed under reduced pressure, and the crude red residue was subjected to flash column chromatography (hexane/ethyl acetate, 80:20), yielding ester **291** as a clear oil which was used without further purification (1.394 g, 87%): ν_{max}/cm^{-1} (NaCl) 2948, 2840, 1737, 1592, 1508, 1127; δ_H (300 MHz, $CDCl_3$) 3.57 [2H, s, C$\underline{H}_2$COOCH$_3$], 3.71 [3H, s, *p*-OCH$_3$], 3.83 [3H, s, NCH$_3$], 3.86 [6H, s, 2 x *m*-OCH$_3$], 6.50 [2H, s, C-H$_{2,6}$]; δ_C (75 MHz, $CDCl_3$) 41.4 (CH_2, $\underline{C}H_2COOCH_3$), 52.1 (CH_3, COO$\underline{C}$H$_3$), 56.1 (2CH_3, 2 x *m*-OCH$_3$), 60.8 (CH_3, *p*-OCH$_3$), 106.2 (2CH, 2 x aromatic CH), 129.5 (C, aromatic C), 137.0 (C, aromatic C), 153.2 (2C, 2 x aromatic C), 172.0 (C, C=O); m/z (ES+) 241.1 $[M+H]^+$ (100%).

Methyl 3-(1-methyl-1*H*-pyrrolo[2,3-*b*]pyridin-3-yl)-3-oxo-2-(3,4,5-trimethoxyphenyl)propanoate (292)

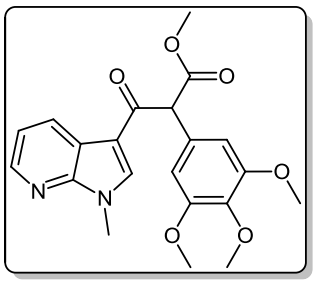

Under a nitrogen atmosphere, a solution of methyl 2-(3,4,5-trimethoxyphenyl)acetate **291** (0.737 g, 3.1 mmol) in THF (5 mL) was added to a stirred solution of LDA (3.8 mL, 6.8 mmol) in THF (20 mL), which had previously been cooled to -78 ^{o}C. The resulting mixture was maintained at -78 ^{o}C and stirred for 1 hour. A suspension of 1-methyl-1*H*-pyrrolo[2,3-*b*]pyridine-3-carbonyl chloride **266** (0.722 g, 3.7 mmol) in THF (10 mL) was added to the reaction mixture in a dropwise manner over a period of 20 minutes. Once complete, the reaction mixture was warmed to 35 ^{o}C and stirred for 14 hours, still under an inert atmosphere. The solvent was evaporated under reduced pressure, and the resulting residue was dissolved in ethyl acetate (50 mL), before being washed with saturated aqueous sodium bicarbonate solution (40 mL), water (40 mL) and then brine (40 mL). Upon drying over magnesium sulfate, the solvent was removed under reduced pressure, affording the crude product as a brown solid. Purification via flash column chromatography (hexane/ethyl acetate, 30:70) gave oxopropanoate **292** as a yellow crystalline solid (0.622 g, 51%): m.p. 108-110 ^{o}C; ν_{max}/cm^{-1} (KBr) 2938, 2839, 1716, 1650, 1593, 1449, 1128; δ_H (300 MHz, $CDCl_3$) 3.79 [3H, s, $COOCH_3$], 3.83 [3H, s, *p*-OCH_3], 3.87 [6H, s, 2 x *m*-OCH_3], 3.93 [3H, s, NCH_3], 5.32 [1H, s, CH_α], 6.71 [2H, s, C-$H_{2',6'}$], 7.26 [1H, dd, *J* 7.8, 4.8, C-H_5], 7.82 [1H, s, C-H_2], 8.41 [1H, dd, *J* 4.8, 1.6, C-H_6], 8.65 [1H, dd, *J* 7.9, 1.6, C-H_4]; δ_C (75 MHz, $CDCl_3$) 32.1 (CH_3, NCH_3), 52.8 (CH_3, $COO\underline{C}H_3$), 56.3 ($2CH_3$, 2 x *m*-OCH_3), 60.8 (CH_3, *p*-OCH_3), 61.5 (CH, $\underline{C}HCOOCH_3$), 106.6 (2CH, 2 x aromatic CH), 113.6 (C, aromatic C), 119.0 (CH, aromatic CH), 119.2 (C, aromatic C), 129.2 (C, aromatic C), 131.2 (CH, aromatic CH), 135.7 (CH, aromatic CH), 137.9 (C, aromatic C), 145.0 (CH, aromatic CH), 153.4 (2C, 2 x aromatic C), 169.4 (C, C=O), 187.4 (C, C=O); m/z (ES+) 399.2 $[M+H]^+$ (100%); HRMS (ES+): HRMS (ES+): Exact mass calculated for $C_{21}H_{23}N_2O_6$ 399.1556. Found 399.1546.

7.2.2.2 Routes towards oxopropanenitriles

2-(1-Methyl-1*H*-indol-3-yl)acetonitrile (275)[6]

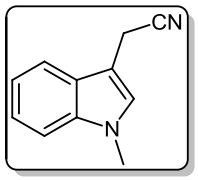

Indole-3-acetonitrile **274** (6.005 g, 38.4 mmol) was dissolved in DMF (80 mL), with the resulting solution being cooled to 0 °C. Sodium hydride (55 wt.% oil dispersion, 2.524 g, 57.6 mmol) was then added slowly in a portionwise manner. The reaction mixture was stirred for 30 minutes, with the temperature maintained at 0 °C. A solution of iodomethane (3.6 mL, 57.6 mmol) in DMF (10 mL) was then added dropwise to the reaction mixture, which was subsequently allowed to warm to room temperature and stirred for 2 hours. Water (50 mL) was cautiously added to quench the reaction, which was then extracted with ethyl acetate (3 x 60 mL). The combined organic extracts were washed with water (4 x 100 mL) and brine (100 mL), and then dried over magnesium sulfate. The solvent was removed under reduced pressure and the crude reddish residue was purified by flash column chromatography (hexane/ethyl acetate, 75:25), yielding the product **275** as an off-white crystalline material (5.503 g, 84%): m.p. 57-59 °C (lit.[6] 59-60 °C) ν_{max}/cm^{-1} (KBr) 2954, 2247, 1657, 1553, 1464, 1377; δ_H (400 MHz, $CDCl_3$) 3.78 [3H, s, NCH_3], 3.82 [2H, s, $C\underline{H}_2CN$], 7.09 [1H, s, C-H_2], 7.17 [1H, t, *J* 7.5, C-H_5], 7.25-7.34 [2H, m, C-$H_{6,7}$], 7.57 [1H, d, *J* 7.9, C-H_4]; δ_C (75 MHz, $CDCl_3$) 14.2 (CH_2, $\underline{C}H_2CN$), 32.8 (CH_3, NCH_3), 103.0 (C, aromatic C), 109.8 (CH, aromatic CH), 118.3 (CH, aromatic CH), 118.6 (C, C≡N), 119.8 (CH, aromatic CH), 122.4 (CH, aromatic CH), 126.5 (C, aromatic C), 127.5 (CH, aromatic CH), 137.3 (C, aromatic C); m/z (ES+) 171.1 $[M+H]^+$ (100%).

2-(1-Methyl-1*H*-indol-3-yl)-3-(1-methyl-1*H*-pyrrolo[2,3-*b*]pyridin-3-yl)-3-oxopropanenitrile (276)

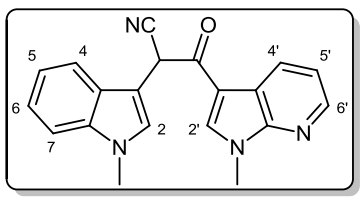

A solution of LDA (1.8 M, 29.0 mL, 52.1 mmol) in THF (100 mL) was cooled to -78 °C under a nitrogen atmosphere. A second solution of 2-(1-methyl-1*H*-indol-3-yl)acetonitrile **275** (4.029 g, 23.7 mmol) in THF (15 mL) was then added in a

dropwise fashion, with the resulting mixture being stirred for 1 hour at -78 ^{o}C. 1-Methyl-1*H*-pyrrolo[2,3-*b*]pyridine-3-carbonyl chloride **266** (5.533 g, 28.4 mmol) was suspended in THF (60 mL) and slowly added to the reaction mixture over a 20 minute period. Once the addition was complete, the reaction mixture was warmed to 35 ^{o}C and left to stir under a nitrogen atmosphere for 12 hours. The solvent was removed under reduced pressure and the residue was dissolved in ethyl acetate (150 mL), and then washed successively with a saturated aqueous sodium bicarbonate solution (120 mL), water (120 mL) and then brine (120 mL). Removal of the organic solvent under reduced pressure yielded the crude product as a brown solid, which was then subjected to flash column chromatography (hexane/ethyl acetate, 30:70) to yield the pure oxopropanenitrile **276** as a reddish crystalline solid (4.218 g, 54%): m.p. 96-98 ^{o}C; ν_{max}/cm^{-1} (KBr) 3053, 2920, 2243, 1652, 1597, 1533, 1448, 1368; δ_H (300 MHz, $CDCl_3$) 3.75 [3H, s, NCH_3], 3.87 [3H, s, NCH_3], 5.55 [1H, s, CH_α], 7.16-7.33 [5H, m, C-$H_{2,5,5',6,7}$], 7.71 [1H, d, *J* 7.6, C-H_4], 7.96 [1H, s, C-$H_{2'}$], 8.38 [1H, dd, *J* 4.7, 1.6, C-$H_{6'}$], 8.58 [1H, dd, *J* 7.9, 1.6, C-$H_{4'}$]; δ_C (75 MHz, $CDCl_3$) 32.2 (CH_3, NCH_3), 33.0 (CH_3, NCH_3), 39.6 (CH, CHCN), 104.8 (C, aromatic C), 109.9 (CH, aromatic CH), 111.3 (C, aromatic C), 117.6 (C, aromatic C), 118.6 (CH, aromatic CH), 119.1 (CH, aromatic CH), 119.3 (C, C≡N), 120.4 (CH, aromatic CH), 122.7 (CH, aromatic CH), 125.7 (C, aromatic C), 128.1 (CH, aromatic CH), 131.1 (CH, aromatic CH), 136.0 (CH, aromatic CH), 137.1 (C, aromatic C), 145.1 (CH, aromatic CH), 148.2 (C, aromatic C), 183.3 (C, C=O); m/z (ES+) 327.2 $[M-H]^-$ (100%); HRMS (ES+): Exact mass calculated for $C_{20}H_{17}N_4O$ 329.1402. Found 329.1407.

N,N-Diethyl-1-(1*H*-pyrrolo[2,3-*b*]pyridin-3-yl)methyl)methanamine (282)

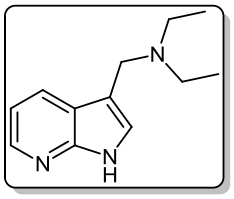

A solution of diethylamine hydrochloride (0.604 g, 5.5 mmol) and water (5 mL) was cooled in an ice bath to 0 ^{o}C. This was treated with 37 wt.% aqueous formaldehyde (0.36 mL, 4.8 mmol) and stirred for 30 minutes. A solution of 7-azaindole **139** (0.500 g, 4.2 mmol) in ethanol (10 mL) was then added, with the resulting mixture maintained at 0 ^{o}C for 30 minutes, before being heated to reflux for 20 hours. Once cooled to room temperature, the reaction mixture was diluted with water (20 mL), then adjusted to pH 11 using 50 wt.% aqueous

NaOH. Extraction with dichloromethane (3 x 20 mL) was then performed, and the combined organic extracts were dried over magnesium sulfate, filtered and evaporated under reduced pressure to yield a yellow/orange residue. The crude product was purified by flash column chromatography (ethyl acetate/methanol, 80:20), giving amine **282** as a light orange solid (0.755 g, 88%): m.p. 62-64 ^{o}C; ν_{max}/cm^{-1} (KBr) 3142, 2970, 2931, 2787, 1583, 1544, 1454, 1421, 1298, 1048; δ_H (300 MHz, DMSO-d_6) 0.98 [6H, t, J 7.1, 2 x NCH$_2$C<u>H</u>$_3$], 2.43 [4H, q, J 7.1, 2 x NC<u>H</u>$_2$CH$_3$], 3.66 [2H, s, CH$_2$], 7.01 [1H, dd, J 7.8, 4.7, C-H$_5$], 7.32 [1H, s, C-H$_2$], 7.99 [1H, dd, J 7.8, 1.2, C-H$_4$], 8.18 [1H, dd, J 4.6, 1.4, C-H$_6$], 11.44 [1H, bs, NH]; δ_C (75 MHz, DMSO-d_6) 11.8 (CH$_3$, 2 x NCH$_2$<u>C</u>H$_3$), 45.9 (CH$_2$, 2 x N<u>C</u>H$_2$CH$_3$), 48.1 (CH$_2$, <u>C</u>H$_2$N(CH$_2$CH$_3$)$_2$), 110.9 (C, aromatic C), 114.8 (CH, aromatic CH), 119.7 (C, aromatic C), 124.5 (CH, aromatic CH), 127.3 (CH, aromatic CH), 142.3 (CH, aromatic CH), 148.8 (C, aromatic C); m/z (ES+) 204.1 [M+H]$^+$ (100%). HRMS (ES+) Exact mass calculated for C$_{12}$H$_{18}$N$_3$ [M+H]$^+$, 204.1501. Found 204.1498.

N,N-Dimethyl-1-(1*H*-pyrrolo[2,3-*b*]pyridin-3-yl)methanamine (284)[7]

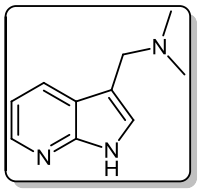

A mixture of dimethylamine (33 wt.% in ethanol, 9.8 mL, 55.2 mmol), acetic acid (2.7 mL, 48 mmol) and water (10 mL) was cooled in an ice bath to 0 ^{o}C. The resulting solution was subsequently treated with 37 wt.% aqueous formaldehyde (3.6 mL, 48.1 mmol) and stirred for 30 minutes. 7-Azaindole **139** (5.004 g, 42.4 mmol) in ethanol (20 mL) was then added, with the resulting solution stirred at 0 ^{o}C for 30 minutes, before being heated to 100 ^{o}C for 18 hours. At this point, TLC analysis showed complete consumption of starting material, and the reaction mixture was cooled to room temperature. The solution was diluted with water (40 mL) and adjusted to pH 11 using 50 wt.% aqueous NaOH. After extraction with dichloromethane (3 x 30 mL), the organic extracts were dried over magnesium sulfate, filtered and evaporated under reduced pressure to give the crude product as a pale yellow solid. Purification was carried out by flash column chromatography (ethyl acetate/methanol, 80:20) to yield amine **284** as a white crystalline solid (6.052 g, 82%): m.p. 157-158 ^{o}C (lit.[7] 144-152 ^{o}C); ν_{max}/cm^{-1} (KBr) 3079, 2947, 2775, 1604, 1528, 1412, 1334, 1002; δ_H (300 MHz, DMSO-

d_6) 2.13 [6H, s, N(C<u>H</u>$_3$)$_2$], 3.51 [2H, s, C<u>H</u>$_2$N(CH$_3$)$_2$], 7.02 [1H, dd, *J* 7.9, 4.7, C-H$_5$], 7.33 [1H, s, C-H$_2$], 7.98 [1H, dd, *J* 7.9, 1.5, C-H$_4$], 8.19 [1H, dd, *J* 4.7, 1.5, C-H$_6$], 11.46 [1H, bs, NH]; δ_C (75 MHz, DMSO-d_6) 44.8 (CH$_3$, 2 x NCH$_3$), 54.4 (CH$_2$, <u>C</u>H$_2$N(CH$_3$)$_2$), 110.6 (C, aromatic C), 114.9 (CH, aromatic CH), 119.7 (C, aromatic C), 124.7 (CH, aromatic CH), 127.2 (CH, aromatic CH), 142.4 (CH, aromatic CH), 148.7 (C, aromatic C); m/z (ES+) 176.1 $[M+H]^+$ (100%).

2-(1*H*-Pyrrolo[2,3-*b*]pyridin-3-yl)acetonitrile (283)[8]

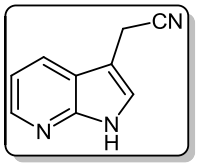

To a solution of *N*,*N*-dimethyl-1-(1*H*-pyrrolo[2,3-*b*]pyridin-3-yl)methanamine **284** (5.603 g, 32.0 mmol) in DMF (20 mL) was added a solution of sodium cyanide (2.35 g, 48.2 mmol) in water (16 mL). Acetic acid (5 mL) was then added in a dropwise manner, and the resulting solution was heated to 110 ^oC for 8 hours. After cooling to room temperature, the solution was diluted with saturated aqueous potassium carbonate (30 mL), then extracted with ethyl acetate (3 x 40 mL). The organic extracts were dried over magnesium sulfate, filtered and evaporated under reduced pressure to yield the crude product. Purification by flash column chromatography (hexane/ethyl acetate, 40:60) gave acetonitrile **283** as a white crystalline solid (2.589 g, 52%), m.p. 135-137 ^oC (lit.[8] 136-138 ^oC); ν_{max}/cm^{-1} (KBr) 3089, 2888, 2248, 1611, 1585, 1538, 1420, 1337; δ_H (300 MHz, CDCl$_3$) 3.85 [2H, s, CH$_2$], 7.16 [1H, dd, *J* 7.9, 4.8, C-H$_5$], 7.40 [1H, s, C-H$_2$], 7.99 [1H, dd, *J* 7.9, 1.5, C-H$_4$], 8.38 [1H, dd, *J* 4.8, 1.5, C-H$_6$], 11.92 [1H, bs, NH]; δ_C (75 MHz, CDCl$_3$) 14.6 (CH$_2$, <u>C</u>H$_2$CN), 102.8 (C, aromatic C), 116.0 (CH, aromatic CH), 117.8 (C, CN), 119.0 (C, aromatic C), 124.0 (CH, aromatic CH), 127.1 (CH, aromatic CH), 143.1 (CH, aromatic CH), 148.9 (C, aromatic C); m/z (ES+) 158.0 $[M+H]^+$ (100%).

2-(1-Methyl-1*H*-pyrrolo[2,3-*b*]pyridin-3-yl)acetonitrile (285)[9]

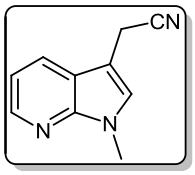

2-(1*H*-Pyrrolo[2,3-*b*]pyridin-3-yl)acetonitrile **283** (2.106 g, 13.4 mmol) was dissolved in anhydrous DMF (30 mL) and the resulting solution was cooled to 0 ^{o}C in an ice bath. Sodium hydride (55 wt.% oil dispersion, 0.585 g, 13.4 mmol) was added slowly in a portionwise manner. Once the addition was complete, the resulting mixture was allowed to stir at 0 ^{o}C for 20 minutes. At this point, a solution of iodomethane (0.83 mL, 13.4 mmol) in DMF (5 mL) was added in a dropwise fashion. The reaction mixture was then allowed to warm to room temperature, with stirring, over 2 hours. Water (20 mL) was cautiously added to quench to reaction. Following extraction with ethyl acetate (3 x 30 mL), the combined organic extracts were washed with water (4 x 50 mL) and brine (50 mL), then dried over magnesium sulfate. The solvent was evaporated under reduced pressure to yield the crude product as a brown solid, which was then purified by flash column chromatography (hexane/ethyl acetate, 70:30) to give acetonitrile **285** as a reddish solid (1.059 g, 46%): m.p. 82-84 ^{o}C (lit.[9] 81-82.5 ^{o}C); ν_{max}/cm^{-1} (KBr) 2941, 2360, 2249, 1602, 1542, 1463, 1410, 1301, 1144; δ_H (400 MHz, $CDCl_3$) 3.83 [2H, s, CH_2], 3.89 [3H, s, CH_3], 7.13 [1H, dd, *J* 7.9, 4.7, C-H_5], 7.22 [1H, s, C-H_2], 7.92 [1H, dd, *J* 7.9, 1.5, C-H_4], 8.40 [1H, dd, *J* 4.7, 1.5, C-H_6]; δ_C (75 MHz, $CDCl_3$) 14.5 (CH_2, $\underline{C}H_2CN$), 31.3 (CH_3, NCH_3), 101.5 (C, aromatic C), 115.8 (CH, aromatic CH), 117.8 (C, CN), 118.8 (C, aromatic C), 126.6 (CH, aromatic CH), 127.5 (CH, aromatic CH), 143.8 (CH, aromatic CH), 147.9 (C, aromatic C); m/z (ES+) 172.1 $[M+H]^+$ (100%).

3,4,5-Trimethoxybenzoyl chloride (286)[10]

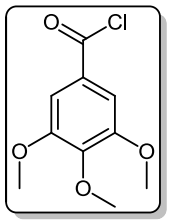

To a suspension of 3,4,5-trimethoxybenzoic acid (8.002 g, 37.7 mmol) in chloroform (30 mL) was added thionyl chloride (13.7 mL, 189 mmol) in a dropwise manner. Upon completion of addition, the mixture was heated to reflux for four hours before being cooled to room temperature. The solvent and excess thionyl chloride were removed under reduced pressure to yield acyl chloride **286** in quantitative yield as a white crystalline solid, which was subsequently used without further purification: ν_{max}/cm^{-1} (KBr) 2947, 2836, 1751, 1591, 1503, 1415, 1127.

2-(1-Methyl-1*H*-pyrrolo[2,3-*b*]pyridin-3-yl)-3-oxo-3-(3,4,5-trimethoxyphenyl)propanenitrile (287)

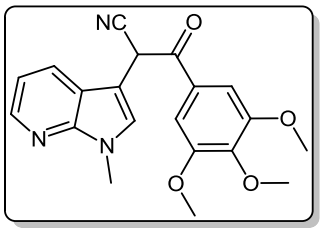

A solution of LDA (1.8 M, 6.49 mL, 11.7 mmol) in THF (40 mL) was cooled to -78 ^{o}C under a nitrogen atmosphere. Another solution of 2-(1-methyl-1*H*-pyrrolo[2,3-*b*]pyridin-3-yl)acetonitrile **285** (0.910 g, 5.3 mmol) in THF (5 mL) was then added in a dropwise manner and the reaction mixture was stirred for 1 hour, with the temperature maintained at -78 ^{o}C. After 1 hour, 3,4,5-trimethoxybenzoyl chloride **286** (1.475 g, 6.4 mmol) in THF (10 mL) was added dropwise to the reaction mixture, which was then allowed to slowly warm to room temperature under stirring over 12 hours. The solvent was removed under reduced pressure, and the residue dissolved in ethyl acetate (50 mL), followed by washings with saturated aqueous sodium bicarbonate solution (40 mL), water (40 mL) and brine (40 mL). After being dried over magnesium sulfate, the solvent was removed under reduced pressure. The crude residue was subjected to flash column chromatography (hexane/ethyl acetate, 20:80), yielding pure oxopropanenitrile **287** as a yellow solid (0.956 g, 49%): m.p. 80-82 ^{o}C; ν_{max}/cm^{-1} (KBr) 2940, 2201, 1684, 1583, 1505, 1461, 1415, 1333, 1127; δ_H (400 MHz, $CDCl_3$) 3.83 [6H, s, 2 x *m*-OCH_3], 3.87 [3H, s, *p*-OCH_3], 3.89 [3H, s, NCH_3], 5.82 [1H, s, CH_α], 7.15 [1H, dd, *J* 8.0, 4.7, C-H_5], 7.22 [2H, s, C-$H_{2',6'}$], 7.30 [1H, s, C-H_2], 8.05 [1H, dd, *J* 8.0, 1.5, C-H_4], 8.38 [1H, dd, *J* 4.7, 1.3, C-H_6]; δ_C (75 MHz, $CDCl_3$) 31.5 (CH_3, NCH_3), 38.6 (CH, CHCN), 56.4 ($2CH_3$, 2 x *m*-OCH_3), 61.0 (CH_3, *p*-OCH_3), 102.4 (C, aromatic C), 105.6 (C, aromatic C), 106.8 (2CH, 2 x aromatic CH), 116.5 (CH, aromatic CH), 118.0 (C, CN), 127.1 (CH, aromatic CH), 128.3 (CH, aromatic CH), 128.3 (C, aromatic C), 143.8 (C, aromatic C), 144.2 (CH, aromatic CH), 147.8 (C, aromatic C), 153.1 (2C, 2 x aromatic C), 187.2 (C, C=O); m/z (ES+) 366.1 $[M+H]^+$ (100%); HRMS (ES+): Exact mass calculated for $C_{20}H_{20}N_3O_4$ 366.1454. Found 366.1448.

3-(1-Methyl-1*H*-pyrrolo[2,3-*b*]pyridin-3-yl)-3-oxo-2-(3,4,5-trimethoxyphenyl)propanenitrile (289)

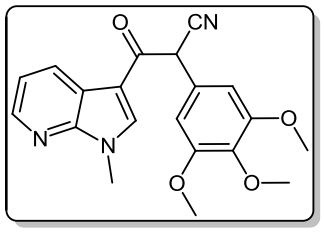

A solution of LDA (1.8 M, 9.8 mL, 17.7 mmol) in THF (10 mL) was then cooled to -78 ^{o}C under a nitrogen atmosphere. A second solution of 3,4,5-trimethoxyphenyl acetonitrile **288** (1.356 g, 6.5 mmol) in THF (5 mL) was then added in a dropwise manner, with the resulting mixture stirred for 1 hour at -78 ^{o}C. A suspension of 1-methyl-1*H*-pyrrolo[2,3-*b*]pyridine-3-carbonyl chloride **266** (1.401 g, 7.2 mmol) in THF (25 mL) was slowly added to the reaction mixture over a 20 minute period. Once the addition was complete, the reaction mixture was warmed to 35 ^{o}C and allowed to stir at this temperature, still under an inert atmosphere, for 12 hours. The solvent was evaporated under reduced pressure and the resultant residue was dissolved in ethyl acetate (40 mL). The organic phase was washed with a saturated aqueous sodium bicarbonate solution (50 mL), water (50 mL) and then brine (50 mL), before being dried over magnesium sulfate. The solvent was removed under reduced pressure and the crude residue was subjected to flash column chromatography (hexane/ethyl acetate, 30:70) to yield oxopropanenitrile **289** as a yellow solid (1.094 g, 46%): m.p. 137-140 ^{o}C; ν_{max}/cm^{-1} (KBr) 2933, 2243, 1728, 1643, 1595, 1450, 1130; δ_H (400 MHz, $CDCl_3$) 3.83 [3H, s, *p*-OCH_3], 3.87 [6H, s, 2 x *m*-OCH_3], 3.94 [3H, s, NCH_3], 5.23 [1H, s, CH_α], 6.70 [2H, s, C-$H_{2',6'}$], 7.28 [1H, dd, *J* 7.9, 4.8, C-H_5], 7.97 [1H, s, C-H_2], 8.43 [1H, dd, *J* 4.8, 1.6, C-H_6], 8.60 [1H, dd, *J* 7.9, 1.6, C-H_4]; δ_C (75 MHz, $CDCl_3$) 32.3 (CH_3, NCH_3), 47.8 (CH, CHCN), 56.4 ($2CH_3$, 2 x *m*-OCH_3), 60.9 (CH_3, *p*-OCH_3), 105.1 (2CH, 2 x aromatic CH), 111.4 (C, aromatic C), 117.3 (C, aromatic C), 119.3 (C, C≡N), 119.4 (CH, aromatic CH), 126.5 (C, aromatic C), 131.2 (CH, aromatic CH), 136.0 (CH, aromatic CH), 138.5 (C, aromatic C), 145.4 (CH, aromatic CH), 148.2 (C, aromatic C), 154.0 (2C, 2 x aromatic C), 182.6 (C, C=O); m/z (ES+) 364.1 $[M-H]^-$ (100%); HRMS (ES+): Exact mass calculated for $C_{20}H_{20}N_3O_4$ 366.1454. Found 366.1472.

7.2.3 Synthesis and derivatisation of 5-aminopyrazole 293

4-(1-Methyl-1*H*-pyrrolo[2,3-*b*]pyridin-3-yl)-3-(3,4,5-trimethoxyphenyl)-1*H*-pyrazol-5-amine (293)

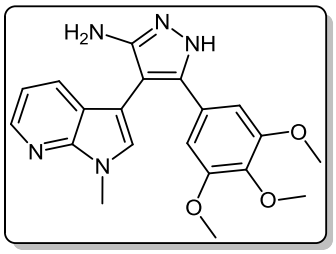

To a solution of 2-(1-methyl-1*H*-pyrrolo[2,3-*b*]pyridin-3-yl)-3-oxo-3-(3,4,5-trimethoxyphenyl)propanenitrile **287** (0.806 g, 2.2 mmol) in absolute alcohol (30 mL), 12 M aqueous HCl (1 mL) was slowly added. Hydrazine hydrate (50% aqueous solution, 0.69 mL, 11.0 mmol) was then added and the resulting mixture was heated to reflux for 20 hours. Once the reaction mixture was cooled to room temperature, the solvent was removed under reduced pressure. The residue was dissolved in ethyl acetate (40 mL) and then washed with saturated aqueous sodium bicarbonate solution (30 mL), water (30 mL) and brine (30 mL), before being dried over magnesium sulfate. The solvent was evaporated under reduced pressure, and the crude product was then purified by flash column chromatography (ethyl acetate/methanol, 90:10) to yield pure aminopyrazole **293** as a brown solid (0.586 g, 70 %): m.p. 266-267 ^{o}C; ν_{max}/cm^{-1} (KBr) 3357, 3205, 2935, 1579, 1516, 1459, 1410, 1248, 1124; δH (400 MHz, DMSO-d_6) 3.37 [6H, s, 2 x *m*-OCH_3], 3.59 [3H, s, *p*-OCH_3], 3.86 [3H, s, NCH_3], 4.51 [2H, bs, NH_2], 6.71 [2H, s, C-$H_{2',6'}$], 6.97 [1H, dd, *J* 7.9, 4.7, C-H_5], 7.36 [1H, dd, *J* 7.8, 1.5, C-H_4], 7.56 [1H, s, C-H_2], 8.24 [1H, dd, *J* 4.6, 1.5, C-H_6], 11.97 [1H, bs, NH]; δ_C (75 MHz, DMSO-d_6) 30.8 (CH_3, NCH_3), 55.3 ($2CH_3$, 2 x *m*-OCH_3), 60.1 (CH_3, *p*-OCH_3), 95.2 (C, broad aromatic C), 103.9 (2CH, 2 x aromatic CH), 104.4 (C, aromatic C), 115.1 (CH, aromatic CH), 119.5 (C, aromatic C), 126.9 (C, broad aromatic C), 128.0 (CH, aromatic CH), 129.2 (CH, aromatic CH), 136.9 (C, aromatic C), 141.8 (C, broad aromatic C), 142.4 (CH, aromatic CH), 147.5 (C, aromatic C), 152.3 (C, broad aromatic C), 152.5 (2C, 2 x aromatic C); m/z (ES+) 380.1 $[M+H]^+$ (100%); HRMS (ES+): Exact mass calculated for $C_{20}H_{22}N_5O_3$ 380.1723. Found 380.1725.

*7.2.3.1 Formation of bicyclic derivatives of 5-aminopyrazole **293***

8-(1-Methyl-1*H*-pyrrolo[2,3-*b*]pyridin-3-yl)-7-(3,4,5-trimethoxyphenyl)pyrazolo[1,5-*a*][1,3,5]triazine-2,4(1*H*,3*H*)-dione (295)

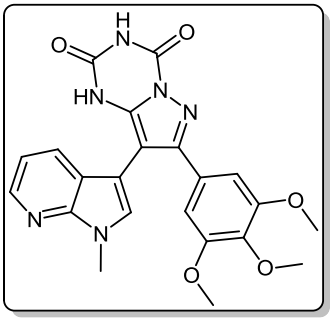

To a solution of 4-(1-methyl-1*H*-pyrrolo[2,3-*b*]pyridin-3-yl)-3-(3,4,5-trimethoxyphenyl)-1*H*-pyrazol-5-amine **293** (0.080 g, 0.21 mmol) in DCM (10 mL) was added two drops of triethylamine, and the resulting mixture was cooled to 0 ^{o}C in an ice bath. This solution was then treated, while stirring, with *N*-chlorocarbonyl isocyanate (0.02 mL, 0.23 mmol). The reaction mixture was allowed to warm to room temperature and was stirred for 15 hours. After careful addition of water (3 mL), the precipitate formed was filtered and subsequently washed with water (4 x 5 mL) and ether (2 x 5 mL). The precipitate was desiccated at 50 ^{o}C overnight to give pure pyrazolotriazinedione **295** as a white solid (0.053 g, 56%): m.p. 301-303 ^{o}C; ν_{max}/cm^{-1} (KBr) 3516, 2834, 1765, 1703, 1648, 1583, 1549, 1421, 1332, 1123; δ_H (400 MHz, DMSO-d_6) 3.37 [6H, s, 2 x *m*-OCH_3], 3.61 [3H, s, *p*-OCH_3], 3.88 [3H, s, NCH_3], 6.84 [2H, s, C-$H_{2',6'}$], 7.04 [1H, dd, *J* 7.8, 4.6, C-H_5], 7.50 [1H, d, *J* 7.8, C-H_4], 7.64 [1H, s, C-H_2], 8.29 [d, 1H, *J* 4.5, C-H_6], 11.66 [2H, bs, 2 x NH]; δ_C (75 MHz, DMSO-d_6) 30.9 (CH_3, NCH_3), 55.2 (2CH_3, 2 x *m*-OCH_3), 60.0 (CH_3, *p*-OCH_3), 94.2 (C, aromatic C), 100.4 (C, aromatic C), 104.5 (2CH, 2 x aromatic CH), 115.6 (CH, aromatic CH), 119.9 (C, aromatic C), 127.2 (C, aromatic C), 127.6 (CH, aromatic CH), 131.0 (CH, aromatic CH), 137.9 (C, aromatic C), 140.1 (C, aromatic C), 142.7 (CH, aromatic CH), 144.3 (C, aromatic C), 147.6 (C, aromatic C), 148.6 (C, C=O), 152.5 (2C, 2 x aromatic C), 153.4 (C, C=O); m/z (ES-) 447.1 [M-H]$^-$, (100%); HRMS (ES+): Exact mass calculated for $C_{22}H_{21}N_6O_5$ 449.1573. Found 449.1554.

5,7-Bis(trifluoromethyl)-3-(1-methyl-1*H*-pyrrolo[2,3-*b*]pyridin-3-yl)-2-(3,4,5-trimethoxyphenyl)pyrazolo[1,5-*a*]pyrimidine (297)

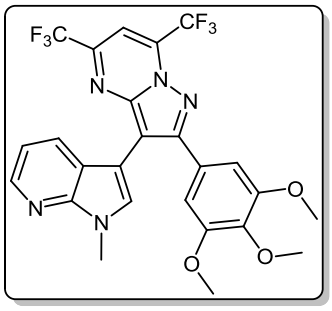

To a stirred mixture of 4-(1-methyl-1*H*-pyrrolo[2,3-*b*]pyridin-3-yl)-3-(3,4,5-trimethoxyphenyl)-1*H*-pyrazol-5-amine **293** (0.080 g, 0.21 mmol) in acetic acid (10 mL), was added hexafluoroacetylacetone (0.60 mL, 4.20 mmol). This mixture was then heated to 80 ^{o}C for 20 hours. After cooling to room temperature, the acetic acid and excess hexafluoroacetylacetone were removed under reduced pressure, and the residue was dissolved in ethyl acetate (30 mL) and then washed with water (20 mL) and brine (20 mL), and dried over magnesium sulfate. Evaporation of the solvent under reduced pressure left the crude product as a red/brown solid. Purification via flash column chromatography (hexane/ethyl acetate, 50:50) gave the pyrimidine **297** as an orange solid (0.062 g, 54%): m.p. 174-176 ^{o}C; ν_{max}/cm^{-1} (KBr) 2926, 1590, 1481, 1419, 1271, 1127, 1010; δ_H (400MHz, $CDCl_3$) 3.55 [6H, s, 2 x *m*-OCH_3], 3.86 [3H, s, *p*-OCH_3], 4.02 [3H, s, NCH_3], 6.96 [1H, dd, *J* 7.6, 4.6, C-H_5], 7.04 [2H, s, C-$H_{2',6'}$], 7.38 [1H, d, *J* 7.8, C-H_4], 7.46 [1H, s, (CF_3)C-CH=C(CF_3)], 7.56 [1H, s, C-H_2], 8.35 [1H, bs, C-H_4]; δ_C (125 MHz, $CDCl_3$) 31.6 (CH_3, NCH_3), 55.9 ($2CH_3$, 2 x *m*-OCH_3), 60.9 (CH_3, *p*-OCH_3), 102.0 (C, aromatic C), 102.3 (CH, aromatic CH), 106.2 (C, aromatic C), 106.3 (2CH, 2 x aromatic CH), 115.9 (CH, aromatic CH), 115.9-122.4 (C, q, *J* 275.4, CF_3), 117.0-123.5 (C, q, *J* 275.2, CF_3), 119.2 (C, aromatic C), 127.1 (C, aromatic C), 129.3 (CH, aromatic CH), 129.4 (CH, aromatic CH), 134.6-135.5 (C, q, *J* 34.7, aromatic C), 139.3 (C, aromatic C), 143.4 (CH, aromatic CH), 144.5-145.4 (C, q, *J* 37.8, aromatic C), 146.7 (C, aromatic C), 148.0 (C, aromatic C), 153.3 (2C, 2 x aromatic C), 156.0 (C, aromatic C); m/z (ES+) 552.1 $[M+H]^+$ (100%); HRMS (ES+): Exact mass calculated for $C_{25}H_{20}N_5O_3F_6$ 552.1470. Found 552.1469.

*7.2.3.2 Reaction of 5-aminopyrazole **293** with monodentate electrophiles*

2,2,2-Trifluoro-*N*-(4-(1-methyl-1*H*-pyrrolo[2,3-*b*]pyridin-3-yl)-5-(3,4,5-trimethoxyphenyl)-1*H*-pyrazol-3-yl)acetamide (300)

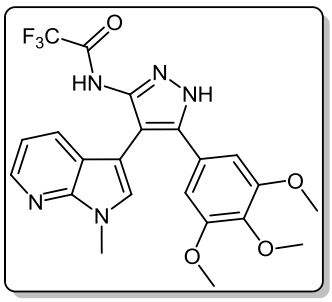

To a solution of 4-(1-methyl-1*H*-pyrrolo[2,3-*b*]pyridin-3-yl)-3-(3,4,5-trimethoxyphenyl)-1*H*-pyrazol-5-amine **293** (0.080 g, 0.21 mmol) in acetonitrile (10 mL) was added trifluoroacetic anhydride (0.04 mL, 0.25 mmol). The reaction mixture was then heated to reflux for 28 hours before being left to cool to room temperature. Evaporation of the solvent under reduced pressure left the crude product as a brown residue. This residue was then purified by flash column chromatography (hexane/ethyl acetate, 40:60), yielding trifluoroacetamide **300** as a pale yellow solid (0.041 g, 41%): m.p. 230-231 ^{o}C; ν_{max}/cm^{-1} (KBr) 3307, 2939, 1714, 1579, 1507, 1464, 1407, 1173, 1129; δ_H (300 MHz, DMSO-d_6) 3.49 [6H, s, 2 x *m*-OCH_3], 3.69 [3H, s, *p*-OCH_3], 3.92 [3H, s, NCH_3], 6.82 [2H, s, C-$H_{2',6'}$], 7.05 (1H, dd, *J* 7.9, 4.7, C-H_5], 7.44 [1H, dd, *J* 7.9, 1.5, C-H_4], 7.54 [1H, s, C-H_2], 8.33 [1H, dd, *J* 4.6, 1.4, C-H_6], 11.23 [1H, bs, $NHCOCF_3$], 13.52 [1H, bs, C=N-NH-C]; δ_C (75 MHz, DMSO-d_6) 30.8 (CH_3, NCH_3), 55.4 ($2CH_3$, 2 x *m*-OCH_3), 60.0 (CH_3, *p*-OCH_3), 102.8 (C, aromatic C), 104.0 (2CH, 2 x aromatic CH), 106.5 (C, aromatic C), 106.7 (C, aromatic C), 110.0-121.5 (C, q, J_{F-C} 288.4, CF_3), 115.3 (CH, aromatic CH), 118.7 (C, aromatic C), 124.5 (C, aromatic C), 127.8 (CH, aromatic CH), 128.8 (CH, aromatic CH), 137.3 (C, aromatic C), 142.6 (CH, aromatic CH), 147.4 (C, aromatic C), 152.7 (2C, 2 x aromatic C), 153.1 (C, aromatic C), 155.6-157.1 (C, q, J_{F-C} 36.7, C=O); m/z (ES+) 476.1 $[M+H]^+$ (100%); HRMS (ES+): Exact mass calculated for $C_{22}H_{21}N_5O_4F_3$ 476.1546. Found 476.1540.

1-[5-Amino-4-(1-methyl-1*H*-pyrrolo[2,3-*b*]pyridin-3-yl)-3-(3,4,5-trimethoxyphenyl)-1*H*-pyrazol-1-yl]ethanone (302)

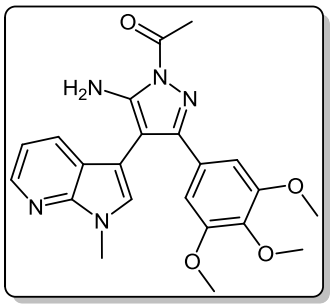

To a solution of 4-(1-methyl-1*H*-pyrrolo[2,3-*b*]pyridin-3-yl)-3-(3,4,5-trimethoxyphenyl)-1*H*-pyrazol-5-amine **293** (0.080 g, 0.21 mmol) in acetonitrile (10 mL) was added acetic anhydride (0.021 mL, 0.22 mmol). The reaction mixture was heated to reflux for 24 hours before being cooled to room temperature. The solvent and excess acetic anhydride was then removed under reduced pressure. The crude residue was subjected to flash column chromatography (hexane/ethyl acetate, 40:60), yielding the pure acetylated product **302** as a pale yellow crystalline solid (0.0547 g, 62%): m.p. 138-140^{o}C; ν_{max}/cm^{-1} (KBr) 3435, 2939, 1702, 1636, 1597, 1577, 1470, 1421, 1380, 1351, 1128; δ_H (300MHz, $CDCl_3$) 2.79 [3H, s, $NCOCH_3$], 3.48 [6H, s, 2 x *m*-OCH_3], 3.79 [3H, s, *p*-OCH_3], 3.90 [3H, s, NCH_3], 5.60 [2H, bs, NH_2], 6.81 [2H, s, C-$H_{2',6'}$], 7.02 [1H, dd, *J* 7.9, 4.7, C-H_5], 7.15 [1H, s, C-H_2], 7.62 [1H, dd, *J* 7.9, 1.5, C-H_4], 8.35 [1H, dd, *J* 4.7, 1.4, C-H_6]; δ_C (75 MHz, $CDCl_3$) 23.3 (CH_3, NCO<u>C</u>H_3), 31.3 (CH_3, NCH_3), 55.7 ($2CH_3$, 2 x *m*-OCH_3), 60.9 (CH_3, *p*-OCH_3), 93.9 (C, aromatic C), 103.5 (C, aromatic C), 104.9 (2CH, 2 x aromatic CH), 115.9 (CH, aromatic CH), 119.9 (C, aromatic C), 127.8 (C, aromatic C), 128.5 (2CH, 2 x aromatic CH), 138.5 (C, aromatic C), 143.6 (CH, aromatic CH), 147.9 (C, aromatic C), 148.7 (C, aromatic C), 152.9 (2C, 2 x aromatic C), 153.1 (C, aromatic C), 173.9 (C, C=O); m/z (ES+) 422.2 $[M+H]^+$ (100%); HRMS (ES+): Exact mass calculated for $C_{22}H_{23}N_5O_4$ 422.1828. Found 422.1812.

5-Amino-*N*-methyl-4-(1-methyl-1*H*-pyrrolo[2,3-*b*]pyridin-3-yl)-3-(3,4,5-trimethoxyphenyl)-1*H*-pyrazole-1-carbothioamide (304)

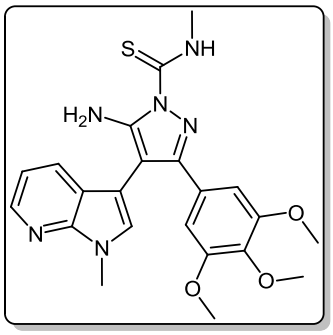

To a solution of 4-(1-methyl-1*H*-pyrrolo[2,3-*b*]pyridin-3-yl)-3-(3,4,5-trimethoxyphenyl)-1*H*-pyrazol-5-amine **293** (0.080 g, 0.21 mmol) in acetonitrile (10 mL) was added methyl isothiocyanate (0.016 g, 0.22 mmol). The reaction mixture was heated to reflux for 26 hours before being cooled to room temperature. The solvent was removed under reduced pressure to give a crude brown residue. Subjection to flash column chromatography (hexane/ethyl acetate, 50:50) gave pure carbothioamide **304** as a white solid (0.044 g, 47%): m.p. 169-171 ^{o}C; ν_{max}/cm^{-1} (KBr) 3320, 2933, 1626, 1594, 1523, 1469, 1423, 1361, 1284, 1123; δ_H (300 MHz, DMSO-d_6) 3.16 [3H, bd, *J* 3.8, NHC<u>H</u>$_3$], 3.37 [6H, s, 2 x *m*-OCH$_3$], 3.59 [3H, s, *p*-OCH$_3$], 3.88 [3H, s, NCH$_3$], 6.90 [2H, s, C-H$_{2',6'}$], 7.03 [1H, dd, *J* 7.8, 4.6, C-H$_5$], 7.14 [2H, bs, NH$_2$], 7.51 [1H, dd, *J* 7.8, 1.5, C-H$_4$], 7.60 [1H, s, C-H$_2$], 8.28 [1H, dd, *J* 4.6, 1.5, C-H$_6$], 10.15 [1H, bd, *J* 4.2, N<u>H</u>CH$_3$]; δ_C (75 MHz, DMSO-d_6) 30.8 (CH$_3$, NCH$_3$), 31.1 (CH$_3$, NHCH$_3$), 55.2 (2CH$_3$, 2 x *m*-OCH$_3$), 60.0 (CH$_3$, *p*-OCH$_3$), 92.7 (C, aromatic C), 102.8 (C, aromatic C), 104.9 (2CH, 2 x aromatic CH), 115.4 (CH, aromatic CH), 119.9 (C, aromatic C), 127.5 (C, aromatic C), 127.6 (CH, aromatic CH), 130.3 (CH, aromatic CH), 137.7 (C, aromatic C), 142.6 (CH, aromatic CH), 147.7 (C, aromatic C), 148.9 (C, aromatic C), 150.2 (C, aromatic C), 152.3 (2C, 2 x aromatic C), 175.7 (C, C=S); m/z (ES+) 453.1 [M+H]$^+$ (100%); HRMS (ES+): Exact mass calculated for $C_{22}H_{25}N_6O_3S$ 453.1709. Found 453.1700.

7.2.4 Synthesis and derivatisation of 5-aminopyrazole **312**

5-(1-Methyl-1*H*-pyrrolo[2,3-*b*]pyridin-3-yl)-4-(3,4,5-trimethoxyphenyl)-1*H*-pyrazol-3-amine (312)

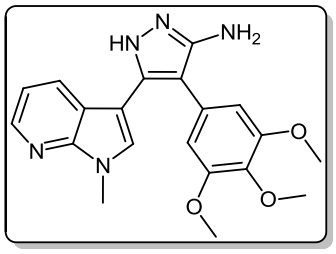

To a solution of 3-(1-methyl-1*H*-pyrrolo[2,3-*b*]pyridin-3-yl)-3-oxo-2-(3,4,5-trimethoxyphenyl)propanenitrile **289** (1.015 g, 2.8 mmol) in absolute alcohol (30 mL), was added 12 M aqueous HCl (1 mL) in a dropwise manner. Hydrazine hydrate (50% aqueous solution, 0.87 mL, 13.9 mmol) was then added, and the resulting mixture was heated to reflux for 26 hours. Once cooled to room temperature, the solvent was evaporated under reduced pressure. The residue was dissolved in ethyl actetate (50 mL), then washed successively with saturated aqueous sodium bicarbonate solution (40 mL), water (40 mL) and then brine (40 mL), before being dried over magnesium sulfate. The solvent was removed under reduced pressure and the crude brown residue was subjected to flash column chromatography (ethyl acetate/methanol, 90:10) to yield pure aminopyrazole **312** as a light brown solid (0.661 g, 62%): m.p. 135-137 ^{o}C; ν_{max}/cm^{-1} (KBr) 3199, 2931, 1602, 1518, 1470, 1351, 1115; δ_H (300 MHz, DMSO-d_6) 3.53 [6H, s, 2 x *m*-OCH_3], 3.64 [3H, s, *p*-OCH_3], 3.82 [3H, s, NCH_3], 4.68 [2H, bs, NH_2], 6.53 [2H, s, C-$H_{2',6'}$], 6.98 [1H, dd, *J* 7.9, 4.6, C-H_5], 7.55 [2H, m, C-$H_{2,4}$], 8.24 [1H, dd, *J* 4.6, 1.3, C-H_6], 11.73 [1H, bs, NH]; δ_C (75 MHz, DMSO-d_6) 30.8 (C, NCH_3), 55.5 (2C, 2 x *m*-OCH_3), 60.0 (C, *p*-OCH_3), 94.9 (C, broad aromatic C), 106.1 (2CH, 2 x aromatic CH), 115.5 (CH, aromatic CH), 117.9 (C, aromatic C), 125.4 (C, broad aromatic C), 128.2 (CH, aromatic CH), 128.8 (CH, aromatic CH), 129.4 (C, aromatic C), 135.4 (C, aromatic C), 141.9 (C, broad aromatic C), 142.7 (CH, aromatic CH), 147.2 (C, aromatic C), 151.8 (C, aromatic C), 152.7 (2C, 2 x aromatic C); m/z (ES+) 380.2 $[M+H]^+$ (100%); HRMS (ES+): Exact mass calculated for $C_{20}H_{22}N_5O_3$ 380.1723. Found 380.1724.

*7.2.4.1 Formation of bicyclic derivatives of 5-aminopyrazole **312***

7-(1-Methyl-1*H*-pyrrolo[2,3-*b*]pyridin-3-yl)-8-(3,4,5-trimethoxyphenyl)pyrazolo[1,5-*a*][1,3,5]triazine-2,4(1*H*,3*H*)-dione (313)

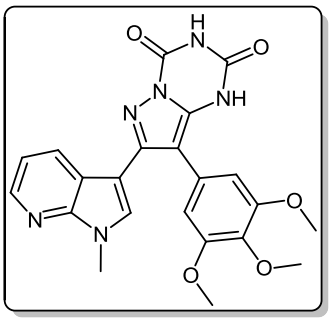

5-(1-Methyl-1*H*-pyrrolo[2,3-*b*]pyridin-3-yl)-4-(3,4,5-trimethoxyphenyl)-1*H*-pyrazol-3-amine **312** (0.100 g, 0.26 mmol) was dissolved in DCM (5 mL) containing three drops of triethylamine, and the resulting solution was cooled to 0 ^{o}C in an ice bath. This solution was then treated, while stirring, with *N*-chlorocarbonyl isocyanate (0.03 mL, 0.29 mmol). The reaction mixture was subsequently allowed to warm to room temperature and was stirred for 15 hrs. After careful addition of water (3 mL), a solid precipitated, which was filtered off and then washed with water (4 x 10 mL), followed by ether (2 x 10 mL). The precipitate was desiccated at 50 ^{o}C overnight to give the desired pyrazolotriazinedione **313** as a white solid (0.051 g, 45%): m.p. 284-285 ^{o}C; ν_{max}/cm^{-1} (KBr) 3215, 3067, 1761, 1713, 1647, 1586, 1411, 1127; δ_H (300MHz, DMSO-d_6) 3.72 [6H, s, 2 x *m*-OCH_3], 3.74 [3H, s, *p*-OCH_3], 3.78 [3H, s, NCH_3], 6.64 [2H, s, C-$H_{2',6'}$], 7.18 [1H, dd, *J* 7.8, 4.9, C-H_5], 7.31 [1H, s, C-H_2], 8.32-8.34 [2H, m, C-$H_{4,6}$], 11.59 [1H, bs, C=C-N<u>H</u>CO], 11.74 [1H, bs, CON<u>H</u>CO]; δ_C (75 MHz, DMSO-d_6) 31.0 (CH_3, NCH_3), 55.8 ($2CH_3$, 2 x *m*-OCH_3), 60.1 (CH_3, *p*-OCH_3), 102.0 (C, aromatic C), 104.8 (C, aromatic C), 107.9 (2CH, 2 x aromatic CH), 116.5 (CH, aromatic CH), 118.0 (C, aromatic C), 124.9 (C, aromatic C), 129.5 (CH, aromatic CH), 130.0 (CH, aromatic CH), 137.2 (C, aromatic C), 138.1 (C, aromatic C), 143.3 (CH, aromatic CH), 144.1 (C, aromatic C), 147.2 (C, aromatic C), 148.7 (C, C=O), 149.7 (C, C=O), 153.0 (2C, 2 x aromatic C); m/z (ES+) 447.2 $[M-H]^-$ (100%); HRMS (ES+): Exact mass calculated for $C_{22}H_{21}N_6O_5$ 449.1573. Found 449.1587.

2-(1-Methyl-1*H*-pyrrolo[2,3-*b*]pyridin-3-yl)-5,7-bis(trifluoromethyl)-3-(3,4,5-trimethoxyphenyl)pyrazolo[1,5-*a*]pyrimidine (314)

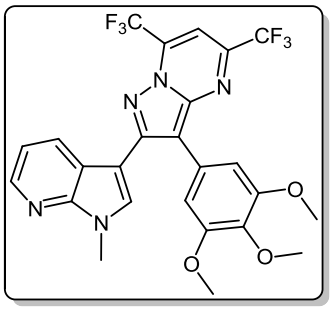

To a stirred solution of 5-(1-methyl-1*H*-pyrrolo[2,3-*b*]pyridin-3-yl)-4-(3,4,5-trimethoxyphenyl)-1*H*-pyrazol-3-amine **312** (0.060 g, 0.16 mmol) in acetic acid (5 mL), was added hexafluoroacetylacetone (0.44 mL, 3.2 mmol). The mixture was then heated to 80 ^{o}C for 22 hours. Once cooled to room temperature, the excess solvent was removed under reduced pressure. The residue was dissolved in ethyl acetate (20 mL), then washed with water (20 mL) and brine (20 mL), before being dried over magnesium sulfate. The solvent was removed under reduced pressure and the crude residue was subjected to flash column chromatography (hexane/ethyl acetate, 60:40) to yield **314** as an orange solid (0.069 g, 78%): m.p. 176-178 ^{o}C; ν_{max}/cm^{-1} (KBr) 2923, 2841, 1586, 1560, 1509, 1279, 1131; δ_H (300MHz, $CDCl_3$) 3.71 [6H, s, 2 x *m*-OCH_3], 3.81 [3H, s, *p*-OCH_3], 3.88 [3H, s, NCH_3], 6.82 [2H, s, C-$H_{2',6'}$], 7.11 [1H, dd, *J* 8.0, 4.8, C-H_5], 7.33 [1H, s, C-H_2], 7.44 [1H, s, C$\underline{H}$CCF_3], 8.33-8.38 [2H, m, C-$H_{4,6}$]; δ_C (75 MHz, $CDCl_3$) 30.6 (CH_3, NCH_3), 55.1 (2CH_3, 2 x *m*-OCH_3), 60.0 (CH_3, *p*-OCH_3), 100.4 (CH, aromatic CH), 104.3 (C, aromatic C), 106.2 (2CH, 2 x aromatic CH), 110.0 (C, aromatic C), 116.2 (CH, aromatic CH), 112.8-123.7 (C, q, J_{F-C} 274.9, CF_3), 113.8-124.8 (C, q, J_{F-C} 274.6, CF_3), 117.8 (C, aromatic C), 124.5 (C, aromatic C), 129.1 (CH, aromatic CH), 129.7 (CH, aromatic CH), 132.8-134.4 (C, q, J_{F-C} 39.0, aromatic C), 137.0 (C, aromatic C), 143.0 (CH, aromatic CH), 143.6-145.1 (C, q, J_{F-C} 38.2, aromatic C), 145.3 (C, aromatic C), 147.0 (C, aromatic C), 151.8 (C, aromatic C), 152.6 (2C, 2 x aromatic C); m/z (ES+) 552.2 $[M+H]^+$ (100%); HRMS (ES+): Exact mass calculated for $C_{25}H_{20}N_5O_3F_6$ 552.1470. Found 552.1493.

*7.2.4.2 Reaction of 5-aminopyrazole **312** with monodentate electrophiles*

2,2,2-Trifluoro-*N*-(5-(1-methyl-1*H*-pyrrolo[2,3-*b*]pyridin-3-yl)-4-(3,4,5-trimethoxyphenyl)-1*H*-pyrazol-3-yl)acetamide (315)

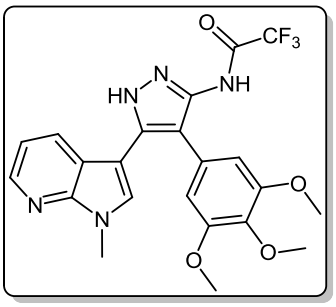

To a solution of 5-(1-methyl-1*H*-pyrrolo[2,3-*b*]pyridin-3-yl)-4-(3,4,5-trimethoxyphenyl)-1*H*-pyrazol-3-amine **312** (0.060 g, 0.16 mmol) in acetonitrile (10 mL), was added trifluoroacetic anhydride (0.03 mL, 0.19 mmol). The resulting mixture was heated to reflux for 28 hours. Once cooled to room temperature, the solvent was evaporated under reduced pressure, and the crude brown residue was subjected to flash column chromatography (hexane/ethyl acetate, 30:70), yielding trifluoroacetamide **315** as an-off white solid (0.518 g, 68%): m.p. 129-131 ^{o}C; ν_{max}/cm^{-1} (KBr) 3215, 3067, 1713, 1603, 1586, 1411; δ_H (300 MHz, DMSO-d_6) 3.49 [6H, s, 2 x *m*-OCH_3], 3.66 [3H, s, *p*-OCH_3], 3.91 [3H, s, NCH_3], 6.53 [2H, s, C-$H_{2',6'}$], 7.03 [1H, dd, *J* 7.9, 4.6, C-H_5], 7.32 [1H, d, *J* 6.5, C-H_4], 7.86 [1H, s, C-H_2], 8.31 [1H, d, *J* 3.5, C-H_6], 11.37 [1H, bs, $NHCOCF_3$], 13.30 [1H, bs, C=N-NH-C]; δ_C (75 MHz, DMSO-d_6) 31.0 (CH_3, NCH_3), 55.4 ($2CH_3$, 2 x *m*-OCH_3), 60.0 (CH_3, *p*-OCH_3), 102.0 (C, aromatic C), 105.8 (2CH, 2 x aromatic CH), 110.2-121.6 (C, q, J_{F-C} 288.0, CF_3), 113.9 (C, aromatic C), 115.9 (CH, aromatic CH), 117.3 (C, aromatic C), 127.1 (C, aromatic C), 128.2 (CH, aromatic CH), 129.4 (CH, aromatic CH), 136.2 (C, aromatic C), 143.1 (CH, aromatic CH), 147.2 (C, aromatic C), 152.7 (2C, 2 x aromatic C), 152.9 (C, aromatic C), 155.8-157.2 (C, q, J_{F-C} 36.2, C=O); m/z (ES+) 474.3 $[M-H]^-$ (100%); HRMS (ES+): Exact mass calculated for $C_{22}H_{21}N_5O_4F_3$ 476.1546. Found 476.1532.

1-(5-Amino-3-(1-methyl-1*H*-pyrrolo[2,3-*b*]pyridin-3-yl)-4-(3,4,5-trimethoxyphenyl)-1*H*-pyrazol-1-yl)ethanone (316)

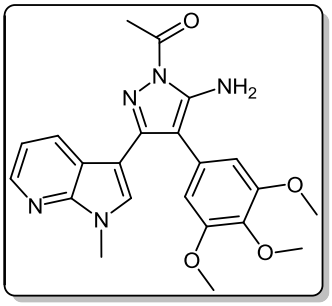

To a solution of 5-(1-methyl-1*H*-pyrrolo[2,3-*b*]pyridin-3-yl)-4-(3,4,5-trimethoxyphenyl)-1*H*-pyrazol-3-amine **312** (0.060 g, 0.16 mmol) in acetonitrile (10 mL), was added acetic anhydride (0.016 mL, 0.17 mmol). The resulting mixture was then heated to reflux for 20 hours. Once cooled to room temperature, the solvent was removed under reduced pressure. The crude residue was purified by flash column chromatography (hexane/ethyl acetate, 50:50) to yield acetylated product **316** as an off-white solid (0.048 g, 71%): m.p. 171-172 ^{o}C; ν_{max}/cm^{-1} (KBr) 3454, 3358, 2927, 1704, 1624, 1509, 1404, 1124; δ_H (300MHz, $CDCl_3$) 2.80 [3H, s, $NCOCH_3$], 3.79 [3H, s, *p*-OCH_3], 3.79 [6H, s, 2 x *m*-OCH_3], 3.92 [3H, s, NCH_3], 5.56 [2H, bs, NH_2], 6.59 [2H, s, C-$H_{2',6'}$], 7.05 [1H, s, C-H_2], 7.14 [1H, dd, *J* 7.9, 4.7, C-H_5], 8.36 [1H, dd, *J* 4.7, 1.5, C-H_6], 8.47 [1H, dd, *J* 7.9, 1.6, C-H_4]; δ_C (75 MHz, $CDCl_3$) 23.3 (CH_3, NCO<u>C</u>H_3), 31.4 (CH_3, NCH_3), 56.2 (CH_3, 2 x *m*-OCH_3), 61.0 (CH_3, *p*-OCH_3), 101.9 (C, aromatic C), 105.9 (C, aromatic C), 107.1 (CH, 2 x aromatic CH), 116.6 (CH, aromatic CH), 118.8 (C, aromatic C), 127.4 (C, aromatic C), 129.3 (CH, aromatic CH), 130.7 (CH, aromatic CH), 137.5 (C, aromatic C), 143.7 (CH, aromatic CH), 147.0 (C, aromatic C), 147.9 (C, aromatic C), 148.5 (C, aromatic C), 153.9 (C, 2 x aromatic C), 173.7 (C, C=O); m/z (ES+) 422.3 $[M+H]^+$ (100%); HRMS (ES+): Exact mass calculated for $C_{22}H_{24}N_5O_4$ 422.1828. Found 422.1813.

5-Amino-*N*-methyl-3-(1-methyl-1*H*-pyrrolo[2,3-*b*]pyridin-3-yl)-4-(3,4,5-trimethoxyphenyl)-1*H*-pyrazole-1-carbothioamide (317)

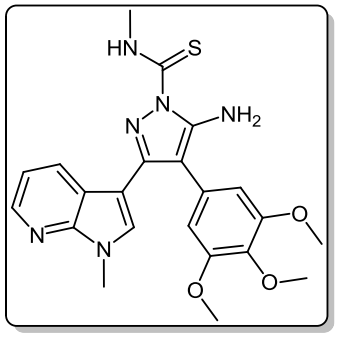

To a solution of 5-(1-methyl-1*H*-pyrrolo[2,3-*b*]pyridin-3-yl)-4-(3,4,5-trimethoxyphenyl)-1*H*-pyrazol-3-amine **312** (0.060 g, 0.16 mmol) in acetonitrile (10 mL), was added methyl isothiocyanate (0.014 g, 0.19 mmol). The mixture was heated to reflux for 22 hours, before then being cooled to room temperature. The solvent was evaporated under reduced pressure and the crude residue was subjected to flash column chromatography (hexane/ethyl acetate, 50:50), yielding pure carbothioamide **317** as a white solid (0.055 g, 76%): m.p. 162-164 ^{o}C; ν_{max}/cm^{-1} (KBr) 3378, 2931, 1601, 1523, 1406, 1362, 1129; δ_H (300 MHz, $CDCl_3$) 3.33 [3H, d, *J* 5.0, NHC<u>H</u>$_3$], 3.78 [6H, s, 2 x *m*-OCH_3], 3.80 [3H, s, *p*-OCH_3], 3.92 [3H, s, NCH_3], 6.47 [2H, bs, NH_2], 6.59 [2H, s, C-$H_{2',6'}$], 7.08 [1H, s, C-H_2], 7.12 [1H, dd, *J* 7.9, 4.7, C-H_5], 8.27 [1H, dd, *J* 7.9, 1.6, C-H_4], 8.36 [1H, dd, *J* 4.7, 1.5, C-H_6], 9.24 [1H, bd, *J* 4.7, N<u>H</u>CH_3]; δ_C (75 MHz, $CDCl_3$) 30.9 (CH_3, $NHCH_3$), 31.4 (CH_3, NCH_3), 56.2 ($2CH_3$, 2 x *m*-OCH_3), 61.0 (CH_3, *p*-OCH_3), 102.5 (C, aromatic C), 105.4 (C, aromatic C), 107.2 (2CH, 2 x aromatic CH), 116.5 (CH, aromatic CH), 118.6 (C, aromatic C), 127.6 (C, aromatic C), 129.7 (CH, aromatic CH), 130.2 (CH, aromatic CH), 137.5 (C, aromatic C), 143.7 (CH, aromatic CH), 145.7 (C, aromatic C), 147.8 (C, aromatic C), 148.1 (C, aromatic C), 153.9 (2C, 2 x aromatic C), 176.8 (C, C=S); m/z (ES+) 453.2 $[M+H]^+$ (100%); HRMS (ES+): Exact mass calculated for $C_{22}H_{25}N_6O_3S$ 453.1709. Found 453.1718.

7.2.5 Synthesis and derivatisation of 5-aminopyrazole **318**

4-(1-Methyl-1*H*-indol-3-yl)-5-(1-methyl-1*H*-pyrrolo[2,3-*b*]pyridin-3-yl)-1*H*-pyrazol-3-amine (318)

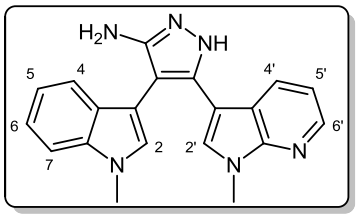

To a solution of 2-(1-methyl-1*H*-indol-3-yl)-3-(1-methyl-1*H*-pyrrolo[2,3-*b*]pyridin-3-yl)-3-oxopropanenitrile **276 (**3.951 g, 12.0 mmol) in absolute alcohol (100 mL), was carefully added 12 M aqueous HCl (2 mL) in a dropwise fashion. Hydrazine hydrate (50% aqueous solution, 3.74 mL, 60.0 mmol) was then added, with the resulting mixture subsequently heated to reflux for 22 hours. Once cooled to room temperature, the solvent was evaporated under reduced pressure. The residue was dissolved in ethyl acetate (100 mL) and washed with saturated aqueous sodium bicarbonate solution (80 mL), water (80 mL) and brine (80 mL), before being dried over magnesium sulfate. The solvent was removed under reduced pressure, leaving the crude product as a dark brown solid, which was then purified by flash column chromatography (ethyl acetate/methanol, 90:10) to yield aminopyrazole **318** as a light brown crystalline solid (2.656 g, 64%): m.p. 136-139 ^{o}C; ν_{max}/cm^{-1} (KBr) 3197, 2928, 1611, 1561, 1487, 1405, 1374, 1298; δ_H (300 MHz, CD_3OD) 3.71 [3H, s, NCH_3], 3.77 [3H, s, NCH_3], 4.64 [2H, bs, NH_2], 6.84-6.90 [2H, m, C-$H_{5,5'}$], 7.10 [1H, s, C-H_2], 7.11-7.18 [2H, m, C-$H_{6,7}$], 7.28 [1H, s, C-$H_{2'}$], 7.35 [1H, d, *J* 8.3, C-H_4], 7.67 [1H, dd, *J* 7.9, 1.2, C-$H_{4'}$], 8.14 [1H, dd, *J* 4.8, 1.5, C-$H_{6'}$]; δ_C (75 MHz, CD_3OD) 31.6 (CH_3, NCH_3), 32.9 (CH_3, NCH_3), 99.0 (C, aromatic C), 100.1 (C, aromatic C), 101.9 (C, aromatic C), 107.1 (C, aromatic C), 110.4 (CH, aromatic CH), 116.8 (CH, aromatic CH), 120.1 (CH, aromatic CH), 120.3 (C, aromatic C), 120.9 (CH, aromatic CH), 122.7 (CH, aromatic CH), 128.9 (C, aromatic C), 129.5 (CH, aromatic CH), 129.6 (CH, aromatic CH), 130.8 (CH, aromatic CH), 138.6 (C, aromatic C), 143.6 (CH, aromatic CH), 148.4 (C, aromatic C), 150.2 (C, aromatic C); m/z (ES+) 343.2 $[M+H]^+$, (100%).

*7.2.5.1 Formation of bicyclic derivatives of 5-aminopyrazole **318***

8-(1-Methyl-1*H*-indol-3-yl)-7-(1-methyl-1*H*-pyrrolo[2,3-*b*]pyridin-3-yl)pyrazolo[1,5-a][1,3,5]triazine-2,4(1*H*,3*H*)-dione (319)

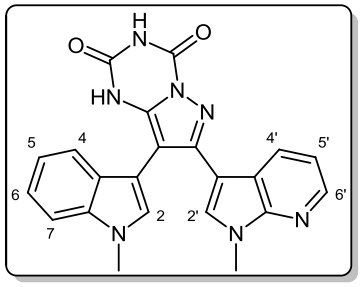

4-(1-Methyl-1*H*-indol-3-yl)-5-(1-methyl-1*H*-pyrrolo[2,3-*b*]pyridin-3-yl)-1*H*-pyrazol-3-amine **318** (0.160 g, 0.47 mmol) was dissolved in DCM (15 mL) containing four drops of triethylamine, and the resulting solution was cooled to 0 ^{o}C in an ice bath. This solution was then treated, while stirring, with *N*-chlorocarbonyl isocyanate (0.04 mL, 0.52 mmol). The reaction mixture was allowed to warm to room temperature and stirred for 15 hours. After careful addition of water (5 mL), the precipitate formed was filtered off before subsequently being washed with water (4 x 20 mL) and ether (2 x 20 mL). The precipitate was desiccated at 50 ^{o}C overnight to yield pyrazolotriazinedione **319** as a grey solid (0.127 g, 66%): m.p. 220-222 ^{o}C; ν_{max}/cm^{-1} (KBr) 3219, 2818, 1753, 1717, 1604, 1559, 1447, 1297; δ_H (400 MHz, DMSO-d_6) 3.58 [3H, s, NCH_3], 3.87 [3H, s, NCH_3], 6.94 [1H, t, *J* 7.3, C-H_5], 7.10 [1H, s, C-H_2], 7.13-7.20 [3H, m, C-$H_{5',6,7}$], 7.39 [1H, s, C-$H_{2'}$], 7.51 [1H, d, C-H_4], 8.29 [1H, dd, *J* 4.6, 1.6, C-$H_{6'}$], 8.55 [1H, dd, *J* 7.9, 1.6, C-$H_{4'}$], 10.75 [1H, bs, C=C-N<u>H</u>CO], 11.12 [1H, bs, CON<u>H</u>CO]; δ_C (150 MHz, DMSO-d_6) 30.8 (CH_3, NCH_3), 32.5 (CH_3, NCH_3), 93.8 (C, aromatic C), 106.1 (C, aromatic C), 109.8 (CH, aromatic CH), 116.3 (CH, aromatic CH), 118.1 (C, aromatic C), 118.7 (CH, aromatic CH), 119.8 (CH, aromatic CH), 121.1 (CH, aromatic CH), 126.8 (C, aromatic C), 129.2 (CH, aromatic CH), 130.2 (CH, aromatic CH), 130.3 (CH, aromatic CH), 136.4 (C, aromatic C), 136.7 (C, aromatic C), 143.1 (CH, aromatic CH), 147.0 (C, aromatic C), 147.1 (C, aromatic C), 150.5 (C, C=O), 162.5 (C, C=O); m/z (ES+) 412.1 $[M+H]^+$ (30%); HRMS (ES+): Exact mass calculated for $C_{22}H_{18}N_7O_2$ 412.1522. Found 412.1531.

3-(1-Methyl-1*H*-indol-3-yl)-2-(1-methyl-1*H*-pyrrolo[2,3-*b*]pyridin-3-yl)-5,7-bis(trifluoromethyl)pyrazolo[1,5-*a*]pyrimidine (320)

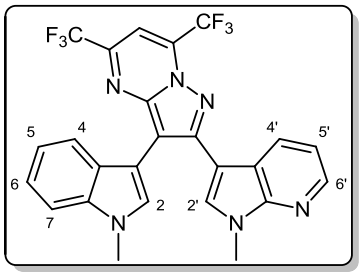

To a stirred mixture of 4-(1-methyl-1*H*-indol-3-yl)-5-(1-methyl-1*H*-pyrrolo[2,3-*b*]pyridin-3-yl)-1*H*-pyrazol-3-amine **318** (0.160 g, 0.47 mmol) in acetic acid (15 mL), was added hexafluoroacetylacetone (1.31 mL, 9.34 mmol). The resulting mixture was heated to 80 ^{o}C for 20 hours. After cooling to room temperature, the acetic acid and excess hexafluoroacetylacetone was removed under reduced pressure. The residue was dissolved in ethyl acetate (30 mL), then washed with water (2 x 20 mL) and brine (20 mL), before being dried over magnesium sulfate. Evaporation of the solvent under reduced pressure yielded the crude product as a red/brown solid. Purification via flash column chromatography (hexane/ethyl acetate, 60:40) gave the pure pyrimidine product **320** as an orange solid (0.115 g, 47%): m.p. 234-235 ^{o}C; ν_{max}/cm^{-1} (KBr) 3118, 2916, 1601, 1559, 1487, 1393, 1274, 1159; δ_H (300 MHz, $CDCl_3$) 3.68 [3H, s, NCH_3], 3.93 [3H, s, NCH_3], 7.03 [1H, t, *J* 7.6, C-H_5], 7.21-7.31 [4H, m, C-$H_{2,4,5',6}$], 7.37 [2H, s, C-$H_{2'}$, (CF_3)C-C<u>H</u>=C(CF_3)], 7.45 [1H, d, *J* 8.3, C-H_7], 8.40 [1H, dd, *J* 4.7, 1.5, C-$H_{6'}$], 8.78 [1H, dd, *J* 7.9, 1.6, C-$H_{4'}$]; δ_C (75 MHz, $CDCl_3$) 31.5 (CH_3, NCH_3), 33.2 (CH_3, NCH_3), 101.1 (CH, C(CF_3)CH=C(CF_3)), 103.3 (C, aromatic C), 104.7 (C, aromatic C), 105.7 (C, aromatic C), 109.8 (CH, aromatic CH), 113.9-124.9 (C, q, J_{F-C} 275.2, CF_3), 115.0-125.9 (C, q, J_{F-C} 275.7, CF_3), 117.2 (CH, aromatic CH), 119.0 (C, aromatic C), 119.6 (CH, aromatic CH), 121.0 (CH, aromatic CH), 122.1 (CH, aromatic CH), 126.6 (C, aromatic C), 129.4 (CH, aromatic CH), 131.1 (2CH, 2 x aromatic CH), 133.6-135.1 (C, q, J_{F-C} 38.1, aromatic C), 137.3 (C, aromatic C), 143.8 (CH, aromatic CH), 143.9-145.4 (C, q, J_{F-C} 37.4, aromatic C), 146.9 (C, aromatic C), 147.9 (C, aromatic C), 153.6 (C, aromatic C); m/z (ES+) 515.1 (100%); HRMS (ES+): Exact mass calculated for $C_{25}H_{17}N_6F_6$ 515.1419. Found 515.1425.

*7.2.5.2 Reaction of 5-aminopyrazole **318** with monodentate electrophiles*

2,2,2-Trifluoro-*N*-(4-(1-methyl-1*H*-indol-3-yl)-5-(1-methyl-1*H*-pyrrolo[2,3-*b*]pyridin-3-yl)-1*H*-pyrazol-3-yl)acetamide (321)

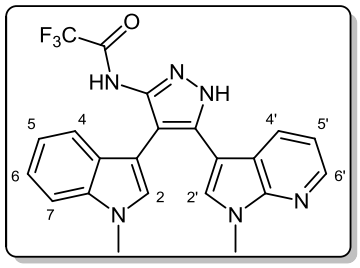

To a solution of 4-(1-methyl-1*H*-indol-3-yl)-5-(1-methyl-1*H*-pyrrolo[2,3-*b*]pyridin-3-yl)-1*H*-pyrazol-3-amine **318** (0.160 g, 0.47 mmol) in acetonitrile (15 mL) was added trifluoroacetic anhydride (0.08 mL, 0.56 mmol). The reaction mixture was then refluxed for 20 hours before being left to cool to room temperature. Evaporation of the solvent under reduced pressure left the crude product as a brown residue, which was then purified by flash column chromatography (hexane/ethyl acetate, 30:70) to yield trifluoroacetamide **321** as a white crystalline solid (0.073 g, 35%): m.p. 127-129 ^{o}C; ν_{max}/cm^{-1} (KBr) 3326, 2922, 1724, 1601, 1564, 1484, 1299, 1211, 1157; δ_H (300 MHz, $CDCl_3$) 3.66 [3H, s, NCH_3], 3.77 [3H, s, NCH_3], 6.89 [1H, dd, *J* 7.9, 4.7, C-$H_{5'}$], 6.97 [1H, s, C-H_2], 7.05 [1H, t, *J* 7.3, C-H_5], 7.11 [1H, s, C-$H_{2'}$], 7.24-7.39 [2H, m, C-$H_{6,7}$], 7.37 [1H, d, *J* 8.2, C-H_4], 7.84 [1H, d, *J* 7.7, C-$H_{4'}$], 8.23 [1H, dd, *J* 4.6, 1.1, C-$H_{6'}$], 8.51 [1H, bs, N<u>H</u>COCF_3]; δ_C (75 MHz, $CDCl_3$) 31.3 (CH_3, NCH_3), 33.0 (CH_3, NCH_3), 102.3 (C, aromatic C), 103.6 (C, aromatic C), 103.9 (C, aromatic C), 109.8 (CH, aromatic CH), 109.9-121.3 (C, q, J_{F-C} 288.6, CF_3), 116.2 (CH, aromatic CH), 117.4 (C, aromatic C), 118.2 (C, aromatic C), 119.5 (CH, aromatic CH), 120.1 (CH, aromatic CH), 122.4 (CH, aromatic CH), 127.0 (C, aromatic C), 128.2 (CH, aromatic CH), 128.3 (CH, aromatic CH), 129.1 (CH, aromatic CH), 137.1 (C, aromatic C), 139.9 (C, aromatic C), 143.3 (CH, aromatic CH), 147.5 (C, aromatic C), 154.0-155.5 (C, q, J_{F-C} 38.0, C=O); m/z (ES+) 439.1 $[M+H]^+$ (100%); HRMS (ES+): Exact mass calculated for $C_{22}H_{18}N_6OF_3$ 439.1494. Found 439.1485.

1-(5-Amino-4-(1-methyl-1*H*-indol-3-yl)-3-(1-methyl-1*H*-pyrrolo[2,3-*b*]pyridin-3-yl)-1*H*-pyrazol-1-yl)ethanone (322)

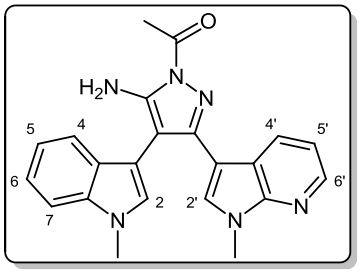

To a solution of 4-(1-methyl-1*H*-indol-3-yl)-5-(1-methyl-1*H*-pyrrolo[2,3-*b*]pyridin-3-yl)-1*H*-pyrazol-3-amine **318** (0.160 g, 0.47 mmol) in acetonitrile (15 mL), was added acetic anhydride (0.05 mL, 0.52 mmol). The resulting mixture was heated to reflux for 22 hours before being cooled to room temperature. The solvent and excess acetic anhydride was then removed under reduced pressure. The crude residue was subjected to flash column chromatography (hexane/ethyl acetate, 50:50), yielding the pure acetylated product **322** as a white crystalline solid (0.126 g, 70%): m.p. 206-207 ^{o}C; ν_{max}/cm^{-1} (KBr) 3444, 3360, 2929, 1703, 1603, 1558, 1406, 1385, 1314, 1135; δ_H (300 MHz, $CDCl_3$) 2.84 [3H, s, $COCH_3$], 3.64 [1H, s, NCH_3], 3.87 [1H, s, NCH_3], 5.44 [2H, bs, NH_2], 6.99 [1H, s, C-H_2], 7.08-7.17 [3H, m, C-$H_{2',5,5'}$], 7.30 [1H, t, *J* 7.0, C-H_6], 7.41-7.45 [2H, m, C-$H_{4,7}$], 8.35 [1H, dd, *J* 4.7, 1.5, C-$H_{6'}$], 8.62 [1H, dd, *J* 7.9, 1.6, C-$H_{4'}$]; δ_C (75 MHz, $CDCl_3$) 23.3 (CH_3, CO<u>C</u>H_3), 31.3 (CH_3, NCH_3), 33.1 (CH_3, NCH_3), 93.8 (C, aromatic C), 104.7 (C, aromatic C), 106.2 (C, aromatic C), 109.6 (CH, aromatic CH), 116.6 (CH, aromatic CH), 118.9 (C, aromatic C), 119.7 (CH, aromatic CH), 120.3 (CH, aromatic CH), 122.2 (CH, aromatic CH), 127.5 (C, aromatic C), 128.6 (CH, aromatic CH), 129.6 (CH, aromatic CH), 130.8 (CH, aromatic CH), 137.3 (C, aromatic C), 143.5 (CH, aromatic CH), 147.8 (C, aromatic C), 148.1 (C, aromatic C), 149.9 (C, aromatic C), 173.6 (C, C=O); m/z (ES+) 385.4 $[M+H]^+$ (100%); HRMS (ES+): Exact mass calculated for $C_{22}H_{21}N_6O$ 385.1777. Found 385.1796.

5-Amino-*N*-methyl-4-(1-methyl-1*H*-indol-3-yl)-3-(1-methyl-1*H*-pyrrolo[2,3-*b*]pyridin-3-yl)-1*H*-pyrazole-1-carbothioamide (323)

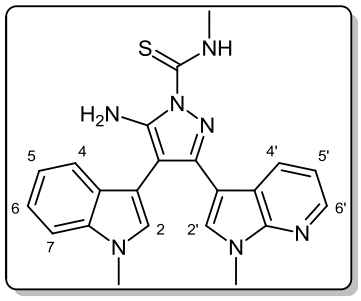

To a solution of 4-(1-methyl-1*H*-indol-3-yl)-5-(1-methyl-1*H*-pyrrolo[2,3-*b*]pyridin-3-yl)-1*H*-pyrazol-3-amine **318** (0.160 g, 0.47 mmol) in acetonitrile (15 mL), was added methyl isothiocyanate (0.038 g, 0.52 mmol). The reaction mixture was then heated to reflux for 26 hours before being cooled to room temperature. The solvent was removed under reduced pressure to give a crude brown residue. Purification was achieved by flash column chromatography (hexane/ethyl acetate, 50:50) to yield carbothioamide **323** as a white solid (0.062 g, 32%): m.p. 185-186 ^{o}C; ν_{max}/cm^{-1} (KBr) 3424, 3277, 2930, 1627, 1603, 1559, 1516, 1485, 1297; δ_H (300 MHz, $CDCl_3$) 3.34 [3H, bd, *J* 5.0, NHC$\underline{H}_3$], 3.64 [3H, s, NCH_3], 3.86 [3H, s, NCH_3], 6.34 [2H, bs, NH_2], 7.01 [1H, s, C-H_2], 7.07 [1H, s, C-$H_{2'}$], 7.09-7.15 [2H, m, C-$H_{5,5'}$], 7.29 [1H, t, *J* 7.0, 1.1, C-H_6], 7.40-7.44 [2H, m, C-$H_{4,7}$], 8.34 [1H, dd, *J* 4.7, 1.6, C-$H_{6'}$], 8.43 [1H, dd, *J* 7.9, 1.6, C-$H_{4'}$], 9.29 [1H, bd, *J* 4.6, N$\underline{H}$CH$_3$); δ_C (75 MHz, $CDCl_3$) 30.9 (CH_3, $NHCH_3$), 31.3 (CH_3, NCH_3), 33.0 (CH_3, NCH_3), 94.3 (C, aromatic C), 104.9 (C, aromatic C), 105.7 (C, aromatic C), 109.5 (CH, aromatic CH), 116.4 (CH, aromatic CH), 118.7 (C, aromatic C), 119.7 (CH, aromatic CH), 120.3 (CH, aromatic CH), 122.2 (CH, aromatic CH), 127.5 (C, aromatic C), 128.8 (CH, aromatic CH), 130.0 (CH, aromatic CH), 130.3 (CH, aromatic CH), 137.2 (C, aromatic C), 143.4 (CH, aromatic CH), 147.1 (C, aromatic C), 147.7 (C, aromatic C), 149.2 (C, aromatic C), 176.8 (C, C=S); m/z (ES+) 416.2 $[M+H]^+$ (100%); HRMS (ES+): Exact mass calculated for $C_{22}H_{22}N_7S$ 416.1657. Found 416.1672.

7.2.6 Cyclocondensation of oxopropanoate intermediates

*7.2.6.1 Synthesis of pyrazolone **326***

5-(1-Benzyl-1*H*-pyrrolo[2,3-*b*]pyridin-3-yl)-4-(1-methyl-1*H*-indol-3-yl)-1*H*-pyrazol-3(2*H*)-one (326)

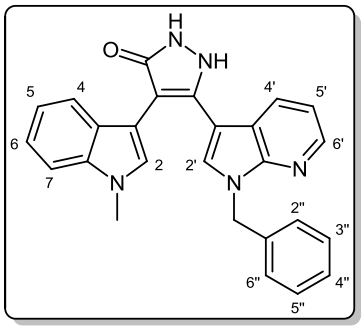

Camphoric acid (0.162 g, 0.8 mmol) was added to a solution of methyl 3-(1-benzyl-1*H*-pyrrolo[2,3-*b*]pyridin-3-yl)-2-(1-methyl-1*H*-indol-3-yl)-3-oxopropanoate **273** (0.350 g, 0.8 mmol) in absolute alcohol (10 mL). Hydrazine hydrate (50% aqueous solution, 0.05 mL, 0.8 mmol) was then added dropwise to the stirred mixture. Once the addition was complete, the mixture was heated to reflux for 2 hours. At this point, a further portion of hydrazine hydrate (50% aqueous solution, 0.20 mL, 3.2 mmol) was added to the reaction mixture, which was then heated once more to the point of reflux. After 22 hours, TLC analysis indicated the total consumption of starting material, following which the reaction mixture was cooled to room temperature. The solvent was removed under reduced pressure and the residue was dissolved in ethyl acetate (30 mL). The organic phase was washed successively with 10% aqueous sodium bicarbonate solution (20 mL), water (20 mL) and brine (20 mL), before being dried over magnesium sulfate. Once the solvent was removed under reduced pressure, the crude product was subjected to flash column chromatography (dichloromethane/methanol, 98:2) to yield the pure product **326** as a brown solid (0.175 g, 52%): m.p. 177-179 ^{o}C; ν_{max}/cm^{-1} (KBr) 3054, 2932, 1719, 1601, 1567, 1512, 1471, 1302; δ_H (300 MHz, DMSO-d_6) 3.75 [3H, s, NCH_3], 5.41 [2H, s, C$\underline{H}_2$Ph], 6.78 [1H, t, *J* 7.0, C-H_5], 6.99 [1H, dd, *J* 7.9, 4.7, C-$H_{5'}$], 7.05-7.10 [4H, m, C-$H_{2,2'',6''}$], 7.22-7.25 [4H, m, C-$H_{7,3'',5''}$], 7.37 [1H, d, *J* 8.2, C-H_4], 7.55 [1H, s, C-$H_{2'}$], 7.77 [1H, d, *J* 7.2, C-$H_{4'}$], 8.21 [1H, dd, *J* 4.7, 1.5, C-$H_{6'}$]; δ_H (150 MHz, DMSO-d_6) 32.4 (CH_3, NCH_3), 47.1 (CH_2, $\underline{C}H_2$Ph), 105.5 (C, aromatic C), 109.4 (CH, aromatic CH), 112.2 (C, aromatic C), 116.0 (CH, aromatic CH), 117.0 (C, aromatic C), 117.9 (C, aromatic C), 118.6 (CH, aromatic CH), 120.1 (CH, aromatic CH), 120.8 (CH, aromatic CH), 126.6 (C, aromatic C), 127.3 (CH, aromatic CH), 128.3 (2CH, 2 x aromatic CH), 128.4 (CH, aromatic CH), 128.6 (2CH, 2 x aromatic CH), 130.0 (CH,

aromatic CH), 135.6 (CH, aromatic CH), 136.2 (C, aromatic C), 136.4 (C, aromatic C), 146.4 (CH, aromatic CH), 146.6 (C, aromatic C), 147.1 (C, aromatic C), 156.6 (C, C=O); m/z (ES+) 420.1 $[M+H]^+$ (100%); HRMS (ES+): Exact mass calculated for $C_{26}H_{22}N_5O$ 420.1824. Found 420.1833.

*7.2.6.2 Synthesis and alkylation of isoxazolone **327***

4-(1-Methyl-1*H*-indol-3-yl)-3-(1-methyl-1*H*-pyrrolo[2,3-*b*]pyridin-3-yl)isoxazol -5(2H)-one (327)

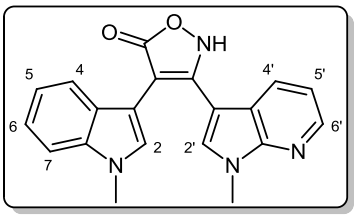

To a solution of methyl 2-(1-methyl-1*H*-indol-3-yl)-3-(1-methyl-1*H*-pyrrolo[2,3-*b*]pyridin-3-yl)-3-oxopropanoate **267** (1.205 g, 3.3 mmol) in methanol (30 mL) was added hydroxylammonium chloride (1.160 g, 16.7 mmol). The resulting mixture was heated to reflux for 14 hours, at which time it was cooled to room temperature. The solvent was removed under reduced pressure, and the resulting brown residue was treated with water (25 mL), before being extracted with ethyl acetate (2 x 30 mL). The combined organic extracts were washed with water (40 mL) and brine (40 mL), then dried over magnesium sulfate and evaporated under reduced pressure. The crude product was purified by flash column chromatography (hexane/ethyl acetate, 20:80) to yield isoxazolone **327** as a light brown solid (0.738 g, 64%): m.p. 138-140 ^oC; ν_{max}/cm^{-1} (KBr) 3419, 3051, 2927, 1718, 1609, 1551, 1464, 1378; δ_H (400 MHz, DMSO-d_6) 3.76 [3H, s, NCH_3], 3.82 [3H, s, NCH_3], 6.87 [1H, t, *J* 7.3, C-H_5], 7.07-7.15 [3H, m, C-$H_{5',6,7}$], 7.46 [1H, s, C-$H_{2'}$], 7.47 [1H, s, C-H_2], 7.74 [2H, m, C-$H_{4,4'}$], 8.31 [1H, dd, *J* 4.7, 1.4, $CH_{6'}$]; δ_C (125 MHz, DMSO-d_6) 31.2 (CH_3, NCH_3), 32.5 (CH_3, NCH_3), 101.1 (C, aromatic C), 103.0 (C, aromatic C), 109.0 (CH, aromatic CH), 116.8 (CH, aromatic CH), 117.0 (C, aromatic C), 118.8 (CH, aromatic CH), 119.9 (CH, aromatic CH), 121.2 (CH, aromatic CH), 126.2 (C, aromatic C), 129.1 (CH, aromatic CH), 129.5 (CH, aromatic CH), 131.3 (CH, aromatic CH), 136.5 (C, aromatic C), 143.7 (CH, aromatic CH), 147.2 (C, aromatic C), 156.8 (C, aromatic C), 171.9 (C, C=O); m/z (ES+) 345.3 $[M+H]^+$ (100%); HRMS (ES+): Exact mass calculated for $C_{20}H_{17}N_4O_2$ 345.1352. Found 345.1349.

2-Methyl-4-(1-methyl-1*H*-indol-3-yl)-3-(1-methyl-1*H*-pyrrolo[2,3-*b*]pyridin-3-yl)isoxazol-5(2*H*)-one (328)

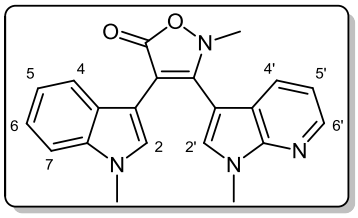

A solution of 4-(1-Methyl-1*H*-indol-3-yl)-3-(1-methyl-1*H*-pyrrolo[2,3-*b*]pyridin-3-yl)isoxazol-5(2H)-one **327** (0.310 g, 0.90 mmol) in DMF (20 mL) was cooled to 0 ^{o}C in an ice bath. Sodium hydride (0.044 g, 1.1 mmol) was added to the solution in a portionwise manner, with the resulting mixture stirred at 0 ^{o}C for 30 minutes. A solution of iodomethane (0.07 mL, 1.1 mmol) in DMF (5 mL) was subsequently added, and the reaction mixture was then allowed warm to room temperature over three hours while stirring. Water (20 mL) was carefully added to quench the reaction, and the resulting solution was extracted with ethyl acetate (3 x 20 mL). The combined organic extracts were washed with water (3 x 25 mL) and brine (25 mL), before being dried over magnesium sulfate and evaporated under reduced pressure. The crude product was purified by flash column chromatography (hexane/ethyl acetate, 50:50) to give *N*-methyl isoxazolone **328** as an off-white solid (0.283 g, 88%): m.p. 109-111 ^{o}C; ν_{max}/cm^{-1} (KBr) 3053, 2926, 1711, 1612, 1532, 1469, 1375; δ_H (400 MHz, $CDCl_3$) 3.24 [3H, s, NCH_3], 3.78 [3H, s, NCH_3], 3.82 [3H, s, NCH_3], 6.76-6.83 [2H, m, C-$H_{5,6}$], 7.12-7.17 [2H, m, C-$H_{5',6,7}$], 7.46 [1H, s, C-$H_{2'}$], 7.47 [1H, s, C-H_2], 7.74 [2H, m, C-$H_{4,4'}$], 8.31 [1H, dd, *J* 4.7, 1.4, $CH_{6'}$]; δ_C (150 MHz, $CDCl_3$) 31.7 (CH_3, NCH_3), 33.0 (CH_3, NCH_3), 42.5 (CH_3, NCH_3), 101.5 (C, aromatic C), 102.9 (C, aromatic C), 109.4 (CH, aromatic CH), 117.5 (CH, aromatic CH), 117.9 (C, aromatic C), 119.2 (CH, aromatic CH), 120.9 (CH, aromatic CH), 121.7 (CH, aromatic CH), 125.3 (C, aromatic C), 129.0 (CH, aromatic CH), 129.6 (CH, aromatic CH), 131.7 (CH, aromatic CH), 137.0 (C, aromatic C), 144.0 (CH, aromatic CH), 147.8 (C, aromatic C), 159.3 (C, aromatic C), 171.4 (C, C=O). m/z (ES+) 359.2 $[M+H]^+$ (100%); HRMS (ES+): Exact mass calculated for $C_{21}H_{19}N_4O_2$ 359.1508. Found 359.1517.

7.2.6.3 Routes towards aza BIM derivatives containing 6-membered F-rings

2-Amino-5-(1-methyl-1*H*-indol-3-yl)-6-(1-methyl-1*H*-pyrrolo[2,3-*b*]pyridin-3-yl)pyrimidin-4(3*H*)-one (332)

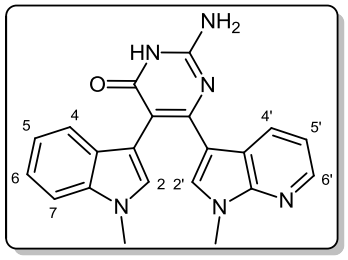

Sodium metal (0.628 g, 27.3 mmol) was carefully added in a portionwise manner over a 30 minute period to dry methanol (20 mL) under a nitrogen atmosphere. Once the sodium had fully reacted, guanidine carbonate (2.463 g, 13.7 mmol) was added to the solution, and the resulting mixture was stirred at room temperature for 30 minutes. Methyl 2-(1-methyl-1*H*-indol-3-yl)-3-(1-methyl-1*H*-pyrrolo[2,3-*b*]pyridin-3-yl)-3-oxopropanoate **267** (0.988 g, 2.7 mmol) was then added to the mixture, which was subsequently heated to reflux for 36 hours. Once cooled to room temperature, the solvent was removed under reduced pressure and the residue was dissolved in water (30 mL). The pH of the strongly basic solution was adjusted to 7 using 2 M HCl, and the precipitate formed was filtered and washed with water. The crude brown solid was subjected to flash column chromatography (ethyl acetate/methanol, 90:10) to yield aminopyrimidinone **332** as a light brown solid (0.424 g, 42%): m.p. 164-166 ^{o}C; ν_{max}/cm^{-1} (KBr) 3338, 2927, 1635, 1524, 1460, 1378; δ_H (300 MHz, DMSO-d_6) 3.50 [3H, s, N-CH_3], 3.86 [3H, s, N-CH_3], 6.50 [2H, bs, NH_2], 6.85-6.89 [2H, m, C-$H_{2,5}$], 7.02-7.15 [3H, m, C-$H_{5',6,7}$], 7.25 [1H, s, C-$H_{2'}$], 7.47 [1H, d, *J* 8.2, C-H_4], 8.24 [1H, dd, *J* 4.6, 1.6, C-$H_{6'}$], 8.64 [1H, dd, *J* 7.9, 1.3, C-$H_{4'}$], 10.90 [1H, bs, NH]; δ_C (75 MHz, DMSO-d_6) 30.8 (CH_3, NCH_3), 32.4 (CH_3, NCH_3), 103.1 (C, aromatic C), 108.5 (C, aromatic C), 109.5 (CH, aromatic CH), 111.9 (C, aromatic C), 116.0 (CH, aromatic CH), 118.4 (CH, aromatic CH), 119.3 (C, aromatic C), 119.6 (CH, aromatic CH), 120.7 (CH, aromatic CH), 127.1 (C, aromatic C), 129.7 (CH, aromatic CH), 131.5 (CH, aromatic CH), 131.9 (CH, aromatic CH), 136.6 (C, aromatic C), 142.5 (CH, aromatic CH), 146.9 (C, aromatic C), 153.5 (C, aromatic C), 157.4 (C, aromatic C), 163.0 (C, C=O); m/z (ES+) 371.1 $[M+H]^+$ (100%); HRMS (ES+): Exact mass calculated for $C_{21}H_{19}N_6O$ 371.1620. Found 371.1613.

2-Amino-5,6-bis(1-methyl-1*H*-pyrrolo[2,3-*b*]pyridin-3-yl)pyrimidin-4(3*H*)-one (337)

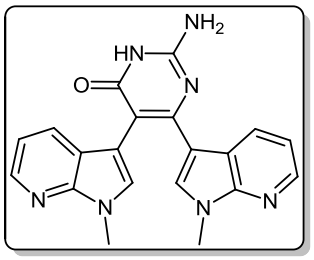

Sodium metal (0.204 g, 8.9 mmol) was added portionwise over 20 minutes to dry methanol (15 mL) under a nitrogen atmosphere. Upon complete reaction of the metal, guanidine carbonate (0.798 g, 4.4 mmol) was added to the solution, and the resulting mixture was stirred at room temperature for 30 minutes. Methyl 2,3-bis(1-methyl-1*H*-pyrrolo[2,3-*b*]pyridin-3-yl)-3-oxopropanoate **281** (0.161 g, 0.44 mmol) was added to the mixture, which was then heated to reflux for 48 hours. At this point, TLC evidence indicated the presence of predominantly starting material in the reaction mixture. Upon workup, spectroscopic analysis indicated that desired pyrimidinone **337** had not been formed.

7.2.7 Synthesis of novel aza ICZs

*7.2.7.1 Synthesis of aza ICZ **239** containing 6-membered F-ring*

6-Amino-13,14-dimethyl-13,14-dihydropyrido[3',2':4,5]pyrrolo[2,3-*a*]pyrimido[4,5-*c*]carbazol-8(7*H*)-one (239)

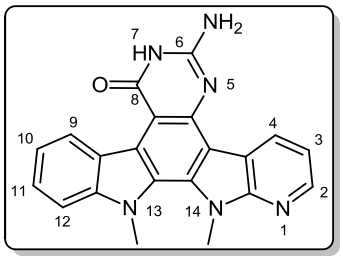

To a solution of 2-amino-5-(1-methyl-1*H*-indol-3-yl)-6-(1-methyl-1*H*-pyrrolo[2,3-*b*]pyridin-3-yl)pyrimidin-4(3*H*)-one **332** (0.080 g, 0.22 mmol) in a mixture of acetonitrile (120 mL) and methanol (80 mL) was added a spatula tip of iodine. The resulting mixture was then irradiated by means of a medium pressure mercury lamp for 18 hours. Once cooled to room temperature, the solvent was removed under reduced pressure. The crude residue was then dissolved in ethyl acetate (60 mL), before being washed with saturated aqueous sodium thiosulfate (50 mL), water (50 mL) and brine (50 mL). After being dried over magnesium sulfate, the solvent was evaporated under reduced pressure and the residue was subjected to flash column chromatography (ethyl acetate/methanol, 99:1) to yield aza ICZ **239** as an off-white solid (0.041 g, 51%): m.p. 289-292 ^{o}C; ν_{max}/cm^{-1} (KBr) 3426, 2923, 1654, 1601, 1566,

1394, 1084; δ_H (300 MHz, DMSO-d_6) 4.22 [3H, s, N-CH_3], 4.34 [3H, s, N-CH_3], 6.46 [2H, bs, NH_2], 7.23 [1H, t, *J* 7.6, aromatic C-H_{10}], 7.38 [1H, dd, *J* 7.7, 4.8, aromatic C-H_3], 7.49 [1H, t, *J* 7.7, aromatic C-H_{11}], 7.66 [1H, d, *J* 8.1, aromatic C-H_{12}], 8.54 [1H, dd, *J* 4.8, 1.7, aromatic C-H_2], 9.26 [1H, dd, *J* 7.7, 1.7, aromatic C-H_4], 9.71 [1H, d, *J* 8.2, aromatic C-H_9], 11.00 [1H, bs, NH]; δ_C (75 MHz, DMSO-d_6) 34.4 (CH_3, NCH_3), 36.9 (CH_3, NCH_3), 105.2 (C, aromatic C), 110.2 (CH, aromatic CH), 112.8 (C, aromatic C), 116.6 (CH, aromatic CH), 117.2 (C, aromatic C), 118.9 (CH, aromatic CH), 120.0 (C, aromatic C), 123.7 (C, aromatic C), 125.4 (CH, aromatic CH), 125.8 (C, aromatic C), 127.3 (CH, aromatic CH), 131.1 (CH, aromatic CH), 132.0 (C, aromatic C), 143.8 (C, aromatic C), 144.7 (CH, aromatic CH), 147.2 (C, aromatic C), 151.8 (C, aromatic C), 152.6 (C, aromatic C), 162.0 (C, C=O); m/z (ES+) 369.4 $[M+H]^+$ (20%); HRMS (ES+): Exact mass calculated for $C_{21}H_{17}N_6O$ 369.1464. Found 369.1462.

7.2.7.2 Route towards monoazaindolyl maleimide precursors

2-(1-Methyl-1*H*-indol-3-yl)acetic acid (350)[11]

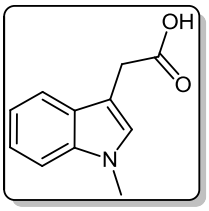

A stirred suspension of sodium hydride (60 wt.% oil dispersion, 6.002 g, 150.1 mmol) in THF (150 mL) was cooled to 0 ^oC in an ice bath. A solution of indole-3-acetic acid **261** (5.250 g, 30.0 mmol) in THF (50 mL) was then added. Following stirring for 30 minutes at 0 ^oC, a solution of iodomethane (6.23 mL, 100.1 mmol) in THF (30 mL) was added to the reaction mixture in a dropwise manner. The mixture was allowed to warm slowly to room temperature and stirred for 16 hours. Methanol (5 mL) was then cautiously added to the mixture, followed by water (100 mL), in order to quench the reaction. Ether (100 mL) was added to the resulting clear yellow solution, after which the phases were separated. The aqueous phase was then acidified to pH 2 using 6M aqueous HCl and extracted with DCM (3 x 100 mL). The combined DCM extracts were dried over magnesium sulfate and concentrated to a volume of roughly 50 mL. Hexane was then added until a brownish solid precipitated out of solution. The crude solid was recrystallised from ethanol to give acetic acid **350** as a light brown solid (4.784 g, 84%): m.p. 126-128 ^oC (lit.[11] 127-129 ^oC); ν_{max}/cm^{-1} (KBr) 2930, 2676,

1698, 1547, 1474, 1412, 1305; δ_H (300 MHz, DMSO-d_6) 3.64 [2H, s, C$\underline{H_2}$COOH], 3.75 [3H, s, NCH_3], 7.03 [1H, t, *J* 7.5, C-H_5], 7.15 [1H, t, *J* 7.6, C-H_6], 7.21 [1H, s, C-H_2], 7.40 [1H, d, *J* 8.2, C-H_7], 7.52 [1H, d, *J* 7.8, C-H_4], 12.17 (1H, bs, COOH]; δ_C (75 MHz, DMSO-d_6) 30.7 (CH_2, $\underline{C}H_2$COOH), 32.2 (CH_3, NCH_3), 106.9 (C, aromatic C), 109.5 (CH, aromatic CH), 118.5 (CH, aromatic CH), 118.7 (CH, aromatic CH), 121.1 (CH, aromatic CH), 127.5 (C, aromatic C), 128.2 (CH, aromatic CH), 136.5 (C, aromatic C), 173.0 (C, C=O). m/z (ES+) 190.4 $[M+H]^+$ (100%).

3-(1-Methyl-1*H*-indol-3-yl)-4-(1-methyl-1*H*-pyrrolo[2,3-*b*]pyridin-3-yl)furan -2,5-dione (355)

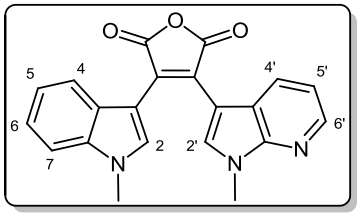

A solution of 1-methyl-1*H*-pyrrolo[2,3-*b*]pyridine **277** (1.808 g, 13.7 mmol) in diethyl ether (80 mL) was cooled to 0 ^oC in an ice bath. Oxalyl chloride (1.39 mL, 16.4 mmol) was then added in a dropwise manner over a period of 20 minutes. The resulting mixture was stirred for 3 hours, whilst being allowed to slowly return to room temperature in that time. The solvent and excess oxalyl chloride was removed under reduced pressure and the solid residue was dissolved in DCM (60 mL). This was then added to a stirred solution containing 2-(1-methyl-1*H*-indol-3-yl)acetic acid **350** (2.592 g, 13.7 mmol) and triethylamine (3.82 mL, 27.4 mmol) in DCM (30 mL). The reaction mixture was stirred at room temperature for 14 hours, after which time the solvent was removed under reduced pressure. The dark red residue was subjected to flash column chromatography (hexane/ethyl acetate, 70:30), yielding maleic anhydride **355** as a red solid (1.796 g, 37%): m.p. 222-224 ^oC; ν_{max}/cm^{-1} (KBr) 2919, 1819, 1747, 1523, 1371, 1254; δ_H (300 MHz, $CDCl_3$) 3.91 [3H, s, NCH_3], 3.94 [3H, s, NCH_3], 6.75 [1H, dd, *J* 8.0, 4.7, C-$H_{5'}$], 6.77-6.79 [2H, m, C-$H_{5,6}$], 7.13-7.19 [1H, m, C-H_7], 7.30 [1H, dd, *J* 8.0, 1.5, C-$H_{4'}$], 7.34 [1H, d, *J* 8.3, C-H_4], 7.85 [1H, s, C-H_2], 7.86 [1H, s, C-$H_{2'}$], 8.25 [1H, dd, *J* 4.7, 1.5, C-$H_{6'}$]; δ_C (75 MHz, $CDCl_3$) 31.9 (CH_3, NCH_3), 33.6 (CH_3, NCH_3), 103.6 (C, aromatic C), 104.8 (C, aromatic C), 109.9 (CH, aromatic CH), 116.5 (CH, aromatic CH), 118.6 (C, aromatic C), 120.9 (CH, aromatic CH), 122.3 (CH, aromatic CH), 123.0 (CH, aromatic CH), 125.5 (C, aromatic C), 126.4 (C,

aromatic C), 128.1 (C, aromatic C), 130.5 (CH, aromatic CH), 133.6 (CH, aromatic CH), 134.0 (CH, aromatic CH), 137.0 (C, aromatic C), 144.0 (CH, aromatic CH), 147.8 (C, aromatic C), 166.6 (C, C=O), 166.8 (C, C=O); m/z (ES+) 358.1 $[M+H]^+$ (100%); HRMS (ES+): Exact mass calculated for $C_{21}H_{16}N_3O_3$ 358.1192. Found 358.1185.

3-(1-Methyl-1*H*-indol-3-yl)-4-(1-methyl-1*H*-pyrrolo[2,3-*b*]pyridin-3-yl)-1*H*-pyrrole -2,5-dione (357)[12]

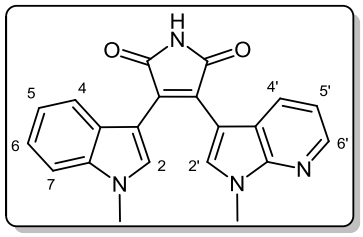

To a stirred solution of 3-(1-methyl-1*H*-indol-3-yl)-4-(1-methyl-1*H*-pyrrolo[2,3-*b*]pyridin-3-yl)furan-2,5-dione **355** (0.801 g, 2.2 mmol) in DMF (10 mL) was added 1,1,1,3,3,3-hexamethyldisilazane (4.70 mL, 22.4 mmol), followed by methanol (0.45 mL, 11.2 mmol). The mixture was then stirred at room temperature for 24 hours. Water (100 mL) was added to the reaction mixture, which was then subsequently extracted with ethyl acetate (3 x 50 mL). The combined organic extracts were washed with water (4 x 100 mL) and brine (100 mL), then dried over magnesium sulfate. The solvent was removed under reduced pressure and the crude residue was subjected to flash column chromatography (hexane/ethyl acetate, 50:50) to yield pure maleimide **357** as a bright red solid (0.709 g, 88%): m.p. 238-239 ^oC; ν_{max}/cm^{-1} (KBr) 3221, 3049, 1754, 1712, 1593, 1530, 1334, 1231; δ_H (300 MHz, $CDCl_3$) 3.85 [3H, s, NCH_3], 3.93 [3H, s, NCH_3], 6.68 [1H, dd, *J* 8.0, 4.7, C-$H_{5'}$], 6.73 [1H, t, *J* 7.5, C-H_5], 6.81 [1H, d, *J* 7.7, C-H_7], 7.10 [1H, t, *J* 7.7, C-H_6], 7.23 [1H, dd, *J* 8.0, 1.6, C-$H_{4'}$], 7.29 [1H, d, *J* 8.3, C-H_4], 7.74 [1H, s, C-H_2], 7.82 [1H, s, C-$H_{2'}$], 8.23 [1H, dd, *J* 4.7, 1.5, C-$H_{6'}$], 8.35 [1H, bs, NH]; δ_C (75 MHz, $CDCl_3$) 31.8 (CH_3, NCH_3), 33.4 (CH_3, NCH_3), 104.2 (C, aromatic C), 105.3 (C, aromatic C), 109.5 (CH, aromatic CH), 116.1 (CH, aromatic CH), 118.9 (C, aromatic C), 120.3 (CH, aromatic CH), 122.0 (CH, aromatic CH), 122.4 (CH, aromatic CH), 125.9 (C, aromatic C), 126.5 (C, aromatic C), 128.1 (C, aromatic C), 130.4 (CH, aromatic CH), 132.7 (CH, aromatic CH), 133.0 (CH, aromatic CH), 136.9 (C, aromatic C), 143.4 (CH, aromatic CH), 147.7 (C, aromatic C), 172.3 (C, C=O), 172.4 (C, C=O). m/z (ES+) 357.2

$[M+H]^+$ (100%); HRMS (ES+): Exact mass calculated for $C_{21}H_{17}N_4O_2$ 357.1352. Found 357.1349.

1-Hydroxy-3-(1-methyl-1*H*-indol-3-yl)-4-(1-methyl-1*H*-pyrrolo[2,3-*b*]pyridin-3-yl)-1*H*-pyrrole-2,5-dione (356)

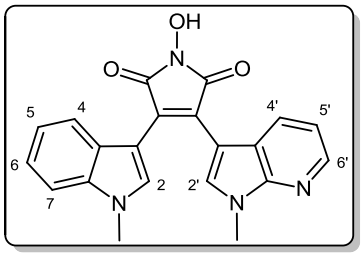

To a solution of 3-(1-methyl-1*H*-indol-3-yl)-4-(1-methyl-1*H*-pyrrolo[2,3-*b*]pyridin-3-yl)furan-2,5-dione **355** (0.200 g, 0.56 mmol) in dry pyridine (5 mL) was added hydroxylammonium chloride (0.389 g, 5.6 mmol). The resulting mixture was heated to reflux for 14 hours before being cooled to room temperature. The solvent was removed under reduced pressure and the residue was dissolved in ethyl acetate (50 mL), before being washed with water (4 x 50 mL) and brine (50 mL), then dried over magnesium sulfate. The solvent was again removed under reduced pressure and the crude residue was subjected to flash column chromatography (hexane/ethyl acetate, 50:50), yielding hydroxymaleimide **356** as a red solid (0.147 g, 71%): m.p. 214-216 ^oC; ν_{max}/cm^{-1} (KBr) 3423, 2919, 1771, 1714, 1530, 1473, 1371, 1102; δ_H (300 MHz, $CDCl_3$) 3.82 [3H, s, NCH_3], 3.96 [3H, s, NCH_3], 6.64-6.72 [3H, m, C-$H_{5,5',6}$], 7.06 [1H, t, *J* 7.1, C-H_7], 7.22 [1H, dd, *J* 8.0, 1.5, C-$H_{4'}$], 7.26 [1H, d, *J* 8.3, C-H_4], 7.74 [1H, s, C-H_2], 7.75 [1H, s, C-$H_{2'}$], 8.22 [1H, dd, *J* 4.8, 1.4, C-$H_{6'}$]; δ_C (75 MHz, $CDCl_3$) 32.3 (CH_3, NCH_3), 33.4 (CH_3, NCH_3), 104.3 (C, aromatic C), 105.2 (C, aromatic C), 109.6 (CH, aromatic CH), 116.1 (CH, aromatic CH), 119.4 (C, aromatic C), 120.5 (CH, aromatic CH), 122.0 (CH, aromatic CH), 122.6 (CH, aromatic CH), 125.2 (C, aromatic C), 125.7 (C, aromatic C), 127.9 (C, aromatic C), 131.1 (CH, aromatic CH), 133.1 (CH, aromatic CH), 133.2 (CH, aromatic CH), 136.9 (C, aromatic C), 143.0 (CH, aromatic CH), 147.0 (C, aromatic C), 169.1 (C, C=O), 169.2 (C, C=O). m/z (ES+) 373.1 $[M+H]^+$ (100%); HRMS (ES+): Exact mass calculated for $C_{21}H_{17}N_4O_3$ 373.1302. Found 373.1301.

7.2.7.3 Route towards bis(7-azaindol-3-yl)maleimide precursors

Potassium 2-(1-methyl-1*H*-pyrrolo[2,3-*b*]pyridin-3-yl)-2-oxoacetate (359)

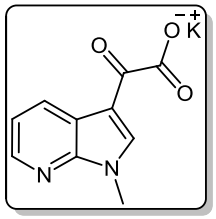

A solution of 2-(1-methyl-1*H*-pyrrolo[2,3-*b*]pyridin-3-yl)-2-oxoacetic acid **278** (1.003 g, 4.9 mmol) in ethanol (15 mL) was treated with potassium hydroxide (0.324 g, 4.9 mmol). The subsequent mixture was left to stir at room temperature for 4 hours before the solvent was removed under reduced pressure. The residue was desiccated at 50 ^{o}C overnight to yield potassium oxoacetate **359** as a white solid (1.193 g, 100%): m.p. 294-296 ^{o}C (decomp.); ν_{max}/cm^{-1} (KBr) 3411, 3177, 1647, 1606, 1526, 1456, 1412, 1342; δ_H (300 MHz, DMSO-d_6) 3.86 [3H, s, NCH_3], 7.24 [1H, dd, *J* 7.8, 4.7, C-H_5], 8.32-8.34 [2H, m, C-$H_{2,6}$], 8.46 [1H, dd, *J* 7.8, 1.4, C-H_4]; δ_C (75 MHz, DMSO-d_6) 31.2 (CH_3, NCH_3), 111.5 (C, aromatic C), 117.7 (CH, aromatic CH), 118.4 (C, aromatic C), 129.5 (CH, aromatic CH), 138.7 (CH, aromatic CH), 143.4 (CH, aromatic CH), 147.8 (C, aromatic C), 169.1 (C, C=O), 192.8 (C, C=O); m/z (ES+) 205.4 $[M+H_2-K]^+$ (100%).

3,4-Bis(1-methyl-1*H*-pyrrolo[2,3-*b*]pyridin-3-yl)furan-2,5-dione (358)

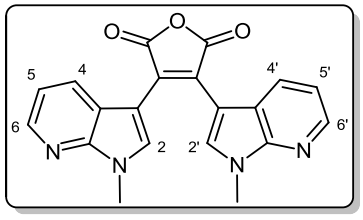

A mixture of 2-(1-methyl-1*H*-pyrrolo[2,3-*b*]pyridin-3-yl)acetic acid **279** (0.603 g, 3.2 mmol), potassium 2-(1-methyl-1*H*-pyrrolo[2,3-*b*]pyridin-3-yl)-2-oxoacetate **359** (0.764 g, 3.2 mmol) and acetic anhydride (30 mL) was heated to 130 ^{o}C for 4 hours. After being cooled to room temperature, the solvent was evaporated under reduced pressure. The ensuing residue was dissolved in ethyl acetate (80 mL) before being washed with saturated aqueous sodium bicarbonate (2 x 50 mL), water (50 mL) and brine (50 mL). The organic phase was then dried over magnesium sulfate and evaporated under reduced pressure, yielding a deep red residue. This residue was subjected to flash column chromatography (hexane/ethyl acetate, 40:60) to yield maleic anhydride **358** as a dark red solid (0.503 g, 45%): m.p. 237-238 ^{o}C; ν_{max}/cm^{-1} (KBr) 2921, 1816, 1745, 1527, 1461, 1256, 1113; δ_H (300 MHz, $CDCl_3$) 3.90 [6H, s, 2 x NCH_3], 6.68 [2H, dd, *J* 8.0, 4.7, C-

$H_{5,5'}$], 7.10 [2H, dd, *J* 8.0, 1.5, C-$H_{4,4'}$], 7.87 [2H, s, C-$H_{2,2'}$], 8.20 [2H, dd, *J* 4.7, 1.5, C-$H_{6,6'}$]; δ_C (75 MHz, $CDCl_3$) 31.9 ($2CH_3$, 2 x NCH_3), 103.1 (2C, 2 x aromatic C), 116.7 (2CH, 2 x aromatic CH), 118.1 (2C, 2 x aromatic C), 127.4 (2C, 2 x aromatic C), 130.3 (2CH, 2 x aromatic CH), 133.9 (2CH, 2 x aromatic CH), 144.2 (2CH, 2 x aromatic CH), 147.9 (2C, 2 x aromatic C), 166.3 (2C, 2 x C=O); m/z (ES+) 359.3 $[M+H]^+$ (100%); HRMS (ES+): Exact mass calculated for $C_{20}H_{15}N_4O_3$ 359.1144. Found 359.1141.

3,4-Bis(1-methyl-1*H*-pyrrolo[2,3-*b*]pyridin-3-yl)-1*H*-pyrrole-2,5-dione (361)[12]

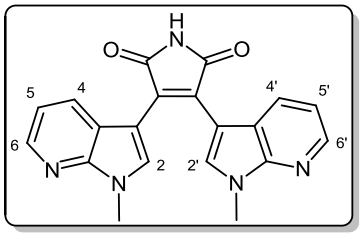

To a stirred solution of 3,4-bis(1-methyl-1*H*-pyrrolo[2,3-*b*]pyridin-3-yl)furan-2,5-dione **358** (0.403 g, 1.12 mmol) in DMF (5 mL) was added 1,1,1,3,3,3-hexamethyldisilazane (2.36 mL, 11.2 mmol), followed by methanol (0.23 mL, 5.6 mmol). The reaction mixture was then stirred at room temperature for 24 hours. Water (50 mL) was added to the reaction mixture, which was subsequently extracted with ethyl acetate (3 x 30 mL). The combined organic extracts were washed with water (4 x 100 mL) and brine (100 mL), and then dried over magnesium sulfate. The solvent was removed under reduced pressure and the crude residue was subjected to flash column chromatography (hexane/ethyl acetate, 20:80), yielding pure maleimide **361** as an orange-red solid (0.368 g, 92%): m.p. 260-262 ^oC (decomp.); ν_{max}/cm^{-1} (KBr) 2929, 2728, 1716, 1530, 1465, 1336, 1301; δ_H (300 MHz, DMSO-d_6) 3.86 [6H, s, 2 x NCH_3], 6.74 [2H, dd, *J* 8.0, 4.7, C-$H_{5,5'}$], 7.06 [2H, dd, *J* 8.0, 1.5, C-$H_{4,4'}$], 8.00 [2H, s, C-$H_{2,2'}$], 8.15 [2H, dd, *J* 4.6, 1.5, C-$H_{6,6'}$], 11.03 [1H, bs, NH]; δ_C (75 MHz, DMSO-d_6) 31.2 ($2CH_3$, 2 x NCH_3), 102.8 (2C, 2 x aromatic C), 115.9 (2CH, 2 x aromatic CH), 117.8 (2C, 2 x aromatic C), 126.9 (2C, 2 x aromatic C), 129.1 (2CH, 2 x aromatic CH), 133.2 (2CH, 2 x aromatic CH), 143.1 (2CH, 2 x aromatic CH), 147.3 (2C, 2 x aromatic C), 172.5 (2C, 2 x C=O); m/z (ES+) 358.4 $[M+H]^+$ (100%); HRMS (ES+): Exact mass calculated for $C_{20}H_{16}N_5O_2$ 358.1304. Found 358.1290.

1-Hydroxy-3,4-bis(1-methyl-1*H*-pyrrolo[2,3-*b*]pyridin-3-yl)-1*H*-pyrrole-2,5-dione (360)

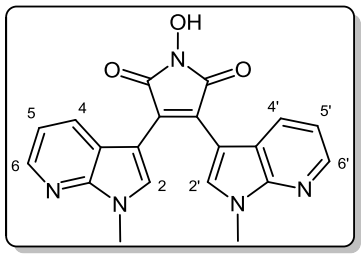

To a solution of 3,4-bis(1-methyl-1*H*-pyrrolo[2,3-*b*]pyridin-3-yl)furan-2,5-dione **358** (0.201g, 0.56 mmol) in dry pyridine (5 mL) was added hydroxylammonium chloride (0.392 g, 5.6 mmol). The resulting mixture was heated to reflux for 16 hours before being cooled to room temperature. The solvent was removed under reduced pressure and the residue was dissolved in ethyl acetate (50 mL), before being washed with water (3 x 50 mL) and brine (50 mL), then dried over magnesium sulfate. The solvent was again removed under reduced pressure and the crude residue was subjected to flash column chromatography (hexane/ethyl acetate, 30:70), yielding pure hydroxymaleimide **360** as a red solid (0.124 g, 59%): m.p. 235-237 ^{o}C; ν_{max}/cm^{-1} (KBr) 3378, 2924, 2853, 1716, 1594, 1532, 1466, 1109; δ_H (300 MHz, DMSO-d_6) 3.95 [6H, s, 2 x NCH_3], 6.83 [2H, dd, *J* 8.0, 4.6, C-$H_{5,5'}$], 7.13 [2H, dd, *J* 8.0, 1.6, C-$H_{4,4'}$], 8.12 [2H, s, C-$H_{2,2'}$], 8.24 [2H, dd, *J* 4.6, 1.5, C-$H_{6,6'}$], 10.57 [1H, bs, OH]; δ_C (75 MHz, DMSO-d_6) 31.3 ($2CH_3$, 2 x NCH_3), 102.7 (2C, 2 x aromatic C), 116.0 (2CH, 2 x aromatic CH), 117.7 (2C, 2 x aromatic C), 123.7 (2C, 2 x aromatic C), 129.2 (2CH, 2 x aromatic CH), 133.4 (2CH, 2 x aromatic CH), 143.2 (2CH, 2 x aromatic CH), 147.3 (2C, 2 x aromatic C), 167.9 (2C, 2 x C=O); m/z (ES+) 374.3 $[M+H]^+$ (100%); HRMS (ES+): Exact mass calculated for $C_{20}H_{16}N_5O_3$ 374.1253. Found 374.1254.

7.2.7.4 Synthesis and derivatisation of monoaza ICZs

12,13-Dimethyl-12,13-dihydro-5*H*-pyrido[3',2':4,5]pyrrolo[2,3-*a*]pyrrolo[3,4-*c*]carbazole-5,7(6*H*)-dione (364)

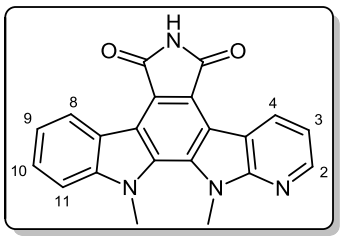

A spatula tip of iodine was added to a stirred solution of 3-(1-methyl-1*H*-indol-3-yl)-4-(1-methyl-1*H*-pyrrolo[2,3-*b*]pyridin-3-yl)-1*H*-pyrrole-2,5-dione **357** (0.100 g, 0.28 mmol) in acetonitrile (300 mL). The resulting mixture was then irradiated using a medium pressure mercury lamp, in the presence of air, for 15 hours, at which point TLC analysis confirmed complete consumption of starting material. A solution of saturated aqueous sodium thiosulfate (100 mL) was subsequently added to the reaction mixture, resulting in the formation of a yellow precipitate. The biphasic mixture was stirred for 20 minutes at room temperature before the precipitate was filtered off, washed with water and desiccated overnight at 50 ^{o}C to yield pure aza ICZ **364** as a yellow solid (0.081 g, 81%): m.p. >300 ^{o}C; ν_{max}/cm^{-1} (KBr) 3436, 1718, 1571, 1470, 1322, 750; δ_H (300 MHz, DMSO-d_6) 4.25 [3H, s, NCH$_3$], 4.31 [3H, s, NCH$_3$], 7.29-7.36 [2H, m, C-H$_{3,9}$], 7.60 [1H, t, *J* 7.5, C-H$_{10}$], 7.74 [1H, d, *J* 8.2, C-H$_{11}$], 8.60 [1H, dd, *J* 4.8, 1.7, C-H$_2$], 9.00 [1H, d, *J* 7.8, C-H$_8$], 9.17 [1H, dd, *J* 7.8, 1.6, C-H$_4$], 11.05 [1H, bs, NH]; δ_C (150 MHz, DMSO-d_6, 47 ^{o}C) 34.9 (CH$_3$, NCH$_3$), 36.9 (CH$_3$, NCH$_3$), 110.7 (CH, aromatic CH), 114.0 (C, aromatic C), 115.2 (C, aromatic C), 116.9 (CH, aromatic CH), 118.6 (C, aromatic C), 120.3 (C, aromatic C), 120.3 (C, aromatic C), 120.7 (CH, aromatic CH), 121.1 (C, aromatic C), 124.4 (CH, aromatic CH), 127.5 (CH, aromatic CH), 130.6 (C, aromatic C), 131.7 (C, aromatic C), 132.5 (CH, aromatic CH), 143.7 (C, aromatic C), 147.4 (CH, aromatic CH), 153.2 (C, aromatic C), 170.5 (C, C=O), 170.5 (C, C=O). m/z (ES+) 355.3 [M+H]$^+$ (100%); HRMS (ES+): Exact mass calculated for $C_{21}H_{15}N_4O_2$ 355.1195. Found 355.1185.

tert-Butyl 12,13-dimethyl-5,7-dioxo-12,13-dihydro-5*H*-pyrido[3',2':4,5]pyrrolo[2,3-*a*]pyrrolo[3,4-*c*]carbazole-6(7*H*)-carboxylate (368)

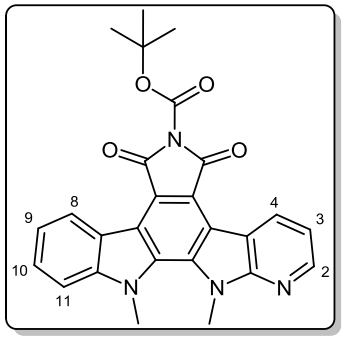

To a suspension of 12,13-dimethyl-12,13-dihydro-5*H*-pyrido[3',2':4,5]pyrrolo[2,3-*a*]pyrrolo[3,4-*c*]carbazole-5,7(6*H*)-dione **364** (0.080 g, 0.23 mmol) in acetonitrile (30 mL) was added di-*tert*-butyl dicarbonate (0.110 g, 0.51 mmol), followed by DMAP (0.003 g, 0.02 mmol, 10 mol.%). The resulting mixture was stirred at room temperature for 1 hour, before the solvent and excess anhydride was evaporated under reduced pressure. The crude product was initially washed with an aliquot of water (100 mL) containing 0.5 mL of 2M aqueous HCl, before further copious water washes. Following overnight desiccation at 50 ^{o}C, pure Boc-protected aza ICZ **368** was afforded as a bright yellow solid (0.101 g, 97%): m.p. >300 ^{o}C (decomp.); ν_{max}/cm^{-1} (KBr) 2982, 1791, 1748, 1568, 1477, 1294; δ_H (400 MHz, $CDCl_3$) 1.73 [9H, s, $C(CH_3)_3$], 4.30 [3H, s, NCH_3], 4.41 [3H, s, NCH_3], 7.36 [1H, dd, *J* 7.9, 4.8, C-H_3], 7.38 [1H, t, *J* 7.5, C-H_9], 7.55 [1H, d, *J* 8.2, C-H_{11}], 7.64 [1H, t, *J* 7.6, C-H_{10}], 8.66 [1H, dd, *J* 4.8, 1.6, C-H_2], 9.23 [1H, d, *J* 8.0, C-H_8], 9.46 [1H, dd, *J* 7.9, 1.6, C-H_4]; δ_C (125 MHz, $CDCl_3$) 28.1 ($3CH_3$, $C(\underline{C}H_3)_3$), 35.4 (CH_3, NCH_3), 37.3 (CH_3, NCH_3), 84.7 (C, $\underline{C}(CH_3)_3$), 110.0 (CH, aromatic CH), 115.2 (C, aromatic C), 116.8 (C, aromatic C), 117.5 (CH, aromatic CH), 119.3 (C, aromatic C), 119.4 (C, aromatic C), 120.3 (C, aromatic C), 121.7 (CH, aromatic CH), 122.1 (C, aromatic C), 125.8 (CH, aromatic CH), 128.1 (CH, aromatic CH), 131.8 (C, aromatic C), 133.1 (C, aromatic C), 133.9 (CH, aromatic CH), 144.6 (C, aromatic C), 147.4 (C, aromatic C), 147.8 (CH, aromatic CH), 154.4 (C, C=O), 165.3 (C, C=O), 165.6 (C, C=O); m/z (ES+) 455.3 $[M+H]^+$ (60%); HRMS (ES+): Exact mass calculated for $C_{26}H_{23}N_4O_4$ 455.1719. Found 455.1714.

6-Hydroxy-12,13-dimethyl-12,13-dihydro-5*H*-pyrido[3',2':4,5]pyrrolo[2,3-*a*]pyrrolo[3,4-*c*]carbazole-5,7(6*H*)-dione (363)

Method A:

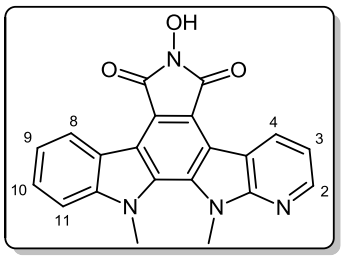

Hydroxylammonium chloride (0.061 g, 0.88 mmol) was added to a suspension of *tert*-butyl 12,13-dimethyl-5,7-dioxo-12,13-dihydro-5*H*-pyrido[3',2':4,5]pyrrolo[2,3-*a*]pyrrolo[3,4-*c*]carbazole-6(7*H*)-carboxylate **368** (0.080 g, 0.18 mmol) in pyridine (25 mL). The resulting mixture was stirred at 80 ^{o}C for 10 hours, before cooling to room temperature. Water (120 mL) was added to the reaction mixture, causing the precipitation of an orange solid, which was subsequently filtered off and washed with copious amounts of water. Recrystallisation of the crude orange product from absolute ethanol gave pure hydroxymaleimide **363** as a bright yellow solid (0.063 g, 94%): m.p. >300 ^{o}C; ν_{max}/cm^{-1} (KBr) 2928, 2738, 1706, 1575, 1474, 1006; δ_H (300 MHz, DMSO-d_6) 4.28 [3H, s, NCH_3], 4.33 [3H, s, NCH_3], 7.27-7.35 [2H, m, C-$H_{3,9}$], 7.62 [1H, t, *J* 7.8, C-H_{10}], 7.77 [1H, d, *J* 8.4, C-H_{11}], 8.62 [1H, dd, *J* 4.6, 1.5, C-H_2], 8.98 [1H, d, *J* 7.8, C-H_8], 9.16 [1H, d, *J* 7.8, C-H_4], 10.91 [1H, bs, OH]; δ_C (150 MHz, DMSO-d_6, 47 ^{o}C) 34.9 (CH_3, NCH_3), 36.9 (CH_3, NCH_3), 110.8 (CH, aromatic CH), 113.9 (C, aromatic C), 115.4 (C, aromatic C), 116.0 (C, aromatic C), 116.0 (C, aromatic C), 116.9 (CH, aromatic CH), 118.8 (C, aromatic C), 120.8 (CH, aromatic CH), 120.9 (C, aromatic C), 124.3 (CH, aromatic CH), 127.7 (CH, aromatic CH), 130.6 (C, aromatic C), 131.7 (C, aromatic C), 132.4 (CH, aromatic CH), 143.8 (C, aromatic C), 147.6 (CH, aromatic CH), 153.3 (C, aromatic C), 165.8 (C, C=O), 165.9 (C, C=O). m/z (ES+) 371.1 $[M+H]^+$ (100%); HRMS (ES+): Exact mass calculated for $C_{21}H_{15}N_4O_3$ 371.1144. Found 371.1138.

Method B:

Sodium hydroxide (0.423 g, 10.6 mmol) was added to a suspension of 12,13-dimethyl-12,13-dihydro-5*H*-pyrido[3',2':4,5]pyrrolo[2,3-*a*]pyrrolo[3,4-*c*]carbazole-5,7(6*H*)-dione **364** (0.075 g, 0.21 mmol) in water (20 mL). The resulting mixture was heated to reflux for 8 hours, before being allowed cool to room temperature. The basic solution was acidified to pH 2 by treatment with 2 M aqueous HCl in a dropwise manner, resulting in the formation of a yellow

precipitate. Following filtration, water washes and desiccation overnight at 50 ^{o}C, anhydride **362** was isolated as a yellow solid (0.063 g, 84%), and used without further purification or full characterisation: m.p. >300 ^{o}C; ν_{max}/cm^{-1} (KBr) 2919, 1819, 1747, 1524, 1254, 1104; m/z (ES+) 356.2 $[M+H]^+$ (20%). Hydroxylammonium chloride (0.049 g, 0.70 mmol) was added to a stirred suspension of anhydride **362** (0.050 g, 0.14 mmol) in pyridine (20 mL). The resulting mixture was heated to reflux for 12 hours before being cooled to room temperature and diluted with water (100 mL). The resulting precipitate was filtered off and washed with copious amounts of water. Recrystallisation from absolute alcohol afforded hydroxymaleimide **363** as a yellow solid (0.046 g, 88%).

Method C:

To a stirred solution of 1-hydroxy-3-(1-methyl-1*H*-indol-3-yl)-4-(1-methyl-1*H*-pyrrolo[2,3-*b*]pyridin-3-yl)-1*H*-pyrrole-2,5-dione **356** (0.080 g, 0.21 mmol) in acetonitrile (150 mL) was added a spatula tip of iodine. The resulting mixture was subsequently irradiated using a medium pressure mercury lamp for 16 hours. Following cooling to room temperature and removal of the solvent under reduced pressure, spectroscopic analysis indicated that desired aza ICZ **363** had not formed, and the crude mixture comprised predominantly of starting material, hydroxymalemide **356**.

Method D:

A mixture of 1-hydroxy-3-(1-methyl-1*H*-indol-3-yl)-4-(1-methyl-1*H*-pyrrolo[2,3-*b*]pyridin-3-yl)-1*H*-pyrrole-2,5-dione **356** (0.025 g, 0.07 mmol) and palladium(II) trifluoroacetate (0.109 g, 0.33 mmol) in DMF (5 mL) was heated to 90 ^{o}C for 12 hours. The reaction mixture was cooled to room temperature, diluted with ethyl acetate (30 mL) and washed with 1M aqueous HCl (60 mL) before being filtered through celite. The solvent was evaporated under reduced pressure to leave a crude brown residue. Spectroscopic analysis indicated that aromatisation towards aza ICZ **363** had not been achieved, and only hydroxymaleimide starting material **356** was present.

7-Amino-13,14-dimethyl-13,14-dihydropyrido[3',2':4,5]pyrrolo[2,3-*a*]pyrimido[4,5-*c*]carbazole-6,8(5*H*,7*H*)-dione (369)

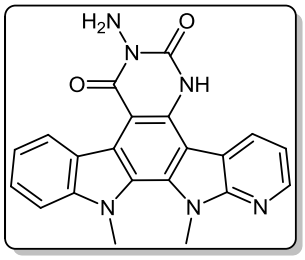

To a suspension of 6-hydroxy-12,13-dimethyl-12,13-dihydro-5*H*-pyrido[3',2':4,5]pyrrolo[2,3-*a*]pyrrolo[3,4-*c*]carbazole-5,7(6*H*)-dione **363** (0.050 g, 0.14 mmol) in a mixture of DMSO (8 mL) and pyridine (0.5 mL), DMAP (0.070 g, 0.57 mmol) was added. The resulting mixture was stirred for 15 minutes at room temperature, before *para*-toluenesulfonyl chloride (0.086 g, 0.45 mmol) was added. The yellow reaction mixture was then stirred at room temperature for 2 hours, until water (100 mL) was added. The yellow precipitate was filtered off, washed with water and desiccated overnight at 50 ^{o}C, at which point it was suspended in ethanol (30 mL). Under stirring, hydrazine hydrate (50% aqueous solution, 0.09 mL, 1.5 mmol) was added to the mixture, which was then heated to reflux for 14 hours. Once cooled to room temperature, the solvent was removed under reduced pressure. Spectroscopic analysis indicated the presence of not only pyrimidinone **369**, but also its regioisomer **370**. Separation of the two regioisomers was undertaken using preparative HPLC, however, sufficient purification was not achieved to allow for full characterisation of either aza ICZ.

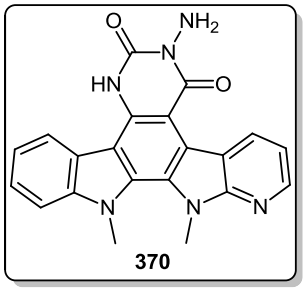

370

7.2.7.5 Synthesis and derivatisation of bisaza ICZs

12,13-Dimethyl-12,13-dihydro-5*H*-pyrido[2,3-*b*]pyrido[3',2':4,5]pyrrolo[3,2-*g*]pyrrolo[3,4-*e*]indole-5,7(6*H*)-dione (371)

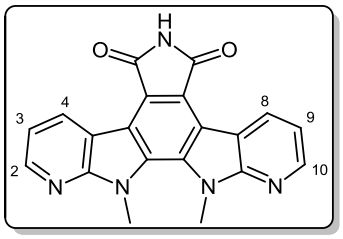

3,4-Bis(1-methyl-1*H*-pyrrolo[2,3-*b*]pyridin-3-yl)-1*H*-pyrrole-2,5-dione **361** (0.100 g, 0.28 mmol) was dissolved in acetonitrile (300 mL), with a spatula tip of iodine then added to the stirred solution. The resulting mixture was irradiated using a medium pressure mercury lamp for 16 hours, after which time it was

cooled to room temperature. A saturated aqueous sodium thiosulfate solution (100 mL) was added to the reaction mixture, leading to the precipitation of a yellow solid. After being stirred at room temperature for 20 minutes, the precipitate was filtered off, washed with water and desiccated at 50 ^{o}C overnight to yield pure aza ICZ **371** as a bright yellow solid (0.088 g, 88%): m.p. >300 ^{o}C; ν_{max}/cm^{-1} (KBr) 3143, 3033, 2755, 1721, 1572, 1469, 1287; δ_H (400 MHz, DMSO-d_6) 4.43 [6H, s, 2 x NCH$_3$], 7.41 [2H, dd, *J* 7.8, 4.7, C-H$_{3,9}$], 8.67 [2H, dd, *J* 4.7, 1.6, C-H$_{2,10}$], 9.25 [2H, dd, *J* 7.8, 1.6, C-H$_{4,8}$], 11.03 [1H, bs, NH]; δ_C (150 MHz, DMSO-d_6) 34.9 (2CH$_3$, 2 x NCH$_3$), 113.8 (2C, 2 x aromatic C), 115.7 (2C, 2 x aromatic C), 117.2 (2CH, 2 x aromatic CH), 120.9 (2C, 2 x aromatic C), 130.6 (2C, 2 x aromatic C), 133.0 (2CH, 2 x aromatic CH), 147.9 (2CH, 2 x aromatic CH), 152.8 (2C, 2 x aromatic C), 170.7 (2C, 2 x C=O); m/z (ES+) 356.2 [M+H]$^+$ (20%); HRMS (ES+): Exact mass calculated for $C_{20}H_{14}N_5O_2$ 356.1147. Found 356.1133.

tert-Butyl 12,13-dimethyl-5,7-dioxo-12,13-dihydro-5*H*-pyrido[2,3-*b*]pyrido[3',2':4,5]pyrrolo[3,2-*g*]pyrrolo[3,4-*e*]indole-6(7*H*)-carboxylate (372)

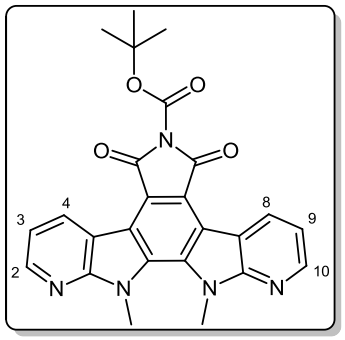

To a suspension of 12,13-dimethyl-12,13-dihydro-5*H*-pyrido[2,3-*b*]pyrido[3',2':4,5]pyrrolo[3,2-*g*]pyrrolo[3,4-*e*]indole-5,7(6*H*)-dione **371** (0.085 g, 0.24 mmol) in acetonitrile (50 mL) was added di-*tert*-butyl dicarbonate (0.115 g, 0.53 mmol) followed by DMAP (0.003 g, 0.02 mmol, 10 mol.%). The resulting mixture was stirred for 90 minutes at room temperature, before the solvent and excess anhydride was removed under reduced pressure. The crude product was then washed with an aliquot of water (100 mL) containing 0.5 mL of 2M aqueous HCl, followed by further copious washes with water. Desiccation at 50 ^{o}C overnight afforded Boc-protected maleimide **372** as a yellow solid (0.103 g, 94%): m.p. 290-292 ^{o}C (decomp.); ν_{max}/cm^{-1} (KBr) 2980, 1790, 1748, 1569, 1473, 1364, 1291; δ_H (400 MHz, CDCl$_3$) 1.73 [9H, s, C(CH$_3$)$_3$], 4.48 [6H, s, 2 x NCH$_3$], 7.36 [2H, dd, *J* 7.8, 4.8, C-H$_{3,9}$], 8.67 [2H, dd, *J* 4.8, 1.7, C-H$_{2,10}$], 9.44 [2H, dd, *J* 7.9, 1.7, C-H$_{4,8}$]; δ_C (125 MHz, CDCl$_3$) 28.1 (3CH$_3$, C(<u>C</u>H$_3$)$_3$), 35.4 (2CH$_3$, 2 x NCH$_3$), 85.0 (C, <u>C</u>(CH$_3$)$_3$), 114.7 (2C, 2

x aromatic C), 117.2 (2C, 2 x aromatic C), 117.7 (2CH, 2 x aromatic CH), 119.5 (2C, 2 x aromatic C), 131.5 (2C, 2 x aromatic C), 134.0 (2CH, 2 x aromatic CH), 147.2 (2C, 2 x aromatic C), 148.2 (2CH, 2 x aromatic CH), 153.8 (C, C=O), 165.4 (2C, 2 x C=O); m/z (ES+) 456.3 $[M+H]^+$ (100%); HRMS (ES+): Exact mass calculated for $C_{25}H_{22}N_5O_4$ 456.1688. Found 456.1682.

6-Hydroxy-12,13-dimethyl-12,13-dihydro-5*H*-pyrido[2,3-*b*]pyrido[3',2':4,5]pyrrolo[3,2-*g*]pyrrolo[3,4-*e*]indole-5,7(6*H*)-dione (373)

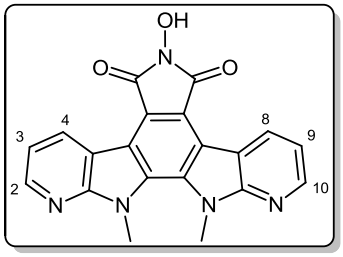

To a stirred suspension of *tert*-butyl 12,13-dimethyl-5,7-dioxo-12,13-dihydro-5*H*-pyrido[2,3-*b*]pyrido[3',2':4,5]pyrrolo[3,2-*g*]pyrrolo[3,4-*e*]indole-6(7*H*)-carboxylate **372** (0.090 g, 0.20 mmol) in pyridine (20 mL) was added hydroxylammonium chloride (0.069 g, 0.99 mmol). The resulting mixture was heated at 80 ^oC for 14 hours before being cooled to room temperature. Water (150 mL) was added to the reaction mixture, and the resulting precipitate was filtered and washed with copious amounts of water. The crude product was recrystallised from absolute alcohol, yielding pure hydroxymaleimide **373** as a yellow solid (0.068 g, 93%): m.p. >300 ^oC; ν_{max}/cm^{-1} (KBr) 3159, 2925, 1717, 1574, 1367, 1287; δ_H (400 MHz, DMSO-d_6) 4.40 [3H, s, NCH_3], 4.42 [3H, s, NCH_3], 7.37 [1H, q, *J* 7.8, 4.7, C-H_3], 7.38 [1H, dd, *J* 7.8, 4.8, C-H_9], 8.65 [1H, dd, *J* 4.7, 1.7, C-H_2], 8.66 [1H, dd, *J* 4.7, 1.6, C-H_{10}], 9.18 [1H, dd, C-H_4], 9.21 [1H, dd, C-H_8], 11.17 [1H, bs OH]; δ_C (150 MHz, DMSO-d_6, 47 ^oC) 34.6 ($2CH_3$, 2 x NCH_3), 113.5 (C, aromatic C), 113.7 (C, aromatic C), 115.7 (C, aromatic C), 115.9 (C, aromatic C), 116.4 (C, aromatic C), 117.1 (2CH, 2 x aromatic CH), 120.7 (C, aromatic C), 130.5 (2C, 2 x aromatic C), 132.6 (2CH, 2 x aromatic CH), 148.0 (2CH, 2 x aromatic CH), 152.8 (C, aromatic C), 152.9 (2C, 2 x aromatic C), 165.7 (2C, 2 x C=O); m/z (ES+) 372.1 $[M+H]^+$ (68%); HRMS (ES+): Exact mass calculated for $C_{20}H_{14}N_5O_3$ 372.1097. Found 372.1087.

7-Amino-13,14-dimethyl-13,14-dihydropyrido[3',2':4,5]pyrrolo[3,2-*f*]pyrido[3',2':4,5]pyrrolo[2,3-*h*]quinazoline-6,8(5*H*,7*H*)-dione (374)

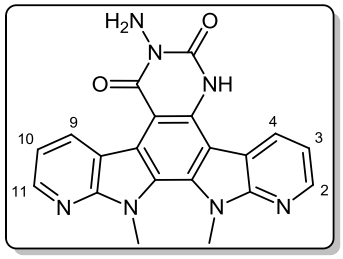

DMAP (0.034 g, 0.28 mmol) was added, at room temperature, to a mixture of 6-hydroxy-12,13-dimethyl-12,13-dihydro-5*H*-pyrido[2,3-*b*]pyrido[3',2':4,5]pyrrolo[3,2-*g*]pyrrolo[3,4-*e*]indole-5,7(6*H*)-dione **373** (0.025 g, 0.07 mmol) in DMSO (10 mL) and pyridine (2.5 mL). Following stirring for 15 minutes, *para*-toluenesulfonyl chloride (0.042 g, 0.22 mmol) was added, with the resulting mixture then stirred for 2 hours at room temperature. Water (80 mL) was added to the reaction mixture, and the resulting yellow precipitate was filtered, washed with water and desiccated overnight at 50 ^{o}C. This precipitate was suspended in ethanol (20 mL), and hydrazine hydrate (50% aqueous solution, 0.06 mL, 1 mmol) was added. The stirred reaction mixture was heated to reflux for 16 hours before being cooled to room temperature. The solvent was removed under reduced pressure, and the crude yellow precipitate was subjected to flash column chromatography (dichloromethane/methanol, 95:5), yielding desired product **374** as an off-white solid (0.013 g, 48%). Due to solubility issues with **374** it was not possible to obtain a fully characterised ^{13}C spectrum - this shall be a focus of future investigation: m.p. >300 ^{o}C; ν_{max}/cm^{-1} (KBr) 3309, 2924, 1722, 1659, 1579, 1448; δ_H (600 MHz, DMSO-d_6) 4.36 [3H, s, NCH_3], 4.40 [3H, s, NCH_3], 4.46 [2H, s, NH_2], 7.34 [1H, dd, *J* 7.8, 4.6, C-H_3], 7.46 [1H, dd, *J* 7.8, 4.7, C-H_{10}], 8.59 [1H, d, *J* 4.5, C-H_2], 8.63 [1H, d, *J* 4.6, C-H_{11}], 9.14 [1H, d, *J* 7.7, C-H_4], 9.93 [1H, d, *J* 7.6, C-H_9], 11.97 [1H, bs, N<u>H</u>CO]; m/z (ES+) 386.2 $[M+H]^+$ (40%); HRMS (ES+): Exact mass calculated for $C_{20}H_{16}N_7O_2$ 386.1365. Found 386.1355.

7.3 Protocol for biological evaluation

7.3.1 NCI-60 experimental methodology

The reported experimental methodology involves initial growth of the tumour cell lines in RPMI 1640 medium containing 5% foetal bovine serum and 2 mM L-glutamine.[13] For a typical screening experiment, cells are inoculated into 96 well microtiter plates in 100 µL of medium at plating densities ranging from 5,000 to 40,000 cells/well, depending on the doubling time of individual cell lines. After cell inoculation, the microtiter plates are incubated at 37 °C, 5% CO_2, 95% air and 100% relative humidity for 24 hours prior to addition of candidate compounds.

After 24 hours, two plates of each cell line are fixed *in situ* with trichloroacetic acid (TCA), to represent a measurement of the cell population for each cell line at the time of drug addition (Tz). Candidate compounds are dissolved in DMSO at 400-fold the desired final maximum test concentration and stored frozen prior to use. Initial single dose screening is carried out at a concentration of 10 µM, with the second phase of testing involving the examination of five different drug concentrations.

Following drug addition, the plates are incubated for an additional 48 hours at 37 °C, 5% CO_2, 95% air, and 100% relative humidity. For adherent cells, the assay is terminated by the addition of cold TCA. Cells are fixed *in situ* by the gentle addition of 50 µL of cold 50% (w/v) TCA and incubated for 60 minutes at 4 °C. Sulforhodamine B (SRB) solution (100 µL) at 0.4% (w/v) in 1% acetic acid is added to each well, and plates are incubated for 10 minutes at room temperature. Absorbance is read on an automated plate reader at a wavelength of 515 nm, and using seven absorbance measurements (time zero (Tz), control growth (C), and test growth in the presence of drug at the five concentration levels (Ti)), the percentage growth is calculated at each of the drug concentration levels. The response parameters GI_{50} (concentration required for 50% inhibition of growth) and LC_{50} (concentration required for 50% cell death) are extracted from concentration-response curves by linear interpolation, while TGI (total growth inhibition) is read as the x-axis intercept from the five different drug concentrations.[13]

7.3.2 COMPARE analysis

The use of the COMPARE algorithm towards the mechanistic investigation of cell growth inhibition consists of calculating the linear correlation coefficient between the data over the cell lines tested for a particular compound and all sets of data in the NCI database to be searched.[14] The calculation of the correlation coefficient involves three steps: (i) choosing the seed (the pattern of interest), (ii) choosing the parameters and (iii) choosing the database.

In running a COMPARE calculation via the Developmental Therapeutics Program (DTP) branch of the NCI website, a number of key parameters can be modified in order to allow for more efficient or user-relevant analyses. For example, the data set used as the seed for the calculation can comprise any of the growth inhibition measurements for a particular compound, such as the GI_{50}, TGI or LC_{50}. There are a number of different databases within the NCI that can be used to perform a COMPARE calculation, such as standard chemotherapeutic agents or synthetic compounds, and it is possible to return only corresponding data sets with a minimum correlation threshold against the seed. It is also possible to specify a minimum number of cell lines with which to run the calculation, rather than using the entire 60 cell panel.[14] For COMPARE calculations run in this project, either standard agents or synthetic compounds were chosen as the target set. Minimum correlation was set at 0.4, minimum count of common cell lines was set at 40, and minimum standard deviation was set at 0.05.

7.3.3 Topoisomerase I assay experimental methodology

The human topo I assay kit was purchased from Inspiralis, Norwich Bioincubator, Norwich Research Park, Colney, Norwich, UK. The kit contained: (i) dilution buffer (10 mM Tris.HCl (pH 7.5), 1 mM DTT, 1 mM EDTA, 100 mM NaCl, 50% (v/v) glycerol and 100 µg/mL albumin); (ii) 10x assay buffer (20 mM Tris.HCl (pH 7.5), 200 mM NaCl, 0.25 mM EDTA, 5% (v/v) glycerol, 50 µg/mL albumin); (iii) supercoiled pBR322 DNA in 0.01% Tris.HCl and 0.03% EDTA; (iv) topo I enzyme (human expressed in *baculovirus* supplied at a minimum

concentration of 10 U per 1 µL) in 0.6% (w/v) Tris.HCl (pH 7.9), 0.015% (w/v) DTT, 0.03% (w/v) EDTA, 50% (w/v) glycerol and 0.01% BSA.

Increasing concentrations of the various aza ICZs were assayed on a cleavage assay adapted from the Inspiralis technical data sheet supplied with the kit and the protocol of Marminon *et al*.[15] The activity each aza ICZ was compared to that of camptothecin **37** (20 µM and 50 µM), positive control (water) and DNA control (no topo I added).

A pBR322 stock containing sufficient material for the assay was prepared in the following ratio: 1 µg (1 µL) pBR322, 3 µL assay buffer and 17 µL deionised water. An aliquot of 21 µL of this stock was added to each eppendorf containing 3 µL of each concentration to be tested, along with the controls. This material was incubated for 30 minutes at 37 ^{o}C to insure binding equilibrium before the addition of topo I. An aliquot of 6 µL human topo I (minimum 6 U) was added to each eppendorf, bringing the final assay volume to 30 µL, and incubated for a further 30 minutes at 37 ^{o}C. The cleavage reactions were then stopped by the addition of SDS and proteinase K to a final concentration of 0.25% and 250 µg/mL, and incubated for 30 min at 50 ^{o}C. To assess topo I induced cleavage, 12 µL of loading buffer was added to each sample, and an aliquot of 20 µL of each sample was loaded onto a 1% agarose gel containing 20 µL Safe View stain (NBS Biologicals, Cambridgeshire, England) per 100 mL gel. The gel was run at 20 Volts for 4 hours at room temperature to separate the DNA. The gels were viewed under UV light using a DNR Bio-Imaging System and photographed using GelCapture software. To compare and quantify the intensity of the cleavage bands produced, the image was inverted and analysed using GelQuant software (v. 1.7.8).

7.3.4 Topoisomerase II assay experimental methodology

The decatenation assay kit was obtained from Inspiralis (Norwich, UK) and comprised of the following: (i) 10x assay buffer containing 50 mM Tris.HCl (pH 7.5), 125 mM NaCl, 10 mM $MgCl_2$, 5 mM DTT and 100 µg/mL albumin; (ii) dilution buffer containing 50 mM Tris.HCl (pH 7.5), 100 mM NaCl, 1 mM DTT, 0.5 mM EDTA, 50% (v/v) glycerol, 50 µg/ml albumin; (iii) ATP 30 mM; (iv) kDNA (100 ng/µL); (v) 10 U/µL human topo II in dilution buffer; (vi)

5x stop buffer containing 2.5% SDS, 15% Ficoll-400, 0.05% bromophenol blue, 0.05% xylene cyanol and 25 mM EDTA. Tris-acetate-EDTA buffer (supplied as 10x buffer) and agarose were obtained from Sigma Life Sciences (Dublin, Ireland).

The topo II decatenation assay protocol involved initial incubation of each inhibitor candidate (100 µM) along with a stock solution containing water, ATP, assay buffer, kDNA obtained from the mitochondrial DNA of *Crithidia fasciculate*, and topo II, at 37 ^{o}C for 1 hour. Following addition of stop buffer, agarose DNA gel electrophoresis was run at 50 V for 2 hours using a Consort EV243 power pack, to determine the relative amounts of decatenated DNA bands obtained in each compound lane. Positive (water), as well as negative controls (ellipticine) were incorporated in order to validate the results of each run. The resulting gels were viewed under UV light using a DNR Bio-Imaging System and photographed using GelCapture software.

7.4 References

1. Allegretti, M; Anacardio, R.; Candida Cesta, M.; Curti, R.; Mantovanini, M.; Nano, G.; Topai, A.; Zampella, G. *Org. Process Res. Dev.* **2003**, 7, 209-213
2. Cassidy, F.; Hughes, I.; Rahman, S.S.; Hunter, D.J. *International Patent*, **1996**, WO/9611929
3. Jiang, X.; Tiwari, A.; Thompson, M.; Chen, Z.; Cleary, T.P.; Lee, T.B.K. *Org. Process Res. Dev.* **2001**, 5, 604-608
4. Diana, P.; Carbone, A.; Barraja, P.; Montalbano, A.; Parrino, B.; Lopergolo, A.; Pennat, M.; Zaffaroni, N.; Cirrincione, G. *ChemBioChem* **2011**, 6, 1300-1309
5. Sober, D.J.; Chang, J.; Fairchild, E.H.; Fowble, J.W.; Mukhopadhyay, A.; Feller, D.R.; Miller, D.D. *J. Med. Chem.* **1981**, 24, 970-974
6. Bellemin, R.; Decerprit, J.; Festal, D. *Eur. J. Med. Chem.* **1996**, 31, 123-132
7. Robison, M.M.; Robison, B.L. *J. Am. Chem. Soc.* **1955**, 77, 457-460
8. Robison, M.M.; Robison, B.L. *J. Am. Chem. Soc.* **1956**, 78, 1247-1251
9. Bell, M.R. *United States Patent* **1967**, Patent no. 3354174
10. Jin, Y.; Zhou, Z.Y.; Tian, W.; Yu, Q.; Long, Y.Q. *Bioorg. Med. Chem. Lett.* **2006**, 16, 5864-5869
11. Roy, S.; Eastman, A.; Gribble, G.W. *Tetrahedron* **2006**, 62, 7838-7845
12. Bone, H.K.; Damiano, T.; Bartlett, S.; Perry, A.; Letchford, J.; Sanchez Ripoll, Y.; Nelson, A.S.; Welham, M.J. *Chem. & Biol.* **2009**, 16, 15-27
13. Alley, M.C.; Scudiero, D.A.; Monks, P.A.; Hursey, M.L.; Czerwinski, M.J.; Fine, D.L.; Abbott, B.J.; Mayo, J.G.; Shoemaker, R.H.; Boyd, M.R. *Cancer Res.* **1988**, 48, 589-601
14. Zaharevitz, D.W.; Holbeck, S.L.; Bowerman, C.; Svetlik, P.A. *J. Mol. Graph. Mod.* **2002**, 20, 297-303
15. Marminon, C.; Anizon, F.; Moreau, P.; Pfeiffer, B.; Pierré, A.; Golsteyn, R.M.; Peixoto, P.; Hildebrand, M.P.; David-Cordonnier, M.H.; Lozach, O.; Meijer, L.; Prudhomme, M. *Mol. Pharmacol.* **2008**, 74, 1620-1629

Appendices

4-(1-Methyl-1*H*-pyrrolo[2,3-*b*]pyridin-3-yl)-3-(3,4,5-trimethoxyphenyl)-1*H*-pyrazol-5-amine (293)

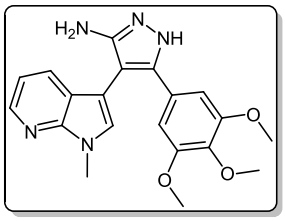

Developmental Therapeutics Program
One Dose Mean Graph

NSC: D-754616 / 1	Conc: 1.00E-5 Molar	Test Date: Oct 18, 2010
Experiment ID: 1010OS37		Report Date: Nov 17, 2010

Panel/Cell Line	Growth Percent
Leukemia	
CCRF-CEM	70.84
HL-60(TB)	46.76
K-562	67.26
MOLT-4	82.67
RPMI-8226	44.69
SR	74.03
Non-Small Cell Lung Cancer	
A549/ATCC	79.88
EKVX	90.35
HOP-62	69.39
HOP-92	30.91
NCI-H226	79.21
NCI-H23	87.36
NCI-H322M	85.16
NCI-H460	94.04
NCI-H522	50.25
Colon Cancer	
COLO 205	74.17
HCC-2998	88.03
HCT-116	69.84
HCT-15	82.16
HT29	63.59
KM12	89.97
SW-620	82.52
CNS Cancer	
SF-268	96.39
SF-295	84.44
SF-539	74.96
SNB-19	86.53
SNB-75	38.05
U251	85.67
Melanoma	
LOX IMVI	72.23
MALME-3M	72.35
M14	69.94
MDA-MB-435	66.78
SK-MEL-2	89.03
SK-MEL-28	80.78
SK-MEL-5	86.51
UACC-257	70.24
UACC-62	51.81
Ovarian Cancer	
IGROV1	84.14
OVCAR-3	93.60
OVCAR-4	74.83
OVCAR-5	85.12
OVCAR-8	83.32
NCI/ADR-RES	102.96
SK-OV-3	80.66
Renal Cancer	
786-0	67.41
A498	79.88
ACHN	80.68
CAKI-1	50.02
RXF 393	87.22
SN12C	86.58
TK-10	62.94
UO-31	51.67
Prostate Cancer	
PC-3	69.11
DU-145	107.66
Breast Cancer	
MCF7	48.88
MDA-MB-231/ATCC	68.92
HS 578T	72.89
BT-549	81.10
T-47D	77.86
MDA-MB-468	80.59
Mean	75.11
Delta	44.20
Range	76.75

Mean Growth Percent - Growth Percent

150 100 50 0 -50 -100 -150

[i]

8-(1-Methyl-1*H*-pyrrolo[2,3-*b*]pyridin-3-yl)-7-(3,4,5-trimethoxyphenyl)pyrazolo[1,5-*a*][1,3,5]triazine-2,4(1*H*,3*H*)-dione (295)

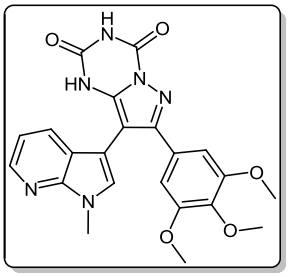

Developmental Therapeutics Program
One Dose Mean Graph

NSC: D-754617 / 1 | Conc: 1.00E-5 Molar | Test Date: Oct 18, 2010
Experiment ID: 1010OS37 | Report Date: Nov 17, 2010

Panel/Cell Line	Growth Percent
Leukemia	
CCRF-CEM	94.56
HL-60(TB)	111.20
K-562	100.36
MOLT-4	106.78
RPMI-8226	94.77
SR	103.83
Non-Small Cell Lung Cancer	
A549/ATCC	94.43
EKVX	115.52
HOP-62	102.35
HOP-92	53.52
NCI-H226	98.50
NCI-H23	101.80
NCI-H322M	103.06
NCI-H460	103.92
NCI-H522	89.48
Colon Cancer	
COLO 205	127.65
HCC-2998	110.09
HCT-116	114.56
HCT-15	106.92
HT29	97.10
KM12	107.96
SW-620	113.33
CNS Cancer	
SF-268	110.15
SF-295	121.78
SF-539	112.14
SNB-19	99.55
SNB-75	99.67
U251	104.97
Melanoma	
LOX IMVI	104.10
MALME-3M	115.54
M14	101.75
MDA-MB-435	104.69
SK-MEL-2	93.23
SK-MEL-28	106.24
SK-MEL-5	102.75
UACC-257	98.83
UACC-62	92.66
Ovarian Cancer	
IGROV1	109.44
OVCAR-3	115.84
OVCAR-4	107.08
OVCAR-5	119.04
OVCAR-8	102.95
NCI/ADR-RES	112.23
SK-OV-3	108.57
Renal Cancer	
786-0	101.56
A498	95.83
ACHN	100.00
CAKI-1	118.39
RXF 393	113.71
SN12C	90.43
TK-10	96.55
UO-31	94.81
Prostate Cancer	
PC-3	90.94
DU-145	122.63
Breast Cancer	
MCF7	99.66
MDA-MB-231/ATCC	110.52
HS 578T	118.55
BT-549	105.74
T-47D	103.14
MDA-MB-468	103.27
Mean	104.34
Delta	50.82
Range	74.13

Mean Growth Percent - Growth Percent

150 100 50 0 -50 -100 -150

5,7-Bis(trifluoromethyl)-3-(1-methyl-1*H*-pyrrolo[2,3-*b*]pyridin-3-yl)-2-(3,4,5-trimethoxyphenyl)pyrazolo[1,5-*a*]pyrimidine (297)

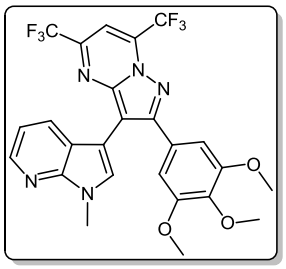

Developmental Therapeutics Program
One Dose Mean Graph

NSC: D-754618 / 1	Conc: 1.00E-5 Molar	Test Date: Oct 18, 2010
Experiment ID: 1010OS37		Report Date: Nov 17, 2010

Panel/Cell Line	Growth Percent
Leukemia	
CCRF-CEM	81.41
HL-60(TB)	110.55
K-562	81.55
MOLT-4	75.10
RPMI-8226	66.26
SR	88.21
Non-Small Cell Lung Cancer	
A549/ATCC	92.32
HOP-62	101.07
HOP-92	-3.08
NCI-H226	91.11
NCI-H23	98.41
NCI-H322M	96.73
NCI-H460	96.90
NCI-H522	89.53
Colon Cancer	
COLO 205	134.17
HCC-2998	117.21
HCT-116	95.16
HCT-15	104.04
HT29	107.00
KM12	105.50
SW-620	104.58
CNS Cancer	
SF-268	92.24
SF-539	100.61
SNB-19	93.28
SNB-75	67.20
U251	88.72
Melanoma	
LOX IMVI	97.68
MALME-3M	105.63
M14	106.84
SK-MEL-2	90.81
SK-MEL-28	105.72
SK-MEL-5	93.00
UACC-257	97.77
UACC-62	91.18
Ovarian Cancer	
IGROV1	97.24
OVCAR-3	113.52
OVCAR-4	84.07
OVCAR-5	108.93
OVCAR-8	90.67
NCI/ADR-RES	91.30
SK-OV-3	103.02
Renal Cancer	
786-0	99.04
A498	85.68
ACHN	95.57
RXF 393	102.48
SN12C	83.96
TK-10	107.21
UO-31	73.66
Prostate Cancer	
PC-3	78.70
DU-145	106.57
Breast Cancer	
MCF7	78.03
MDA-MB-231/ATCC	87.74
HS 578T	111.58
BT-549	100.53
T-47D	81.20
MDA-MB-468	117.78
Mean	93.98
Delta	97.06
Range	137.25

Mean Growth Percent - Growth Percent

150 100 50 0 -50 -100 -150

1-[5-Amino-4-(1-methyl-1*H*-pyrrolo[2,3-*b*]pyridin-3-yl)-3-(3,4,5-trimethoxyphenyl)-1*H*-pyrazol-1-yl]ethanone (302)

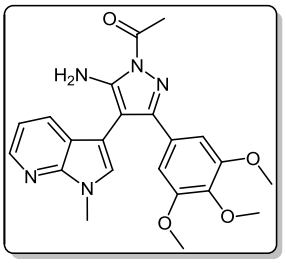

Developmental Therapeutics Program
One Dose Mean Graph

NSC: D-763899 / 1	Conc: 1.00E-5 Molar	Test Date: Feb 27, 2012
Experiment ID: 1202OS23		Report Date: Apr 02, 2012

Panel/Cell Line	Growth Percent
Leukemia	
CCRF-CEM	102.06
HL-60(TB)	99.61
K-562	114.39
MOLT-4	103.28
RPMI-8226	92.11
SR	87.19
Non-Small Cell Lung Cancer	
A549/ATCC	104.85
EKVX	100.63
HOP-62	107.04
HOP-92	86.44
NCI-H23	99.47
NCI-H322M	113.75
NCI-H460	100.58
NCI-H522	90.70
Colon Cancer	
COLO 205	103.69
HCC-2998	110.09
HCT-116	104.81
HCT-15	113.71
HT29	103.78
KM12	112.91
SW-620	111.16
CNS Cancer	
SF-268	118.67
SF-295	105.78
SF-539	103.02
SNB-19	109.22
SNB-75	101.88
U251	104.91
Melanoma	
LOX IMVI	93.66
MALME-3M	124.54
M14	110.57
MDA-MB-435	105.57
SK-MEL-2	117.55
SK-MEL-28	104.21
UACC-257	109.82
UACC-62	108.10
Ovarian Cancer	
IGROV1	118.22
OVCAR-3	114.24
OVCAR-4	110.53
OVCAR-5	100.29
OVCAR-8	98.67
NCI/ADR-RES	101.45
SK-OV-3	114.70
Renal Cancer	
786-0	98.35
A498	81.16
ACHN	97.21
CAKI-1	80.96
RXF 393	109.58
SN12C	103.65
TK-10	117.45
UO-31	92.77
Prostate Cancer	
PC-3	96.10
DU-145	128.54
Breast Cancer	
MCF7	92.60
MDA-MB-231/ATCC	101.35
HS 578T	93.69
BT-549	92.06
T-47D	110.27
MDA-MB-468	111.66
Mean	104.23
Delta	23.27
Range	47.58

Mean Growth Percent - Growth Percent

150 100 50 0 -50 -100 -150

5-Amino-*N*-methyl-4-(1-methyl-1*H*-pyrrolo[2,3-*b*]pyridin-3-yl)-3-(3,4,5-trimethoxyphenyl)-1*H*-pyrazole-1-carbothioamide (304)

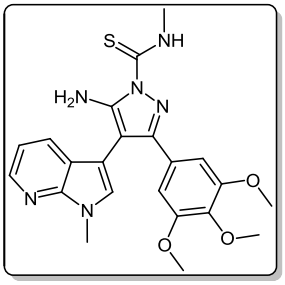

Developmental Therapeutics Program
One Dose Mean Graph

NSC: D-763898 / 1	Conc: 1.00E-5 Molar	Test Date: Feb 27, 2012
Experiment ID: 1202OS23		Report Date: Apr 02, 2012

Panel/Cell Line	Growth Percent
Leukemia	
CCRF-CEM	66.47
HL-60(TB)	62.92
K-562	75.51
MOLT-4	89.75
RPMI-8226	44.88
SR	51.13
Non-Small Cell Lung Cancer	
A549/ATCC	75.48
EKVX	71.31
HOP-62	55.81
NCI-H226	62.14
NCI-H23	66.45
NCI-H322M	67.78
NCI-H460	77.57
NCI-H522	42.17
Colon Cancer	
COLO 205	51.78
HCC-2998	97.31
HCT-116	68.43
HCT-15	54.43
HT29	52.66
KM12	81.79
SW-620	83.16
CNS Cancer	
SF-268	95.69
SF-295	54.47
SF-539	80.79
SNB-19	71.01
SNB-75	39.71
U251	79.27
Melanoma	
LOX IMVI	55.30
MALME-3M	73.71
M14	66.42
MDA-MB-435	61.68
SK-MEL-2	86.08
SK-MEL-28	75.36
UACC-257	72.81
UACC-62	37.56
Ovarian Cancer	
IGROV1	69.58
OVCAR-3	88.01
OVCAR-4	69.13
OVCAR-5	82.54
OVCAR-8	71.14
NCI/ADR-RES	63.83
SK-OV-3	69.71
Renal Cancer	
786-0	69.39
A498	57.93
ACHN	79.80
CAKI-1	18.20
RXF 393	107.78
SN12C	80.71
TK-10	52.43
UO-31	25.34
Prostate Cancer	
PC-3	68.76
DU-145	97.80
Breast Cancer	
MCF7	37.99
MDA-MB-231/ATCC	60.24
HS 578T	48.99
BT-549	69.01
T-47D	62.73
MDA-MB-468	56.95
Mean	66.50
Delta	48.30
Range	89.58

Mean Growth Percent - Growth Percent

150 100 50 0 -50 -100 -150

5-(1-Methyl-1*H*-pyrrolo[2,3-*b*]pyridin-3-yl)-4-(3,4,5-trimethoxyphenyl)-1*H*-pyrazol-3-amine (312)

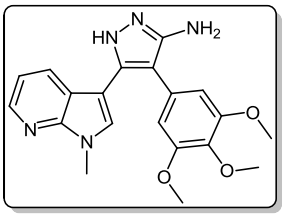

Developmental Therapeutics Program
One Dose Mean Graph

NSC: D-763892 / 1	Conc: 1.00E-5 Molar	Test Date: Feb 27, 2012
Experiment ID: 1202OS23		Report Date: Apr 02, 2012

Panel/Cell Line	Growth Percent
Leukemia	
CCRF-CEM	74.89
HL-60(TB)	76.66
K-562	78.54
MOLT-4	90.19
RPMI-8226	69.95
SR	60.73
Non-Small Cell Lung Cancer	
A549/ATCC	79.49
EKVX	92.27
HOP-62	66.50
HOP-92	47.90
NCI-H23	85.75
NCI-H322M	92.36
NCI-H460	88.70
NCI-H522	56.85
Colon Cancer	
COLO 205	70.18
HCT-116	90.24
HCT-15	94.84
HT29	68.31
KM12	88.29
SW-620	86.56
CNS Cancer	
SF-268	104.05
SF-295	78.37
SF-539	87.26
SNB-19	87.26
SNB-75	34.43
U251	80.44
Melanoma	
LOX IMVI	84.45
MALME-3M	80.57
M14	89.71
MDA-MB-435	74.30
SK-MEL-2	89.87
SK-MEL-28	82.79
UACC-257	77.88
UACC-62	52.99
Ovarian Cancer	
IGROV1	112.92
OVCAR-3	102.22
OVCAR-4	76.38
OVCAR-5	89.37
OVCAR-8	81.80
NCI/ADR-RES	100.68
SK-OV-3	79.07
Renal Cancer	
786-0	91.80
A498	64.75
ACHN	95.64
CAKI-1	48.94
RXF 393	104.09
SN12C	80.12
TK-10	76.57
UO-31	49.60
Prostate Cancer	
PC-3	81.93
DU-145	110.19
Breast Cancer	
MCF7	63.01
MDA-MB-231/ATCC	77.02
HS 578T	61.50
BT-549	97.29
T-47D	70.53
MDA-MB-468	70.69
Mean	79.82
Delta	45.39
Range	78.49

Mean Growth Percent - Growth Percent

150 100 50 0 -50 -100 -150

7-(1-Methyl-1*H*-pyrrolo[2,3-*b*]pyridin-3-yl)-8-(3,4,5-trimethoxyphenyl)pyrazolo[1,5-*a*][1,3,5]triazine-2,4(1*H*,3*H*)-dione (313)

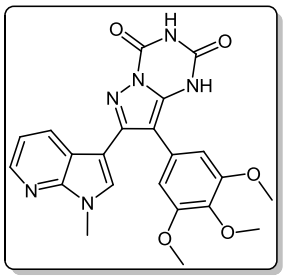

Developmental Therapeutics Program
One Dose Mean Graph

NSC: D-763893 / 1	Conc: 1.00E-5 Molar	Test Date: Feb 27, 2012
Experiment ID: 1202OS23		Report Date: Apr 02, 2012

Panel/Cell Line	Growth Percent
Leukemia	
CCRF-CEM	90.21
HL-60(TB)	97.77
K-562	106.96
MOLT-4	94.52
RPMI-8226	88.39
SR	82.16
Non-Small Cell Lung Cancer	
A549/ATCC	99.23
EKVX	109.20
HOP-62	108.54
HOP-92	87.70
NCI-H23	95.25
NCI-H322M	115.45
NCI-H460	104.31
NCI-H522	82.43
Colon Cancer	
COLO 205	104.73
HCC-2998	99.87
HCT-116	111.99
HCT-15	108.21
HT29	102.08
KM12	108.33
SW-620	106.74
CNS Cancer	
SF-268	114.78
SF-295	89.91
SF-539	103.04
SNB-19	96.97
SNB-75	67.20
U251	102.77
Melanoma	
LOX IMVI	99.06
MALME-3M	117.81
M14	112.19
MDA-MB-435	100.76
SK-MEL-2	105.39
SK-MEL-28	93.43
UACC-257	101.09
UACC-62	92.46
Ovarian Cancer	
IGROV1	134.61
OVCAR-3	119.99
OVCAR-4	94.98
OVCAR-5	111.62
OVCAR-8	101.50
NCI/ADR-RES	106.22
SK-OV-3	105.70
Renal Cancer	
786-0	114.85
A498	79.85
ACHN	113.77
CAKI-1	89.78
RXF 393	109.73
SN12C	101.70
TK-10	101.92
UO-31	94.15
Prostate Cancer	
PC-3	96.21
DU-145	114.91
Breast Cancer	
MCF7	87.21
MDA-MB-231/ATCC	98.24
HS 578T	89.90
BT-549	118.67
T-47D	101.55
MDA-MB-468	98.09
Mean	101.48
Delta	34.28
Range	67.41

Mean Growth Percent - Growth Percent

150 100 50 0 -50 -100 -150

2-(1-Methyl-1*H*-pyrrolo[2,3-*b*]pyridin-3-yl)-5,7-bis(trifluoromethyl)-3-(3,4,5-trimethoxyphenyl)pyrazolo[1,5-*a*]pyrimidine (314)

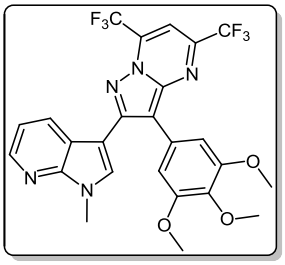

Developmental Therapeutics Program
One Dose Mean Graph

NSC: D-763894 / 1	Conc: 1.00E-5 Molar	Test Date: Feb 27, 2012
Experiment ID: 1202OS23		Report Date: Apr 02, 2012

Panel/Cell Line	Growth Percent
Leukemia	
CCRF-CEM	89.32
HL-60(TB)	103.42
K-562	103.13
MOLT-4	93.25
RPMI-8226	70.57
SR	85.31
Non-Small Cell Lung Cancer	
A549/ATCC	91.78
EKVX	75.49
HOP-62	98.88
NCI-H23	90.32
NCI-H322M	102.84
NCI-H460	102.45
NCI-H522	83.64
Colon Cancer	
COLO 205	99.17
HCC-2998	101.04
HCT-116	95.01
HCT-15	100.95
HT29	104.54
KM12	103.08
SW-620	99.39
CNS Cancer	
SF-268	104.30
SF-295	104.02
SF-539	105.20
SNB-19	94.81
SNB-75	73.15
U251	98.11
Melanoma	
LOX IMVI	83.00
MALME-3M	117.38
M14	109.96
MDA-MB-435	100.94
SK-MEL-2	88.13
SK-MEL-28	99.49
UACC-257	94.53
UACC-62	90.94
Ovarian Cancer	
IGROV1	101.10
OVCAR-3	115.86
OVCAR-4	76.03
OVCAR-5	121.15
OVCAR-8	91.85
NCI/ADR-RES	86.71
SK-OV-3	104.16
Renal Cancer	
786-0	115.54
A498	74.49
ACHN	95.55
CAKI-1	82.28
RXF 393	95.74
SN12C	88.16
TK-10	117.49
UO-31	71.23
Prostate Cancer	
PC-3	81.22
DU-145	111.62
Breast Cancer	
MCF7	91.67
MDA-MB-231/ATCC	73.09
HS 578T	84.95
BT-549	117.21
T-47D	90.63
MDA-MB-468	92.09
Mean	95.39
Delta	24.82
Range	50.58

Mean Growth Percent - Growth Percent

150 100 50 0 -50 -100 -150

1-(5-Amino-3-(1-methyl-1*H*-pyrrolo[2,3-*b*]pyridin-3-yl)-4-(3,4,5-trimethoxyphenyl)-1*H*-pyrazol-1-yl)ethanone (316)

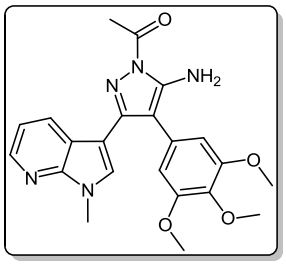

Developmental Therapeutics Program
One Dose Mean Graph

NSC: D-763896 / 1	Conc: 1.00E-5 Molar	Test Date: Feb 27, 2012
Experiment ID: 1202OS23		Report Date: Apr 02, 2012

Panel/Cell Line	Growth Percent
Leukemia	
CCRF-CEM	75.31
HL-60(TB)	80.46
K-562	90.81
MOLT-4	92.82
RPMI-8226	73.44
SR	57.82
Non-Small Cell Lung Cancer	
A549/ATCC	80.11
EKVX	84.85
HOP-62	63.11
NCI-H23	77.77
NCI-H322M	76.92
NCI-H460	93.03
NCI-H522	63.35
Colon Cancer	
COLO 205	76.45
HCT-116	94.89
HCT-15	92.13
HT29	67.88
KM12	87.84
SW-620	87.18
CNS Cancer	
SF-268	95.94
SF-295	75.30
SF-539	79.27
SNB-19	74.92
SNB-75	8.48
U251	88.38
Melanoma	
LOX IMVI	77.28
MALME-3M	66.23
M14	86.81
MDA-MB-435	73.31
SK-MEL-2	98.75
SK-MEL-28	79.86
UACC-257	80.76
UACC-62	55.43
Ovarian Cancer	
IGROV1	92.81
OVCAR-3	101.31
OVCAR-4	58.36
OVCAR-5	90.13
OVCAR-8	83.87
NCI/ADR-RES	88.65
SK-OV-3	79.33
Renal Cancer	
786-0	86.35
A498	54.72
ACHN	80.54
CAKI-1	39.74
RXF 393	98.72
SN12C	74.57
TK-10	82.02
UO-31	33.10
Prostate Cancer	
PC-3	80.93
DU-145	103.16
Breast Cancer	
MCF7	54.68
MDA-MB-231/ATCC	63.67
HS 578T	51.08
BT-549	90.91
T-47D	77.48
MDA-MB-468	64.98
Mean	76.57
Delta	68.09
Range	94.68

Mean Growth Percent - Growth Percent

150 100 50 0 -50 -100 -150

5-Amino-*N*-methyl-3-(1-methyl-1*H*-pyrrolo[2,3-*b*]pyridin-3-yl)-4-(3,4,5-trimethoxyphenyl)-1*H*-pyrazole-1-carbothioamide (317)

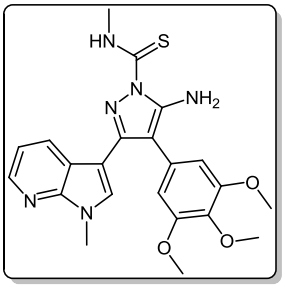

Developmental Therapeutics Program
One Dose Mean Graph

NSC: D-763895 / 1 | Conc: 1.00E-5 Molar | Test Date: Feb 27, 2012
Experiment ID: 1202OS23 | Report Date: Apr 02, 2012

Panel/Cell Line	Growth Percent
Leukemia	
CCRF-CEM	72.87
HL-60(TB)	86.24
K-562	81.84
MOLT-4	93.36
RPMI-8226	70.87
SR	54.33
Non-Small Cell Lung Cancer	
A549/ATCC	84.93
EKVX	71.97
HOP-62	69.93
NCI-H23	81.39
NCI-H322M	84.97
NCI-H460	89.00
NCI-H522	57.43
Colon Cancer	
COLO 205	79.66
HCC-2998	90.09
HCT-116	82.70
HCT-15	87.96
HT29	68.77
KM12	89.29
SW-620	89.23
CNS Cancer	
SF-268	98.33
SF-295	70.27
SF-539	91.32
SNB-19	79.84
SNB-75	26.49
U251	85.81
Melanoma	
LOX IMVI	73.89
MALME-3M	81.38
M14	96.94
MDA-MB-435	76.42
SK-MEL-2	92.29
SK-MEL-28	85.50
UACC-257	79.65
UACC-62	55.04
Ovarian Cancer	
IGROV1	108.05
OVCAR-3	105.22
OVCAR-4	69.30
OVCAR-5	99.03
OVCAR-8	81.32
NCI/ADR-RES	74.10
SK-OV-3	89.63
Renal Cancer	
786-0	94.66
A498	69.00
ACHN	83.59
CAKI-1	34.14
RXF 393	91.16
SN12C	74.68
TK-10	85.87
UO-31	35.90
Prostate Cancer	
PC-3	75.18
DU-145	107.57
Breast Cancer	
MCF7	63.66
MDA-MB-231/ATCC	62.14
HS 578T	55.15
BT-549	90.96
T-47D	76.39
MDA-MB-468	70.35
Mean	78.55
Delta	52.06
Range	81.56

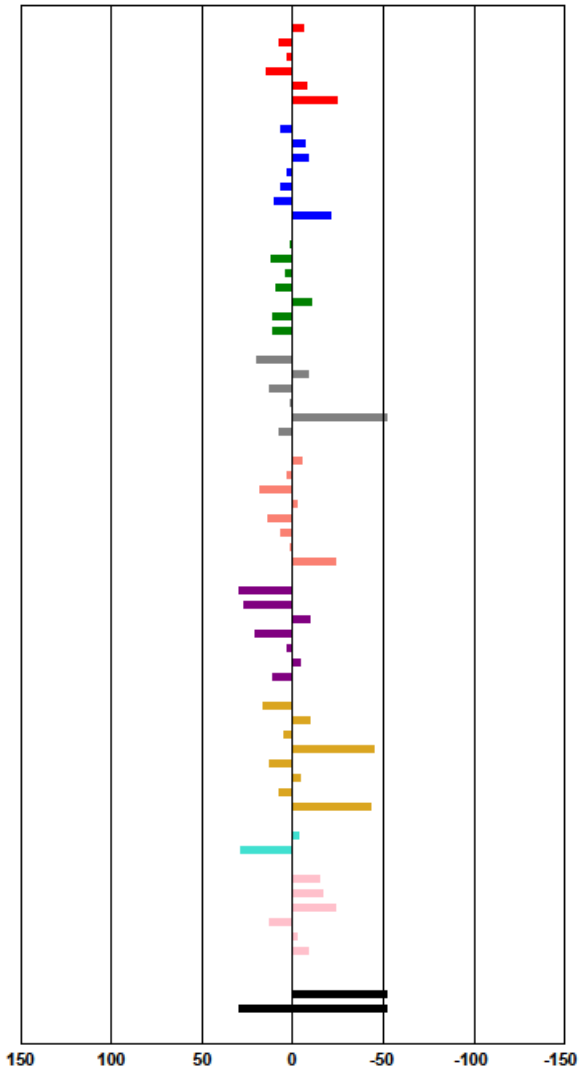

4-(1-Methyl-1*H*-indol-3-yl)-5-(1-methyl-1*H*-pyrrolo[2,3-*b*]pyridin-3-yl)-1*H*-pyrazol-3-amine (318)

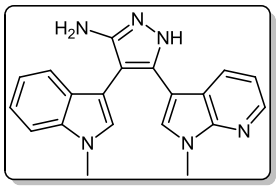

Developmental Therapeutics Program
One Dose Mean Graph

NSC: D-754612 / 1	Conc: 1.00E-5 Molar	Test Date: Oct 18, 2010
Experiment ID: 1010OS37		Report Date: Nov 17, 2010

Panel/Cell Line	Growth Percent
Leukemia	
CCRF-CEM	62.63
HL-60(TB)	96.51
K-562	62.05
MOLT-4	53.74
RPMI-8226	79.02
SR	18.48
Non-Small Cell Lung Cancer	
A549/ATCC	75.13
EKVX	98.33
HOP-62	82.96
NCI-H226	71.19
NCI-H23	89.36
NCI-H322M	91.57
NCI-H460	54.80
NCI-H522	51.38
Colon Cancer	
COLO 205	93.42
HCC-2998	103.74
HCT-116	81.02
HCT-15	86.18
HT29	82.38
KM12	88.37
SW-620	69.74
CNS Cancer	
SF-268	71.44
SF-295	56.69
SF-539	100.55
SNB-19	87.45
SNB-75	54.66
U251	48.43
Melanoma	
LOX IMVI	77.17
MALME-3M	110.79
M14	119.56
MDA-MB-435	84.56
SK-MEL-2	106.92
SK-MEL-28	108.81
SK-MEL-5	92.40
UACC-257	93.63
UACC-62	65.10
Ovarian Cancer	
IGROV1	81.52
OVCAR-3	102.40
OVCAR-5	111.78
OVCAR-8	77.05
NCI/ADR-RES	90.41
SK-OV-3	93.69
Renal Cancer	
786-0	95.03
A498	75.84
ACHN	71.22
CAKI-1	66.16
RXF 393	103.56
SN12C	92.48
TK-10	103.81
UO-31	68.54
Prostate Cancer	
DU-145	102.26
Breast Cancer	
MCF7	47.72
MDA-MB-231/ATCC	86.23
HS 578T	87.63
BT-549	87.54
T-47D	81.63
MDA-MB-468	75.72
Mean	81.97
Delta	63.49
Range	101.08

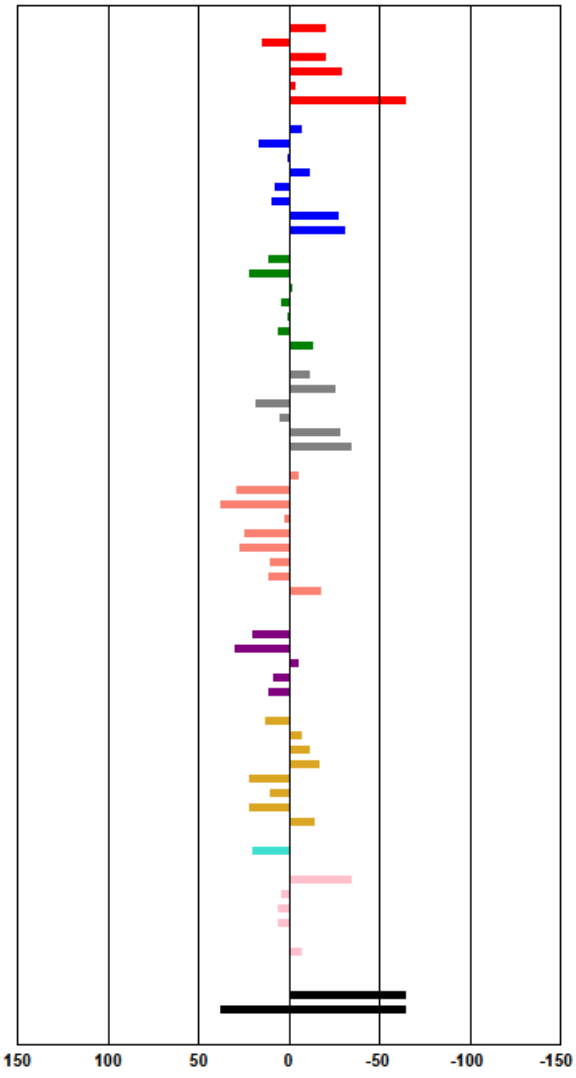

8-(1-Methyl-1*H*-indol-3-yl)-7-(1-methyl-1*H*-pyrrolo[2,3-*b*]pyridin-3-yl)pyrazolo[1,5-a][1,3,5]triazine-2,4(1*H*,3*H*)-dione (319)

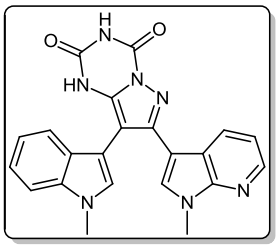

Developmental Therapeutics Program
One Dose Mean Graph

NSC: D-754613 / 1 | Conc: 1.00E-5 Molar | Test Date: Oct 18, 2010
Experiment ID: 1010OS37 | Report Date: Nov 17, 2010

Panel/Cell Line	Growth Percent
Leukemia	
CCRF-CEM	90.37
HL-60(TB)	102.93
K-562	91.41
MOLT-4	85.99
RPMI-8226	81.15
SR	61.37
Non-Small Cell Lung Cancer	
A549/ATCC	105.34
EKVX	101.99
HOP-62	95.10
NCI-H226	79.75
NCI-H23	93.27
NCI-H322M	98.69
NCI-H460	88.10
NCI-H522	72.15
Colon Cancer	
COLO 205	105.85
HCC-2998	105.58
HCT-116	103.25
HCT-15	99.14
HT29	97.98
KM12	97.08
SW-620	93.99
CNS Cancer	
SF-268	96.10
SF-295	102.70
SF-539	107.65
SNB-19	99.90
SNB-75	73.40
U251	73.90
Melanoma	
LOX IMVI	96.20
MALME-3M	102.28
M14	117.39
MDA-MB-435	104.93
SK-MEL-2	100.15
SK-MEL-28	112.97
SK-MEL-5	95.80
UACC-257	102.37
UACC-62	90.18
Ovarian Cancer	
IGROV1	75.27
OVCAR-3	96.98
OVCAR-5	108.56
OVCAR-8	95.18
NCI/ADR-RES	101.17
SK-OV-3	101.56
Renal Cancer	
786-0	106.43
A498	84.83
ACHN	92.89
CAKI-1	86.97
RXF 393	117.29
SN12C	98.37
TK-10	88.38
UO-31	72.63
Prostate Cancer	
PC-3	85.05
DU-145	110.15
Breast Cancer	
MCF7	55.95
MDA-MB-231/ATCC	83.32
HS 578T	99.49
BT-549	97.34
T-47D	96.56
MDA-MB-468	103.08
Mean	94.55
Delta	38.60
Range	61.44

Mean Growth Percent - Growth Percent

150 100 50 0 -50 -100 -150

3-(1-Methyl-1*H*-indol-3-yl)-2-(1-methyl-1*H*-pyrrolo[2,3-*b*]pyridin-3-yl)-5,7-bis(trifluoromethyl)pyrazolo[1,5-*a*]pyrimidine (320)

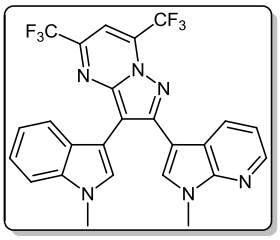

Developmental Therapeutics Program
One Dose Mean Graph

NSC: D-754614 / 1	Conc: 1.00E-5 Molar	Test Date: Oct 18, 2010
Experiment ID: 1010OS37		Report Date: Nov 17, 2010

Panel/Cell Line	Growth Percent
Leukemia	
CCRF-CEM	87.47
HL-60(TB)	93.83
K-562	86.17
MOLT-4	85.06
RPMI-8226	75.47
SR	86.31
Non-Small Cell Lung Cancer	
A549/ATCC	64.94
EKVX	105.28
HOP-62	19.47
NCI-H226	66.41
NCI-H23	86.81
NCI-H322M	90.99
NCI-H460	81.61
NCI-H522	70.90
Colon Cancer	
COLO 205	29.88
HCC-2998	95.86
HCT-116	90.34
HCT-15	88.82
HT29	63.08
KM12	85.74
SW-620	68.33
CNS Cancer	
SF-268	79.23
SF-295	81.70
SF-539	79.32
SNB-19	80.33
SNB-75	9.11
U251	49.05
Melanoma	
LOX IMVI	94.21
MALME-3M	87.99
M14	12.82
MDA-MB-435	85.51
SK-MEL-2	85.50
SK-MEL-28	91.10
SK-MEL-5	95.17
UACC-257	73.06
UACC-62	92.16
Ovarian Cancer	
IGROV1	65.68
OVCAR-3	100.13
OVCAR-5	115.94
OVCAR-8	58.75
NCI/ADR-RES	77.68
SK-OV-3	72.41
Renal Cancer	
786-0	99.08
A498	91.68
ACHN	36.95
CAKI-1	81.24
RXF 393	88.38
SN12C	77.13
TK-10	62.12
UO-31	102.23
Prostate Cancer	
PC-3	78.64
DU-145	78.45
Breast Cancer	
MCF7	77.56
MDA-MB-231/ATCC	24.65
HS 578T	80.56
BT-549	101.90
T-47D	89.03
MDA-MB-468	82.37
Mean	76.92
Delta	67.81
Range	106.83

Mean Growth Percent - Growth Percent

150 100 50 0 -50 -100 -150

1-(5-Amino-4-(1-methyl-1*H*-indol-3-yl)-3-(1-methyl-1*H*-pyrrolo[2,3-*b*]pyridin-3-yl)-1*H*-pyrazol-1-yl)ethanone (322)

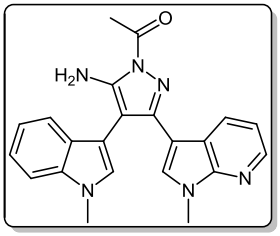

Developmental Therapeutics Program
One Dose Mean Graph

NSC: D-762132 / 1	Conc: 1.00E-5 Molar	Test Date: Nov 07, 2011
Experiment ID: 1111OS59		Report Date: Dec 09, 2011

Panel/Cell Line	Growth Percent
Leukemia	
CCRF-CEM	89.12
HL-60(TB)	71.52
K-562	53.92
MOLT-4	78.55
RPMI-8226	89.15
SR	28.25
Non-Small Cell Lung Cancer	
A549/ATCC	95.77
EKVX	91.59
HOP-62	74.68
HOP-92	36.75
NCI-H226	70.63
NCI-H23	88.12
NCI-H460	92.84
NCI-H522	74.64
Colon Cancer	
HCC-2998	95.99
HCT-116	86.15
HCT-15	84.80
HT29	84.69
SW-620	86.54
CNS Cancer	
SF-268	86.21
SF-295	78.77
SF-539	85.06
SNB-19	95.39
SNB-75	53.99
U251	99.10
Melanoma	
LOX IMVI	79.22
MALME-3M	78.51
M14	73.17
MDA-MB-435	33.20
SK-MEL-2	91.25
SK-MEL-28	98.26
SK-MEL-5	59.05
UACC-257	109.79
UACC-62	86.07
Ovarian Cancer	
IGROV1	75.80
OVCAR-3	89.02
OVCAR-4	81.73
OVCAR-5	98.20
OVCAR-8	85.26
NCI/ADR-RES	86.07
SK-OV-3	80.04
Renal Cancer	
A498	55.46
ACHN	79.96
CAKI-1	65.96
RXF 393	70.78
SN12C	86.35
TK-10	92.30
UO-31	41.53
Prostate Cancer	
PC-3	67.82
DU-145	83.76
Breast Cancer	
MCF7	54.87
MDA-MB-231/ATCC	70.45
HS 578T	64.98
BT-549	76.34
T-47D	74.62
MDA-MB-468	50.45
Mean	77.01
Delta	48.76
Range	81.54

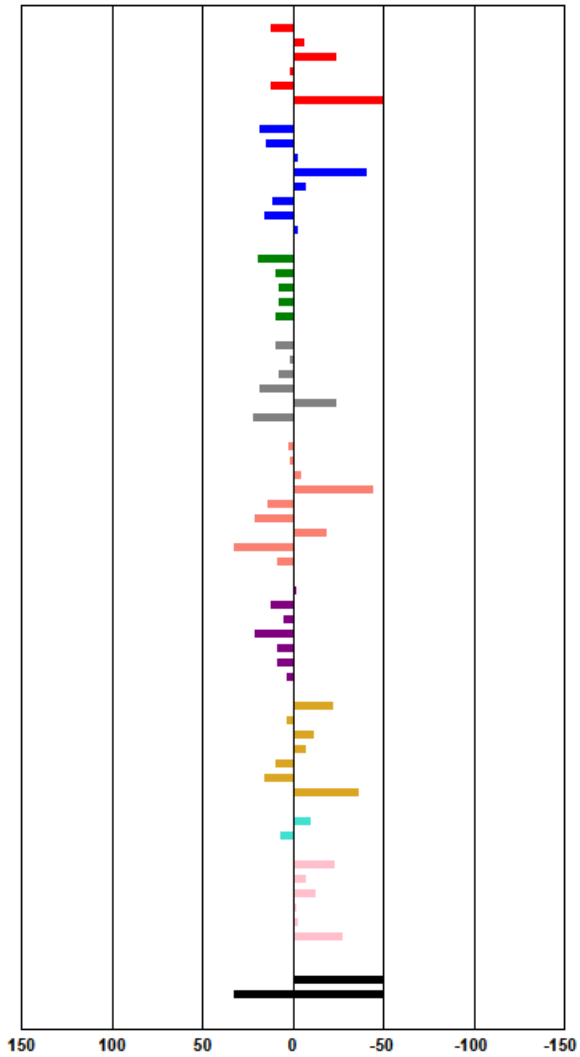

5-Amino-*N*-methyl-4-(1-methyl-1*H*-indol-3-yl)-3-(1-methyl-1*H*-pyrrolo[2,3-*b*]pyridin-3-yl)-1*H*-pyrazole-1-carbothioamide (323)

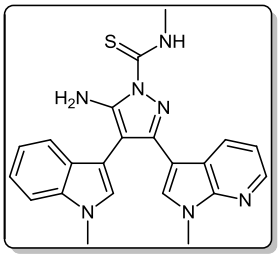

Developmental Therapeutics Program
One Dose Mean Graph

NSC: D-754615 / 1	Conc: 1.00E-5 Molar	Test Date: Oct 18, 2010
Experiment ID: 1010OS37		Report Date: Nov 17, 2010

Panel/Cell Line	Growth Percent
Leukemia	
CCRF-CEM	65.09
HL-60(TB)	65.15
K-562	37.08
MOLT-4	55.45
RPMI-8226	65.45
SR	46.24
Non-Small Cell Lung Cancer	
A549/ATCC	79.33
EKVX	85.74
HOP-62	83.22
NCI-H226	84.85
NCI-H23	88.42
NCI-H322M	80.75
NCI-H460	92.36
NCI-H522	49.33
Colon Cancer	
COLO 205	96.52
HCC-2998	95.12
HCT-116	89.24
HCT-15	72.08
HT29	74.49
KM12	66.47
SW-620	79.47
CNS Cancer	
SF-268	81.69
SF-295	50.94
SF-539	76.60
SNB-19	99.88
SNB-75	53.34
U251	59.37
Melanoma	
LOX IMVI	85.39
MALME-3M	94.17
M14	27.52
MDA-MB-435	25.62
SK-MEL-2	68.52
SK-MEL-28	85.72
SK-MEL-5	83.58
UACC-257	74.18
UACC-62	52.21
Ovarian Cancer	
IGROV1	70.65
OVCAR-3	84.65
OVCAR-5	101.05
OVCAR-8	81.62
NCI/ADR-RES	69.50
SK-OV-3	98.81
Renal Cancer	
786-0	96.51
A498	98.19
ACHN	66.22
CAKI-1	50.00
RXF 393	54.79
SN12C	85.73
TK-10	85.59
UO-31	52.43
Prostate Cancer	
PC-3	56.83
DU-145	97.73
Breast Cancer	
MCF7	62.00
MDA-MB-231/ATCC	69.79
HS 578T	71.92
BT-549	99.48
T-47D	72.58
MDA-MB-468	80.64
Mean	73.75
Delta	48.13
Range	75.43

Mean Growth Percent - Growth Percent

150 100 50 0 -50 -100 -150

5-(1-Benzyl-1*H*-pyrrolo[2,3-*b*]pyridin-3-yl)-4-(1-methyl-1*H*-indol-3-yl)-1*H*-pyrazol-3(2*H*)-one (326)

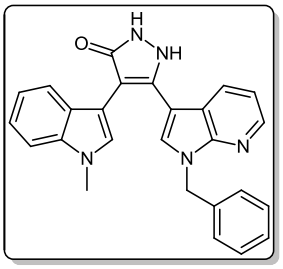

Developmental Therapeutics Program
One Dose Mean Graph

NSC: D-762134 / 1	Conc: 1.00E-5 Molar	Test Date: Nov 07, 2011
Experiment ID: 1111OS59		Report Date: Dec 09, 2011

Panel/Cell Line	Growth Percent
Leukemia	
CCRF-CEM	97.71
HL-60(TB)	97.56
K-562	106.30
MOLT-4	83.15
RPMI-8226	87.67
SR	91.34
Non-Small Cell Lung Cancer	
A549/ATCC	102.75
EKVX	89.49
HOP-62	99.41
NCI-H226	99.32
NCI-H23	100.64
NCI-H460	106.02
NCI-H522	72.26
Colon Cancer	
HCC-2998	109.27
HCT-116	87.22
HCT-15	99.19
HT29	103.73
KM12	93.26
SW-620	104.37
CNS Cancer	
SF-268	93.32
SF-295	94.26
SF-539	104.40
SNB-19	91.87
SNB-75	49.53
U251	111.27
Melanoma	
LOX IMVI	91.40
MALME-3M	91.26
M14	100.41
MDA-MB-435	104.79
SK-MEL-28	98.42
SK-MEL-5	104.77
UACC-257	127.67
UACC-62	80.09
Ovarian Cancer	
IGROV1	83.81
OVCAR-3	100.78
OVCAR-4	91.31
OVCAR-5	98.40
OVCAR-8	104.10
NCI/ADR-RES	102.88
SK-OV-3	93.45
Renal Cancer	
A498	118.11
ACHN	97.21
CAKI-1	80.61
RXF 393	108.87
SN12C	91.01
TK-10	109.33
UO-31	60.06
Prostate Cancer	
PC-3	81.38
DU-145	104.27
Breast Cancer	
MCF7	85.08
MDA-MB-231/ATCC	79.87
HS 578T	105.30
BT-549	99.61
T-47D	75.36
MDA-MB-468	98.03
Mean	95.33
Delta	45.80
Range	78.14

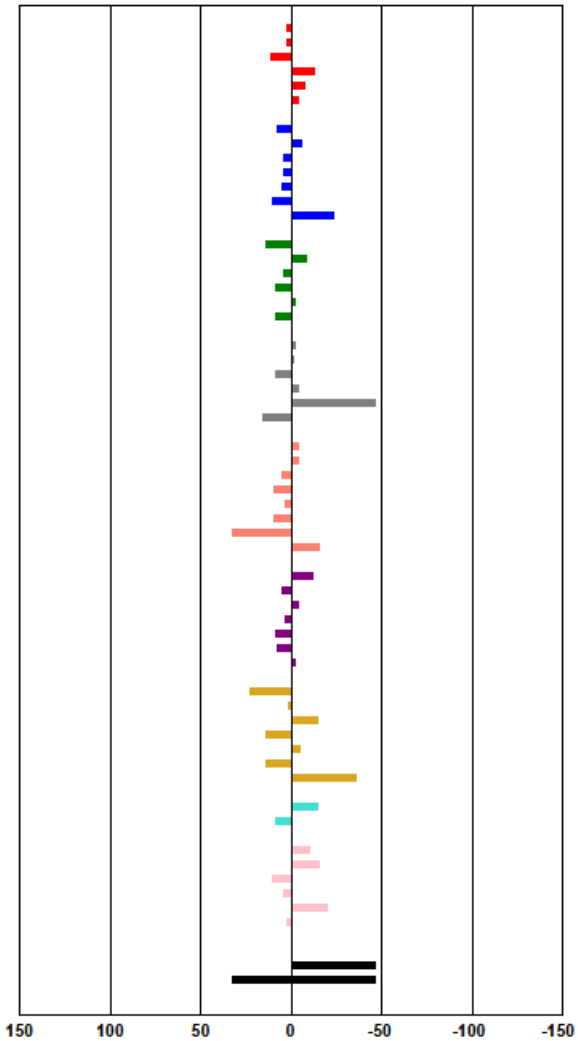

4-(1-Methyl-1*H*-indol-3-yl)-3-(1-methyl-1*H*-pyrrolo[2,3-*b*]pyridin-3-yl)isoxazol-5(2H)-one (327)

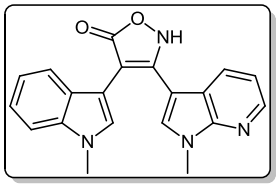

Developmental Therapeutics Program
One Dose Mean Graph

NSC: D-762131 / 1	Conc: 1.00E-5 Molar	Test Date: Nov 07, 2011
Experiment ID: 1111OS59		Report Date: Dec 01, 2011

Panel/Cell Line	Growth Percent
Leukemia	
CCRF-CEM	83.22
HL-60(TB)	67.13
K-562	29.84
MOLT-4	66.67
RPMI-8226	73.36
SR	9.28
Non-Small Cell Lung Cancer	
A549/ATCC	54.16
EKVX	73.01
HOP-62	58.64
NCI-H226	66.33
NCI-H23	53.41
NCI-H460	52.13
NCI-H522	27.00
Colon Cancer	
HCC-2998	79.50
HCT-116	59.41
HCT-15	65.18
HT29	25.95
SW-620	57.77
CNS Cancer	
SF-268	85.51
SF-295	51.62
SF-539	82.14
SNB-19	95.75
SNB-75	49.21
U251	75.85
Melanoma	
LOX IMVI	67.36
MALME-3M	64.70
M14	51.35
MDA-MB-435	2.61
SK-MEL-2	35.98
SK-MEL-28	80.29
SK-MEL-5	47.97
UACC-257	83.80
UACC-62	59.25
Ovarian Cancer	
IGROV1	59.94
OVCAR-3	42.94
OVCAR-4	70.42
OVCAR-5	94.08
OVCAR-8	78.25
NCI/ADR-RES	34.56
SK-OV-3	70.57
Renal Cancer	
A498	79.40
ACHN	77.07
CAKI-1	47.49
RXF 393	76.89
SN12C	88.25
TK-10	88.87
UO-31	36.70
Prostate Cancer	
PC-3	48.94
DU-145	84.45
Breast Cancer	
MCF7	39.81
MDA-MB-231/ATCC	53.43
HS 578T	83.23
BT-549	61.72
T-47D	63.79
MDA-MB-468	34.36
Mean	60.92
Delta	58.31
Range	93.14

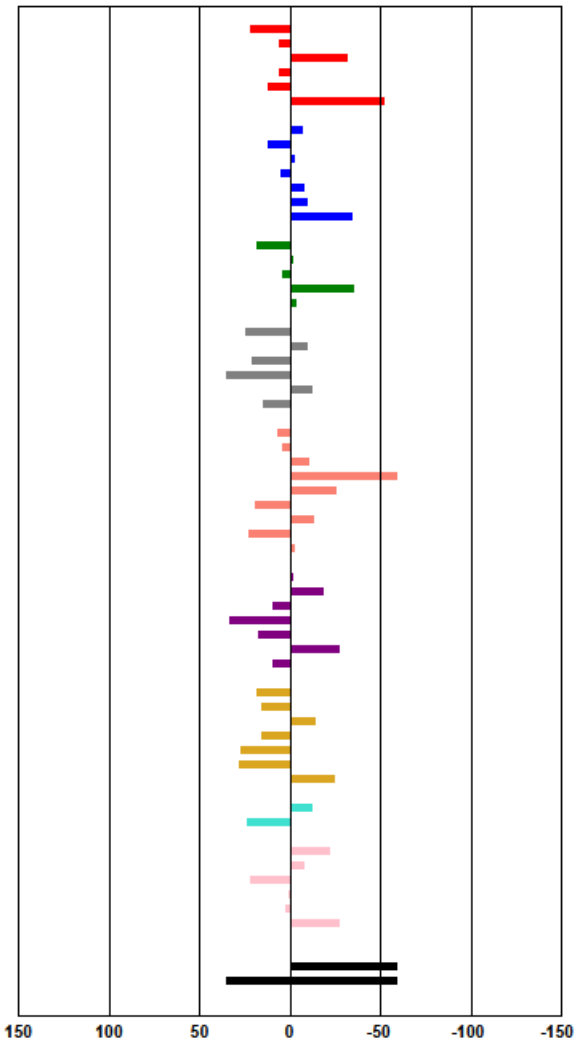

2-Methyl-4-(1-methyl-1*H*-indol-3-yl)-3-(1-methyl-1*H*-pyrrolo[2,3-*b*]pyridin-3-yl)isoxazol-5(2*H*)-one (328)

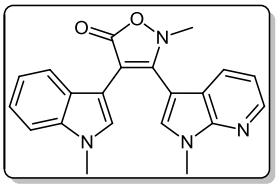

Developmental Therapeutics Program
One Dose Mean Graph

NSC: D-762133 / 1 | Conc: 1.00E-5 Molar | Test Date: Nov 07, 2011
Experiment ID: 1111OS59 | Report Date: Dec 09, 2011

Panel/Cell Line	Growth Percent
Leukemia	
CCRF-CEM	100.32
HL-60(TB)	89.68
K-562	97.34
MOLT-4	88.53
RPMI-8226	93.78
SR	83.51
Non-Small Cell Lung Cancer	
A549/ATCC	91.86
EKVX	83.30
HOP-62	97.44
HOP-92	78.25
NCI-H226	87.67
NCI-H23	94.37
NCI-H460	96.96
NCI-H522	77.06
Colon Cancer	
HCC-2998	99.85
HCT-116	90.67
HCT-15	81.72
HT29	97.77
SW-620	106.23
CNS Cancer	
SF-268	95.03
SF-295	92.23
SF-539	95.27
SNB-19	102.19
SNB-75	73.27
U251	101.74
Melanoma	
LOX IMVI	89.12
MALME-3M	89.22
M14	89.76
MDA-MB-435	100.72
SK-MEL-2	86.96
SK-MEL-28	115.44
SK-MEL-5	98.55
UACC-257	103.08
UACC-62	98.32
Ovarian Cancer	
IGROV1	90.42
OVCAR-3	108.38
OVCAR-4	100.39
OVCAR-5	109.16
OVCAR-8	93.35
NCI/ADR-RES	90.16
SK-OV-3	102.73
Renal Cancer	
A498	105.87
ACHN	99.14
CAKI-1	91.07
RXF 393	114.67
SN12C	99.79
TK-10	111.62
UO-31	52.91
Prostate Cancer	
PC-3	83.74
DU-145	114.67
Breast Cancer	
MCF7	51.27
MDA-MB-231/ATCC	71.99
HS 578T	100.94
BT-549	91.21
T-47D	79.20
MDA-MB-468	48.23
Mean	92.47
Delta	44.24
Range	67.21

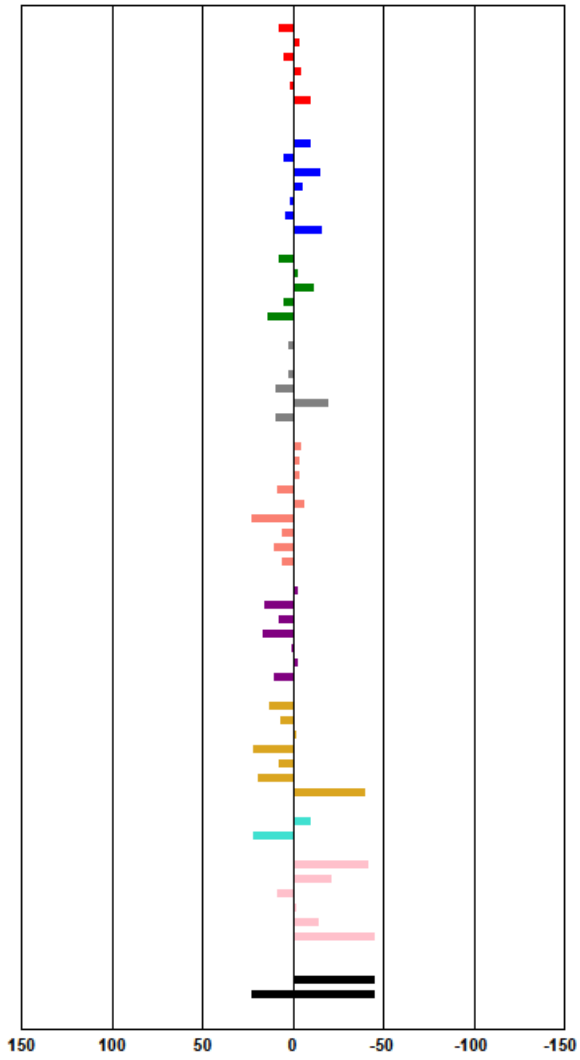

2-Amino-5-(1-methyl-1*H*-indol-3-yl)-6-(1-methyl-1*H*-pyrrolo[2,3-*b*]pyridin-3-yl)pyrimidin-4(3*H*)-one (332)

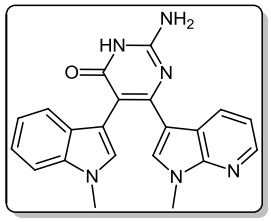

Developmental Therapeutics Program
One Dose Mean Graph

NSC: D-754611 / 1	Conc: 1.00E-5 Molar	Test Date: Oct 18, 2010
Experiment ID: 1010OS37		Report Date: Nov 17, 2010

Panel/Cell Line	Growth Percent
Leukemia	
CCRF-CEM	92.52
HL-60(TB)	105.27
K-562	95.03
MOLT-4	97.12
RPMI-8226	85.14
SR	90.42
Non-Small Cell Lung Cancer	
A549/ATCC	101.61
EKVX	96.34
HOP-62	91.46
NCI-H226	84.15
NCI-H23	92.63
NCI-H322M	95.33
NCI-H460	98.41
NCI-H522	87.95
Colon Cancer	
COLO 205	105.85
HCC-2998	109.08
HCT-116	97.99
HCT-15	103.22
HT29	98.47
KM12	102.16
SW-620	97.53
CNS Cancer	
SF-268	100.59
SF-295	98.19
SF-539	103.86
SNB-19	110.66
SNB-75	87.55
U251	77.55
Melanoma	
LOX IMVI	99.87
MALME-3M	107.12
M14	102.93
MDA-MB-435	98.77
SK-MEL-2	105.11
SK-MEL-28	111.01
SK-MEL-5	96.47
UACC-257	102.72
UACC-62	96.95
Ovarian Cancer	
IGROV1	87.12
OVCAR-3	99.67
OVCAR-4	88.05
OVCAR-5	105.60
OVCAR-8	95.85
NCI/ADR-RES	100.63
SK-OV-3	98.30
Renal Cancer	
786-0	105.52
A498	85.65
ACHN	87.57
CAKI-1	89.98
RXF 393	123.55
SN12C	103.87
TK-10	112.80
UO-31	79.03
Prostate Cancer	
PC-3	84.21
DU-145	107.06
Breast Cancer	
MCF7	85.95
MDA-MB-231/ATCC	96.44
HS 578T	100.63
BT-549	95.85
T-47D	83.01
MDA-MB-468	115.55
Mean	97.61
Delta	20.06
Range	46.00

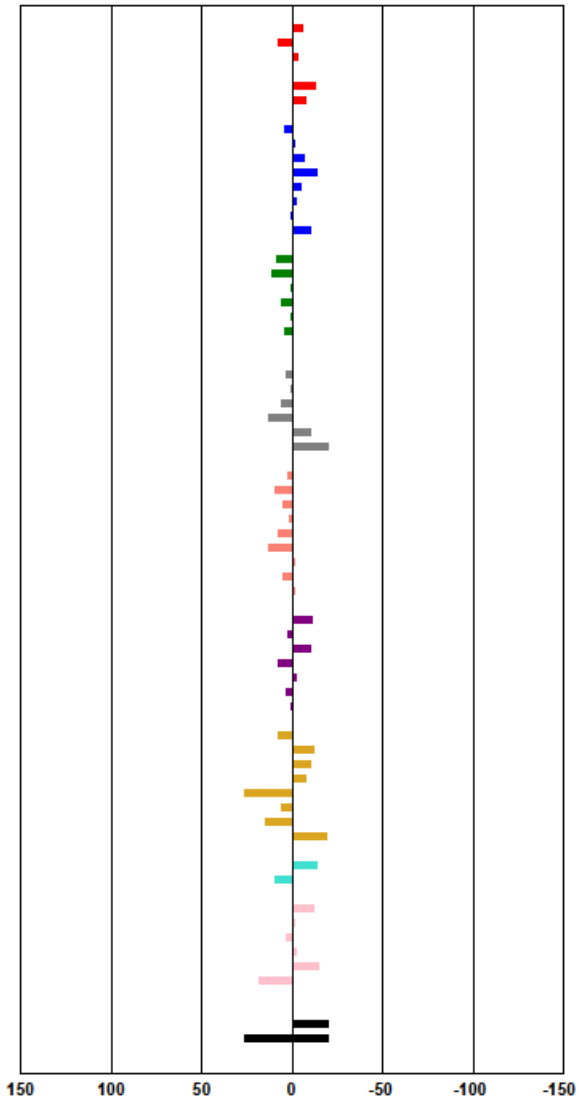

1-Hydroxy-3-(1-methyl-1*H*-indol-3-yl)-4-(1-methyl-1*H*-pyrrolo[2,3-*b*]pyridin-3-yl)-1*H*-pyrrole-2,5-dione (356)

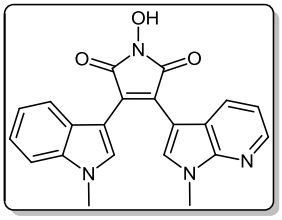

Developmental Therapeutics Program
One Dose Mean Graph

NSC: D-762130 / 1	Conc: 1.00E-5 Molar	Test Date: Nov 07, 2011
Experiment ID: 1111OS59		Report Date: Dec 09, 2011

Panel/Cell Line	Growth Percent
Leukemia	
CCRF-CEM	100.40
HL-60(TB)	98.75
K-562	91.42
MOLT-4	97.62
RPMI-8226	94.32
SR	53.12
Non-Small Cell Lung Cancer	
A549/ATCC	108.24
EKVX	95.26
HOP-62	76.41
NCI-H226	86.83
NCI-H23	99.71
NCI-H460	102.73
NCI-H522	81.36
Colon Cancer	
HCC-2998	105.68
HCT-116	98.15
HCT-15	105.85
HT29	105.40
SW-620	98.68
CNS Cancer	
SF-268	96.98
SF-295	93.11
SF-539	96.93
SNB-19	111.45
SNB-75	79.78
U251	110.37
Melanoma	
LOX IMVI	83.00
MALME-3M	94.72
M14	90.82
MDA-MB-435	104.85
SK-MEL-2	109.82
SK-MEL-28	110.74
SK-MEL-5	101.04
UACC-257	117.01
UACC-62	101.96
Ovarian Cancer	
IGROV1	101.00
OVCAR-3	99.47
OVCAR-4	107.38
OVCAR-5	104.42
OVCAR-8	100.51
NCI/ADR-RES	101.05
SK-OV-3	102.04
Renal Cancer	
A498	113.07
ACHN	98.67
CAKI-1	94.41
RXF 393	106.18
SN12C	102.12
TK-10	114.90
UO-31	66.00
Prostate Cancer	
PC-3	97.81
DU-145	104.06
Breast Cancer	
MCF7	87.43
MDA-MB-231/ATCC	98.60
HS 578T	99.20
BT-549	86.42
T-47D	96.83
MDA-MB-468	94.39
Mean	97.79
Delta	44.67
Range	63.89

Mean Growth Percent - Growth Percent

150 100 50 0 -50 -100 -150

3-(1-Methyl-1*H*-indol-3-yl)-4-(1-methyl-1*H*-pyrrolo[2,3-*b*]pyridin-3-yl)-1*H*-pyrrole-2,5-dione (357)

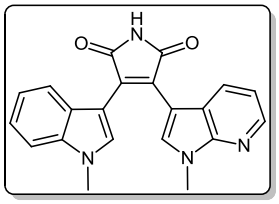

Developmental Therapeutics Program

One Dose Mean Graph

NSC: D-762129 / 1	Conc: 1.00E-5 Molar	Test Date: Nov 07, 2011
Experiment ID: 1111OS59		Report Date: Dec 01, 2011

Panel/Cell Line	Growth Percent
Leukemia	
CCRF-CEM	6.61
HL-60(TB)	3.55
K-562	19.89
MOLT-4	12.62
RPMI-8226	45.39
SR	12.12
Non-Small Cell Lung Cancer	
A549/ATCC	28.82
EKVX	62.74
HOP-62	40.63
NCI-H226	8.44
NCI-H23	49.32
NCI-H460	19.54
NCI-H522	14.30
Colon Cancer	
HCC-2998	58.85
HCT-116	21.95
HCT-15	33.36
HT29	2.28
KM12	8.78
SW-620	12.89
CNS Cancer	
SF-268	50.23
SF-295	9.52
SF-539	-11.83
SNB-19	64.98
SNB-75	10.44
U251	26.97
Melanoma	
LOX IMVI	41.00
MALME-3M	20.34
M14	17.47
MDA-MB-435	12.89
SK-MEL-2	-13.82
SK-MEL-28	51.33
SK-MEL-5	31.16
UACC-257	84.78
UACC-62	36.57
Ovarian Cancer	
IGROV1	70.77
OVCAR-3	50.25
OVCAR-4	58.97
OVCAR-5	54.64
OVCAR-8	53.76
NCI/ADR-RES	53.45
SK-OV-3	22.13
Renal Cancer	
A498	-19.91
ACHN	26.51
CAKI-1	35.04
RXF 393	14.35
SN12C	30.68
TK-10	26.27
UO-31	22.63
Prostate Cancer	
PC-3	44.57
DU-145	63.19
Breast Cancer	
MCF7	22.69
MDA-MB-231/ATCC	56.32
HS 578T	-7.79
BT-549	-7.12
T-47D	24.25
MDA-MB-468	25.16
Mean	28.84
Delta	48.75
Range	104.69

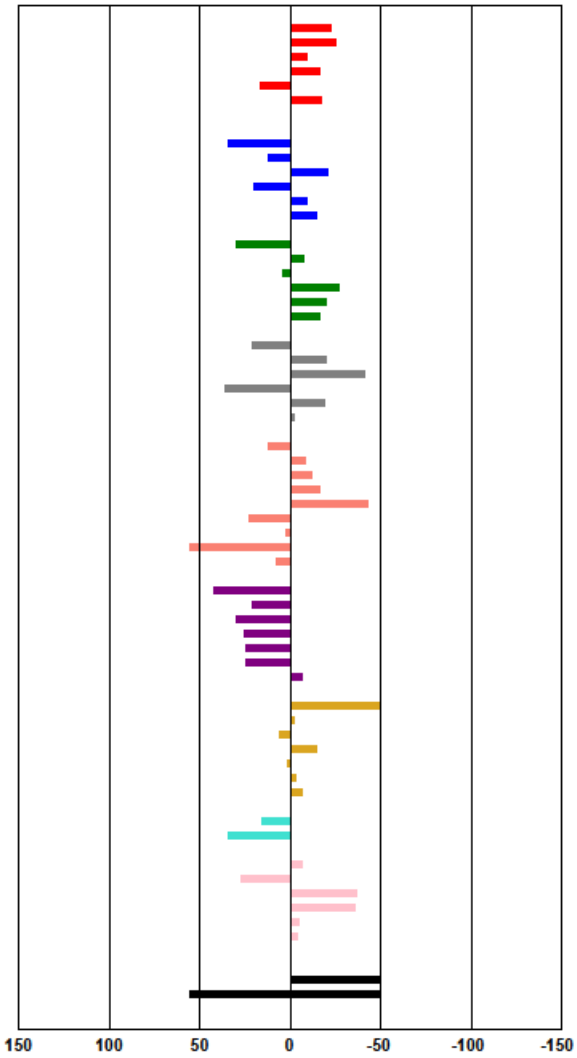

3,4-Bis(1-methyl-1*H*-pyrrolo[2,3-*b*]pyridin-3-yl)-1*H*-pyrrole-2,5-dione (361)

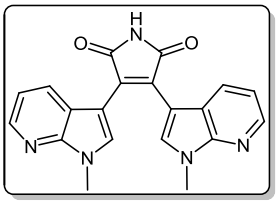

Developmental Therapeutics Program
One Dose Mean Graph

NSC: D-763897 / 1 | Conc: 1.00E-5 Molar | Test Date: Feb 27, 2012
Experiment ID: 1202OS23 | Report Date: Apr 02, 2012

Panel/Cell Line	Growth Percent
Leukemia	
CCRF-CEM	34.93
HL-60(TB)	96.98
K-562	83.60
MOLT-4	60.61
RPMI-8226	72.85
SR	9.03
Non-Small Cell Lung Cancer	
A549/ATCC	62.86
EKVX	59.77
HOP-62	66.77
NCI-H23	65.40
NCI-H322M	67.06
NCI-H460	52.64
NCI-H522	60.68
Colon Cancer	
COLO 205	52.83
HCT-116	70.88
HCT-15	78.80
HT29	52.51
KM12	67.89
SW-620	65.09
CNS Cancer	
SF-268	79.44
SF-295	-14.06
SF-539	29.97
SNB-19	84.90
SNB-75	-12.07
U251	67.86
Melanoma	
LOX IMVI	61.65
MALME-3M	13.81
M14	94.31
MDA-MB-435	67.07
SK-MEL-2	94.49
SK-MEL-28	83.12
UACC-257	86.62
UACC-62	58.07
Ovarian Cancer	
IGROV1	66.78
OVCAR-3	88.32
OVCAR-4	42.02
OVCAR-5	82.92
OVCAR-8	72.93
NCI/ADR-RES	68.42
SK-OV-3	52.44
Renal Cancer	
786-0	79.62
A498	-15.67
ACHN	47.01
CAKI-1	23.20
RXF 393	61.35
SN12C	61.80
TK-10	38.20
UO-31	31.41
Prostate Cancer	
PC-3	58.66
DU-145	94.85
Breast Cancer	
MCF7	47.86
MDA-MB-231/ATCC	58.01
HS 578T	6.64
BT-549	24.58
T-47D	38.89
MDA-MB-468	37.24
Mean	56.14
Delta	71.81
Range	112.65

Mean Growth Percent - Growth Percent

150 100 50 0 -50 -100 -150

6-Amino-13,14-dimethyl-13,14-dihydropyrido[3',2':4,5]pyrrolo[2,3-*a*]pyrimido[4,5-*c*]carbazol-8(7*H*)-one (239)

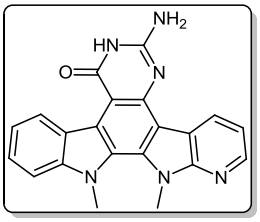

Developmental Therapeutics Program
One Dose Mean Graph

NSC: D-762128 / 1	Conc: 1.00E-5 Molar	Test Date: Nov 07, 2011
Experiment ID: 1111OS59		Report Date: Dec 09, 2011

Panel/Cell Line	Growth Percent
Leukemia	
CCRF-CEM	65.33
HL-60(TB)	72.81
K-562	73.99
MOLT-4	74.38
RPMI-8226	64.42
SR	63.29
Non-Small Cell Lung Cancer	
A549/ATCC	92.90
EKVX	82.19
HOP-62	84.06
NCI-H226	65.05
NCI-H23	86.28
NCI-H460	65.53
NCI-H522	35.05
Colon Cancer	
HCC-2998	104.02
HCT-116	63.01
HCT-15	67.39
HT29	78.05
KM12	59.02
SW-620	71.95
CNS Cancer	
SF-268	95.56
SF-295	94.08
SF-539	111.27
SNB-19	102.73
SNB-75	74.13
U251	81.25
Melanoma	
LOX IMVI	66.04
MALME-3M	119.26
M14	68.83
MDA-MB-435	87.02
SK-MEL-2	68.46
SK-MEL-28	119.75
SK-MEL-5	74.70
UACC-257	128.72
UACC-62	86.95
Ovarian Cancer	
IGROV1	94.20
OVCAR-3	98.25
OVCAR-4	80.14
OVCAR-5	98.79
OVCAR-8	60.12
NCI/ADR-RES	80.23
SK-OV-3	87.23
Renal Cancer	
A498	97.51
ACHN	54.13
CAKI-1	60.13
RXF 393	87.37
SN12C	91.01
TK-10	76.41
UO-31	39.40
Prostate Cancer	
PC-3	71.01
DU-145	83.23
Breast Cancer	
MCF7	45.71
MDA-MB-231/ATCC	79.41
HS 578T	127.82
BT-549	66.05
T-47D	48.67
MDA-MB-468	75.14
Mean	79.45
Delta	44.40
Range	93.67

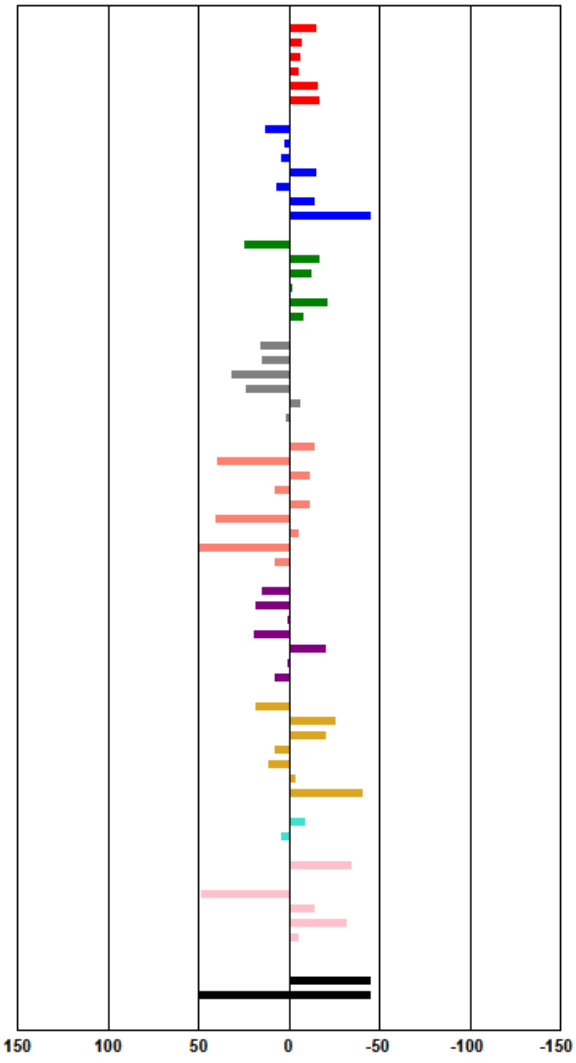

12,13-Dimethyl-12,13-dihydro-5*H*-pyrido[3',2':4,5]pyrrolo[2,3-*a*]pyrrolo[3,4-*c*]carbazole-5,7(6*H*)-dione (364)

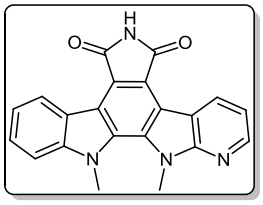

Developmental Therapeutics Program
One Dose Mean Graph

NSC: D-762125 / 1	Conc: 1.00E-5 Molar	Test Date: Nov 07, 2011
Experiment ID: 1111OS59		Report Date: Dec 01, 2011

Panel/Cell Line	Growth Percent
Leukemia	
CCRF-CEM	55.47
HL-60(TB)	84.25
K-562	83.41
MOLT-4	61.51
RPMI-8226	93.93
SR	10.24
Non-Small Cell Lung Cancer	
A549/ATCC	70.53
EKVX	70.83
HOP-62	68.16
HOP-92	76.94
NCI-H226	48.45
NCI-H23	73.37
NCI-H460	19.91
NCI-H522	21.36
Colon Cancer	
HCC-2998	83.19
HCT-116	55.24
HCT-15	76.80
HT29	49.22
SW-620	57.89
CNS Cancer	
SF-268	67.00
SF-295	69.52
SF-539	83.86
SNB-19	88.13
SNB-75	61.27
U251	66.86
Melanoma	
LOX IMVI	62.41
MALME-3M	72.76
M14	61.33
MDA-MB-435	63.45
SK-MEL-2	78.44
SK-MEL-28	105.39
SK-MEL-5	63.24
UACC-257	88.85
UACC-62	71.62
Ovarian Cancer	
IGROV1	59.86
OVCAR-3	106.13
OVCAR-4	32.54
OVCAR-5	74.65
OVCAR-8	36.67
NCI/ADR-RES	64.02
SK-OV-3	88.27
Renal Cancer	
A498	72.17
ACHN	48.97
CAKI-1	52.38
RXF 393	67.76
SN12C	78.85
TK-10	40.51
UO-31	45.40
Prostate Cancer	
PC-3	70.19
DU-145	83.52
Breast Cancer	
MCF7	15.91
MDA-MB-231/ATCC	46.94
HS 578T	86.02
BT-549	43.26
T-47D	34.93
MDA-MB-468	20.51
Mean	63.11
Delta	52.87
Range	95.89

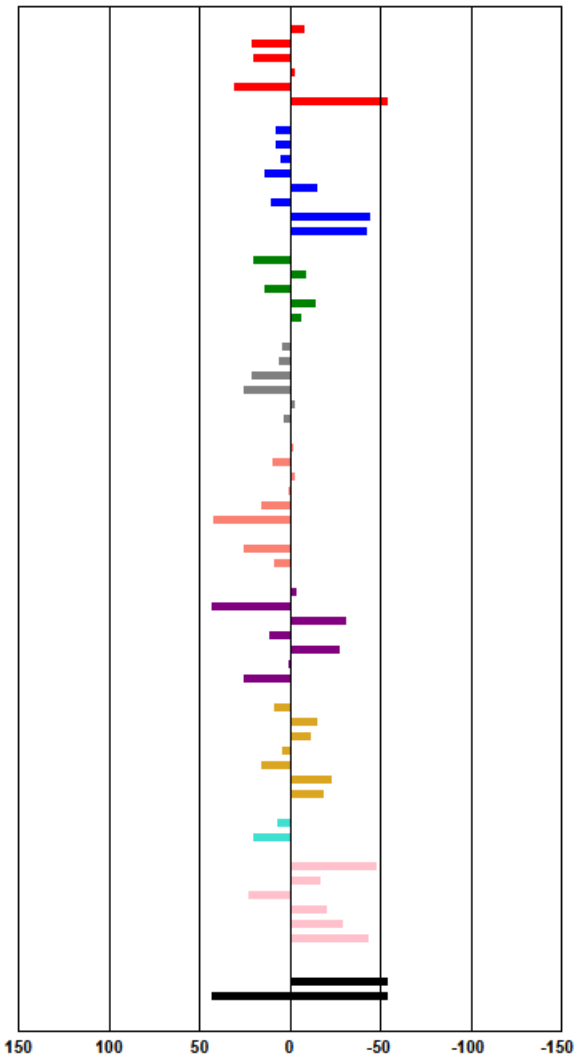

6-Hydroxy-12,13-dimethyl-12,13-dihydro-5*H*-pyrido[3',2':4,5]pyrrolo[2,3-*a*]pyrrolo[3,4-*c*]carbazole-5,7(6*H*)-dione (363)

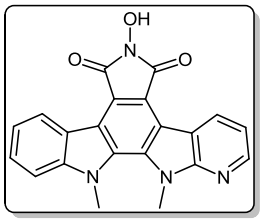

Developmental Therapeutics Program
One Dose Mean Graph

NSC: D-762126 / 1	Conc: 1.00E-5 Molar	Test Date: Nov 07, 2011
Experiment ID: 1111OS59		Report Date: Dec 01, 2011

Panel/Cell Line	Growth Percent
Leukemia	
CCRF-CEM	3.44
HL-60(TB)	9.35
K-562	46.59
MOLT-4	-8.58
RPMI-8226	62.61
SR	3.27
Non-Small Cell Lung Cancer	
A549/ATCC	50.53
EKVX	76.84
HOP-62	-3.66
NCI-H226	74.77
NCI-H23	34.49
NCI-H460	2.11
NCI-H522	4.02
Colon Cancer	
HCC-2998	76.78
HCT-116	34.51
HCT-15	65.90
HT29	63.09
KM12	38.10
SW-620	44.53
CNS Cancer	
SF-268	21.80
SF-295	18.22
SF-539	-4.19
SNB-19	34.64
SNB-75	-6.41
U251	17.20
Melanoma	
LOX IMVI	8.25
MALME-3M	54.42
M14	11.88
MDA-MB-435	41.62
SK-MEL-28	63.52
SK-MEL-5	9.04
UACC-257	134.92
UACC-62	25.82
Ovarian Cancer	
IGROV1	51.59
OVCAR-3	90.58
OVCAR-4	65.49
OVCAR-5	94.52
OVCAR-8	39.64
NCI/ADR-RES	35.99
SK-OV-3	17.59
Renal Cancer	
A498	82.41
ACHN	1.89
CAKI-1	5.71
RXF 393	63.34
SN12C	14.53
TK-10	53.92
UO-31	7.46
Prostate Cancer	
PC-3	62.67
DU-145	3.69
Breast Cancer	
MCF7	3.30
MDA-MB-231/ATCC	95.17
HS 578T	120.45
BT-549	21.09
T-47D	-7.71
MDA-MB-468	41.54
Mean	37.71
Delta	46.29
Range	143.50

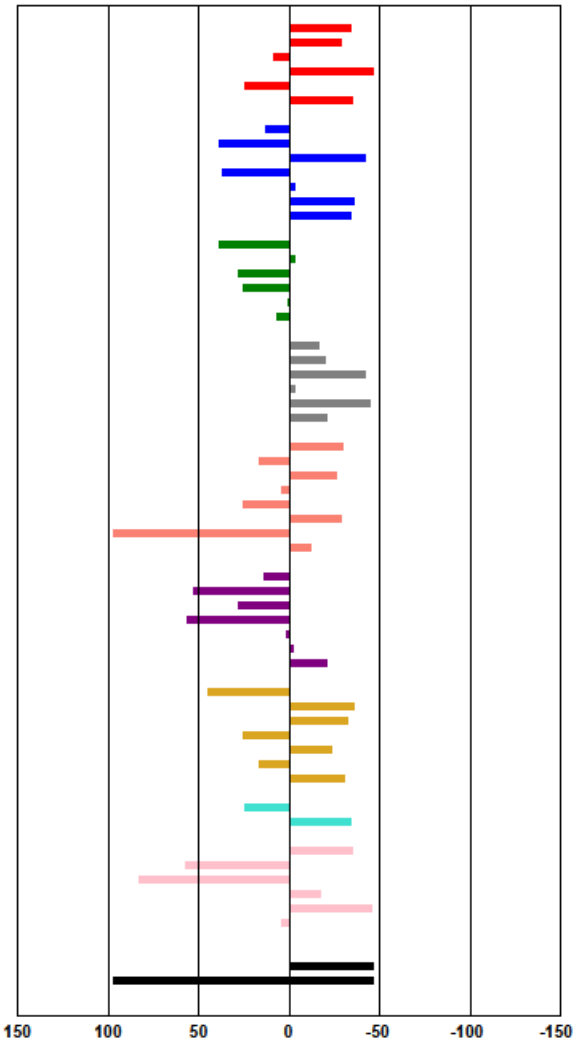

***tert*-Butyl 12,13-dimethyl-5,7-dioxo-12,13-dihydro-5*H*-pyrido[3',2':4,5]pyrrolo[2,3-*a*]pyrrolo[3,4-*c*]carbazole-6(7*H*)-carboxylate (368)**

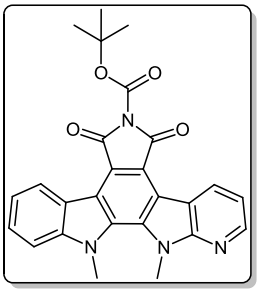

Developmental Therapeutics Program
One Dose Mean Graph

NSC: D-762127 / 1 | Conc: 1.00E-5 Molar | Test Date: Nov 07, 2011
Experiment ID: 1111OS59 | Report Date: Dec 01, 2011

Panel/Cell Line	Growth Percent
Leukemia	
CCRF-CEM	61.30
HL-60(TB)	84.95
K-562	81.25
MOLT-4	60.96
RPMI-8226	89.32
SR	5.87
Non-Small Cell Lung Cancer	
A549/ATCC	63.36
EKVX	58.69
HOP-62	15.17
NCI-H226	44.13
NCI-H23	65.85
NCI-H460	15.23
NCI-H522	8.12
Colon Cancer	
HCC-2998	70.90
HCT-116	40.05
HCT-15	78.32
HT29	46.35
KM12	32.11
SW-620	53.12
CNS Cancer	
SF-268	34.17
SF-295	52.26
SF-539	72.54
SNB-19	88.00
SNB-75	28.86
U251	60.30
Melanoma	
LOX IMVI	50.68
MALME-3M	49.90
M14	56.26
MDA-MB-435	59.02
SK-MEL-2	88.35
SK-MEL-28	80.39
SK-MEL-5	47.79
UACC-257	64.22
UACC-62	62.17
Ovarian Cancer	
IGROV1	47.64
OVCAR-3	63.26
OVCAR-4	9.41
OVCAR-5	72.54
OVCAR-8	36.17
NCI/ADR-RES	42.89
SK-OV-3	63.91
Renal Cancer	
A498	68.57
ACHN	41.12
CAKI-1	51.93
RXF 393	54.23
SN12C	58.96
TK-10	41.68
UO-31	35.83
Prostate Cancer	
PC-3	65.70
DU-145	50.57
Breast Cancer	
MCF7	4.41
MDA-MB-231/ATCC	60.12
HS 578T	83.03
BT-549	12.24
T-47D	-0.58
MDA-MB-468	5.45
Mean	50.70
Delta	51.28
Range	89.90

Mean Growth Percent - Growth Percent

150 100 50 0 -50 -100 -150

12,13-Dimethyl-12,13-dihydro-5*H*-pyrido[2,3-*b*]pyrido[3',2':4,5]pyrrolo[3,2-*g*]pyrrolo[3,4-*e*]indole-5,7(6*H*)-dione (371)

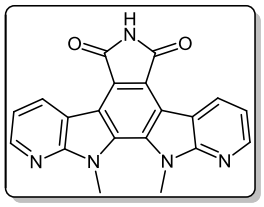

Developmental Therapeutics Program
One Dose Mean Graph

NSC: D-763889 / 1 | Conc: 1.00E-5 Molar | Test Date: Feb 27, 2012
Experiment ID: 1202OS23 | Report Date: Apr 02, 2012

Panel/Cell Line	Growth Percent
Leukemia	
CCRF-CEM	37.30
HL-60(TB)	100.34
K-562	68.70
MOLT-4	-7.55
RPMI-8226	66.54
SR	-30.20
Non-Small Cell Lung Cancer	
A549/ATCC	58.87
EKVX	78.30
HOP-62	25.79
NCI-H23	56.99
NCI-H322M	64.43
NCI-H460	14.51
NCI-H522	36.52
Colon Cancer	
COLO 205	66.45
HCT-116	49.18
HCT-15	72.12
HT29	51.73
KM12	68.57
SW-620	51.59
CNS Cancer	
SF-268	45.49
SF-295	6.51
SF-539	70.19
SNB-19	82.59
SNB-75	16.07
U251	43.76
Melanoma	
LOX IMVI	53.09
MALME-3M	76.69
M14	70.00
MDA-MB-435	83.65
SK-MEL-2	85.91
SK-MEL-28	92.41
UACC-257	87.71
UACC-62	44.13
Ovarian Cancer	
IGROV1	45.90
OVCAR-3	88.86
OVCAR-4	61.97
OVCAR-5	96.76
OVCAR-8	62.97
NCI/ADR-RES	64.75
SK-OV-3	58.45
Renal Cancer	
786-0	52.75
A498	43.43
ACHN	17.64
CAKI-1	17.29
RXF 393	53.16
SN12C	77.45
TK-10	57.91
UO-31	67.04
Prostate Cancer	
PC-3	71.61
DU-145	82.22
Breast Cancer	
MCF7	20.34
MDA-MB-231/ATCC	77.65
HS 578T	93.36
BT-549	43.49
T-47D	61.75
MDA-MB-468	24.31
Mean	55.88
Delta	86.08
Range	130.54

Mean Growth Percent - Growth Percent

150 100 50 0 -50 -100 -150

***tert*-Butyl 12,13-dimethyl-5,7-dioxo-12,13-dihydro-5*H*-pyrido[2,3-*b*]pyrido[3',2':4,5]pyrrolo[3,2-*g*]pyrrolo[3,4-*e*]indole-6(7*H*)-carboxylate (372)**

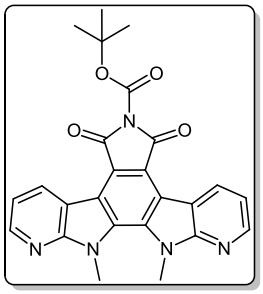

Developmental Therapeutics Program
One Dose Mean Graph

NSC: D-763890 / 1	Conc: 1.00E-5 Molar	Test Date: Feb 27, 2012
Experiment ID: 1202OS23		Report Date: Apr 02, 2012

Panel/Cell Line	Growth Percent
Leukemia	
CCRF-CEM	34.92
HL-60(TB)	102.87
K-562	70.17
MOLT-4	-5.76
RPMI-8226	62.80
SR	1.84
Non-Small Cell Lung Cancer	
A549/ATCC	52.30
EKVX	76.27
HOP-62	55.63
NCI-H226	48.01
NCI-H23	52.17
NCI-H322M	69.00
NCI-H460	14.88
NCI-H522	39.80
Colon Cancer	
COLO 205	68.28
HCC-2998	98.66
HCT-116	50.92
HCT-15	74.15
HT29	46.59
KM12	56.65
SW-620	46.88
CNS Cancer	
SF-268	56.45
SF-295	16.76
SF-539	82.17
SNB-19	74.32
SNB-75	85.29
U251	56.20
Melanoma	
LOX IMVI	49.41
MALME-3M	74.99
M14	71.37
MDA-MB-435	76.54
SK-MEL-2	102.35
SK-MEL-28	89.21
UACC-257	75.02
UACC-62	39.76
Ovarian Cancer	
IGROV1	53.98
OVCAR-3	92.67
OVCAR-4	67.95
OVCAR-5	98.03
OVCAR-8	58.96
NCI/ADR-RES	64.92
SK-OV-3	90.30
Renal Cancer	
786-0	88.11
A498	54.18
ACHN	35.21
CAKI-1	22.73
RXF 393	72.25
SN12C	65.29
TK-10	72.35
UO-31	59.91
Prostate Cancer	
PC-3	59.31
DU-145	81.81
Breast Cancer	
MCF7	24.72
MDA-MB-231/ATCC	81.47
HS 578T	87.28
BT-549	63.37
T-47D	57.07
MDA-MB-468	31.40
Mean	61.21
Delta	66.97
Range	108.63

Mean Growth Percent - Growth Percent

150 100 50 0 -50 -100 -150

6-Hydroxy-12,13-dimethyl-12,13-dihydro-5*H*-pyrido[2,3-*b*]pyrido[3',2':4,5]pyrrolo[3,2-*g*]pyrrolo[3,4-*e*]indole-5,7(6*H*)-dione (373)

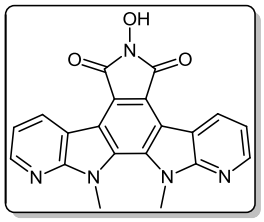

Developmental Therapeutics Program
One Dose Mean Graph

NSC: D-763891 / 1	Conc: 1.00E-5 Molar	Test Date: Feb 27, 2012
Experiment ID: 1202OS23		Report Date: Apr 02, 2012

Panel/Cell Line	Growth Percent
Leukemia	
CCRF-CEM	14.13
HL-60(TB)	14.11
K-562	28.47
MOLT-4	-33.04
RPMI-8226	-3.25
SR	-25.08
Non-Small Cell Lung Cancer	
A549/ATCC	15.15
EKVX	42.79
HOP-62	13.32
HOP-92	2.39
NCI-H23	-14.43
NCI-H322M	23.96
NCI-H460	3.84
NCI-H522	4.92
Colon Cancer	
COLO 205	50.24
HCC-2998	55.72
HCT-116	13.34
HCT-15	52.98
HT29	18.33
KM12	37.98
SW-620	30.31
CNS Cancer	
SF-268	16.65
SF-295	-17.75
SF-539	11.20
SNB-19	29.70
SNB-75	10.33
U251	13.42
Melanoma	
LOX IMVI	0.61
MALME-3M	17.03
M14	5.45
MDA-MB-435	21.21
SK-MEL-2	61.78
SK-MEL-28	43.93
UACC-257	45.27
UACC-62	2.78
Ovarian Cancer	
IGROV1	24.38
OVCAR-3	30.70
OVCAR-4	28.83
OVCAR-5	80.52
OVCAR-8	23.36
NCI/ADR-RES	14.35
SK-OV-3	29.46
Renal Cancer	
786-0	-24.75
A498	49.34
ACHN	8.89
CAKI-1	-6.85
RXF 393	7.28
SN12C	14.42
TK-10	63.42
UO-31	-0.58
Prostate Cancer	
PC-3	38.57
DU-145	6.84
Breast Cancer	
MCF7	5.44
MDA-MB-231/ATCC	67.79
HS 578T	73.04
BT-549	6.25
T-47D	25.25
MDA-MB-468	-14.88
Mean	19.98
Delta	53.02
Range	113.56

Mean Growth Percent - Growth Percent

150 100 50 0 -50 -100 -150

4-(1-Methyl-1*H*-indol-3-yl)-3-(1-methyl-1*H*-pyrrolo[2,3-*b*]pyridin-3-yl)isoxazol-5(2H)-one (327)

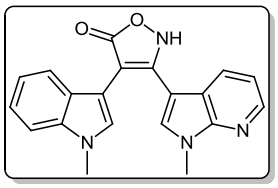

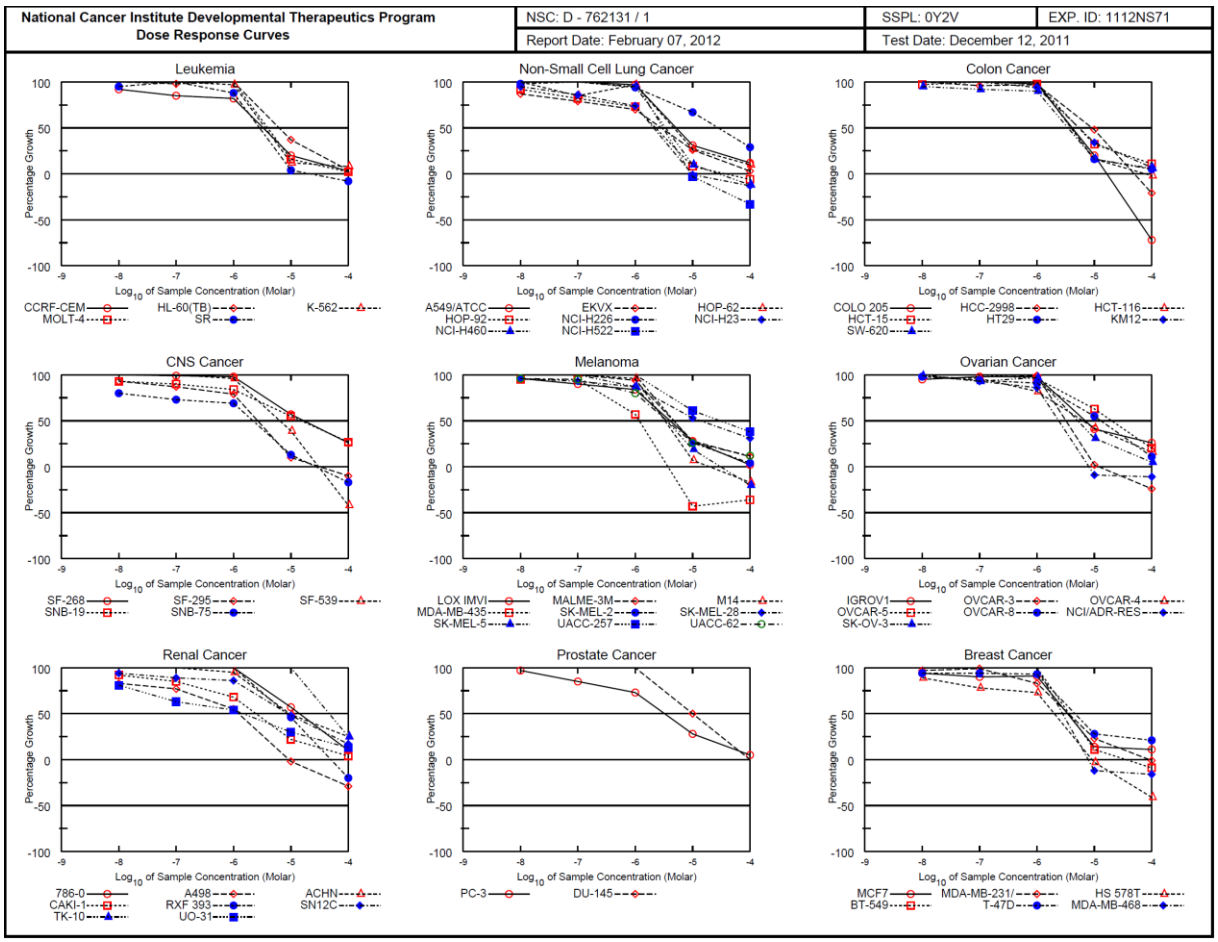

4-(1-Methyl-1*H*-indol-3-yl)-3-(1-methyl-1*H*-pyrrolo[2,3-*b*]pyridin-3-yl)isoxazol-5(2H)-one (327)

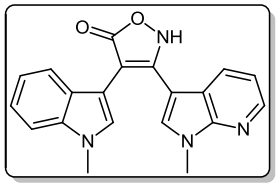

National Cancer Institute Developmental Therapeutics Program
In-Vitro Testing Results

NSC : D - 762131 / 1	Experiment ID : 1112NS71	Test Type : 08	Units : Molar
Report Date : February 07, 2012	Test Date : December 12, 2011	QNS :	MC :
COMI : MC-4-323 (111508)	Stain Reagent : SRB Dual-Pass Related	SSPL : 0Y2V	

		Log10 Concentration												
	Time	Mean Optical Densities						Percent Growth						
Panel/Cell Line	Zero	Ctrl	-8.0	-7.0	-6.0	-5.0	-4.0	-8.0	-7.0	-6.0	-5.0	-4.0	GI50	TGI	LC50
Leukemia															
CCRF-CEM	0.438	2.083	1.955	1.837	1.793	0.767	0.495	92	85	82	20	3	3.30E-6	> 1.00E-4	> 1.00E-4
HL-60(TB)	0.860	2.628	2.692	2.598	2.791	1.512	0.928	104	98	109	37	4	6.58E-6	> 1.00E-4	> 1.00E-4
K-562	0.167	1.390	1.426	1.433	1.350	0.309	0.269	103	103	97	12	8	3.54E-6	> 1.00E-4	> 1.00E-4
MOLT-4	0.461	1.879	1.915	1.998	1.946	0.684	0.492	103	108	105	16	2	4.12E-6	> 1.00E-4	> 1.00E-4
SR	0.316	1.791	1.722	1.813	1.619	0.381	0.290	95	101	88	4	-8	2.86E-6	2.21E-5	> 1.00E-4
Non-Small Cell Lung Cancer															
A549/ATCC	0.314	1.418	1.436	1.435	1.387	0.661	0.443	102	102	97	31	12	5.21E-6	> 1.00E-4	> 1.00E-4
EKVX	0.576	1.239	1.152	1.098	1.041	0.747	0.594	87	79	70	26	3	2.84E-6	> 1.00E-4	> 1.00E-4
HOP-62	0.303	0.691	0.693	0.633	0.681	0.406	0.343	100	85	97	27	10	4.67E-6	> 1.00E-4	> 1.00E-4
HOP-92	0.988	1.386	1.354	1.315	1.277	1.019	0.930	92	82	73	8	-6	2.23E-6	3.68E-5	> 1.00E-4
NCI-H226	0.638	1.272	1.262	1.275	1.232	1.062	0.820	98	101	94	67	29	2.76E-5	> 1.00E-4	> 1.00E-4
NCI-H23	0.861	2.235	2.162	2.049	1.882	0.857	0.749	95	86	74	-1	-13	2.11E-6	9.84E-6	> 1.00E-4
NCI-H460	0.285	2.290	2.291	2.286	2.187	0.492	0.250	100	100	95	10	-12	3.39E-6	2.84E-5	> 1.00E-4
NCI-H522	0.678	1.392	1.488	1.441	1.434	0.656	0.451	113	107	106	-3	-33	3.25E-6	9.32E-6	> 1.00E-4
Colon Cancer															
COLO 205	0.279	0.955	0.999	0.999	0.943	0.411	0.080	106	106	98	20	-72	4.10E-6	1.64E-5	5.80E-5
HCC-2998	0.591	1.600	1.597	1.561	1.572	1.080	0.466	100	96	97	48	-21	9.28E-6	4.97E-5	> 1.00E-4
HCT-116	0.219	1.514	1.527	1.658	1.544	0.430	0.214	101	111	102	16	-2	4.05E-6	7.53E-5	> 1.00E-4
HCT-15	0.292	1.807	1.755	1.844	1.774	0.781	0.459	97	102	98	32	11	5.36E-6	> 1.00E-4	> 1.00E-4
HT29	0.198	1.114	1.167	1.174	1.166	0.345	0.248	106	106	106	16	5	4.17E-6	> 1.00E-4	> 1.00E-4
KM12	0.493	2.032	2.092	2.104	1.943	1.013	0.602	104	105	94	34	7	5.39E-6	> 1.00E-4	> 1.00E-4
SW-620	0.244	1.548	1.482	1.442	1.417	0.451	0.318	95	92	90	16	6	3.46E-6	> 1.00E-4	> 1.00E-4
CNS Cancer															
SF-268	0.496	1.531	1.574	1.521	1.512	1.088	0.766	104	99	98	57	26	1.70E-5	> 1.00E-4	> 1.00E-4
SF-295	0.819	2.664	2.536	2.421	2.269	0.997	0.738	93	87	79	10	-10	2.60E-6	3.10E-5	> 1.00E-4
SF-539	0.695	1.677	1.698	1.681	1.642	1.082	0.403	102	100	96	39	-42	6.51E-6	3.05E-5	> 1.00E-4
SNB-19	0.650	1.873	1.784	1.747	1.675	1.329	0.977	93	90	84	55	27	1.55E-5	> 1.00E-4	> 1.00E-4
SNB-75	0.735	1.285	1.177	1.136	1.112	0.809	0.609	80	73	69	13	-17	2.17E-6	2.74E-5	> 1.00E-4
Melanoma															
LOX IMVI	0.255	1.506	1.456	1.381	1.307	0.600	0.286	96	90	84	28	2	4.00E-6	> 1.00E-4	> 1.00E-4
MALME-3M	0.588	1.793	1.910	1.861	1.717	0.922	0.724	110	106	94	28	11	4.59E-6	> 1.00E-4	> 1.00E-4
M14	0.415	1.237	1.265	1.266	1.202	0.474	0.345	103	103	96	7	-17	3.28E-6	1.99E-5	> 1.00E-4
MDA-MB-435	0.473	1.925	1.848	1.852	1.305	0.272	0.305	95	95	57	-43	-36	1.18E-6	3.75E-6	> 1.00E-4
SK-MEL-2	0.861	1.601	1.705	1.751	1.689	1.054	0.892	114	120	112	26	4	5.26E-6	> 1.00E-4	> 1.00E-4
SK-MEL-28	0.507	1.416	1.381	1.349	1.298	0.987	0.790	96	93	87	53	31	1.34E-5	> 1.00E-4	> 1.00E-4
SK-MEL-5	0.523	2.479	2.578	2.486	2.224	0.902	0.417	105	100	87	19	-20	3.52E-6	3.07E-5	> 1.00E-4
UACC-257	0.550	1.136	1.158	1.180	1.146	0.907	0.774	104	107	102	61	38	3.02E-5	> 1.00E-4	> 1.00E-4
UACC-62	0.579	1.948	1.893	1.884	1.674	0.938	0.739	96	95	80	26	12	3.61E-6	> 1.00E-4	> 1.00E-4
Ovarian Cancer															
IGROV1	0.590	1.284	1.248	1.268	1.269	0.876	0.770	95	98	98	41	26	6.97E-6	> 1.00E-4	> 1.00E-4
OVCAR-3	0.517	1.310	1.345	1.354	1.303	0.536	0.394	104	105	99	2	-24	3.22E-6	1.23E-5	> 1.00E-4
OVCAR-4	0.534	1.141	1.126	1.120	1.029	0.791	0.633	98	96	82	42	16	6.38E-6	> 1.00E-4	> 1.00E-4
OVCAR-5	0.597	1.453	1.454	1.477	1.422	1.134	0.765	100	103	96	63	20	1.97E-5	> 1.00E-4	> 1.00E-4
OVCAR-8	0.417	1.651	1.628	1.573	1.540	1.101	0.548	98	94	91	55	11	1.32E-5	> 1.00E-4	> 1.00E-4
NCI/ADR-RES	0.532	1.678	1.674	1.597	1.513	0.482	0.475	100	93	86	-9	-11	2.37E-6	7.95E-6	> 1.00E-4
SK-OV-3	0.487	1.113	1.110	1.071	1.095	0.680	0.521	99	93	97	31	5	5.13E-6	> 1.00E-4	> 1.00E-4
Renal Cancer															
786-0	0.834	2.220	2.308	2.376	2.260	1.618	0.977	106	111	103	57	10	1.38E-5	> 1.00E-4	> 1.00E-4
A498	1.307	1.744	1.672	1.646	1.548	1.286	0.927	83	77	55	-2	-29	1.23E-6	9.35E-6	> 1.00E-4
ACHN	0.312	1.277	1.302	1.279	1.226	0.789	0.553	103	100	95	49	25	9.71E-6	> 1.00E-4	> 1.00E-4
CAKI-1	0.638	1.856	1.764	1.677	1.470	0.904	0.684	92	85	68	22	4	2.48E-6	> 1.00E-4	> 1.00E-4
RXF 393	0.656	1.086	1.097	1.109	1.100	0.856	0.528	103	105	103	46	-20	8.64E-6	5.06E-5	> 1.00E-4
SN12C	0.466	1.816	1.737	1.661	1.624	1.110	0.691	94	89	86	48	17	8.70E-6	> 1.00E-4	> 1.00E-4
TK-10	0.738	1.246	1.285	1.372	1.512	1.265	0.866	108	125	152	104	25	4.83E-5	> 1.00E-4	> 1.00E-4
UO-31	0.555	1.719	1.493	1.292	1.179	0.901	0.701	81	63	54	30	13	1.42E-6	> 1.00E-4	> 1.00E-4
Prostate Cancer															
PC-3	0.513	1.913	1.870	1.706	1.535	0.906	0.576	97	85	73	28	5	3.25E-6	> 1.00E-4	> 1.00E-4
DU-145	0.381	1.201	1.297	1.266	1.264	0.794	0.381	112	108	108	50	.	1.02E-5	9.94E-5	> 1.00E-4
Breast Cancer															
MCF7	0.268	1.555	1.477	1.430	1.435	0.455	0.408	94	90	91	14	11	3.42E-6	> 1.00E-4	> 1.00E-4
MDA-MB-231/ATCC	0.490	0.995	0.982	0.988	0.910	0.605	0.486	97	99	83	23	-1	3.53E-6	9.23E-5	> 1.00E-4
HS 578T	1.204	1.793	1.726	1.662	1.636	1.166	0.711	89	78	73	-3	-41	2.01E-6	9.08E-6	> 1.00E-4
BT-549	0.840	1.393	1.448	1.531	1.422	0.901	0.767	110	125	105	11	-9	3.85E-6	3.61E-5	> 1.00E-4
T-47D	0.624	1.643	1.581	1.583	1.573	0.912	0.839	94	94	93	28	21	4.61E-6	> 1.00E-4	> 1.00E-4
MDA-MB-468	0.549	0.835	0.847	0.834	0.842	0.483	0.460	104	100	102	-12	-16	2.86E-6	7.84E-6	> 1.00E-4

3-(1-Methyl-1*H*-indol-3-yl)-4-(1-methyl-1*H*-pyrrolo[2,3-*b*]pyridin-3-yl)-1*H*-pyrrole-2,5-dione (357)

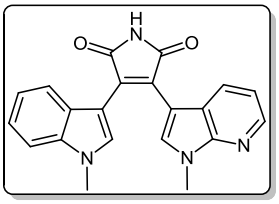

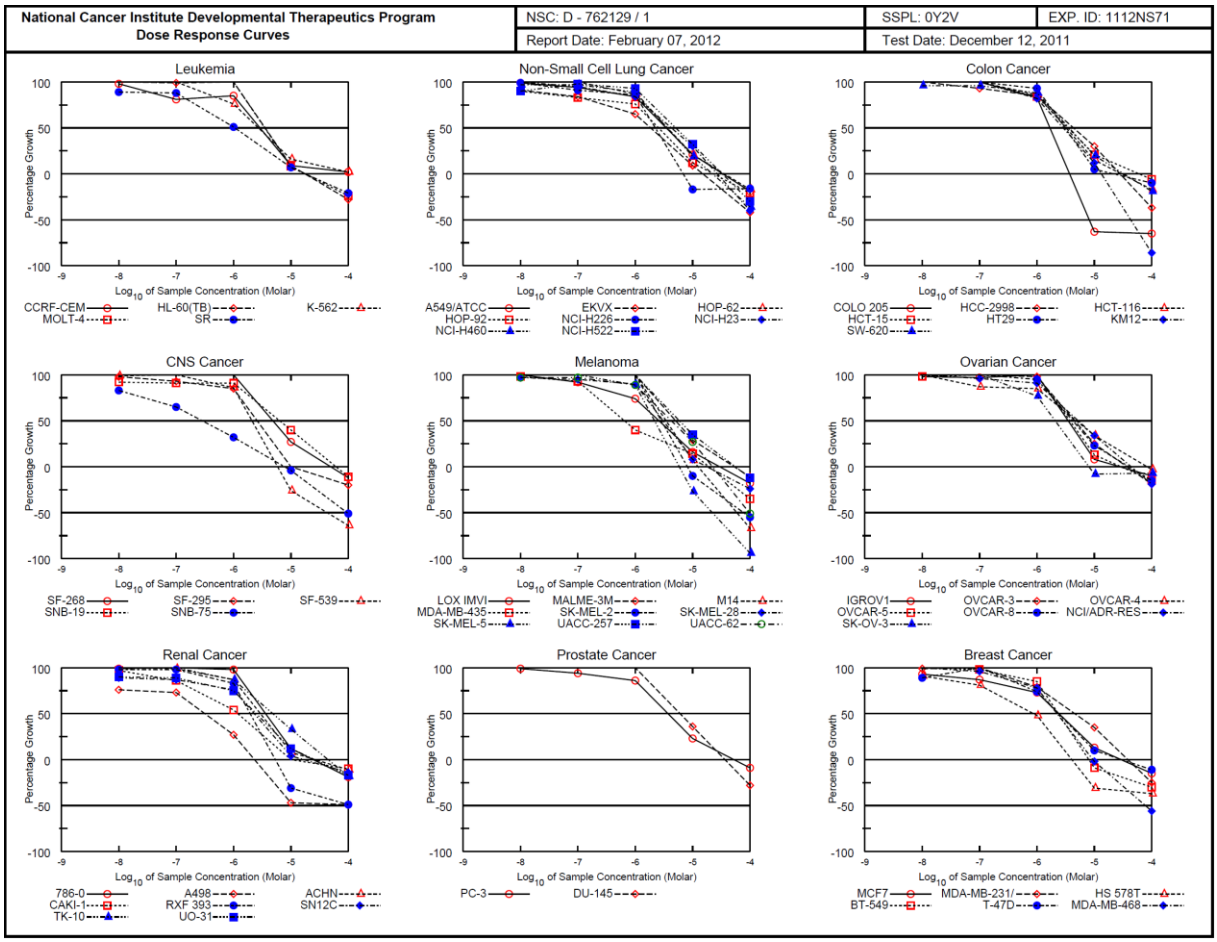

3-(1-Methyl-1*H*-indol-3-yl)-4-(1-methyl-1*H*-pyrrolo[2,3-*b*]pyridin-3-yl)-1*H*-pyrrole-2,5-dione (357)

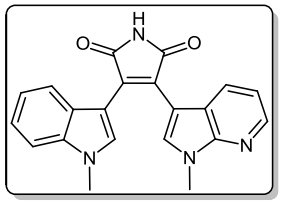

National Cancer Institute Developmental Therapeutics Program
In-Vitro Testing Results

NSC : D - 762129 / 1	Experiment ID : 1112NS71	Test Type : 08	Units : Molar
Report Date : February 07, 2012	Test Date : December 12, 2011	QNS :	MC :
COMI : MC-5-403 (111506)	Stain Reagent : SRB Dual-Pass Related	SSPL : 0Y2V	

		Log10 Concentration												
	Time	Mean Optical Densities					Percent Growth							
Panel/Cell Line	Zero	Ctrl	-8.0	-7.0	-6.0	-5.0	-4.0	-8.0	-7.0	-6.0	-5.0	-4.0	GI50	TGI	LC50
Leukemia															
CCRF-CEM	0.438	1.933	1.902	1.648	1.702	0.573	0.464	98	81	85	9	2	2.86E-6	> 1.00E-4	> 1.00E-4
HL-60(TB)	0.860	2.642	2.743	2.625	2.873	1.026	0.623	106	99	113	9	-28	4.05E-6	1.79E-5	> 1.00E-4
K-562	0.167	1.292	1.386	1.310	1.023	0.352	0.194	108	102	76	16	2	2.74E-6	> 1.00E-4	> 1.00E-4
MOLT-4	0.461	1.720	1.761	1.959	1.735	0.559	0.353	103	119	101	8	-24	3.53E-6	1.77E-5	> 1.00E-4
SR	0.316	1.686	1.537	1.522	1.012	0.419	0.251	89	88	51	7	-21	1.04E-6	1.84E-5	> 1.00E-4
Non-Small Cell Lung Cancer															
A549/ATCC	0.314	1.500	1.484	1.428	1.316	0.563	0.254	99	94	84	21	-19	3.49E-6	3.32E-5	> 1.00E-4
EKVX	0.576	1.264	1.203	1.154	1.021	0.638	0.337	91	84	65	9	-42	1.83E-6	1.51E-5	> 1.00E-4
HOP-62	0.303	0.710	0.751	0.723	0.659	0.390	0.253	110	103	87	21	-17	3.69E-6	3.67E-5	> 1.00E-4
HOP-92	0.988	1.416	1.374	1.341	1.312	1.041	0.781	90	83	76	12	-21	2.54E-6	2.34E-5	> 1.00E-4
NCI-H226	0.638	1.277	1.271	1.222	1.188	0.530	0.538	99	91	86	-17	-16	2.24E-6	6.84E-6	> 1.00E-4
NCI-H23	0.861	2.253	2.254	2.184	2.024	1.273	0.519	100	95	84	30	-40	4.18E-6	2.67E-5	> 1.00E-4
NCI-H460	0.285	2.442	2.382	2.376	2.203	0.695	0.181	97	97	89	19	-36	3.60E-6	2.20E-5	> 1.00E-4
NCI-H522	0.678	1.484	1.405	1.464	1.431	0.933	0.472	90	98	93	32	-30	5.05E-6	3.24E-5	> 1.00E-4
Colon Cancer															
COLO 205	0.279	0.983	1.020	1.049	0.866	0.103	0.099	105	109	83	-63	-65	1.69E-6	3.71E-6	8.14E-6
HCC-2998	0.591	1.664	1.701	1.589	1.508	0.913	0.374	103	93	85	30	-37	4.35E-6	2.82E-5	> 1.00E-4
HCT-116	0.219	1.673	1.767	1.779	1.471	0.443	0.183	106	107	86	15	-17	3.24E-6	3.02E-5	> 1.00E-4
HCT-15	0.292	1.852	1.848	1.891	1.600	0.627	0.275	100	103	84	21	-6	3.49E-6	6.05E-5	> 1.00E-4
HT29	0.198	1.132	1.212	1.202	1.067	0.241	0.178	109	107	93	5	-10	3.07E-6	2.06E-5	> 1.00E-4
KM12	0.493	2.077	2.112	2.111	1.796	0.688	0.071	102	102	82	12	-86	2.89E-6	1.34E-5	4.32E-5
SW-620	0.244	1.645	1.582	1.592	1.475	0.523	0.198	96	96	88	20	-19	3.61E-6	3.26E-5	> 1.00E-4
CNS Cancer															
SF-268	0.496	1.592	1.622	1.609	1.603	0.789	0.435	103	102	101	27	-12	4.86E-6	4.84E-5	> 1.00E-4
SF-295	0.819	2.574	2.536	2.453	2.319	0.824	0.657	98	93	85	.	-20	2.61E-6	1.03E-5	> 1.00E-4
SF-539	0.695	1.802	1.796	1.879	1.645	0.514	0.249	99	107	86	-26	-64	2.09E-6	5.85E-6	4.24E-5
SNB-19	0.650	1.888	1.788	1.780	1.770	1.144	0.580	92	91	91	40	-11	6.31E-6	6.11E-5	> 1.00E-4
SNB-75	0.735	1.273	1.180	1.086	0.909	0.709	0.359	83	65	32	-4	-51	2.91E-7	7.97E-6	9.46E-5
Melanoma															
LOX IMVI	0.255	1.545	1.557	1.443	1.210	0.465	0.210	101	92	74	16	-18	2.61E-6	3.02E-5	> 1.00E-4
MALME-3M	0.588	1.793	1.904	1.935	1.918	0.932	0.523	109	112	110	29	-11	5.47E-6	5.24E-5	> 1.00E-4
M14	0.415	1.307	1.353	1.379	1.399	0.479	0.137	105	108	110	7	-67	3.84E-6	1.25E-5	5.88E-5
MDA-MB-435	0.473	1.989	1.952	1.879	1.081	0.688	0.306	98	93	40	14	-35	6.48E-7	1.93E-5	> 1.00E-4
SK-MEL-2	0.861	1.717	1.796	1.830	1.813	0.776	0.390	109	113	111	-10	-55	3.20E-6	8.28E-6	7.85E-5
SK-MEL-28	0.507	1.407	1.381	1.362	1.314	0.578	0.387	97	95	90	8	-24	3.05E-6	1.77E-5	> 1.00E-4
SK-MEL-5	0.523	2.574	2.616	2.595	2.339	0.380	0.031	102	101	89	-27	-94	2.15E-6	5.80E-6	2.18E-5
UACC-257	0.550	1.235	1.259	1.255	1.314	0.788	0.483	104	103	112	35	-12	6.32E-6	5.48E-5	> 1.00E-4
UACC-62	0.579	1.966	1.926	1.925	1.812	0.949	0.283	97	97	89	27	-51	4.22E-6	2.20E-5	9.67E-5
Ovarian Cancer															
IGROV1	0.590	1.328	1.315	1.309	1.455	0.646	0.533	98	97	117	8	-10	4.10E-6	2.75E-5	> 1.00E-4
OVCAR-3	0.517	1.301	1.358	1.386	1.281	0.711	0.419	107	111	98	25	-19	4.49E-6	3.68E-5	> 1.00E-4
OVCAR-4	0.534	1.124	1.134	1.049	1.034	0.736	0.518	102	87	85	34	-3	4.86E-6	8.31E-5	> 1.00E-4
OVCAR-5	0.597	1.477	1.463	1.498	1.503	0.711	0.508	98	102	103	13	-15	3.88E-6	2.91E-5	> 1.00E-4
OVCAR-8	0.417	1.665	1.732	1.659	1.608	0.703	0.354	105	100	95	23	-15	4.23E-6	3.99E-5	> 1.00E-4
NCI/ADR-RES	0.532	1.743	1.751	1.696	1.633	0.940	0.433	101	96	91	34	-19	5.19E-6	4.40E-5	> 1.00E-4
SK-OV-3	0.487	1.098	1.124	1.108	0.960	0.447	0.453	104	102	77	-8	-7	2.09E-6	8.00E-6	> 1.00E-4
Renal Cancer															
786-0	0.834	2.283	2.268	2.298	2.252	1.003	0.672	99	101	98	12	-19	3.59E-6	2.37E-5	> 1.00E-4
A498	1.307	1.758	1.650	1.637	1.430	0.697	0.668	76	73	27	-47	-49	3.20E-7	2.34E-6	> 1.00E-4
ACHN	0.312	1.314	1.309	1.303	1.183	0.391	0.278	100	99	87	8	-11	2.93E-6	2.62E-5	> 1.00E-4
CAKI-1	0.638	1.927	1.886	1.750	1.336	0.639	0.575	97	86	54	.	-10	1.19E-6	1.02E-5	> 1.00E-4
RXF 393	0.656	1.139	1.128	1.132	1.059	0.450	0.332	98	98	83	-31	-49	1.95E-6	5.32E-6	> 1.00E-4
SN12C	0.466	1.876	1.716	1.687	1.543	0.519	0.400	89	87	76	4	-14	2.31E-6	1.62E-5	> 1.00E-4
TK-10	0.738	1.335	1.338	1.367	1.256	0.935	0.603	100	105	87	33	-18	4.82E-6	4.39E-5	> 1.00E-4
UO-31	0.555	1.746	1.630	1.614	1.444	0.693	0.460	90	89	75	12	-17	2.46E-6	2.53E-5	> 1.00E-4
Prostate Cancer															
PC-3	0.513	1.934	1.923	1.853	1.739	0.836	0.469	99	94	86	23	-9	3.72E-6	5.29E-5	> 1.00E-4
DU-145	0.381	1.273	1.333	1.286	1.308	0.703	0.273	107	102	104	36	-28	6.24E-6	3.62E-5	> 1.00E-4
Breast Cancer															
MCF7	0.268	1.525	1.443	1.367	1.182	0.433	0.229	93	87	73	13	-15	2.40E-6	2.95E-5	> 1.00E-4
MDA-MB-231/ATCC	0.490	1.019	1.012	1.042	0.911	0.678	0.369	99	104	79	35	-25	4.67E-6	3.88E-5	> 1.00E-4
HS 578T	1.204	1.894	1.834	1.762	1.533	0.835	0.760	91	81	48	-31	-37	8.47E-7	4.06E-6	> 1.00E-4
BT-549	0.840	1.497	1.563	1.485	1.397	0.768	0.586	110	98	85	-9	-30	2.36E-6	8.09E-6	> 1.00E-4
T-47D	0.624	1.603	1.499	1.602	1.345	0.726	0.554	89	100	74	10	-11	2.37E-6	3.03E-5	> 1.00E-4
MDA-MB-468	0.549	0.846	0.850	0.834	0.779	0.539	0.239	101	96	78	-2	-56	2.22E-6	9.46E-6	7.61E-5

3,4-Bis(1-methyl-1*H*-pyrrolo[2,3-*b*]pyridin-3-yl)-1*H*-pyrrole-2,5-dione (361)

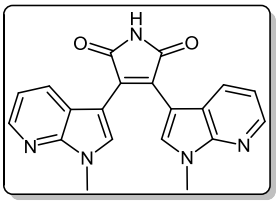

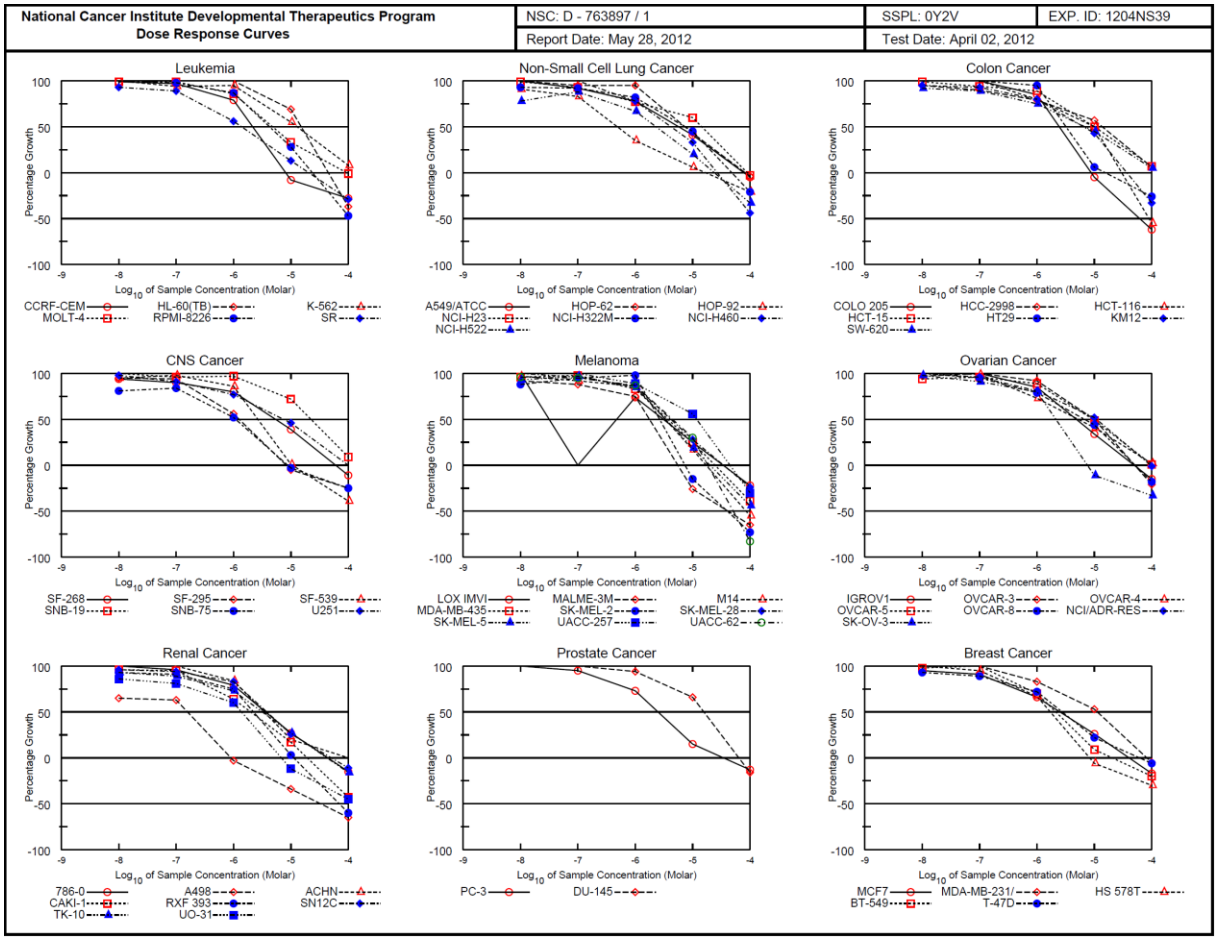

3,4-Bis(1-methyl-1*H*-pyrrolo[2,3-*b*]pyridin-3-yl)-1*H*-pyrrole-2,5-dione (361)

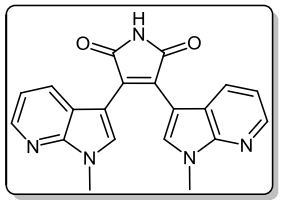

National Cancer Institute Developmental Therapeutics Program
In-Vitro Testing Results

NSC : D - 763897 / 1	Experiment ID : 1204NS39	Test Type : 08	Units : Molar
Report Date : May 28, 2012	Test Date : April 02, 2012	QNS :	MC :
COMI : MC-5-453 (115199)	Stain Reagent : SRB Dual-Pass Related	SSPL : 0Y2V	

		Log10 Concentration												
	Time	Mean Optical Densities						Percent Growth						
Panel/Cell Line	Zero	Ctrl	-8.0	-7.0	-6.0	-5.0	-4.0	-8.0	-7.0	-6.0	-5.0	-4.0	GI50	TGI	LC50
Leukemia															
CCRF-CEM	0.689	2.472	2.454	2.414	2.090	0.637	0.495	99	97	79	-8	-28	2.15E-6	8.16E-6	> 1.00E-4
HL-60(TB)	0.706	2.289	2.472	2.456	2.294	1.792	0.448	112	111	100	69	-37	1.50E-5	4.49E-5	> 1.00E-4
K-562	0.231	1.530	1.537	1.458	1.471	0.945	0.339	100	94	95	55	8	1.28E-5	> 1.00E-4	> 1.00E-4
MOLT-4	0.551	2.032	2.023	2.018	1.819	1.038	0.545	99	99	86	33	-1	4.74E-6	9.29E-5	> 1.00E-4
RPMI-8226	0.724	1.956	1.980	1.934	1.792	1.065	0.386	102	98	87	28	-47	4.18E-6	2.36E-5	> 1.00E-4
SR	0.385	1.373	1.305	1.264	0.940	0.514	0.275	93	89	56	13	-29	1.39E-6	2.06E-5	> 1.00E-4
Non-Small Cell Lung Cancer															
A549/ATCC	0.330	1.502	1.559	1.414	1.245	0.805	0.315	105	92	78	41	-5	5.59E-6	7.93E-5	> 1.00E-4
HOP-62	0.375	1.223	1.233	1.179	1.182	0.738	0.361	101	95	95	43	-4	7.29E-6	8.26E-5	> 1.00E-4
HOP-92	0.898	1.467	1.418	1.368	1.096	0.934	0.707	91	83	35	6	-21	4.80E-7	1.70E-5	> 1.00E-4
NCI-H23	0.511	1.948	1.934	1.843	1.619	1.367	0.496	99	93	77	60	-3	1.42E-5	8.97E-5	> 1.00E-4
NCI-H322M	0.725	1.391	1.344	1.339	1.273	1.023	0.575	93	92	82	45	-21	7.24E-6	4.82E-5	> 1.00E-4
NCI-H460	0.231	2.091	2.105	2.129	1.689	0.844	0.130	101	102	78	33	-44	4.21E-6	2.69E-5	> 1.00E-4
NCI-H522	0.607	1.149	1.027	1.081	0.972	0.714	0.408	78	88	67	20	-33	2.31E-6	2.38E-5	> 1.00E-4
Colon Cancer															
COLO 205	0.259	1.108	1.118	1.104	0.984	0.247	0.098	101	100	85	-5	-62	2.47E-6	8.84E-6	6.10E-5
HCC-2998	0.333	1.371	1.319	1.272	1.156	0.928	0.397	95	90	79	57	6	1.39E-5	> 1.00E-4	> 1.00E-4
HCT-116	0.175	1.645	1.657	1.642	1.358	0.917	0.079	101	100	80	50	-55	1.01E-5	3.01E-5	8.94E-5
HCT-15	0.213	1.717	1.704	1.630	1.549	0.969	0.313	99	94	89	50	7	1.01E-5	> 1.00E-4	> 1.00E-4
HT29	0.221	1.068	1.094	1.088	1.027	0.273	0.163	103	102	95	6	-26	3.22E-6	1.54E-5	> 1.00E-4
KM12	0.468	2.141	2.058	2.023	1.802	1.192	0.316	95	93	80	43	-33	6.53E-6	3.72E-5	> 1.00E-4
SW-620	0.285	1.866	1.744	1.688	1.475	0.994	0.366	92	89	75	45	5	6.76E-6	> 1.00E-4	> 1.00E-4
CNS Cancer															
SF-268	0.608	1.909	1.830	1.780	1.652	1.113	0.540	94	90	80	39	-11	5.37E-6	5.98E-5	> 1.00E-4
SF-295	0.771	2.306	2.223	2.218	1.625	0.733	0.576	95	94	56	-5	-25	1.24E-6	8.27E-6	> 1.00E-4
SF-539	0.601	1.943	1.875	1.914	1.750	0.617	0.367	95	98	86	1	-39	2.64E-6	1.07E-5	> 1.00E-4
SNB-19	0.462	1.305	1.348	1.267	1.283	1.070	0.534	105	96	97	72	9	2.23E-5	> 1.00E-4	> 1.00E-4
SNB-75	0.820	1.654	1.497	1.517	1.257	0.796	0.614	81	84	52	-3	-25	1.10E-6	8.83E-6	> 1.00E-4
U251	0.365	1.711	1.687	1.595	1.407	0.979	0.365	98	91	77	46	.	7.29E-6	> 1.00E-4	> 1.00E-4
Melanoma															
LOX IMVI	0.171	1.315	1.321	.	1.014	0.462	0.133	100	.	74	25	-22	3.10E-6	3.42E-5	> 1.00E-4
MALME-3M	0.674	1.182	1.142	1.123	1.055	0.497	0.233	92	88	75	-26	-65	1.77E-6	5.51E-6	4.04E-5
M14	0.422	1.684	1.652	1.589	1.504	0.633	0.189	97	92	86	17	-55	3.29E-6	1.71E-5	8.46E-5
MDA-MB-435	0.403	1.498	1.454	1.472	1.313	0.674	0.245	96	98	83	25	-39	3.69E-6	2.44E-5	> 1.00E-4
SK-MEL-2	0.883	1.484	1.414	1.452	1.473	0.755	0.237	88	95	98	-15	-73	2.68E-6	7.43E-6	4.02E-5
SK-MEL-28	0.527	1.450	1.446	1.412	1.322	0.789	0.399	100	96	86	28	-24	4.22E-6	3.45E-5	> 1.00E-4
SK-MEL-5	0.400	2.163	2.039	2.102	1.892	0.728	0.223	93	97	85	19	-44	3.35E-6	1.97E-5	> 1.00E-4
UACC-257	0.969	1.849	1.911	1.848	1.755	1.463	0.676	107	100	89	56	-30	1.18E-5	4.47E-5	> 1.00E-4
UACC-62	0.666	2.250	2.180	2.174	2.042	1.134	0.117	96	95	87	30	-83	4.39E-6	1.84E-5	5.13E-5
Ovarian Cancer															
IGROV1	0.561	1.603	1.614	1.663	1.444	0.914	0.475	101	106	85	34	-15	4.82E-6	4.87E-5	> 1.00E-4
OVCAR-3	0.507	1.537	1.509	1.541	1.454	1.024	0.403	97	100	92	50	-21	1.01E-5	5.13E-5	> 1.00E-4
OVCAR-4	0.548	1.340	1.345	1.331	1.126	0.874	0.567	101	99	73	41	2	5.25E-6	> 1.00E-4	> 1.00E-4
OVCAR-5	0.437	1.376	1.320	1.335	1.272	0.896	0.447	94	96	89	49	1	9.36E-6	> 1.00E-4	> 1.00E-4
OVCAR-8	0.429	1.579	1.592	1.524	1.335	0.940	0.350	101	95	79	44	-18	6.88E-6	5.09E-5	> 1.00E-4
NCI/ADR-RES	0.418	1.637	1.632	1.583	1.411	1.047	0.415	100	96	81	52	-1	1.07E-5	9.64E-5	> 1.00E-4
SK-OV-3	0.558	1.238	1.227	1.176	1.099	0.499	0.376	98	91	80	-11	-33	2.13E-6	7.62E-6	> 1.00E-4
Renal Cancer															
786-0	0.585	2.251	2.257	2.178	1.903	1.030	0.498	100	96	79	27	-15	3.59E-6	4.39E-5	> 1.00E-4
A498	1.160	1.785	1.566	1.554	1.121	0.764	0.412	65	63	-3	-34	-65	1.57E-7	8.89E-7	3.32E-5
ACHN	0.296	1.450	1.462	1.449	1.265	0.531	0.296	101	100	84	20	.	3.41E-6	9.81E-5	> 1.00E-4
CAKI-1	0.821	2.214	2.153	2.143	1.714	1.053	0.469	96	95	64	17	-43	1.98E-6	1.90E-5	> 1.00E-4
RXF 393	0.637	1.121	1.087	1.076	1.001	0.654	0.254	93	91	75	3	-60	2.25E-6	1.13E-5	6.91E-5
SN12C	0.510	1.973	1.908	1.880	1.723	0.895	0.453	96	94	83	26	-11	3.81E-6	5.03E-5	> 1.00E-4
TK-10	0.562	1.142	1.103	1.076	0.987	0.719	0.471	93	89	73	27	-16	3.18E-6	4.22E-5	> 1.00E-4
UO-31	0.615	1.496	1.376	1.328	1.144	0.539	0.341	86	81	60	-12	-45	1.37E-6	6.75E-6	> 1.00E-4
Prostate Cancer															
PC-3	0.441	1.802	1.802	1.729	1.433	0.647	0.383	100	95	73	15	-13	2.49E-6	3.42E-5	> 1.00E-4
DU-145	0.350	1.317	1.321	1.330	1.257	0.990	0.294	100	101	94	66	-16	1.57E-5	6.37E-5	> 1.00E-4
Breast Cancer															
MCF7	0.384	2.058	1.970	1.906	1.495	0.825	0.319	95	91	66	26	-17	2.56E-6	4.05E-5	> 1.00E-4
MDA-MB-231/ATCC	0.549	1.374	1.403	1.402	1.238	0.990	0.521	103	103	83	53	-5	1.14E-5	8.15E-5	> 1.00E-4
HS 578T	0.834	1.755	1.763	1.708	1.450	0.786	0.587	101	95	67	-6	-30	1.71E-6	8.33E-6	> 1.00E-4
BT-549	0.827	1.755	1.738	1.771	1.479	0.907	0.662	98	102	70	9	-20	2.13E-6	2.00E-5	> 1.00E-4
T-47D	0.689	1.644	1.580	1.536	1.380	0.898	0.646	93	89	72	22	-6	2.77E-6	6.00E-5	> 1.00E-4

12,13-Dimethyl-12,13-dihydro-5*H*-pyrido[3',2':4,5]pyrrolo[2,3-*a*]pyrrolo[3,4-*c*]carbazole-5,7(6*H*)-dione (364)

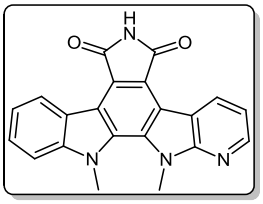

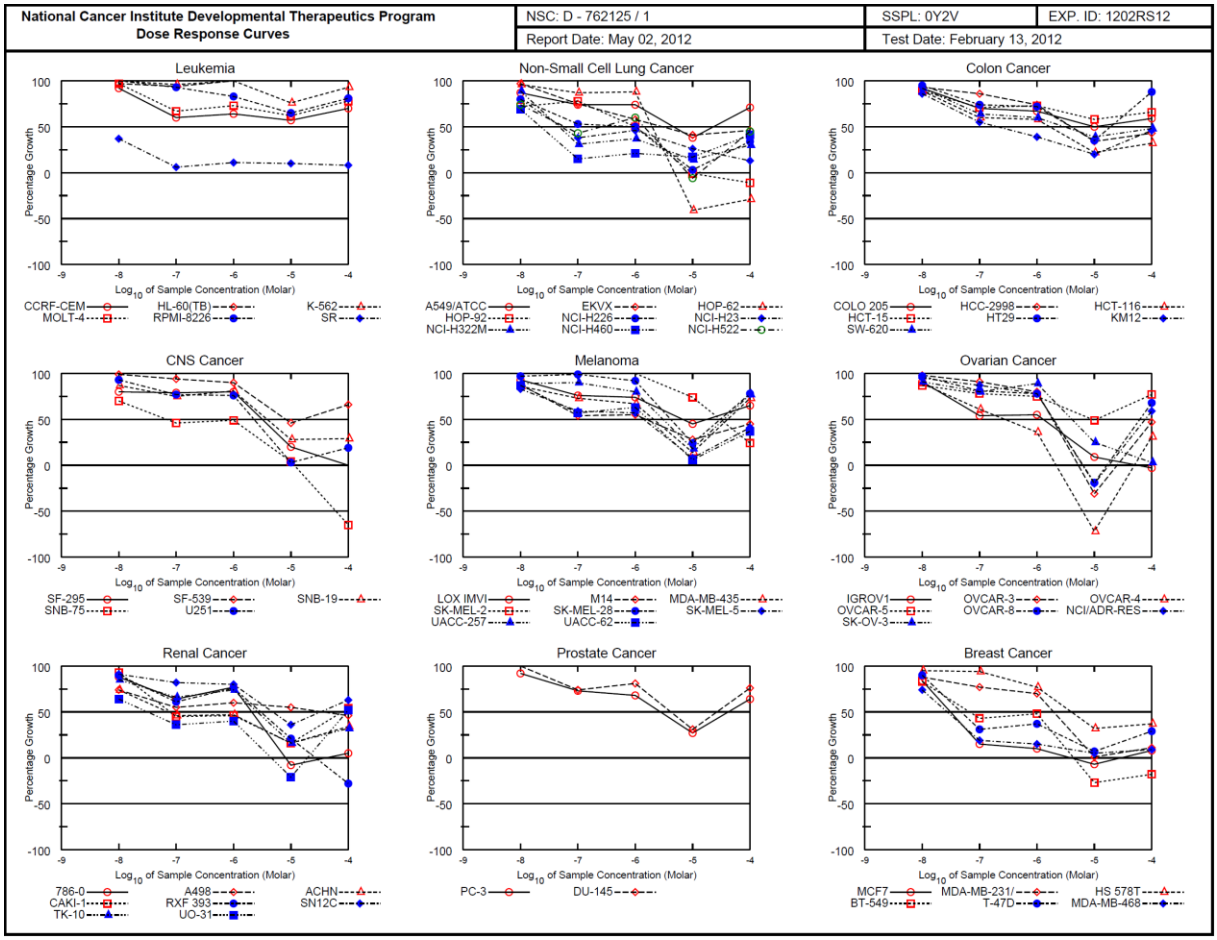

12,13-Dimethyl-12,13-dihydro-5*H*-pyrido[3',2':4,5]pyrrolo[2,3-*a*]pyrrolo[3,4-*c*]carbazole-5,7(6*H*)-dione (364)

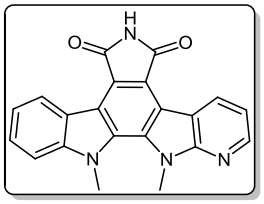

National Cancer Institute Developmental Therapeutics Program
In-Vitro Testing Results

NSC : D - 762125 / 1	Experiment ID : 1202RS12	Test Type : 08	Units : Molar
Report Date : May 02, 2012	Test Date : February 13, 2012	QNS :	MC :
COMI : MC-5-406 (111451)	Stain Reagent : SRB Dual-Pass Related	SSPL : 0Y2V	

			Log10 Concentration											
	Time		Mean Optical Densities					Percent Growth						
Panel/Cell Line	Zero	Ctrl	-8.0	-7.0	-6.0	-5.0	-4.0	-8.0	-7.0	-6.0	-5.0	-4.0	GI50	TGI	LC50
Leukemia															
CCRF-CEM	0.336	1.586	1.488	1.087	1.136	1.044	1.217	92	60	64	57	70	> 1.00E-4	> 1.00E-4	> 1.00E-4
HL-60(TB)	1.226	2.606	2.567	2.517	2.745	2.832	2.771	97	94	110	116	112	> 1.00E-4	> 1.00E-4	> 1.00E-4
K-562	0.402	1.938	2.050	1.877	2.008	1.577	1.834	107	96	105	76	93	> 1.00E-4	> 1.00E-4	> 1.00E-4
MOLT-4	0.745	2.310	2.266	1.789	1.895	1.716	1.969	97	67	73	62	78	> 1.00E-4	> 1.00E-4	> 1.00E-4
RPMI-8226	1.190	2.729	2.726	2.625	2.467	2.195	2.433	100	93	83	65	81	> 1.00E-4	> 1.00E-4	> 1.00E-4
SR	0.361	1.239	0.687	0.417	0.455	0.453	0.431	37	6	11	10	8	< 1.00E-8	> 1.00E-4	> 1.00E-4
Non-Small Cell Lung Cancer															
A549/ATCC	0.400	1.597	1.444	1.287	1.287	0.854	1.249	87	74	74	38	71	.	> 1.00E-4	> 1.00E-4
EKVX	0.953	1.929	1.898	1.683	1.519	1.358	1.404	97	75	58	41	46	3.03E-6	> 1.00E-4	> 1.00E-4
HOP-62	0.284	0.774	0.755	0.709	0.714	0.168	0.201	96	87	88	-41	-29	1.96E-6	4.81E-6	> 1.00E-4
HOP-92	1.091	1.455	1.353	1.375	1.275	1.080	0.975	72	78	50	-1	-11	1.02E-6	9.54E-6	> 1.00E-4
NCI-H226	0.796	1.634	1.463	1.238	1.211	0.822	1.084	80	53	50	3	34	7.11E-7	> 1.00E-4	> 1.00E-4
NCI-H23	0.505	1.394	1.214	0.844	0.912	0.738	0.620	80	38	46	26	13	5.18E-8	> 1.00E-4	> 1.00E-4
NCI-H322M	0.665	1.293	1.225	0.861	0.896	0.755	0.851	89	31	37	14	30	4.73E-8	> 1.00E-4	> 1.00E-4
NCI-H460	0.251	2.201	1.604	0.536	0.652	0.574	1.054	69	15	21	17	41	2.26E-8	> 1.00E-4	> 1.00E-4
NCI-H522	0.660	1.358	1.176	0.958	1.076	0.621	0.976	74	43	60	-6	45	.	.	> 1.00E-4
Colon Cancer															
COLO 205	0.381	1.579	1.488	1.214	1.186	0.975	1.091	92	70	67	50	59	.	> 1.00E-4	> 1.00E-4
HCC-2998	0.568	1.838	1.748	1.665	1.510	1.005	1.112	93	86	74	34	43	4.04E-6	> 1.00E-4	> 1.00E-4
HCT-116	0.200	1.429	1.290	0.935	0.918	0.471	0.595	89	60	58	22	32	1.70E-6	> 1.00E-4	> 1.00E-4
HCT-15	0.345	1.927	1.749	1.463	1.501	1.262	1.385	89	71	73	58	66	> 1.00E-4	> 1.00E-4	> 1.00E-4
HT29	0.195	1.018	0.976	0.801	0.785	0.487	0.916	95	74	72	35	88	.	> 1.00E-4	> 1.00E-4
KM12	0.463	1.795	1.610	1.195	0.977	0.734	1.070	86	55	39	20	46	2.01E-7	> 1.00E-4	> 1.00E-4
SW-620	0.291	1.710	1.595	1.205	1.147	0.841	0.975	92	64	60	39	48	3.01E-6	> 1.00E-4	> 1.00E-4
CNS Cancer															
SF-295	0.521	1.438	1.257	1.244	1.254	0.700	0.522	80	79	80	20	.	3.13E-6	> 1.00E-4	> 1.00E-4
SF-539	0.782	2.051	2.034	1.978	1.928	1.371	1.626	99	94	90	46	66	.	> 1.00E-4	> 1.00E-4
SNB-19	0.623	1.893	1.725	1.581	1.653	0.982	0.987	87	75	81	28	29	3.88E-6	> 1.00E-4	> 1.00E-4
SNB-75	0.647	1.213	1.042	0.906	0.926	0.668	0.230	70	46	49	4	-65	6.65E-8	1.13E-5	6.12E-5
U251	0.269	1.088	1.029	0.897	0.888	0.290	0.423	93	77	76	3	19	2.24E-6	> 1.00E-4	> 1.00E-4
Melanoma															
LOX IMVI	0.293	1.932	1.821	1.532	1.508	1.038	1.359	93	76	74	45	65	.	> 1.00E-4	> 1.00E-4
M14	0.351	1.300	1.186	0.866	0.871	0.621	0.775	88	54	55	28	45	1.52E-6	> 1.00E-4	> 1.00E-4
MDA-MB-435	0.420	1.724	1.543	1.366	1.291	0.596	1.366	86	73	67	14	73	.	> 1.00E-4	> 1.00E-4
SK-MEL-2	0.597	0.935	0.951	0.946	0.979	0.847	0.677	105	103	113	74	24	2.99E-5	> 1.00E-4	> 1.00E-4
SK-MEL-28	0.505	1.354	1.329	1.345	1.287	0.706	1.166	97	99	92	24	78	.	> 1.00E-4	> 1.00E-4
SK-MEL-5	0.390	1.339	1.180	0.951	0.930	0.468	0.783	83	59	57	8	41	1.39E-6	> 1.00E-4	> 1.00E-4
UACC-257	0.718	1.414	1.341	1.348	1.275	0.846	1.254	89	90	80	18	77	.	> 1.00E-4	> 1.00E-4
UACC-62	0.576	2.029	1.836	1.400	1.487	0.659	1.109	87	57	63	6	37	1.67E-6	> 1.00E-4	> 1.00E-4
Ovarian Cancer															
IGROV1	0.644	1.576	1.490	1.147	1.157	0.728	0.622	91	54	55	9	-3	1.29E-6	5.26E-5	> 1.00E-4
OVCAR-3	0.456	1.192	1.181	1.126	1.046	0.315	0.805	98	91	80	-31	47	1.87E-6	.	> 1.00E-4
OVCAR-4	0.494	1.058	0.996	0.839	0.696	0.140	0.671	89	61	36	-72	31	2.74E-7	.	.
OVCAR-5	0.746	1.647	1.534	1.450	1.424	1.191	1.438	87	78	75	49	77	.	> 1.00E-4	> 1.00E-4
OVCAR-8	0.321	1.218	1.190	1.050	1.017	0.259	0.935	97	81	78	-19	68	.	.	> 1.00E-4
NCI/ADR-RES	0.431	1.401	1.353	1.279	1.189	0.346	1.008	95	87	78	-20	59	.	.	> 1.00E-4
SK-OV-3	0.452	1.058	1.003	0.936	0.994	0.605	0.468	91	80	89	25	3	4.10E-6	> 1.00E-4	> 1.00E-4
Renal Cancer															
786-0	0.527	1.955	1.782	1.440	1.631	0.486	0.597	88	64	77	-8	5	2.09E-6	.	> 1.00E-4
A498	1.374	2.179	1.968	1.818	1.854	1.814	1.745	74	55	60	55	46	3.48E-5	> 1.00E-4	> 1.00E-4
ACHN	0.353	1.342	1.082	0.806	0.814	0.512	0.689	74	46	47	16	34	7.06E-8	> 1.00E-4	> 1.00E-4
CAKI-1	0.704	2.047	1.947	1.309	1.325	0.913	1.428	93	45	46	16	54	.	> 1.00E-4	> 1.00E-4
RXF 393	0.556	0.973	0.933	0.809	0.875	0.645	0.403	90	61	76	21	-28	3.02E-6	2.72E-5	> 1.00E-4
SN12C	0.807	2.712	2.547	2.375	2.327	1.495	2.001	91	82	80	36	63	.	> 1.00E-4	> 1.00E-4
TK-10	0.654	1.414	1.302	1.158	1.220	0.779	0.896	85	66	74	16	32	2.64E-6	> 1.00E-4	> 1.00E-4
UO-31	0.622	1.395	1.119	0.899	0.932	0.489	1.028	64	36	40	-21	52	.	.	> 1.00E-4
Prostate Cancer															
PC-3	0.670	1.897	1.793	1.560	1.498	0.997	1.459	92	73	68	27	64	.	> 1.00E-4	> 1.00E-4
DU-145	0.377	1.240	1.243	1.019	1.072	0.648	1.037	100	74	81	31	76	.	> 1.00E-4	> 1.00E-4
Breast Cancer															
MCF7	0.308	1.559	1.359	0.493	0.432	0.286	0.407	84	15	10	-7	8	3.10E-8	.	> 1.00E-4
MDA-MB-231/ATCC	0.540	1.411	1.307	1.213	1.148	0.547	0.639	88	77	70	1	11	1.94E-6	> 1.00E-4	> 1.00E-4
HS 578T	0.865	1.744	1.698	1.693	1.546	1.149	1.187	95	94	77	32	37	4.05E-6	> 1.00E-4	> 1.00E-4
BT-549	0.680	1.433	1.303	1.003	1.039	0.494	0.558	83	43	48	-27	-18	6.61E-8	4.32E-6	> 1.00E-4
T-47D	0.701	1.451	1.375	0.931	0.982	0.752	0.916	90	31	37	7	29	4.71E-8	> 1.00E-4	> 1.00E-4
MDA-MB-468	0.573	1.075	0.947	0.667	0.650	0.598	0.620	74	19	15	5	9	2.74E-8	> 1.00E-4	> 1.00E-4

6-Hydroxy-12,13-dimethyl-12,13-dihydro-5*H*-pyrido[3',2':4,5]pyrrolo[2,3-*a*]pyrrolo[3,4-*c*]carbazole-5,7(6*H*)-dione (363)

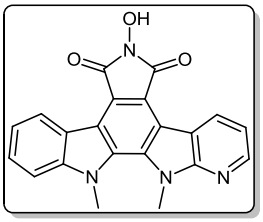

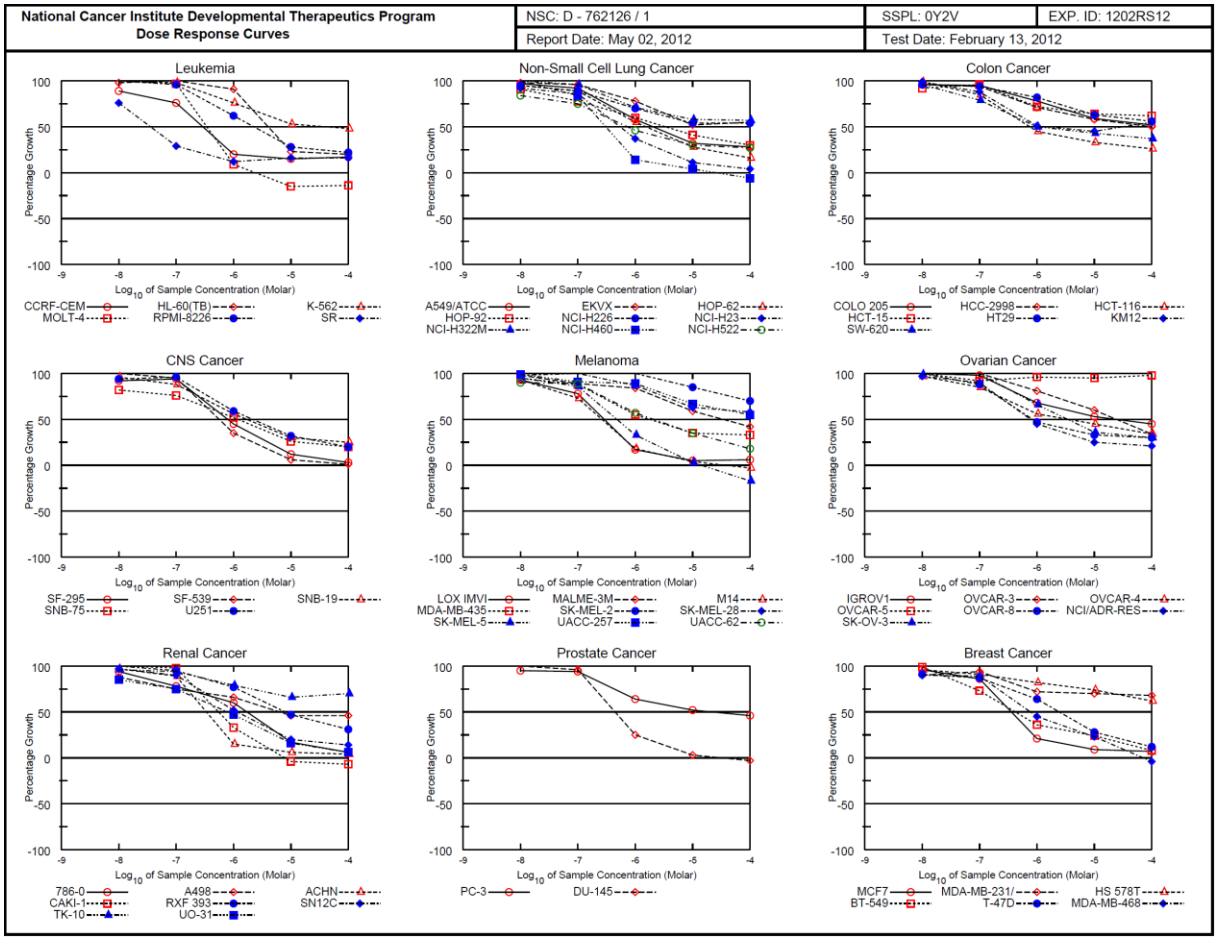

6-Hydroxy-12,13-dimethyl-12,13-dihydro-5*H*-pyrido[3',2':4,5]pyrrolo[2,3-*a*]pyrrolo[3,4-*c*]carbazole-5,7(6*H*)-dione (363)

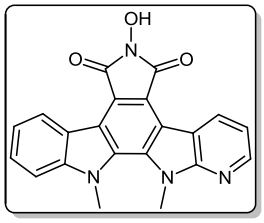

National Cancer Institute Developmental Therapeutics Program
In-Vitro Testing Results

NSC : D - 762126 / 1	Experiment ID : 1202RS12	Test Type : 08	Units : Molar
Report Date : May 02, 2012	Test Date : February 13, 2012	QNS :	MC :
COMI : MC-5-431 (111452)	Stain Reagent : SRB Dual-Pass Related	SSPL : 0Y2V	

			Log10 Concentration											
	Time		Mean Optical Densities					Percent Growth						
Panel/Cell Line	Zero	Ctrl	-8.0	-7.0	-6.0	-5.0	-4.0	-8.0	-7.0	-6.0	-5.0	-4.0	GI50	TGI	LC50
Leukemia															
CCRF-CEM	0.336	1.660	1.513	1.336	0.607	0.535	0.564	89	76	20	15	17	2.91E-7	> 1.00E-4	> 1.00E-4
HL-60(TB)	1.226	2.737	2.703	2.760	2.598	1.566	1.536	98	102	91	23	20	3.96E-6	> 1.00E-4	> 1.00E-4
K-562	0.402	2.212	2.256	2.183	1.769	1.356	1.272	102	98	76	53	48	3.81E-5	> 1.00E-4	> 1.00E-4
MOLT-4	0.745	2.495	2.512	2.444	0.898	0.634	0.640	101	97	9	-15	-14	3.41E-7	2.33E-6	> 1.00E-4
RPMI-8226	1.190	2.733	2.729	2.665	2.148	1.624	1.532	100	96	62	28	22	2.27E-6	> 1.00E-4	> 1.00E-4
SR	0.361	1.329	1.094	0.640	0.474	0.515	0.516	76	29	12	16	16	3.53E-8	> 1.00E-4	> 1.00E-4
Non-Small Cell Lung Cancer															
A549/ATCC	0.400	1.778	1.740	1.669	1.198	0.843	0.783	97	92	58	32	28	2.02E-6	> 1.00E-4	> 1.00E-4
EKVX	0.953	2.083	2.057	2.038	1.835	1.544	1.576	98	96	78	52	55	> 1.00E-4	> 1.00E-4	> 1.00E-4
HOP-62	0.284	0.856	0.827	0.796	0.600	0.446	0.373	95	89	55	28	16	1.56E-6	> 1.00E-4	> 1.00E-4
HOP-92	1.091	1.555	1.514	1.454	1.372	1.282	1.228	91	78	60	41	30	3.49E-6	> 1.00E-4	> 1.00E-4
NCI-H226	0.796	1.774	1.729	1.671	1.482	1.326	1.321	95	89	70	54	54	> 1.00E-4	> 1.00E-4	> 1.00E-4
NCI-H23	0.505	1.499	1.424	1.358	0.872	0.611	0.545	92	86	37	11	4	5.40E-7	> 1.00E-4	> 1.00E-4
NCI-H322M	0.665	1.521	1.532	1.487	1.276	1.158	1.156	101	96	71	58	57	> 1.00E-4	> 1.00E-4	> 1.00E-4
NCI-H460	0.251	2.157	2.151	1.857	0.513	0.328	0.237	100	84	14	4	-6	3.06E-7	2.57E-5	> 1.00E-4
NCI-H522	0.660	1.497	1.361	1.292	1.048	0.908	0.890	84	75	46	30	27	7.45E-7	> 1.00E-4	> 1.00E-4
Colon Cancer															
COLO 205	0.381	1.638	1.592	1.581	1.362	1.120	1.034	96	95	78	59	52	> 1.00E-4	> 1.00E-4	> 1.00E-4
HCC-2998	0.568	1.776	1.731	1.703	1.431	1.271	1.168	96	94	71	58	50	9.11E-5	> 1.00E-4	> 1.00E-4
HCT-116	0.200	1.551	1.538	1.349	0.810	0.648	0.551	99	85	45	33	26	7.55E-7	> 1.00E-4	> 1.00E-4
HCT-15	0.345	1.991	1.867	1.924	1.528	1.400	1.359	92	96	72	64	62	> 1.00E-4	> 1.00E-4	> 1.00E-4
HT29	0.195	1.122	1.083	1.066	0.955	0.779	0.715	96	94	82	63	56	> 1.00E-4	> 1.00E-4	> 1.00E-4
KM12	0.463	1.928	1.907	1.750	1.205	1.128	1.268	99	88	51	45	55	.	> 1.00E-4	> 1.00E-4
SW-620	0.291	1.698	1.648	1.396	0.995	0.890	0.816	96	79	50	43	37	1.01E-6	> 1.00E-4	> 1.00E-4
CNS Cancer															
SF-295	0.521	1.441	1.364	1.382	0.933	0.629	0.550	92	94	45	12	3	7.82E-7	> 1.00E-4	> 1.00E-4
SF-539	0.782	2.098	2.139	2.028	1.241	0.860	0.793	103	95	35	6	1	5.59E-7	> 1.00E-4	> 1.00E-4
SNB-19	0.623	1.906	1.851	1.758	1.343	1.010	0.941	96	88	56	30	25	1.72E-6	> 1.00E-4	> 1.00E-4
SNB-75	0.647	1.223	1.119	1.083	0.944	0.798	0.765	82	76	52	26	20	1.15E-6	> 1.00E-4	> 1.00E-4
U251	0.269	1.237	1.181	1.201	0.844	0.576	0.463	94	96	59	32	20	2.18E-6	> 1.00E-4	> 1.00E-4
Melanoma															
LOX IMVI	0.293	2.244	2.113	1.824	0.616	0.397	0.402	93	78	17	5	6	2.88E-7	> 1.00E-4	> 1.00E-4
MALME-3M	0.520	0.922	0.915	0.877	0.857	0.757	0.689	98	89	84	59	42	3.33E-5	> 1.00E-4	> 1.00E-4
M14	0.351	1.390	1.320	1.106	0.537	0.391	0.342	93	73	18	4	-3	2.59E-7	3.96E-5	> 1.00E-4
MDA-MB-435	0.420	1.837	1.760	1.671	1.195	0.915	0.886	95	88	55	35	33	1.72E-6	> 1.00E-4	> 1.00E-4
SK-MEL-2	0.597	1.048	1.037	1.049	1.059	0.980	0.915	98	100	102	85	70	> 1.00E-4	> 1.00E-4	> 1.00E-4
SK-MEL-28	0.505	1.359	1.366	1.366	1.248	1.047	1.001	101	101	87	63	58	> 1.00E-4	> 1.00E-4	> 1.00E-4
SK-MEL-5	0.390	1.505	1.444	1.346	0.754	0.421	0.324	95	86	33	3	-17	4.70E-7	1.37E-5	> 1.00E-4
UACC-257	0.718	1.521	1.512	1.450	1.430	1.257	1.158	99	91	89	67	55	> 1.00E-4	> 1.00E-4	> 1.00E-4
UACC-62	0.576	1.999	1.857	1.844	1.391	1.076	0.834	90	89	57	35	18	2.13E-6	> 1.00E-4	> 1.00E-4
Ovarian Cancer															
IGROV1	0.644	1.853	1.862	1.832	1.470	1.282	1.193	101	98	68	53	45	2.37E-5	> 1.00E-4	> 1.00E-4
OVCAR-3	0.456	1.270	1.272	1.278	1.114	0.941	0.732	100	101	81	60	34	2.35E-5	> 1.00E-4	> 1.00E-4
OVCAR-4	0.494	1.147	1.130	1.048	0.859	0.790	0.714	97	85	56	45	34	3.61E-6	> 1.00E-4	> 1.00E-4
OVCAR-5	0.746	1.756	1.764	1.671	1.718	1.707	1.736	101	92	96	95	98	> 1.00E-4	> 1.00E-4	> 1.00E-4
OVCAR-8	0.321	1.279	1.294	1.167	0.768	0.640	0.612	102	88	47	33	30	8.29E-7	> 1.00E-4	> 1.00E-4
NCI/ADR-RES	0.431	1.445	1.413	1.341	0.890	0.681	0.641	97	90	45	25	21	7.84E-7	> 1.00E-4	> 1.00E-4
SK-OV-3	0.452	1.083	1.080	1.094	0.866	0.679	0.639	99	102	66	36	30	3.35E-6	> 1.00E-4	> 1.00E-4
Renal Cancer															
786-0	0.527	2.139	2.040	1.780	1.495	0.803	0.626	94	78	60	17	6	1.71E-6	> 1.00E-4	> 1.00E-4
A498	1.374	2.242	2.139	2.027	1.945	1.771	1.773	88	75	66	46	46	6.14E-6	> 1.00E-4	> 1.00E-4
ACHN	0.353	1.389	1.353	1.276	0.508	0.416	0.390	97	89	15	6	4	3.37E-7	> 1.00E-4	> 1.00E-4
CAKI-1	0.704	2.205	2.213	2.176	1.205	0.679	0.655	101	98	33	-4	-7	5.53E-7	7.98E-6	> 1.00E-4
RXF 393	0.556	1.047	1.046	1.025	0.932	0.785	0.708	100	95	77	47	31	7.72E-6	> 1.00E-4	> 1.00E-4
SN12C	0.807	2.650	2.596	2.468	1.769	1.167	1.068	97	90	52	20	14	1.17E-6	> 1.00E-4	> 1.00E-4
TK-10	0.654	1.505	1.473	1.455	1.330	1.220	1.247	96	94	79	66	70	> 1.00E-4	> 1.00E-4	> 1.00E-4
UO-31	0.622	1.530	1.398	1.299	1.047	0.770	0.680	85	75	47	16	6	7.65E-7	> 1.00E-4	> 1.00E-4
Prostate Cancer															
PC-3	0.670	1.996	1.931	1.913	1.523	1.358	1.275	95	94	64	52	46	1.99E-5	> 1.00E-4	> 1.00E-4
DU-145	0.377	1.321	1.350	1.279	0.614	0.406	0.368	103	96	25	3	-3	4.43E-7	3.51E-5	> 1.00E-4
Breast Cancer															
MCF7	0.308	1.676	1.618	1.486	0.598	0.437	0.399	96	86	21	9	7	3.60E-7	> 1.00E-4	> 1.00E-4
MDA-MB-231/ATCC	0.540	1.378	1.295	1.332	1.147	1.124	1.108	90	94	72	70	68	> 1.00E-4	> 1.00E-4	> 1.00E-4
HS 578T	0.865	1.731	1.694	1.654	1.577	1.504	1.403	96	91	82	74	62	> 1.00E-4	> 1.00E-4	> 1.00E-4
BT-549	0.680	1.589	1.583	1.348	1.010	0.897	0.756	99	73	36	24	8	4.28E-7	> 1.00E-4	> 1.00E-4
T-47D	0.701	1.568	1.493	1.458	1.255	0.942	0.806	91	87	64	28	12	2.43E-6	> 1.00E-4	> 1.00E-4
MDA-MB-468	0.573	1.127	1.070	1.069	0.821	0.702	0.548	90	89	45	23	-4	7.64E-7	6.91E-5	> 1.00E-4

tert-Butyl 12,13-dimethyl-5,7-dioxo-12,13-dihydro-5*H*-pyrido[3',2':4,5]pyrrolo[2,3-*a*]pyrrolo[3,4-*c*]carbazole-6(7*H*)-carboxylate (368)

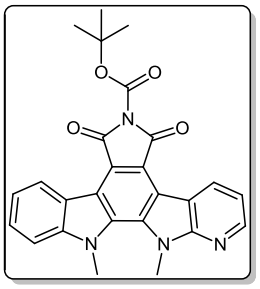

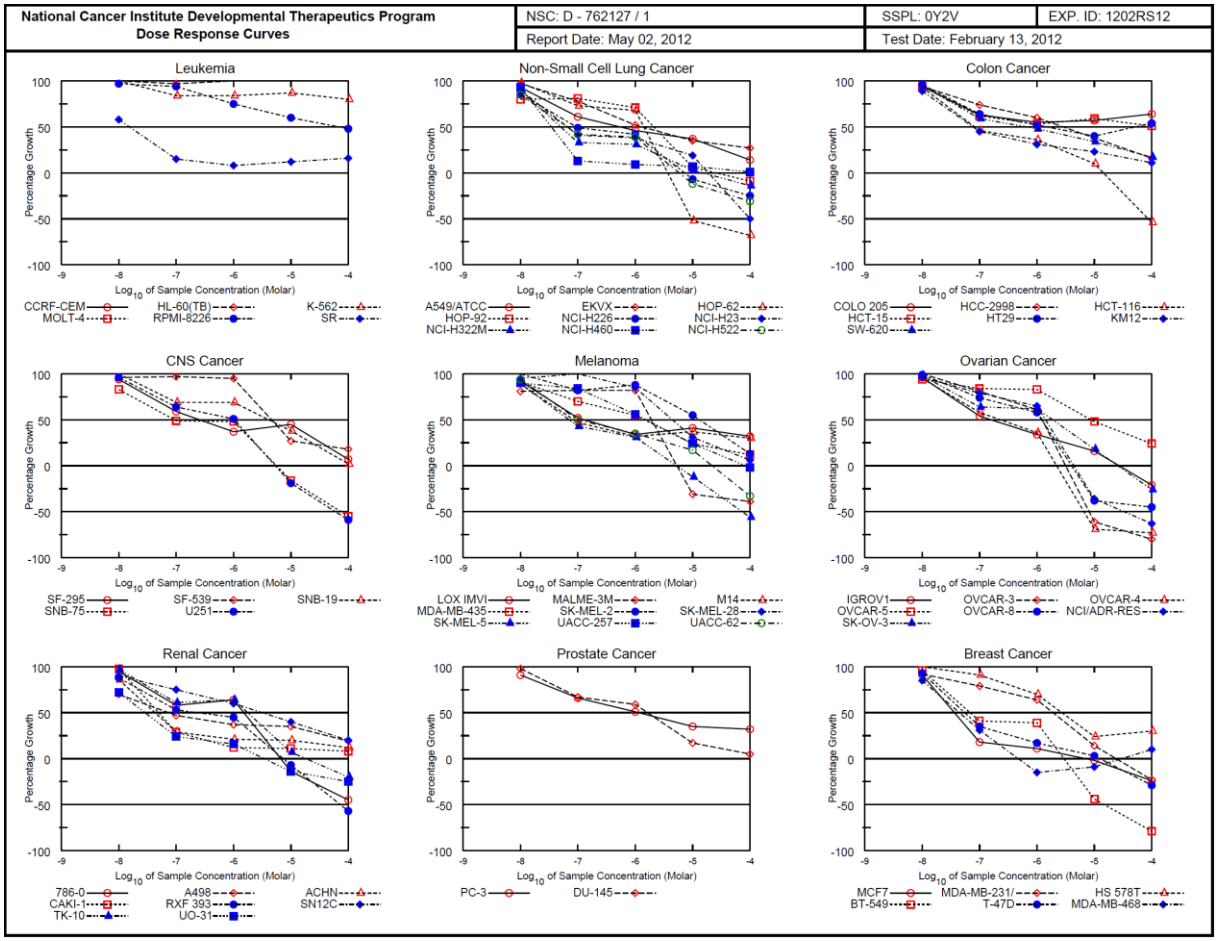

tert-Butyl 12,13-dimethyl-5,7-dioxo-12,13-dihydro-5*H*-pyrido[3',2':4,5]pyrrolo[2,3-*a*]pyrrolo[3,4-*c*]carbazole-6(7*H*)-carboxylate (368)

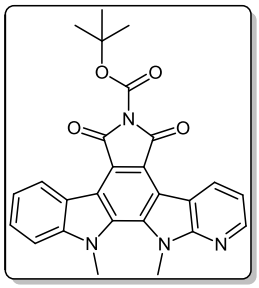

National Cancer Institute Developmental Therapeutics Program
In-Vitro Testing Results

NSC : D - 762127 / 1	Experiment ID : 1202RS12	Test Type : 08	Units : Molar
Report Date : May 02, 2012	Test Date : February 13, 2012	QNS :	MC :
COMI : MC-5-434 (111453)	Stain Reagent : SRB Dual-Pass Related	SSPL : 0Y2V	

			Log10 Concentration											
	Time		Mean Optical Densities					Percent Growth						
Panel/Cell Line	Zero	Ctrl	-8.0	-7.0	-6.0	-5.0	-4.0	-8.0	-7.0	-6.0	-5.0	-4.0	GI50	TGI	LC50
Leukemia															
CCRF-CEM	0.336	1.618													
HL-60(TB)	1.226	2.457	2.468	2.418	2.508	2.804	2.905	101	97	104	128	136	> 1.00E-4	> 1.00E-4	> 1.00E-4
K-562	0.402	1.962	2.064	1.715	1.713	1.764	1.656	107	84	84	87	80	> 1.00E-4	> 1.00E-4	> 1.00E-4
MOLT-4	0.745	2.187													
RPMI-8226	1.190	2.755	2.713	2.657	2.368	2.134	1.948	97	94	75	60	48	7.40E-5	> 1.00E-4	> 1.00E-4
SR	0.361	1.143	0.817	0.476	0.421	0.454	0.486	58	15	8	12	16	1.54E-8	> 1.00E-4	> 1.00E-4
Non-Small Cell Lung Cancer															
A549/ATCC	0.400	1.670	1.587	1.172	0.988	0.865	0.577	93	61	46	37	14	5.52E-7	> 1.00E-4	> 1.00E-4
EKVX	0.953	1.979	1.953	1.757	1.485	1.311	1.229	97	78	52	35	27	1.28E-6	> 1.00E-4	> 1.00E-4
HOP-62	0.284	0.797	0.787	0.661	0.635	0.136	0.090	98	73	68	-52	-68	1.42E-6	3.69E-6	9.57E-6
HOP-92	1.091	1.516	1.431	1.434	1.391	1.117	0.996	80	81	71	6	-9	2.09E-6	2.55E-5	> 1.00E-4
NCI-H226	0.796	1.604	1.490	1.192	1.134	0.743	0.596	86	49	42	-7	-25	9.42E-8	7.27E-6	> 1.00E-4
NCI-H23	0.505	1.455	1.363	0.894	0.870	0.690	0.254	90	41	38	19	-50	6.54E-8	1.91E-5	> 1.00E-4
NCI-H322M	0.665	1.360	1.293	0.892	0.881	0.688	0.573	90	33	31	3	-14	5.00E-8	1.54E-5	> 1.00E-4
NCI-H460	0.251	2.224	2.086	0.500	0.427	0.390	0.274	93	13	9	7	1	3.43E-8	> 1.00E-4	> 1.00E-4
NCI-H522	0.660	1.432	1.319	0.984	0.960	0.582	0.453	85	42	39	-12	-31	6.52E-8	5.83E-6	> 1.00E-4
Colon Cancer															
COLO 205	0.381	1.608	1.531	1.159	1.058	1.083	1.167	94	63	55	57	64	> 1.00E-4	> 1.00E-4	> 1.00E-4
HCC-2998	0.568	1.699	1.636	1.400	1.250	1.001	0.748	94	74	60	38	16	2.93E-6	> 1.00E-4	> 1.00E-4
HCT-116	0.200	1.490	1.400	0.788	0.658	0.327	0.092	93	46	36	10	-54	8.07E-8	1.42E-5	8.58E-5
HCT-15	0.345	1.795	1.708	1.245	1.112	1.198	1.088	94	62	53	59	51	> 1.00E-4	> 1.00E-4	> 1.00E-4
HT29	0.195	1.062	1.029	0.754	0.647	0.540	0.661	96	64	52	40	54		> 1.00E-4	> 1.00E-4
KM12	0.463	1.840	1.694	1.085	0.883	0.775	0.616	89	45	31	23	11	7.76E-8	> 1.00E-4	> 1.00E-4
SW-620	0.291	1.687	1.623	1.116	0.962	0.760	0.525	95	59	48	34	17	6.69E-7	> 1.00E-4	> 1.00E-4
CNS Cancer															
SF-295	0.521	1.420	1.368	1.052	0.850	0.930	0.580	94	59	37	45	7	2.52E-7	> 1.00E-4	> 1.00E-4
SF-539	0.782	2.054	1.997	2.015	1.989	1.131	1.015	96	97	95	27	18	4.63E-6	> 1.00E-4	> 1.00E-4
SNB-19	0.623	1.735	1.760	1.389	1.390	1.048	0.644	102	69	69	38	2	4.14E-6	> 1.00E-4	> 1.00E-4
SNB-75	0.647	1.159	1.071	0.900	0.895	0.547	0.292	83	49	48	-16	-55	9.59E-8	5.72E-6	7.49E-5
U251	0.269	1.114	1.082	0.811	0.703	0.219	0.109	96	64	51	-19	-59	1.04E-6	5.40E-6	5.85E-5
Melanoma															
LOX IMVI	0.293	2.146	1.989	1.249	0.920	1.050	0.892	92	52	34	41	32	1.23E-7	> 1.00E-4	> 1.00E-4
MALME-3M	0.520	0.818	0.761	0.764	0.766	0.357	0.317	81	82	82	-31	-39	1.93E-6	5.30E-6	> 1.00E-4
M14	0.351	1.307	1.205	0.798	0.658	0.704	0.637	89	47	32	37	30	8.38E-8	> 1.00E-4	> 1.00E-4
MDA-MB-435	0.420	1.741	1.624	1.345	1.151	0.742	0.575	91	70	55	24	12	1.48E-6	> 1.00E-4	> 1.00E-4
SK-MEL-2	0.597	0.978	0.979	0.911	0.932	0.807	0.648	100	82	88	55	13	1.32E-5	> 1.00E-4	> 1.00E-4
SK-MEL-28	0.505	1.355	1.311	1.355	1.223	0.771	0.554	95	100	85	31	6	4.45E-6	> 1.00E-4	> 1.00E-4
SK-MEL-5	0.390	1.342	1.234	0.796	0.682	0.343	0.173	89	43	31	-12	-56	6.91E-8	5.20E-6	7.42E-5
UACC-257	0.718	1.487	1.410	1.367	1.151	0.902	0.705	90	84	56	24	-2	1.56E-6	8.46E-5	> 1.00E-4
UACC-62	0.576	1.836	1.763	1.209	1.023	0.794	0.388	94	50	35	17	-33	1.04E-7	2.22E-5	> 1.00E-4
Ovarian Cancer															
IGROV1	0.644	1.640	1.603	1.177	0.980	0.805	0.508	96	54	34	16	-21	1.50E-7	2.71E-5	> 1.00E-4
OVCAR-3	0.456	1.228	1.226	1.082	0.924	0.179	0.090	100	81	61	-61	-80	1.22E-6	3.16E-6	8.16E-6
OVCAR-4	0.494	1.093	1.065	0.841	0.713	0.155	0.135	95	58	36	-69	-73	2.32E-7	2.22E-6	6.65E-6
OVCAR-5	0.746	1.630	1.576	1.487	1.478	1.172	0.958	94	84	83	48	24	8.88E-6	> 1.00E-4	> 1.00E-4
OVCAR-8	0.321	1.219	1.206	0.986	0.846	0.201	0.176	99	74	58	-38	-45	1.22E-6	4.06E-6	> 1.00E-4
NCI/ADR-RES	0.431	1.408	1.370	1.200	1.067	0.277	0.161	96	79	65	-36	-63	1.41E-6	4.42E-6	3.37E-5
SK-OV-3	0.452	1.069	1.055	0.847	0.832	0.566	0.334	98	64	62	18	-26	1.86E-6	2.59E-5	> 1.00E-4
Renal Cancer															
786-0	0.527	1.981	1.902	1.367	1.458	0.452	0.289	95	58	64	-14	-45	1.51E-6	6.58E-6	> 1.00E-4
A498	1.374	2.246	1.988	1.783	1.699	1.679	1.536	70	47	37	35	19	7.34E-8	> 1.00E-4	> 1.00E-4
ACHN	0.353	1.369	1.225	0.647	0.571	0.553	0.478	86	29	21	20	12	4.27E-8	> 1.00E-4	> 1.00E-4
CAKI-1	0.704	2.094	2.063	1.103	0.878	0.853	0.820	98	29	12	11	8	4.91E-8	> 1.00E-4	> 1.00E-4
RXF 393	0.556	0.966	0.916	0.771	0.740	0.517	0.238	88	53	45	-7	-57	2.14E-7	7.33E-6	7.16E-5
SN12C	0.807	2.602	2.431	2.151	1.891	1.526	1.161	90	75	60	40	20	3.24E-6	> 1.00E-4	> 1.00E-4
TK-10	0.654	1.403	1.377	1.114	1.135	0.707	0.523	97	61	64	7	-20	1.77E-6	1.82E-5	> 1.00E-4
UO-31	0.622	1.438	1.209	0.822	0.751	0.535	0.467	72	24	16	-14	-25	2.90E-8	3.38E-6	> 1.00E-4
Prostate Cancer															
PC-3	0.670	2.031	1.915	1.567	1.361	1.144	1.111	91	66	51	35	32	1.11E-6	> 1.00E-4	> 1.00E-4
DU-145	0.377	1.248	1.229	0.957	0.892	0.525	0.418	98	67	59	17	5	1.64E-6	> 1.00E-4	> 1.00E-4
Breast Cancer															
MCF7	0.308	1.541	1.429	0.527	0.446	0.302	0.236	91	18	11	-2	-24	3.62E-8	7.11E-6	> 1.00E-4
MDA-MB-231/ATCC	0.540	1.367	1.298	1.190	1.073	0.659	0.415	92	79	64	14	-23	1.94E-6	2.41E-5	> 1.00E-4
HS 578T	0.865	1.692	1.692	1.617	1.443	1.068	1.112	100	91	70	24	30	2.74E-6	> 1.00E-4	> 1.00E-4
BT-549	0.680	1.403	1.374	0.976	0.961	0.379	0.142	96	41	39	-44	-79	6.84E-8	2.93E-6	1.46E-5
T-47D	0.701	1.558	1.494	1.004	0.846	0.723	0.495	93	35	17	3	-29	5.54E-8	1.20E-5	> 1.00E-4
MDA-MB-468	0.573	1.051	0.981	0.722	0.486	0.519	0.620	85	31	-15	-9	10	4.49E-8		> 1.00E-4

12,13-Dimethyl-12,13-dihydro-5*H*-pyrido[2,3-*b*]pyrido[3',2':4,5]pyrrolo[3,2-*g*]pyrrolo[3,4-*e*]indole-5,7(6*H*)-dione (371)

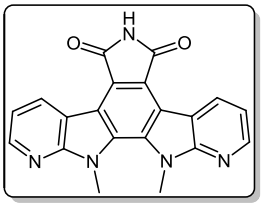

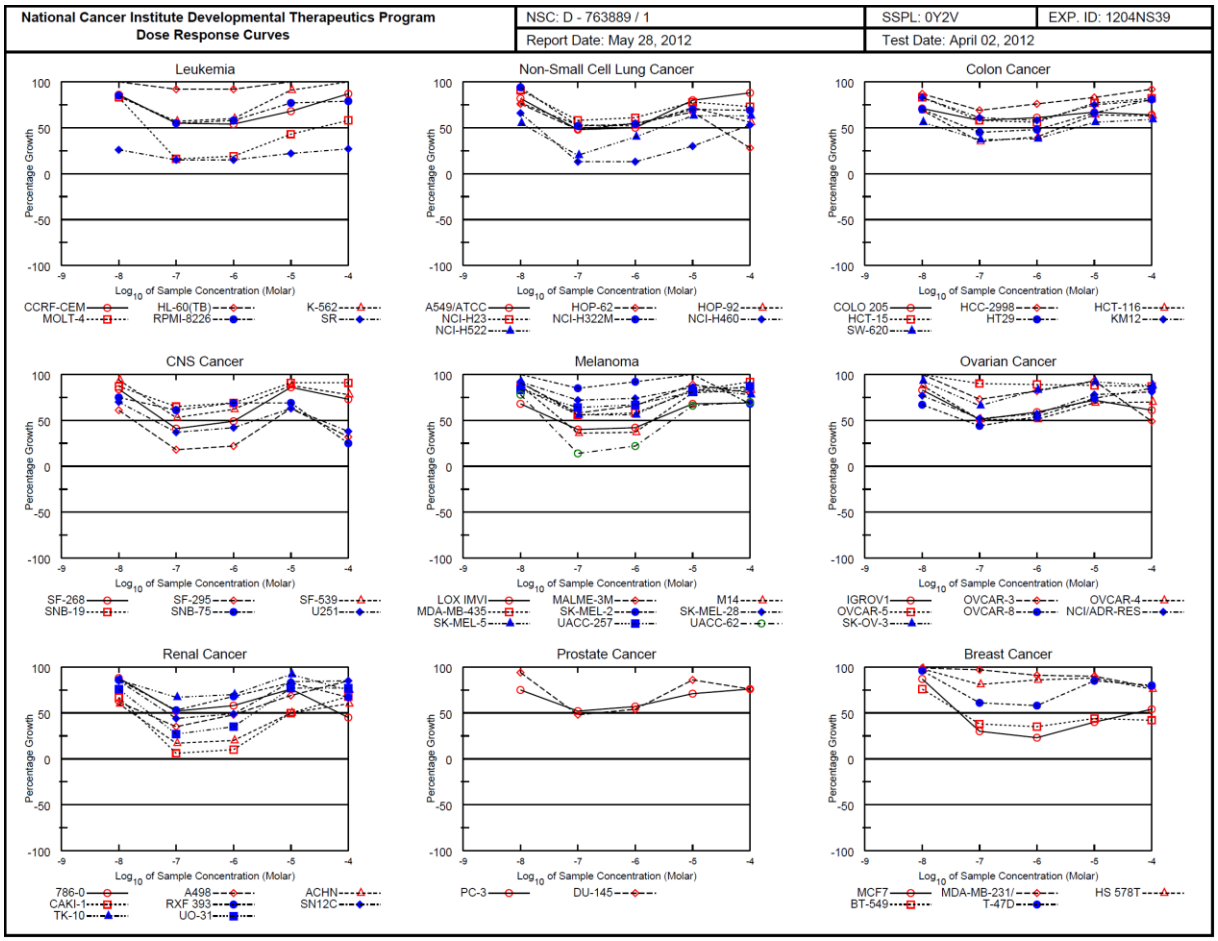

12,13-Dimethyl-12,13-dihydro-5*H*-pyrido[2,3-*b*]pyrido[3',2':4,5]pyrrolo[3,2-*g*]pyrrolo[3,4-*e*]indole-5,7(6*H*)-dione (371)

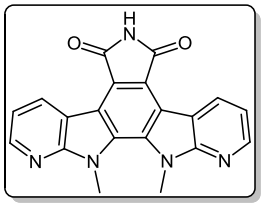

National Cancer Institute Developmental Therapeutics Program
In-Vitro Testing Results

NSC : D - 763889 / 1	Experiment ID : 1204NS39	Test Type : 08	Units : Molar
Report Date : May 28, 2012	Test Date : April 02, 2012	QNS :	MC :
COMI : MC-5-456 (115191)	Stain Reagent : SRB Dual-Pass Related	SSPL : 0Y2V	

			Log10 Concentration											
	Time		Mean Optical Densities					Percent Growth						
Panel/Cell Line	Zero	Ctrl	-8.0	-7.0	-6.0	-5.0	-4.0	-8.0	-7.0	-6.0	-5.0	-4.0	GI50	TGI	LC50
Leukemia															
CCRF-CEM	0.689	2.535	2.272	1.710	1.694	1.951	2.290	86	55	54	68	87	> 1.00E-4	> 1.00E-4	> 1.00E-4
HL-60(TB)	0.706	2.472	2.555	2.336	2.327	2.555	2.538	105	92	92	105	104	> 1.00E-4	> 1.00E-4	> 1.00E-4
K-562	0.231	1.643	1.413	1.031	1.074	1.515	1.639	84	57	60	91	100	> 1.00E-4	> 1.00E-4	> 1.00E-4
MOLT-4	0.551	2.040	1.785	0.783	0.827	1.191	1.420	83	16	19	43	58	.	> 1.00E-4	> 1.00E-4
RPMI-8226	0.724	2.044	1.850	1.449	1.496	1.746	1.764	85	55	58	77	79	> 1.00E-4	> 1.00E-4	> 1.00E-4
SR	0.385	1.279	0.614	0.524	0.521	0.584	0.631	26	15	15	22	27	< 1.00E-8	> 1.00E-4	> 1.00E-4
Non-Small Cell Lung Cancer															
A549/ATCC	0.330	1.422	1.225	0.853	0.876	1.200	1.295	82	48	50	80	88	.	> 1.00E-4	> 1.00E-4
HOP-62	0.375	1.222	1.016	0.784	0.841	0.946	0.608	76	48	55	67	28	.	> 1.00E-4	> 1.00E-4
HOP-92	0.898	1.289	1.201	1.104	1.101	1.180	1.117	77	53	52	72	56	> 1.00E-4	> 1.00E-4	> 1.00E-4
NCI-H23	0.511	2.034	1.895	1.396	1.447	1.693	1.617	91	58	61	78	73	> 1.00E-4	> 1.00E-4	> 1.00E-4
NCI-H322M	0.725	1.423	1.384	1.089	1.105	1.212	1.205	94	52	54	70	69	> 1.00E-4	> 1.00E-4	> 1.00E-4
NCI-H460	0.231	2.116	1.477	0.477	0.481	0.804	1.227	66	13	13	30	53	.	> 1.00E-4	> 1.00E-4
NCI-H522	0.607	1.143	0.901	0.714	0.824	0.947	0.943	55	20	40	63	63	.	> 1.00E-4	> 1.00E-4
Colon Cancer															
COLO 205	0.259	1.143	0.887	0.775	0.798	0.852	0.823	71	58	61	67	64	> 1.00E-4	> 1.00E-4	> 1.00E-4
HCC-2998	0.333	1.472	1.323	1.121	1.198	1.279	1.377	87	69	76	83	92	> 1.00E-4	> 1.00E-4	> 1.00E-4
HCT-116	0.175	1.604	1.166	0.681	0.753	1.096	1.081	69	35	40	64	63	.	> 1.00E-4	> 1.00E-4
HCT-15	0.213	1.676	1.421	1.058	1.036	1.334	1.407	83	58	56	77	82	> 1.00E-4	> 1.00E-4	> 1.00E-4
HT29	0.221	1.116	0.844	0.624	0.655	0.816	0.942	70	45	48	66	81	.	> 1.00E-4	> 1.00E-4
KM12	0.468	2.144	1.859	1.489	1.440	1.720	1.812	83	61	58	75	80	> 1.00E-4	> 1.00E-4	> 1.00E-4
SW-620	0.285	1.863	1.165	0.864	0.878	1.167	1.212	56	37	38	56	59	.	> 1.00E-4	> 1.00E-4
CNS Cancer															
SF-268	0.608	1.831	1.631	1.111	1.203	1.656	1.497	84	41	49	86	73	.	> 1.00E-4	> 1.00E-4
SF-295	0.771	2.193	1.641	1.030	1.090	1.663	1.223	61	18	22	63	32	.	> 1.00E-4	> 1.00E-4
SF-539	0.601	1.946	1.870	1.312	1.439	1.787	1.644	94	53	62	88	78	> 1.00E-4	> 1.00E-4	> 1.00E-4
SNB-19	0.462	1.499	1.369	1.132	1.176	1.404	1.403	87	65	69	91	91	> 1.00E-4	> 1.00E-4	> 1.00E-4
SNB-75	0.820	1.662	1.449	1.333	1.399	1.402	1.031	75	61	69	69	25	2.71E-5	> 1.00E-4	> 1.00E-4
U251	0.365	1.702	1.307	0.860	0.929	1.208	0.879	70	37	42	63	38	.	> 1.00E-4	> 1.00E-4
Melanoma															
LOX IMVI	0.171	1.321	0.949	0.632	0.649	0.949	0.965	68	40	42	68	69	.	> 1.00E-4	> 1.00E-4
MALME-3M	0.674	1.164	1.121	0.957	0.999	1.108	1.065	91	58	66	89	80	> 1.00E-4	> 1.00E-4	> 1.00E-4
M14	0.422	1.654	1.511	0.866	0.879	1.406	1.442	88	36	37	80	83	.	> 1.00E-4	> 1.00E-4
MDA-MB-435	0.403	1.512	1.351	1.024	1.048	1.310	1.419	86	56	58	82	92	> 1.00E-4	> 1.00E-4	> 1.00E-4
SK-MEL-2	0.883	1.547	1.587	1.449	1.495	1.589	1.336	106	85	92	106	68	> 1.00E-4	> 1.00E-4	> 1.00E-4
SK-MEL-28	0.527	1.480	1.407	1.214	1.231	1.344	1.335	92	72	74	86	85	> 1.00E-4	> 1.00E-4	> 1.00E-4
SK-MEL-5	0.400	2.088	1.935	1.350	1.346	1.817	1.709	91	56	56	84	78	> 1.00E-4	> 1.00E-4	> 1.00E-4
UACC-257	0.969	1.881	1.724	1.557	1.579	1.710	1.760	83	64	67	81	87	> 1.00E-4	> 1.00E-4	> 1.00E-4
UACC-62	0.666	2.421	2.028	0.908	1.046	1.825	1.886	78	14	22	66	70	.	> 1.00E-4	> 1.00E-4
Ovarian Cancer															
IGROV1	0.561	1.648	1.463	1.116	1.199	1.340	1.220	83	51	59	72	61	> 1.00E-4	> 1.00E-4	> 1.00E-4
OVCAR-3	0.507	1.489	1.500	1.219	1.317	1.420	0.989	101	73	82	93	49	9.53E-5	> 1.00E-4	> 1.00E-4
OVCAR-4	0.548	1.363	1.268	0.964	0.961	1.110	1.122	88	51	51	69	70	> 1.00E-4	> 1.00E-4	> 1.00E-4
OVCAR-5	0.437	1.305	1.303	1.218	1.206	1.204	1.191	100	90	89	88	87	> 1.00E-4	> 1.00E-4	> 1.00E-4
OVCAR-8	0.429	1.588	1.201	0.937	1.054	1.292	1.418	67	44	54	74	85	.	> 1.00E-4	> 1.00E-4
NCI/ADR-RES	0.418	1.690	1.401	1.084	1.141	1.407	1.447	77	52	57	78	81	> 1.00E-4	> 1.00E-4	> 1.00E-4
SK-OV-3	0.558	1.241	1.191	1.011	1.123	1.188	1.161	93	66	83	92	88	> 1.00E-4	> 1.00E-4	> 1.00E-4
Renal Cancer															
786-0	0.585	2.223	2.023	1.434	1.533	1.829	1.322	88	52	58	76	45	6.90E-5	> 1.00E-4	> 1.00E-4
A498	1.160	1.759	1.531	1.368	1.448	1.576	1.670	62	35	48	69	85	.	> 1.00E-4	> 1.00E-4
ACHN	0.296	1.431	0.972	0.492	0.522	0.867	0.974	60	17	20	50	60	.	> 1.00E-4	> 1.00E-4
CAKI-1	0.821	2.156	1.719	0.906	0.951	1.484	1.729	67	6	10	50	68	.	> 1.00E-4	> 1.00E-4
RXF 393	0.637	1.103	1.036	0.884	0.952	1.025	0.948	86	53	68	83	67	> 1.00E-4	> 1.00E-4	> 1.00E-4
SN12C	0.510	2.029	1.806	1.179	1.253	1.794	1.798	85	44	49	84	85	.	> 1.00E-4	> 1.00E-4
TK-10	0.562	1.189	1.102	0.982	1.003	1.138	1.031	86	67	70	92	75	> 1.00E-4	> 1.00E-4	> 1.00E-4
UO-31	0.615	1.526	1.308	0.865	0.931	1.315	1.321	76	27	35	77	77	.	> 1.00E-4	> 1.00E-4
Prostate Cancer															
PC-3	0.441	1.678	1.364	1.080	1.147	1.318	1.380	75	52	57	71	76	> 1.00E-4	> 1.00E-4	> 1.00E-4
DU-145	0.350	1.310	1.256	0.813	0.870	1.173	1.081	94	48	54	86	76	.	> 1.00E-4	> 1.00E-4
Breast Cancer															
MCF7	0.384	2.029	1.814	0.876	0.761	1.043	1.268	87	30	23	40	54	.	> 1.00E-4	> 1.00E-4
MDA-MB-231/ATCC	0.549	1.461	1.452	1.429	1.379	1.370	1.264	99	97	91	90	78	> 1.00E-4	> 1.00E-4	> 1.00E-4
HS 578T	0.834	1.737	1.721	1.562	1.611	1.627	1.517	98	81	86	88	76	> 1.00E-4	> 1.00E-4	> 1.00E-4
BT-549	0.827	1.799	1.563	1.201	1.170	1.259	1.238	76	38	35	44	42	4.90E-8	> 1.00E-4	> 1.00E-4
T-47D	0.689	1.718	1.674	1.320	1.282	1.559	1.517	96	61	58	85	80	> 1.00E-4	> 1.00E-4	> 1.00E-4

tert-Butyl 12,13-dimethyl-5,7-dioxo-12,13-dihydro-5*H*-pyrido[2,3-*b*]pyrido[3',2':4,5]pyrrolo[3,2-*g*]pyrrolo[3,4-*e*]indole-6(7*H*)-carboxylate (372)

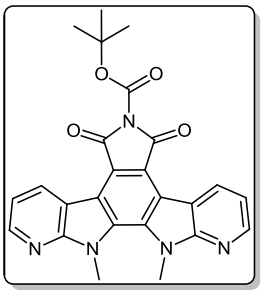

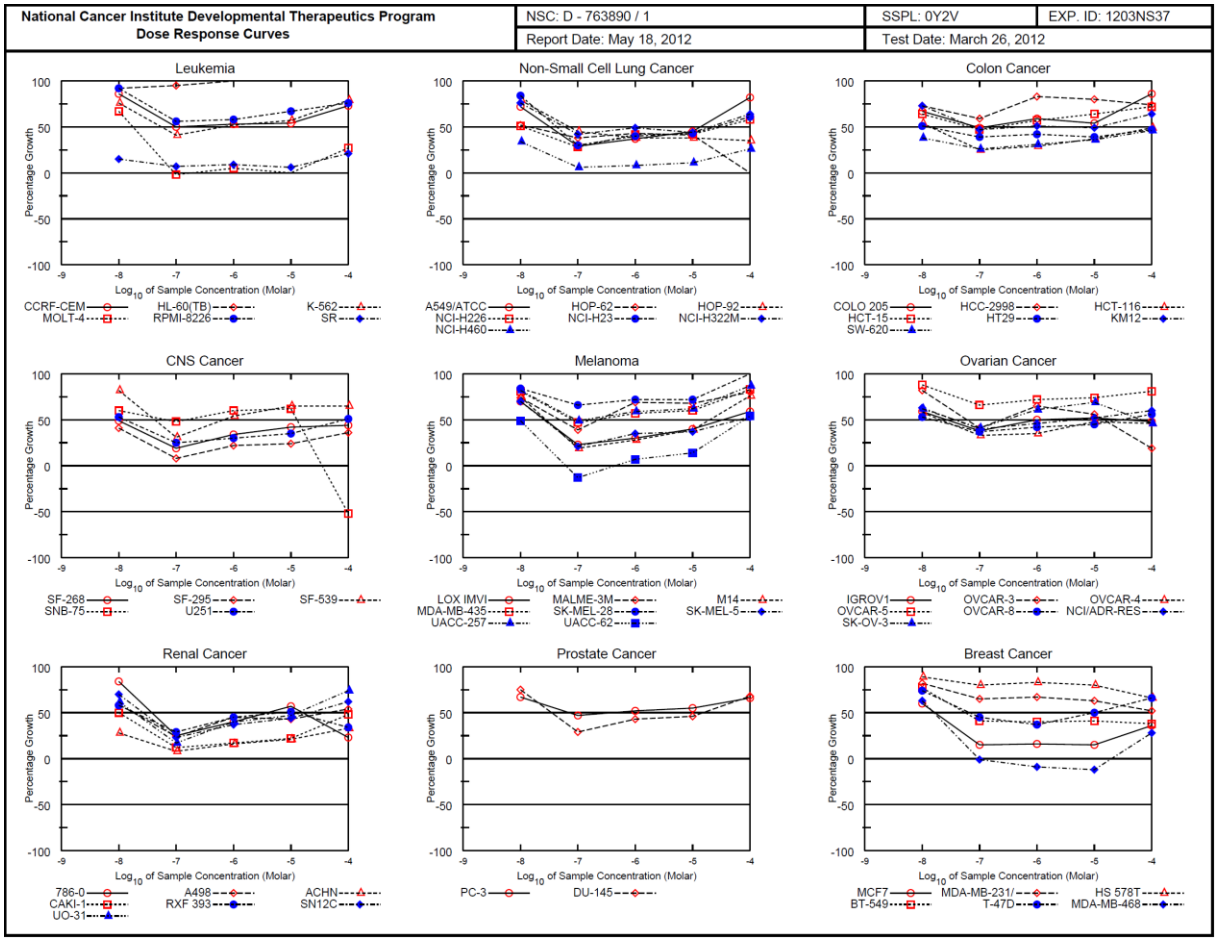

tert-Butyl 12,13-dimethyl-5,7-dioxo-12,13-dihydro-5_H_-pyrido[2,3-_b_]pyrido[3',2':4,5]pyrrolo[3,2-_g_]pyrrolo[3,4-_e_]indole-6(7_H_)-carboxylate (372)

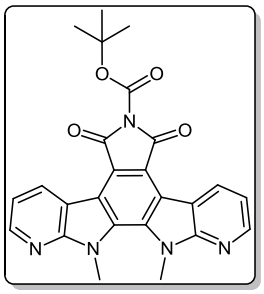

National Cancer Institute Developmental Therapeutics Program
In-Vitro Testing Results

NSC : D - 763890 / 1	Experiment ID : 1203NS37	Test Type : 08	Units : Molar
Report Date : May 18, 2012	Test Date : March 26, 2012	QNS :	MC :
COMI : MC-5-457 (115192)	Stain Reagent : SRB Dual-Pass Related	SSPL : 0Y2V	

		Log10 Concentration												
	Time	Mean Optical Densities					Percent Growth							
Panel/Cell Line	Zero	Ctrl	-8.0	-7.0	-6.0	-5.0	-4.0	-8.0	-7.0	-6.0	-5.0	-4.0	GI50	TGI	LC50
Leukemia															
CCRF-CEM	0.709	2.587	2.332	1.641	1.697	1.721	2.079	86	50	53	54	73	.	> 1.00E-4	> 1.00E-4
HL-60(TB)	0.902	2.230	2.120	2.160	2.316	2.367	2.313	92	95	107	110	106	> 1.00E-4	> 1.00E-4	> 1.00E-4
K-562	0.273	1.725	1.376	0.875	1.027	1.099	1.423	76	41	52	57	79	.	> 1.00E-4	> 1.00E-4
MOLT-4	0.728	2.480	1.895	0.711	0.815	0.736	1.201	67	-2	5	.	27	1.74E-8	.	> 1.00E-4
RPMI-8226	0.911	2.406	2.283	1.742	1.785	1.916	2.047	92	56	58	67	76	> 1.00E-4	> 1.00E-4	> 1.00E-4
SR	0.453	1.587	0.626	0.531	0.554	0.525	0.686	15	7	9	6	21	< 1.00E-8	> 1.00E-4	> 1.00E-4
Non-Small Cell Lung Cancer															
A549/ATCC	0.256	1.233	0.955	0.542	0.618	0.693	1.053	72	29	37	45	82	.	> 1.00E-4	> 1.00E-4
HOP-62	0.332	0.990	0.675	0.585	0.613	0.605	0.335	52	38	43	41	.	1.43E-8	> 1.00E-4	> 1.00E-4
HOP-92	1.339	1.658	1.593	1.483	1.461	1.461	1.451	79	45	38	38	35	7.15E-8	> 1.00E-4	> 1.00E-4
NCI-H226	0.563	1.148	0.863	0.728	0.806	0.810	0.903	51	28	42	42	58	.	> 1.00E-4	> 1.00E-4
NCI-H23	0.598	1.820	1.622	0.967	1.081	1.129	1.338	84	30	40	43	61	.	> 1.00E-4	> 1.00E-4
NCI-H322M	0.849	1.605	1.427	1.169	1.217	1.179	1.330	76	42	49	44	64	.	> 1.00E-4	> 1.00E-4
NCI-H460	0.255	2.199	0.909	0.374	0.415	0.462	0.770	34	6	8	11	26	< 1.00E-8	> 1.00E-4	> 1.00E-4
Colon Cancer															
COLO 205	0.321	1.108	0.851	0.706	0.782	0.744	1.001	67	49	59	54	86	.	> 1.00E-4	> 1.00E-4
HCC-2998	0.364	1.136	0.930	0.820	1.006	0.984	0.934	73	59	83	80	74	> 1.00E-4	> 1.00E-4	> 1.00E-4
HCT-116	0.227	1.776	1.060	0.607	0.675	0.793	0.984	54	25	29	37	49	1.34E-8	> 1.00E-4	> 1.00E-4
HCT-15	0.311	1.843	1.286	1.032	1.192	1.291	1.409	64	47	57	64	72	.	> 1.00E-4	> 1.00E-4
HT29	0.223	1.231	0.739	0.616	0.644	0.621	0.696	51	39	42	39	47	1.25E-8	> 1.00E-4	> 1.00E-4
KM12	0.443	2.121	1.669	1.224	1.303	1.265	1.518	73	47	51	49	64	.	> 1.00E-4	> 1.00E-4
SW-620	0.288	1.811	0.869	0.687	0.764	0.833	0.985	38	26	31	36	46	< 1.00E-8	> 1.00E-4	> 1.00E-4
CNS Cancer															
SF-268	0.605	1.743	1.166	0.825	0.994	1.079	1.103	49	19	34	42	44	< 1.00E-8	> 1.00E-4	> 1.00E-4
SF-295	0.963	2.536	1.610	1.083	1.303	1.339	1.536	41	8	22	24	36	< 1.00E-8	> 1.00E-4	> 1.00E-4
SF-539	0.954	2.388	2.127	1.405	1.730	1.891	1.880	82	31	54	65	65	.	> 1.00E-4	> 1.00E-4
SNB-75	0.687	1.247	1.024	0.954	1.025	1.033	0.330	60	48	60	62	-52	.	3.49E-5	9.60E-5
U251	0.326	1.537	0.969	0.634	0.688	0.756	0.944	53	25	30	35	51	.	> 1.00E-4	> 1.00E-4
Melanoma															
LOX IMVI	0.300	2.016	1.509	0.688	0.816	0.985	1.305	70	23	30	40	59	.	> 1.00E-4	> 1.00E-4
MALME-3M	0.686	1.246	1.103	0.904	1.075	1.070	1.132	74	39	69	68	80	.	> 1.00E-4	> 1.00E-4
M14	0.454	1.460	1.204	0.647	0.735	0.850	1.215	75	19	28	39	76	.	> 1.00E-4	> 1.00E-4
MDA-MB-435	0.461	1.936	1.652	1.161	1.298	1.350	1.685	81	47	57	60	83	.	> 1.00E-4	> 1.00E-4
SK-MEL-28	0.371	0.957	0.862	0.756	0.794	0.795	1.023	84	66	72	72	111	> 1.00E-4	> 1.00E-4	> 1.00E-4
SK-MEL-5	0.681	2.385	1.875	1.033	1.273	1.314	1.576	70	21	35	37	53	.	> 1.00E-4	> 1.00E-4
UACC-257	0.558	1.256	1.133	0.897	0.969	0.991	1.168	82	49	59	62	87	.	> 1.00E-4	> 1.00E-4
UACC-62	0.917	2.062	1.479	0.795	0.998	1.081	1.530	49	-13	7	14	54	.	.	> 1.00E-4
Ovarian Cancer															
IGROV1	0.652	1.809	1.340	1.088	1.228	1.252	1.207	59	38	50	52	48	.	> 1.00E-4	> 1.00E-4
OVCAR-3	0.521	1.446	1.279	0.904	1.122	1.036	0.694	82	41	65	56	19	.	> 1.00E-4	> 1.00E-4
OVCAR-4	0.418	0.801	0.640	0.546	0.551	0.602	0.594	58	33	35	48	46	2.12E-8	> 1.00E-4	> 1.00E-4
OVCAR-5	0.453	1.248	1.155	0.980	1.024	1.041	1.097	88	66	72	74	81	> 1.00E-4	> 1.00E-4	> 1.00E-4
OVCAR-8	0.282	1.289	0.817	0.654	0.708	0.733	0.850	53	37	42	45	56	.	> 1.00E-4	> 1.00E-4
NCI/ADR-RES	0.393	1.463	1.070	0.824	0.882	0.950	1.034	63	40	46	52	60	.	> 1.00E-4	> 1.00E-4
SK-OV-3	0.531	1.070	0.867	0.753	0.861	0.906	0.777	62	41	61	69	46	.	> 1.00E-4	> 1.00E-4
Renal Cancer															
786-0	0.774	2.381	2.131	1.174	1.419	1.692	1.142	84	25	40	57	23	.	> 1.00E-4	> 1.00E-4
A498	1.111	1.685	1.451	1.252	1.367	1.357	1.421	59	24	45	43	54	.	> 1.00E-4	> 1.00E-4
ACHN	0.344	1.429	0.653	0.434	0.517	0.570	0.700	28	8	16	21	33	< 1.00E-8	> 1.00E-4	> 1.00E-4
CAKI-1	0.809	2.317	1.562	0.994	1.066	1.141	1.532	50	12	17	22	48	< 1.00E-8	> 1.00E-4	> 1.00E-4
RXF 393	0.682	1.145	0.953	0.815	0.892	0.917	0.838	58	29	45	51	34	.	> 1.00E-4	> 1.00E-4
SN12C	0.545	1.828	1.438	0.846	1.024	1.114	1.344	70	23	37	44	62	.	> 1.00E-4	> 1.00E-4
UO-31	0.897	2.046	1.608	1.093	1.355	1.434	1.744	62	17	40	47	74	.	> 1.00E-4	> 1.00E-4
Prostate Cancer															
PC-3	0.466	1.728	1.311	1.055	1.126	1.160	1.305	67	47	52	55	66	.	> 1.00E-4	> 1.00E-4
DU-145	0.365	1.353	1.110	0.653	0.789	0.817	1.041	75	29	43	46	68	.	> 1.00E-4	> 1.00E-4
Breast Cancer															
MCF7	0.330	1.726	1.173	0.546	0.548	0.545	0.830	60	15	16	15	36	1.70E-8	> 1.00E-4	> 1.00E-4
MDA-MB-231/ATCC	0.599	1.154	1.055	0.962	0.970	0.949	0.890	82	65	67	63	52	> 1.00E-4	> 1.00E-4	> 1.00E-4
HS 578T	0.853	1.509	1.435	1.379	1.394	1.376	1.284	89	80	83	80	66	> 1.00E-4	> 1.00E-4	> 1.00E-4
BT-549	0.908	1.816	1.606	1.278	1.271	1.278	1.256	77	41	40	41	38	5.54E-8	> 1.00E-4	> 1.00E-4
T-47D	0.558	1.240	1.066	0.862	0.812	0.900	1.008	74	45	37	50	66	.	> 1.00E-4	> 1.00E-4
MDA-MB-468	0.551	1.262	0.998	0.545	0.502	0.488	0.748	63	-1	-9	-12	28	1.59E-8	.	> 1.00E-4

6-Hydroxy-12,13-dimethyl-12,13-dihydro-5*H*-pyrido[2,3-*b*]pyrido[3',2':4,5]pyrrolo[3,2-*g*]pyrrolo[3,4-*e*]indole-5,7(6*H*)-dione (373)

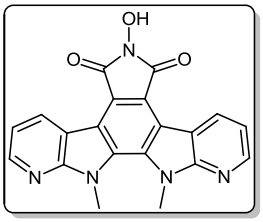

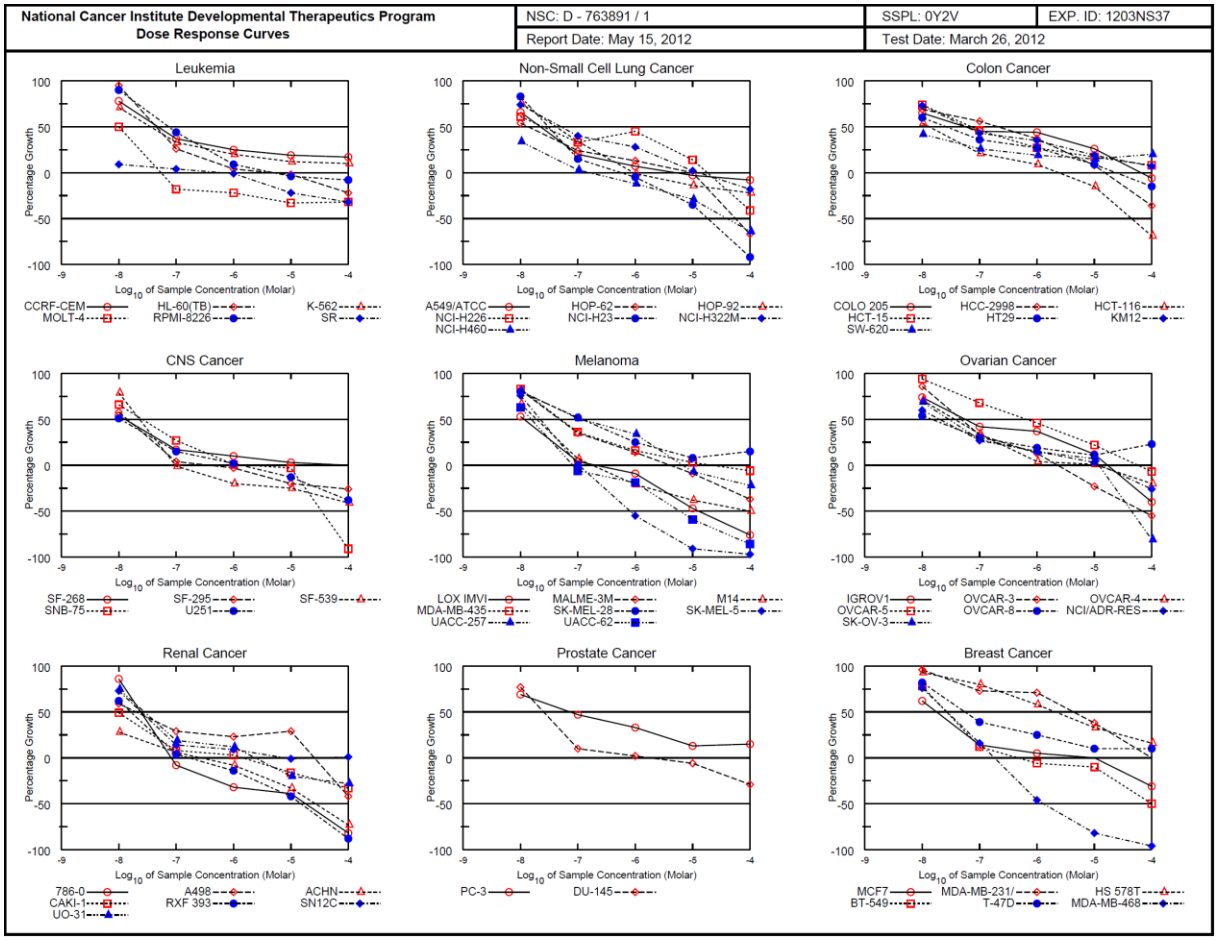

6-Hydroxy-12,13-dimethyl-12,13-dihydro-5*H*-pyrido[2,3-*b*]pyrido[3',2':4,5]pyrrolo[3,2-*g*]pyrrolo[3,4-*e*]indole-5,7(6*H*)-dione (373)

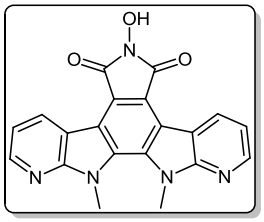

National Cancer Institute Developmental Therapeutics Program
In-Vitro Testing Results

NSC : D - 763891 / 1	Experiment ID : 1203NS37	Test Type : 08	Units : Molar
Report Date : May 15, 2012	Test Date : March 26, 2012	QNS :	MC :
COMI : MC-5-458 (115193)	Stain Reagent : SRB Dual-Pass Related	SSPL : 0Y2V	

			Log10 Concentration											
	Time		Mean Optical Densities					Percent Growth						
Panel/Cell Line	Zero	Ctrl	-8.0	-7.0	-6.0	-5.0	-4.0	-8.0	-7.0	-6.0	-5.0	-4.0	GI50	TGI	LC50
Leukemia															
CCRF-CEM	0.709	2.669	2.239	1.430	1.206	1.079	1.049	78	37	25	19	17	4.78E-8	> 1.00E-4	> 1.00E-4
HL-60(TB)	0.902	2.514	2.433	1.316	0.963	0.881	0.700	95	26	4	-2	-22	4.46E-8	4.16E-6	> 1.00E-4
K-562	0.273	1.770	1.338	0.770	0.566	0.451	0.421	71	33	20	12	10	3.60E-8	> 1.00E-4	> 1.00E-4
MOLT-4	0.728	2.437	1.591	0.594	0.571	0.489	0.499	50	-18	-22	-33	-32	1.02E-8	5.40E-8	> 1.00E-4
RPMI-8226	0.911	2.498	2.332	1.610	1.048	0.874	0.842	90	44	9	-4	-8	7.39E-8	4.76E-6	> 1.00E-4
SR	0.453	1.590	0.557	0.495	0.448	0.354	0.307	9	4	-1	-22	-32	< 1.00E-8	5.89E-7	> 1.00E-4
Non-Small Cell Lung Cancer															
A549/ATCC	0.256	1.257	0.912	0.458	0.327	0.250	0.235	66	20	7	-3	-8	2.20E-8	5.43E-6	> 1.00E-4
HOP-62	0.332	0.954	0.667	0.482	0.411	0.335	0.109	54	24	13	.	-67	1.35E-8	1.01E-5	5.55E-5
HOP-92	1.339	1.696	1.610	1.462	1.323	1.150	1.045	76	34	-1	-14	-22	4.20E-8	9.25E-7	> 1.00E-4
NCI-H226	0.563	1.104	0.893	0.741	0.806	0.640	0.331	61	33	45	14	-41	2.46E-8	1.80E-5	> 1.00E-4
NCI-H23	0.598	1.838	1.628	0.788	0.568	0.387	0.048	83	15	-5	-35	-92	3.07E-8	5.62E-7	1.81E-5
NCI-H322M	0.849	1.703	1.484	1.194	1.090	0.866	0.695	74	40	28	2	-18	5.21E-8	1.25E-5	> 1.00E-4
NCI-H460	0.255	2.118	0.893	0.304	0.224	0.181	0.092	34	3	-12	-29	-64	< 1.00E-8	1.49E-7	3.96E-5
Colon Cancer															
COLO 205	0.321	1.065	0.805	0.653	0.647	0.512	0.302	65	45	44	26	-6	5.44E-8	6.43E-5	> 1.00E-4
HCC-2998	0.364	1.123	0.884	0.791	0.646	0.422	0.233	69	56	37	8	-36	2.13E-7	1.49E-5	> 1.00E-4
HCT-116	0.227	1.749	1.043	0.540	0.360	0.192	0.071	54	21	9	-15	-69	1.29E-8	2.30E-6	4.45E-5
HCT-15	0.311	1.819	1.428	1.005	0.720	0.575	0.430	74	46	27	17	8	7.22E-8	> 1.00E-4	> 1.00E-4
HT29	0.223	1.285	0.863	0.601	0.513	0.322	0.190	60	36	27	9	-15	2.60E-8	2.41E-5	> 1.00E-4
KM12	0.443	2.042	1.610	1.138	1.002	0.752	0.551	73	43	35	19	7	6.00E-8	> 1.00E-4	> 1.00E-4
SW-620	0.288	1.777	0.913	0.671	0.575	0.518	0.588	42	26	19	15	20	< 1.00E-8	> 1.00E-4	> 1.00E-4
CNS Cancer															
SF-268	0.605	1.840	1.275	0.811	0.734	0.639	0.611	54	17	10	3	.	1.30E-8	> 1.00E-4	> 1.00E-4
SF-295	0.963	2.440	1.815	1.015	0.935	0.773	0.713	58	4	-3	-20	-26	1.39E-8	3.53E-7	> 1.00E-4
SF-539	0.954	2.333	2.046	0.947	0.763	0.717	0.560	79	-1	-20	-25	-41	2.32E-8	9.78E-8	> 1.00E-4
SNB-75	0.687	1.232	1.044	0.837	0.690	0.669	0.062	66	27	1	-3	-91	2.56E-8	1.49E-6	3.44E-5
U251	0.326	1.550	0.956	0.511	0.351	0.284	0.204	51	15	2	-13	-38	1.10E-8	1.37E-6	> 1.00E-4
Melanoma															
LOX IMVI	0.300	1.951	1.173	0.369	0.275	0.158	0.073	53	4	-9	-47	-76	1.15E-8	2.14E-7	1.24E-5
MALME-3M	0.686	1.249	1.146	0.881	0.768	0.623	0.430	82	35	14	-9	-37	4.73E-8	4.09E-6	> 1.00E-4
M14	0.454	1.504	1.155	0.525	0.360	0.284	0.229	67	7	-21	-38	-50	1.90E-8	1.76E-7	> 1.00E-4
MDA-MB-435	0.461	1.906	1.660	0.984	0.698	0.500	0.433	83	36	16	3	-6	5.06E-8	2.00E-5	> 1.00E-4
SK-MEL-28	0.371	0.950	0.833	0.675	0.516	0.415	0.456	80	52	25	8	15	1.22E-7	> 1.00E-4	> 1.00E-4
SK-MEL-5	0.681	2.385	1.982	0.705	0.306	0.059	0.020	76	1	-55	-91	-97	2.25E-8	1.06E-7	8.13E-7
UACC-257	0.558	1.285	1.146	0.927	0.808	0.517	0.436	81	51	34	-7	-22	1.10E-7	6.67E-6	> 1.00E-4
UACC-62	0.917	2.080	1.647	0.861	0.741	0.373	0.129	63	-6	-19	-59	-86	1.53E-8	8.15E-8	5.85E-6
Ovarian Cancer															
IGROV1	0.652	1.815	1.515	1.144	1.081	0.795	0.391	74	42	37	12	-40	5.73E-8	1.72E-5	> 1.00E-4
OVCAR-3	0.521	1.424	1.298	0.820	0.634	0.401	0.235	86	33	13	-23	-55	4.79E-8	2.24E-6	7.01E-5
OVCAR-4	0.418	0.782	0.676	0.541	0.434	0.423	0.333	71	34	4	1	-20	3.64E-8	1.16E-5	> 1.00E-4
OVCAR-5	0.453	1.274	1.225	1.008	0.834	0.631	0.423	94	68	46	22	-7	6.78E-7	5.83E-5	> 1.00E-4
OVCAR-8	0.282	1.261	0.813	0.575	0.465	0.387	0.506	54	30	19	11	23	1.49E-8	> 1.00E-4	> 1.00E-4
NCI/ADR-RES	0.393	1.446	1.024	0.678	0.551	0.427	0.292	60	27	15	3	-26	2.00E-8	1.29E-5	> 1.00E-4
SK-OV-3	0.531	1.075	0.905	0.682	0.610	0.567	0.104	69	28	15	7	-81	2.86E-8	1.19E-5	4.46E-5
Renal Cancer															
786-0	0.774	2.295	2.079	0.713	0.523	0.472	0.139	86	-8	-32	-39	-82	2.41E-8	8.23E-8	1.79E-5
A498	1.111	1.622	1.411	1.258	1.230	1.259	0.645	59	29	23	29	-42	1.95E-8	2.56E-5	> 1.00E-4
ACHN	0.344	1.443	0.655	0.415	0.316	0.232	0.092	28	6	-8	-33	-73	< 1.00E-8	2.76E-7	2.68E-5
CAKI-1	0.809	2.225	1.506	0.917	0.851	0.676	0.544	49	8	3	-16	-33	< 1.00E-8	1.42E-6	> 1.00E-4
RXF 393	0.682	1.077	0.928	0.697	0.584	0.396	0.083	62	4	-14	-42	-88	1.61E-8	1.61E-7	1.50E-5
SN12C	0.545	1.810	1.472	0.718	0.661	0.542	0.558	73	14	9	-1	1	2.46E-8	.	> 1.00E-4
UO-31	0.897	2.025	1.744	1.115	1.036	0.719	0.643	75	19	12	-20	-28	2.82E-8	2.42E-6	> 1.00E-4
Prostate Cancer															
PC-3	0.466	1.748	1.347	1.065	0.890	0.629	0.656	69	47	33	13	15	7.11E-8	> 1.00E-4	> 1.00E-4
DU-145	0.365	1.332	1.107	0.460	0.387	0.343	0.259	77	10	2	-6	-29	2.51E-8	1.86E-6	> 1.00E-4
Breast Cancer															
MCF7	0.330	1.733	1.200	0.530	0.399	0.329	0.228	62	14	5	.	-31	1.78E-8	8.23E-6	> 1.00E-4
MDA-MB-231/ATCC	0.599	1.175	1.155	1.018	1.011	0.821	0.598	96	73	71	38	.	4.47E-6	9.85E-5	> 1.00E-4
HS 578T	0.853	1.501	1.458	1.374	1.232	1.067	0.957	93	80	58	33	16	2.15E-6	> 1.00E-4	> 1.00E-4
BT-549	0.908	1.699	1.525	1.006	0.858	0.814	0.459	78	12	-6	-10	-50	2.67E-8	4.92E-7	> 1.00E-4
T-47D	0.558	1.279	1.152	0.841	0.737	0.628	0.627	82	39	25	10	10	5.62E-8	> 1.00E-4	> 1.00E-4
MDA-MB-468	0.551	1.304	1.122	0.671	0.298	0.100	0.023	76	16	-46	-82	-96	2.70E-8	1.81E-7	1.30E-6